

FEMA 307

EVALUATION OF EARTHQUAKE DAMAGED CONCRETE AND MASONRY WALL BUILDINGS

Technical Resources

Prepared by:



The Applied Technology Council

555 Twin Dolphin Drive, Suite 550
Redwood City, California 94065

Prepared for:

The Partnership for Response and Recovery

Washington, D.C.

Funded by:

Federal Emergency Management Agency

1998

Applied Technology Council

The Applied Technology Council (ATC) is a nonprofit, tax-exempt corporation established in 1971 through the efforts of the Structural Engineers Association of California. ATC is guided by a Board of Directors consisting of representatives appointed by the American Society of Civil Engineers, the Structural Engineers Association of California, the Western States Council of Structural Engineers Associations, and four at-large representatives concerned with the practice of structural engineering. Each director serves a three-year term.

The purpose of ATC is to assist the design practitioner in structural engineering (and related design specialty fields such as soils, wind, and earthquake) in the task of keeping abreast of and effectively using technological developments. ATC also identifies and encourages needed research and develops consensus opinions on structural engineering issues in a nonproprietary format. ATC thereby fulfills a unique role in funded information transfer.

Project management and administration are carried out by a full-time Executive Director and support staff. Project work is conducted by a wide range of highly qualified consulting professionals, thus incorporating the experience of many individuals from academia, research, and professional practice who would not be available from any single organization. Funding for ATC projects is obtained from government agencies and from the private sector in the form of tax-deductible contributions.

1998-1999 Board of Directors

Charles H. Thornton, President
Edwin T. Dean, Vice President
Andrew T. Merovich, Secretary/
Treasurer
C. Mark Saunders, Past President
James R. Cagley
Arthur N. L. Chiu
Robert G. Dean

Edwin H. Johnson
Kenneth A. Luttrell
Newland J. Malmquist
Stephen H. Pelham
Richard J. Phillips
Charles W. Roeder
Jonathan G. Shipp

Notice

This report was prepared under Contract EMW-95-C-4685 between the Federal Emergency Management Agency and the Partnership for Response and Recovery.

Any opinions, findings, conclusions, or recommendations expressed in this publication do not necessarily reflect the views of the Applied Technology Council (ATC), the Partnership for Response and Recovery (PaRR), or the Federal Emergency Management Agency (FEMA). Additionally, neither ATC, PaRR, FEMA, nor any of their employees makes any warranty, expressed or implied, nor assumes any legal liability or responsibility for the accuracy, completeness, or usefulness of any information, product, or process included in this publication. Users of information from this publication assume all liability arising from such use.

For further information concerning this document or the activities of the ATC, contact the Executive Director, Applied Technology Council, 555 Twin Dolphin Drive, Suite 550, Redwood City, California 94065; phone 650-595-1542; fax 650-593-2320; e-mail atc@atcouncil.org.

Preface

Following the two damaging California earthquakes in 1989 (Loma Prieta) and 1994 (Northridge), many concrete wall and masonry wall buildings were repaired using federal disaster assistance funding. The repairs were based on inconsistent criteria, giving rise to controversy regarding criteria for the repair of cracked concrete and masonry wall buildings. To help resolve this controversy, the Federal Emergency Management Agency (FEMA) initiated a project on evaluation and repair of earthquake damaged concrete and masonry wall buildings in 1996. The project was conducted through the Partnership for Response and Recovery (PaRR), a joint venture of Dewberry & Davis of Fairfax, Virginia, and Woodward-Clyde Federal Services of Gaithersburg, Maryland. The Applied Technology Council (ATC), under subcontract to PaRR, was responsible for developing technical criteria and procedures (the ATC-43 project).

The ATC-43 project addresses the investigation and evaluation of earthquake damage and discusses policy issues related to the repair and upgrade of earthquake-damaged buildings. The project deals with buildings whose primary lateral-force-resisting systems consist of concrete or masonry bearing walls with flexible or rigid diaphragms, or whose vertical-load-bearing systems consist of concrete or steel frames with concrete or masonry infill panels. The intended audience is design engineers, building owners, building regulatory officials, and government agencies.

The project results are reported in three documents. The FEMA 306 report, *Evaluation of Earthquake Damaged Concrete and Masonry Wall Buildings, Basic Procedures Manual*, provides guidance on evaluating damage and analyzing future performance. Included in the document are component damage classification guides, and test and inspection guides. FEMA 307, *Evaluation of Earthquake Damaged Concrete and Masonry Wall Buildings, Technical Resources*, contains supplemental information including results from a theoretical analysis of the effects of prior damage on single-degree-of-freedom mathematical models, additional background information on the component guides, and an example of the application of the basic procedures. FEMA 308, *The Repair of Earthquake Damaged Concrete and Masonry Wall Buildings*, discusses the policy issues pertaining to the repair of earthquake damaged buildings and illustrates how the procedures developed for the project can be used to provide a technically sound basis for policy decisions. It

also provides guidance for the repair of damaged components.

The project also involved a workshop to provide an opportunity for the user community to review and comment on the proposed evaluation and repair criteria. The workshop, open to the profession at large, was held in Los Angeles on June 13, 1997 and was attended by 75 participants.

The project was conducted under the direction of ATC Senior Consultant Craig Comartin, who served as Co-Principal Investigator and Project Director. Technical and management direction were provided by a Technical Management Committee consisting of Christopher Rojahn (Chair), Craig Comartin (Co-Chair), Daniel Abrams, Mark Doroudian, James Hill, Jack Moehle, Andrew Merovich (ATC Board Representative), and Tim McCormick. The Technical Management Committee created two Issue Working Groups to pursue directed research to document the state of the knowledge in selected key areas: (1) an Analysis Working Group, consisting of Mark Aschheim (Group Leader) and Mete Sozen (Senior Consultant) and (2) a Materials Working Group, consisting of Joe Maffei (Group Leader and Reinforced Concrete Consultant), Greg Kingsley (Reinforced Masonry Consultant), Bret Lizundia (Unreinforced Masonry Consultant), John Mander (Infilled Frame Consultant), Brian Kehoe and other consultants from Wiss, Janney, Elstner and Associates (Tests, Investigations, and Repairs Consultant). A Project Review Panel provided technical overview and guidance. The Panel members were Gregg Borchelt, Gene Corley, Edwin Huston, Richard Klingner, Vilas Mujumdar, Hassan Sassi, Carl Schulze, Daniel Shapiro, James Wight, and Eugene Zeller. Nancy Sauer and Peter Mork provided technical editing and report production services, respectively. Affiliations are provided in the list of project participants.

The Applied Technology Council and the Partnership for Response and Recovery gratefully acknowledge the cooperation and insight provided by the FEMA Technical Monitor, Robert D. Hanson.

Tim McCormick
PaRR Task Manager

Christopher Rojahn
ATC-43 Principal Investigator
ATC Executive Director

Table of Contents

Preface	iii
List of Figures	ix
List of Tables	xiii
Prologue	xv
1. Introduction	1
1.1 Purpose And Scope	1
1.2 Materials Working Group	1
1.2.1 Tests and Investigations	1
1.2.2 Component Behavior and Modeling	1
1.2.3 Repair Techniques	2
1.3 Analysis Working Group	3
1.4 References	4
2. Reinforced Concrete Components	7
2.1 Commentary and Discussion	7
2.1.1 Development of Component Guides and λ -Factors	7
2.2 Typical Force-Displacement Hysteretic Behavior	10
2.3 Tabular Bibliography	28
2.4 Symbols for Reinforced Concrete	33
2.5 References for Reinforced Concrete	35
3. Reinforced Masonry	39
3.1 Commentary and Discussion	39
3.1.1 Typical Hysteretic Behavior	39
3.1.2 Cracking and Damage Severity	39
3.1.3 Interpretation of Tests	46
3.2 Tabular Bibliography for Reinforced Masonry	46
3.3 Symbols for Reinforced Masonry	53
3.4 References for Reinforced Masonry	54
4. Unreinforced Masonry	59
4.1 Commentary and Discussion	59
4.1.1 Hysteretic Behavior of URM Walls Subjected to In-Plane Demands	59
4.1.2 Comments on FEMA 273 Component Force/Displacement Relationships	72
4.1.3 Development of λ -factors	75
4.2 Tabular Bibliography for Unreinforced Masonry	77
4.3 Symbols for Unreinforced Masonry	80

4.4	References for Unreinforced Masonry	81
5.	Infilled Frames	85
5.1	Commentary And Discussion	85
5.1.1	Development of λ -Factors for Component Guides	85
5.1.2	Development of Stiffness Deterioration— λ_K	85
5.1.3	The Determination of λ_Q for Strength Deterioration	86
5.1.4	Development of λ_D —Reduction in Displacement Capability	87
5.2	Tabular Bibliography for Infilled Frames	89
5.3	References for Infilled Frames	91
6.	Analytical Studies	95
6.1	Overview	95
6.2	Summary of Previous Findings	95
6.2.1	Hysteresis Models	95
6.2.2	Effect of Ground Motion Duration	98
6.2.3	Residual Displacement	98
6.2.4	Repeated Loading	98
6.3	Dynamic Analysis Framework	99
6.3.1	Overview	99
6.3.2	Dynamic Analysis Approach	99
6.3.3	Ground Motions	100
6.3.4	Force/Displacement Models	120
6.3.5	Undamaged Oscillator Parameters	122
6.3.6	Damaged Oscillator Parameters	123
6.3.7	Summary of Dynamic Analysis Parameters	125
6.3.8	Implementation of Analyses	126
6.4	Results Of Dynamic Analyses	126
6.4.1	Overview and Nomenclature	126
6.4.2	Response of Bilinear Models	127
6.4.3	Response of Takeda Models	127
6.4.4	Response Statistics	151
6.5	Nonlinear Static Procedures	155
6.5.1	Introduction	155
6.5.2	Description of Nonlinear Static Procedures	156
6.5.3	Comments on Procedures	159
6.5.4	Application of Procedures to Undamaged and Damaged Oscillators	160
6.6	Comparison of NSP and Dynamic Analysis Results	160
6.6.1	Introduction	160
6.6.2	Displacement Estimation	160
6.6.3	Displacement Ratio Estimation	161
6.7	Conclusions and Implications	177
6.8	References	178

7.	Example Application	181
7.1	Introduction	181
7.1.1	Objectives	181
7.1.2	Organization	181
7.2	Investigation	183
7.2.1	Building Description	183
7.2.2	Postearthquake Damage Observations	183
7.2.3	Preliminary Classification (by Observation) of Component Types, Behavior Modes, and Damage Severity	189
7.2.4	Final Classification (by Analysis) of Component Type, Behavior Mode and Damage Severity	190
7.2.5	Other Damage Observations	195
7.2.6	Summary of Component Classifications	195
7.3	Evaluation by the Direct Method	199
7.3.1	Structural Restoration Measures	199
7.3.2	Nonstructural Restoration Measures	201
7.3.3	Restoration Summary and Cost	201
7.4	Evaluation by Performance Analysis	201
7.4.1	Performance Objectives	202
7.4.2	Nonlinear Static Analysis	203
7.4.3	Force-Displacement Capacity (Pushover Analysis) Results	206
7.4.4	Estimation of Displacement, d_e , Caused by Damaging Earthquake	209
7.4.5	Displacement Demand	210
7.4.6	Analysis of Restored Structure	212
7.4.7	Performance Restoration Measures	214
7.5	Discussion of Results	214
7.5.1	Discussion of Building Performance	214
7.5.2	Discussion of Methodology and Repair Costs	215
7.6	References	215
	Appendix A. Component Damage Records for Building Evaluated in Example Application	217
	ATC-43 Project Participants	237
	Applied Technology Council Projects And Report Information	241

List of Figures

Figure 1-1	Component Force-Deformation Relationships	2
Figure 1-2	Generalized Undamaged and Damaged Component Curves	3
Figure 1-3	Effect of Damage on Building Response	4
Figure 1-4	Global Load-Displacement Relationships	5
Figure 2-1	Diagram of process used to develop component guides and component modification factors.	8
Figure 4-1	Bed-joint sliding force/displacement relationship	73
Figure 4-2	Relationship Between Toe Crushing and Bed-Joint Sliding	74
Figure 4-3	Developing the initial portion of the damaged force/displacement relationship	76
Figure 5-1	Energy-based damage analysis of strength reduction to define λ_Q	88
Figure 6-1	Effect of Hysteretic Properties on Response to 1940 NS El Centro Record (from Nakamura, 1988)	97
Figure 6-2	Characteristics of the WN87MWLN.090 (Mount Wilson) Ground Motion	102
Figure 6-3	Characteristics of the BB92CIVC.360 (Big Bear) Ground Motion	103
Figure 6-4	Characteristics of the SP88GUKA.360 (Spitak) Ground Motion	104
Figure 6-5	Characteristics of the LP89CORR.090 (Corralitos) Ground Motion	105
Figure 6-6	Characteristics of the NR94CENT.360 (Century City) Ground Motion	106
Figure 6-7	Characteristics of the IV79ARY7.140 (Imperial Valley Array) Ground Motion	107
Figure 6-8	Characteristics of the CH85LLEO.010 (Llolleo) Ground Motion	108
Figure 6-9	Characteristics of the CH85VALP.070 (Valparaiso University) Ground Motion	109
Figure 6-10	Characteristics of the IV40ELCN.180 (El Centro) Ground Motion	110
Figure 6-11	Characteristics of the TB78TABS.344 (Tabas) Ground Motion	111
Figure 6-12	Characteristics of the LN92JOSH.360 (Joshua Tree) Ground Motion	112
Figure 6-13	Characteristics of the MX85SCT1.270 (Mexico City) Ground Motion	113
Figure 6-14	Characteristics of the LN92LUCN.250 (Lucerne) Ground Motion	114
Figure 6-15	Characteristics of the IV79BRWY.315 (Brawley Airport) Ground Motion	115
Figure 6-16	Characteristics of the LP89SARA.360 (Saratoga) Ground Motion	116
Figure 6-17	Characteristics of the NR94NWHL.360 (Newhall) Ground Motion	117
Figure 6-18	Characteristics of the NR94SYLH.090 (Sylmar Hospital) Ground Motion	118
Figure 6-19	Characteristics of the KO95TTRI.360 (Takatori) Ground Motion	119
Figure 6-20	Force-Displacement Hysteretic Models	120
Figure 6-21	Degrading Models Used in the Analyses	121
Figure 6-22	Bilinear Model Used to Determine Strengths of Degrading Models	122
Figure 6-23	Specification of the Pinching Point for the Takeda Pinching Model	122
Figure 6-24	Specification of the Uncracked Stiffness, Cracking Strength, and Unloading Stiffness for the Takeda Models	123
Figure 6-25	Construction of Initial Force-Displacement Response for Prior Ductility Demand > 0 and Reduced Strength Ratio = 1	123
Figure 6-26	Construction of Initial Force-Displacement Response for PDD > 0 and RSR < 1 for Takeda5 and Takeda10 Models	124

Figure 6-27	Strength Degradation for Takeda Pinching Model	125
Figure 6-28	Construction of Initial Force-Displacement Response for $PDD > 0$ and $RSR < 1$ for Takeda Pinching Model	126
Figure 6-29	Response of Bilinear Oscillators to Short Duration Records ($DDD = 8$)	128
Figure 6-30	Response of Bilinear Oscillators to Long Duration Records ($DDD = 8$)	129
Figure 6-31	Response of Bilinear Oscillators to Forward Directive Records ($DDD = 8$)	130
Figure 6-32	Displacement Response of Takeda Models Compared with Elastic Response and Bilinear Response, for Short-Duration Records ($DDD = 8$ and $RSR = 1$)	131
Figure 6-33	Displacement Response of Takeda Models Compared with Elastic Response and Bilinear Response for Long-Duration Records ($DDD = 8$ and $RSR = 1$)	132
Figure 6-34	Displacement Response of Takeda Models Compared with Elastic Response and Bilinear Response for Forward Directive Records ($DDD = 8$ and $RSR = 1$)	133
Figure 6-35	Effect of Cracking Without and With Strength Reduction on Displacement Response of Takeda5 Models, for Short-Duration Records ($DDD = 8$ and $PDD = 1$)	135
Figure 6-36	Effect of Cracking Without and With Strength Reduction on Displacement Response of Takeda5 Models, for Long-Duration Records ($DDD = 8$ and $PDD = 1$)	136
Figure 6-37	Effect of Cracking Without and With Strength Reduction on Displacement Response of Takeda5 Models, for Forward Directive Records ($DDD = 8$ and $PDD = 1$)	137
Figure 6-38	Effect of Large Prior Ductility Demand Without and With Strength Reduction on Displacement Response of Takeda5 Models, for Short Duration Records ($DDD = 8$ and $PDD = 8$)	138
Figure 6-39	Effect of Large Prior Ductility Demand Without and With Strength Reduction on Displacement Response of Takeda5 Models, for Long Duration Records ($DDD = 8$ and $PDD = 8$)	139
Figure 6-40	Effect of Large Prior Ductility Demand Without and With Strength Reduction on Displacement Response of Takeda5 Models, for Forward Directive Records ($DDD = 8$ and $PDD = 8$)	140
Figure 6-41	Effect of Damage on Response to El Centro (IV40ELCN.180) for Takeda5, $T = 0.2$ sec ($DDD = 8$)	141
Figure 6-42	Effect of Damage on Response to El Centro (IV40ELCN.180) for Takeda5, $T = 0.5$ sec ($DDD = 8$)	142
Figure 6-43	Effect of Damage on Response to El Centro (IV40ELCN.180) for Takeda5, $T = 1.0$ sec ($DDD = 8$)	143
Figure 6-44	Effect of Damage on Response to El Centro (IV40ELCN.180) for Takeda5, $T = 1.5$ sec ($DDD = 8$)	144
Figure 6-45	Effect of Damage on Response to El Centro (IV40ELCN.180) for Takeda5, $T = 2.0$ sec ($DDD = 8$)	145
Figure 6-46	Effect of Large Prior Ductility Demand Without and With Strength Reduction on Displacement Response of TakPinch Models, for Short Duration Records ($DDD = 8$ and $PDD = 8$)	146
Figure 6-47	Effect of Large Prior Ductility Demand Without and With Strength Reduction on Displacement Response of TakPinch Models, for Long Duration Records ($DDD = 8$ and $PDD = 8$)	147
Figure 6-48	Effect of Large Prior Ductility Demand Without and With Strength Reduction on Displacement Response of TakPinch, for Forward Directive Records ($DDD = 8$ and $PDD = 8$)	148
Figure 6-49	Effect of Damage on Response of TakPinch Model to El Centro (IV40ELCN.180) for	

	T=1.0 sec and RSR= 1 (DDD= 8)	149
Figure 6-50	Effect of Damage on Response of TakPinch Model to El Centro (IV40ELCN.180) for T=1.0 sec and RSR = 0.6 (DDD= 8)	150
Figure 6-51	Effect of Cracking on Displacement Response of Takeda10 Model for Short Duration Records (DDD= 8 and PDD=1)	151
Figure 6-52	Effect of Cracking on Displacement Response of Takeda10 Model for Long-Duration Records (DDD= 8 and PDD=1)	152
Figure 6-53	Effect of Cracking on Displacement Response of Takeda10 Model for Forward Directive Records (DDD= 8 and PDD=1)	152
Figure 6-54	Effect of Damage on Response of Takeda10 Model to El Centro (IV40ELCN.180) for T=1.0 sec and RSR= 1 (DDD= 8)	153
Figure 6-55	Mean and Standard Deviation Values of d'_d/d_d for Takeda5 Model.	154
Figure 6-56	Mean and Standard Deviation Values of d'_d/d_d for TakPinch Model.	155
Figure 6-57	Percent of Takeda10 Oscillators that Collapsed	156
Figure 6-58	Construction of Effective Stiffness for use with the Displacement Coefficient Method	157
Figure 6-59	Initial Effective Stiffness and Capacity Curves Used in the Secant and Capacity Spectrum Methods	158
Figure 6-60	Schematic Depiction of Secant Method Displacement Estimation	158
Figure 6-61	Schematic Depiction of Successive Iterations to Estimate Displacement Response Using the Secant Method for Single-Degree-of-Freedom Oscillators	159
Figure 6-62	Schematic Depiction of Successive Iterations to Estimate Displacement Response Using the Capacity Spectrum Method	159
Figure 6-63	Values of $d_{d,NSP}/d_d$ for the Takeda5 Model	162
Figure 6-64	Mean values of $d_{d,NSP}/d_d$ for all ground motions for each NSP method, for short and long-period Takeda5 Models. See text in Section 6.6.3.	163
Figure 6-65	Coefficient Method Estimates of Ratio of Damaged and Undamaged Oscillator Displacement Normalized by Computed Ratio, for Short-Duration Records	163
Figure 6-66	Coefficient Method Estimates of Ratio of Damaged and Undamaged Oscillator Displacement Normalized by Computed Ratio, for Long-Duration Records	164
Figure 6-67	Coefficient Method Estimates of Ratio of Damaged and Undamaged Oscillator Displacement Normalized by Computed Ratio, for Forward Directive Records	164
Figure 6-68	Secant Method Estimates of Ratio of Damaged and Undamaged Oscillator Displacement Normalized by Computed Ratio, for Short-Duration Records	165
Figure 6-69	Secant Method Estimates of Ratio of Damaged and Undamaged Oscillator Displacement Normalized by Computed Ratio, for Long-Duration Records	165
Figure 6-70	Secant Method Estimates of Ratio of Damaged and Undamaged Oscillator Displacement Normalized by Computed Ratio, for Forward Directive Records	166
Figure 6-71	Capacity Spectrum Method Estimates of Ratio of Damaged and Undamaged Oscillator Displacement Normalized by Computed Ratio, for Short-Duration Records	166
Figure 6-72	Capacity Spectrum Method Estimates of Ratio of Damaged and Undamaged Oscillator Displacement Normalized by Computed Ratio, for Long-Duration Records	167
Figure 6-73	Capacity Spectrum Method Estimates of Ratio of Damaged and Undamaged Oscillator Displacement Normalized by Computed Ratio, for Forward Directive Records	167
Figure 6-74	Coefficient Method Estimates of Displacement Ratio of RSR=0.6 and RSR=1.0 Takeda5 Oscillators having DDD= 8 and PDD= 1	168
Figure 6-75	Coefficient Method Estimates of Displacement Ratio of RSR=0.6 and RSR=1.0	

	Takeda5 Oscillators having DDD= 8 and PDD= 1	169
Figure 6-76	Coefficient Method Estimates of Displacement Ratio of RSR=0.6 and RSR=1.0 Takeda5 Oscillators having DDD= 8 and PDD= 1	170
Figure 6-77	Secant Method Estimates of Displacement Ratio of RSR=0.6 and RSR=1.0 Takeda5 Oscillators having DDD= 8 and PDD= 1	171
Figure 6-78	Secant Method Estimates of Displacement Ratio of RSR=0.6 and RSR=1.0 Takeda5 Oscillators having DDD= 8 and PDD= 1	172
Figure 6-79	Secant Method Estimates of Displacement Ratio of RSR=0.6 and RSR=1.0 Takeda5 Oscillators having DDD= 8 and PDD= 1	173
Figure 6-80	Capacity Spectrum Method Estimates of Displacement Ratio of RSR=0.6 and RSR=1.0 Takeda5 Oscillators having DDD= 8 and PDD= 1	174
Figure 6-81	Capacity Spectrum Method Estimates of Displacement Ratio of RSR=0.6 and RSR=1.0 Takeda5 Oscillators having DDD= 8 and PDD= 1	175
Figure 6-82	Capacity Spectrum Method Estimates of Displacement Ratio of RSR=0.6 and RSR=1.0 Takeda5 Oscillators having DDD= 8 and PDD= 1	176
Figure 7-1	Flowchart for Example	182
Figure 7-2	Floor Plans	184
Figure 7-3	Building Cross-section	185
Figure 7-4	Example Solid Wall Detail	185
Figure 7-5	Example Coupled Wall Detail	186
Figure 7-6	Solid Wall Example	187
Figure 7-7	Coupled Wall Example	188
Figure 7-8	Detail of Coupling Beam Replacement	202
Figure 7-9	Response Spectra for Selected Performance Levels	203
Figure 7-10	Mathematical Model of Coupled Shear Wall	204
Figure 7-11	Mathematical Model of Full Building	205
Figure 7-12	Component Force-Displacement Curves for Coupling Beams	207
Figure 7-13	Comparison of Pre-event and Post-event Pushover Curves	208
Figure 7-14	Response Spectra from Damaging Earthquake	209
Figure 7-15	Comparison of Pre-event and Repaired Pushover Curves	213

List of Tables

Table 2-1	Ranges of Reinforced Concrete Component Displacement Ductility, μ_{Δ} , Associated with Damage Severity Levels and λ Factors	9
Table 2-2	Key References on Reinforced Concrete Wall Behavior.	29
Table 3-1	Damage Patterns and Hysteretic Response for Reinforced Masonry Components	40
Table 3-2	Ranges of Reinforced Masonry Component Displacement Ductility, μ_{Δ} , Associated with Damage Severity Levels and λ Factors	47
Table 3-3	Annotated Bibliography for Reinforced Masonry	48
Table 4-1	Summary of Significant Experimental Research or Research Summaries	78
Table 5-1	Tabular Bibliography for Infilled Frames	89
Table 6-1	Recorded Ground Motions Used in the Analyses	101
Table 7-1	Capacity of Potential Behavior Modes for Typical Solid Wall	191
Table 7-2	Capacity of Potential Behavior Modes for Typical Coupling Beam	193
Table 7-3	Shear Capacities for Potential Behavior Modes of Wall Pier (RC1) Components in Coupled Wall	194
Table 7-4	Summary of Component Type, Behavior Mode, and Damage Severity for Wall Components (North-South Direction)	200
Table 7-5	Summary of Component Type, Behavior Mode, and Damage Severity for Wall Components (East-West Direction)	201
Table 7-6	Restoration Cost Estimate by the Direct Method	202
Table 7-7	Performance Indices for Pre-event and Post-event Structures	212
Table 7-8	Restoration Cost Estimate by the Relative Performance Method	214

Prologue

This document is one of three to result from the ATC-43 project funded by the Federal Emergency Management Agency (FEMA). The goal of the project is to develop technically sound procedures to evaluate the effects of earthquake damage on buildings with primary lateral-force-resisting systems consisting of concrete or masonry bearing walls or infilled frames. The procedures are based on the knowledge derived from research and experience in engineering practice regarding the performance of these types of buildings and their components. The procedures require thoughtful examination and review prior to implementation. The ATC-43 project team strongly urges individual users to read all of the documents carefully to form an overall understanding of the damage evaluation procedures and repair techniques.

Before this project, formalized procedures for the investigation and evaluation of earthquake-damaged buildings were limited to those intended for immediate use in the field to identify potentially hazardous conditions. ATC-20, *Procedures for Postearthquake Safety Evaluation of Buildings*, and its addendum, ATC-20-2 (ATC, 1989 and 1995) are the definitive documents for this purpose. Both have proven to be extremely useful in practical applications. ATC-20 recognizes and states that in many cases, detailed structural engineering evaluations are required to investigate the implications of earthquake damage and the need for repairs. This project provides a framework and guidance for those engineering evaluations.

What have we learned?

The project team for ATC-43 began its work with a thorough review of available analysis techniques, field observations, test data, and emerging evaluation and design methodologies. The first objective was to understand the effects of damage on future building performance. The main points are summarized below.

- **Component behavior controls global performance.**

Recently developed guidelines for structural engineering seismic analysis and design techniques focus on building displacement, rather than forces as the primary parameter for the characterization of

seismic performance. This approach models the building as an assembly of its individual components. Force-deformation properties (e.g., elastic stiffness, yield point, ductility) control the behavior of wall panels, beams, columns, and other components. The component behavior, in turn, governs the overall displacement of the building and its seismic performance. Thus, the evaluation of the effects of damage on building performance must concentrate on how component properties change as a result of damage.

- **Indicators of damage (e.g., cracking, spalling) are meaningful only in light of the mode of component behavior.**

Damage affects the behavior of individual components differently. Some exhibit ductile modes of post-elastic behavior, maintaining strength even with large displacements. Others are brittle and lose strength abruptly after small inelastic displacements. The post-elastic behavior of a structural component is a function of material properties, geometric proportions, details of construction, and the combination of demand actions (axial, flexural, shearing, torsional) imposed upon it. As earthquake shaking imposes these actions on components, the components tend to exhibit predominant modes of behavior as damage occurs. For example, if earthquake shaking and its associated inertial forces and frame distortions cause a reinforced concrete wall panel to rotate at each end, statics defines the relationship between the associated bending moments and shear force. The behavior of the panel depends on its strength in flexure relative to that in shear. Cracks and other signs of damage must be interpreted in the context of the mode of component behavior. A one-eighth-inch crack in a wall panel on the verge of brittle shear failure is a very serious condition. The same size crack in a flexurally-controlled panel may be insignificant with regard to future seismic performance. This is, perhaps, the most important finding of the ATC-43 project: the significance of cracks and other signs of damage, with respect to the future performance of a building, depends on the mode of behavior of the components in which the damage is observed.

- **Damage may reveal component behavior that differs from that predicted by evaluation and design methodologies.**

When designing a building or evaluating an undamaged building, engineers rely on theory and their own experience to visualize how earthquakes will affect the structure. The same is true when they evaluate the effects of actual damage after an earthquake, with one important difference. If engineers carefully observe the nature and extent of the signs of the damage, they can greatly enhance their insight into the way the building actually responded to earthquake shaking. Sometimes the actual behavior differs from that predicted using design equations or procedures. This is not really surprising, since design procedures must account conservatively for a wide range of uncertainty in material properties, behavior parameters, and ground shaking characteristics. Ironically, actual damage during an earthquake has the potential for improving the engineer's knowledge of the behavior of the building. When considering the effects of damage on future performance, this knowledge is important.

- **Damage may not significantly affect displacement demand in future larger earthquakes.**

One of the findings of the ATC-43 project is that prior earthquake damage does not affect maximum displacement response in future, larger earthquakes in many instances. At first, this may seem illogical. Observing a building with cracks in its walls after an earthquake and visualizing its future performance in an even larger event, it is natural to assume that it is worse off than if the damage had not occurred. It seems likely that the maximum displacement in the future, larger earthquake would be greater than if it had not been damaged. Extensive nonlinear time-history analyses performed for the project indicated otherwise for many structures. This was particularly true in cases in which significant strength degradation did not occur during the prior, smaller earthquake. Careful examination of the results revealed that maximum displacements in time histories of relatively large earthquakes tended to occur after the loss of stiffness and strength would have taken place even in an undamaged structure. In other words, the damage that occurs in a prior,

smaller event would have occurred early in the subsequent, larger event anyway.

What does it mean?

The ATC-43 project team has formulated performance-based procedures for evaluating the effects of damage. These can be used to quantify losses and to develop repair strategies. The application of these procedures has broad implications.

- **Performance-based damage evaluation uses the actual behavior of a building, as evidenced by the observed damage, to identify specific deficiencies.**

The procedures focus on the connection between damage and component behavior and the implications for estimating actual behavior in future earthquakes. This approach has several important benefits. First, it provides a meaningful engineering basis for measuring the effects of damage. It also identifies performance characteristics of the building in its pre-event and damaged states. The observed damage itself is used to calibrate the analysis and to improve the building model. For buildings found to have unacceptable damage, the procedures identify specific deficiencies at a component level, thereby facilitating the development of restoration or upgrade repairs.

- **Performance-based damage evaluation provides an opportunity for better allocation of resources.**

The procedures themselves are technical engineering tools. They do not establish policy or prescribe rules for the investigation and repair of damage. They may enable improvements in both private and public policy, however. In past earthquakes, decisions on what to do about damaged buildings have been hampered by a lack of technical procedures to evaluate the effects of damage and repairs. It has also been difficult to investigate the risks associated with various repair alternatives. The framework provided by performance-based damage evaluation procedures can help to remove some of these roadblocks. In the long run, the procedures may tend to reduce the prevailing focus on the loss caused by damage from its pre-event conditions and to increase the focus on what the damage reveals about future building performance. It makes little

sense to implement unnecessary repairs to buildings that would perform relatively well even in a damaged condition. Nor is it wise to neglect buildings in which the component behavior reveals serious hazards regardless of the extent of damage.

- **Engineering judgment and experience are essential to the successful application of the procedures.**

ATC-20 and its addendum, ATC-20-2, were developed to be used by individuals who might be somewhat less knowledgeable about earthquake building performance than practicing structural engineers. In contrast, the detailed investigation of damage using the performance-based procedures of this document and the companion FEMA 306 report (ATC, 1998a) and FEMA 308 report (ATC, 1998b) must be implemented by an experienced engineer. Although the documents include information in concise formats to facilitate field operations, they must not be interpreted as a “match the pictures” exercise for unqualified observers. Use of these guideline materials requires a thorough understanding of the underlying theory and empirical justifications contained in the documents. Similarly, the use of the simplified direct method to estimate losses has limitations. The decision to use this method and the interpretation of the results must be made by an experienced engineer.

- **The new procedures are different from past damage evaluation techniques and will continue to evolve in the future.**

The technical basis of the evaluation procedures is essentially that of the emerging performance-based

seismic and structural design procedures. These will take some time to be assimilated in the engineering community. The same is true for building officials. Seminars, workshops, and training sessions are required not only to introduce and explain the procedures but also to gather feedback and to improve the overall process. Additionally, future materials-testing and analytical research will enhance the basic framework developed for this project. Current project documents are initial editions to be revised and improved over the years.

In addition to the project team, a Project Review Panel has reviewed the damage evaluation and repair procedures and each of the three project documents. This group of experienced practitioners, researchers, regulators, and materials industry representatives reached a unanimous consensus that the products are technically sound and that they represent the state of knowledge on the evaluation and repair of earthquake-damaged concrete and masonry wall buildings. At the same time, all who contributed to this project acknowledge that the recommendations depart from traditional practices. Owners, design professionals, building officials, researchers, and all others with an interest in the performance of buildings during earthquakes are encouraged to review these documents and to contribute to their continued improvement and enhancement. Use of the documents should provide realistic assessments of the effects of damage and valuable insight into the behavior of structures during earthquakes. In the long run, they hopefully will contribute to sensible private and public policy regarding earthquake-damaged buildings.

Prologue

1. Introduction

1.1 Purpose And Scope

The purpose of this document is to provide supplemental information for evaluating earthquake damage to buildings with primary lateral-force-resisting systems consisting of concrete and masonry bearing walls and infilled frames. This document includes background and theoretical information to be used in conjunction with the practical evaluation guidelines and criteria given in *FEMA 306: Evaluation of Earthquake Damaged Concrete and Masonry Wall Buildings - Basics Procedures Manual* (ATC, 1998a). In both documents, concrete and masonry wall buildings include those with vertical-load-bearing wall panels, with and without intermediate openings. In these documents, shear wall buildings also include those with vertical-load-bearing frames of concrete or steel that incorporate masonry or concrete infill panels to resist horizontal forces. The FEMA 306 procedures for these building types address:

- a. The investigation and documentation of damage caused by earthquakes.
- b. The classification of the damage to building components, according to mode of structural behavior and severity.
- c. The evaluation of the effects of the damage on the performance of the building during future earthquakes.
- d. The development of hypothetical measures that would restore the performance to that of the undamaged building.

Supplemental data in this document, FEMA 307, includes the results of the efforts of two issues working groups that focused on the key aspects of adapting and enhancing existing technology for the purposes of the evaluation and repair of earthquake-damaged buildings. The general scope of work for each group is briefly outlined in the following two sections.

1.2 Materials Working Group

The Materials Working Group effort was a part of the overall ATC-43 project. The primary objectives of the Materials Working Group were:

- a. To summarize tests and investigative techniques that can be used to document and evaluate existing structural conditions, particularly the

effects of earthquake damage, in concrete and masonry wall buildings.

- b. To recommend modifications to component force-deformation relationships currently used in nonlinear structural analysis, based on the documented effects of damage similar to that caused by earthquakes.
- c. To describe the specification and efficacy of methods for repair of component damage in a coordinated format suitable for inclusion in the final document.

Figure 1-1 illustrates the idealization of the force-deformation relationships from actual structural component hysteretic data for use in nonlinear analysis. The focus of the Materials Working Group was the generalized force-deformation relationship for structural components of concrete and masonry wall buildings, shown in Figure 1-2.

1.2.1 Tests and Investigations

The scope included review of experimental and analytical research reports, technical papers, standards, and manufacturers' specifications. Practical example applications relating to the documentation, measurement, and quantification of the structural condition of concrete and masonry walls and in-fill frame walls were also reviewed. The reviews focused on tests and investigative techniques for identifying and evaluating cracking, crushing, deterioration, strength, and general quality of concrete or masonry and yielding, fracture, deterioration, strength, and location of reinforcing steel. Based on this review of existing information, practical guidelines for appropriate tests and investigative techniques were developed and are included in FEMA 306. These guidelines consist of outline specifications for equipment, materials, and procedures required to execute the tests, as well as criteria for documenting and interpreting the results.

1.2.2 Component Behavior and Modeling

The members of the group reviewed experimental and analytical research reports, technical papers, and practical example applications relating to the force-deformation behavior of concrete and masonry walls and in-fill frame walls. Of particular interest were the effects of damage of varying nature and extent on the hysteretic characteristics of elements and components

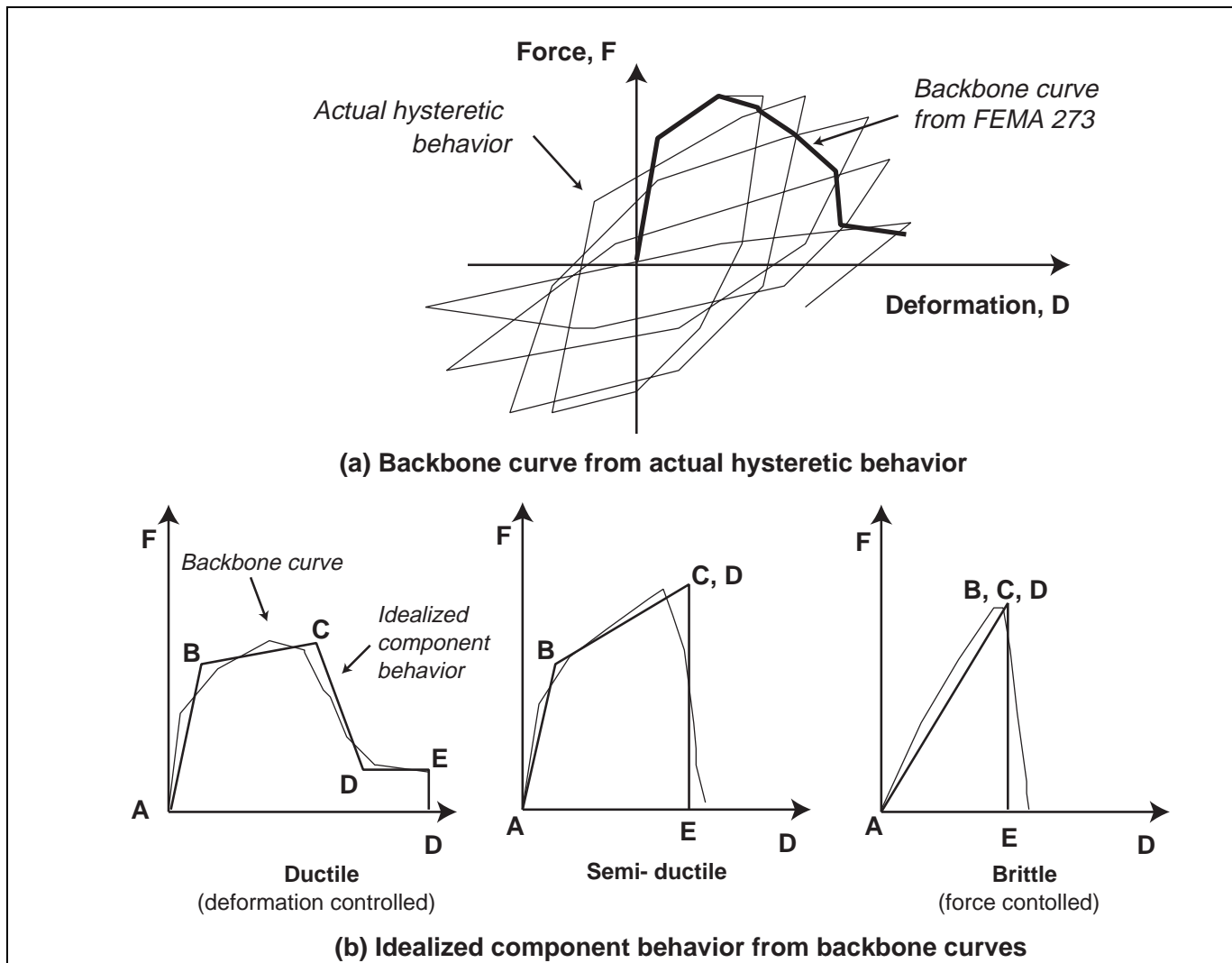


Figure 1-1 Component Force-Deformation Relationships

subject to cyclic lateral loads. The types of damage investigated included cracking and crushing of concrete or masonry and yielding and fracture of reinforcing steel. Components included a wide variety of configurations for vertical-load-bearing and infilled-frame elements. Materials included reinforced concrete, reinforced masonry, and unreinforced masonry.

Based on the review, practical guidelines for identifying and modeling the force-deformation characteristics of damaged components were developed and included in FEMA 306. These consist of modifications (B', C', D', E') to the generalized force-deformation relationships for undamaged components, as shown in Figure 1-2. Supplemental information on these modifications is included in this volume in Chapters 2 (Concrete), 3

(Reinforced Masonry), 4 (Unreinforced Masonry), and 5 (Infilled Frames).

1.2.3 Repair Techniques

The Materials Group also reviewed experimental and analytical research reports, technical papers, standards, manufacturers' specifications, and practical example applications relating to the repair of damage in concrete and masonry walls and infilled-frame walls. The primary interest was the repair of earthquake damage to structural components. The review focused on materials and methods of installation and tests of the effectiveness of repair techniques for cracking, crushing, and deterioration of concrete or masonry and yielding, fracture, and deterioration of reinforcing steel.

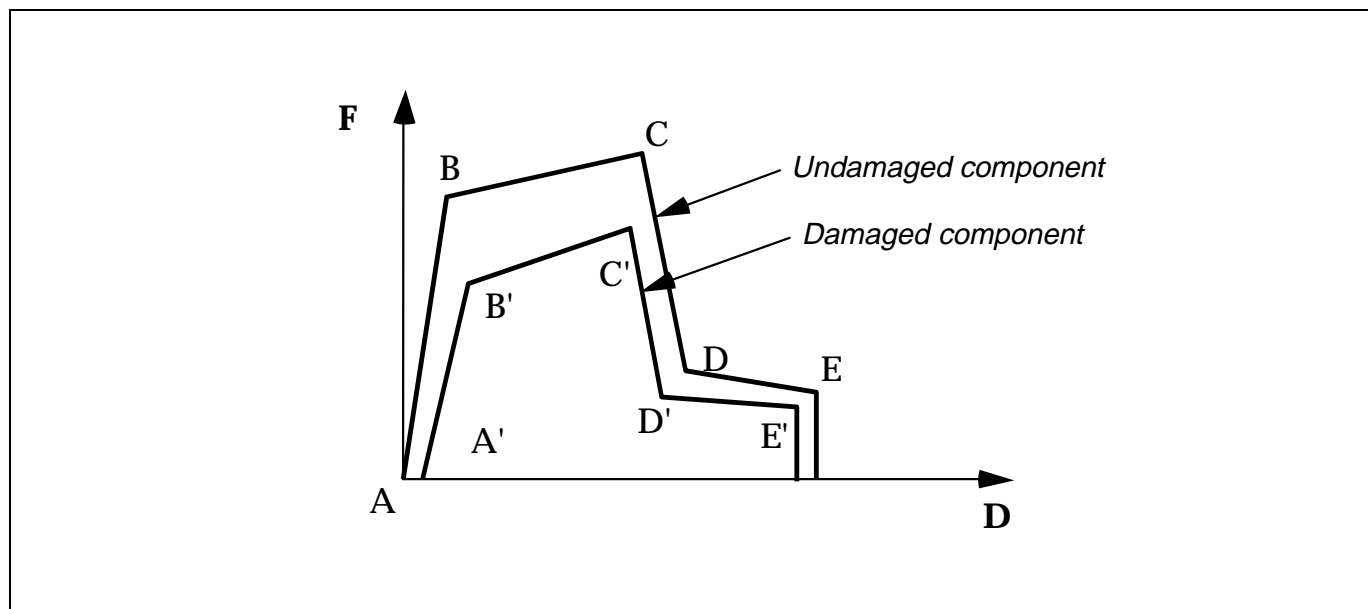


Figure 1-2 Generalized Undamaged and Damaged Component Curves

Based on the review, practical guidelines for damage repair were developed and are contained in *FEMA 308: The Repair of Earthquake Damaged Concrete and Masonry Wall Buildings* (ATC, 1998b). These guidelines consist of outline specifications for equipment, materials, and procedures required to execute the repairs, as well as criteria for quality control and verification of field installations.

1.3 Analysis Working Group

The work of the Analysis Working Group was a sub-project of the overall ATC-43 project. The primary objectives of the group were:

- To determine whether existing structural analysis techniques are capable of capturing the global effects of previous earthquake damage on future seismic performance
- To formulate practical guidance for the use of these analysis techniques in design-oriented evaluation and repair of damaged masonry and concrete wall buildings.

Chapter 6 summarizes the results of the Analysis Working Group efforts. Work consisted primarily of analytical studies of representative single-degree-of-freedom (SDOF) oscillators subjected to a range of earthquake ground motions. The study was formulated

so that the following question might be answered (see Figure 1-3): If a building has experienced damage in an earthquake (the *damaging earthquake*), and if that intermediate damage state can be characterized in terms of its effect on the global force-displacement relationship, how will the damage influence global response to a subsequent earthquake (the *Performance Earthquake*)?

The SDOF oscillators had force-displacement relationships that represent the effects of earthquake damage on the global dynamic response of hypothetical buildings to earthquake ground motions. Types of global force-displacement relationships considered included those shown in Figure 1-4.

The results obtained using existing simplified analyses methods were compared to the time-history results. The group was particularly interested in understanding how nonlinear static analysis methods might be used to represent the findings. Regarding the nonlinear static methods, consideration was given to the applicability of the coefficient method, the capacity-spectrum method, and the secant method of analysis, as summarized in *FEMA-273 NEHRP Guidelines for the Seismic Rehabilitation of Buildings* (ATC, 1997a) and *ATC-40 Seismic Evaluation and Retrofit of Concrete Buildings* (ATC, 1996). The work included a study of the accuracy of the various methods in terms of predicting future performance. The study included an assessment of the

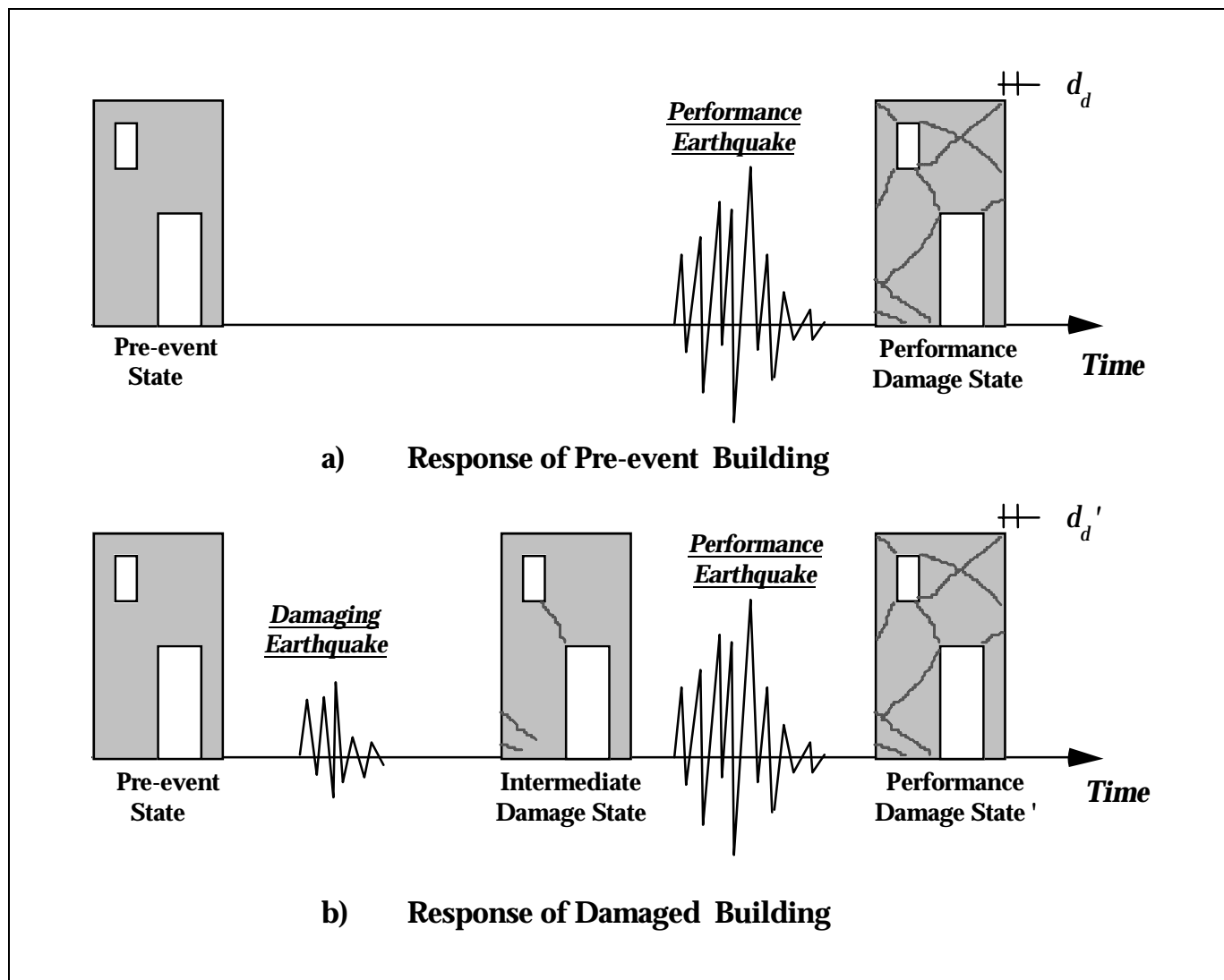


Figure 1-3 Effect of Damage on Building Response

sensitivity of the predictions to variations in global load-deformation characteristics and to variations in ground motion characteristics. The results are reflected in the procedures presented in FEMA 306.

1.4 References

- ATC, 1996, *The Seismic Evaluation and Retrofit of Concrete Buildings*, Applied Technology Council, ATC-40 Report, Redwood City, California.
- ATC, 1997a, *NEHRP Guidelines for the Seismic Rehabilitation of Buildings*, prepared by the Applied Technology Council (ATC-33 project) for the Building Seismic Safety Council, published by the Federal Emergency Management Agency, Report No. FEMA 274, Washington, D.C.
- ATC, 1997b, *NEHRP Commentary on the Guidelines for the Seismic Rehabilitation of Buildings*, prepared by the Applied Technology Council (ATC-33 project) for the Building Seismic Safety Council, published by the Federal Emergency Management Agency, Report No. FEMA 274, Washington, D.C.
- ATC, 1998a, *Evaluation of Earthquake Damaged Concrete and Masonry Wall Buildings, Basic Procedures Manual*, prepared by the Applied Technology Council (ATC-43 project) for the Partnership for Response and Recovery, published by the Federal

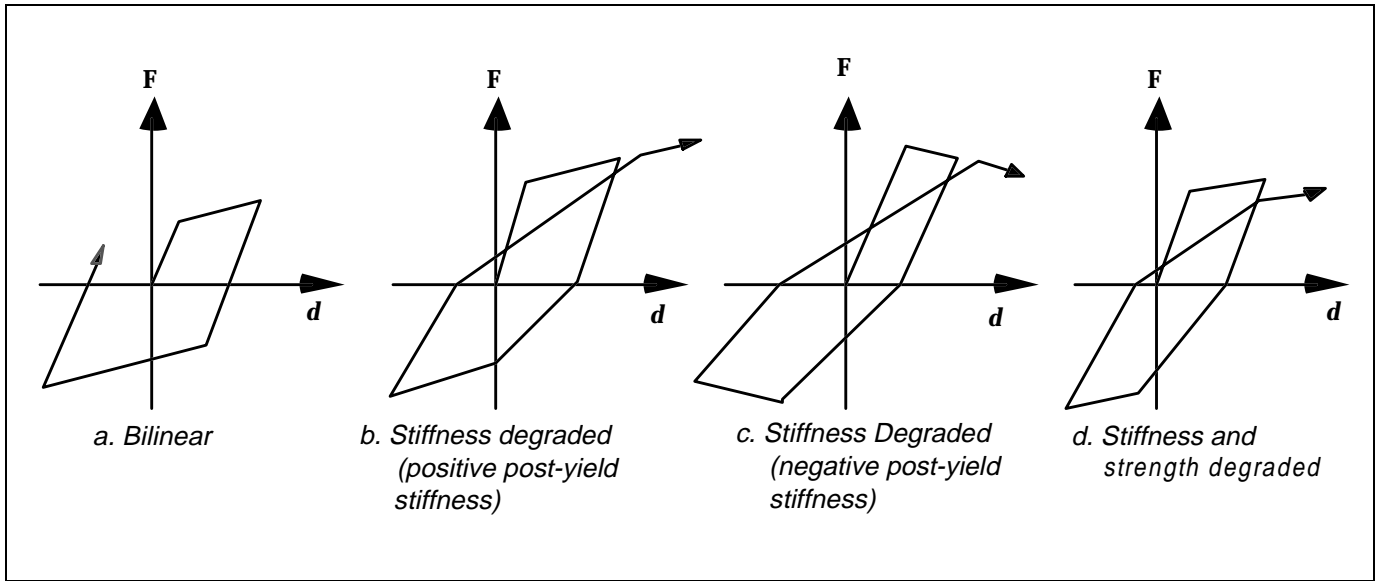


Figure 1-4 Global Load-Displacement Relationships

Emergency Management Agency, Report No. FEMA 306, Washington D.C.

ATC, 1998b, *Repair of Earthquake Damaged Concrete and Masonry Wall Buildings*, prepared by the Applied Technology Council (ATC-43 project) for

the Partnership for Response and Recovery, published by the Federal Emergency Management Agency, Report No. FEMA 308, Washington D.C.

2. Reinforced Concrete Components

2.1 Commentary and Discussion

2.1.1 Development of Component Guides and λ Factors

The Component Damage Classification Guides (Component Guides) and component modification factors (λ factors) for reinforced concrete walls were developed based on an extensive review of the research. The main references used are listed in the tabular bibliography of Section 2.3.

2.1.1.1 Identical Test Specimens Subjected to Different Load Histories

As indicated in FEMA 306, the ideal way to establish λ factors would be from structural tests designed specifically for that purpose. Two identical test specimens would be required for each structural component of interest. One specimen would be tested to represent the component in its *post-event* condition subjected to the performance earthquake; the second specimen would be tested to represent the component in its *pre-event* condition subjected to the performance earthquake. The λ values would be derived from the differences in the force-displacement response between the two specimens.

Research to date on reinforced concrete walls does not include test programs as described above. There are only a few tests of identical wall specimens subjected to different loading histories, and typically this is only a comparison of monotonic versus cyclic behavior. For reinforced concrete columns, there are more studies of the effects of load history (El-Bahy et al., 1997; Kawashima and Koyama, 1988) but these studies have not focused on the specific problem of comparing previously damaged components to undamaged components.

2.1.1.2 Interpretation of Individual Tests

In the absence of tests directly designed to develop λ factors, the factors can be inferred from individual cyclic-static tests. This is done by examining the change in force-displacement response from cycle to cycle as displacements are increased. Initial cycles can be considered representative of the damaging earthquake, and subsequent cycles representative of the behavior of an initially damaged component.

The general process of interpreting the test data is outlined in the diagram of Figure 2-1. Each structural test is considered according to the component type and behavior mode represented by the test. At intervals along the load-displacement history of the test the critical damage indicators, such as spalling, cracking, etc., are noted. The damage indicators at each interval are correlated with the displacement ductility reached at that point of the test and with the characteristics of subsequent cycles of the test. From the comparisons of initial and subsequent cycles, λ values are estimated. Critical damage indicators and the associated λ factors are then discretized into different damage severity levels.

The ranges of component displacement ductility, μ_{Δ} , associated with damage severity levels and λ factors and for each Component Guide are given in Table 2-1. The range of ductility values are the result of the differences in test procedures, specimen details, and relative values of coincident loading (shear, moment, axial load). See the remarks column of Table 2-1 for specific factors affecting individual components. Typical force-displacement hysteresis loops from wall tests are given in Section 2.2. A discussion of the relationship between cracking and damage severity for reinforced masonry is given in Section 3.1.2. This discussion is largely applicable to reinforced concrete as well as reinforced masonry.

In estimating the λ values, it was considered that some stiffness and strength degradation would occur in a structural component in the course of the Performance Earthquake, whether or not it was previously subjected to a damaging earthquake. As discussed in FEMA 306, the λ factors refer to the difference in the stiffness, strength, and displacement capacity of the performance earthquake response, between a pre-event component and a post-event component.

2.1.1.3 Accuracy

The λ factors are considered accurate to one significant digit, as presented in the Component Damage Classification Guides. In the case of component types and behavior modes which are not well covered in the research, engineering judgment and comparisons to similar component types or behavior modes were used

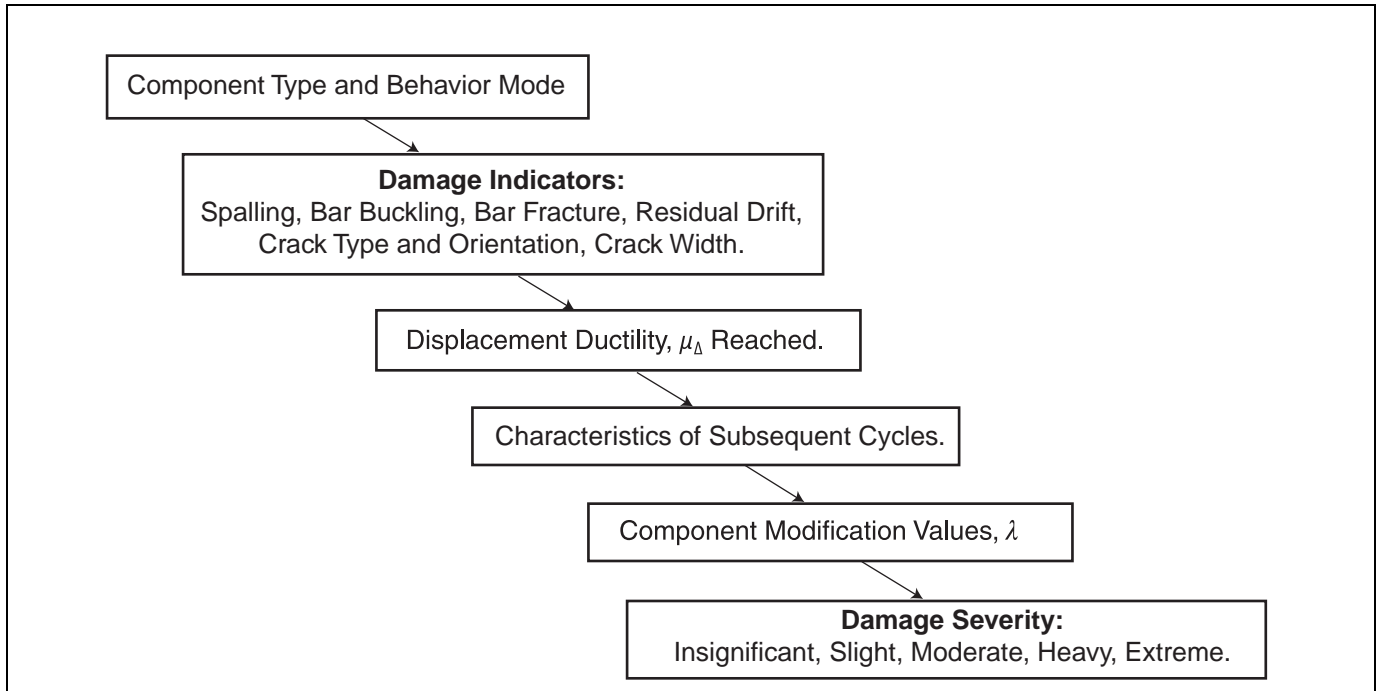


Figure 2-1 Diagram of process used to develop component guides and component modification factors.

to establish λ factors. In cases of uncertainty, the recommended λ factors and severity classifications are designed to be conservative — that is, the factors and classifications may overestimate the effect of damage on future performance.

Only limited research is available from which to infer specific λ_D values. However, a number of tests support the general idea that ultimate displacement capacity can be reduced because of previous damaging cycles. Comparisons of monotonic to cyclic-static wall tests show greater displacement capacities for monotonic loading, and Oesterle et al. (1976) conclude, “structural

wall performance under load reversals is a function of load history. The previous level of maximum deformation is critical.”

For reinforced concrete columns, Mander et al. (1996) have shown a correlation between strength degradation and cumulative plastic drift. El-Bahy et al. (1997) have shown similar results. This research generally supports the λ_D values recommended for reinforced concrete, which are 0.9 at moderate damage and 0.7 to 0.8 at heavy damage.

Chapter 2: Reinforced Concrete Components

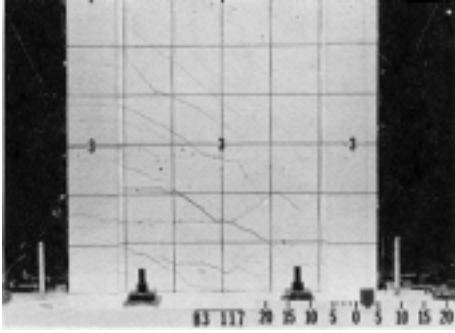
Table 2-1 Ranges of reinforced concrete component displacement ductility, μ_{Δ} , associated with damage severity levels and λ factors

Component Guide	Damage Severity				Remarks on Ductility Ranges
	Insignif.	Slight	Moderate	Heavy	
RC1A Ductile Flexural	$\mu_{\Delta} \leq 3$ $\lambda_K = 0.8$ $\lambda_Q = 1.0$ $\lambda_D = 1.0$	$\mu_{\Delta} \approx 4 - 8$ $\lambda_K = 0.6$ $\lambda_Q = 1.0$ $\lambda_D = 1.0$	$\mu_{\Delta} \approx 3 - 10$ $\lambda_K = 0.5$ $\lambda_Q = 0.8$ $\lambda_D = 0.9$	Heavy not used	Slight category will only occur for low axial loads, where concrete does not spall until large ductilities develop
RC1B Flexure/ Diagonal Tension	$\mu_{\Delta} \leq 3$ $\lambda_K = 0.8$ $\lambda_Q = 1.0$ $\lambda_D = 1.0$	Slight not used	$\mu_{\Delta} \approx 2 - 6$ $\lambda_K = 0.5$ $\lambda_Q = 0.8$ $\lambda_D = 0.9$	$\mu_{\Delta} \approx 2 - 8$ $\lambda_K = 0.2$ $\lambda_Q = 0.3$ $\lambda_D = 0.7$	Ductility depends on ratio of flexural to shear strength. Lower ductility indicates behavior similar to preemptive diagonal tension. Higher ductility indicates behavior similar to ductile flexural.
RC1C Flexure/ Web Crushing	$\mu_{\Delta} \leq 3$ See RC1B	Slight not used	$\mu_{\Delta} \approx 2 - 6$ $\lambda_K = 0.5$ $\lambda_Q = 0.8$ $\lambda_D = 0.9$	$\mu_{\Delta} \approx 3 - 8$ $\lambda_K = 0.2$ $\lambda_Q = 0.3$ $\lambda_D = 0.7$	Ductility depends on ratio of flexural to web crushing strength. Lower ductility indicates behavior similar to preemptive web crushing. Higher ductility indicates behavior similar to ductile flexural.
RC1D Flexure/ Sliding Shear	$\mu_{\Delta} \leq 3$ See RC1A	$\mu_{\Delta} \approx 4 - 6$ See RC1A	Moderate not used	$\mu_{\Delta} \approx 4 - 8$ $\lambda_K = 0.4$ $\lambda_Q = 0.5$ $\lambda_D = 0.8$	Ductility depends on ratio of flexural to sliding shear strength.
RC1E Flexure/ Boundary Compression	$\mu_{\Delta} \leq 3$ See RC1A	$\mu_{\Delta} \approx 4 - 6$ See RC1A	$\mu_{\Delta} \approx 3 - 6$ See RC1A	$\mu_{\Delta} \approx 4 - 8$ $\lambda_K = 0.4$ $\lambda_Q = 0.6$ $\lambda_D = 0.7$	Slight category will only occur for lower axial loads, where concrete does not spall until large ductilities develop. Lower ductility relates poorer confinement conditions. Higher ductility indicates behavior similar to ductile flexural
RC2A Ductile Flexural	$\mu_{\Delta} \leq 3$ See RC1A	$\mu_{\Delta} \approx 4 - 6$ See RC1A	$\mu_{\Delta} \approx 3 - 10$ $\lambda_K = 0.5$ $\lambda_Q = 0.8$ $\lambda_D = 0.9$	Heavy not used	See RC1A
RC2H Preemptive Diagonal Shear	$\mu_{\Delta} \leq 1$ $\lambda_K = 0.9$ $\lambda_Q = 1.0$ $\lambda_D = 1.0$	Slight not used	$\mu_{\Delta} \leq 1.5$ $\lambda_K = 0.5$ $\lambda_Q = 0.8$ $\lambda_D = 0.9$	$\mu_{\Delta} \leq 2$ $\lambda_K = 0.2$ $\lambda_Q = 0.3$ $\lambda_D = 0.7$	Force controlled behavior associated with low ductility levels.
RC3B Flexure/ Diagonal Tension	$\mu_{\Delta} \leq 3$ See RC1B	Slight not used	$\mu_{\Delta} \approx 2 - 6$ See RC1B	$\mu_{\Delta} \approx 2 - 8$ $\lambda_K = 0.2$ $\lambda_Q = 0.3$ $\lambda_D = 0.7$	See RC1B
RC3D Flexure/ Sliding Shear	$\mu_{\Delta} \leq 3$ See RC1D	$\mu_{\Delta} \approx 4 - 6$ See RC1D	Moderate not used	$\mu_{\Delta} \approx 3 - 8$ $\lambda_K = 0.2$ $\lambda_Q = 0.3$ $\lambda_D = 0.7$	Sliding shear may occur at lower ductility levels than RC1D because of less axial load.

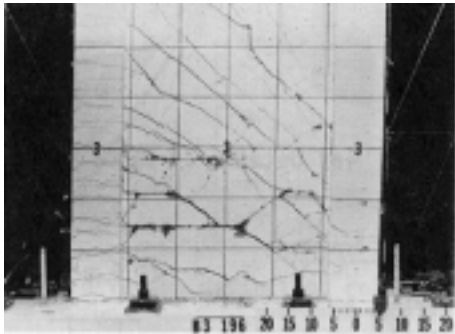
2.2 Typical Force-Displacement Hysteretic Behavior

DAMAGE PATTERNS AND HYSTERETIC RESPONSE	
System:	Reinforced Concrete
Component Type:	Isolated Wall or Stronger Wall Pier
Predominant Behavior Mode:	Ductile Flexure
Secondary Behavior Mode:	—
Reference:	Corley, Fioralo, Oesterle (1981), Oesterle et al. (1976), Oesterle et al. (1979)
Specimen:	B3

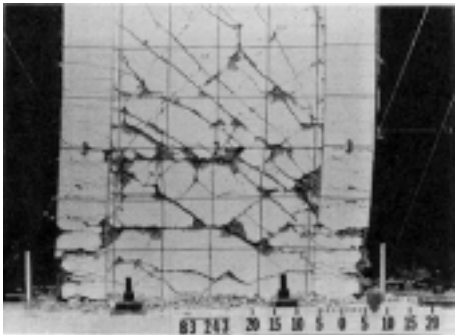
RC1A

 Example 1 of 1


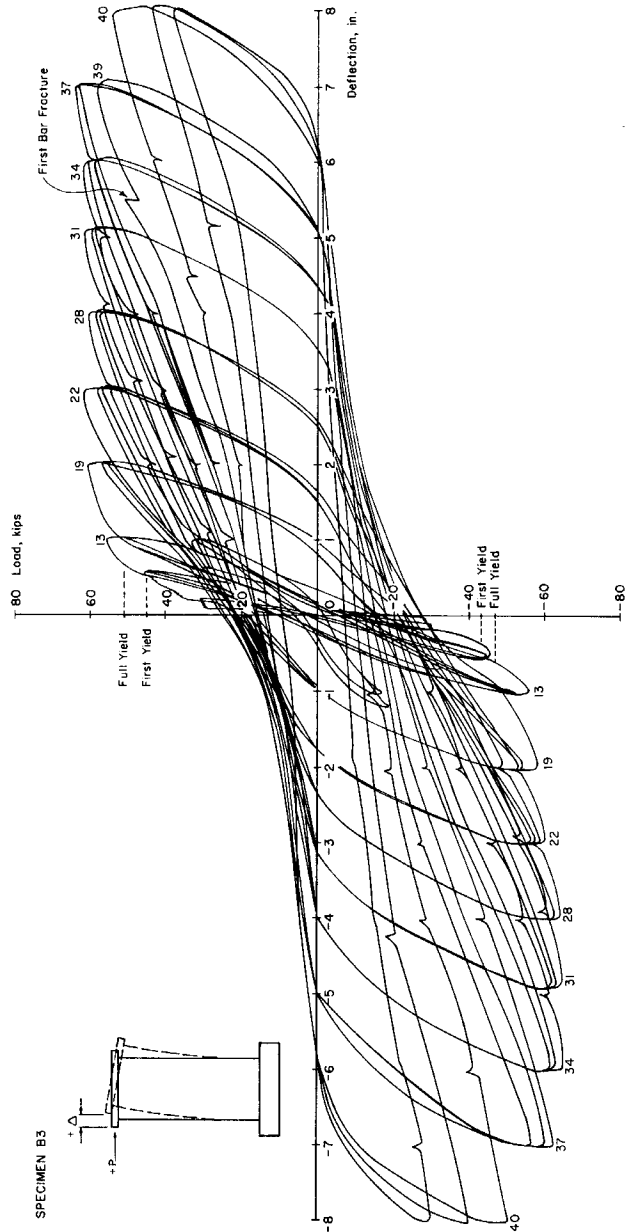
Damage at +3-in. deflection
 $\Delta = 3$ in $\Delta/h_w = 0.017$ $\lambda_Q = 1.0$



Damage at +6-in. deflection
 $\Delta = 6$ in $\Delta/h_w = 0.033$ $\lambda_Q = 1.0$



Damage at +8-in. deflection
 $\Delta = 8$ in $\Delta/h_w = 0.044$ $\lambda_Q = 0.7$

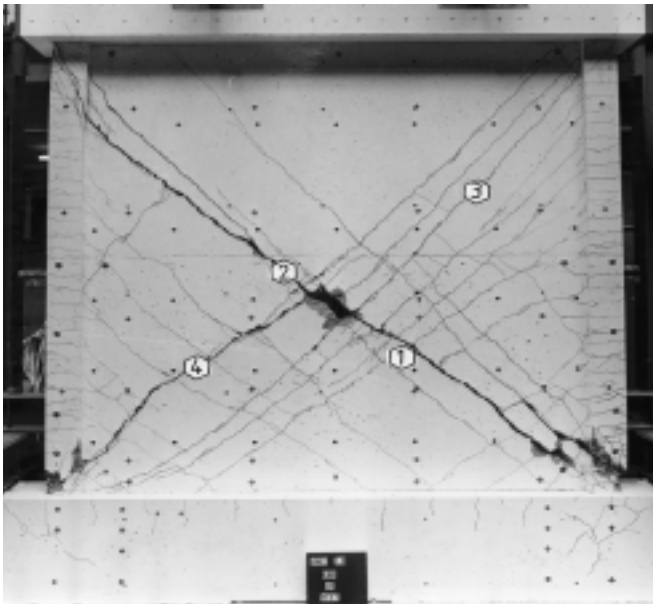


DAMAGE PATTERNS AND HYSTERETIC RESPONSE

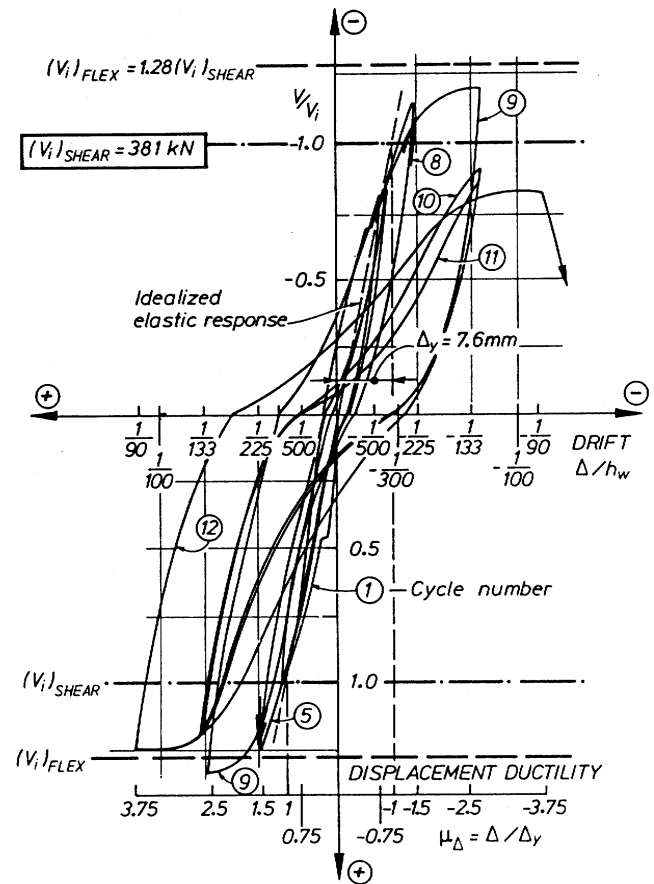
System: **Reinforced Concrete**
 Component Type: **Isolated Wall or Stronger Wall Pier**
 Predominant Behavior Mode: **Flexure/Diagonal Tension**
 Secondary Behavior Mode: **—**

RC1B Example 1 of 2

Reference: Paulay and Priestley (1992)
 Specimen: Figure 8.3 of reference



Failure of a squat wall due to diagonal tension after reversed cyclic loading.



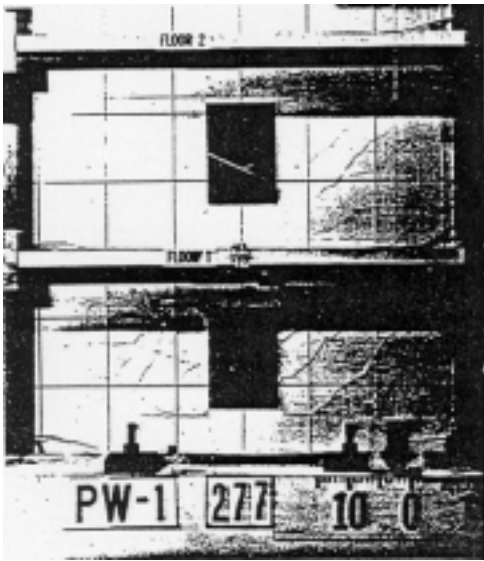
Hysteretic response of a squat wall that eventually failed in shear.

DAMAGE PATTERNS AND HYSTERETIC RESPONSE

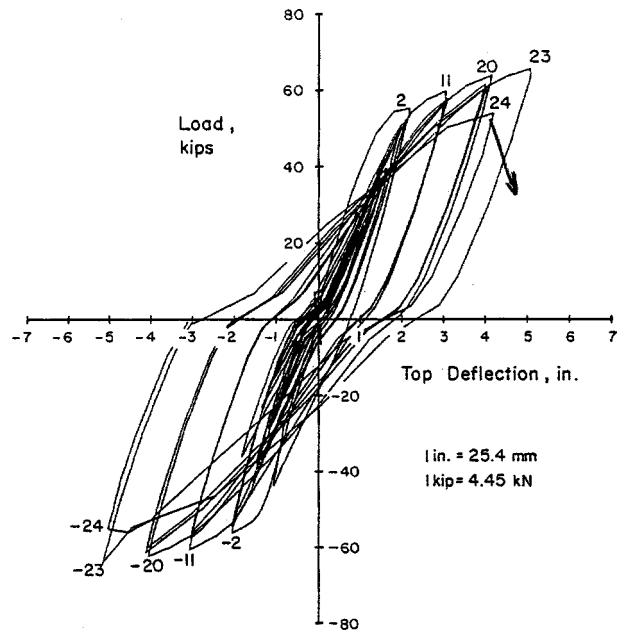
System: **Reinforced Concrete**
 Component Type: **Isolated Wall or Stronger Wall Pier**
 Predominant Behavior Mode: **Flexure/Diagonal Tension**
 Secondary Behavior Mode: **Flexure/Web Crushing**

RC1B Example 2 of 2

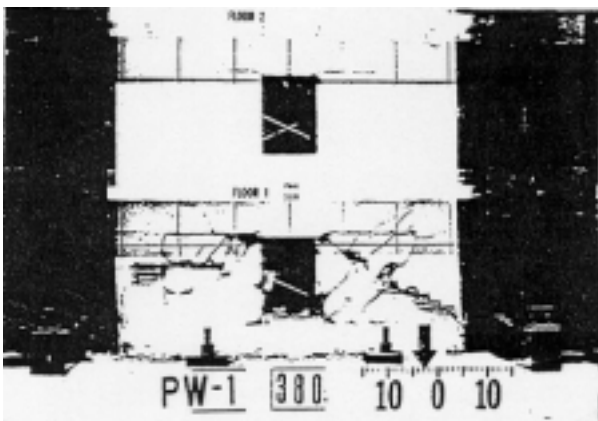
Reference: Shiu et al. (1981)
 Specimen: PW-1



Crack pattern of specimen PW-1 at end of Phase II.



Load versus top deflection relationship for specimen PW-1.



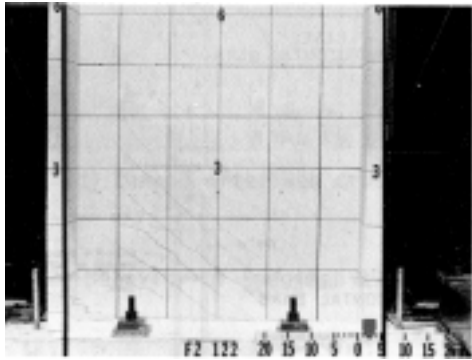
Specimen PW-1 at end of test.

DAMAGE PATTERNS AND HYSTERETIC RESPONSE

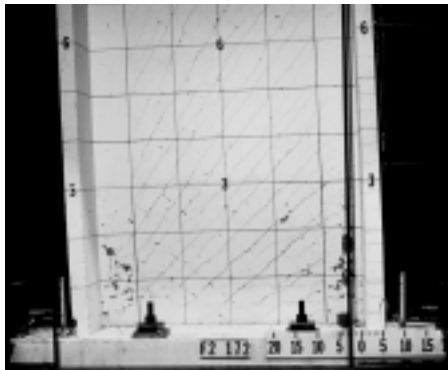
System: **Reinforced Concrete**
 Component Type: **Isolated Wall or Stronger Wall Pier**
 Predominant Behavior Mode: **Flexure/Web Crushing**
 Secondary Behavior Mode: **—**

RC1C Example 1 of 3

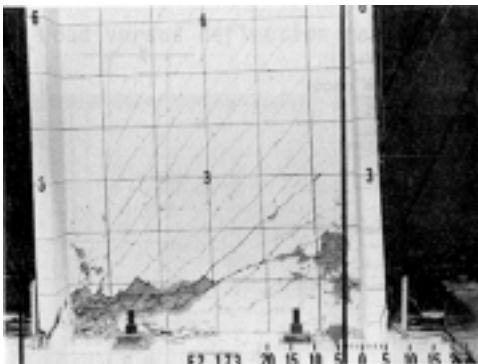
Reference: Corley, Fioralo, Oesterle (1981), Oesterle et al. (1976), Oesterle et al. (1979)
 Specimen: F2



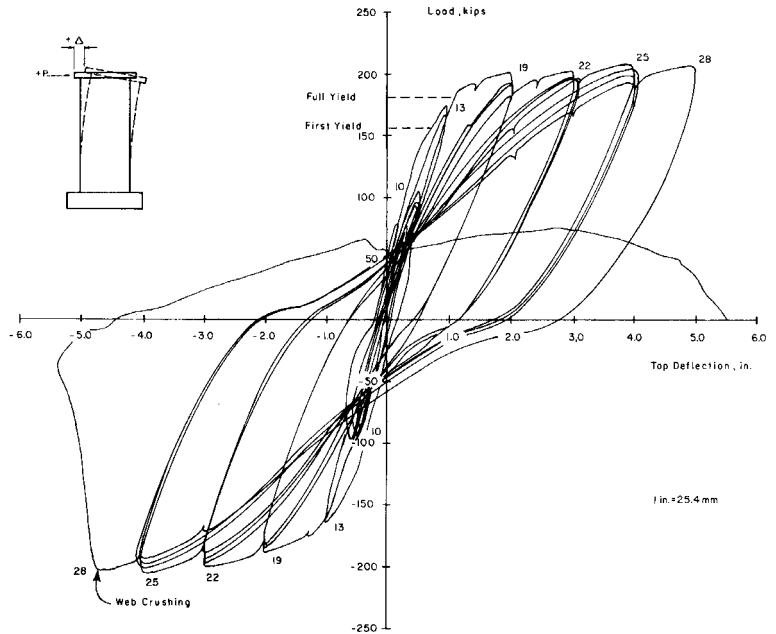
Damage at +3-in. deflection
 $\Delta = 3$ in $\Delta/h_w = 0.017$ $\lambda_Q = 1.0$



Damage prior to web crushing
 $\Delta = 4$ in $\Delta/h_w = 0.022$ $\lambda_Q = 1.0$



Damage after web crushing
 $\Delta = 5$ in $\Delta/h_w = 0.028$ $\lambda_Q = 0.3$



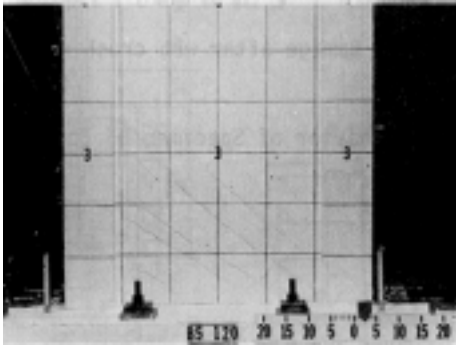
Load versus deflection relationship

DAMAGE PATTERNS AND HYSTERETIC RESPONSE

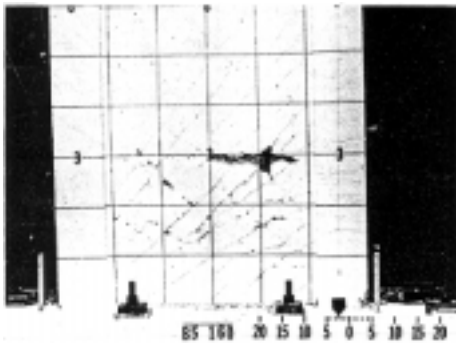
System: **Reinforced Concrete**
 Component Type: **Isolated Wall or Stronger Wall Pier**
 Predominant Behavior Mode: **Flexure/Web Crushing**
 Secondary Behavior Mode: **—**

RC1C Example 2 of 3

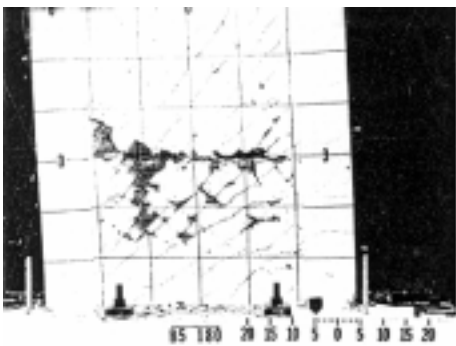
Reference: Corley, Fioralo, Oesterle (1981), Oesterle et al. (1976), Oesterle et al. (1979)
 Specimen: B5



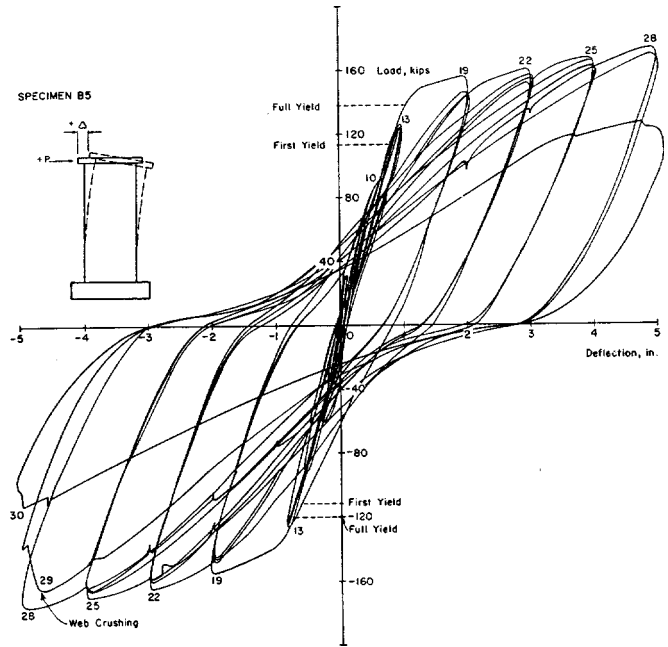
Damage at +3-in. deflection
 $\Delta = 3 \text{ in}$ $\Delta/h_w = 0.017$ $\lambda_Q = 1.0$



Damage at -3-in. deflection
 $\Delta = 3 \text{ in}$ $\Delta/h_w = 0.017$ $\lambda_Q = 1.0$



Damage after web crushing
 $\Delta = 5 \text{ in}$ $\Delta/h_w = 0.028$ $\lambda_Q = 0.6$



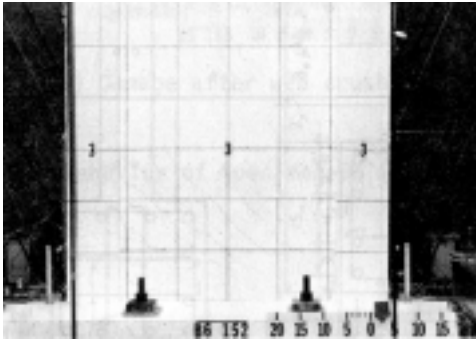
Load versus deflection relationship

DAMAGE PATTERNS AND HYSTERETIC RESPONSE

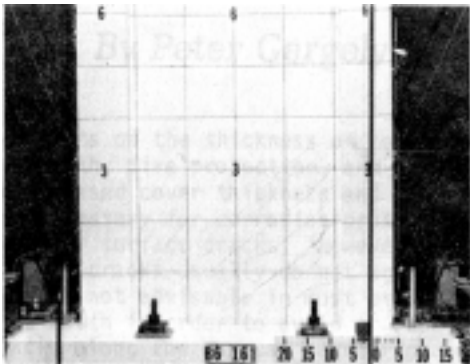
System: **Reinforced Concrete**
 Component Type: **Isolated Wall or Stronger Wall Pier**
 Predominant Behavior Mode: **Flexure/Web Crushing**
 Secondary Behavior Mode: **—**

RC1C Example 3 of 3

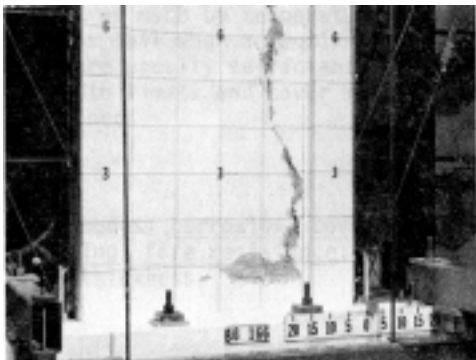
Reference: Corley, Fioralo, Oesterle (1981), Oesterle et al. (1976), Oesterle et al. (1979)
 Specimen: B6



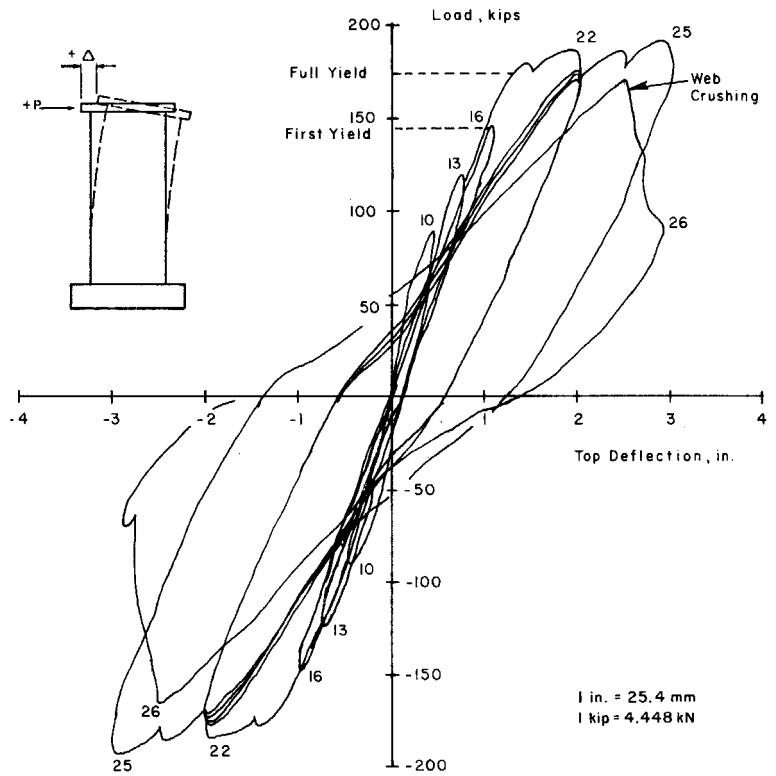
Damage at +3-in. deflection
 $\Delta = 3 \text{ in}$ $\Delta/h_w = 0.017$ $\lambda_Q = 1.0$



Damage at -3-in. deflection
 $\Delta = 3 \text{ in}$ $\Delta/h_w = 0.017$ $\lambda_Q = 1.0$



Damage after web crushing
 $\Delta = 3 \text{ in}$ $\Delta/h_w = 0.017$ $\lambda_Q = 0.3$



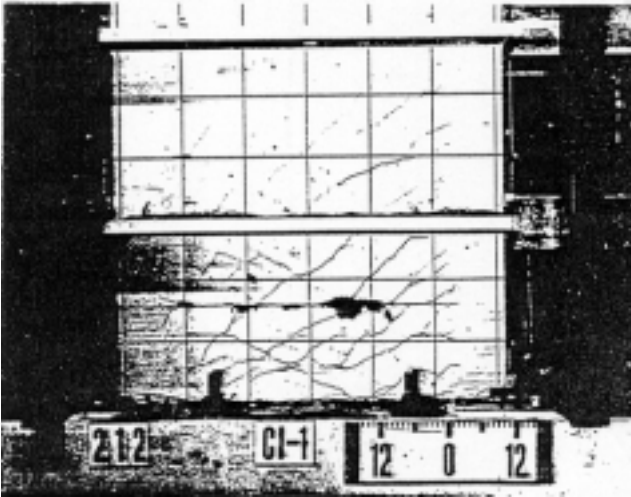
Load versus deflection relationship

DAMAGE PATTERNS AND HYSTERETIC RESPONSE

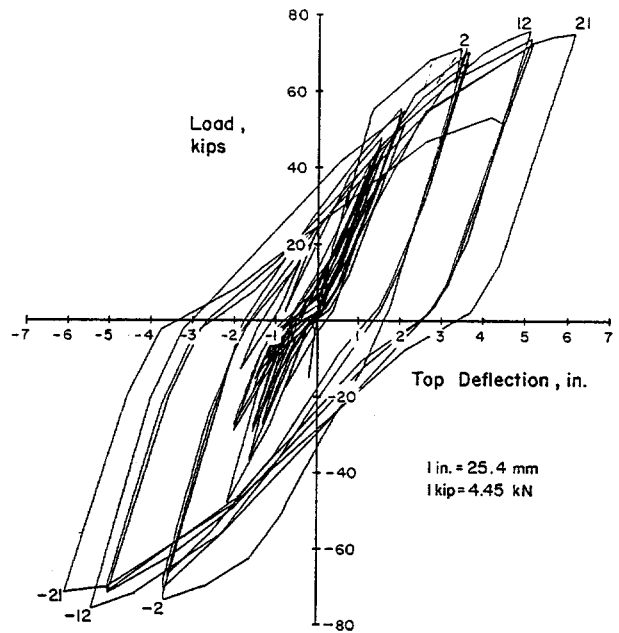
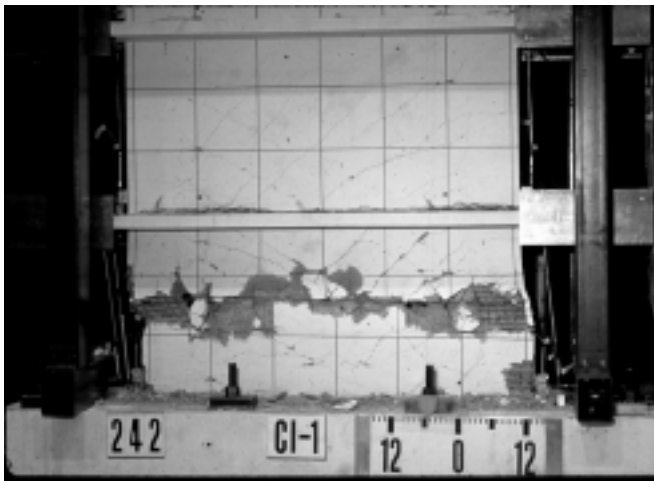
System: **Reinforced Concrete**
 Component Type: **Isolated Wall or Stronger Wall Pier**
 Predominant Behavior Mode: **Flexure/Sliding Shear**
 Secondary Behavior Mode: **—**

RC1D Example 1 of 2

Reference: Corley, Fioralo, Oesterle (1981), Shiu et al. (1981)
 Specimen: CI-1



Crack pattern of specimen CI-1 at end of phase II.



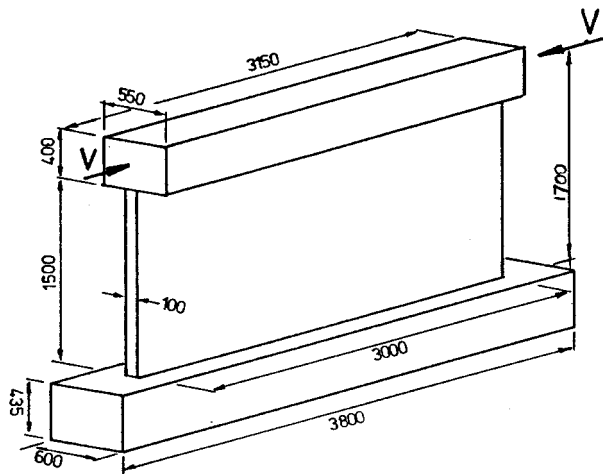
Load versus top deflection relationship for specimen CI-1.

DAMAGE PATTERNS AND HYSTERETIC RESPONSE

System: **Reinforced Concrete**
 Component Type: **Isolated Wall or Stronger Wall Pier**
 Predominant Behavior Mode: **Flexure/Sliding Shear**
 Secondary Behavior Mode: **—**

RC1D Example 2 of 3

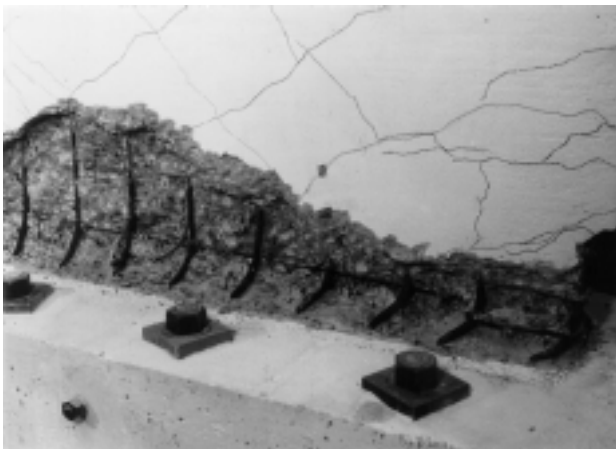
Reference: Paulay, Priestley, and Syngé (1982)
 Specimen: Wall 1



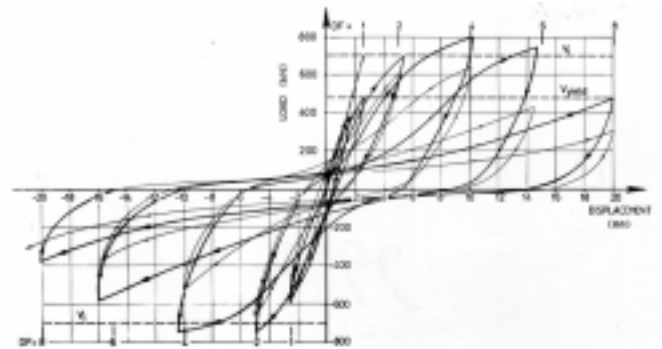
Overall dimensions of typical test units.



Splitting and Crushing of Concrete at Base of Wall



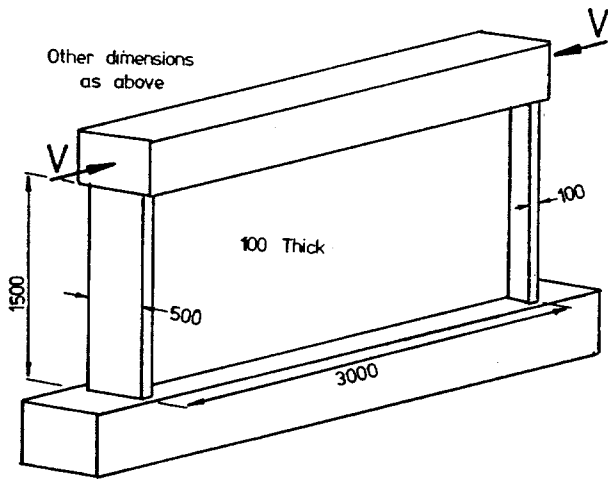
Compression Toe



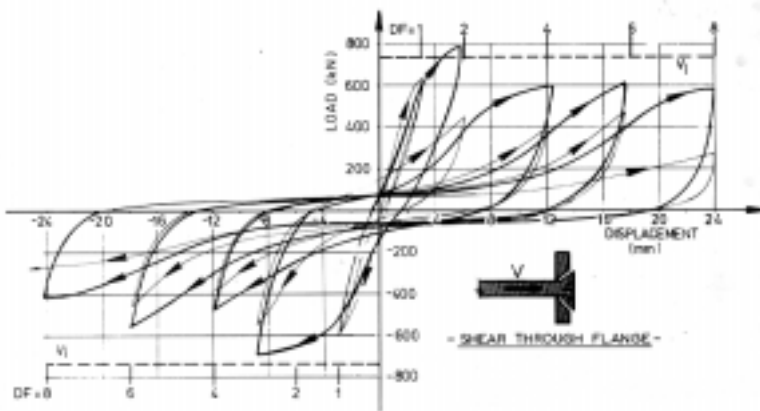
Load-deflection relationship for wall 1.

DAMAGE PATTERNS AND HYSTERETIC RESPONSE

System: Reinforced Concrete	RC1D Example 3 of 3
Component Type: Isolated Wall or Stronger Wall Pier	
Predominant Behavior Mode: Flexure/Sliding Shear	
Secondary Behavior Mode: —	
Reference: Paulay, Priestley, and Syngé (1982))	
Specimen: Wall 3	



Overall Dimensions for Walls 3 and 4.



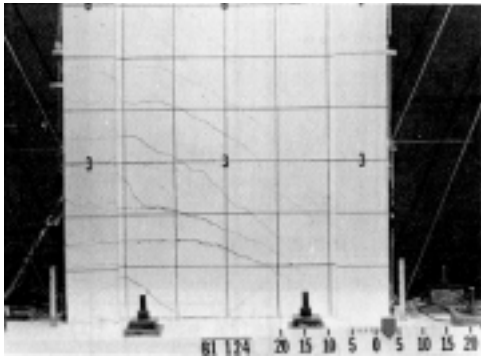
Load-Deflection Relationship for Flanged Wall

DAMAGE PATTERNS AND HYSTERETIC RESPONSE

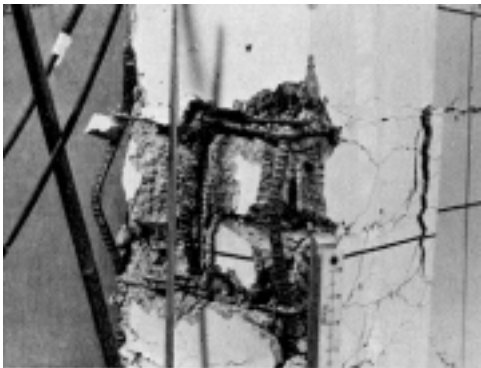
System: **Reinforced Concrete**
 Component Type: **Isolated Wall or Stronger Wall Pier**
 Predominant Behavior Mode: **Flexure/Boundary Compression**
 Secondary Behavior Mode: **—**

RC1E Example 1 of 1

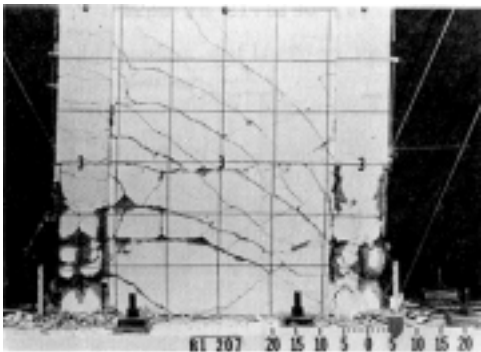
Reference: Corley, Fioralo, Oesterle (1981), Oesterle et al. (1976), Oesterle et al. (1979)
 Specimen: B1



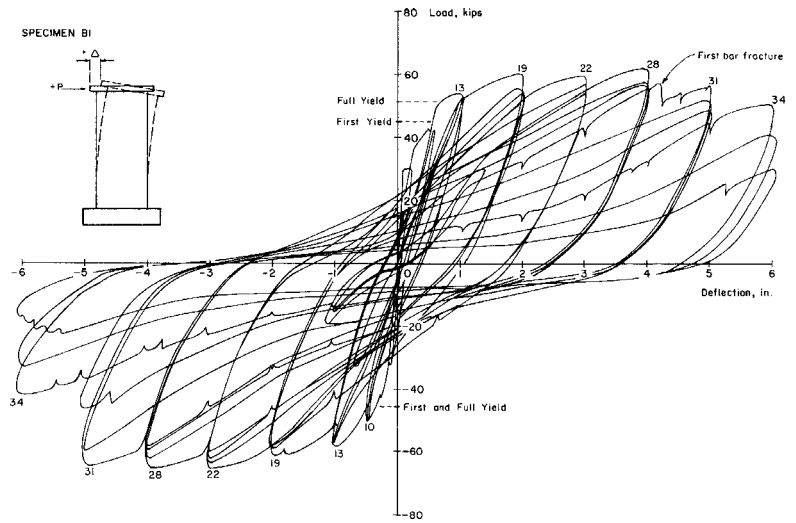
Damage at +3-in. deflection
 $\Delta = 3$ in $\Delta/h_w = 0.017$ $\lambda_Q = 1.0$



Buckled reinforcement after Load Cycle 30
 $\Delta = 4$ in $\Delta/h_w = 0.022$ $\lambda_Q = 0.9$



Damage during Load Cycle 34
 $\Delta = 6$ in $\Delta/h_w = 0.033$ $\lambda_Q = 0.6$



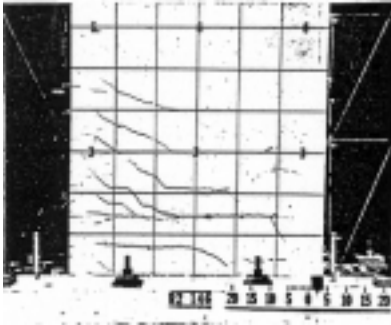
Load versus deflection relationship

DAMAGE PATTERNS AND HYSTERETIC RESPONSE

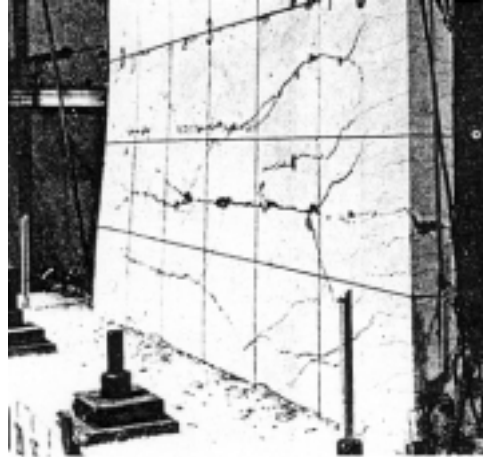
System: **Reinforced Concrete**
 Component Type: **Isolated Wall or Stronger Wall Pier**
 Predominant Behavior Mode: **Flexure/Out-of-Plane Wall Buckling**
 Secondary Behavior Mode: **—**

RC1G Example 1 of 2

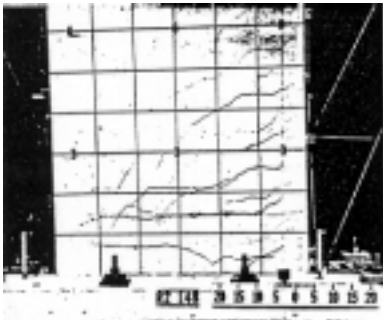
Reference: Corley, Fioralo, Oesterle (1981), Oesterle et al. (1976), Oesterle et al. (1979)
 Specimen: R2



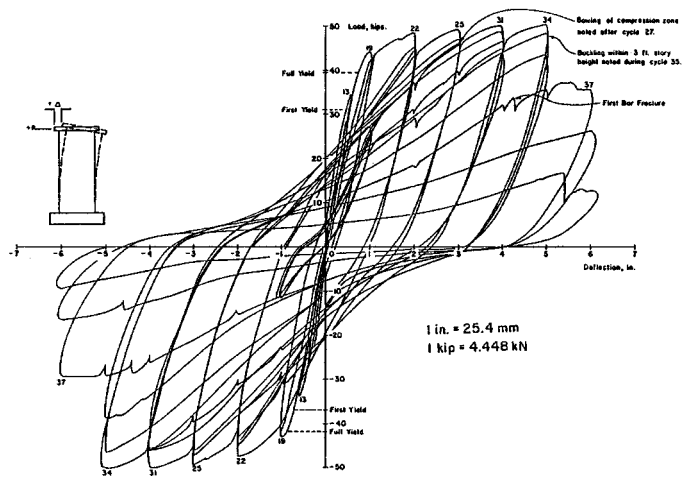
Cracking pattern at +3 in. deflection for Specimen R2



Inelastic instability of compression zone



Cracking pattern at -3 in. deflection for Specimen R2



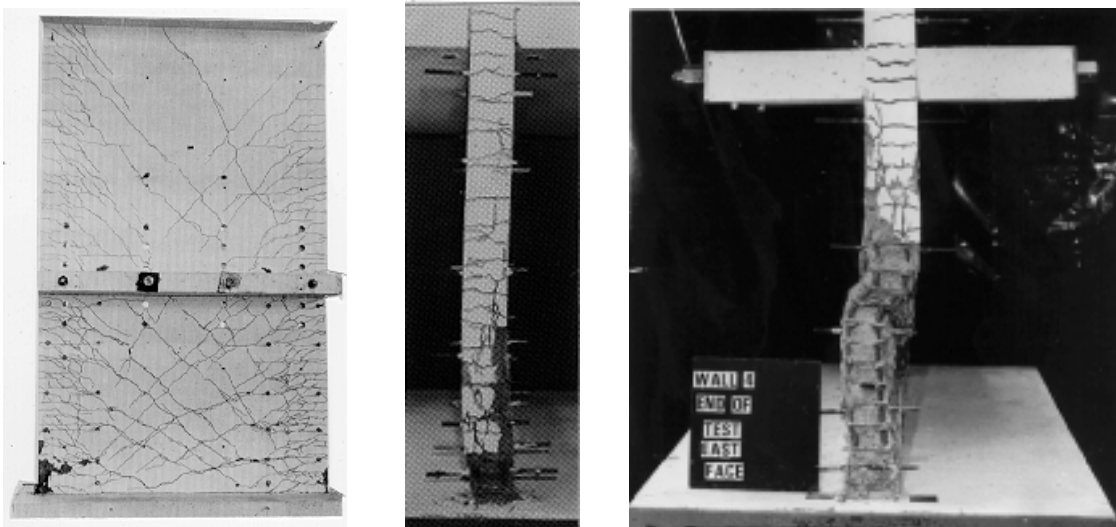
Continuous load-deflection plot for Specimen R2

DAMAGE PATTERNS AND HYSTERETIC RESPONSE

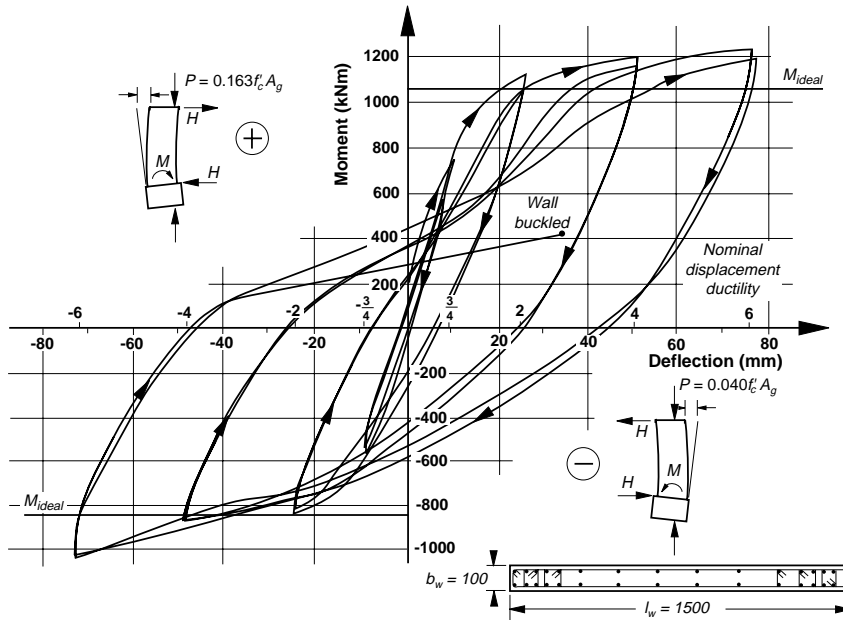
System: **Reinforced Concrete**
 Component Type: **Isolated Wall or Stronger Wall Pier**
 Predominant Behavior Mode: **Flexure/Out-of-Plane Wall Buckling**
 Secondary Behavior Mode: **—**

RC1G Example 2 of 2

Reference: Paulay and Priestley (1992)
 Specimen: Wall 2 and Wall 4, Figure 5.37 of reference



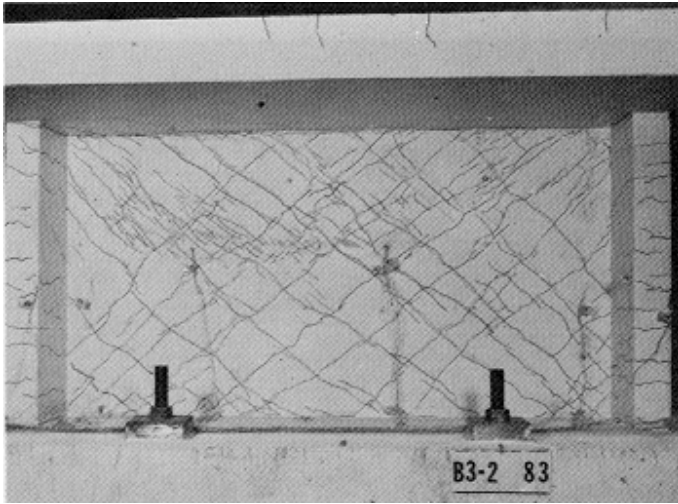
Diagonal cracking and buckling in the plastic hinge region of a structural wall (G1).



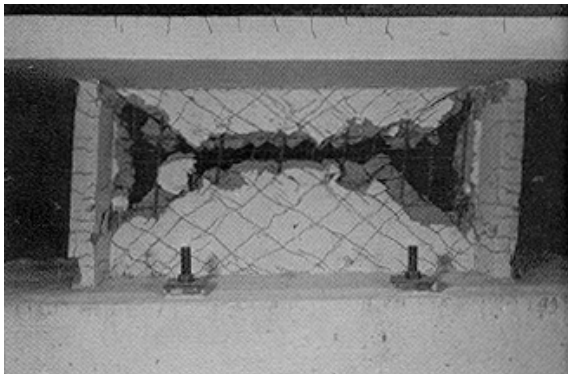
Stable hysteretic response of a ductile wall structure (G1).

DAMAGE PATTERNS AND HYSTERETIC RESPONSE

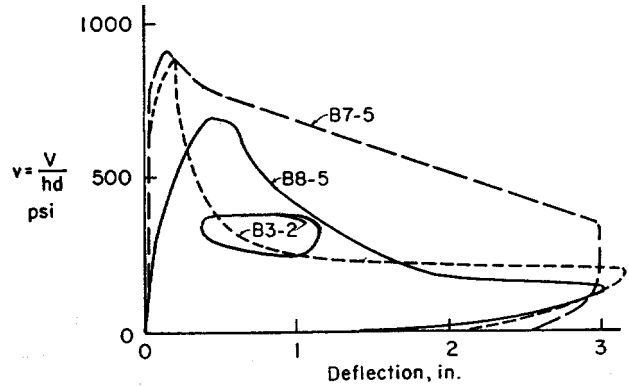
System: Reinforced Concrete	RC11 Example 1 of 2
Component Type: Isolated Wall or Stronger Wall Pier	
Predominant Behavior Mode: Preemptive Web Crushing	
Secondary Behavior Mode: —	
Reference: Barda (1972), Barda, Hanson, & Corley (1976) (Lehigh Univ.)	
Specimen: B3-2	



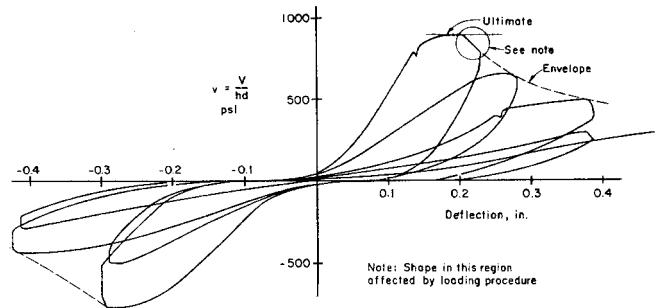
Test specimen at ultimate load
 $\Delta = 0.2$ in $\Delta/h_w = 0.005$ $\lambda_Q = 1.0$



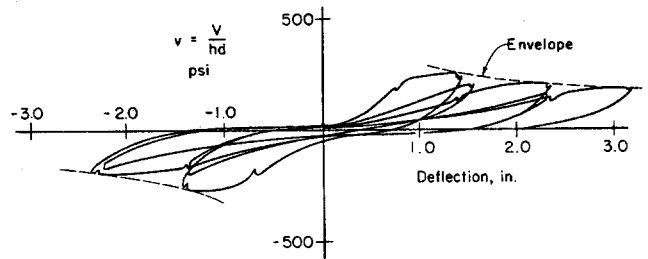
Test specimen at conclusion of loading
 $\Delta = 3.0$ in $\Delta/h_w = 0.080$ $\lambda_Q = 0.2$



Envelope of response



Hysteretic response



Provided Information	Calculated Values
$h_w = 37.5$ "	$P = 4.9$ k
$f_y = 60$ ksi	$M_n = 1700$ k-1
$f'_c = 3920$ psi	$\frac{V}{b_w l_w}$ corresponding to $M_n = 1810$ psi

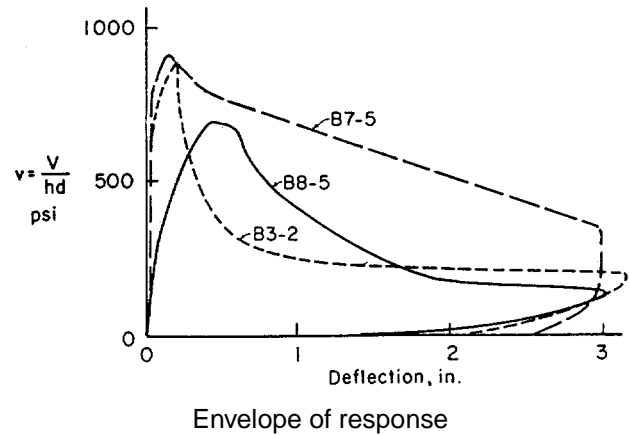
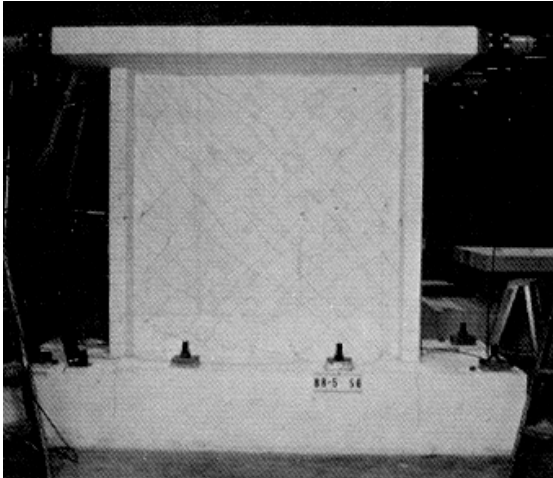
Δ	Δ/h_w	λ_Q
0.20	0.005	1.0
0.23	0.006	0.9
0.28	0.007	0.7
0.40	0.011	0.5
0.80	0.021	0.3
3.00	0.080	0.2

DAMAGE PATTERNS AND HYSTERETIC RESPONSE

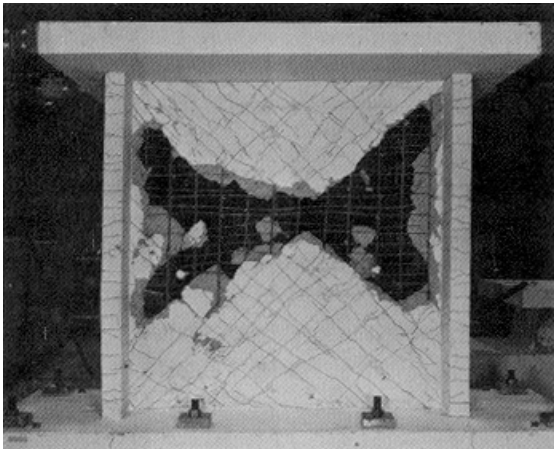
System: **Reinforced Concrete**
 Component Type: **Isolated Wall or Stronger Wall Pier**
 Predominant Behavior Mode: **Preemptive Web Crushing**
 Secondary Behavior Mode: **—**

RC11 Example 2 of 2

Reference: Barda (1972), Barda, Hanson, & Corley (1976)
 Specimen: B8-5



Test specimen at ultimate load
 $\Delta = 0.2$ in $\Delta/h_w = 0.005$ $\lambda_Q = 1.0$



Test specimen at conclusion of loading
 $\Delta = 3.0$ in $\Delta/h_w = 0.040$ $\lambda_Q = 0.2$

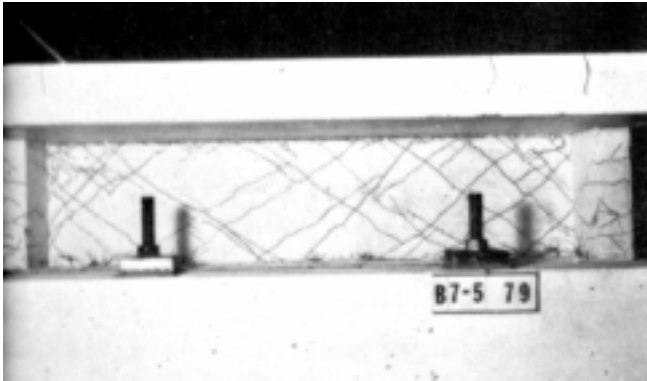
Provided Information	Calculated Values	Δ	Δ/h_w	λ_Q
$h_w = 75$ "	$P = 7.5$ k	0.45	0.006	1.0
$f_y = 71$ ksi	$M_n = 2000$ k-1	0.60	0.008	0.9
		0.80	0.011	0.7
		1.20	0.016	0.5
$f'_c = 3400$ psi	$\frac{V}{b_w l_w}$ corresponding to $M_n = 1070$ psi	1.70	0.023	0.3
		3.00	0.040	0.2

DAMAGE PATTERNS AND HYSTERETIC RESPONSE

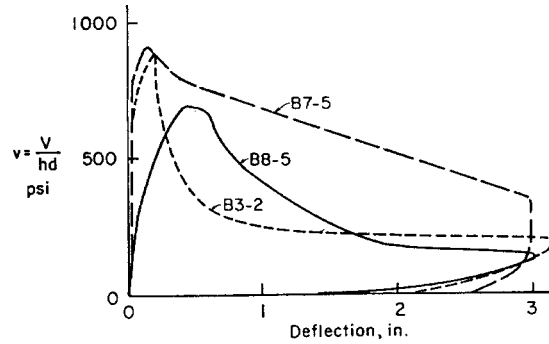
System: **Reinforced Concrete**
 Component Type: **Isolated Wall or Stronger Wall Pier**
 Predominant Behavior Mode: **Preemptive Sliding Shear**
 Secondary Behavior Mode: **Web Crushing**

RC1J Example 1 of 1

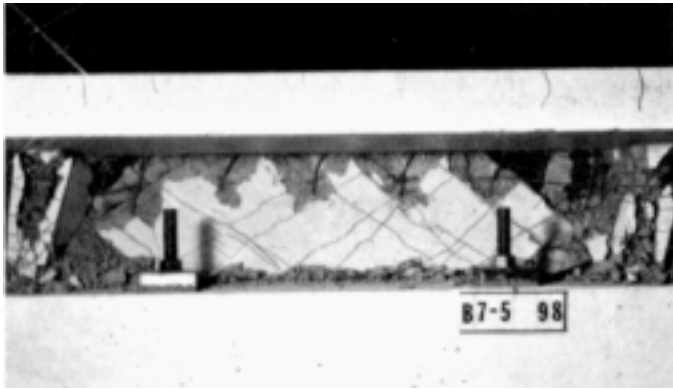
Reference: Barda (1972), Barda, Hanson, & Corley (1976) (Lehigh Univ.)
 Specimen: B7-5



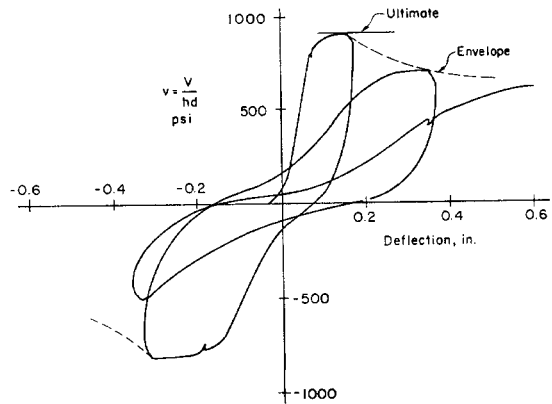
Test specimen at ultimate load
 $\Delta = 0.15$ in $\Delta/h_w = 0.008$ $\lambda_Q = 1.0$



Envelope of response



Test specimen at conclusion of loading
 $\Delta = 3.0$ in $\Delta/h_w = 0.160$ $\lambda_Q = 0.4$



Hysteretic response to 0.6in.

Provided Information

$h_w = 18.75$ "

$f_y = 78$ ksi

$f'_c = 3730$ psi

Calculated Values

$P = 3.6$ k

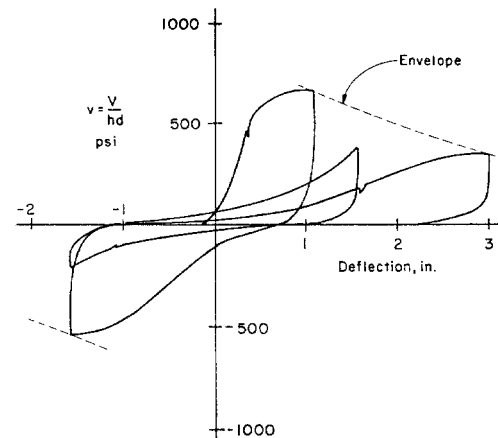
$M_n = 2180$ k-in

$\frac{V}{b_w l_w}$ corresponding to

$M_n = 4600$ psi

λ_Q values from response plot

Δ	Δ/h_w	λ_Q
0.15	0.008	1.0
0.30	0.016	0.9
0.70	0.037	0.8
1.80	0.096	0.6
3.00	0.160	0.4



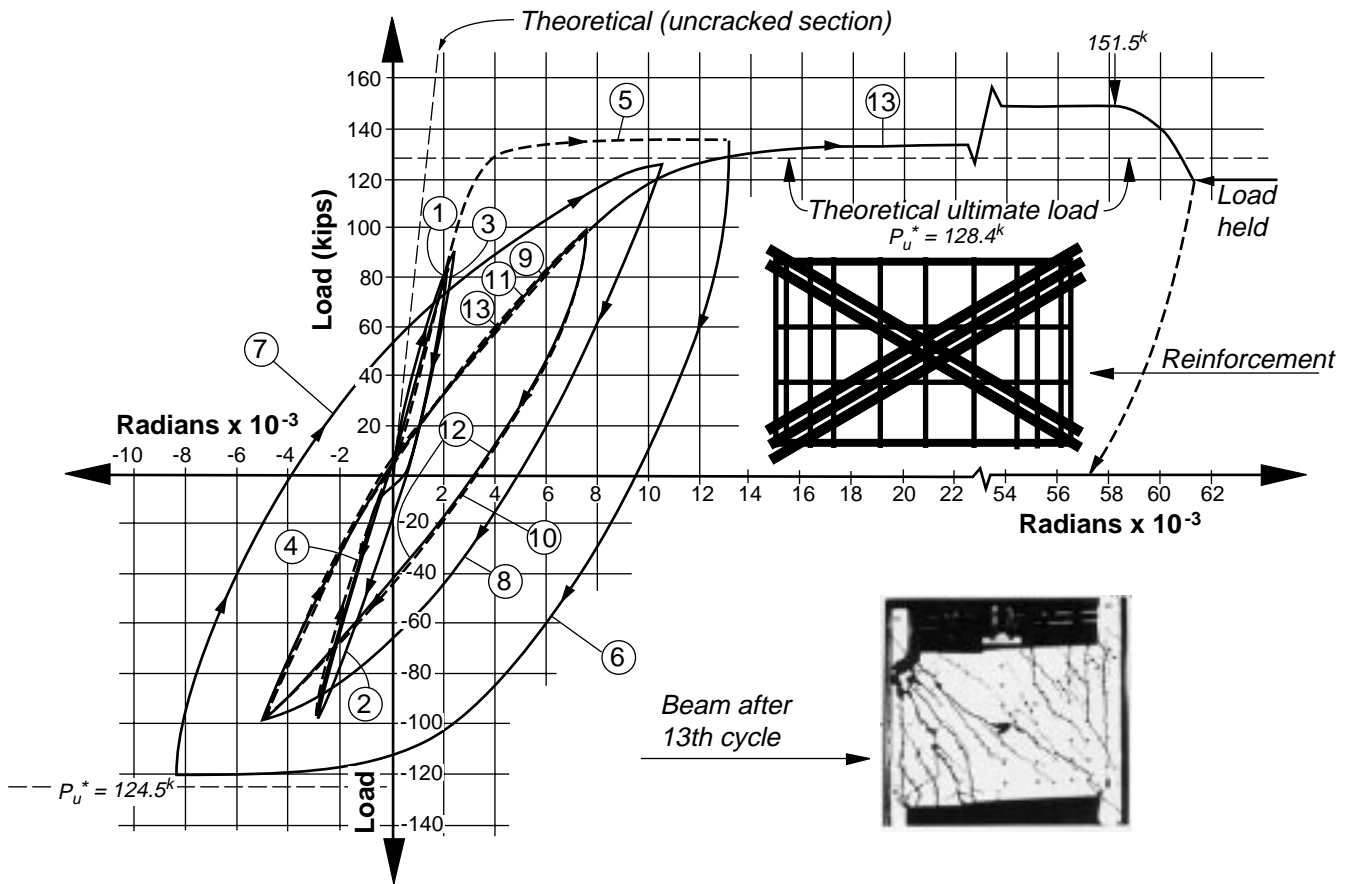
Hysteretic response to 3.0 in.

DAMAGE PATTERNS AND HYSTERETIC RESPONSE

System: **Reinforced Concrete**
 Component Type: **Weaker Spandrel or Coupling Beam**
 Predominant Behavior Mode: **Ductile Flexure**
 Secondary Behavior Mode: **—**

RC3A Example 1 of 1

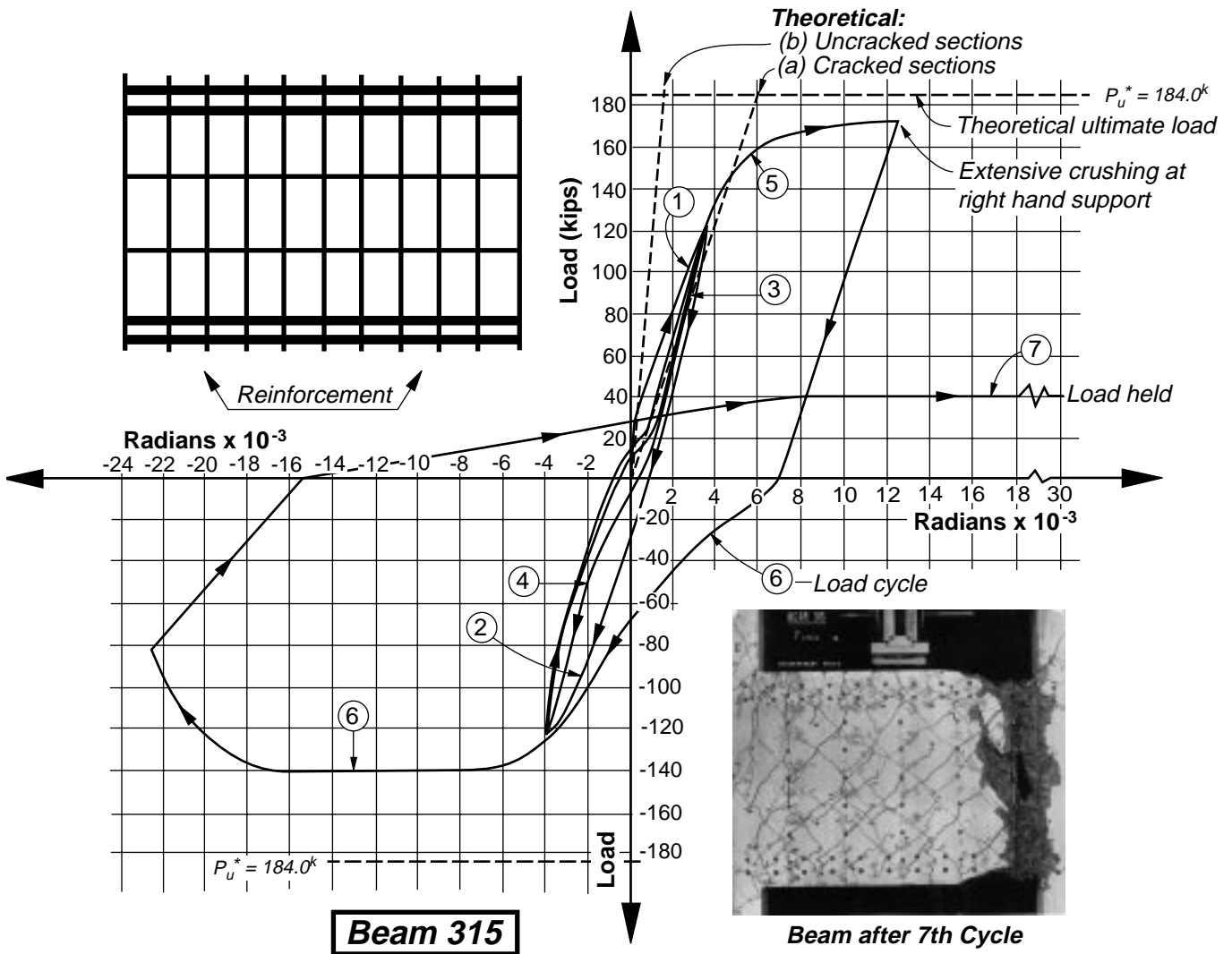
Reference: Paulay & Binney (1974)
 Specimen: Beam 316



Load-rotation relationship for Beam 316.

DAMAGE PATTERNS AND HYSTERETIC RESPONSE

System: Reinforced Concrete	RC3D Example 1 of 1
Component Type: Weaker Spandrel or Coupling Beam	
Predominant Behavior Mode: Flexure/Sliding Shear	
Secondary Behavior Mode: —	
Reference: Paulay & Binney (1974)	
Specimen: Beam 315	



Load-rotation relationship for a conventional coupling beam.

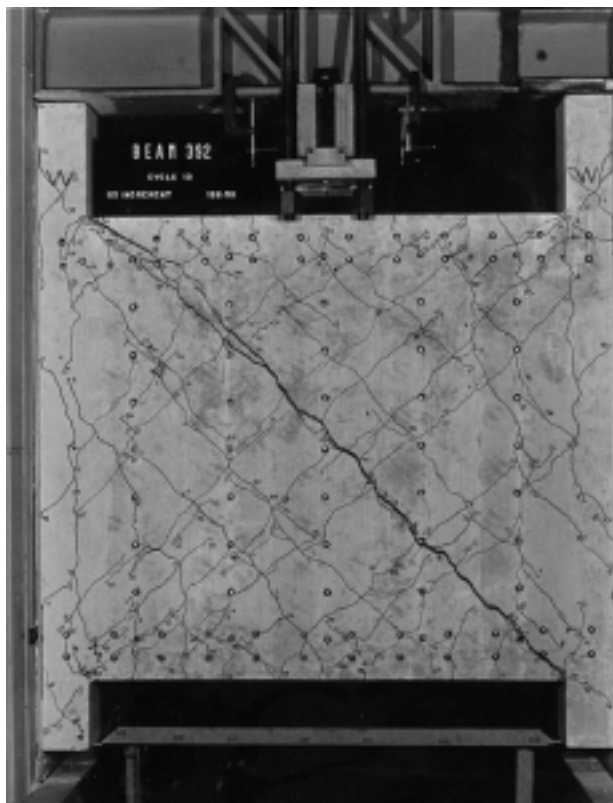
DAMAGE PATTERNS AND HYSTERETIC RESPONSE

System: **Reinforced Concrete**
Component Type: **Weaker Spandrel or Coupling Beam**
Predominant Behavior Mode: **Preemptive Diagonal Tension**
Secondary Behavior Mode: —

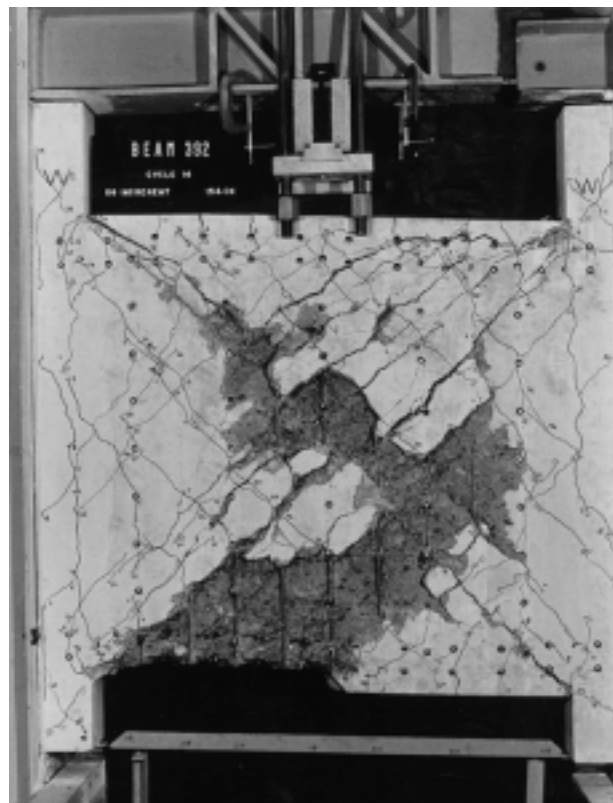
RC3H

Example 1 of 1

Reference: Paulay (1977), Paulay (1986)
Specimen: Beam 392



Beam 392 after being subjected to seismic-type loading: Cycle 13.



Beam 392, Cycle 14.

2.3 Tabular Bibliography

Table 2-2 contains a brief description of the key technical reports that address specific reinforced concrete component behavior. The component types and their

behavior modes are indicated. The full references can be found in Section 2.5.

Table 2-2 Key References on Reinforced Concrete Wall Behavior.

Reference	Description	Comp. Types	Behavior modes Addressed												
			A	B	C	D	E	F	G	H	I	J	K	L	
<i>EVALUATION AND DESIGN RECOMMENDATIONS:</i>															
ACI 318 (1995)	Code provisions for the design of r/c walls. Distinct behavior modes are often not considered explicitly.	RC1 – RC4													
Paulay & Priestley (1992)	Comprehensive recommendations for the design of r/c walls. Considers all component types and prevalent behavior modes.	RC1 – RC4	•	•	•	•	•		•	•				•	
Oesterle et al (1983)	Development of a design equation for web crushing strength. Strength is related to story drift and correlation with research results is shown.	RC1			•										
<i>OVERVIEWS OF TEST RESULTS:</i>															
Wood (1991)	Review of 27 specimens. 24 cyclic-static loading, 3 monotonic loading. “Slender” walls: $1.1 < M/VL < 2.9$, All specimens reached flexural yield. Failure categorized as either “shear” or “flexure”.	RC1													
Wood (1990)	Review of 143 specimens. 50 cyclic-static loading, 89 monotonic loading, 4 repeated unidirectional loading. “Short” walls: $0.23 < M/VL < 1.7$. Review focuses on maximum strength. Failure modes and displacement capacity not addressed	RC1													
ATC-11(1983)	Commentary on implications of r/c wall test results and design issues.	RC1, RC3													
Sozen & Moehle (1993)	Review of wall test results applicable to nuclear power plant structures. Focused on predicting initial stiffness.	RC1													

¹ Behavior modes:

A Ductile Flexural Response

B Flexure/Diagonal Tension

C Flexure/Diagonal Compression (Web Crushing)

D Flexure/Sliding Shear

E Flexure/Boundary-Zone Compression

F Flexure/Lap-Splice Slip

G Flexure/Out-of-Plane Wall Buckling

H Preemptive Diagonal Tension

I Preemptive Web Crushing

J Preemptive Sliding Shear

K Preemptive Boundary Zone Compression Failure

L Preemptive Lap-Splice Failure

M Global foundation rocking of wall

N Foundation rocking of individual piers

Table 2-1 Key References on Reinforced Concrete Wall Behavior (continued)

Reference	Description	Comp. Types	Behavior modes Addressed											
			A	B	C	D	E	F	G	H	I	J	K	L
<i>DETAILED TEST RESULTS:</i>														
Barda (1972) Barda, Hanson & Corley (1976) (Lehigh Univ.)	8 test specimens: 6 cyclic-static loading, 2 monotonic loading, Small axial load. Approx. 1/3 scale, flanged walls. Low-rise: $M/VL = 1.0, 0.5, 0.25$. Wall vertical & horiz. reinf. and flange longit. reinf. varied 1 specimen repaired by replacement of web concrete and tested.	RC1												
Oesterle et al (1976) Oesterle et al (1979) (Portland Cement Association)	16 test specimens: 2 rectangular, 12 barbell, 2 flanged. $M/VL = 2.4$. Approx. 1/3 scale. Variables include boundary longit. and hoop reinf., wall horiz. reinf., axial load, load history 2 specimens repaired and tested.	RC1	•		•		•		•					
Shiu et al (1981) (Portland Cement Association)	2 test specimens. One solid wall and one wall with openings. Approx. 1/3 scale. Rectangular sections. Solid wall governed by sliding shear. Wall with openings was governed by diagonal compression in the piers. Coupling beams were not significantly damaged.	RC1, RC2, RC4			•	•								
Wang, Bertero & Popov (1975) Valle- nas, Bertero & Popov (1979) (U.C. Berkeley)	10 test specimens: 6 barbell and 4 rectangular. 5 cyclic-static loading, 5 monotonic. 1/3 scale, modeled bottom 3 stories of 10-story barbell wall and 7-story rectangular wall. 5 specimens repaired with replacement of damaged rebar and crushed concrete.	RC1			•		•	•	•					
Iliya & Bertero (1980) (U.C. Berkeley)	2 test specimens. Barbell-shaped sections. Combination of cyclic-static and monotonic loading. 1/3 scale, modeled bottom 3 stories of 10-story barbell wall. Specimens repaired with epoxy injection of cracks after minor damage then subsequently repaired (after major damage) with replacement of damaged rebar and crushed concrete.	RC1			•			•						

¹ Behavior modes:

A Ductile Flexural Response

B Flexure/Diagonal Tension

C Flexure/Diagonal Compression (Web Crushing)

D Flexure/Sliding Shear

E Flexure/Boundary-Zone Compression

F Flexure/Lap-Splice Slip

G Flexure/Out-of-Plane Wall Buckling

H Preemptive Diagonal Tension

I Preemptive Web Crushing

J Preemptive Sliding Shear

K Preemptive Boundary Zone Compression Failure

L Preemptive Lap-Splice Failure

M Global foundation rocking of wall

N Foundation rocking of individual piers

Table 2-1 Key References on Reinforced Concrete Wall Behavior (continued)

Reference	Description	Comp. Types	Behavior modes Addressed														
			A	B	C	D	E	F	G	H	I	J	K	L			
Paulay, Priestley & Syngé (1982)	4 test specimens, 2 rectangular, 2 flanged. Low-rise walls, $M/VL = 0.57$ Approx. 1/2 scale. Two specimens with diagonal bars to prevent sliding shear.	RC1	•			•											
Paulay & Binney (1974) Paulay (1971a, 1971b)	12 coupling-beam test specimens, 3 monotonic loading, 9 cyclic-static loading. $M/VL = 0.51, 0.65$. Approx. 1/2 scale. Varied amount of stirrup reinforcement, and amount and arrangement of longitudinal reinf., 3 specimens with diagonal bars.	RC3	•	•	•	•											
Paulay and Santhakumar (1976)	Two 7-story coupled wall specimens. Cyclic-static loading 1/4 scale. One specimen with diagonally reinforced coupling beams.	RC1 RC3	•			•											
Barney et al (1978) (Portland Cement Association)	8 coupling beam test specimens, Cyclic-static loading. $M/VL = 1.25, 2.5$. Approximately 1/3-scale specimens with conventional longitudinal reinforcement, diagonal bars in hinge zones, and full length diagonal bars. Full length diagonal reinforcement significantly improved performance.	RC3	•	•		•											
Wight (Editor) (1985)	7-story building, two bays by three bays with beam and slab floors, cyclic-static loading full scale. One wall acting parallel to moment frames. Parallel and perpendicular frames increased the capacity of the structure. Test structure repaired with epoxy injection and re-tested	RC1				•											
Alexander, Heidebrcht, and Tso (1973) (McMaster University)	$M/VL = 2.0, 1.33, 0.67$ Cyclic-static loading. 1/2 scale. Axial load varied.	RC1	•			•											
Shiga, Shibata, and Takahashi (1973, 1975) (Tohoku University)	8 test specimens, 6 cyclic-static loading, 2 monotonic. Approx. 1/4 scale. Barbell section. Load history, web reinforcement, and axial load varied. $M/VL = 0.63$.	RC1				•											
Maier (1991)	10 test specimens, 2 cyclic-static loading, 8 monotonic. 7 flanged sections, 3 rectangular. Approx. 1/3 scale. Reinforcement and axial load varied. $M/VL = 1.12$.	RC1		•	•												

¹ Behavior modes:

A Ductile Flexural Response

B Flexure/Diagonal Tension

C Flexure/Diagonal Compression (Web Crushing)

D Flexure/Sliding Shear

E Flexure/Boundary-Zone Compression

F Flexure/Lap-Splice Slip

G Flexure/Out-of-Plane Wall Buckling

H Preemptive Diagonal Tension

I Preemptive Web Crushing

J Preemptive Sliding Shear

K Preemptive Boundary Zone Compression Failure

L Preemptive Lap-Splice Failure

M Global foundation rocking of wall

N Foundation rocking of individual piers

Table 2-1 Key References on Reinforced Concrete Wall Behavior (continued)

Reference	Description	Comp. Types	Behavior modes Addressed													
			A	B	C	D	E	F	G	H	I	J	K	L		
Mansur, Balendra, and H'ng (1991)	4 successful test specimens, cyclic-static loading. Approx. 1/4 scale. Flanged section. Web reinforced with welded wire mesh or expanded metal. $M/VL = 0.68$.	RC1		•	•											
Saatcioglu (1991)	3 test specimens, cyclic-static loading. Approx. 1/3 scale. Rectangular section. Horizontal and sliding-shear dowel reinforcement varied. $M/VL = 0.50$.	RC1		•	•	•										
Aristizabal-Ochoa, Dario, & Sozen (1976) (University of Illinois)	4 shake-table specimens. Approx. 1/12 scale. 10-story coupled walls, rectangular pier and beam sections. Discusses reduced stiffness of coupling beams resulting from bond slip, and redistribution of demands between wall piers.	RC1 RC3	•													
Lybas & Sozen (1977) (University of Illinois)	6 test specimens, 5 shake-table and 1 cyclic static. Approx. 1/12 scale. 6-story coupled walls, rectangular pier and beam sections.	RC1 RC3	•													
Azizinamini et al. (1994) (Portland Cement Association)	Out-of-plane tests on tilt-up walls. 6 test specimens. Approx. 3/5 scale. Monotonic out-of-plane loading. Report shows typical crack patterns resulting from out-of-plane forces.	RC1														
ACI-SEAOSC Task Force (1982)	Out-of-plane tests on tilt-up walls, 12 reinforced concrete specimens (Also, 18 reinforced masonry specimens). Full scale monotonic out-of-plane loading and constant axial loading h/t ratios of 30 to 60.	RC1														

¹ Behavior modes:

A Ductile Flexural Response

B Flexure/Diagonal Tension

C Flexure/Diagonal Compression (Web Crushing)

D Flexure/Sliding Shear

E Flexure/Boundary-Zone Compression

F Flexure/Lap-Splice Slip

G Flexure/Out-of-Plane Wall Buckling

H Preemptive Diagonal Tension

I Preemptive Web Crushing

J Preemptive Sliding Shear

K Preemptive Boundary Zone Compression Failure

L Preemptive Lap-Splice Failure

M Global foundation rocking of wall

N Foundation rocking of individual piers

2.4 Symbols for Reinforced Concrete

Symbols that are used in this chapter are defined below. Further information on some of the variables used (particularly those noted “per ACI”) may be found by looking up the symbol in Appendix D of *ACI 318-95*.

A_{ch} = Cross sectional area of confined core of wall boundary region, measured out-to-out of confining reinforcement and contained within a length c' from the end of the wall, FEMA 306, Section A2.3.7	h_w = Height of wall or segment of wall considered (per ACI)
A_{cv} = Net area of concrete section bounded by web thickness and length of section in the direction of shear force considered, in ² (per ACI)	k_{rc} = Coefficient accounting the effect of ductility demand on V_c per FEMA 306, Section A2.3.6.b
A_g = Gross cross sectional area of wall boundary region, taken over a length c' from the end of the wall, FEMA 306, Section A2.3.7	l_p = Equivalent plastic hinge length, determined according to FEMA 306, Section A2.3.3.
A_{sh} = Total cross-sectional area of transverse reinforcement (including crossties) within spacing s and perpendicular to dimension h_c . (per ACI)	l_u = Unsupported length considered for wall buckling, determined according to FEMA 306, Section A2.3.9
b = Width of compression face of member, in (per ACI)	l_n = Beam clear span (per ACI)
b_w = Web width, in (per ACI)	l_w = Length of entire wall or segment of wall considered in direction of shear force (per ACI). (For isolated walls and wall piers equals horizontal length, for spandrels and coupling beams equals vertical dimension i.e., overall depth)
c = Distance from extreme compressive fiber to neutral axis (per ACI)	M_{cr} = Cracking moment (per ACI)
c' = Length of wall section over which boundary ties are required, per FEMA 306, Section A2.3.7	M_e = Expected moment strength at section, equal to nominal moment strength considering expected material strengths.
d_b = Bar diameter (per ACI)	M_n = Nominal moment strength at section (per ACI)
d_{bt} = Bar diameter of tie or loop	M_u = Factored moment at section (per ACI)
f'_c = Specified compressive strength of concrete, psi (per ACI)	M/V = Ratio of moment to shear at a section. When moment or shear results from gravity loads in addition to seismic forces, can be taken as M_u/V_u
f_y = Specified yield strength of nonprestressed reinforcement, psi. (per ACI)	N_u = Factored axial load normal to cross section occurring simultaneously with V_u ; to be taken as positive for compression, negative for tension (per ACI)
f_{yh} = Specified yield strength of transverse reinforcement, psi (per ACI)	s = Spacing of transverse reinforcement measured along the longitudinal axis of the structural member (per ACI)
h_c = Cross sectional dimension of confined core of wall boundary region, measured out-to-out of confining reinforcement	s_l = spacing of vertical reinforcement in wall (per ACI)
h_d = Height over which horizontal reinforcement contributes to V_s per FEMA 306, Section A2.3.6.b	V_c = Nominal shear strength provided by concrete (per ACI)
	V_n = Nominal shear strength (per ACI)
	V_p = Nominal shear strength related to axial load per Section

V_s	= Nominal shear strength provided by shear reinforcement (per ACI)	μ_{Δ}	= Displacement ductility demand for a component, used in FEMA 306, Section A2.3.4, as discussed in Section 6.4.2.4 of <i>FEMA-273</i> . Equal to the component deformation corresponding to the global target displacement, divided by the effective yield displacement of the component (which is defined in Section 6.4.1.2B of <i>FEMA-273</i>).
V_u	= Factored shear force at section (per ACI)	ρ_g	= Ratio of total reinforcement area to cross-sectional area of wall.
V_{wc}	= Web crushing shear strength per FEMA 306, Section A2.3.6.c	ρ_l	= Local reinforcement ratio in boundary region of wall according to FEMA 306, Section A2.3.7
α	= Coefficient accounting for wall aspect ratio effect on V_c per FEMA 306, Section A2.3.6.b	ρ_n	= Ratio of distributed shear reinforcement on a plane perpendicular to plane of A_{cv} (per ACI). (For typical wall piers and isolated walls indicates amount of horizontal reinforcement.)
β	= Coefficient accounting for longitudinal reinforcement effect on V_c per FEMA 306, Section A2.3.6.b		
δ	= Story drift ratio for a component, corresponding to the global target displacement, used in the computation of V_{wc} , FEMA 306, Section A2.3.6.c		
μ	= Coefficient of friction (per ACI)		

2.5 References for Reinforced Concrete

This list contains references from the reinforced concrete chapters of both FEMA 306 and 307.

- ACI, 1995, *Building Code Requirements for Reinforced Concrete*, American Concrete Institute, Report ACI 318-95, Detroit, Michigan.
- ACI-SEAOSC, 1982, *Test Report on Slender Walls*, Task Committee on slender Walls, American Concrete Institute, Southern California Chapter, and Structural Engineers of Southern California.
- Alexander, C.M., Heidebrecht, A.C., and Tso, W.K., 1973, "Cyclic Load Tests on Shear Wall Panels, Proceedings," *Fifth World Conference on Earthquake Engineering*, Rome, pp. 1116–1119.
- Ali, Aejaz and Wight, J. K., 1991, "R/C Structural Walls with Staggered Door Openings," *Journal of Structural Engineering*, ASCE, Vol. 117, No. 5, pp. 1514-1531.
- Antebi, J., Utku, S., and Hansen, R.J., 1960, *The Response of Shear Walls to Dynamic Loads*, MIT Department of Civil and Sanitary Engineering, Report DASA-1160, Cambridge, Massachusetts.
- Aristizabal-Ochoa, D., J., and Sozen, M.A., 1976, *Behavior of Ten-Story Reinforced Concrete Walls Subjected to Earthquake Motions*, Civil Engineering Studies Structural Research Series No. 431, Report UILU-ENG-76-2017, University of Illinois, Urbana, Illinois.
- ASCE/ACI Task Committee 426, 1973, "The Shear Strength of Reinforced Concrete Members," *ASCE Journal of Structural Engineering*, Vol. 99, No. ST6, pp 1091-1187.
- ATC, 1983, *Seismic Resistance of Reinforced Concrete Shear Walls and Frame Joints: Implication of Recent Research for Design Engineers*, Applied Technology Council, ATC-11 Report, Redwood City, California.
- ATC, 1996, *The Seismic Evaluation and Retrofit of Concrete Buildings*, Applied Technology Council, ATC-40 Report, Redwood City, California.
- ATC, 1997a, *NEHRP Guidelines for the Seismic Rehabilitation of Buildings*, prepared by the Applied Technology Council (ATC-33 project) for the Building Seismic Safety Council, published by the Federal Emergency Management Agency, Report No. FEMA 273, Washington, D.C.
- ATC, 1997b, *NEHRP Commentary on the Guidelines for the Seismic Rehabilitation of Buildings*, prepared by the Applied Technology Council (ATC-33 project) for the Building Seismic Safety Council, published by the Federal Emergency Management Agency, Report No. FEMA 274, Washington, D.C.
- Azizinamini, A., Glikin, J.D., and Oesterle, R.G., 1994, *Tilt-up Wall Test Results*, Portland Cement Association, Report RP322D, Skokie, Illinois.
- Barda, Felix, 1972, *Shear Strength of Low-Rise Walls with Boundary Elements*, Ph.D. University, Lehigh University, Bethlehem, Pennsylvania.
- Barda, Felix, Hanson, J.W., and Corley, W.G., 1976, *Shear Strength of Low-Rise Walls with Boundary Elements*, Research and Development Bulletin RD043.01D, preprinted with permission from ACI Symposium Reinforced Concrete Structures in Seismic Zones, American Concrete Institute.
- Barney, G.B., Shiu, K.N., Rabbat, B.G., Fiorako, A.E., Russell, H.G., and Corley, W.G., 1978, *Earthquake Resistant Structural Walls — Test of Coupling Beams*, Report to National Science Foundation, Portland Cement Association, Skokie, Illinois.
- Benjamin, J.R., and Williams, H.A., 1958a, "The Behavior of One-Story Reinforced Concrete Shear Walls," *Journal of the Structural Division*, ASCE, Vol. 83, No. ST3.
- Benjamin, J.R., and Williams, H.A., 1958b, Behavior of One-Story Reinforced Concrete Shear Walls Containing Openings, *ACI Journal*, Vol. 55, pp. 605-618.
- BSSC, 1992, *NEHRP Handbook for the Seismic Evaluation of Existing Buildings*, prepared by the Building Seismic Safety Council for the Federal Emergency Management Agency, Report No. FEMA-178, Washington, D.C.
- BSSC, 1997, *NEHRP Recommended Provisions for Seismic Regulations for New Buildings and Other Structures*, prepared by the Building Seismic Safety Council for the Federal Emergency Management Agency, Report No. FEMA 302, Composite Draft Copy, Washington, D.C.
- Cardenas, Alex E., 1973, "Shear Walls -- Research and Design Practice," *Proceedings, Fifth World Conference on Earthquake Engineering*, Rome Italy.

- Corley, W.G., Fiorato, A.E., and Oesterle, R.G., 1981, *Structural Walls*, American Concrete Institute, Publication SP-72, Detroit, Michigan, pp. 77-131.
- CRSI, No publication date given, *Evaluation of Reinforcing Steel in Old Reinforced Concrete Structures*, Concrete Reinforcing Steel Institute, Engineering Data Report No. 11, Chicago, Illinois.
- CSI, 1997, *SAP2000*, Computers and Structures, Inc., Berkeley, California.
- El-Bahy, A., Kunath, S.K., Taylor, A.W., and Stone, W.C., 1997, *Cumulative Seismic Damage of Reinforced Concrete Bridge Piers*, Building and Fire Research Laboratory, National Institute of Standards and Technology (NIST), Draft Report, Gaithersburg, Maryland.
- Hill, James A, 1997, "Summary of Finite Element Studies of Walls," oral communication
- ICBO, 1994, 1997, *Uniform Building Code*, International Conference of Building Officials, Whittier, California.
- Iliya, R., and Bertero, V.V., 1980, *Effects of Amount and Arrangement of Wall-Panel Reinforcement on Behavior of Reinforced Concrete Walls*, Earthquake Engineering Research Center, University of California at Berkeley, Report UCB-EERC-82-04.
- Kawashima, K., and Koyama, T., 1988, "Effect of Number of Loading Cycles on Dynamic Characteristics of Reinforced Concrete Bridge Pier Columns," *Proceedings of the Japan Society of Civil Engineers, Structural Eng./Earthquake Eng.*, Vol. 5, No. 1.
- Lybas, J.M. and Sozen, M.A., 1977, *Effect of Beam Strength and Stiffness on Dynamic Behavior of Reinforce Concrete Coupled Walls*, University of Illinois Civil Engineering Studies, Structural Research Series No. 444, Report UILU-ENG-77-2016 (two volumes), Urbana, Illinois.
- Maier, Johannes, 1991, "Shear Wall Tests," *Preliminary Proceedings, International Workshop on Concrete Shear in Earthquake*, Houston Texas.
- Mander, J.B., Mahmoodzadegan, B., Bhadra, S., and Chen, S.S., 1996, *Seismic Evaluation of a 30-Year-Old Highway Bridge Pier and Its Retrofit*, Department of Civil Engineering, State University of New York, Technical Report NCEER-96-0008, Buffalo NY.
- Mansur, M.A., Balendra, T., and H'Ng, S.C., 1991, "Tests on Reinforced Concrete Low-Rise Shear Walls Under Cyclic Loading," *Preliminary Proceedings, International Workshop on Concrete Shear in Earthquake*, Houston Texas.
- Oesterle, R.G., Fiorato, A.E., Johal, L.S., Carpenter, J.E., Russell, H.G., and Corley, W.G., 1976, *Earthquake Resistant Structural Walls -- Tests of Isolated Walls*, Report to National Science Foundation, Portland Cement Association, Skokie, Illinois, 315 pp.
- Oesterle, R.G., Aristizabal-Ochoa, J.D., Fiorato, A.E., Russell, H.G., and Corley, W.G., 1979, *Earthquake Resistant Structural Walls -- Tests of Isolated Walls -- Phase II*, Report to National Science Foundation, Portland Cement Association, Skokie, Illinois.
- Oesterle, R.G., Aristizabal, J.D., Shiu, K.N., and Corley, W.G., 1983, *Web Crushing of Reinforced Concrete Structural Walls*, Portland Cement Association, Project HR3250, PCA R&D Ser. No. 1714, Draft Copy, Skokie, Illinois.
- Ogata, K., and Kabeyasawa, T., 1984, "Experimental Study on the Hysteretic Behavior of Reinforced Concrete Shear Walls Under the Loading of Different Moment-to-Shear Ratios," *Transactions, Japan Concrete Institute*, Vol. 6, pp. 274-283.
- Park, R., 1996, "A Static Force-Based Procedure for the Seismic Assessment of Existing R/C Moment Resisting Frames," *Proceedings of the Annual Technical Conference*, New Zealand National Society for Earthquake Engineering.
- Park, R. and Paulay, T., 1975, *Reinforced Concrete Structures*, John Wiley & Sons, New York.
- Paulay, T., 1971a, "Coupling Beams of Reinforced-Concrete Shear Walls," *Journal of the Structural Division*, ASCE, Vol. 97, No. ST3, pp. 843-862.
- Paulay, T., 1971b, "Simulated Seismic Loading of Spandrel Beams," *Journal of the Structural Division*, ASCE, Vol. 97, No. ST9, pp. 2407-2419.
- Paulay, T., 1977, "Ductility of Reinforced Concrete Shearwalls for Seismic Areas," *Reinforced Concrete Structures in Seismic Zones*, American Concrete Institute, ACI Publication SP-52, Detroit, Michigan, pp. 127-147.
- Paulay, T., 1980, "Earthquake-Resisting Shearwalls -- New Zealand Design Trends," *ACI Journal*, pp. 144-152.

- Paulay, T., 1986, "A Critique of the Special Provisions for Seismic Design of the Building Code Requirements for Reinforced Concrete," *ACI Journal*, pp. 274-283.
- Paulay, T., and Binney, J.R., 1974, "Diagonally Reinforced Coupling Beams of Shear Walls," *Shear in Reinforced Concrete*, ACI Publication SP-42, American Concrete Institute, Detroit, Michigan, pp. 579-598.
- Paulay, T. and Priestley, M.J.N., 1992, *Seismic Design of Reinforced Concrete and Masonry Buildings*, John Wiley & Sons, New York.
- Paulay, T., and Priestley, M.J.N., 1993, "Stability of Ductile Structural Walls," *ACI Structural Journal*, Vol. 90, No. 4.
- Paulay, T., Priestley, M.J.N., and Syngé, A.J., 1982, "Ductility in Earthquake Resisting Squat Shear Walls," *ACI Journal*, Vol. 79, No. 4, pp.257-269.
- Paulay, T., and Santhakumar, A.R., 1976, "Ductile Behavior of Coupled Shear Walls," *Journal of the Structural Division, ASCE*, Vol. 102, No. ST1, pp. 93-108.
- Priestley M.J.N., Evison, R.J., and Carr, A.J., 1978, "Seismic Response of Structures Free to Rock on their Foundations," *Bulletin of the New Zealand National Society for Earthquake Engineering*, Vol. 11, No. 3, pp. 141-150.
- Priestley, M.J.N., Seible, F., and Calvi, G.M., 1996, *Seismic Design and Retrofit of Bridges*, John Wiley & Sons, New York, 686 pp.
- Saatcioglu, Murat, 1991, "Hysteretic Shear Response of Low-rise Walls," *Preliminary Proceedings, International Workshop on Concrete Shear in Earthquake*, Houston Texas.
- SANZ, Standards Association of New Zealand, 1995, *Code of Practice for the Design of Concrete Structures*, NZS3101.
- SEAOC, 1996, *Recommended Lateral Force Requirements and Commentary* ("Blue Book"), 6th Edition, Seismology Committee, Structural Engineers Association of California, Sacramento, California.
- Shiga, Shibata, and Takahashi, 1973, "Experimental Study on Dynamic Properties of Reinforced Concrete Shear Walls," *Proceedings, Fifth World Conference on Earthquake Engineering*, Rome, pp. 107-117.
- Shiga, Shibata, and Takahashi, 1975, "Hysteretic Behavior of Reinforced Concrete Shear Walls," *Proceedings of the Review Meeting, US-Japan Cooperative Research Program in Earthquake Engineering with Emphasis on the Safety of School Buildings*, Honolulu Hawaii, pp. 1157-1166.
- Shiu, K.N., Daniel, J.I., Aristizabal-Ochoa, J.D., A.E. Fiorato, and W.G. Corley, 1981, *Earthquake Resistant Structural Walls -- Tests of Wall With and Without Openings*, Report to National Science Foundation, Portland Cement Association, Skokie, Illinois.
- Sozen, M.A., and Moehle, J.P., 1993, *Stiffness of Reinforced Concrete Walls Resisting In-Plane Shear*, Electric Power Research Institute, EPRI TR-102731, Palo Alto, California.
- Vallenas, J.M., Bertero, V.V., Popov, E.P., 1979, *Hysteretic Behavior of Reinforced Concrete Structural Walls*, Earthquake Engineering Research Center, University of California, Report No. UCB/EERC-79/20, Berkeley, California, 234 pp.
- Wallace, J. W., 1996, "Evaluation of UBC-94 Provisions for Seismic Design of RC Structural Walls," *Earthquake Spectra*, EERI, Oakland, California.
- Wallace, J. W. and Moehle, J.P., 1992, "Ductility and Detailing Requirements for Bearing Wall Buildings," *Journal of Structural Engineering, ASCE*, Vol. 118, No. 6, pp. 1625-1644.
- Wallace, J. W. and Thomsen IV, J.H., 1995, "Seismic Design of RC Shear Walls (Parts I and II)," *Journal of Structural Engineering, -ASCE*, pp. 75-101.
- Wang, T.Y., Bertero, V.V., Popov, E.P., 1975, *Hysteretic Behavior of Reinforced Concrete Framed Walls*, Earthquake Engineering Research Center, University of California at Berkeley, Report No. UCB/EERC-75/23, Berkeley, California, 367 pp.
- Wight, James K. (editor), 1985, *Earthquake Effects on Reinforced Concrete Structures*, US-Japan Research, ACI Special Publication SP-84, American Concrete Institute, Detroit Michigan.
- Wiss, Janney, Elstner and Associates, 1970, *Final Report on Bar Tests*, for the Committee of Concrete Reinforcing Bar Producers, American Iron and Steel Institute (Job #70189), Northbrook, Illinois.
- Wood, S. L., 1990, "Shear Strength of Low-Rise Reinforced Concrete Walls," *ACI Structural Journal*, Vol. 87, No. 1, pp 99-107.

Wood, S. L., 1991, "Observed Behavior of Slender Reinforced Concrete Walls Subjected to Cyclic Loading," *Earthquake-Resistant Concrete Structures, Inelastic Response and Design*, ACI Special

Publication SP-127, S.K. Ghosh, Editor, American Concrete Institute, Detroit Michigan, pp. 453–478

3. Reinforced Masonry

3.1 Commentary and Discussion

Several topics that are relevant to the development of the reinforced masonry component guides are addressed in this chapter.

3.1.1 Typical Hysteretic Behavior

The behavior modes described for reinforced masonry in FEMA 306, Section A3.2 are based on experimental research and field observation of earthquake damaged masonry buildings. Typical damage patterns and hysteretic response representative of different components and behavior modes are presented in Table 3-1

3.1.2 Cracking and Damage Severity

Cracks in a structural wall can provide information about previous displacements and component response. Aspects of cracking that relate to component behavior include:

- The orientation of cracks
- The number (density) of cracks
- The spacing of cracks
- The width of individual cracks
- The relative size of crack widths

In reinforced masonry with a flexural behavior mode, flexural cracks generally form in the mortar bed joints. At the base of a tall cantilever wall, flexural cracks may propagate across the entire length of the wall. Following an earthquake, flexural cracks tend to close due to gravity loads, and they may be particularly hard to locate in mortar joints. They are generally associated with ductile response and the natural engagement of vertical reinforcement; as a result, they do not provide a good measure of damage. When such cracks are visible, they are only used to identify behavior modes, not to assess the severity of damage.

Diagonal cracks reflect associated shear stresses, but they may be a natural part of ductile flexural action. In

fully-grouted hollow brick or block masonry, diagonal cracks typically propagate through the units with short deviations along the mortar joints. Stair-step diagonal cracks are rare, and would indicate partial grouting and low-strength mortar. In plastic-hinge zones undergoing flexural response, diagonal cracks propagate from the ends of flexural cracks. In shear-dominated panels, diagonal cracks are more independent of flexural cracks.

In a flexurally-controlled wall, diagonal cracks are well-distributed and of uniform, small width. In a wall undergoing the transition from flexural response to shear response, one or two diagonal cracks, typically at the center of the wall, will grow wider than the others, dominating the response and concentrating shear deformations in a small area. A poorly-detailed wall undergoing preemptive shear behavior may have very few cracks until a critical, single diagonal crack opens.

In the investigation of earthquake-damaged concrete and masonry wall structures, cracks are the most visible evidence of damage. Because cracks are a striking and easily observed indication of the effect of earthquakes on walls, there is a strong temptation to overemphasize the relationship between crack width and the associated decrease (if any) in the strength and deformation capacity of a wall. Hanson (1996), has made the case that crack width alone is a poor indicator of damage severity. In recognition of this, the Component Damage Classification Guides in FEMA 306 do not rely on crack width as the only description of damage—numerous indicators of damage severity in reinforced masonry walls are described, among which crack width is only one. Cracking patterns can provide a wealth of information about the performance of a structural wall, but the location, orientation, number, and distribution of the cracks must be considered as important as, if not more important than, the crack width.

With the understanding that crack width must be considered in the context of all of the other parameters that can affect the behavior mode and damage severity of a wall, a rational approach is required to understand the influence of crack width on damage. This section outlines the basis of crack width limits specified in the Component Damage Classification Guides.

Table 3-1 Damage Patterns and Hysteretic Response for Reinforced Masonry Components

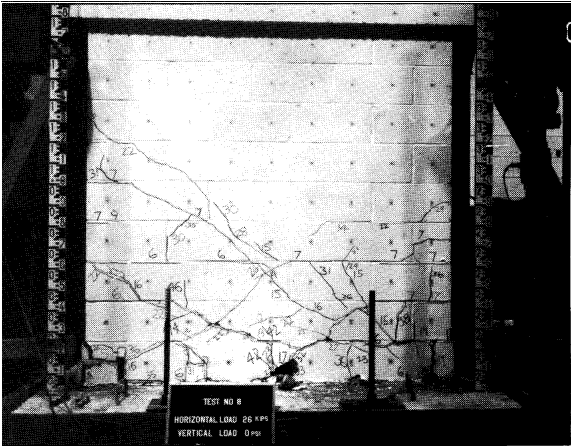
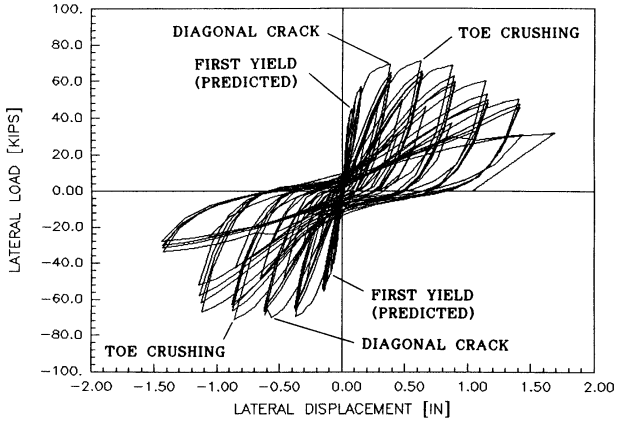
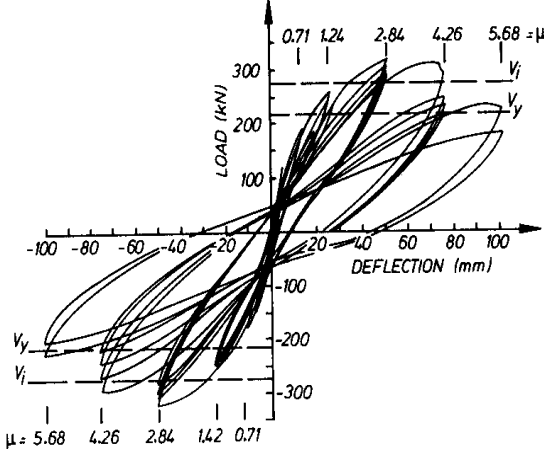
Component and Behavior Mode	Reference	Crack / Damage Pattern	Hysteretic Response
RM1 Flexure <i>See Guide RM1A</i>	Shing et al., 1991 Specimen 12		
RM1 Flexure <i>See Guide RM1A</i>	Priestley and Elder 1982		 <p>(b) Confined Wall</p>

Table 3-1 *Damage Patterns and Hysteretic Response for Reinforced Masonry Components (continued)*

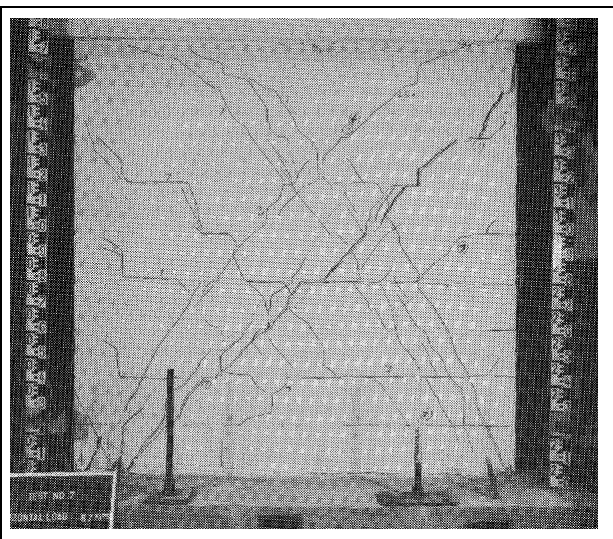
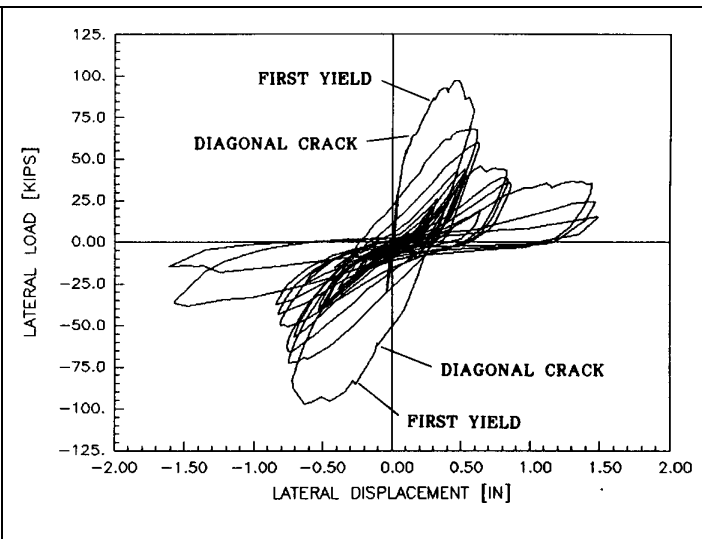
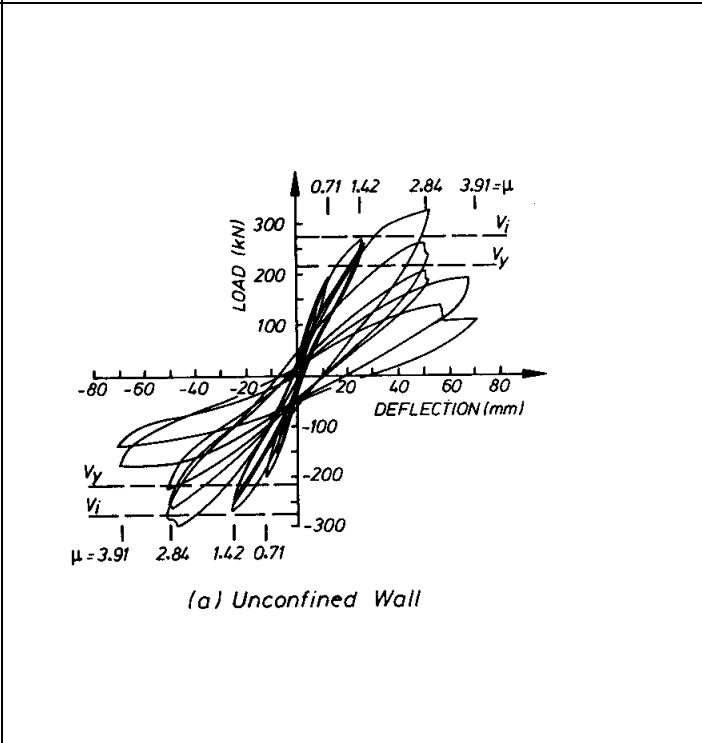
<p>RM1</p> <p>Flexure / Shear</p> <p><i>See Guides RM1B and RM2B</i></p>	<p>Shing et al., 1991</p> <p>Specimen 7</p>		
<p>RM1</p> <p>Flexure / Shear</p> <p><i>See Guides RM1B and RM2B</i></p>	<p>Priestley and Elder 1982</p>		 <p>(a) Unconfined Wall</p>

Table 3-1 Damage Patterns and Hysteretic Response for Reinforced Masonry Components (continued)

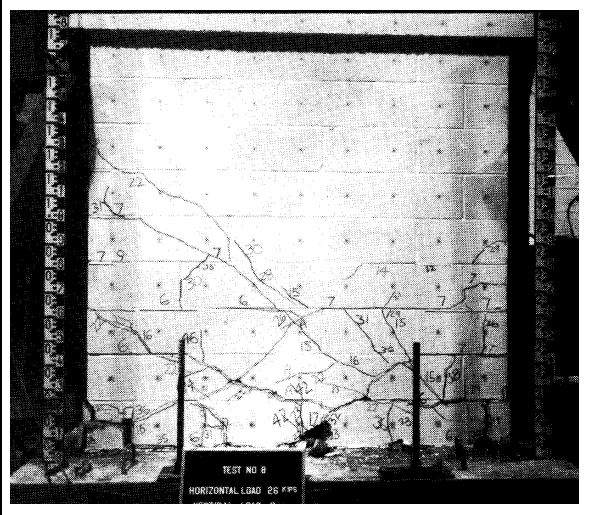
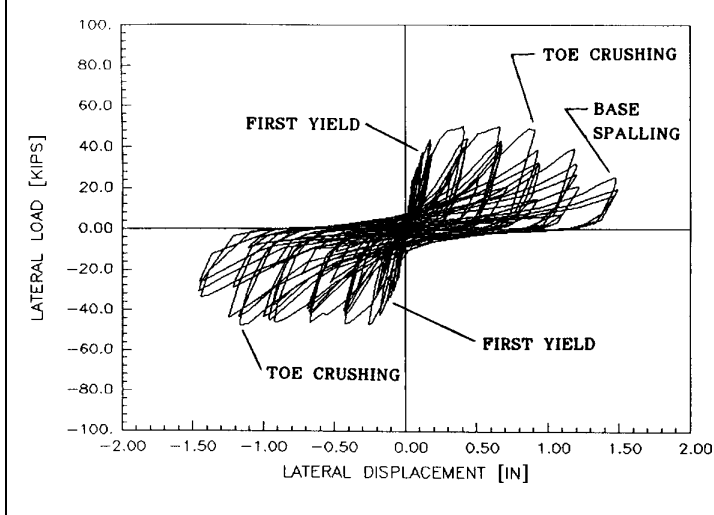
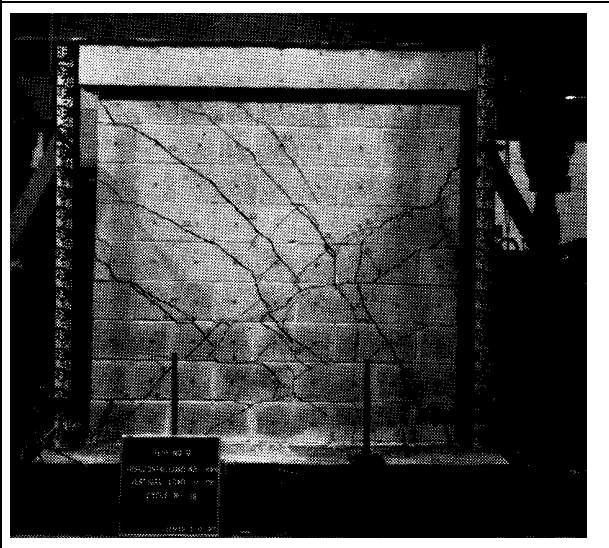
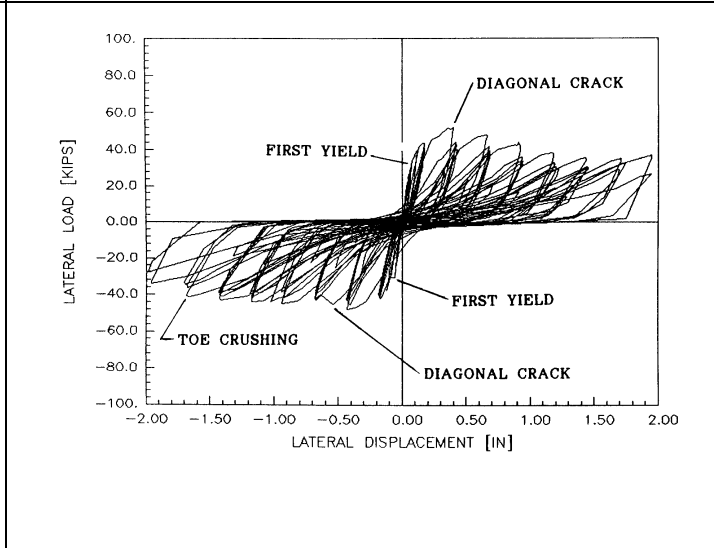
<p>RM1</p> <p>Flexure / Sliding Shear</p> <p>See Guide RM1C</p>	<p>Shing et al., 1991</p> <p>Specimen 8</p>		
<p>RM1</p> <p>Flexure / Shear / Sliding Shear</p> <p>See Guides RM1B and RM1C</p>	<p>Shing et al., 1991</p> <p>Specimen 6</p>		

Table 3-1 *Damage Patterns and Hysteretic Response for Reinforced Masonry Components (continued)*

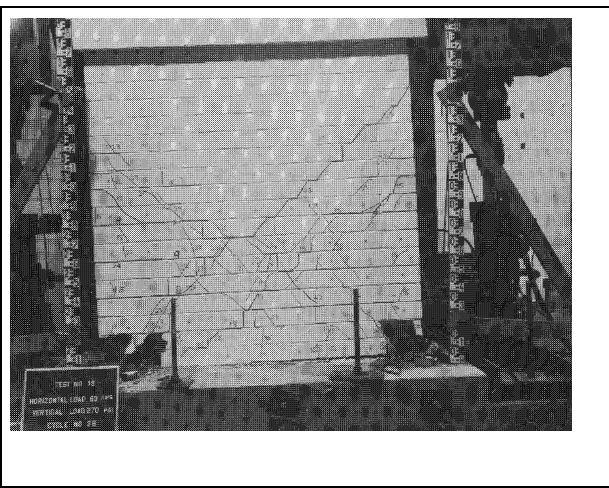
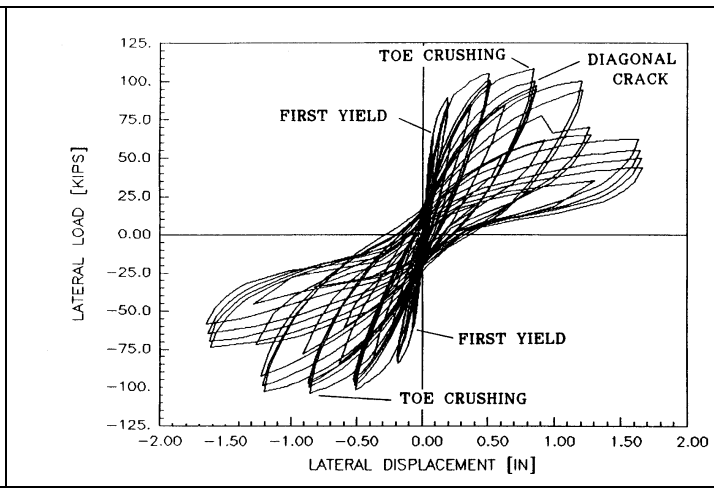
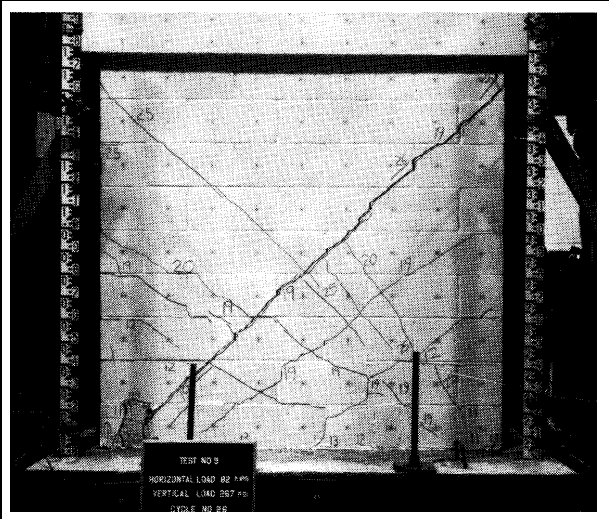
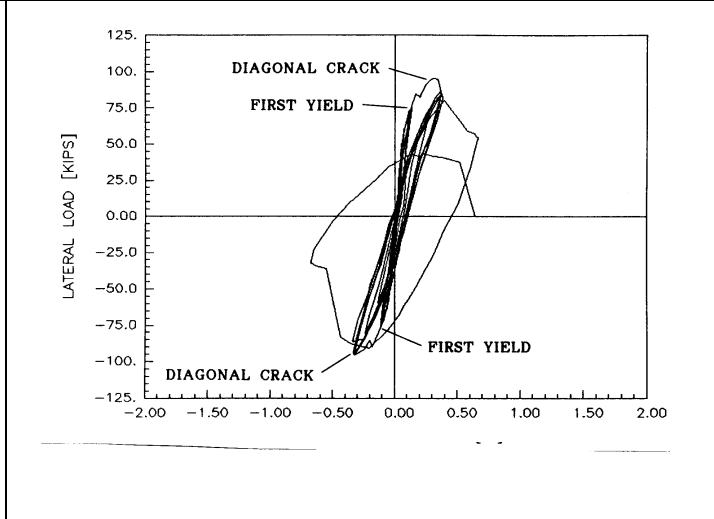
<p>RM1</p> <p>Flexure /lap splice slip</p> <p><i>See Guide RM1E</i></p>	<p>Shing et al., 1991</p> <p>Specimen 19</p>		
<p>RM1 or RM2</p> <p>Preemptive Shear</p> <p><i>See Guide RM2G</i></p>	<p>Shing et al., 1991</p> <p>Specimen 9</p>		

Table 3-1 Damage Patterns and Hysteretic Response for Reinforced Masonry Components (continued)

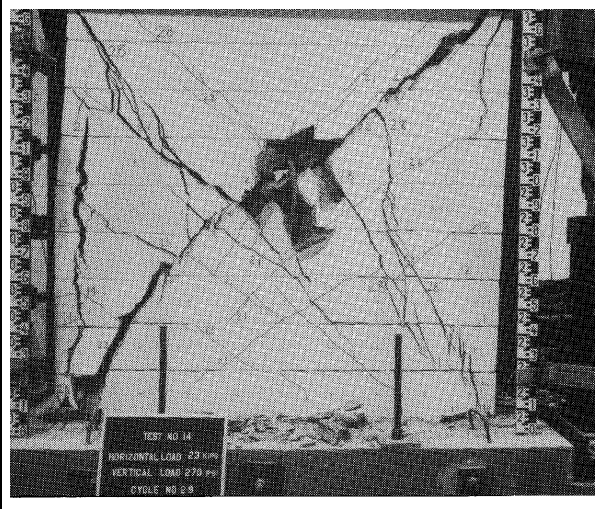
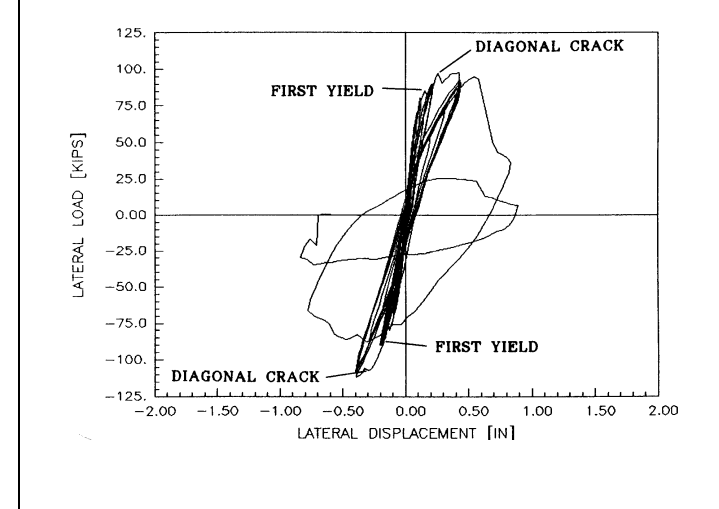
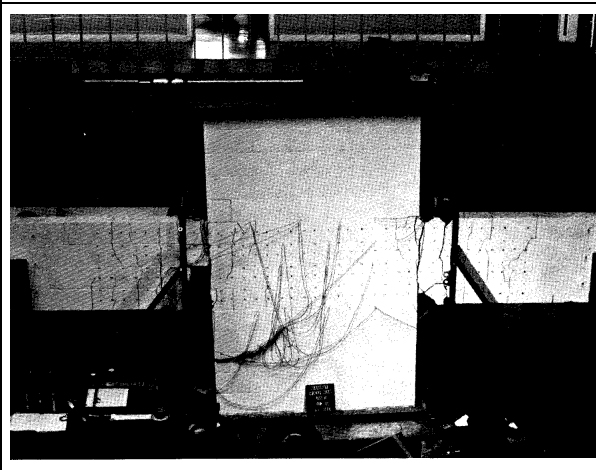
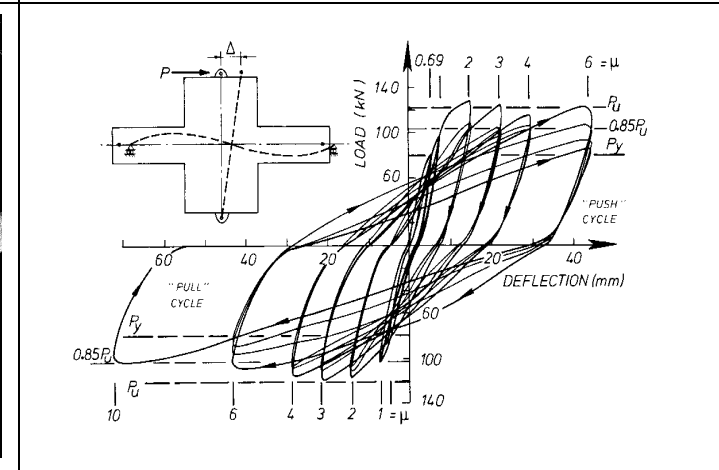
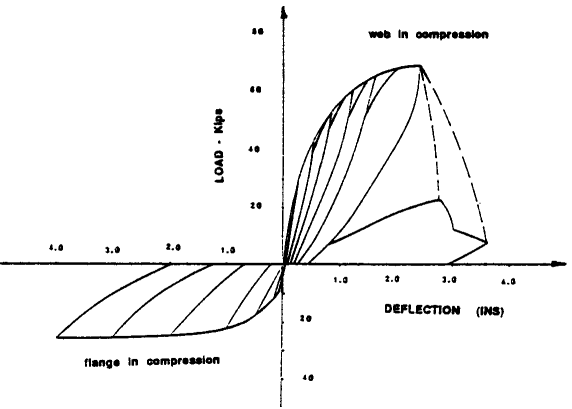
<p>RM1 or RM2</p> <p>Preemptive Shear</p> <p>See Guide RM2G</p>	<p>Shing et al., 1991</p> <p>Specimen 14</p>		
<p>RM3</p> <p>Flexure</p> <p>See Guide RM3A</p>	<p>Priestley and Hon, 1985</p>		

Table 3-1 *Damage Patterns and Hysteretic Response for Reinforced Masonry Components (continued)*

<p>RM1 or RM2 with flange.</p> <p>Flexure / Shear</p> <p><i>See Guides RM1A, RM1B, and / or RM2G</i></p>	<p>Priestley and He, 1990</p>		 <p>The figure is a load-deflection hysteresis loop for a reinforced masonry component with a flange. The vertical axis is labeled 'LOAD - kips' and ranges from -4.0 to 8.0. The horizontal axis is labeled 'DEFLECTION (INS)' and ranges from -4.0 to 4.0. The plot shows several loading and unloading cycles. The loading curves (solid lines) show a peak load of approximately 7.5 kips at a deflection of about 2.5 inches. The unloading curves (dashed lines) show a residual load of about 2.0 kips at a deflection of 4.0 inches. The region of positive deflection is labeled 'web in compression' and the region of negative deflection is labeled 'flange in compression'.</p>

Research has been conducted to evaluate the relationship between crack width, crack spacing, and reinforcing bar strain. A partial review of the literature on crack width is provided by Noakowski, (1985). Research indicates that the width of a crack crossing a reinforcing bar at first yield of the reinforcement depends on the bar diameter, the reinforcement yield stress, the reinforcement ratio, the reinforcement elastic modulus, and on the characteristics of the bond stress-slip relationship. However, most research in this area has focused on nearly elastic systems (prior to yield in reinforcement), and flexural cracking in beams and uniaxial tension specimens. It is difficult to extrapolate quantitative expressions for crack width and spacing prior to yield to reinforced masonry specimens with sufficient damage to reduce strength or deformation capacity.

Sassi and Ranous (1996) have suggested criteria to relate crack width to damage, but they have not provided sufficient information to associate crack patterns with specific behavior modes, which is essential when determining damage severity.

In the guides for reinforced masonry components, the crack width limits for each damage severity level have

been determined empirically, using crack widths reported in the literature and photographs of damaged specimens. Consideration has been given to the theoretical crack width required to achieve yield of reinforcement under a variety of conditions. A fundamental presumption is that the width of shear cracks is related to damage severity, while flexural crack widths are not closely related to damage severity.

3.1.3 Interpretation of Tests

Interpretation of test results for reinforced masonry was similar to that for reinforced concrete as described in Section 2.1.1.2. The ranges of component ductility and l-factors are presented in Table 3-2.

3.2 Tabular Bibliography for Reinforced Masonry

Table 3-3 contains a brief description of the key technical reports which address specific reinforced masonry component behavior. The component types and their behavior modes are indicated. The full references can be found in Section 3.4.

Chapter 3: Reinforced Masonry

Table 3-2 Ranges of reinforced masonry component displacement ductility, μ_{Δ} , associated with damage severity levels and λ factors

Damage Guide	Damage Severity			
	Insignificant	Slight	Moderate	Heavy
RM1A Ductile Flexural	$\mu_{\Delta} \leq 3$ $\lambda_K = 0.8$ $\lambda_Q = 1.0$ $\lambda_D = 1.0$	$\mu_{\Delta} \approx 2 - 4$ $\lambda_K = 0.6$ $\lambda_Q = 1.0$ $\lambda_D = 1.0$	$\mu_{\Delta} \approx 3 - 8$ $\lambda_K = 0.4$ $\lambda_Q = 0.9$ $\lambda_D = 1.0$	Heavy not used
RM1B Flexure/Shear	$\mu_{\Delta} \leq 2$ $\lambda_K = 0.8$ $\lambda_Q = 1.0$ $\lambda_D = 1.0$	$\mu_{\Delta} \approx 2 - 3$ $\lambda_K = 0.6$ $\lambda_Q = 1.0$ $\lambda_D = 1.0$	$\mu_{\Delta} \approx 3 - 5$ $\lambda_K = 0.4$ $\lambda_Q = 0.8$ $\lambda_D = 0.9$	
RM1C Flexure/ Sliding Shear	See RM1A	$\mu_{\Delta} \approx 2 - 4$ $\lambda_K = 0.5$ $\lambda_Q = 0.9$ $\lambda_D = 1.0$	$\mu_{\Delta} \approx 3 - 8$ $\lambda_K = 0.2$ $\lambda_Q = 0.8$ $\lambda_D = 0.9$	
RM1D Flexure/ Out-of-Plane Instability	See RM1A	See RM1A	See RM1A	$\mu_{\Delta} \approx 8 - 10$ $\lambda_K = 0.4$ $\lambda_Q = 0.5$ $\lambda_D = 0.5$
RM1E Flexure/ Lap Splice Slip	See RM1A or RM1B	See RM1A or RM1B	$\mu_{\Delta} \approx 3 - 4$ $\lambda_K = 0.4$ $\lambda_Q = 0.5$ $\lambda_D = 0.8$	
RM2B Flexure/Shear	$\mu_{\Delta} \leq 2$ $\lambda_K = 0.8$ $\lambda_Q = 1.0$ $\lambda_D = 1.0$	$\mu_{\Delta} \approx 2 - 3$ $\lambda_K = 0.6$ $\lambda_Q = 1.0$ $\lambda_D = 1.0$	$\mu_{\Delta} \approx 3 - 5$ $\lambda_K = 0.4$ $\lambda_Q = 0.8$ $\lambda_D = 0.9$	Heavy not used
RM2G Preemptive Shear	$\mu_{\Delta} \leq 1$ $\lambda_K = 0.9$ $\lambda_Q = 1.0$ $\lambda_D = 1.0$	$\mu_{\Delta} \approx 1 - 2$ $\lambda_K = 0.8$ $\lambda_Q = 1.0$ $\lambda_D = 1.0$	$\mu_{\Delta} \approx 1 - 2$ $\lambda_K = 0.5$ $\lambda_Q = 0.8$ $\lambda_D = 0.9$	$\mu_{\Delta} \approx 2 - 3$ $\lambda_K = 0.3$ $\lambda_Q = 0.4$ $\lambda_D = 0.5$
RM3A Flexure	$\mu_{\Delta} \leq 2$ $\lambda_K = 0.9$ $\lambda_Q = 1.0$ $\lambda_D = 1.0$	$\mu_{\Delta} \leq 3$ $\lambda_K = 0.8$ $\lambda_Q = 0.9$ $\lambda_D = 1.0$	$\mu_{\Delta} \approx 6$ $\lambda_K = 0.6$ $\lambda_Q = 0.8$ $\lambda_D = 1.0$	
RM3G Preemptive Shear (No μ values for RM3G)	$\lambda_K = 0.9$ $\lambda_Q = 1.0$ $\lambda_D = 1.0$	$\lambda_K = 0.8$ $\lambda_Q = 0.8$ $\lambda_D = 1.0$	$\lambda_K = 0.3$ $\lambda_Q = 0.5$ $\lambda_D = 0.9$	

Table 3-3 Annotated Bibliography for Reinforced Masonry

Reference(s)	Description	Comp. Type(s)	Behavior modes Addressed							
			a	b	c	d	e	f	g	
<i>EVALUATION AND DESIGN RECOMMENDATIONS</i>										
Paulay and Priestley (1992)	Overview of capacity-design principles for reinforced concrete and masonry structures. Thorough description of R/C failure modes, and, to a lesser extent, R/M failure modes.	Description of R/M component response in terms of displacement and ductility.	RM1 RM2 RM3 RM4	•	•	•	•	•	•	•
<i>OVERVIEWS OF EXPERIMENTAL TEST RESULTS</i>										
Drysdale, Hamid, and Baker (1994)	Textbook for design of masonry structures. Includes complete bibliography and selected results from experimental research.		RM1 RM2 RM4	•	•					•
<i>EXPERIMENTAL TEST RESULTS</i>										
Abrams and Paulson (1989) Abrams and Paulson (1990)	<u>2 specimens</u> 1/4-scale model		RM2	•	•	•				
Foltz and Yancy (1993)	<u>10 Specimens</u> 8" CMU 56" tall by 48" wide Axial load 200+ psi	No vertical reinforcement $\rho_v = 0.0\%$ $\rho_h = 0.024\% - 0.22\%$ Axial load increased w/ displacement. Clear improvement in displacement and crack distribution w/ increased horizontal reinforcement.	Many damage photos. No hysteresis curves. Joint reinforcement improved ultimate displacement from $\mu=1$ to $\mu=3$.	RM2						•

Table 3-3 Annotated Bibliography for Reinforced Masonry (continued)

Matsuno et al. (1987)	<u>1 grouted hollow clay specimen</u> 3-stories 3-coupled flanged walls	Limited ductility, significant strength degradation associated w/ preemptive shear failure of coupling beams.	Flexure response in long wall (RM1) Flexure/shear in short walls (RM2)	RM1 RM2 RM4	•				•	•
Merryman et al (1990) Leiva and Klingner (1991)	<u>6 fully-grouted, 2-story wall specimens</u> 2-story walls with openings 2-story pairs of wall coupled by slab only 2-story pairs of walls coupled by slab and R/M lintel	Flexural design by 1985 UBC. Shear design to ensure flexure hinging. $\rho_v = 0.22\%$ $\rho_h = 0.22\% - 0.44\%$	Stable flexural response in coupled walls, limited by compression toe spalling, fracture of reinforcement, and sliding. No significant load degradation even at end of test. One specimen inadvertently loaded to 60% of max base shear in single pulse prior to test, with no clear effect on response.	RM1	•		•			
Okada and Kumazawa (1987)	Concrete block beams 32"x90"	Similar to concrete. Rotation capacity of 1/100	Damage for lap splices limited to splice zone. More distributed without laps.	RM4	•	•				
Priestley and Elder (1982)				RM1	•	•				
Schultz, (1996)	<u>6 partially-grouted specimens</u> concrete masonry	Minimum vertical reinf $\rho_h = .05\% - .12\%$ Moderately ductile response w/ initial peak and drop to degrading plateau at approx. 75% of max.	Drift = 0.3%-1% at 75% of max strength. Behavior characterized by vertical cracks at junction of grouted and ungrouted cells. Few if any diagonal cracks except in one specimen.	RM2		•				

Table 3-3 Annotated Bibliography for Reinforced Masonry (continued)

Seible et al. (1994) Seible et al. (1995) Kingsley (1994) Kingsley et al. (1994) Kürkchübasche et al. (1994)	<u>1 fully grouted, 5-story building specimen</u> 6" hollow concrete block 5-story full-scale flanged walls coupled by topped, precast plank floor system $\rho_v = 0.23\% - 0.34\%$ $\rho_h = 0.11\% - 0.44\%$	Flexural design by 1991 <i>NEHRP Recommended Provisions for the Development of Seismic Regulations for New Buildings</i> . Shear design to ensure flexural hinging.	Ductile flexural response with some sliding to $\mu=6$ and 9, (drift = 1% and 1.5%). Distributed cracking. Significant influence of flanges and coupling slabs.	RM1	•	•					
Shing et al. (1990a) Shing et al. (1990b) Shing et al. (1991)	<u>24 fully-grouted test specimens:</u> 6 6-inch hollow clay brick 18 6-inch hollow concrete block 2 monotonic loading 22 cyclic-static loading. 4 levels of axial load	Full-scale walls, 6-ft square, loaded in single curvature. $M/VL = 1$ Uniformly distributed vertical & horizontal reinforcement. $\rho_v = 0.38\% - 0.74\%$ $\rho_h = 0.14\% - 0.26\%$	2 specimens with lap splices at base, others with continuous reinforcement. 1 specimen w/ confinement comb at wall toe. Most comprehensive tests on reinforced masonry wall components to date	RM1 RM2	•	•	•				•
Tomazevic and Zarnic (1985) Tomazevic and Lutman (1988) Tomazevic and Modena (1988) Tomazevic et al. (1993)	<u>32 wall specimens</u> Concrete block walls and complete structures Static and shaking table	$\rho_v = 0.26\% - 0.52\%$ $\rho_h = 0.00\% - 0.52\%$		RM2	•	•					•
Yamazaki et al. (1988a) Yamazaki et al. (1988b)	<u>1 fully-grouted 5-story building specimen</u> 8" hollow concrete block 5-story full-scale flanged walls coupled by cast-in-place 6" and 8" R/C floor slabs	First damage in masonry lintel beams of many different geometries.	Flexural modes degraded to shear failing modes at 0.75% building drift (1.4% first story drift).	RM1 RM2 RM4		•					•

Table 3-3 Annotated Bibliography for Reinforced Masonry (continued)

<i>EXPERIMENTAL TEST RESULTS – REPAIRED OR RETROFITTED WALLS</i>											
Innamorato (1994)	<u>3 fully-grouted test specimens</u> Designed to match Shing (1991) Preemptive shear failure Flexure failure	Tested in “original” and “repaired” condition	Repair by epoxy injection and carbon fiber overlay	RM1 RM2	•	•					•
Laursen et al. (1995)	<u>2 in-plane specimens</u> Designed to match Shing (1991) specimen preemptive shear failure. <u>2 out-of-plane specimens</u>	Tested in “original,” “repaired,” and “retrofit” con- figurations.	Repair by epoxy injection and carbon fiber overlays in horizon- tal or vertical direction to enhance ductility or strength	RM1 RM2	•						•
Weeks et al. (1994)	5-story building tested previously by Seible et al. (1994) repaired and retested.		Repair by epoxy injection and carbon fiber overlay	RM1							

¹ Behavior modes:

a Ductile Flexural Response:

b Flexure/Diagonal Shear

c Flexure/Sliding Shear

d Flexure/Out-of-Plane Wall Buckling

e Flexure/Lap-Splice Slip

f Foundation rocking of individual piers

g Preemptive Diagonal Shear Failure

3.3 Symbols for Reinforced Masonry

A_g	= Gross crosssectional area of wall	s	= Spacing of reinforcement
A_{si}	= Area of reinforcing bar i	t	= Wall thickness
A_v	= Area of shear reinforcing bar	V_e	= Expected shear strength of a reinforced masonry wall
A_{vf}	= Area of reinforcement crossing perpendicular to the sliding plane	V_m	= Portion of the expected shear strength of a wall attributed to masonry
a	= Depth of the equivalent stress block	V_s	= Portion of the expected shear strength of a wall attributed to steel
c	= Depth to the neutral axis	V_p	= Portion of the expected shear strength of a wall attributed to axial compression effects
C_m	= Compression force in the masonry	V_{se}	= Expected sliding shear strength of a masonry wall
f_{me}	= Expected compressive strength of masonry	x_i	= Location of reinforcing bar i
f_{ye}	= Expected yield strength of reinforcement	Δ_p	= Maximum inelastic displacement capacity
h_e	= Effective height of the wall (height to the resultant of the lateral force) = M/V	Δ_y	= Displacement at first yield
l_d	= Lap splice development length	ϕ_m	= Maximum inelastic curvature of a masonry section
l_p	= Effective plastic hinge length	ϕ_y	= Yield curvature of a masonry section
l_w	= Length of the wall	μ_Δ	= Displacement ductility
M/V	= Ratio of moment to shear (shear span) at a section	μ	= Coefficient of friction at the sliding plane
M_e	= Expected moment capacity of a masonry section		
P_u	= Wall axial load		

3.4 References for Reinforced Masonry

This list contains references from the reinforced masonry chapters of both FEMA 306 and 307.

- Abrams, D.P., and Paulson, T.J., 1989, "Measured Non-linear Dynamic Response of Reinforced Concrete Masonry Building Systems," *Proceedings of the Fifth Canadian Masonry Symposium*, University of British Columbia, Vancouver, B.C., Canada.
- Abrams, D.P., and Paulson, T.J., 1990, "Perceptions and Observations of Seismic Response for Reinforced Masonry Building Structures," *Proceedings of the Fifth North American Masonry Conference*, University of Illinois at Urbana-Champaign.
- Agbabian, M., Adham, S., Masri, S., and Avanesian, V., *Out-of-Plane Dynamic Testing of Concrete Masonry Walls*, U.S. Coordinated Program for Masonry Building Research, Report Nos. 3.2b-1 and 3.2b-2.
- Anderson, D.L., and Priestley, M.J.N., 1992, "In Plane Shear Strength of Masonry Walls," *Proceedings of the 6th Canadian Masonry Symposium*, Saskatoon, Saskatchewan.
- Atkinson, R.H., Amadei, B.P., Saeb, S., and Sture, S., 1989, "Response of Masonry Bed Joints in Direct Shear," *American Society of Civil Engineers Journal of the Structural Division*, Vol. 115, No. 9.
- Atkinson, R.H., and Kingsley, G.R., 1985, *A Comparison of the Behavior of Clay and Concrete Masonry in Compression*, U.S. Coordinated Program for Masonry Building Research, Report No. 1.1-1.
- Atkinson, R.H., Kingsley, G.R., Saeb, S., B. Amadei, B., and Sture, S., 1988, "A Laboratory and In-situ Study of the Shear Strength of Masonry Bed Joints," *Proceedings of the 8th International Brick/Block Masonry Conference*, Dublin.
- BIA, 1988, *Technical Notes on Brick Construction, No. 17*, Brick Institute of America, Reston, Virginia.
- Blakeley, R.W.G., Cooney, R.C., and Megget, L.M., 1975, "Seismic Shear Loading at Flexural Capacity in Cantilever Wall Structures," *Bulletin of the New Zealand National Society for Earthquake Engineering*, Vol. 8, No. 4.
- Calvi, G.M., Macchi, G., and Zanon, P., 1985, "Random Cyclic Behavior of Reinforced Masonry Under Shear Action," *Proceedings of the Seventh International Brick Masonry Conference*, Melbourne, Australia.
- Chen, S.J., Hidalgo, P.A., Mayes, R.L., and Clough, R.W., 1978, *Cyclic Loading Tests of Masonry Single Piers, Volume 2 – Height to Width Ratio of 1*, Earthquake Engineering Research Center Report No. UCB/EERC-78/28, University of California, Berkeley, California.
- Drysdale, R.G., Hamid, A.A., and Baker, L.R., 1994, *Masonry Structures, Behavior and Design*, Prentice Hall, New Jersey.
- Fattal, S.G., 1993, *Strength of Partially-Grouted Masonry Shear Walls Under Lateral Loads*, National Institute of Standards and Technology, NISTIR 5147, Gaithersburg, Maryland.
- Foltz, S., and Yancy, C.W.C., 1993, "The Influence of Horizontal Reinforcement on the Shear Performance of Concrete Masonry Walls", *Masonry: Design and Construction, Problems and Repair*, ASTM STP 1180, American Society for Testing and Materials, Philadelphia, Pennsylvania.
- Ghanem, G.M., Elmagd, S.A., Salama, A.E., and Hamid, A.A., 1993, "Effect of Axial Compression on the Behavior of Partially Reinforced Masonry Shear Walls," *Proceedings of the Sixth North American Masonry Conference*, Philadelphia, Pennsylvania.
- Hamid, A., Assis, G., and Harris, H., 1988, *Material Models for Grouted Block Masonry*, U.S. Coordinated Program for Masonry Building Research, Report No. 1.2a-1.
- Hamid, A., Abboud, B., Farah, M., Hatem, K., and Harris, H., 1989, *Response of Reinforced Block Masonry Walls to Out-of-Plane Static Loads*, U.S. Coordinated Program for Masonry Building Research, Report No. 3.2a-1.
- Hammons, M.I., Atkinson, R.H., Schuller, M.P., and Tikalsky, P.J., 1994, *Masonry Research for Limit-States Design, Construction Productivity Advancement Research (CPAR)* U.S. Army Corps of Engineers Waterways Experiment Station, Program Report CPAR-SL-94-1, Vicksburg Mississippi.
- Hanson, R.D., 1996, "The Evaluation of Reinforced Concrete Members Damaged by Earthquakes", *Earthquake Spectra*, Vol. 12, No. 3, Earthquake Engineering Research Institute.

- Hart, G.C., and Priestley, M.J.N., 1989, *Design Recommendations for Masonry Moment-Resisting Wall Frames*, UC San Diego Structural Systems Research Project Report No. 89/02.
- Hart, G.C., Priestley, M.J.N., and Seible, F., 1992, "Masonry Wall Frame Design and Performance," *The Structural Design of Tall Buildings*, John Wiley & Sons, New York.
- He, L., and Priestley, M.J.N., 1992, *Seismic Behavior of Flanged Masonry Walls*, University of California, San Diego, Department of Applied Mechanics and Engineering Sciences, Report No. SSRP-92/09.
- Hegemier, G.A., Arya, S.K., Nunn, R.O., Miller, M.E., Anvar, A., and Krishnamoorthy, G., 1978, *A Major Study of Concrete Masonry Under Seismic-Type Loading*, University of California, San Diego Report No. AMES-NSF TR-77-002.
- Hidalgo, P.A., Mayes, R.L., McNiven, H.D., and Clough, R.W., 1978, *Cyclic Loading Tests of Masonry Single Piers, Volume 1 – Height to Width Ratio of 2*, University of California, Berkeley, Earthquake Engineering Research Center Report No. UCB/EERC-78/27.
- Hidalgo, P.A., Mayes, R.L., McNiven, H.D., and Clough, R.W., 1979, *Cyclic Loading Tests of Masonry Single Piers, Volume 3 – Height to Width Ratio of 0.5*, University of California, Berkeley, Earthquake Engineering Research Center Report No. UCB/EERC-79/12.
- Hon, C.Y., and Priestley, M.J.N., 1984, *Masonry Walls and Wall Frames Under Seismic Loading*, Department of Civil Engineering, University of Canterbury, Research Report 84-15, New Zealand.
- Igarashi, A., F. Seible, and Hegemier, G.A., 1993, *Development of the Generated Sequential Displacement Procedure and the Simulated Seismic Testing of the TCCMAR 3-Story In-plane Walls*, U.S. Coordinated Program for Masonry Building Research Report No. 3.1(b)-2.
- Innamorato, D., 1994, *The Repair of Reinforced Structural Masonry Walls using a Carbon Fiber, Polymeric Matrix Composite Overlay*, M.Sc. Thesis in Structural Engineering, University of California, San Diego.
- Kariotis, J.C., Rahman, M. A., El-mustapha, A. M., 1993, "Investigation of Current Seismic Design Provisions for Reinforced Masonry Shear Walls," *The Structural Design of Tall Buildings*, Vol. 2, 163-191.
- Kingsley, G.R., 1994, *Seismic Design and Response of a Full-scale Five-Story Reinforced Masonry Research Building*, Doctoral Dissertation, University of California, San Diego, School of Structural Engineering.
- Kingsley, G.R., Noland, J.L., and Atkinson, R.H., 1987, "Nondestructive Evaluation of Masonry Structures Using Sonic and Ultrasonic Pulse Velocity Techniques," *Proceedings of the Fourth North American Masonry Conference*, University of California at Los Angeles.
- Kingsley, G.R., Seible, F., Priestley, M.J.N., and Hegemier, G.A., 1994, *The U.S.-TCCMAR Full-scale Five-Story Masonry Research Building Test, Part II: Design, Construction, and Test Results*, Structural Systems Research Project, Report No. SSRP-94/02, University of California at San Diego.
- Kubota, T., and Murakami, M., 1988, "Flexural Failure Test of Reinforced Concrete Masonry Walls -- Effect of Lap Joint of Reinforcement," *Proceedings of the Fourth Meeting of the U.S.-Japan Joint Technical Coordinating Committee on Masonry Research*, San Diego, California.
- Kubota, T., Okamoto, S., Nishitani, Y., and Kato, S., 1985, "A Study on Structural Behavior of Brick Panel Walls," *Proceedings of the Seventh International Brick Masonry Conference*, Melbourne, Australia.
- Kürkchübasche, A.G., Seible, F., and Kingsley, G.R., 1994, *The U.S.-TCCMAR Five-story Full-scale Reinforced Masonry Research Building Test: Part IV, Analytical Models*, Structural Systems Research Project, Report No. TR - 94/04, University of California at San Diego.
- Laursen, P. T., Seible, F., and Hegemier, G. A., 1995, *Seismic Retrofit and Repair of Reinforced Concrete with Carbon Overlays*, Structural Systems Research Project, Report No. TR - 95/01, University of California at San Diego.
- Leiva, G., and Klingner, R.E., 1991, *In-Plane Seismic Resistance of Two-story Concrete Masonry Shear Walls with Openings*, U.S. Coordinated Program for Masonry Building Research, Report No. 3.1(c)-2.
- Leiva, G., and Klingner, R.E., 1994, "Behavior and Design of Multi-Story Masonry Walls under In-

- plane Seismic Loading," *The Masonry Society Journal*, Vol. 13, No. 1.
- Matsumura, A., 1988, "Effectiveness of Shear Reinforcement in Fully Grouted Hollow Clay Masonry Walls," *Proceedings of the Fourth Meeting of the U.S.-Japan Joint Technical Coordinating Committee on Masonry Research*, San Diego, California.
- Matsuno, M., Yamazaki, Y., Kaminosono, T., Teshigawara, M., 1987, "Experimental and Analytical Study of the Three Story Reinforced Clay Block Specimen," *Proceedings of the Third Meeting of the U.S.-Japan Joint Technical Coordinating Committee on Masonry Research*, Tomamu, Hokkaido, Japan.
- Mayes, R.L., 1993, Unpublished study in support of the U.S. Coordinated Program for Masonry Building Research Design and Criteria Recommendations for Reinforced Masonry.
- Merryman, K.M., Leiva, G., Antrobus, N., and Klingner, 1990, *In-plane Seismic Resistance of Two-story Concrete Masonry Coupled Shear Walls*, U.S. Coordinated Program for Masonry Building Research, Report No. 3.1(c)-1.
- Modena, C., 1989, "Italian Practice in Evaluating, Strengthening, and Retrofitting Masonry Buildings," *Proceedings of the International Seminar on Evaluating, Strengthening, and Retrofitting Masonry Buildings*, University of Texas, Arlington, Texas.
- Noakowski, Piotr, 1985, *Continuous Theory for the Determination of Crack Width under the Consideration of Bond*, Beton-Und Stahlbetonbau, 7 u..
- Noland, J.L., 1990, "1990 Status Report: U.S. Coordinated Program for Masonry Building Research," *Proceedings of the Fifth North American Masonry Conference*, Urbana-Champaign, Illinois.
- Ohkubo, M., 1991, *Current Japanese System on Seismic Capacity and Retrofit Techniques for Existing Reinforced Concrete Buildings and Post-Earthquake Damage Inspection and Restoration Techniques*, University of California, San Diego Structural Systems Research Project Report No. SSRP-91/02.
- Okada, T., and Kumazawa, F., 1987, "Flexural Behavior of Reinforced Concrete Block Beams with Spirally-Reinforced Lap Splices," *Proceedings of the Third Meeting of the U.S.-Japan Joint Technical Coordinating Committee on Masonry Research*, Tomamu, Hokkaido, Japan.
- Park, R. and T. Paulay, 1975, *Reinforced Concrete Structures*, John Wiley & Sons, New York.
- Paulay T., and Priestley, M.J.N, 1992, *Seismic Design of Reinforced Concrete and Masonry Structures*, John Wiley & Sons, New York.
- Paulay, T., and Priestley, M.J.N, 1993, "Stability of Ductile Structural Walls," *ACI Structural Journal*, Vol. 90, No. 4.
- Paulay, T., Priestley, M.J.N., and Syngé, A.J., 1982, "Ductility in Earthquake Resisting Squat Shearwalls," *ACI Journal*, Vol. 79, No. 4, pp.257-269.
- Priestley, M.J.N., 1977, "Seismic Resistance of Reinforced Concrete Masonry Shear Walls with High Steel Percentages," *Bulletin of the New Zealand National Society for Earthquake Engineering*, Vol. 10, No. 1, pp.1-16.
- Priestley, M.J.N., 1986, "Flexural Strength of Rectangular Unconfined Shear Walls with Distributed Reinforcement," *The Masonry Society Journal*, Vol. 5, No. 2.
- Priestley, M.J.N., 1990, *Masonry Wall-Frame Joint Test*, Report No. 90-5, Sequad Consulting Engineers, Solana Beach, California.
- Priestley, M.J.N. and Elder, D.M., 1982, *Seismic Behavior of Slender Concrete Masonry Shear Walls*, Dept. of Civil Engineering, University of Canterbury, Christchurch, Research Report ISSN 0110-3326, New Zealand.
- Priestley M.J.N., Evison, R.J., and Carr, A.J., 1978, "Seismic Response of Structures Free to Rock on their Foundations," *Bulletin of the New Zealand National Society for Earthquake Engineering*, Vol. 11, No. 3, pp. 141-150.
- Priestley, M.J.N., and Hart, G.C., 1989, *Design Recommendations for the Period of Vibration of Masonry Wall Buildings*, Structural Systems Research Project, Report No. SSRP 89/05, University of California at San Diego.
- Priestley, M.J.N., and Hon, C.Y., 1985, "Seismic Design of Reinforced Concrete Masonry Moment-Resisting Frames," *The Masonry Society Journal*, Vol. 4., No. 1.

- Priestley, M.J.N., and Limin, He, 1990, "Seismic Response of T-Section Masonry Shear Walls," *The Masonry Society Journal*, Vol. 9, No. 1.
- Priestley, M.J.N., Verma, R., and Xiao, Y., 1994, "Seismic Shear Strength of Reinforced Concrete Columns," *ASCE Journal of Structural Engineering*, Vol. 120, No. 8.
- Sassi, H., and Ranous, R., 1996, "Shear Failure in Reinforced Concrete Walls," *From Experience*, Structural Engineers Association of Southern California, Whittier, California.
- Schuller, M.P., Atkinson, R.H., and Borgsmiller, J.T., 1994, "Injection Grouting for Repair and Retrofit of Unreinforced Masonry," *Proceedings of the 10th International Brick and Block Masonry Conference*, Calgary, Alberta, Canada.
- Schultz, A.E., 1996 "Seismic Resistance of Partially-Grouted Masonry Shear Walls," *Worldwide Advances in Structural Concrete and Masonry*, A.E. Schultz and S.L. McCabe, Eds., American Society of Civil Engineers, New York.
- Seible, F., Hegemier, G.A., Igarashi, A., and Kingsley, G.R., 1994a, "Simulated Seismic-Load Tests on Full-Scale Five-Story Masonry Building," *ASCE Journal of Structural Engineering*, Vol. 120, No. 3.
- Seible, F., Kingsley, G.R., and Kürkchübasche, A.G., 1995, "Deformation and Force Capacity Assessment Issues in Structural Wall Buildings," *Recent Developments in Lateral Force Transfer in Buildings – Thomas Paulay Symposium*, ACI SP-157.
- Seible, F., Okada, T., Yamazaki, Y., and Teshigawara, M., 1987, "The Japanese 5-story Full Scale Reinforced Concrete Masonry Test — Design and Construction of the Test Specimen," *The Masonry Society Journal*, Vol. 6, No. 2.
- Seible, F., Priestley, M.J.N., Kingsley, G.R., and Kürkchübasche, A.G., 1991, *Flexural coupling of Topped Hollow Core Plank Floor Systems in Shear Wall Structures*, Structural Systems Research Project, Report No. SSRP-91/10, University of California at San Diego.
- Seible, F., Priestley, M.J.N., Kingsley, G.R., and Kürkchübasche, A.G., 1994b, "Seismic Response of a Five-story Full-scale RM Research Building", *ASCE Journal of Structural Engineering*, Vol. 120, No. 3.
- Seible, F., Yamazaki, Y., Kaminosono, T., and Teshigawara, M., 1987, "The Japanese 5-story Full Scale Reinforced Concrete Masonry Test -- Loading and Instrumentation of the Test Building," *The Masonry Society Journal*, Vol. 6, No. 2.
- Shing, P.B., Brunner, J., and Lofti, H.R., 1993, "Analysis of Shear Strength of Reinforced Masonry Walls," *Proceedings of the Sixth North American Masonry Conference*, Philadelphia, Pennsylvania.
- Shing, P.B., Noland, J.L., Spaeh, H.P., Klamerus, E.W., and Schuller, M.P., 1991, *Response of Single Story Reinforced Masonry Shear Walls to In-plane Lateral Loads*, TCCMAR Report No. 3.1(a)-2.
- Shing, P., Schuller, M., Hoskere, V., and Carter, E., 1990a, "Flexural and Shear Response of Reinforced Masonry Walls," *ACI Structural Journal*, Vol. 87, No. 6.
- Shing, P., Schuller, M., and Hoskere, V., 1990b, "In-plane Resistance of Reinforced Masonry Shear Walls," *Proceedings of ASCE Journal of the Structural Division*, Vol 116, No. 3.
- Soric, Z. and Tulin, L.E., 1987, "Bond in Reinforced Concrete Masonry," *Proceedings Fourth North American Masonry Conference*, Los Angeles, California.
- Thurston, S., and Hutchinson, D., 1982, "Reinforced Masonry Shear Walls Cyclic Load Tests in Contraflexure," *Bulletin of the New Zealand Society for Earthquake Engineering*, Vol. 15, No. 1.
- TMS, 1994, *Performance of Masonry Structures in the Northridge, California Earthquake of January 17, 1994*, Richard E. Klingner, ed., The Masonry Society.
- Tomazevic, M., and Lutman, M., 1988, "Design of Reinforced Masonry Walls for Seismic Actions," *Brick and Block Masonry*, J.W. DeCourcy, Ed., Elsevier Applied Science, London.
- Tomazevic, M., Lutman, M., and Velechovsky, T., 1993, "The Influence of Lateral Load Time-history on the Behavior of Reinforced-Masonry Walls Failing in Shear," *Proceedings of the Sixth North American Masonry Conference*, Philadelphia, Pennsylvania.
- Tomazevic, M., and Modena, C., 1988, "Seismic Behavior of Mixed, Reinforced Concrete, Reinforced Masonry Structural Systems," *Brick and Block Masonry*, J.W. DeCourcy, Ed., Elsevier Applied Science, London.

- Tomazevic, M., and Zarnic, R., 1985, "The Effect of Horizontal Reinforcement on the Strength and Ductility of Masonry Walls at Shear Failure," *Proceedings of the Seventh International Brick Masonry Conference*, Melbourne, Australia.
- Vulcano A., and Bertero, V.V., 1987, *Analytical Models for Predicting the Lateral Response of RC Shear Walls*, University of California, UCB/EERC Report No. 87-19, Berkeley, California.
- Weeks, J., Seible, F., Hegemier, G., and Priestley, M.J.N., 1994, *The U.S.-TCCMAR Full-scale Five-story Masonry Research Building Test, Part V - Repair and Retest*, University of California Structural Systems Research Project Report No. SSRP-94/05.
- Yamamoto, M., and Kaminosono, T., 1986, "Behavior of Reinforced Masonry Walls with Boundary Beams," *Proceedings of the Second Meeting of the Joint Technical Coordinating Committee on Masonry Research*, Keystone, Colorado.
- Yamazaki, Y., F. Seible, H., Mizuno, H., Kaminosono, T., Teshigawara, M., 1988b, "The Japanese 5-story Full Scale Reinforced Concrete Masonry Test -- Forced Vibration and Cyclic Load Test Results," *The Masonry Society Journal*, Vol. 7, No. 1.
- Yamazaki, Y., Kaminosono, T., Teshigawara, M., and Seible, F., 1988a, "The Japanese 5-story Full Scale Reinforced Concrete Masonry Test -- Pseudo Dynamic and Ultimate Load Test Results," *The Masonry Society Journal*, Vol. 7, No. 2.
- Young, J.M., and Brown, R.H., 1988, *Compressive Stress Distribution of Grouted Hollow Clay Masonry Under Stain Gradient*, U.S. Coordinated Program for Masonry Building Research, Report No. 1.2b-1.

4. Unreinforced Masonry

4.1 Commentary and Discussion

4.1.1 Hysteretic Behavior of URM Walls Subjected to In-Plane Demands

A search of the available literature was performed to identify experimental and analytical research relevant to unreinforced masonry bearing-wall damage. Because URM buildings have performed poorly in past earthquakes, there is an extensive amount of anecdotal information in earthquake reconnaissance reports; there have also been several studies that took a more statistical approach and collected damage information in a consistent format for a comprehensive population of buildings. These studies help to confirm the prevalence of the damage types listed in FEMA 306, and they help to indicate the intensity of shaking required to produce certain damage types.

The proposed methodology for this document, however, requires moving beyond anecdotal and qualitative discussions of component damage and instead obtaining quantitative information on force/displacement relationships for various components. The focus of research on URM buildings has been on the in-plane behavior of walls. Most of the relevant research has been done in China, the former Yugoslavia, Italy, and the United States. This stands in contrast to the elements in URM buildings that respond to ground shaking with essentially brittle or force-controlled behavior: parapets, appendages, wall-diaphragm ties, out-of-plane wall capacity, and, possibly, archaic diaphragms such as brick arch floors. While there has been very little research on most of these elements, it is less important because performance of these elements is not deformation-controlled.

Unfortunately, research on in-plane wall behavior is rarely consistent—materials, experimental techniques, modes of reporting, and identified inelastic mechanisms all vary widely. Placing the research in a format consistent with FEMA 273 and this project’s emphasis on components, damage types, hysteresis curves, nonlinear force/displacement relationships, and performance levels is difficult. Almost no experimental tests have been done on damaged URM walls; typically, tests were done on undamaged walls and stopped. In some cases, the damaged wall was repaired and retested. Most of the research does not provide simple

predictive equations for strength and stiffness (particularly post-elastic stiffness); when analysis has been done, it has usually used fairly sophisticated finite element modelling techniques.

Hysteresis loops for in-plane wall behavior are shown on the following pages, Sections 4.1.1.1 to 4.1.1.6, organized by behavior mode. Research shows that the governing behavior mode depends upon a number of variables including material properties, aspect ratio, and axial stress. To aid in comparing the curves, basic data given in the research report are provided, including the average compressive strength of prism tests and the masonry unit, the pier aspect ratio, the nominal axial stress, and whether the specimen was free to rotate at the top (cantilever condition) or was fixed (double-curvature condition). For many of the specimens, independent calculations have been carried out for this document to allow comparison between the evaluation procedure predictions in Section 7.3 of FEMA 306 and the actual experimental results. Predictions using FEMA 273 are also noted. In several cases, engineering judgment has been exercised to make these calculations, since not all of the necessary information is available. Material properties that were assumed for the purposes of the calculation are identified. It is expected that predicted results could vary significantly if different assumptions are made. In addition, the experimental research in URM piers is difficult to synthesize for several reasons:

- Some researchers do not report a measure of bed-joint sliding-shear strength. Others use triplet tests rather than in-place push tests to measure bed-joint sliding capacity. Comparisons between triplet tests and in-place push tests are not well established. Several different assumptions were investigated for this project, and the approach shown below was found to correlate best with the data.
- Descriptions of cracking can be inconsistent and overly vague. Diagonal cracking, for example, is often reported, but it can be unclear if the report refers to diagonal tension cracking, toe crushing with diagonally-oriented cracks, or stair-stepped bed-joint sliding.
- Observed damage is often not linked to points on the force/displacement hysteresis loops.
- Final drift values are not always given; when they are, it is often unclear why the test was stopped and

whether additional stable deformation capacity remained.

- In many tests, the applied axial load varies significantly from the desired nominal value at different times during the test. Thus, lateral capacities can be affected.

- There is no direct test for f'_{dt1} . FEMA 273 equations use v_{me} for f'_{dt} . This gives the value for V_{dt1} . As an additional check, 1/30th of the value of flat-wise compressive strength of the masonry units was also used; this results in the value for V_{dt2} .

4.1.1.1 Rocking

Reference: Anthoine et al. (1995)

Specimen: High wall, first run

Material: Brick

Loading: Reversed quasistatic cyclic

Provided Information:

Prism $f'_m=6.2$ MPa, brick $f'_m=16$ MPa

$L/h_{eff}=1m/2m=0.5$

Nominal $f_a=0.60$ MPa

Fixed-fixed end conditions

Assumed Values:

$v_{me1}=(0.75/1.5)*(0.23+0.57f_a)$ MPa

$v_{me2}=(0.75/1.5)*(0.57f_a)$ MPa

Calculated Values (kN):

$V_r=68$ $V_{tc}=65$

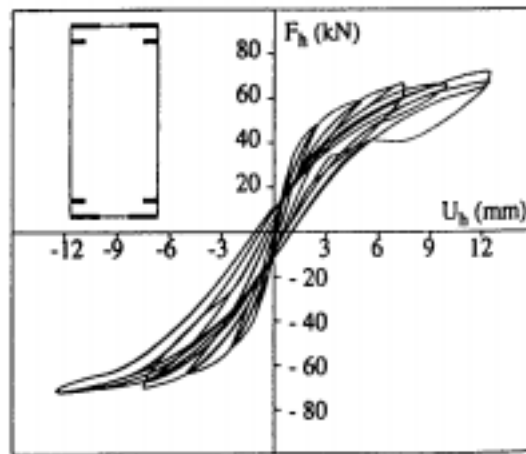
$V_{bjs1}=73$ $V_{bjs2}=43$

$V_{dt1}=85$ $V_{dt2}=130$

FEMA 273 Predicted Mode: Toe crushing

ATC-43 Predicted Behavior: Rocking at 68 kN with drift “d”=0.8%

Actual Behavior: Rocking at 72 kN with test stopped at 0.6%. Slight cracks at mid-pier. Axial load increased for second run (see below).



Hysteretic response of the high wall, first run.

Reference: Anthoine et al. (1995)

Specimen: High wall, second run

Material: Brick

Loading: Reversed quasistatic cyclic

Provided Information:

Prism $f'_m=6.2$ MPa, brick $f'_m=16$ MPa

$L/h_{eff}=1m/2m=0.5$

Nominal $f_a=0.80$ MPa

Fixed-fixed end conditions

Assumed Values:

$v_{me1}=(0.75/1.5)*(0.23+0.57f_a)$ MPa

$v_{me2}=(0.75/1.5)*(0.57f_a)$ MPa

Calculated Values (kN):

$V_r=90$ $V_{tc}=82$

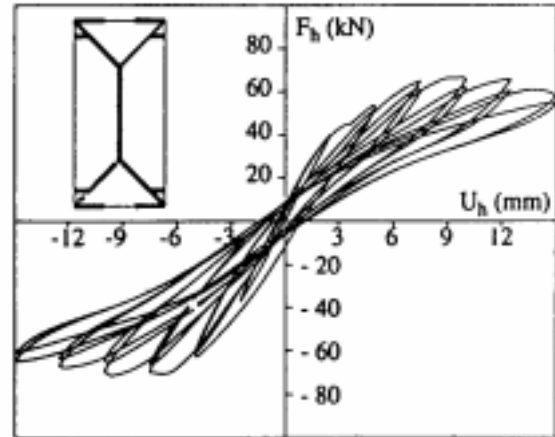
$V_{bjs1}=85$ $V_{bjs2}=58$

$V_{dt1}=104$ $V_{dt2}=141$

FEMA 273 Predicted Mode: Toe crushing

ATC-43 Predicted Behavior: Same as FEMA 273

Actual Behavior: Rocking, then stair-stepped bed-joint sliding at a drift of 0.75%



Hysteretic response of the high wall, second run.

Reference: Magenes & Calvi (1995)

Specimen: 3, runs 7-12

Material: Brick

Loading: Shaketable

Provided Information:

Prism $f'_m=8.6$ MPa, brick $f'_m=18.2$ MPa

$L/h_{eff}=1m/2m=0.5$

Nominal $f_a=0.63$ MPa

Fixed-fixed end conditions

Assumed Values:

$v_{me1}=(0.75/1.5)*(1.15+0.57f_a)$ MPa

$v_{me2}=(0.75/1.5)*(0.57f_a)$ MPa

Calculated Values (kN):

$V_r=71$ $V_{tc}=70$

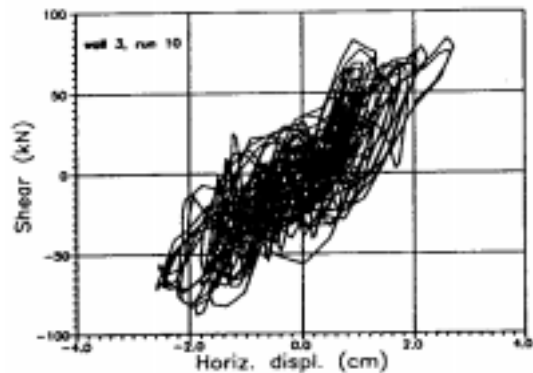
$V_{bjs1}=189$ $V_{bjs2}=45$

$V_{dt1}=171$ $V_{dt2}=145$

FEMA 273 Predicted Mode: Toe crushing

ATC-43 Predicted Behavior: Rocking at 71 kN with drift "d" = 0.8%.

Actual Behavior: Rocking at 87 kN with drift of 1.3% in run 10.



Shear-displacement curve characterized by rocking (wall 3, run 10). The figure does not show final runs 11 and 12.

Reference: Costley & Abrams (1996)

Specimen: S1 Door Wall

Material: Brick

Loading: 3/8th-scale building on shaketable

Provided Information:

Prism $f'_m=1960$ psi, brick $f'_m=6730$ psi

Fixed-fixed end conditions

Assumed Values:

$v_{me1}=(0.75/1.5)*(0.75*361+f_a)$ psi

$v_{me2}=(0.75/1.5)*(f_a)$ psi

Outer Piers:

$L/h_{eff}=1.44\text{ft}/2.67\text{ft}=0.54$

Nominal $f_a=33$ psi

Calculated Values (kips):

$V_r=1.0$ $V_{tc}=1.1$

$V_{bjs1}=9.7$ $V_{bjs2}=1.1$

$V_{dt1}=7.2$ $V_{dt2}=10.3$

Inner Pier:

$L/h_{eff}=0.79\text{ft}/1.50\text{ft}=0.53$

Nominal $f_a=40$ psi

Calculated Values (kips):

$V_r=2.7$ $V_{tc}=2.9$

$V_{bjs1}=15.3$ $V_{bjs2}=1.8$

$V_{dt1}=14.3$ $V_{dt2}=20.4$

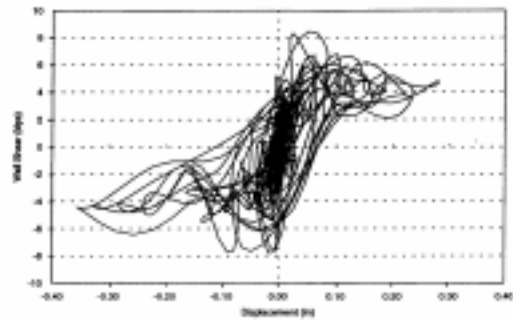
FEMA 273 Predicted Behavior of Wall Line: Rocking at 4.7 kips with inner-pier drift “d”=0.5%

ATC-43 Predicted Behavior of Wall Line: Same as FEMA 273

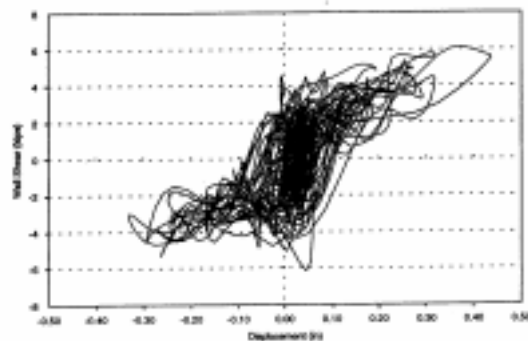
Actual Behavior of the Wall Line:

Run 14: Rocking up to 8 kips, then stable at 4-6 kips.
Drift up to 1.1%.

Run 15: Rocking at 4-6 kips with drift up to 1.3%



Door-wall shear vs. first-level door-wall displacement from Test Run 14



Door-wall shear vs. first-level door-wall displacement from Test Run 15

Reference: Costley & Abrams (1996)

Specimen: S2 Door Wall

Material: Brick

Loading: 3/8th-scale building on shaketable

Provided Information:

Prism $f'_m=1960$ psi, brick $f'_m=6730$ psi

Fixed-fixed end conditions

Assumed Values:

$v_{me1}=(0.75/1.5)*(0.75*361+f_a)$ psi

$v_{me2}=(0.75/1.5)*(f_a)$ psi

Outer Piers:

$L/h_{eff}=0.79\text{ft}/2.67\text{ft}=0.30$

Nominal $f_a=40$ psi

Calculated Values (kips):

$V_r=0.4$ $V_{tc}=0.4$

$V_{bjs1}=5.5$ $V_{bjs2}=0.7$

$V_{dt1}=4.1$ $V_{dt2}=5.7$

Inner Piers:

$L/h_{eff}=1.12\text{ft}/2.67\text{ft}=0.42$

Nominal $f_a=48$ psi

Calculated Values (kips):

$V_r=0.9$ $V_{tc}=1.0$

$V_{bjs1}=7.9$ $V_{bjs2}=1.2$

$V_{dt1}=6.1$ $V_{dt2}=8.2$

FEMA 273 Predicted Behavior of Wall Line: Rocking at 2.6 kips with inner-pier drift “d”=1.0%

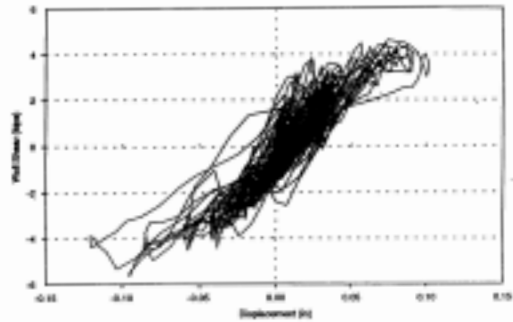
ATC-43 Predicted Behavior of Wall Line: Same as FEMA 273

Actual Behavior of the Wall Line:

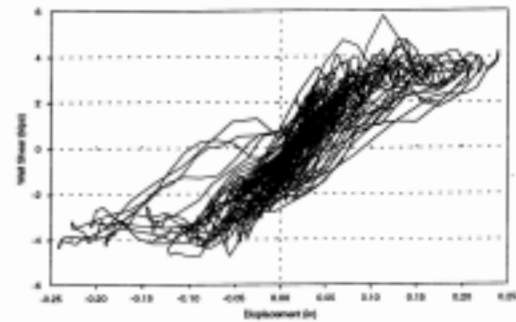
Run 22: Rocking at 4 kips, up to a 0.3% drift

Run 23: Rocking at 4 kips, up to a 0.8% drift

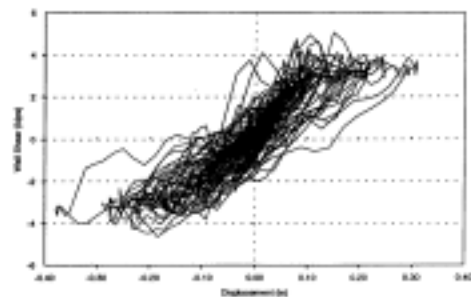
Run 24: Rocking at 4 kips, up to a 1.1% drift



Door-wall shear vs. first-level door-wall displacement from Test Run 22



Door-wall shear vs. first-level door-wall displacement from Test Run 23



Door-wall shear vs. first-level door-wall displacement from Test Run 24

4.1.1.2 Bed-joint Sliding

Reference: Magenes & Calvi (1992)

Specimen: MI4

Material: Brick

Loading: Reversed quasistatic cyclic

Provided Information:

Prism $f'_m=7.9$ MPa, brick $f'_m=19.7$ MPa

$L/h_{eff}=1.5m/3m = 0.5$

Nominal $f_a = 0.69$ MPa

Fixed-fixed end conditions

Assumed Values:

$v_{me1}=(0.75/1.5)*(0.206+0.813f_a)$ MPa

$v_{me2}=(0.75/1.5)*(0.813f_a)$ MPa

Calculated Values (kN):

$V_r=177$ $V_{tc}=172$

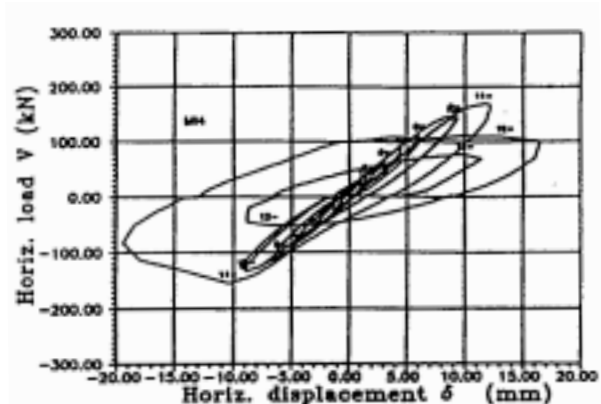
$V_{bjs1}=219$ $V_{bjs2}=160$

$V_{dt1}=245$ $V_{dt2}=360$

FEMA 273 Predicted Behavior: Toe crushing at 172 kN

ATC-43 Predicted Behavior: Rocking at 177kN with drift "d" = 0.8%

Actual Behavior: Stair-stepped bed-joint sliding at 153 kN with a final drift of 0.6%



Specimen MI4

Reference: Abrams & Shah (1992)

Specimen: W1

Material: Brick

Loading: Reversed quasistatic cyclic

Provided Information:

Prism $f'_m=911$ psi, brick $f'_m=3480$ psi

$L/h_{eff}=12ft/6ft = 2$

Nominal $f_a = 75$ psi

Cantilever conditions

Assumed Values:

$v_{me1}=(0.75/1.5)*(0.75*100+f_a)$ psi

$v_{me2}=(0.75/1.5)*(f_a)$ psi

Calculated Values (kips):

$V_r=76$ $V_{tc}=74$

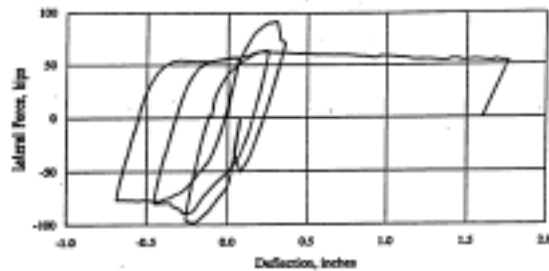
$V_{bjs1}=84$ $V_{bjs2}=42$

$V_{dt1}=149$ $V_{dt2}=167$

FEMA 273 Predicted Behavior: Toe crushing at 74 kips

ATC-43 Predicted Behavior: Flexural cracking/toe crushing/bed-joint sliding with a peak load of 74 kips with "d" drift of 0.4%

Actual Behavior: Bed-joint sliding at 92 kips with test stopped at a drift of 2.4%.



Test Wall W1

Reference: Magenes & Calvi (1995)

Specimen: 5

Material: Brick

Loading: Shaketable

Provided Information:

Prism $f'_m=6.2$ MPa, brick $f'_m=16$ MPa

$L/h_{eff}=1\text{m}/1.35\text{m} = 0.74$

Nominal $f_a = 0.63$ MPa

Fixed-fixed end conditions

Assumed Values:

$v_{me1}=(0.75/1.5)*(0.23+0.57f_a)$ MPa

$v_{me2}=(0.75/1.5)*(0.57f_a)$ MPa

Calculated Values (kN):

$V_r=105$ $V_{tc}=102$

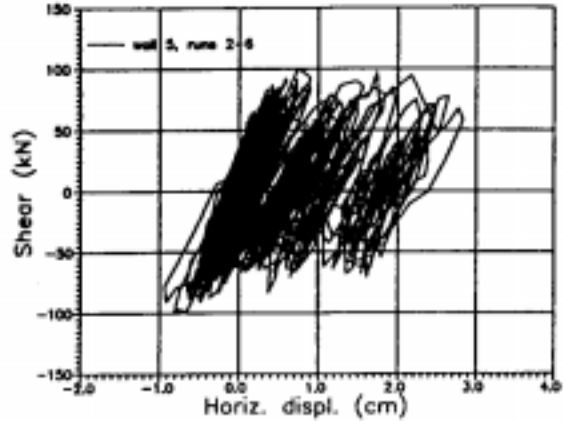
$V_{bjs1}=74$ $V_{bjs2}=45$

$V_{dt1}=97$ $V_{dt2}=160$

FEMA 273 Predicted Behavior: Bed-joint sliding at 74 kN with “d” drift of 0.4%

ATC-43 Predicted Behavior: Same as FEMA 273

Actual Behavior: Flexural cracking then horizontal and stepped bed-joint sliding with peak load of 114 kN



Shear-displacement curve characterized by rocking and sliding (wall 5, runs 2-6). The figure does not show final run 7.

Reference: Magenes & Calvi (1992)

Specimen: MI2

Material: Brick

Loading: Reversed quasistatic cyclic

Provided Information:

Prism $f'_m=7.9$ MPa, brick $f'_m=19.7$ MPa

$L/h_{eff}=1.5\text{m}/2\text{m} = 0.74$

Nominal $f_a = 0.67$ MPa

Fixed-fixed end conditions

Assumed Values:

$v_{me1}=(0.75/1.5)*(0.206+0.813f_a)$ MPa

$v_{me2}=(0.75/1.5)*(0.813f_a)$ MPa

Calculated Values (kN):

$V_r=257$ $V_{tc}=251$

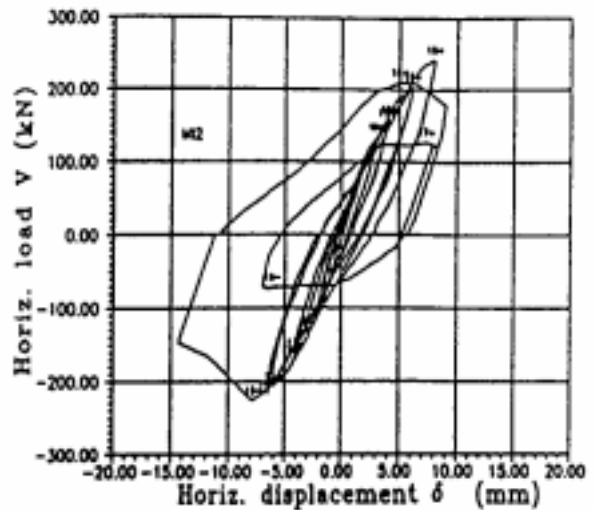
$V_{bjs1}=213$ $V_{bjs2}=155$

$V_{dt1}=267$ $V_{dt2}=399$

FEMA 273 Predicted Behavior: Bed-joint sliding at 213 kN with “d” drift of 0.4%.

ATC-43 Predicted Behavior: Same as FEMA 273

Actual Behavior: Horizontal bed-joint sliding at top course, then stair-stepped bed-joint sliding with a peak load of 227 kN and drift of 0.7%



Specimen MI2

4.1.1.3 Rocking/Toe Crushing

Reference: Abrams & Shah (1992)

Specimen: W3

Material: Brick

Loading: Reversed quasistatic cyclic

Provided Information:

Prism $f'_m = 911$ psi, brick $f'_m = 3480$ psi

$L/h_{eff} = 6\text{ft}/6\text{ft} = 1.0$

Nominal $f_a = 50$ psi

Cantilever conditions

Assumed Values:

$v_{me1} = (0.75/1.5) * (0.75 * 100 + f_a)$ psi

$v_{me2} = (0.75/1.5) * (f_a)$ psi

Calculated Values (kips):

$V_r = 12.6$ $V_{tc} = 12.9$

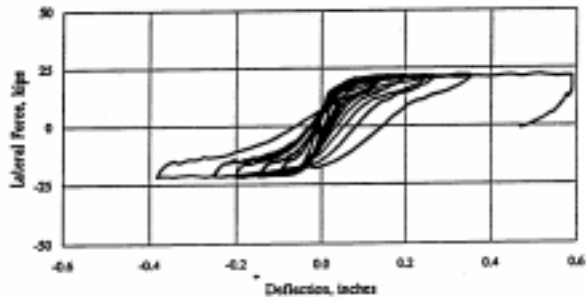
$V_{bjs1} = 35$ $V_{bjs2} = 14$

$V_{dt1} = 69$ $V_{dt2} = 78$

FEMA 273 Predicted Behavior: Rocking at 12.6 kips with drift “d”=0.4%

ATC-43 Predicted Behavior: Same as FEMA 273

Actual Behavior: Rocking at 20 kips then toe crushing at drift of 0.8%



Test Wall W3: Measured relation between lateral force and deflection.

4.1.1.4 Flexural Cracking/Toe Crushing/Bed-Joint Sliding

Reference: Manzouri et al. (1995)

Specimen: W1

Material: Brick

Loading: Reversed quasistatic cyclic

Provided Information:

Prism $f'_m = 2000$ psi, brick $f'_m = 3140$ psi

$L/h_{eff} = 8.5\text{ft}/5\text{ft} = 1.7$

Nominal $f_a = 150$ psi

Cantilever conditions

Assumed Values:

$v_{me1} = (0.75/1.5) * (0.75 * 85 + f_a)$ psi

$v_{me2} = (0.75/1.5) * (f_a)$ psi

Calculated Values (kips):

$V_r = 152$ $V_{tc} = 151$

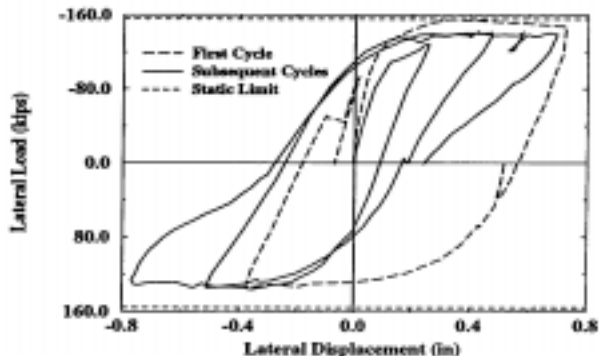
$V_{bjs1} = 156$ $V_{bjs2} = 99$

$V_{dt1} = 235$ $V_{dt2} = 172$

FEMA 273 Predicted Behavior: Toe crushing at 151 kips.

ATC-43 Predicted Behavior: Flexural cracking/toe crushing/bed-joint sliding with a 151 kip peak load, 99 kip load for “c” and a “d” drift of 0.4%.

Actual Behavior: Flexural cracking at 88 kips, toe crushing then bed-joint sliding at 156 kips, with a final drift of 1.3%



Specimen W1

Reference: Manzouri et al. (1995)

Specimen: W2

Material: Brick

Loading: Reversed quasistatic cyclic

Provided Information:

Prism $f'_m = 2200$ psi, brick $f'_m = 3140$ psi

$L/h_{eff} = 8.5\text{ft}/5\text{ft} = 1.7$

Nominal $f_a = 55$ psi

Cantilever conditions

Assumed Values:

$v_{me1} = (0.75/1.5) * (0.75 * 85 + f_a)$ psi

$v_{me2} = (0.75/1.5) * (f_a)$ psi

Calculated Values (kips):

$V_r = 56$ $V_{tc} = 60$

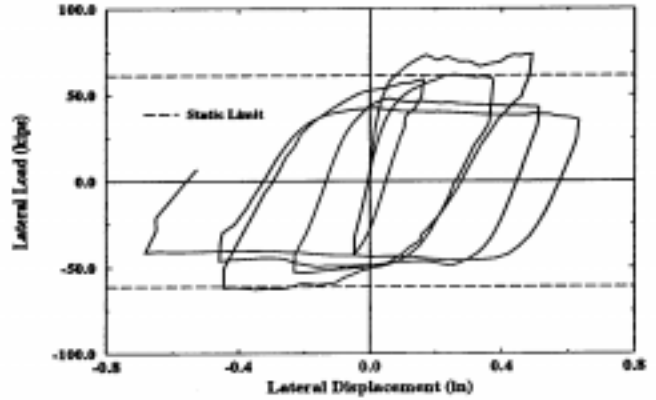
$V_{bjs1} = 93$ $V_{bjs2} = 36$

$V_{dt1} = 124$ $V_{dt2} = 171$

FEMA 273 Predicted Behavior: Rocking at 56 kips.

ATC-43 Predicted Behavior: Flexural cracking/toe crushing at 60 kips.

Actual Behavior: Flexural cracking at 31 kips, toe crushing at 68 kips, diagonal cracking at 62 kips, then bed-joint sliding at 52 kips and below, with a final drift of 1.2%



Specimen W2

Reference: Manzouri et al. (1995)

Specimen: W3

Material: Brick

Loading: Reversed quasistatic cyclic

Provided Information:

Prism $f'_m = 2600$ psi, brick $f'_m = 3140$ psi

$L/h_{eff} = 8.5\text{ft}/5\text{ft} = 1.7$

Nominal $f_a = 85$ psi

Cantilever conditions

Assumed Values:

$v_{me1} = (0.75/1.5) * (0.75 * 85 + f_a)$ psi

$v_{me2} = (0.75/1.5) * (f_a)$ psi

Calculated Values (kips):

$V_r = 86$ $V_{tc} = 91$

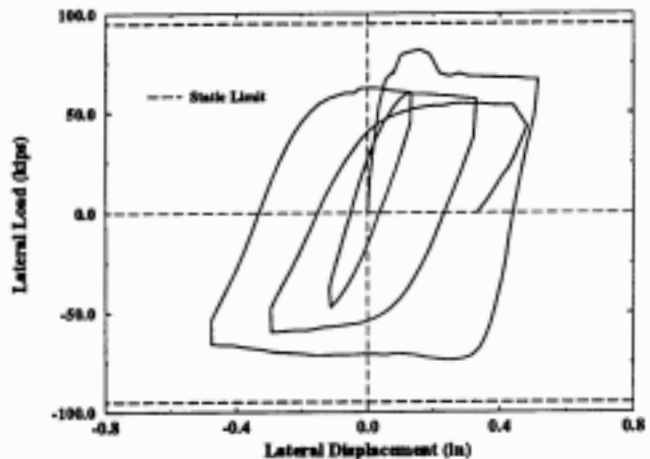
$V_{bjs1} = 113$ $V_{bjs2} = 56$

$V_{dt1} = 159$ $V_{dt2} = 187$

FEMA 273 Predicted Behavior: Rocking at 86 kips.

ATC-43 Predicted Behavior: Flexural cracking/toe crushing/bed-joint sliding with a 91 kip peak load, 56 kip load for “c” and a “d” drift of 0.4%.

Actual Behavior: Flexural cracking at 55 kips, toe crushing at 80 kips, then bed-joint sliding at 80 kips, reducing to 56-62 kips, with some final toe crushing up to final drift of 0.8%



Specimen W3

4.1.1.5 Flexural Cracking/Diagonal Tension

Reference: Anthoine et al. (1995)

Specimen: Low Wall

Material: Brick

Loading: Reversed quasistatic cyclic

Provided Information:

Prism $f'_m=6.2$ MPa, brick $f'_m=16$ MPa

$L/h_{eff}=1\text{m}/1.35\text{m}=0.74$

Nominal $f_a=0.60$ MPa

Fixed-fixed end conditions

Assumed Values:

$v_{me1}=(0.75/1.5)*(0.23+0.57f_a)$ MPa

$v_{me2}=(0.75/1.5)*(0.57f_a)$ MPa

Calculated Values (kN):

$V_r=100$ $V_{ic}=96$

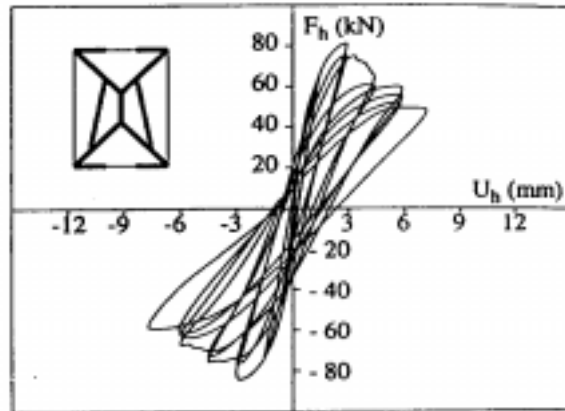
$V_{bjs1}=73$ $V_{bjs2}=43$

$V_{dt1}=94$ $V_{dt2}=144$

FEMA 273 Predicted Behavior: Bed-joint sliding at 73 kips with “d” drift of 0.4%

ATC-43 Predicted Behavior: Same as FEMA 273

Actual Behavior: Flexural cracking then diagonal tension cracking with a peak load of 84 kN and a final drift of 0.5%



Hysteretic response of the low wall.

Reference: Magenes & Calvi (1992)

Specimen: MI3

Material: Brick

Loading: Reversed quasistatic cyclic

Provided Information:

Prism $f'_m=7.9$ MPa, brick $f'_m=19.7$ MPa

$L/h_{eff}=1.5\text{m}/3\text{m}=0.5$

Nominal $f_a=1.245$ MPa

Fixed-fixed end conditions

Assumed Values:

$v_{me1}=(0.75/1.5)*(0.206+0.813f_a)$ MPa

$v_{me2}=(0.75/1.5)*(0.813f_a)$ MPa

Calculated Values (kN):

$V_r=319$ $V_{ic}=275$

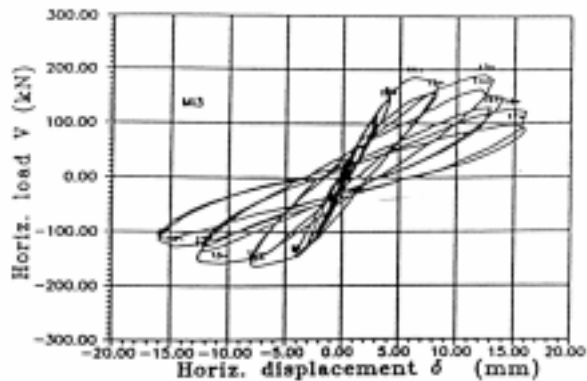
$V_{bjs1}=347$ $V_{bjs2}=288$

$V_{dt1}=406$ $V_{dt2}=427$

FEMA 273 Predicted Behavior: Toe crushing

ATC-43 Predicted Behavior: Flexural cracking/diagonal tension at 275 kN

Actual Behavior: Flexural cracking then diagonal tension cracking with a peak load of 185 kN and a final drift of 0.5%



Specimen MI3

Reference: Magenes & Calvi (1995)

Specimen: 8

Material: Brick

Provided Information:

Prism $f'_m=6.2$ MPa, brick $f'_m=16$ MPa

$L/h_{eff}=1\text{m}/2\text{m} = 0.5$

Nominal $f_a= 1.11$ MPa

Fixed-fixed end conditions

Assumed Values:

$v_{me1}=(0.75/1.5)*(0.23+0.57f_a)$ MPa

$v_{me2}=(0.75/1.5)*(0.57f_a)$ MPa

Calculated Values (kN):

$V_r=125$ $V_{tc}=109$

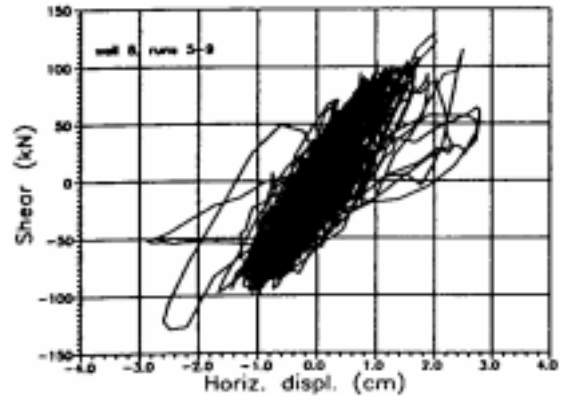
$V_{bjs1}=108$ $V_{bjs2}=79$

$V_{dt1}=137$ $V_{dt2}=171$

FEMA 273 Predicted Behavior: Bed-joint sliding or toe crushing.

ATC-43 Predicted Behavior: Bed-joint sliding or flexural cracking/diagonal tension at 108-109 kN

Actual Behavior: Flexural cracking then diagonal tension cracking with a peak load of 129 kN and a final drift of 0.8-1.3%



Brittle collapse due to diagonal cracking (wall 8, runs 5-9)

Reference: Magenes & Calvi (1992)

Specimen: M11

Material: Brick

Loading: Reversed quasistatic cyclic

Provided Information:

Prism $f'_m=7.9$ MPa, brick $f'_m=19.7$ MPa

$L/h_{eff}=1.5\text{m}/2\text{m}= 0.75$

Nominal $f_a= 1.123$ MPa

Fixed-fixed end conditions

Assumed Values:

$v_{me1}=(0.75/1.5)*(0.206+0.813f_a)$ MPa

$v_{me2}=(0.75/1.5)*(0.813f_a)$ MPa

Calculated Values (kN):

$V_r=432$ $V_{tc}=383$

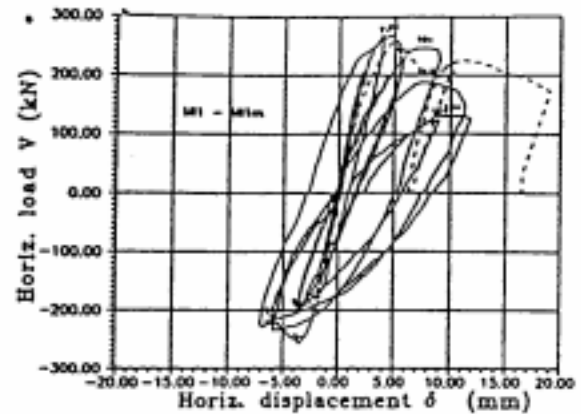
$V_{bjs1}=319$ $V_{bjs2}=260$

$V_{dt1}=415$ $V_{dt2}=462$

FEMA 273 Predicted Behavior: Bed-joint sliding at 319 kN with drift “d”=0.4%

ATC-43 Predicted Behavior of Wall Line: Same as FEMA 273

Actual Behavior: Flexural cracking then diagonal tension at 259 kN, with maximum drift of 0.6%



Test on wall M11 and M11m (dashed line); h = 2m.

4.1.1.6 Flexural Cracking/Toe Crushing

Reference: Abrams & Shah (1992)

Specimen: W2

Material: Brick

Loading: Reversed quasistatic cyclic

Provided Information:

Prism $f'_m = 911$ psi, brick $f'_m = 3480$ psi

$L/h_{eff} = 9\text{ft} / 6\text{ft} = 1.5$

Nominal $f_a = 50$ psi

Cantilever conditions

Assumed Values:

$v_{me1} = (0.75/1.5) * (0.75 * 100 + f_a)$ psi

$v_{me2} = (0.75/1.5) * (f_a)$ psi

Calculated Values (kips):

$V_r = 28$ $V_{tc} = 29$

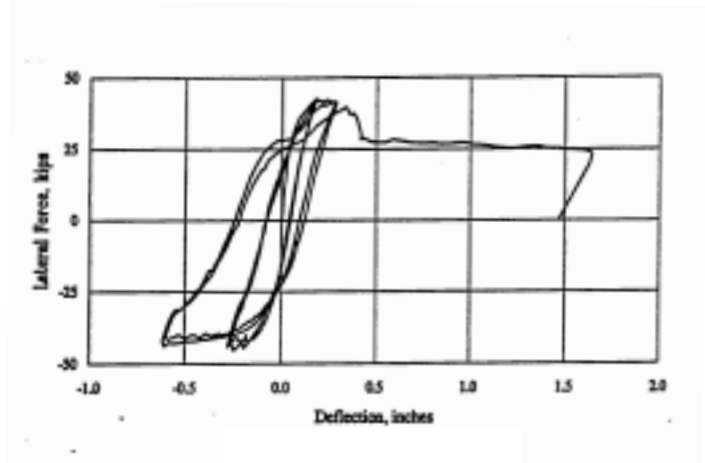
$V_{bjs1} = 53$ $V_{bjs2} = 21$

$V_{dt1} = 155$ $V_{dt2} = 175$

FEMA 273 Predicted Behavior: Rocking at 28 kips with drift “d”=0.3%

ATC-43 Predicted Behavior: Flexural cracking/toe crushing at 29 kips

Actual Behavior: Flexural cracking/toe crushing, with a maximum capacity of 43-45 kips.



Test Wall W2

Reference: Epperson and Abrams (1989)

Specimen: E1

Material: Brick

Loading: Monotonic

Provided Information:

Prism $f'_m = 1740$ psi, brick $f'_m = 8280$ psi

$L/h_{eff} = 7.83\text{ft} / 6\text{ft} = 1.31$

Nominal $f_a = 126$ psi

Cantilever conditions

Assumed Values:

$v_{me1} = (0.75/1.5) * (0.75 * 186 + f_a)$ psi

$v_{me2} = (0.75/1.5) * (f_a)$ psi

Calculated Values (kips):

$V_r = 118$ $V_{tc} = 118$

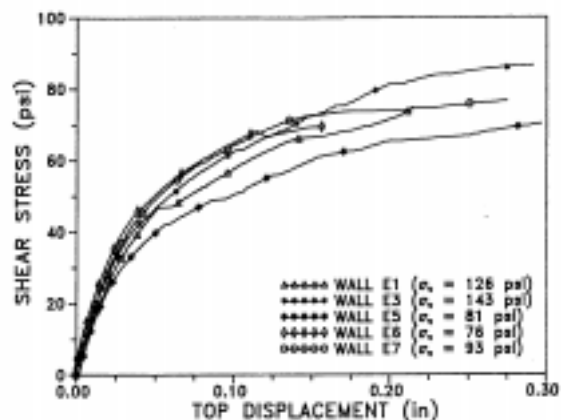
$V_{bjs1} = 250$ $V_{bjs2} = 101$

$V_{dt1} = 336$ $V_{dt2} = 533$

FEMA 273 Predicted Behavior: Rocking or toe crushing

ATC-43 Predicted Behavior: Flexural cracking/toe crushing at 118 kips

Actual Behavior: Flexural cracking/toe crushing, with a maximum capacity of 120 kips and final drift of 0.3%



Summary of measured top level displacement of the Test Walls vs shear stress

Reference: Epperson and Abrams (1989)

Specimen: E3

Material: Brick

Loading: Monotonic

Provided Information:

Prism $f'_m = 1740$ psi, brick $f'_m = 8280$ psi

$L/h_{eff} = 9.5\text{ft} / 6\text{ft} = 1.58$

Nominal $f_a = 141$ psi

Cantilever conditions

Assumed Values:

$v_{me1} = (0.75/1.5) * (0.75 * 186 + f_a)$ psi

$v_{me2} = (0.75/1.5) * (f_a)$ psi

Calculated Values (kips):

$V_r = 190$ $V_{tc} = 186$

$V_{bjs1} = 307$ $V_{bjs2} = 133$

$V_{dt1} = 420$ $V_{dt2} = 635$

FEMA 273 Predicted Behavior: Toe crushing at 186 kips

ATC-43 Predicted Behavior: Flexural cracking/toe crushing at 186 kips

Actual Behavior: Flexural cracking/toe crushing, with a maximum capacity of 164 kips and final drift of 0.4%

Reference: Epperson and Abrams (1989)

Specimen: E5

Material: Brick

Loading: Monotonic

Provided Information:

Prism $f'_m = 1740$ psi, brick $f'_m = 8280$ psi

$L/h_{eff} = 11.42\text{ft} / 6\text{ft} = 1.90$

Nominal $f_a = 81$ psi

Cantilever conditions

Assumed Values:

$v_{me1} = (0.75/1.5) * (0.75 * 186 + f_a)$ psi

$v_{me2} = (0.75/1.5) * (f_a)$ psi

Calculated Values (kips):

$V_r = 150$ $V_{tc} = 156$

$V_{bjs1} = 289$ $V_{bjs2} = 88$

$V_{dt1} = 367$ $V_{dt2} = 680$

FEMA 273 Predicted Behavior: Rocking at 150 kips with "d" drift of 0.2%

ATC-43 Predicted Behavior: Flexural cracking/toe crushing at 156 kips

Actual Behavior: Flexural cracking/toe crushing, with a maximum capacity of 154 kips and final drift of 0.4%

Reference: Epperson and Abrams (1989)

Specimen: E6

Material: Brick

Loading: Monotonic

Provided Information:

Prism $f'_m = 1740$ psi, brick $f'_m = 8280$ psi

$L/h_{eff} = 11.42\text{ft} / 6\text{ft} = 1.90$

Nominal $f_a = 76$ psi

Cantilever conditions

Assumed Values:

$v_{me1} = (0.75/1.5) * (0.75 * 186 + f_a)$ psi

$v_{me2} = (0.75/1.5) * (f_a)$ psi

Calculated Values (kips):

$V_r = 141$ $V_{tc} = 147$

$V_{bjs1} = 284$ $V_{bjs2} = 82$

$V_{dt1} = 357$ $V_{dt2} = 675$

FEMA 273 Predicted Behavior: Rocking at 141 kips with "d" drift of 0.2%

ATC-43 Predicted Behavior: Flexural cracking/toe crushing at 147 kips

Actual Behavior: Flexural cracking/toe crushing, with a maximum capacity of 150 kips and final drift of 0.2%

Reference: Epperson and Abrams (1989)

Specimen: E7

Material: Brick

Loading: Monotonic

Provided Information:

Prism $f'_m = 1740$ psi, brick $f'_m = 8280$ psi

$L/h_{eff} = 11.42\text{ft} / 6\text{ft} = 1.90$

Nominal $f_a = 93$ psi

Cantilever conditions

Assumed Values:

$v_{me1} = (0.75/1.5) * (0.75 * 186 + f_a)$ psi

$v_{me2} = (0.75/1.5) * (f_a)$ psi

Calculated Values (kips):

$V_r = 173$ $V_{tc} = 177$

$V_{bjs1} = 302$ $V_{bjs2} = 101$

$V_{dt1} = 390$ $V_{dt2} = 692$

FEMA 273 Predicted Behavior: Rocking at 173 kips with "d" drift of 0.2%

ATC-43 Predicted Behavior: Flexural cracking/toe crushing at 177 kips

Actual Behavior: Flexural cracking/toe crushing, with a maximum capacity of 157 kips and final drift of 0.4%

4.1.2 Comments on FEMA 273 Component Force/Displacement Relationships

4.1.2.1 Conclusions from Review of the Research and Their Impact on the Evaluation Methodology

As the previous sections indicate, the FEMA 273 methodology leads to successful predictions in certain cases. In other cases, the predictions did not match the observed behavior. To help address this issue, some modifications were made in the Section 7.3 methodology in FEMA 306. Some of these issues and their resolution include:

- Rocking and toe crushing equations often yield very similar values; when they do differ, the lower value does not necessarily predict the governing mode. Section 7.3 in FEMA 306 thus identifies which mode will occur on the basis of aspect ratio, unless the axial stress is very high, since there have been no reported instances of rocking in stocky piers. The $L/h_{eff} > 1.25$ is a somewhat arbitrary threshold based simply on a review of test results.
- Stable rocking generally exceeds the proposed “d” drift value of $0.4h_{eff}/L$. Thus, this value is conservative (see Costley and Abrams, 1996 and Anthoine et al., 1995).
- Rocking does not appear to exhibit the FEMA 273 drop to the “c” capacity value in the above two tests nor, apparently, in the Magenes and Calvi (1995) tests. The only exception is Specimen W3 of Abrams and Shah (1992), which, after rocking for ten cycles at drifts of up to 0.5% ($0.5h_{eff}/L$), was then pushed to 0.8% drift ($0.8h_{eff}/L$) where it experienced toe crushing. The test was stopped at that point. Given the limited number of specimens, it is difficult to determine if this represents the drop from initial load to the “c” level, or a special, sequential mode. For simplicity, this case was combined with the rocking cases, and the “d” drift level was set to account for this level of toe crushing. In most cases, though, rocking capacities will not drop off significantly. The “d” drift value of $0.4h_{eff}/L$ was set based on Costley and Abrams (1996), with some conservatism (Abrams, 1997) to account for Specimen W3. The “c” drift value was conservatively set at 0.6, because of the limited test

data (Abrams, 1997), but aside from Specimen W3, higher “c” values are probably likely.

- There are few pure bed-joint sliding tests. Specimen W1 of Abrams and Shah (1992) is one example, and Specimens MI2 and MI4 of Magenes and Calvi (1992) appear to be examples as well. The drop in lateral strength appears to occur at about 0.3-0.4% drift in W1 and MI4, so the proposed “d” value of 0.4 seems reasonable. The “c” of 0.6 also seems reasonable. The capacity for bed-joint sliding is based on the bond-plus-friction strength. After cracking, the bond capacity will be eroded, and the strength is likely to be based simply on the friction portion of the equation. Cyclic in-place push tests show this behavior; so does Specimen W1 of Abrams and Shah (1992). One could argue that the second cycle backbone curve of FEMA 273 (which, by definition, goes into the nonlinear, post-cracking range) should be limited only to the frictional capacity. But in many cases, other modes will be reached before the full bed-joint sliding capacity is reached. In some of these cases, interestingly, bed-joint sliding occurs after another mode has occurred. Manzouri et al. (1995), for example, show sequences such as initial toe crushing that progresses to bed-joint sliding at higher drift values. One explanation is that toe crushing degenerated into bed-joint sliding because the toe crushing and initial bed-joint sliding values were quite close. See Section 4.1.2.2 for further explanation.
- Mixed modes or, more accurately, sequences of different behavior modes are common in the experiments.

4.1.2.2 The Bed-Joint Sliding and Flexural Cracking/Toe Crushing/Bed-Joint Sliding Modes

The model of bed-joint sliding used in this document is shown in Figure 4-1. For estimating the strength and deformation capacity of the undamaged bed-joint sliding mode, FEMA 273 was used. The idealized relationship has a plateau at the bed-joint capacity V_{bjs1} , which includes the bond and friction components. After bond is lost, the residual strength is limited to 60% of V_{bjs1} . The actual backbone curve is likely to be smoother than the idealized model, since the loss of bond does not occur all at once in the entire masonry section. Instead, more heavily stressed portions crack, and shear demand is redistributed to the remaining

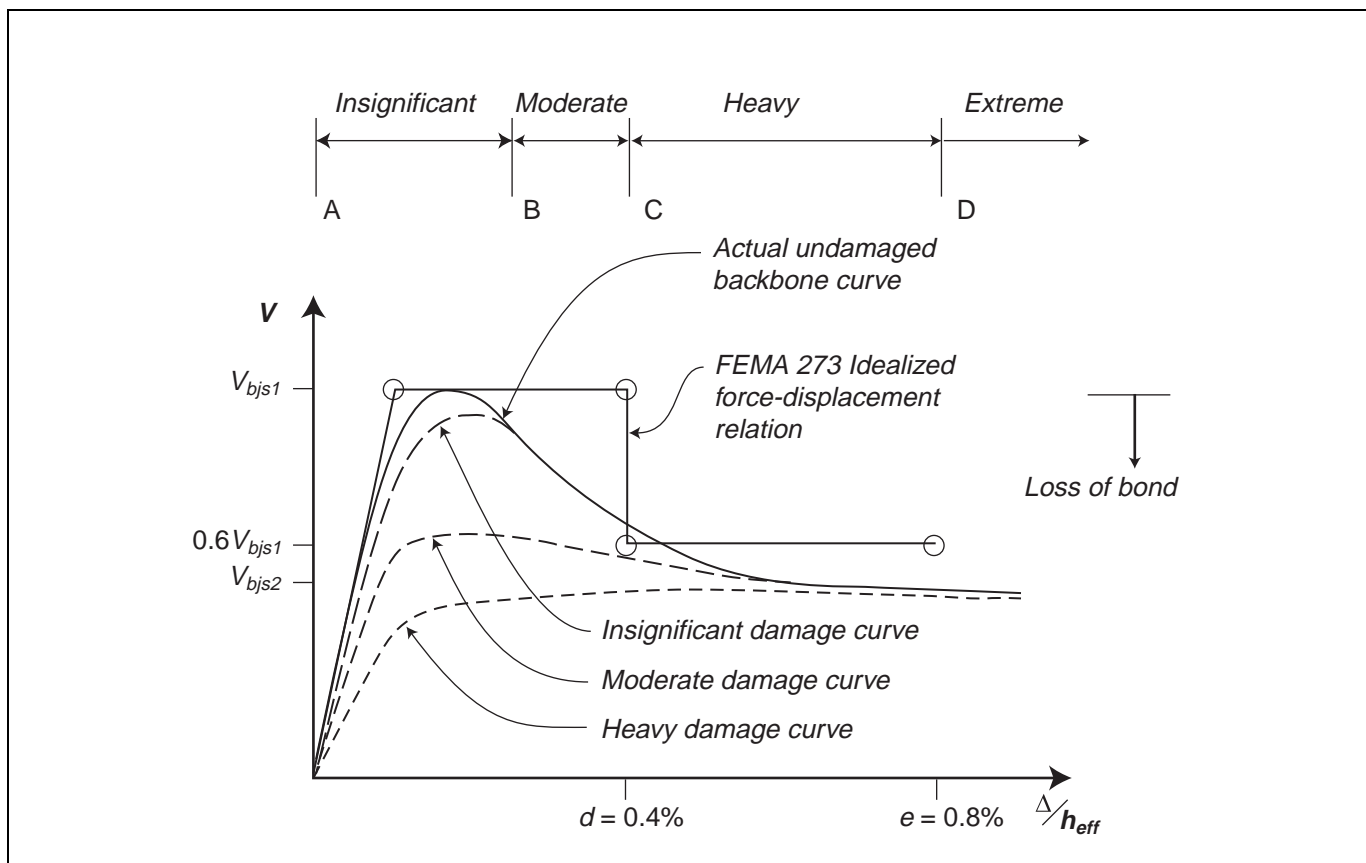


Figure 4-1 Bed-joint sliding force/displacement relationship

sections. The actual residual strength could be higher or lower than $0.6V_{bjs1}$. One measure of the residual capacity is V_{bjs2} .

Figure 4-1 also shows the assumed changes to the force/displacement relationship following the damaging event. *Insignificant* damage is characterized by displacement during the damaging event that is between points A and B. Loss of bond is limited. Following the damaging event, the dashed “Insignificant Damage Curve” represents the force/displacement relationship. For damaging events that reach levels of initial displacement beyond point B, greater loss of bond occurs, and the subsequent damage curve achieves a lower strength. Eventually, with initial displacements beyond point C, the entire bond is lost and only friction remains. Thus, future cycles will no longer be able to achieve the original V_{bjs1} level, reaching only the V_{bjs2} level. With significant cyclic displacements, some erosion of the crack plane and deterioration of the wall

is likely to lead to a small reduction in capacity below the V_{bjs2} level.

The varying level of bed-joint sliding strength is assumed in this document to be a possible explanation for some of the observed testing results in stocky walls, in particular results such as (1) Specimen W1 of Abrams and Shah (1992), in which bed-joint sliding was the only mode observed; (2) Manzouri et al. (1995), in which toe crushing behavior was followed by bed-joint sliding; and (3) Epperson and Abrams (1989), in which toe crushing was not followed by sliding. Figure 4-2 helps to explain the hypothesis.

In the top set of curves, toe-crushing strength substantially exceeds the V_{bjs1} level. As displacement occurs, the bed-joint sliding capacity is reached first, and it becomes the limit state. If displacement is such that *heavy* damage occurs, then in subsequent cycles, the strength will be limited to the V_{bjs2} level.

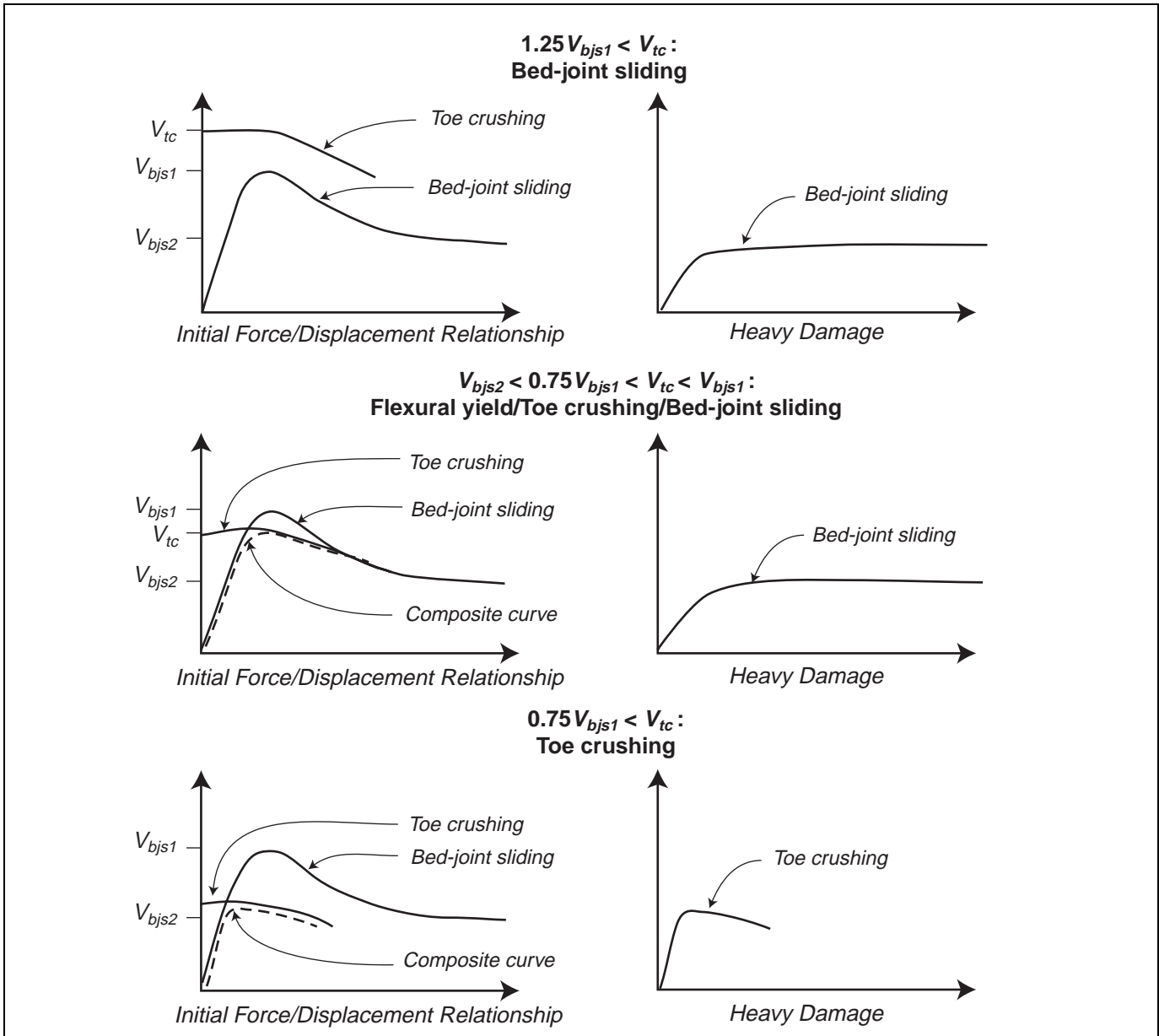


Figure 4-2 Relationship Between Toe Crushing and Bed-Joint Sliding

In the second set of curves, toe-crushing and initial bed-joint sliding strengths are similar. As displacement occurs, the toe-crushing strength is reached first, cracking and movement occur within the wall, some of the bond is lost, and the wall begins to slide. The initial force/displacement curve is thus similar to that for bed-joint sliding, except that the peak is limited by the toe-crushing strength. If displacement is such that *Heavy* damage occurs, then in subsequent cycles, the strength

will be limited to the V_{bjs2} level. This is one possible explanation for the Manzouri et al. (1995) tests.

In the third set of curves, toe-crushing strength is substantially lower than initial bed-joint sliding strength and the ductile mechanism of sliding is not achieved. This is one possible explanation for the Epperson and Abrams (1989) results, in which mortar shear strength was much higher and ductility was lower.

Section 7.3.2 in FEMA 306 makes use of the above hypotheses; cutoff values for the middle set of curves were based in part on review of the results shown in Section 4.1.1. Results are promising, but additional testing and verification of other tests should be done.

4.1.2.3 Out-of-Plane Flexural Response

The most comprehensive set of testing done to date on the out-of-plane response of URM walls was part of the ABK program in the 1980s, and it is documented in ABK (1981c). Input motions used in the ABK (1981c) were based on the following earthquake records: Taft 1954 N21E, Castaic 1971 N69E, Olympia 1949 S04E, and El Centro 1940 S00E. They were scaled in amplitude and were processed to represent the changes caused by diaphragms of varying stiffness to produce the final series of 22 input motion sets. Each set has a motion for the top of the wall and the bottom of the wall. Peak velocities range up to 39.8 in/sec; accelerations, up to 1.42g; and displacements, up to 9.72 inches. In ABK (1984), the mean ground input velocity for UBC Seismic Zone 4 was assumed to be 12 in/sec. For buildings with crosswalls, diaphragm amplification would increase this about 1.75-fold, to 21 in/sec. For buildings without crosswalls, wood roofs were assumed to have a velocity of about 24 in/sec and floors about 27 in/sec.

Since 1981, a significant number of ground motion records have been obtained, including a number of near-field records. In several instances, recent recordings substantially exceed the 12 in/sec value and even exceed the maximum values used by ABK (1981c). Of particular concern are near-field pulse effects and whether they were adequately captured by the original testing. When site-specific spectra and time histories that incorporate these effects are available, it may be possible to address this issue using the original research.

4.1.3 Development of λ -factors

One of the central goals of this document is to develop a method for quantitatively characterizing the effect of damage on the force/displacement relationship of wall components. Ideally, the most accurate approach would be to have two sets of cyclic tests for a component. One test would be of an initially undamaged wall displaced to failure. The second set would include walls initially displaced to various levels of damage (to represent the “damaging event”) and then retested to failure. This would allow for direct determination of the λ -factors

contained in the Component Guides in FEMA 306. Unfortunately, as noted in Section 4.1.1 there have been almost no experimental tests done on damaged URM walls; typically, tests were done on undamaged walls and either stopped or continued only after the damaged wall was repaired.

In the absence of test results on damaged walls, hysteresis curves of initially undamaged walls were reviewed. In reviewing these tests, the goal was to characterize how force/displacement relationships changed from cycle to cycle as displacement was increased. Early cycles were considered to represent “damaging” events, and subsequent cycles represented the behavior of an initially-damaged component. Particular attention was given to tests in which multiple runs on a specimen were performed. In these cases, initial runs (representing not just a damaging cycle, but a damaging earthquake record) were compared with subsequent runs to determine the extent of strength and stiffness deterioration.

Using these tests, the following general approaches were used to estimate λ -factors for this project. The reloading stiffnesses (i.e., the stiffness observed moving from the fourth quadrant to the first) at different cycles or different runs were compared to the initial stiffness to determine λ_K . This variable is estimated to be the ratio of stiffness at higher cycles to the initial stiffness. The assumption made is that if testing had been stopped and the displacement reset to zero and then restarted, the stiffness of the damaged component would have been similar to the reloading stiffness. See Figure 4-3 for an example.

For determining λ_Q , the approach shown in Figure 4-1 and discussed in the previous section is applied where appropriate to determine λ_Q , the ratio of strength at higher cycles to initial strength. The loss of strength is roughly equal to the capacity at high drift levels divided by the peak capacity. FEMA 273 describes both deformation-controlled and force-controlled modes. In a purely force-controlled mode, there is, by definition, little or no ductility. Deformation progresses until a brittle failure results. Thus, there are few, if any, damage states between *Insignificant* and *Extreme*, and there would be little, if any, post-cracking strength. Further, until a brittle mode occurs, the component would be expected to be minimally affected by previous displacement. Review of available hysteresis curves shows, though, that even modes defined as force-

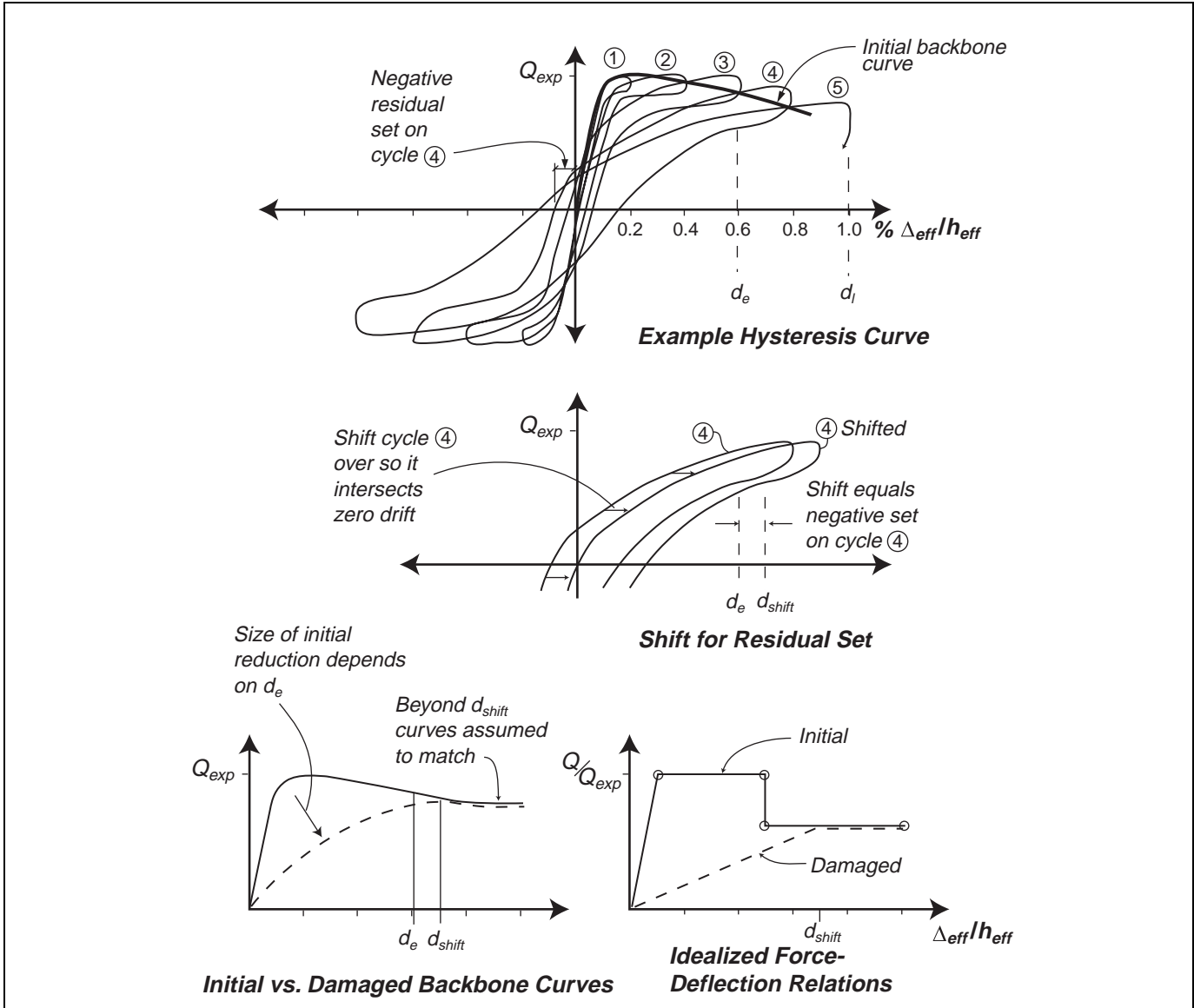


Figure 4-3 Developing the initial portion of the damaged force/displacement relationship

controlled by FEMA 273 (such as diagonal tension) do have some residual strength.

There is little available information for determining λ_{Δ} , because retesting of damaged components to failure has not been done. Values were estimated using engineering judgment. In most cases, less-ductile modes are assumed to have higher λ_{Δ} values, even at higher damage levels. The basis of this assumption is the idea that in more-ductile modes, λ_{Δ} is assumed to be somewhat more dependent on cumulative inelastic deformation. In more-ductile modes, the available

hysteretic energy has been dissipated in part by the damaging earthquake, and there is less available in the subsequent event. The result is the final displacement that can be achieved is reduced.

Values for λ_K^* , λ_Q^* , and λ_{Δ}^* are based, where possible, on tests of repaired walls. The values in URM1F, for example, are set at 1.0 because the hysteresis curves of repaired walls were equal to or better than those of the original walls. In most other cases, repairs typically involve injection of cracks, but since microcracking can never be fully injected, it may not be possible to restore

complete initial stiffness. In the bed-joint sliding modes without tests, it was assumed that the strength could not be fully restored by injection, because the horizontal crack planes are closed and bond cannot be restored in these locations. It is important to recognize that injection of walls with many cracks or unfilled collar joints and cavities, may enhance strength, but it may also lead to less ductile behavior, because other modes may then occur prior to bed-joint sliding.

Values for $\lambda_{h/t}$ are based on a review of the ABK (1981c) document, the model proposed in Priestley (1985), and engineering judgment. At low levels of damage, the portions of wall between the crack planes are essentially undamaged, and the effective thickness,

t , remains unchanged. At higher levels of damage, deterioration, crushing, and spalling of the corners of the masonry at crack locations reduces the effective thickness and the ability of the wall to resist movements imparted by the diaphragm.

4.2 Tabular Bibliography for Unreinforced Masonry

Table 4-1 contains a brief description of the key technical reports that address specific reinforced masonry component behavior. The component types and their behavior modes are indicated. The full references can be found in Section 4.4.

4.3 Symbols for Unreinforced Masonry

Symbols used in the unreinforced masonry sections of FEMA 306 and 307 are the same as those given in Section 7.9 of FEMA 273 except for the following additions and modifications.

C	Resultant compressive force in a spandrel, lb	b_l	Length of masonry unit, in.
L_{sp}	Length of spandrel, in.	b_w	Width of brick unit, in.
M_{spcr}	Expected moment capacity of a cracked spandrel, lb-in.	d_{sp}	Depth of spandrel, in.
M_{spun}	Expected moment capacity of an uncracked spandrel, lb-in.	d_{effcr}	Distance between resultant tensile and compressive forces in a cracked spandrel, in.
V_{spcr}	Expected diagonal tension capacity of a cracked spandrel, lb	d_{effun}	Distance between resultant tensile and compressive forces in an uncracked spandrel, in.
V_{spun}	Expected diagonal tension capacity of an uncracked spandrel, lb	f'_{dt}	Masonry diagonal tension strength, psi
NB	Number of brick wythes in a spandrel	v_{bjcr}	Cracked bed joint shear stress, psi
NR	Number of rows of bed joints in a spandrel	v_{bjun}	Uncracked bed joint shear stress in a spandrel, psi
T	Resultant tensile force in a spandrel, lb	v_{ccr}	Cracked collar joint shear stress in a spandrel, psi
V_{bjs1}	Expected shear strength of wall or pier based on bed joint shear stress, including both the bond and friction components, lb	v_{cun}	Uncracked collar joint shear stress in a spandrel, psi
V_{bjs2}	Expected shear strength of wall or pier based on bed joint shear stress, including only the friction component, lb	β	=0.67 when $L/h_{eff} < 0.67$, = L/h_{eff} when $0.67 \leq L/h_{eff} \leq 1.0$, and = 1.0 when $L/h_{eff} > 1$
V_{sp}	Shear imparted on the spandrel by the pier, lb	Δ_s	Average slip at cracked spandrel (can be estimated as average opening width of open head joint), in.
V_{dt}	Expected shear strength of wall or pier based on diagonal tension using v_{me} for f'_{dt} , lb	ϵ	Factor for estimating the bond strength of the mortar in spandrels
V_{tc}	Expected shear strength of wall or pier based on toe crushing using v_{me} for f'_{dt} , lb	γ	Factor for coefficient of friction in bed joint sliding equation for spandrels
W_w	Expected weight of a wall, lb	η	Factor to estimate average stress in uncracked spandrel. Equal to $NR/2$ or, for more sophistication, use $\sum_{i=1, NR} [(d_{sp}/2 - b_h(i))/(d_{sp}/2 - b_h)]$
b_{effcr}	Effective length of interface for a cracked spandrel, in.	$\lambda_{h/t}$	Factor used to estimate the loss of out-of-plane wall capacity to damaged URM walls
b_{effun}	Effective length of interface for an uncracked spandrel, in.	μ_{Δ}	Displacement ductility demand for a component, used in FEMA 306, Section 5.3.4, and discussed in Section 6.4.2.4 of FEMA 273. Equal to the component deformation corresponding to the global target displacement, divided by the effective yield displacement of the component (which is defined in Section 6.4.1.2B of FEMA 273).
b_h	Height of masonry unit plus bed joint thickness, in.		

4.4 References for Unreinforced Masonry

- ABK, 1981a, *Methodology for Mitigation of Seismic Hazards in Existing Unreinforced Masonry Buildings: Categorization of Buildings*, A Joint Venture of Agbabian Associates, S.B. Barnes and Associates, and Kariotis and Associates (ABK), Topical Report 01, c/o Agbabian Associates, El Segundo, California.
- ABK, 1981b, *Methodology for Mitigation of Seismic Hazards in Existing Unreinforced Masonry Buildings: Diaphragm Testing*, A Joint Venture of Agbabian Associates, S.B. Barnes and Associates, and Kariotis and Associates (ABK), Topical Report 03, c/o Agbabian Associates, El Segundo, California.
- ABK, 1981c, *Methodology for Mitigation of Seismic Hazards in Existing Unreinforced Masonry Buildings: Wall Testing, Out-of-Plane*, A Joint Venture of Agbabian Associates, S.B. Barnes and Associates, and Kariotis and Associates (ABK), Topical Report 04, c/o Agbabian Associates, El Segundo, California.
- ABK, 1984, *Methodology for Mitigation of Seismic Hazards in Existing Unreinforced Masonry Buildings: The Methodology*, A Joint Venture of Agbabian Associates, S.B. Barnes and Associates, and Kariotis and Associates (ABK), Topical Report 08, c/o Agbabian Associates, El Segundo, California.
- Abrams, D.P., 1992, "Strength and Behavior of Unreinforced Masonry Elements," *Proceedings of Tenth World Conference on Earthquake Engineering*, Balkema Publishers, Rotterdam, The Netherlands, pp. 3475-3480.
- Abrams, D.P., 1997, personal communication, May.
- Abrams, D.P., and Epperson, G.S., 1989, "Evaluation of Shear Strength of Unreinforced Brick Walls Based on Nondestructive Measurements," *5th Canadian Masonry Symposium*, Department of Civil Engineering, University of British Columbia, Vancouver, British Columbia., Volume 2.
- Abrams, D.P., and Epperson, G.S., 1989, "Testing of Brick Masonry Piers at Seventy Years", *The Life of Structures: Physical Testing*, Butterworths, London.
- Abrams, D.P., and Shah, N., 1992, *Cyclic Load Testing of Unreinforced Masonry Walls*, College of Engineering, University of Illinois at Urbana, Advanced Construction Technology Center Report #92-26-10.
- Adham, S.A., 1985, "Static and Dynamic Out-of-Plane Response of Brick Masonry Walls," *Proceedings of the 7th International Brick Masonry Conference*, Melbourne, Australia.
- Anthoine, A., Magonette, G., and Magenes, G., 1995, "Shear-Compression Testing and Analysis of Brick Masonry Walls," *Proceedings of the 10th European Conference on Earthquake Engineering*, Duma, editor, Balkema: Rotterdam, The Netherlands.
- ATC, 1997a, *NEHRP Guidelines for the Seismic Rehabilitation of Buildings*, prepared by the Applied Technology Council (ATC-33 project) for the Building Seismic Safety Council, published by the Federal Emergency Management Agency, Report No. FEMA 273, Washington, D.C.
- ATC, 1997b, *NEHRP Commentary on the Guidelines for the Seismic Rehabilitation of Buildings*, prepared by the Applied Technology Council (ATC-33 project) for the Building Seismic Safety Council, published by the Federal Emergency Management Agency, Report No. FEMA 274, Washington, D.C.
- BSSC, 1992, *NEHRP Handbook for the Seismic Evaluation of Existing Buildings*, prepared by the Building Seismic Safety Council for the Federal Emergency Management Agency, Report No. FEMA-178, Washington, D.C.
- Calvi, G.M., Kingsley, G.R., and Magenes, G., 1996, "Testing of Masonry Structures for Seismic Assessment," *Earthquake Spectra*, Earthquake Engineering Research Institute, Oakland, California, Vol. 12, No. 1, pp. 145-162.
- Calvi, G.M, and Magenes, G., 1994, "Experimental Results on Unreinforced Masonry Shear Walls Damaged and Repaired," *Proceedings of the 10th International Brick Masonry Conference*, Vol. 2, pp. 509-518.
- Calvi, G.M., Magenes, G., Pavese, A., and Abrams, D.P., 1994, "Large Scale Seismic Testing of an Unreinforced Brick Masonry Building," *Proceedings of Fifth U.S. National Conference on Earthquake Engineering*, Chicago, Illinois, July 1994, pp.127-136.
- City of Los Angeles, 1985, "Division 88: Earthquake Hazard Reduction in Unreinforced Masonry Buildings," *City of Los Angeles Building Code*, Los Angeles, California.
- City of Los Angeles, 1991, *Seismic Reinforcement Seminar Notes*, City of Los Angeles Department of Building and Safety.

- Costley, A.C., Abrams, D.P., and Calvi, G.M., 1994, "Shaking Table Testing of an Unreinforced Brick Masonry Building," *Proceedings of Fifth U.S. National Conference on Earthquake Engineering*, Chicago, Illinois, July 1994, pp.127-136.
- Costley, A.C., and Abrams, D.P., 1996a, "Response of Building Systems with Rocking Piers and Flexible Diaphragms," *Worldwide Advances in Structural Concrete and Masonry, Proceedings of the Committee on Concrete and Masonry Symposium*, ASCE Structures Congress XIV, Chicago, Illinois.
- Costley, A.C., and Abrams, D.P., 1996b, *Dynamic Response of Unreinforced Masonry Buildings with Flexible Diaphragms*, National Center for Earthquake Engineering Research, Technical Report NCEER-96-0001, Buffalo, New York.
- Epperson, G.S., and Abrams, D.P., 1989, *Nondestructive Evaluation of Masonry Buildings*, College of Engineering, University of Illinois at Urbana, Advanced Construction Technology Center Report No. 89-26-03, Illinois.
- Epperson, G.S., and Abrams, D.P., 1992, "Evaluating Lateral Strength of Existing Unreinforced Brick Masonry Piers in the Laboratory," *Journal of The Masonry Society*, Boulder, Colorado, Vol. 10, No. 2, pp. 86-93.
- Feng, Jianguo, 1986, "The Seismic Shear Strength of Masonry Wall," *Proceedings of the US-PRC Joint Workshop on Seismic Resistance of Masonry Structures*, State Seismological Bureau, PRC and National Science Foundation, USA, Harbin, China.
- Gambarotta, L. and Lagomarsino, S., 1996, "A Finite Element Model for the Evaluation and Rehabilitation of Brick Masonry Shear Walls," *Worldwide Advances in Structural Concrete and Masonry, Proceedings of the Committee on Concrete and Masonry Symposium*, ASCE Structures Congress XIV, Chicago, Illinois.
- ICBO, 1994, *Uniform Code for Building Conservation*, International Conference of Building Officials, Whittier, California.
- Kariotis, J.C., 1986, "Rule of General Application - Basic Theory," *Earthquake Hazard Mitigation of Unreinforced Pre-1933 Masonry Buildings*, Structural Engineers Association of Southern California, Los Angeles, California.
- Kariotis, J.C., Ewing, R.D., and Johnson, A.W., 1985a, "Predictions of Stability for Unreinforced Brick Masonry Walls Shaken by Earthquakes," *Proceedings of the 7th International Brick Masonry Conference*, Melbourne, Australia.
- Kariotis, J.C., Ewing, R.D., and Johnson, A.W., 1985b, "Strength Determination and Shear Failure Modes of Unreinforced Brick Masonry with Low Strength Mortar," *Proceedings of the 7th International Brick Masonry Conference*, Melbourne, Australia.
- Kariotis, J.C., Ewing, R.D., and Johnson, A.W., 1985c, "Methodology for Mitigation of Earthquake Hazards in Unreinforced Brick Masonry Buildings," *Proceedings of the 7th International Brick Masonry Conference*, Melbourne, Australia.
- Kingsley, G.R., 1995, "Evaluation and Retrofit of Unreinforced Masonry Buildings," *Proceedings of the Third National Concrete and Masonry Engineering Conference*, San Francisco, California, pp. 709-728.
- Kingsley, G.R., Mages, G., and Calvi, G.M., 1996, "Measured Seismic Behavior of a Two-Story Masonry Building," *Worldwide Advances in Structural Concrete and Masonry, Proceedings of the Committee on Concrete and Masonry Symposium*, ASCE Structures Congress XIV, Chicago, Illinois.
- Mages, G., 1997, personal communication, May.
- Mages, G., and Calvi, G.M., 1992, "Cyclic Behavior of Brick Masonry Walls," *Proceedings of the Tenth World Conference*, Balkema: Rotterdam, The Netherlands.
- Mages, G. and Calvi, G.M., 1995, "Shaking Table Tests on Brick Masonry Walls," *10th European Conference on Earthquake Engineering*, Duma, editor, Balkema: Rotterdam, The Netherlands.
- Manzouri, T., Shing, P.B., Amadei, B., Schuller, M., and Atkinson, R., 1995, *Repair and Retrofit of Unreinforced Masonry Walls: Experimental Evaluation and Finite Element Analysis*, Department of Civil, Environmental and Architectural Engineering, University of Colorado: Boulder, Colorado, Report CU/SR-95/2.
- Manzouri, T., Shing, P.B., Amadei, B., 1996, "Analysis of Masonry Structures with Elastic/Viscoplastic Models, 1996," *Worldwide Advances in Structural Concrete and Masonry, Proceedings of the Committee on Concrete and Masonry Symposium*, ASCE Structures Congress XIV, Chicago, Illinois.
- Priestley, M.J.N, 1985, "Seismic Behavior of Unreinforced Masonry Walls," *Bulletin of the New*

- Zealand National Society for Earthquake Engineering*, Vol. 18, No. 2.
- Proposal for Change G7-7, 1997, proposal to change the in-plane URM wall provisions of FEMA 273 (1996).
- Rutherford & Chekene, 1990, *Seismic Retrofitting Alternatives for San Francisco's Unreinforced Masonry Buildings: Estimates of Construction Cost and Seismic Damage for the San Francisco Department of City Planning*, Rutherford and Chekene Consulting Engineers: San Francisco, California.
- Rutherford & Chekene, 1997, *Development of Procedures to Enhance the Performance of Rehabilitated Buildings*, prepared by Rutherford & Chekene Consulting Engineers, published by the National Institute of Standards and Technology as Reports NIST GCR 97-724-1 and 97-724-2.
- SEAOC/CALBO, 1990, "Commentary on the SEAOC-CALBO Unreinforced Masonry Building Seismic Strengthening Provisions," *Evaluation and Strengthening of Unreinforced Masonry Buildings*, 1990 Fall Seminar, Structural Engineers Association of Northern California, San Francisco, California.
- SEAOSC, 1986, "RGA (Rule of General Application) Unreinforced Masonry Bearing Wall Buildings (Alternate Design to Division 88)," *Earthquake Hazard Mitigation of Unreinforced Pre-1933 Masonry Buildings*, Structural Engineers Association of Southern California: Los Angeles, California.
- Sheppard, P.F. and Terceelj, S., 1985, "Determination of the Seismic Resistance of an Historical Brick Masonry Building by Laboratory Tests of Cut-Out Wall Elements," *Proceedings of the 7th International Brick Masonry Conference*, Melbourne, Australia.
- Tena-Colunga, A., and Abrams, D.P., 1992, *Response of an Unreinforced Masonry Building During the Loma Prieta Earthquake*, Department of Civil Engineering, University of Illinois at Urbana-Champaign, Structural Research Series No. 576.
- Tomazevic, M., and Anicic, 1989, "Research, Technology and Practice in Evaluating, Strengthening, and Retrofitting Masonry Buildings: Some Yugoslavian Experiences," *Proceedings of the International Seminar on Evaluating, Strengthening and Retrofitting Masonry Buildings*, The Masonry Society: Boulder, Colorado.
- Tomazevic, M., Lutman, M., and Weiss, P., 1996, "Seismic Upgrading of Old Brick-Masonry Urban Houses: Tying of Walls with Steel Ties," *Earthquake Spectra*, EERI: Oakland, California, Volume 12, No. 3.
- Tomazevic, M., and Weiss, P., 1990, "A Rational, Experimentally Based Method for the Verification of Earthquake Resistance of Masonry Buildings," *Proceedings of the Fourth U.S. National Conference on Earthquake Engineering*, EERI: Oakland, California.
- Turnsek, V., and Sheppard, P., 1980, "The Shear and Flexural Resistance of Masonry Walls," *Proceedings of the International Research Conference on Earthquake Engineering*, Skopje, Yugoslavia.
- Willsea, F.J., 1990, "SEAOC/CALBO Recommended Provisions", *Evaluation and Strengthening of Unreinforced Masonry Buildings*, 1990 Fall Seminar, Structural Engineers Association of Northern California, San Francisco, California.
- Xu, W., and Abrams, D.P., 1992, *Evaluation of Lateral Strength and Deflection for Cracked Unreinforced Masonry Walls*, U.S. Army Research Office, Report ADA 264-160, Triangle Park, North Carolina.
- Zsutty, T.C., 1990, "Applying Special Procedures", *Evaluation and Strengthening of Unreinforced Masonry Buildings*, 1990 Fall Seminar, Structural Engineers Association of Northern California, San Francisco, California.

5. Infilled Frames

5.1 Commentary And Discussion

There is a wealth of experimental data reported in the literature on infilled frames. Unfortunately, only a limited amount of the research has been performed under *cyclic* loading and conducted on specimens that reflect U.S. construction practice. For these test results, it is evident that infilled frames can possess stable hysteresis loops and continue to carry substantial lateral loads at significant interstory drifts. This is true in spite of the highly damaged appearance and even complete loss of some of the masonry units within an infill panel.

Most experimental results on infilled-frame systems show a mixture of behavior modes that take place at various stages of loading. At low interstory drift levels (0.2% - 0.4%), corner crushing and some diagonal cracking in the panel tend to occur first. This is followed by frame yielding (0.5% - 1.0% interstory drift) and possible bed-joint sliding. As the drift amplitude increases beyond about 1%, cracking in the infill panel becomes more extensive, along with further frame damage. The frame damage takes the form of cracking, crushing, and spalling of concrete in the case of reinforced concrete frames or prying damage to bolted semi-rigid connections in steel frames. The coexistence of several behavior modes makes it difficult to determine what λ -factors should be used for quantitative strength and deformation analysis. Therefore, it is necessary to resort to individual component tests to assess λ -values. The results of experiments conducted by Aycardi et al. (1994) are illustrative of the performance of nonductile reinforced concrete frames. These tests give results for each of the failure modes (except column shear).

In the experimental studies on infilled frames by Mander et al. (1993a,b), steel frames were used and were instrumented with numerous strain gauges so the behavior of the frame could be uncoupled from the behavior of the infill panel. It was, therefore, possible to plot the net lateral load-drift capacity of the brick masonry infill panel. These results were helpful in identifying the λ -factors for corner crushing, diagonal cracking and general shear-failure behavior modes for masonry. The bed-joint sliding behavior mode tends to occur mostly in steel frames with ungrouted/unreinforced masonry infill with low panel height-to-length aspect ratios. The experimental results of Gergely et al. (1994) were useful for identifying λ -factors for this behavior mode.

When investigating the out-of-plane behavior of infilled frame panels, it is difficult to enforce a complete failure, as evidenced by recent tests by Angel and Abrams (1994). It should be noted that these investigators first loaded their specimens in-plane before conducting their out-of-plane tests. Results of this study indicate that lateral strength capacity is generally well in excess of 200 psf. Thus, it is unlikely that out-of-plane failure should occur for normal infill height-to-thickness aspect ratios. These results suggest that if an out-of-plane failure is observed in the field, then some other (in-plane) behavior mode has contributed to the failure of the infill.

Dealing with infill panels with openings is difficult due to the many potential types of openings that may occur in practice. Evidently, when openings are present, the strength capacity is bounded by that of bare frame (lower bound) and that of a system with solid infill panels (upper bound). Although these results are derived from monotonic tests, they suggest that the deformation capacity is not impaired if openings exist.

5.1.1 Development of λ -Factors for Component Guides

The Component Damage Classification Guides and component modification factors (λ -factors) for infilled frames were based on an extensive review of research in the area of both nonductile reinforced concrete frames, as well as masonry structures. The principal references used in this work are listed in the tabular bibliography presented in Section 5.2. For each component behavior mode, three types of λ -factors are used: stiffness reduction factors (λ_K), strength reduction factor (λ_Q) and a displacement reduction factor (λ_D). Description of how each of these λ -factors were derived from experimental evidence and theoretical considerations is presented in what follows.

5.1.2 Development of Stiffness Deterioration— λ_K

As the displacement ductility of a member progressively increases, the member also softens. Even though the strength may be largely maintained at a nominal yield level, softening is manifest in the form of stiffness reduction. The degree of softening is generally related to the maximum displacement ductility the member has previously achieved.

There are several analytical models that can be used to give guidance on how one can assess the degree of softening in an element. For example, Chang and Mander (1994) describe several computational hysteretic models calibrated for reinforced concrete components. Utilizing their information obtained from a calibrated modified Takeda model, the λ_K -factor for stiffness reduction can be related by the following relationship:

$$\lambda_K = \left(\frac{\Delta_{\max}}{\Delta_y} \right)^{-\alpha} = (\mu_\Delta)^{-\alpha} \quad (5-1)$$

where Δ_{\max} = maximum displacement in the displacement history, Δ_y = yield displacement, μ_Δ = displacement ductility factor, and α = an experimentally calibrated factor that is material- or specimen-dependent.

Strictly, α should be established on a component-by-component basis. However, for reinforced concrete components there is a range of values from $\alpha = 0.25$ to $\alpha = 1$ that may be applicable, $\alpha = 0.5$ being typical for most specimens. Well detailed members tend to have low α values, whereas higher α values are common for poorly detailed members. Although specific research on infill panels is not developed to the same extent, it seems reasonable that similar trends would be found for these components.

5.1.3 The Determination of λ_Q for Strength Deterioration

In structural elements not specifically designed for seismic resistance, there is generally a lack of adequate transverse reinforcement necessary to provide adequate confinement and shear resistance. As a result, under reversed cyclic loading the strength of such elements deteriorates progressively. Furthermore, if the non-seismically designed frame elements have inadequate anchorage for the reinforcing steel, there can be a gradual loss in strength and then a sudden drop in strength when the anchorage zone or lap splice zone fails. An energy approach can be used to assess the loss of strength in a reinforced concrete column or beam element where inadequate transverse reinforcement is found. The energy-based approach advanced by Mander and Dutta (1997) has been used in developing this process. A summary of the underlying theoretical concepts is given below.

Assuming the moment capacity contributed by the concrete is gradually consumed by the propagating level of damage, then at the end of the i -th cycle it can be

shown that the reduced strength $F_i = \lambda_Q F_n$ can be evaluated through

$$\lambda_Q = \frac{F_i}{F_n} = 1 - \frac{M_c}{M_n} \Sigma D_{ci} = 1 - \frac{M_c}{M_n} \frac{\Sigma \theta_{pi}}{\Sigma \theta_{PC}} \quad (5-2)$$

in which ΣD_{ci} = accumulated damage, $\Sigma \theta_{ci}$ = cumulative plastic drift, M_n = nominal moment capacity, M_c = the moment generated by the eccentric concrete stress block and $\Sigma \theta_{PC}$ = cumulative plastic rotation capacity considering concrete fatigue alone. Using energy concepts where it is assumed that the finite energy reserve of an unconfined concrete section is gradually consumed to resist the concrete compression force, a work expression can be formulated as

$$EWD = IWD \quad (5-3)$$

where EWD = external work done on the section by the concrete compression force defined by the left hand side of the equation below, and IWD = internal work or energy absorption capacity of the section defined by the right hand side of the following equation

$$C_c \times \left(\phi_p \frac{c}{2} \right) \times 2N_c = A_g \int_0^{\epsilon_{cu}} f_c d\epsilon \quad (5-4)$$

in which C_c = concrete compression force, ϕ_p = plastic curvature, c = neutral axis depth, $2N_c$ = total number of reversals and A_g = gross area of the concrete section. The integral in the above expression actually denotes the finite energy capacity of an unconfined concrete section which in lieu of a more precise analysis, can be approximated as $0.008 f'_c$. Note also that the term in brackets in the above equation denotes the plastic strain at the location of the concrete compression force.

Assuming that in a cantilever column the plastic rotation is entirely confined to the plastic hinge zone (of length L_p), using the moment-area theorem and rearranging terms in the above equation, it is possible to solve for the cumulative plastic drift capacity as

$$\Sigma \theta_{PC} = \frac{0.016 \left(\frac{L_p}{D} \right)}{\left(\frac{C_c}{f'_c A_g} \right) \left(\frac{c}{D} \right)} \quad (5-5)$$

where $\Sigma \theta_P = 2N_c \theta_p$ is the *cumulative plastic drift* defined as the sum of all positive and negative drift amplitudes up to a given stage of loading; and D = overall depth/diameter of the column.

The concrete damage model described so far is generally applicable to beam and/or column elements with adequate bonding between the longitudinal reinforcement and the surrounding concrete. Thus following Equation 5-2, the concrete strength continues to decay until the moment capacity of the eccentric concrete block is fully exhausted. At this point the residual moment capacity entirely consists of the steel contribution. This is schematically portrayed in Figure 5-1a. However, more often than not, older buildings possess lap splice zones at their column bases. Such splices are not always equipped with adequate lap length to ensure proper development of bond strength. The lap splice thus becomes the weak point in the column which shows a drastic reduction in the strength almost immediately following the lap splice failure. This is depicted in Figure 5-1b where the bond failure in the lap splice is assumed to occur over one complete cycle. The residual strength immediately after F_i is determined by the extent of confinement around the lap splice, if any. Subsequently the lateral strength is entirely dependent on the performance of pure concrete which continues to decay following the same Equation 5-2 until the residual rocking strength F_r is obtained.

This theory has been validated with experimental results as shown in Figures 5-1c and 5-1d. In Figure 5-1c, the lateral strength envelope is compared with test results with instances of unconfined concrete failure only. In Figure 5-1d, the strength envelope is plotted for column specimen with a clear indication of lap splice failure. Satisfactory agreement between theory and experiment is observed.

Therefore, with the mechanism of failure and the progression of strength deterioration clearly identified and quantified, it is possible to assess, analytically, λ_Q factors for reinforced concrete elements with specific detailing. The research has not been developed to the same extent for infill panels, although an examination of test results indicates that similar trends are present.

5.1.4 Development of λ_D —Reduction in Displacement Capability

The reduction in displacement capability is more difficult to ascertain from traditional, quasi-static, reversed-cyclic-loading, laboratory tests on members. Generally such tests are conducted using two cycles at each ductility factor (or drift angle percentages) of ± 1 , ± 2 , ± 6 ... until failure occurs. The reduction in displacement capacity depends on the severity of the

previous loading history—that is, the amount of energy absorbed with respect to the total energy absorption capacity. Strictly this cannot be ascertained without resorting to fatigue type of testing.

Mander et al. (1994, 1995) and Mander and Dutta (1997) have shown that the displacement capability of structural concrete and steel elements follows a well-known Manson-Coffin fatigue relationship that can be written in displacement ductility terms as follows:

$$\mu_{\Delta} = \mu_m N_f^c \quad (5-6)$$

where N_f = number of equi-amplitude cycles required to produce failure at ductility amplitude μ_{Δ} ; μ_m = monotonic ductility capacity; and c = fatigue exponent. Typical values of the latter are $c = -1/3$ for steel failure and $c = -1/2$ for nonductile reinforced concrete.

The above equation can be written in terms of a “damage fraction” ($D = n_d / N_f$) that can be sustained for n_d cycles of loading in the damaging earthquake:

$$D = \frac{n_d}{N_f} = n_d \left(\frac{\mu_{\Delta}^d}{\mu_m} \right)^{-\frac{1}{c}} \quad (5-7)$$

The remaining fatigue life then is $(1 - D)$. The displacement-based λ_D -factor can thus be defined as

$$\lambda_D = \frac{\mu_{\Delta}^r}{\mu_m} = (1 - D)^{-c} = \left[\frac{1}{n_d} - \left(\frac{\mu_{\Delta}^d}{\mu_m} \right)^{-\frac{1}{c}} \right]^{-c} \quad (5-8)$$

In the above two equations superscripts d and r refer to the damaging earthquake and remaining life, respectively.

Thus for nonductile reinforced concrete failure taking $c = -1/2$ gives

$$\lambda_D = \sqrt{\frac{1}{n_d} - \left(\frac{\mu_{\Delta}^d}{\mu_m} \right)^2} \quad (5-9)$$

For frictional or sliding behavior modes such as lap-splice failure of masonry infill panels, there is no limit to the displacement capability. Therefore, for these two behavior modes, $\lambda_D = 1$ at all times.

Although specific research on infill components is less developed, it is reasonable to assume that similar trends would be observed.

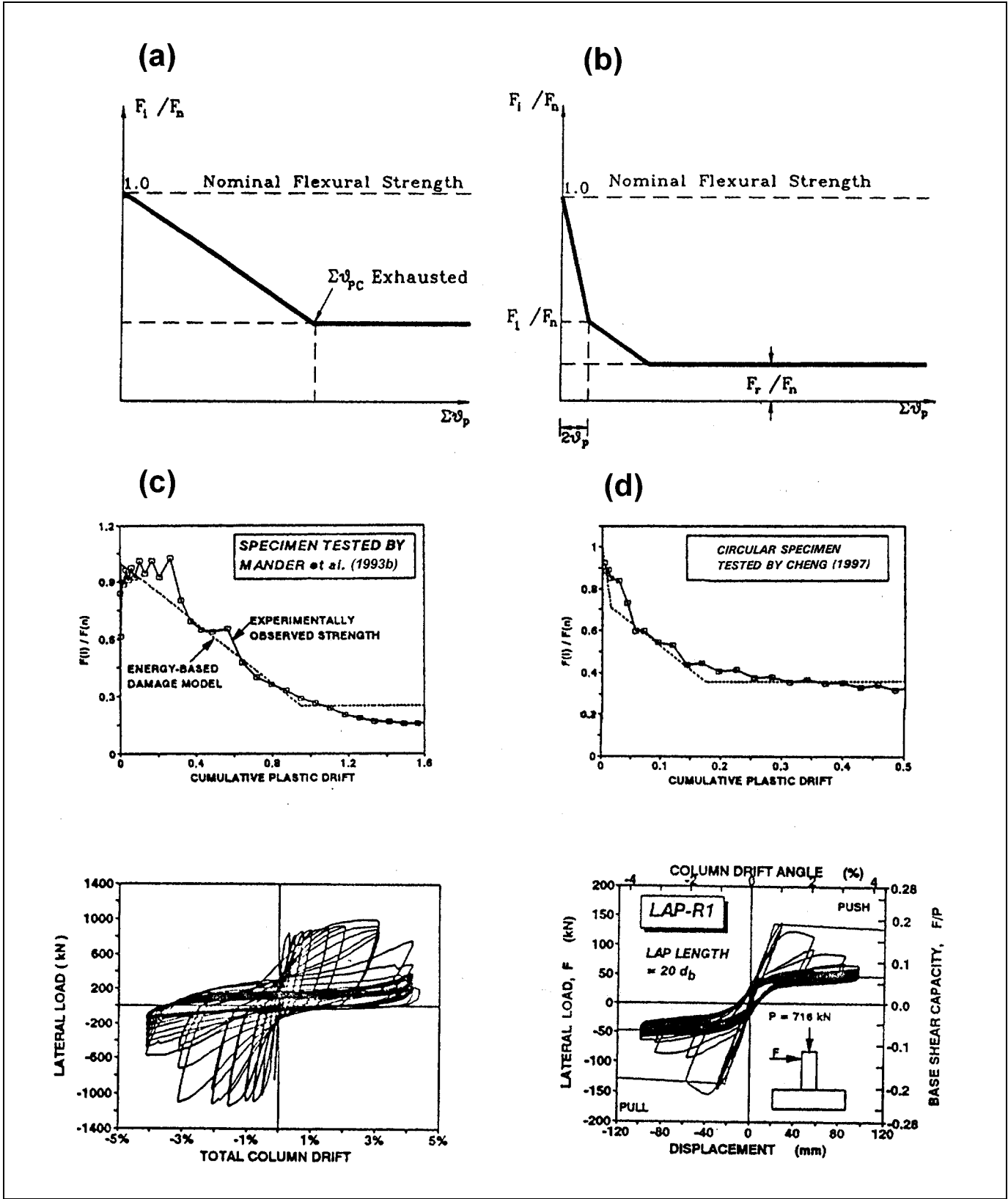


Figure 5-1 Energy-based damage analysis of strength reduction to define λ_Q

5.2 Tabular Bibliography for Infilled Frames

Table 5-1 *Tabular Bibliography for Infilled Frames*

References	Categories*									Remarks
	A	B	C	D	E	F	G	H	I	
Abrams, 1994								✓		
Al-Chaar et al., 1994								✓		
Aycardi et al., 1992									✓	Nonductile concrete frame performance
Aycardi et al., 1994									✓	Nonductile concrete frame performance
Axely and Bertero, 1979	✓							✓		Experiments on multistory frames
Benjamin and Williams, 1958		✓				✓		✓		Classic brick infilled steel frame experiments
Bertero and Brokken, 1983		✓	✓					✓		
Bracci et al., 1995									✓	Emphasis on nonductile frame performance
Brokken and Bertero, 1981								✓		
Coul, 1966						✓				
Crisafully et al., 1995		✓								
Dawe and McBride, 1985		✓				✓		✓		Steel frame with pierced brick infills
Dhanasekar et al., 1985		✓								
Flanagan and Bennett, 1994								✓		Steel frame-clay tile infill
Focardi and Manzini, 1984		✓								
Gergely et al., 1993				✓						Steel frame-clay tile infill
Hamburger and Chakradeo, 1993		✓								
Hill, 1994		✓								
Holmes, 1961						✓				
Kadir, 1974	✓	✓	✓					✓		
Kahn and Hanson, 1977				✓						
Klingner and Bertero, 1976								✓		Multistory infilled frame performance
Klingner and Bertero, 1978								✓		Multistory infilled frame performance
Kodur et al., 1995		✓								
Liau and Lee, 1977	✓	✓				✓				
Liau, 1979	✓							✓		Multistory steel frames-concrete infills
Liau and Kwan, 1983a	✓							✓		Steel frame-concrete infill plastic failure modes
Liau and Kwan, 1983b	✓	✓								Plastic-strength theory
Maghaddam and Dowling, 1987	✓	✓	✓	✓	✓	✓	✓	✓		General treatise on infilled-frame behavior
Mainstone and Weeks, 1970			✓					✓		

*A = Modes of Failure, B = Strength, C = Stiffness, D = Ductility, E = Hysteretic Performance, F = Openings, G = Repairs, H = Experimental Performance of Infilled Frames, I = Steel and Concrete Frame Behavior

Chapter 5: Infilled Frames

Table 5-1 Tabular Bibliography for Infilled Frames (continued)

References	Categories*									Remarks
	A	B	C	D	E	F	G	H	I	
Mainstone, 1971		✓	✓	✓				✓		Classical work on strut methods of analysis
Mallick and Garg, 1971						✓				
Mander and Nair, 1993a	✓				✓			✓		Steel frames-brick infills under cyclic loading
Mander et al., 1993b	✓				✓		✓	✓		Effect of ferrocement repairs
Mander et al., 1994									✓	Low-cycle fatigue of steel frame connections
Mander et al., 1995									✓	
Mehrabi et al., 1996								✓		Concrete frame-block infill experiments
Mosalam et al., 1994				✓						Steel frame brick infills finite-element analysis
Parducci and Mezzi, 1980		✓			✓					
Paulay and Priestley, 1992	✓	✓	✓						✓	Classical text on design
Polyakov, 1956	✓	✓	✓					✓		Earliest work on infills translated from Russian
Prawel and Lee, 1994							✓			Ferrocement repairs for masonry
Priestley, 1996									✓	Most recent work on RC in shear
Priestley et al., 1996									✓	Most recent work on RC in shear
Reinhorn et al., 1995					✓					Advanced analysis methods for infills
Riddington and Stafford-Smith, 1977	✓	✓	✓							Early work on strut methods of analysis
Riddington, 1984		✓						✓		Emphasis on gap effects
Sachanski, 1960								✓		
Saneinejad and Hobbs, 1995	✓	✓	✓							Most up-to-date reference on analysis methods
Shapiro et al., 1994								✓		
Shen and Zhu, 1994								✓		Pseudo-dynamic tests
Shing et al., 1994								✓		
Stafford-Smith, 1966		✓	✓					✓		Early experimental work
Stafford-Smith and Carter, 1969			✓							Pioneering work on analysis using strut methods
Thomas, 1953								✓		Emphasis on brick work
Wood, 1978	✓	✓								Early work on plastic methods of analysis
Yoshimura and Kikuchi, 1995								✓		
Zamic and Tomazevic, 1984				✓	✓			✓		
Zamic and Tomazevic, 1985a				✓	✓			✓		
Zamic and Tomazevic, 1985b		✓		✓	✓			✓		

*A = Modes of Failure, B = Strength, C = Stiffness, D = Ductility, E = Hysteretic Performance, F = Openings, G = Repairs, H = Experimental Performance of Infilled Frames, I = Steel and Concrete Frame Behavior

5.3 References for Infilled Frames

This list contains references from the infilled frames chapters of both FEMA 306 and 307.

- Abrams, D.P. (Ed.), 1994, *Proceedings of the NCEER Workshop on Seismic Response of Masonry Infills*, National Center for Earthquake Engineering Research, Technical Report NCEER-94-0004.
- Al-Chaar, G., Angel, R. and Abrams, D., 1994, "Dynamic testing of unreinforced brick masonry infills," *Proc. of the Structures Congress '94*, Atlanta, Georgia., ASCE, 1: 791-796.
- Angel R., and Abrams, D.P., 1994, "Out-Of-Plane Strength evaluation of URM infill Panels," *Proceedings of the NCEER Workshop on Seismic Response of Masonry Infills*, D.P. Abrams editor, NCEER Technical Report NCEER-94-0004.
- Aycardi, L.E., Mander, J.B., and Reinhorn, A.M., 1992, *Seismic Resistance of RC Frame Structures Designed only for Gravity Loads, Part II: Experimental Performance of Subassemblages*, National Center for Earthquake Engineering Research, Technical Report NCEER-92-0028.
- Aycardi, L.E., Mander, J.B., and Reinhorn, A.M., 1994, "Seismic resistance of reinforced concrete frame structures designed only for gravity loads: Experimental performance of subassemblages", *ACI Structural Journal*, (91)5: 552-563.
- Axely, J.W. and Bertero, V.V., 1979, "Infill panels: their influence on seismic response of buildings," Earthquake Eng. Research Center, University of California at Berkeley, Report No. EERC 79-28.
- Benjamin, J.R., and Williams, H.A., 1958, "The behavior of one-story shear walls," *Proc. ASCE*, ST. 4, Paper 1723: 30.
- Bertero, V.V. and Brokken, S.T., 1983, "Infills in seismic resistant building," *Proc. ASCE*, 109(6).
- Bracci, J.M., Reinhorn, A.M., and Mander, J.B., 1995, "Seismic resistance of reinforced concrete frame structures designed for gravity loads: Performance of structural system", *ACI Structural Journal*, (92)5: 597-609.
- Brokken, S.T., and Bertero, V.V., 1981, *Studies on effects of infills in seismic resistance R/C construction*, Earthquake Engineering Research Centre, University of California at Berkeley, Report No. EERC 81-12.
- Chang, G. A., and Mander, J.B., 1994, *Seismic Energy Based Fatigue Damage Analysis of Bridge Columns: Part I - Evaluation of Seismic Capacity*, Technical Report NCEER-94-0006, and *Part II - Evaluation of Seismic Demand*, Technical Report NCEER-94-0013, National Center for Earthquake Engineering Research, State University of New York at Buffalo.
- Cheng, C.T., 1997, *New Paradigms for the Seismic Design and Retrofit of Bridge Piers*, Ph.D. Dissertation, Science and Engineering Library, State University of New York at Buffalo, Buffalo, New York.
- Chrysostomou, C.Z., Gergely, P. and Abel, J.F., 1988, *Preliminary Studies of the Effect of Degrading Infill Walls on the Nonlinear Seismic Response of Steel Frames*, National Center for Earthquake Engineering Research, Technical Report NCEER-88-0046.
- Coul, A., 1966, "The influence of concrete infilling on the strength and stiffness of steel frames," *Indian Concrete Journal*.
- Crisafulli, F.J., Carr, A.J., and Park, R., 1995, "Shear Strength of Unreinforced Masonry Panels," *Proceedings of the Pacific Conference on Earthquake Engineering*; Melbourne, Australia, Parkville, Victoria, 3: 77-86.
- Dawe, J.L. and McBride, R.T., 1985, "Experimental investigation of the shear resistance of masonry panels in steel frames," *Proceedings of the 7th Brick Masonry Conf.*, Melbourne, Australia.
- Dawe, J.L. and Young, T.C., 1985, "An investigation of factors influencing the behavior of masonry infill in steel frames subjected to in-plane shear," *Proceedings of the 7th International Brick Masonry Conference*, Melbourne, Australia.
- Dhanasekar, K., Page, A.W., and Kleeman, P.W., 1985, "The behavior of brick masonry under biaxial stress with particular reference to infilled frames," *Proceedings of the 7th International Brick Masonry Conference*, Melbourne, Australia.
- Durrani, A.J., and Luo, Y.H., 1994, "Seismic Retrofit of Flat-Slab Buildings with Masonry Infills," in *Proceedings of the NCEER Workshop on Seismic Response of Masonry Infills*, D.P. Abrams editor, National Center for Earthquake Engineering Research, Technical Report NCEER-94-0004.
- Flanagan, R.D. and Bennett, R.M., 1994, "Uniform Lateral Load Capacity of Infilled Frames," *Proceed-*

- ings of the Structures Congress '94*, Atlanta, Georgia, ASCE, 1: 785-790.
- Focardi, F. and Manzini, E., 1984, "Diagonal tension tests on reinforced and non-reinforced brick panels," *Proceedings of the 8th World Conference on Earthquake Engineering*, San Francisco, California, VI: 839-846.
- Freeman S. A., 1994 "The Oakland Experience During Loma Prieta - Case Histories," *Proceedings of the NCEER Workshop on Seismic Response of Masonry Infills*, D.P. Abrams editor, National Center for Earthquake Engineering Research, Technical Report NCEER-94-0004.
- Gergely, P., White, R.N., and Mosalam, K.M., 1994, "Evaluation and Modeling of Infilled Frames," *Proceedings of the NCEER Workshop on Seismic Response of Masonry Infills*, D.P. Abrams editor, National Center for Earthquake Engineering Research, Technical Report NCEER-94-0004, pp. 1-51 to 1-56.
- Gergely, P., White, R.N., Zawilinski, D., and Mosalam, K.M., 1993, "The Interaction of Masonry Infill and Steel or Concrete Frames," *Proceedings of the 1993 National Earthquake Conference, Earthquake Hazard Reduction in the Central and Eastern United States: A Time for Examination and Action*; Memphis, Tennessee, II: 183-191.
- Hamburger, R.O. and Chakradeo, A.S., 1993, "Methodology for seismic capacity evaluation of steel-frame buildings with infill unreinforced masonry," *Proceedings of the 1993 National Earthquake Conference, Earthquake Hazard Reduction in the Central and Eastern United States: A Time for Examination and Action*; Memphis, Tennessee, II: 173-182.
- Hill, James A., 1994, "Lateral Response of Unreinforced Masonry Infill Frame," *Proceedings of the Eleventh Conference* (formerly Electronic Computation Conference) held in conjunction with ASCE Structures Congress '94 and International Symposium '94, Atlanta, Georgia, pp. 77-83.
- Holmes, M., 1961, "Steel frames with brickwork and concrete infilling," *Proceedings of the Institute of Civil Engineers*, 19: 473.
- Kadir, M.R.A., 1974, *The structural behavior of masonry infill panels in framed structures*, Ph.D. thesis, University of Edinburgh.
- Kahn, L.F. and Hanson, R.D., 1977, "Reinforced concrete shear walls for a seismic strengthening," *Proceedings of the 6th World Conf. on Earthquake Engineering*, New Delhi, India, III: 2499-2504.
- Klingner, R.E. and Bertero, V.V., 1976, *Infilled frames in earthquake resistant construction*, Earthquake Engineering Research Centre, University of California at Berkeley, Report No. EERC 76-32.
- Klingner, R.E. and Bertero, V.V., 1978, "Earthquake resistance of infilled frames," *Journal of the Structural Division, Proc. ASCE*, (104)6.
- Kodur, V.K.R., Erki, M.A., and Quenneville, J.H.P., 1995, "Seismic design and analysis of masonry-infilled frames," *Journal of Civil Engineering*, 22: 576-587.
- Liau, T.C. and Lee, S.W., 1977, "On the behavior and the analysis of multi-story infilled frames subjected to lateral loading," *Proceedings of the Institute of Civil Engineers*, 63: 641-656.
- Liau, T.C., 1979, "Tests on multi-storey infilled frames subject to dynamic lateral loading," *ACI Journal*, (76)4: 551-563.
- Liau, T.C. and Kwan, K.H., 1983a, "Plastic theory of infilled frames with finite interface shear strength," *Proceedings of the Institute of Civil Engineers*, (2)75: 707-723.
- Liau, T.C. and Kwan, K.H., 1983b, "Plastic theory of non-integral infilled frames," *Proceedings of the Institute of Civil Engineers*, (2)75: 379-396.
- Maghaddam, H.A. and Dowling, P.J., 1987, *The State of the Art in Infilled Frames*, Civil Engineering Department, Imperial College, ESEE Research Report No. 87-2, London.
- Mainstone, R.J. and Weeks, G.A., 1970, "The influence of bounding frame on the racking stiffness and strength of brick walls," *2nd International Brick Masonry Conference*.
- Mainstone, R.J., 1971, "On the stiffness and strength of infilled frames," *Proceedings of the Institute of Civil Engineers Sup.*, pp. 57-90.
- Mallik, D.V. and Garg, R.P., 1971, "Effect of openings on the lateral stiffness of infilled frames," *Proceedings of the Institute of Civil Engineers*, 49: 193-209.
- Mander J. B., Aycardi, L.E., and Kim, D-K, 1994, "Physical and Analytical Modeling of Brick Infilled Steel Frames," *Proceedings of the NCEER Workshop on Seismic Response of Masonry Infills*, D.P. Abrams editor, National Center for Earthquake Engineering Research, Technical Report NCEER-94-0004.

- Mander, J.B., Chen, S.S., and Pekcan, G., 1994, "Low-cycle fatigue behavior of semi-rigid top-and-seat angle connections," *AISC Engineering Journal*, (31)3: 111-122.
- Mander, J.B., and Dutta, A., 1997, "How Can Energy Based Seismic Design Be Accommodated In Seismic Mapping," *Proceedings of the FHWA/NCEER Workshop on the National Representation of Seismic Ground Motion for New and Existing Highway Facilities, Technical Report*, National Center for Earthquake Engineering Research, NCEER-97-0010, pp 95-114.
- Mander, J.B., and Nair, B., 1993a, "Seismic Resistance of Brick-Infilled Steel Frames With and Without Retrofit," *The Masonry Society Journal*, 12(2): 24-37.
- Mander, J.B., Nair, B., Wojtkowski, K., and Ma, J., 1993b, *An Experimental Study on the Seismic Performance of Brick Infilled Steel Frames*, National Center for Earthquake Engineering Research, Technical Report NCEER-93-0001.
- Mander, J.B., Pekcan, G., and Chen, S.S., 1995, "Low-cycle variable amplitude fatigue modeling of top-and-seat angle connections," *AISC Engineering Journal*, American Institute of Steel Construction, (32)2: 54-62.
- Mander, J.B., Waheed, S.M., Chaudhary, M.T.A., and Chen, S.S., 1993, *Seismic Performance of Shear-Critical Reinforced Concrete Bridge Piers*, National Center for Earthquake Engineering Research, Technical Report NCEER-93-0010.
- Mehrabi, A.B., Shing, P.B., Schuller, M.P. and Noland J.L., 1996, "Experimental evaluation of masonry-infilled RC frames," *Journal of Structural Engineering*.
- Mosalam, K.M., Gergely, P., and White, R., 1994, "Performance and Analysis of Frames with "URM" Infills," *Proceedings of the Eleventh Conference (formerly Electronic Computation Conference) held in conjunction with ASCE Structures Congress '94 and International Symposium '94, Atlanta, Georgia*, pp. 57-66.
- Parducci, A. and Mezzi, M., 1980, "Repeated horizontal displacement of infilled frames having different stiffness and connection systems--Experimental analysis," *Proceedings of the 7th World Conference on Earthquake Engineering*, Istanbul, Turkey, 7: 193-196.
- Paulay, T. and Priestley, M.J.N., 1992, *Seismic Design of Reinforced Concrete and Masonry Buildings*, John Wiley & Sons, New York.
- Polyakov, S.V., 1956, *Masonry in framed buildings*, pub. by Gosudarstvennoe Izdatelstvo po Stroitelstvu I Arkhitekture (Translation into English by G.L.Cairns).
- Prawel, S.P. and Lee, H.H., 1994, "Research on the Seismic Performance of Repaired URM Walls," *Proc. of the US-Italy Workshop on Guidelines for Seismic Evaluation and Rehabilitation of Unreinforced Masonry Buildings*, Department of Structural Mechanics, University of Pavia, Italy, June 22-24, Abrams, D.P. et al. (eds.) National Center for Earthquake Engineering Research, SUNY at Buffalo, pp. 3-17 - 3-25.
- Priestley, M.J.N., 1996, "Displacement-based seismic assessment of existing reinforced concrete buildings," *Bulletin of the New Zealand National Soc. for Earthquake Eng.*, (29)4: 256-271.
- Priestley, M.J.N., Seible, F., and Calvi, G.M., 1996, *Seismic Design and Retrofit of Bridges*, John Wiley & Sons, New York, 686 pp.
- Reinhorn, A.M., Madan, A., Valles, R.E., Reichmann, Y., and Mander, J.B., 1995, *Modeling of Masonry Infill Panels for Structural Analysis*, National Center for Earthquake Engineering Research, Technical Report NCEER-95-0018.
- Riddington, J. and Stafford-Smith, B., 1977, "Analysis of infilled frames subject to racking with design recommendations," *Structural Engineers*, (52)6: 263-268.
- Riddington, J.R., 1984, "The influence of initial gaps on infilled frame behavior," *Proceedings of the Institute of Civil Engineers*, (2)77: 259-310.
- Sachanski, S., 1960, "Analysis of earthquake resistance of frame buildings taking into consideration the carrying capacity of the filling masonry," *Proceedings of the 2nd World Conference on Earthquake Engineering*, Japan, 138: 1-15.
- Saneinejad, A and Hobbs, B., 1995, "Inelastic design of infilled frames," *Journal of Structural Engineering*, (121)4: 634-650.
- Shapiro, D., Uzarski, J., and Webster, M., 1994, *Estimating Out-of-Plane Strength of Cracked Masonry Infills*, University of Illinois at Urbana-Champaign, Report SRS-588, 16 pp.

- Shen, J. and Zhu, R., 1994, "Earthquake response simulation of reinforced concrete frames with infilled brick walls by pseudo-dynamic test," *Proc. of the Second International Conference on Earthquake Resistant Construction and Design*, Berlin, A. Balkema, Rotterdam, pp. 955-962.
- Shing, P.B., Mehrabi, A.B., Schuller, M. and Noland J.D., 1994, "Experimental evaluation and finite element analysis of masonry-infilled R/C frames," *Proc. of the Eleventh Conference (formerly Electronic Computation Conference) held in conjunction with ASCE Structures Congress '94 and International Symposium '94*, Atlanta, Georgia., pp. 84-93.
- Stafford-Smith, B.S., 1966, "Behavior of square infilled frames," *ASCE* (92)1: 381-403.
- Stafford-Smith, B. and Carter, C., 1969, "A method of analysis for infilled frames," *Proceedings of the Institute of Civil Engineers*, 44: 31-48.
- Thiruvengadam, V., 1985, "On the natural frequencies of infilled frames," *Earthquake Engineering and Structural Dynamics*, 13: 401-419.
- Thomas, F.G., 1953, "The strength of brickwork," *J. Instnt. Struct. Engrs.*, (31)2: 35-46.
- Wood, R.H., 1978, "Plasticity, composite action and collapse design of unreinforced shear wall panels in frames," *Proceedings of the Institute of Civil Engineers*, 2: 381-411.
- Yoshimura, K. and Kikuchi, K., 1995, "Experimental study on seismic behavior of masonry walls confined by R/C frames," *Proceedings of the Pacific Conference on Earthquake Engineering*, Melbourne, Australia, Parkville, Victoria, 3: 97-106.
- Zarnic, R. and Tomazevic, M., 1984, "The behavior of masonry infilled reinforced concrete frames subjected to seismic loading," *Proceedings of the 8th World Conference on Earthquake Engineering*, California, VI: 863-870.
- Zarnic, R. and Tomazevic, M., 1985a, "Study of the behavior of masonry infilled reinforced concrete frames subjected to seismic loading," *Proc. 7th Intl. Brick Masonry Conf.*, Melbourne, Australia.
- Zarnic, R. and Tomazevic, M., 1985b, *Study of the behavior of masonry infilled reinforced concrete frames subjected to seismic loading, Part 2. A report to the research community of Slovenia*, ZRMK/IKPI - 8502, Ljubljana.

6. Analytical Studies

6.1 Overview

Analytical studies were conducted as part of this project to serve two broad objectives: (1) to assess the effects of damage from a prior earthquake on the response of single-degree-of-freedom oscillators to a subsequent, hypothetical performance-level earthquake, and (2) to evaluate the utility of simple, design-oriented methods for estimating the response of damaged structures. Previous analytical studies were also reviewed.

To assess the effects of prior damage on response to a performance-level earthquake, damage to a large number of single-degree-of-freedom (SDOF) oscillators was simulated. The initially “damaged” oscillators were then subjected to an assortment of ground motions. The response of the damaged oscillators was compared with that of their undamaged counterparts to identify how the damage affected the response.

The oscillators ranged in initial period from 0.1 to 2.0 seconds, and the strength values were specified such that the oscillators achieved displacement ductility values of 1, 2, 4, and 8 for each of the ground motions when using a bilinear force-displacement model. The effects of damage were computed for these oscillators using several Takeda-based force-displacement models. Damage was parameterized independently in terms of ductility demand and strength reduction.

Ground motions were selected to represent a broad range of frequency characteristics in each of the following categories: Short-duration (SD) records were selected from earthquakes with magnitudes less than about 7, while long-duration (LD) records were generally selected from stronger earthquakes. A third category, forward directivity (FD), consists of ground motions recorded near the fault rupture surface for which a strong velocity pulse may be observed very early in the S-wave portion of the record. Six motions were selected for each category, representing different frequency characteristics, source mechanisms, and earthquakes occurring in locations around the world over the last half-century.

The utility of simple, design-oriented methods for estimating response was evaluated for the damaged and undamaged SDOF oscillators. The displacement coefficient method is presented in FEMA 273 (FEMA, 1997a) and the capacity spectrum and secant stiffness

methods is presented in ATC-40 (ATC, 1996). Estimates of peak displacement response were determined according to these methods and compared with computed values obtained in the dynamic analyses for the damaged and undamaged structures. In addition, the ratio of the peak displacement estimates of damaged and undamaged structures was compared with the ratio obtained from the displacements computed in the nonlinear dynamic analyses.

This chapter summarizes related findings by previous investigators in Section 6.2. The dynamic analysis framework is described in detail in Section 6.3, and results of the nonlinear dynamic analyses are presented in Section 6.4. The design-oriented nonlinear static procedures are described in Section 6.5, and the results of these analyses are compared with the results computed in the dynamic analyses in Section 6.6. Conclusions and implications of the work are presented in Section 6.7.

6.2 Summary of Previous Findings

Previous studies have addressed several issues related to this project. Relevant analytical and experimental findings are reviewed in this section.

6.2.1 Hysteresis Models

Studies of response to recorded ground motions have used many force-displacement models that incorporate various rules for modeling hysteretic response. By far, the most common of these are the bilinear and stiffness-degrading models, which repeatedly attain the strengths given by the monotonic or envelope force-displacement relation. The response of oscillators modeled using bilinear or stiffness-degrading models is discussed below.

6.2.1.1 Bilinear and Stiffness-Degrading Models

Many studies (for example, Iwan, 1977; Newmark and Riddell, 1979; Riddell, 1980; Humar, 1980; Fajfar and Fischinger, 1984; Shimazaki and Sozen, 1984; and Minami and Osawa, 1988) have examined the effect of the hysteresis model on the response of SDOF structures. These studies considered elastic-perfectly-plastic, bilinear (with positive post-yield stiffness), and stiffness-degrading models such as the Takeda model

and the Q model, as well as some lesser-known models. For the nonlinear models used in these studies, the post-yield stiffness of the primary curve ranged between 0 and 10% of the initial stiffness. It is generally found that for long-period structures with positive post-yield stiffness, peak displacement response tends to be independent of the hysteresis model, and it is approximately equal to the peak displacement of linear-elastic oscillators having the same initial stiffness. For shorter-period structures, however, peak displacement response tends to exceed the response of linear-elastic oscillators having the same initial stiffness. The difference in displacement response is exacerbated in lower-strength oscillators. Fajfar and Fischinger (1984), found that for shorter-period oscillators, the peak displacements of elastic-perfectly-plastic models tend to exceed those of degrading-stiffness models (the Q-model), and these peak displacements tend to exceed those of the bilinear model. Riddell (1980), reported that the response of stiffness-degrading systems tends to “go below the peaks and above the troughs” of the spectra obtained for elastoplastic systems.

The dynamic response of reinforced concrete structures tested on laboratory shake tables has been compared with the response computed using different hysteretic models. The Takeda model was shown to give good agreement with measured response characteristics (Takeda et al., 1970). In a subsequent study, the Takeda model was shown to match closely the recorded response; acceptable results were obtained with the less-complicated Q-Hyst model (Saiidi, 1980). Time histories computed by these models were far more accurate than those obtained with the bilinear model.

Studies of a seven-story reinforced concrete moment-resisting frame building damaged in the 1994 Northridge earthquake yield similar conclusions. Moehle et al. (1997) reported that the response computed for plane-frame representations of the structure most nearly matched the recorded response when the frame members were modeled using stiffness-degrading models and strength- and stiffness-degrading force/displacement relationships; dynamic analysis results obtained using bilinear force/displacement relationships were not sufficiently accurate.

Iwan (1973) examined the effect of pinching and yielding on the response of SDOF oscillators to four records. It was found that the maximum displacement response of oscillators having an initial period equal to one second was very nearly equal to that computed for

bilinear systems having the same initial stiffness and yield strength. For one-second oscillators having different system parameters and subjected to different earthquake records, the ratio of mean degrading-system peak displacement response to bilinear system response was 1.06, with standard deviation of 0.14. Iwan noted that for periods appreciably less than one second, the response of degrading systems was significantly greater than that for the corresponding bilinear system, but these effects were not quantified.

Iwan (1977) reported on the effects of a reduction in stiffness caused by cracking. Modeling the uncracked stiffness caused a reduction in peak displacement response for shorter-period oscillators with displacement ductility values less than four, when compared with the response of systems having initial stiffness equal to the yield-point secant stiffness.

Humar (1980) compared the displacement ductility demand calculated for the bilinear and Takeda models for SDOF and multi-degree-of-freedom (MDOF) systems. For the shorter-period SDOF oscillators, the displacement ductility demands exceeded the strength-reduction factor, particularly for the Takeda model. Five- and ten-story frames were designed with girder strengths set equal to 25% of the demands computed in an elastic analysis, and column strengths were set higher than the values computed in an elastic analysis. The Takeda model, which included stiffness degradation, generally led to larger interstory drifts and girder ductility demands than were computed with the bilinear model.

The studies described above considered hysteretic models for which the slope of the post-yield portion of the primary curve was greater than or equal to zero. Where negative post-yield slopes are present, peak displacement response is heightened (Mahin, 1980). The change in peak displacement response tends to be significantly larger for decreases in the post-yield slope below zero than for similar increases above zero. Even post-yield stiffness values equal to negative 1% of the yield stiffness were sufficient to cause collapse. These effects were found to be more pronounced in shorter-period systems and in relatively weak systems.

Rahnama and Krawinkler (1995) reported findings for SDOF structures subjected to 15 records obtained on rock sites. They found that higher lateral strength is required, relative to elastic demands to obtain target displacement ductility demands, for oscillators with

negative post-yield stiffness. The decrease in the strength-reduction factor is relatively independent of vibration period and is more dramatic with increases in target displacement ductility demand. These effects depend on the hysteresis model; the effect of negative post-yield stiffness on the strength-reduction factor is much smaller for stiffness-degrading systems than for bilinear systems. They note that stiffness-degrading systems behave similarly to bilinear systems for positive post-yield stiffness, and they are clearly superior to systems with negative values of post-yield stiffness.

Palazzo and DeLuca (1984) found that the strength required to avoid collapse of SDOF oscillators subjected to the Irpinia earthquake increased as the post-yield stiffness of the oscillator became increasingly negative. Xie and Zhang (1988) compared the response of stiffness-degrading models (having zero post-yield stiffness) with the response of models having a negative post-yield stiffness. The SDOF oscillators were subjected to 40 synthetic records having duration varying from 6 to 30 seconds. It appears that Xie and Zhang found that for shorter-period structures, negative post-yield stiffness models were more likely to result in collapse than were the stiffness-degrading models for all durations considered.

6.2.1.2 Strength-Degrading Models

The response of structures for which the attainable strength is reduced with repeated cyclic loading is discussed below.

Parducci and Mezzi (1984) used elasto-plastic force-displacement models to examine the effects of strength degradation. Yield strength was modeled as decreasing linearly with cumulative plastic deformation. Using accelerograms recorded in Italian earthquakes, The authors found that strength degradation causes an increase in displacement ductility demand for the stronger, shorter-period oscillators. For weaker oscillators, strength degradation amplifies ductility demand over a broader range of periods. The more rapid the degradation of strength, the greater the increase in ductility demand. An analogy can be made with the findings of Shimazaki and Sozen (1984): when strength degradation occurs, the increase in ductility demand can be kept small for shorter-period structures if sufficient strength is provided.

Nakamura and Tanida (1988) examined the effect of strength degradation and slip on the response of SDOF oscillators to white noise and to the 1940 NS El Centro motion. Figure 6-1 plots the force/displacement response curves obtained in this study for various combinations of hysteresis parameters for oscillators with a 0.2-sec period. The parameter D controls the

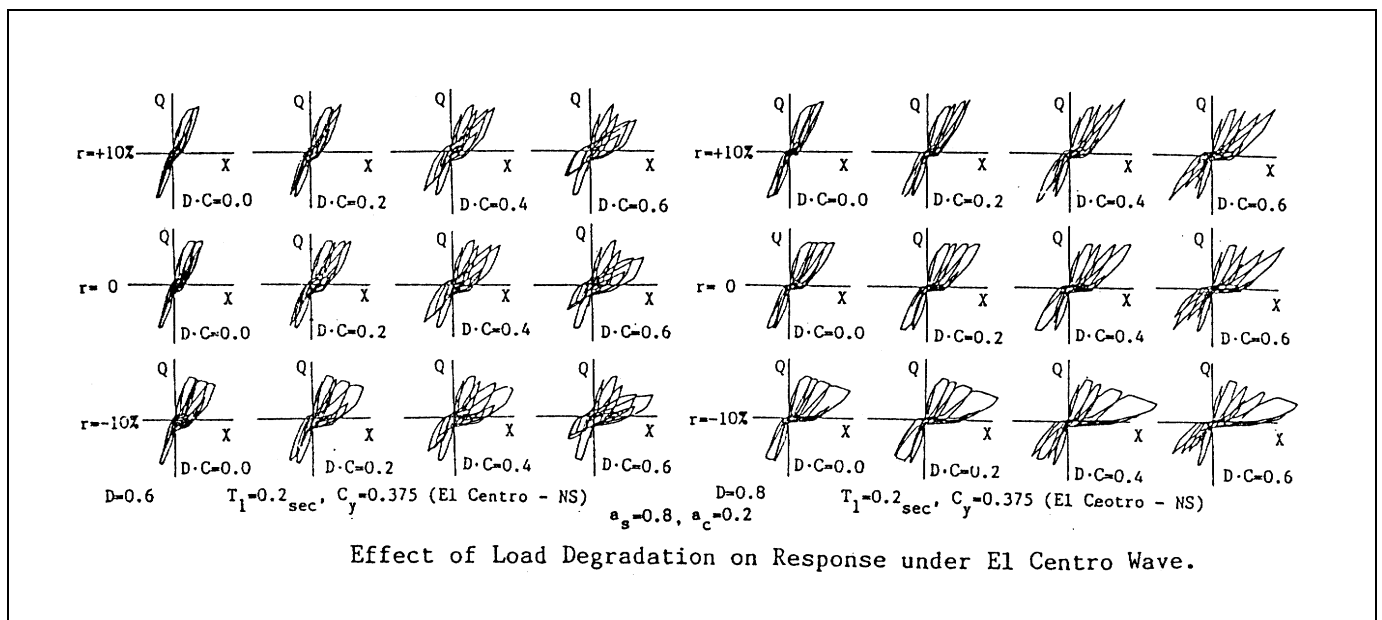


Figure 6-1 Effect of Hysteretic Properties on Response to 1940 NS El Centro Record (from Nakamura, 1988)

amount of slip, C controls the degraded loading stiffness, and a_s and a_c control the unloading stiffness for the slip and degrading components of the model. It is clear that peak displacement response tends to increase as slip becomes more prominent, as post-yield stiffness decreases or even becomes negative, and as loading stiffness decreases.

Rahnama and Krawinkler (1995) modeled strength degradation for SDOF systems as a function of dissipated hysteretic energy. Strength degradation may greatly affect the response of SDOF systems, and the response is sensitive to the choice of parameters by which the strength degradation is modeled. Results of such studies need to be tied to realistic degradation relationships to understand the practical significance of computed results.

6.2.2 Effect of Ground Motion Duration

As described previously, Xie and Zhang (1988) subjected a number of SDOF oscillators to 40 synthetic ground motions, which lasted from 6 to 30 seconds. For stiffness-degrading and negative post-yield stiffness models, the number of collapses increased, as ground motion duration increased. The incidence of collapse tended to be higher for shorter-period structures than longer-period structures. Shorter-duration ground motions that were just sufficient to trigger the collapse of short-period structures did not trigger the collapse of any longer-period structures.

Mahin (1980) reported on the evolution of ductility demand with time for SDOF oscillators subjected to five synthetic records, each having a 60-second duration. Peak evolutionary ductility demands were plotted at 10-second intervals for bilinear oscillators; ductility demand was found to increase asymptotically toward the peak values obtained at 60 seconds. This implies that increases in the duration of ground motion may cause relatively smaller increases in ductility demand.

Sewell (1992) studied the effect of ground-motion duration on elastic demand, constant-ductility strength-reduction factors, and inelastic response intensity, using a set of 262 ground-motion records. He found that the spectral acceleration of elastic and inelastic systems is not correlated with duration, and that strength-reduction factors can be estimated using elastic response ordinates. These findings suggest that the effect of

duration on inelastic response is contained within representations of elastic response quantities.

6.2.3 Residual Displacement

Kawashima et al. (1994) studied the response of bilinear systems with periods between 0.1 and 3 seconds that were subjected to Japanese ground-motion records. According to this study, residual displacement values are strongly dependent on the post-yield stiffness of the bilinear system; that is, systems with larger post-yield stiffness tend to have significantly smaller residual displacements, and systems with zero or negative post-yield stiffness tend to have residual displacements that approach the peak response displacement. They also found that the magnitude of residual displacement, normalized by peak displacement, tends to be independent of displacement ductility demand, based on displacement ductility demands of two, four, and six. The results also indicated that the magnitude of residual displacement is not strongly dependent on the characteristic period of the ground motion, the magnitude of the earthquake, or the distance from the epicenter.

In shake-table tests of reinforced concrete wall and frame/wall structures, Araki et al. (1990) reported that residual drifts for all tests were less than 0.2% of structure height. These tests included wall structures exhibiting displacement ductility demands up to about 12 and frame/wall structures exhibiting displacement ductility demands up to about 14. The small residual drifts in this study were attributed to the presence of restoring forces (acting on the mass of the structure), which are generated as the wall lengthens when displaced laterally. Typical response analyses do not model these restoring forces. These results appear to be applicable to systems dominated by flexural response. However, larger residual displacements have been observed in postearthquake reconnaissance.

6.2.4 Repeated Loading

In the shake-table tests, Araki et al. (1990) also subjected reinforced concrete wall and frame-wall structures to single and repeated motions. It appears that a synthetic ground motion was used. It was found that the low-rise structures subjected to repeated shake-table tests displaced to approximately twice as much as they did in a single test. For the mid-rise and high-rise structures, repeated testing caused peak displacements that were approximately 0 to 10% larger than those obtained in single tests.

Wolschlag (1993) tested three-story reinforced concrete walls on a shake table. In one test series, an undamaged structure was subjected to repeated ground motions of the same intensity. In the repeat tests, the peak displacement response at each floor of the damaged specimen hardly differed from the response measured for the initially undamaged structure.

Cecen (1979) tested two identical ten-story, three-bay, reinforced concrete frame models on a shake table. The two models were subjected to sequences of base motions of differing intensity, followed by a final test using identical base motions. When the structures were subjected to the repeated base motion, the peak displacement response at each story was only slightly affected by the previous shaking of the same intensity. When the two structures were subjected to the same final motion, peak displacement response over the height of the two structures was only slightly affected by the different prior sequences. Floor acceleration response, however, was prone to more variation.

Mahin (1980) investigated the analytical response of SDOF oscillators to repeated ground motions. He reported minor-to-moderate increases in displacement ductility demand across all periods, and weaker structures were prone to the largest increases. For bilinear models with negative post-yield stiffness, increased duration or repeated ground motions tended to cause significant increases in displacement ductility demand (Mahin and Boroschek, 1991).

6.3 Dynamic Analysis Framework

6.3.1 Overview

This section describes the dynamic analyses determining the effects of damage from prior earthquakes on the response to a subsequent performance-level earthquake. In particular, this section describes the ground motion and hysteresis models, the properties of the undamaged oscillators, and the assumptions and constructions used to establish the initially-damaged oscillators. Results of the dynamic analyses are presented in Section 6.4.

6.3.2 Dynamic Analysis Approach

The aim of dynamic analysis was to quantify the effects of a damaging earthquake on the response of a SDOF oscillator to a subsequent, hypothetical, performance-event earthquake. Two obvious approaches may be

taken: the first simulates the damaging earthquake, and the second simulates the damage caused by the damaging earthquake.

To simulate the damaging earthquake, oscillators can be subjected to an acceleration record that is composed of an initial, damaging ground motion record, a quiescent period, and a final ground motion record specified as the performance-level event. This approach appears to simulate reality well, but it is difficult to determine *a priori* how to specify the intensity of the damaging ground motion. One rationale would be to impose damaging earthquakes that cause specified degrees of ductility demand. This would result in oscillators having experienced prior ductility demand and residual displacement at the start of the performance-level ground motion.

In the second approach, taken in this study, the force-displacement curve of the oscillator is modified prescriptively to simulate prior ductility demand, and these analytically “damaged” oscillators are subjected to only the performance-level ground motion. To identify the effects of damage (through changes in stiffness and strength of the oscillator force/displacement response), the possibility of significant residual displacements resulting from the damaging earthquake was neglected. Thus, the damaging earthquake is considered to have imposed prior ductility demands (PDD), possibly in conjunction with strength reduction or strength degradation, on an initially-undamaged oscillator. Initial stiffness, initial unloading stiffness, and strength of the oscillators at the start of the performance-level ground motion may be affected. Response of the initially-damaged structure is compared with the response of the undamaged structure under the performance-level motion. This approach presumes that an engineer will be able to assess changes in lateral stiffness and strength of a real structure based on the nature of damage observed after the damaging earthquake.

While a number of indices may be used to compare response intensity, peak displacement response is preferred here because of its relative simplicity, its immediate physical significance, and its use as the basic parameter in the nonlinear static procedures (described in Section 6.5). The utility of the nonlinear static procedures is assessed vis-a-vis their ability to estimate accurately the peak displacement response.

It should be recognized that predicting the capacity of wall and infill elements may be difficult and prone to uncertainty, whether indexed by displacement, energy,

or other measures. When various modes of response may contribute significantly to an element's behavior, existing models may not reliably identify which mode will dominate. Uncertainty in the dominant mode necessarily leads to uncertainty in estimates of the various capacity measures.

6.3.3 Ground Motions

Several issues were considered when identifying ground motion records to be used in the analyses. First, the relative strength of the oscillators and the duration of ground motion are thought to be significant because these parameters control the prominence of inelastic response. Second, it is known that ground motions rich in frequencies just below the initial frequency of the structure tend to exacerbate damage, because the period of the structure lengthens as yielding progresses. Third, information is needed on the characteristics of structural response to near-field motions having forward-directivity effects.

The analyses were intended to identify possible effects of duration and forward directivity on the response of damaged structures. Therefore, three categories of ground motions were established: short duration (SD), long duration (LD), and Forward Directivity (FD). The characteristics of several hundred ground motions were considered in detail in order to select the records used in each category. Ground motions within a category were selected to represent a broad range of frequency content. In addition, it was desired to use some records that were familiar to the research community, and to use some records obtained from the Loma Prieta, Northridge, and Kobe earthquakes. Within these constraints, records were selected from a diverse worldwide set of earthquakes in order to avoid systematic biases that might otherwise occur. Six time series were used in each category to provide a statistical base on which to interpret response trends and variability. Table 6-1 identifies the ground motions that compose each category, sorted by characteristic period.

Record duration was judged qualitatively in order to sort the records into the short duration and long duration categories. The categorization is intended to discriminate broadly between records for which the duration of inelastic response is short or long. Because the duration of inelastic response depends fundamentally on the oscillator period, the relative strength, and the force/displacement model, a suitable scalar index of record duration is not available.

The physical rupture process tends to correlate ground-motion duration and earthquake magnitude. It can be observed that earthquakes with magnitudes less than 7 tended to produce records that were categorized as short-duration motions, while those with magnitudes greater than 7 tended to be categorized as long-duration motions.

Ground motions recorded near a rupturing fault may contain relatively large velocity pulses if the fault rupture progresses toward the recording station. Motions selected for the forward directivity category were identified by others as containing near-field pulses (Somerville et al., 1997). Recorded components aligned most nearly with the direction perpendicular to the fault trace were selected for this category.

The records shown in Table 6-1 are known to come from damaging earthquakes. The peak ground acceleration values shown in Table 6-1 are in units of the acceleration of gravity. The actual value of peak ground acceleration does not bear directly on the results of this study, because oscillator strength is determined relative to the peak ground acceleration in order to obtain specified displacement ductility demands.

Identifiers in Table 6-1 are formulated using two characters to represent the earthquake, followed by two digits representing the year, followed by four characters representing the recording station, followed by three digits representing the compass bearing of the ground-motion component. Thus, IV40ELCN.180 identifies the South-North component recorded at El Centro in the 1940 Imperial Valley earthquake. Various magnitude measures are reported in the literature and repeated here for reference: M_L represents the traditional local or Richter magnitude, M_W represents moment magnitude, and M_S represents the surface-wave magnitude.

Detailed plots of the ground motions listed in Table 6-1 are presented in Figures 6-2 through 6-19. The plots present ground motion acceleration, velocity, and displacement time-series data, as well as spectral-response quantities. In all cases, ground acceleration data were used in the response computations, assuming zero initial velocity and displacement. For most records, the ground velocity and displacement data presented in the figures were prepared by others. For the four records identified with an asterisk (*) in Table 6-1, informal integration procedures were used to obtain the ground velocity and displacement values shown.

(Text continued on page 120)

Chapter 6: Analytical Studies

Table 6-1 Recorded Ground Motions Used in the Analyses

Identifier	Earthquake Date	Mag.	Station	Component	PGA (g)	Epic. Dist. (km)	Char. Period (sec)
Short Duration (SD)							
WN87MWLN.090	Whittier Narrows 1 Oct 87	$M_L=6.1$	Mount Wilson Caltech Seismic Station	90	0.175	18	0.20
BB92CIVC.360	Big Bear 28 Jun 92	$M_s=6.6$	Civic Center Grounds	360	0.544	12	0.40
SP88GUKA.360 *	Spitak 7 Dec 88	$M_s=6.9$	Gukasyan, Armenia	360	0.207	57	0.55
LP89CORR.090	Loma Prieta 17 Oct 89	$M_s=7.1$	Corralitos Eureka Canyon Rd.	90	0.478	8	0.85
NR94CENT.360	Northridge 17 Jan 94	$M_w=6.7$	Century City	360	0.221	19	1.00
IV79ARY7.140	Imperial Valley 15 Oct 79	$M_L=6.6$	Array #7-14	140	0.333	27	1.20
Long Duration (LD)							
CH85LLEO.010	Central Chile 3 Mar 85	$M_s=7.8$	Llolleo-Baseament of 1- Story Building	010	0.711	60	0.30
CH85VALP.070	Central Chile 3 Mar 85	$M_s=7.8$	Valparaiso University of Santa Maria	070	0.176	26	0.55
IV40ELCN.180	Imperial Valley 18 May 40	$M_L=6.3$	El Centro Irrigation District	180	0.348	12	0.65
TB78TABS.344 *	Tabas 16 Sep 78	$M=7.4$	Tabas	344	0.937	<3	0.80
LN92JOSH.360	Landers 28 Jun 92	$M=7.5$	Joshua Tree	360	0.274	15	1.30
MX85SCT1.270	Michoacan 19 Sep 85	$M_s=8.1$	SCT1-Secretary of Com- munication and Transpor- tation	270	0.171	376	2.00
Forward Directivity (FD)							
LN92LUCN.250 *	Landers 28 Jun 92	$M=7.5$	Lucerne	250	0.733	42	0.20
IV79BRWY.315	Imperial Valley 15 Oct 79	$M_L=6.6$	Brawley Municipal Airport	315	0.221	43	0.35
LP89SARA.360	Loma Prieta 17 Oct 89	$M_s=7.1$	Saratoga Aloha Avenue	360	0.504	28	0.40
NR94NWHL.360	Northridge 17 Jan 94	$M_w=6.7$	Newhall LA County Fire Station	360	0.589	19	0.80
NR94SYLH.090	Northridge 17 Jan 94	$M_w=6.7$	Sylmar County Hospital Parking Lot	090	0.604	15	0.90
KO95TTRI.360 *	Hyogo-Ken Nambu 17 Jan 95	$M_L=7.2$	Takatori-kisu	360	0.617	11	1.40
* Indicates that informal integration procedures were used to calculate the velocity and displacement histories shown in Figures 6-2 through 6-19.							

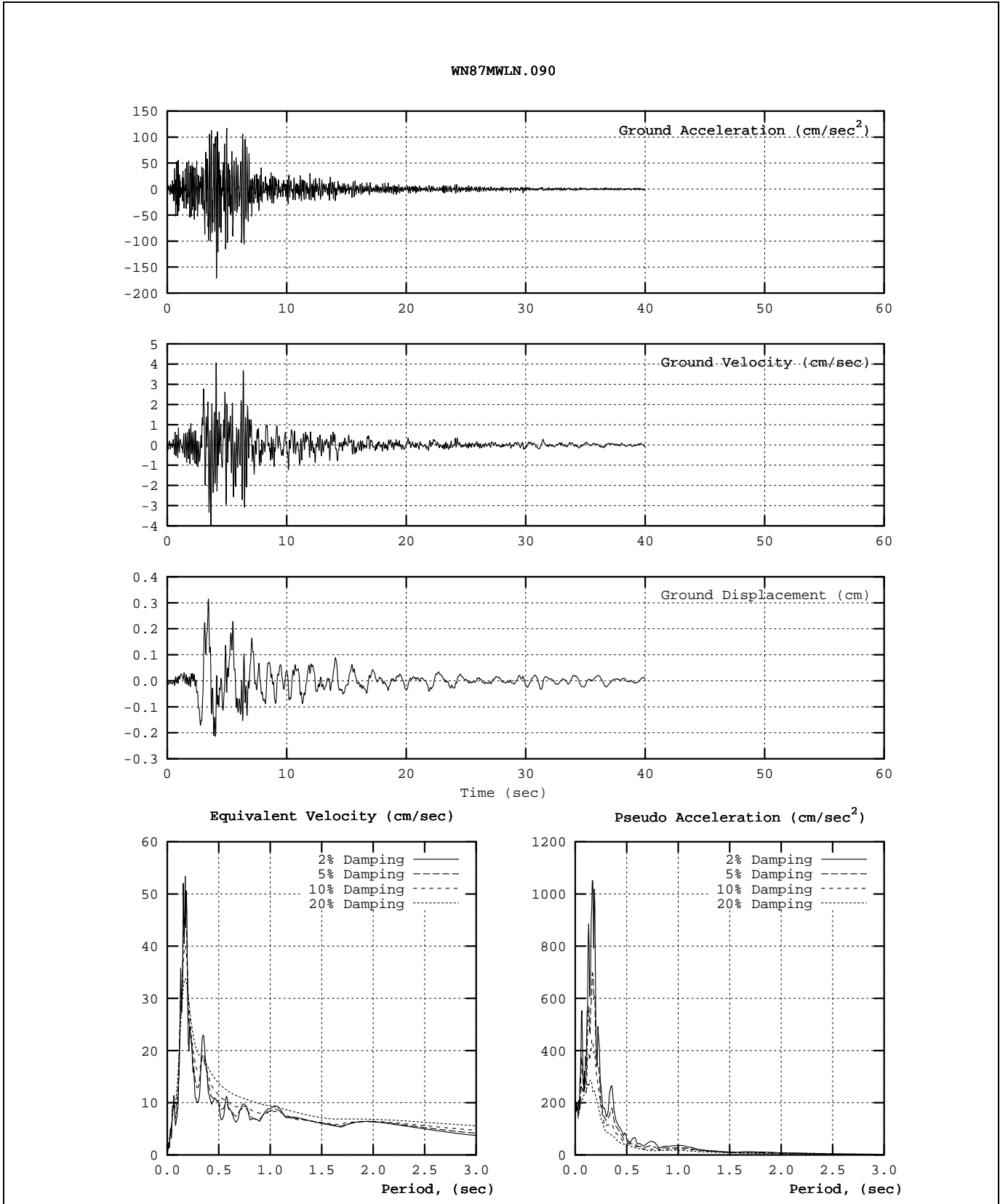


Figure 6-2 Characteristics of the WN87MWLN.090 (Mount Wilson) Ground Motion

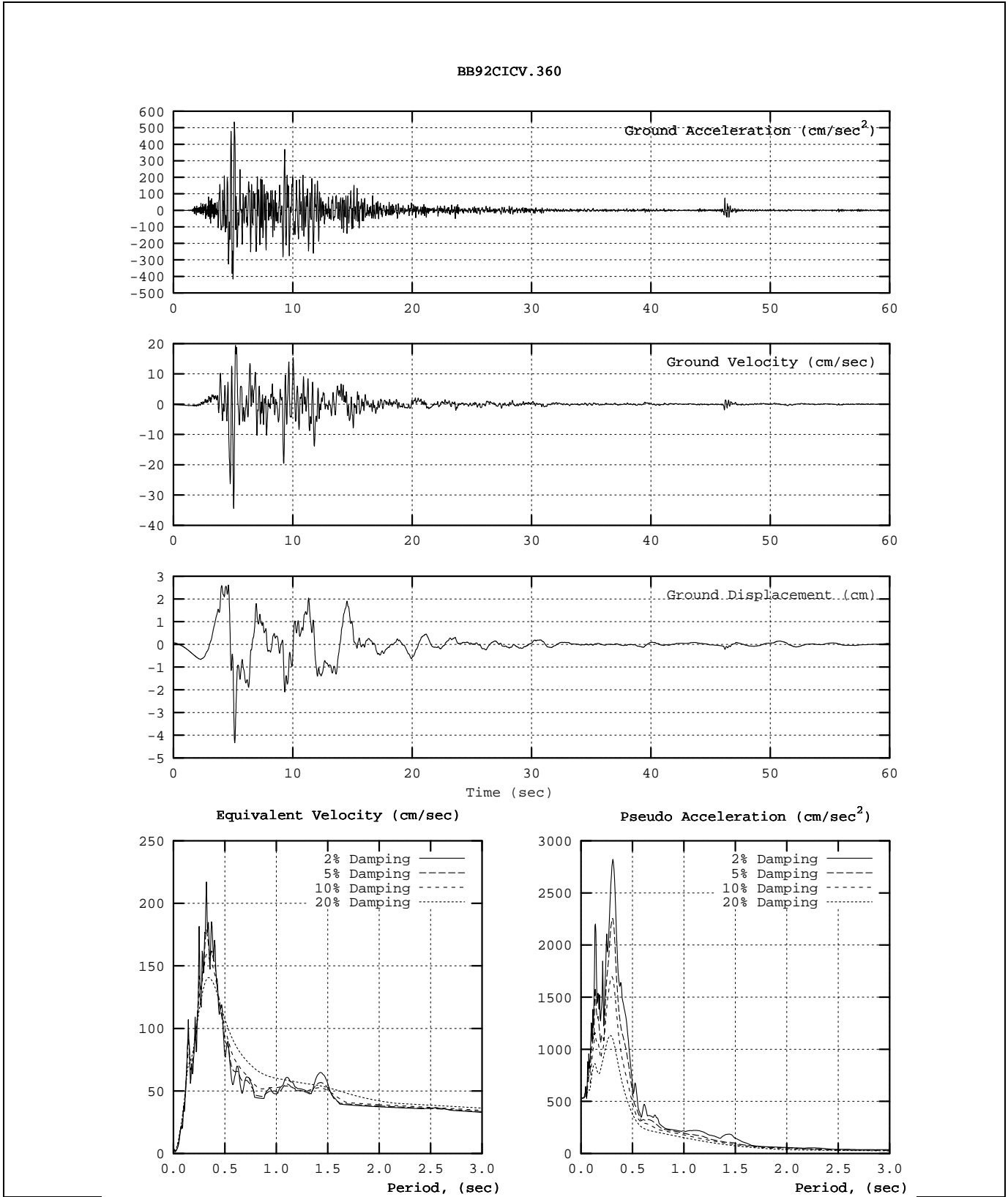


Figure 6-3 Characteristics of the BB92CIVC.360 (Big Bear) Ground Motion

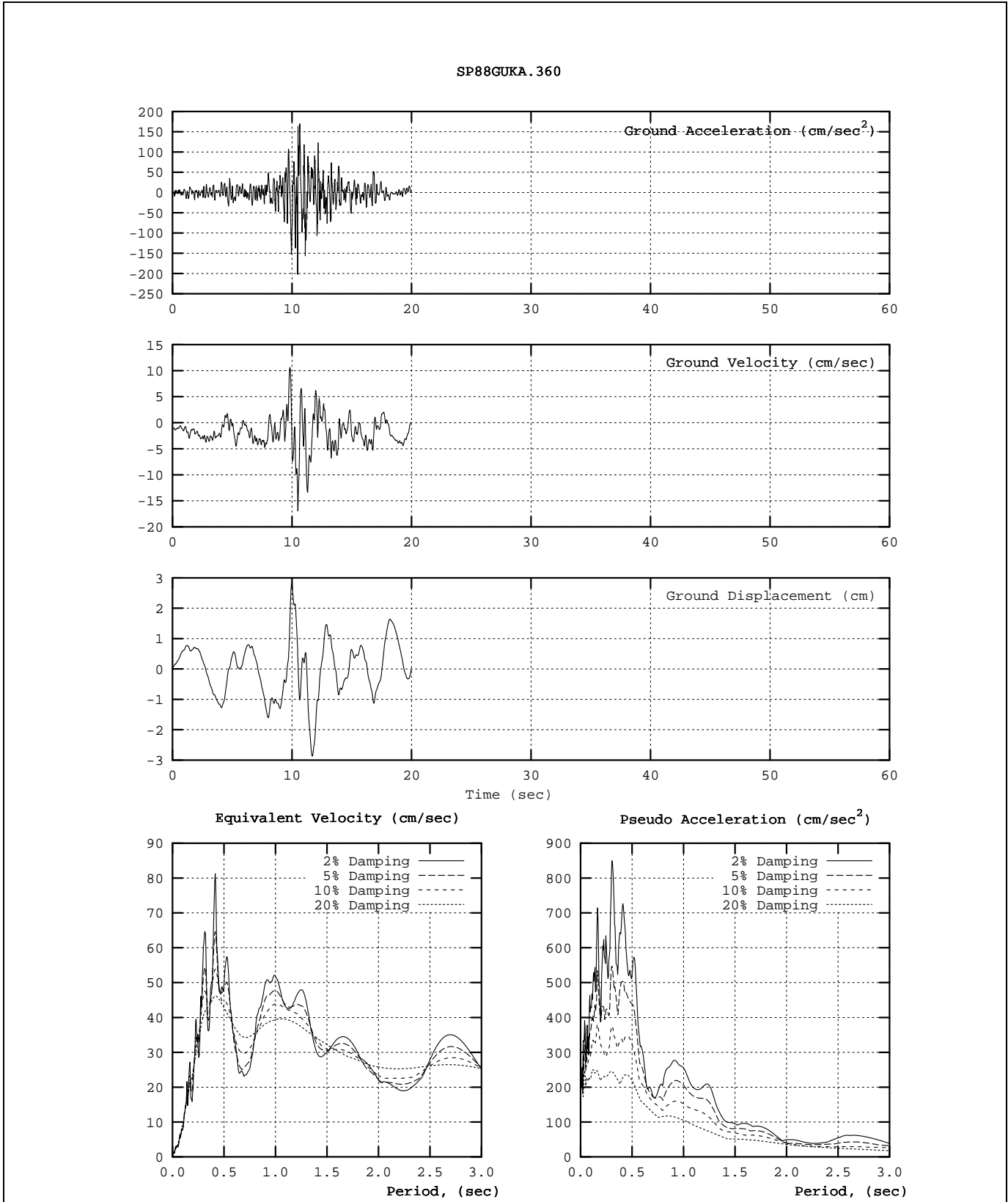


Figure 6-4 Characteristics of the SP88GUKA.360 (Spitak) Ground Motion

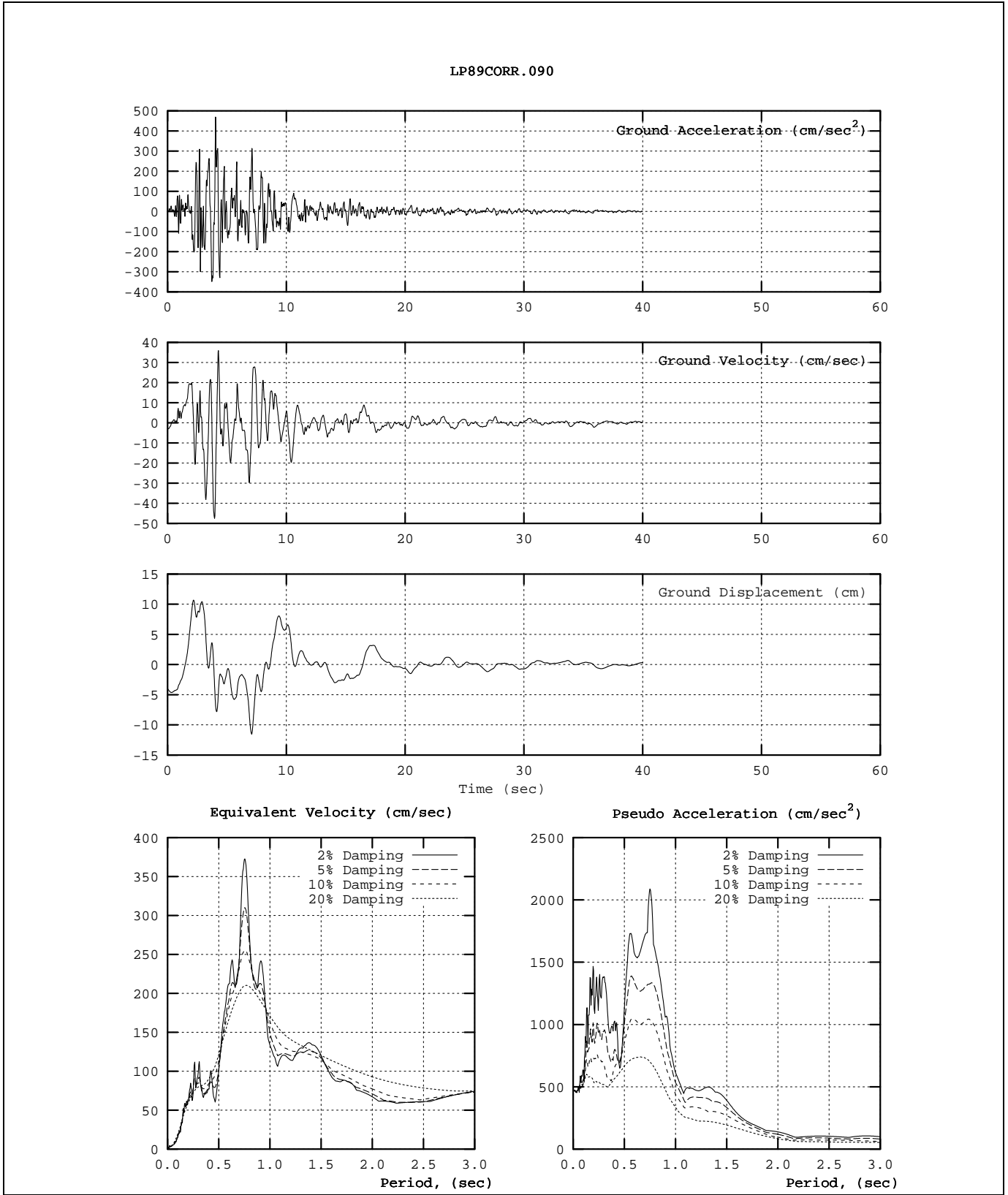


Figure 6-5 Characteristics of the LP89CORR.090 (Corralitos) Ground Motion

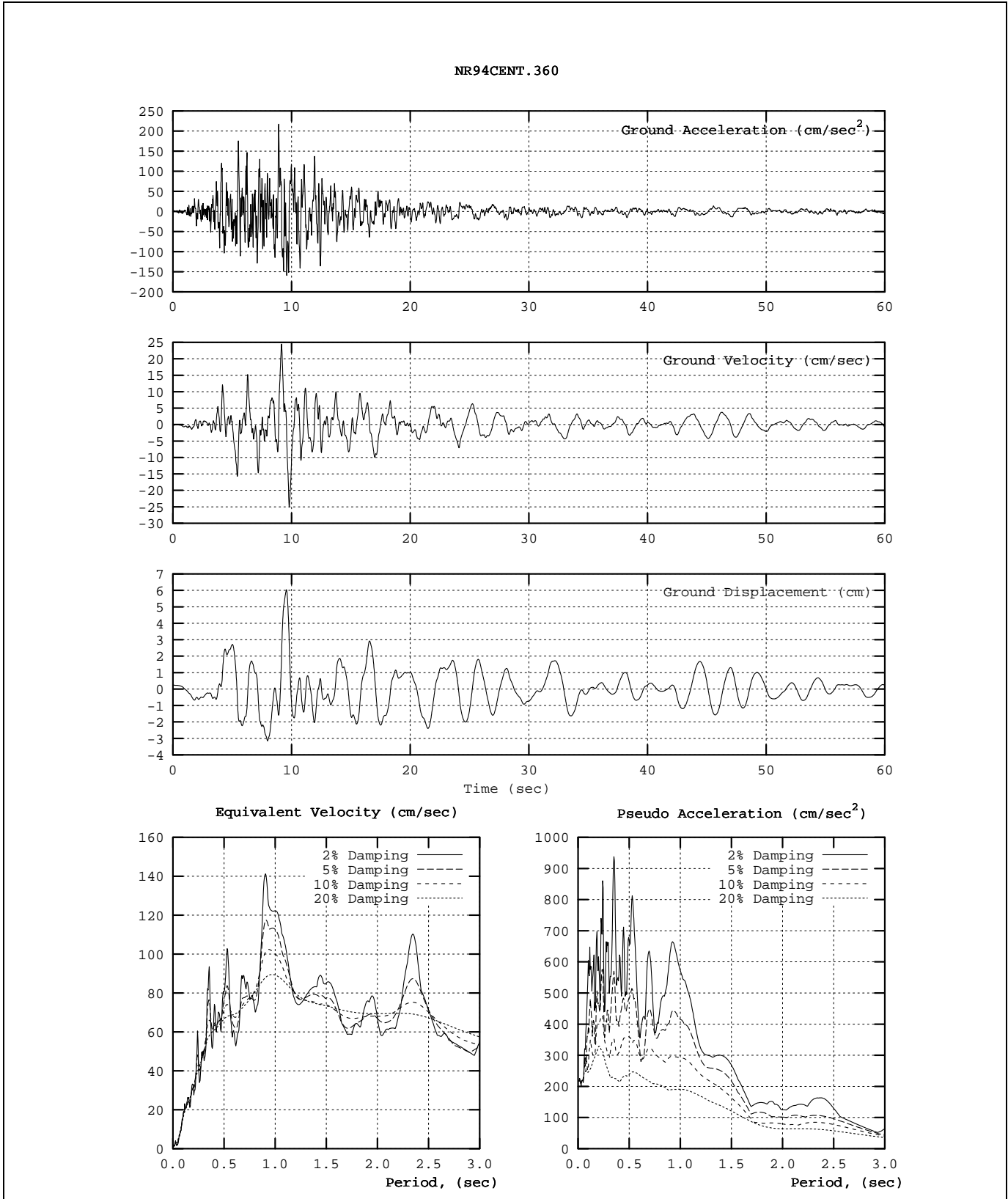


Figure 6-6 Characteristics of the NR94CENT.360 (Century City) Ground Motion

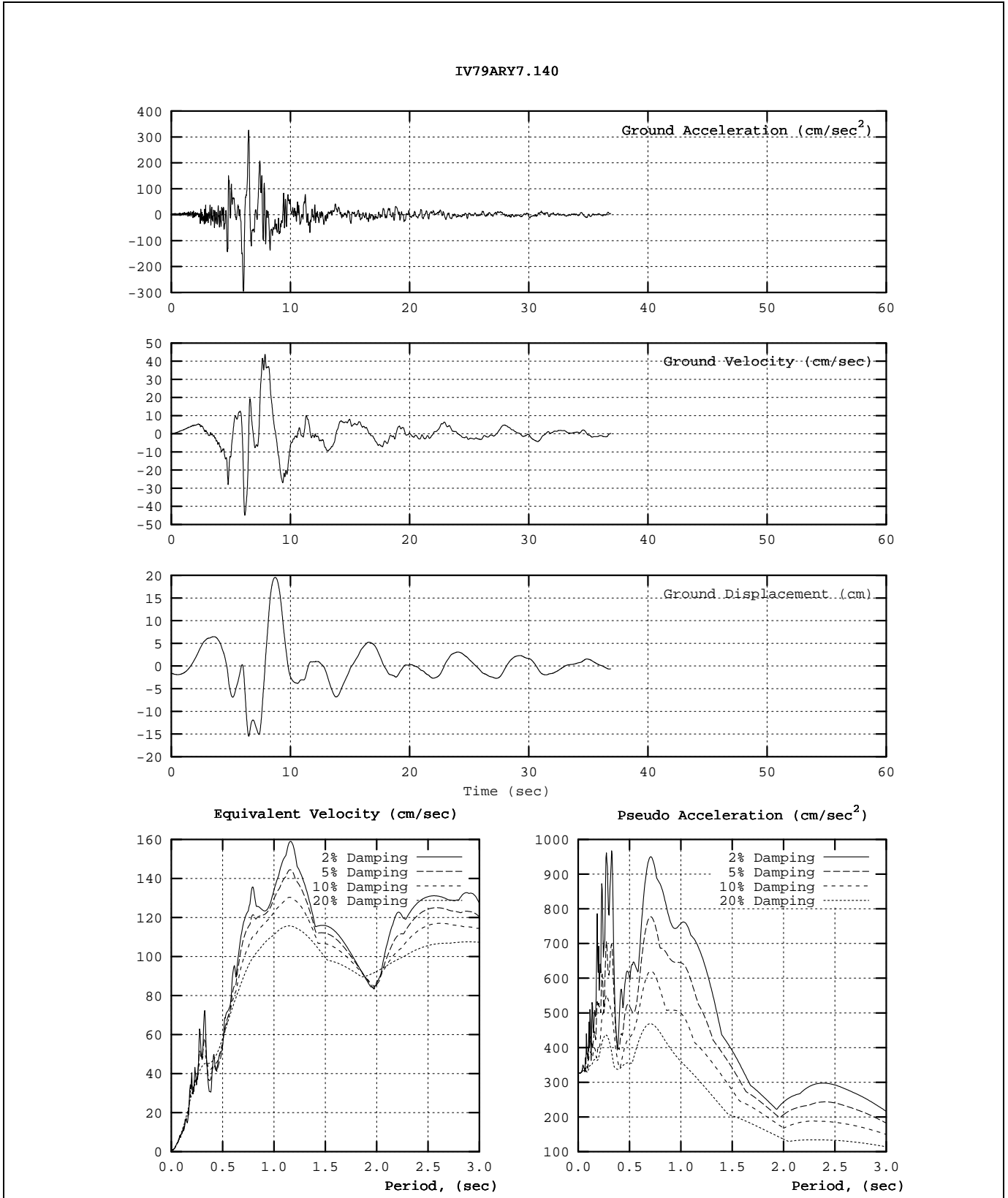


Figure 6-7 Characteristics of the IV79ARY7.140 (Imperial Valley Array) Ground Motion

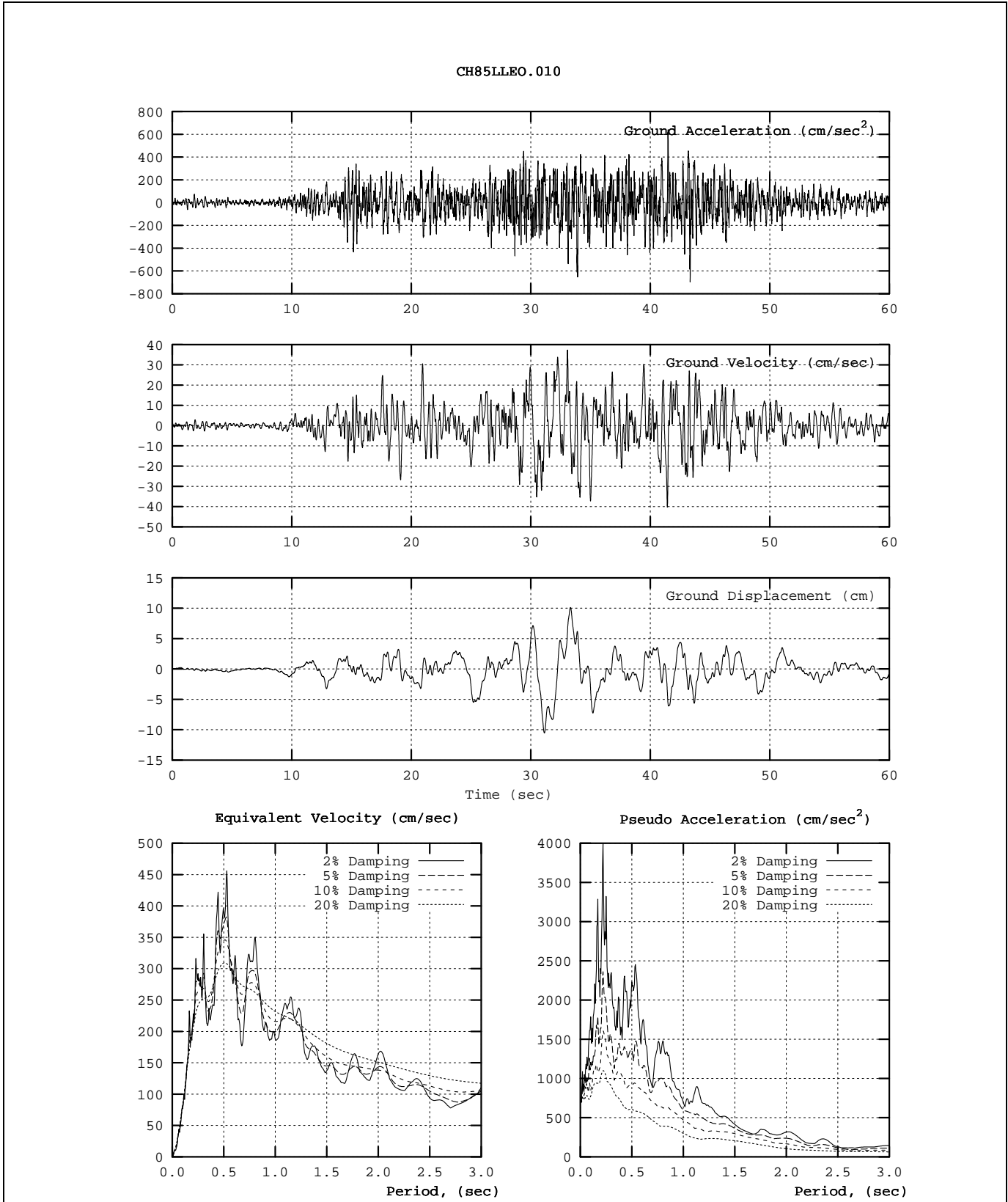


Figure 6-8 Characteristics of the CH85LLEO.010 (Llolleo) Ground Motion

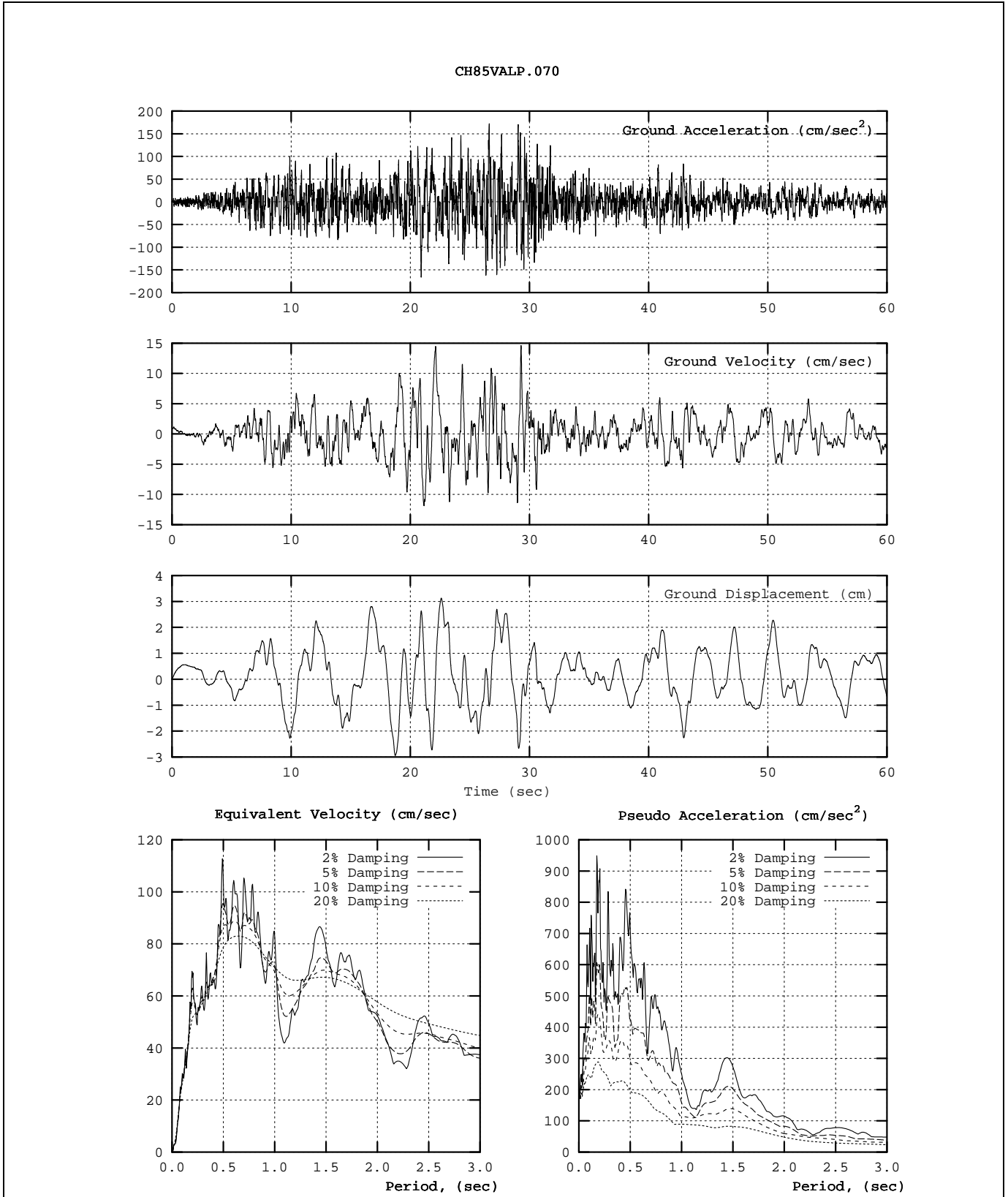


Figure 6-9 Characteristics of the CH85VALP.070 (Valparaiso University) Ground Motion

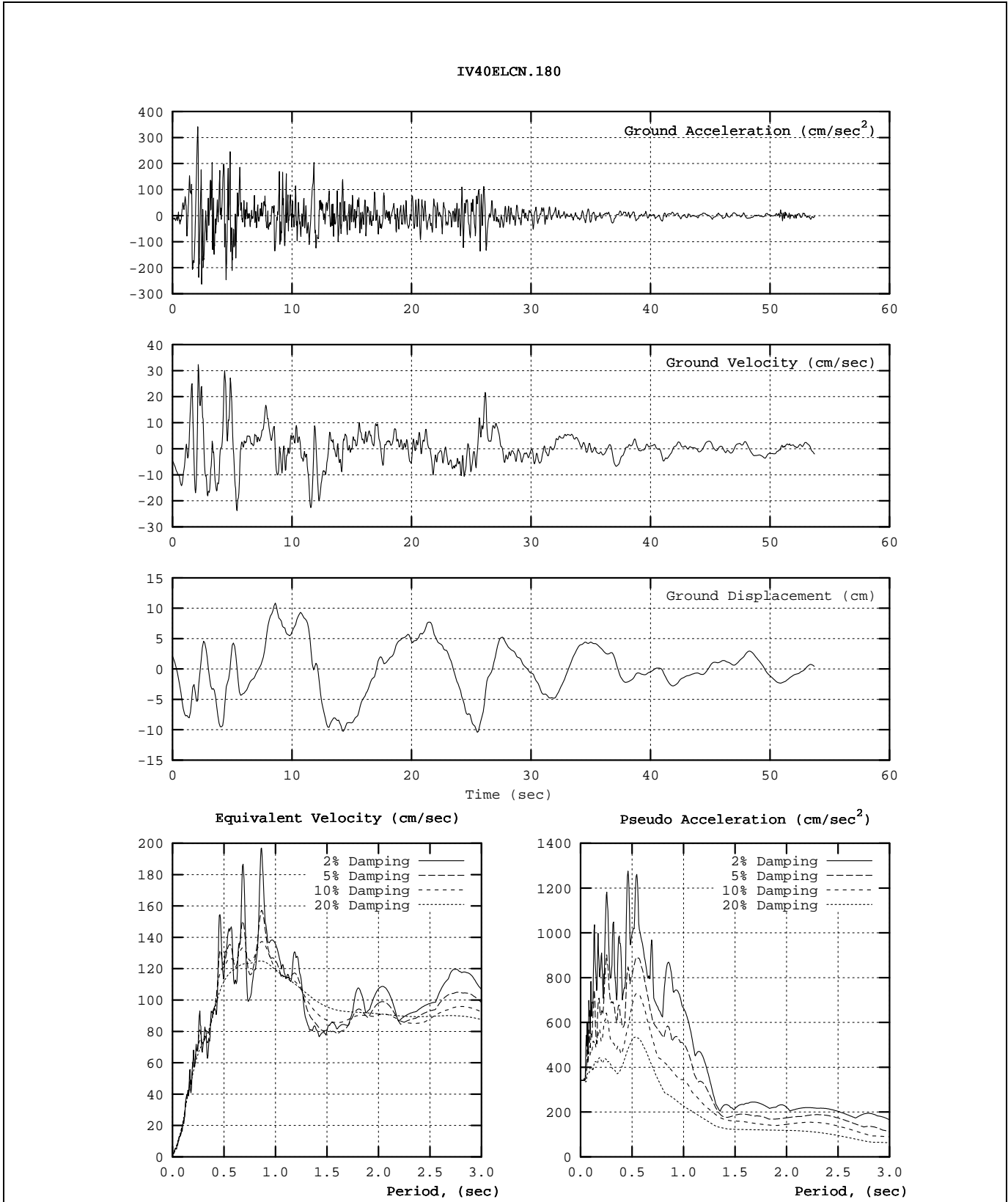


Figure 6-10 Characteristics of the IV40ELCN.180 (El Centro) Ground Motion

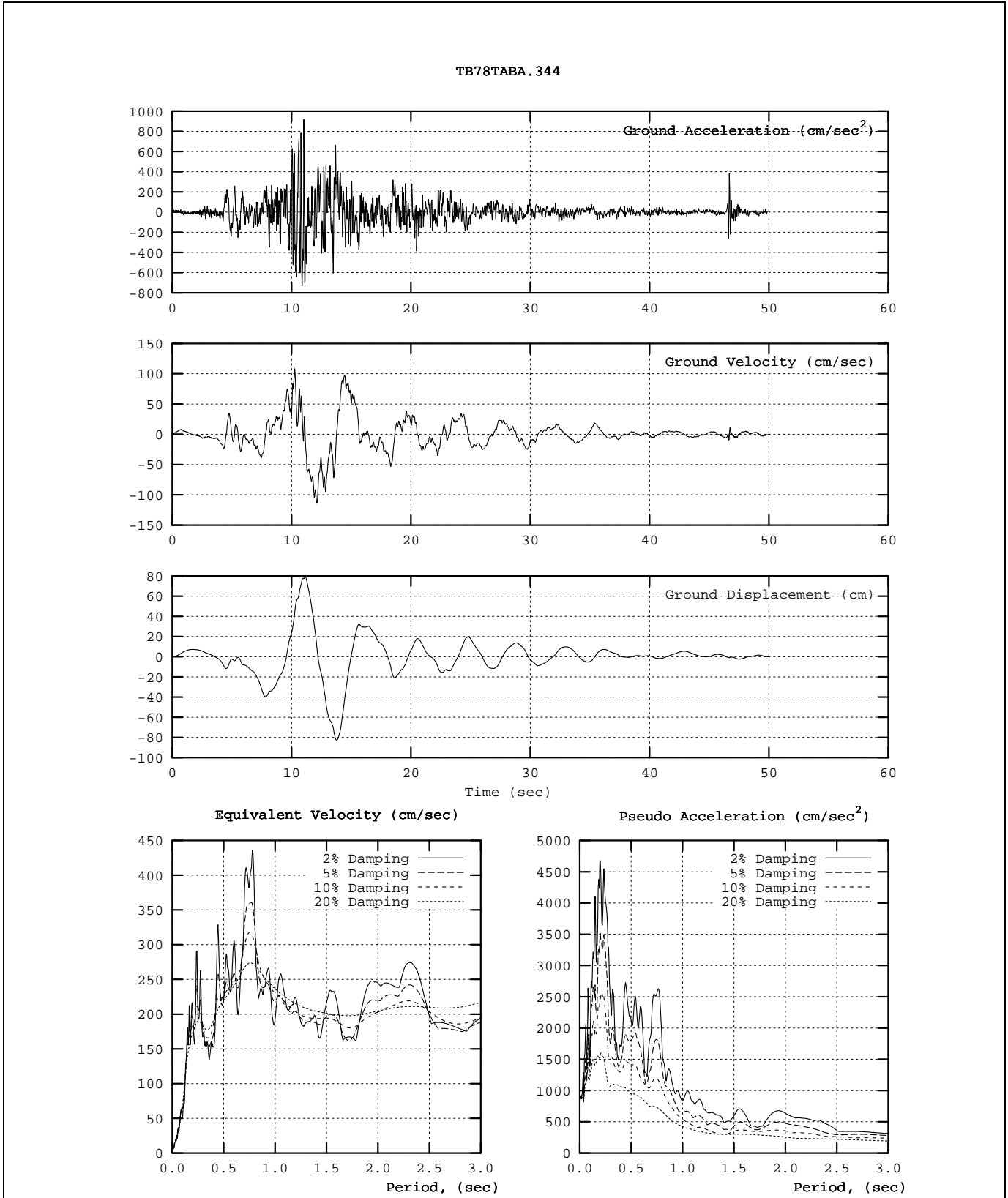


Figure 6-11 Characteristics of the TB78TABS.344 (Tabas) Ground Motion

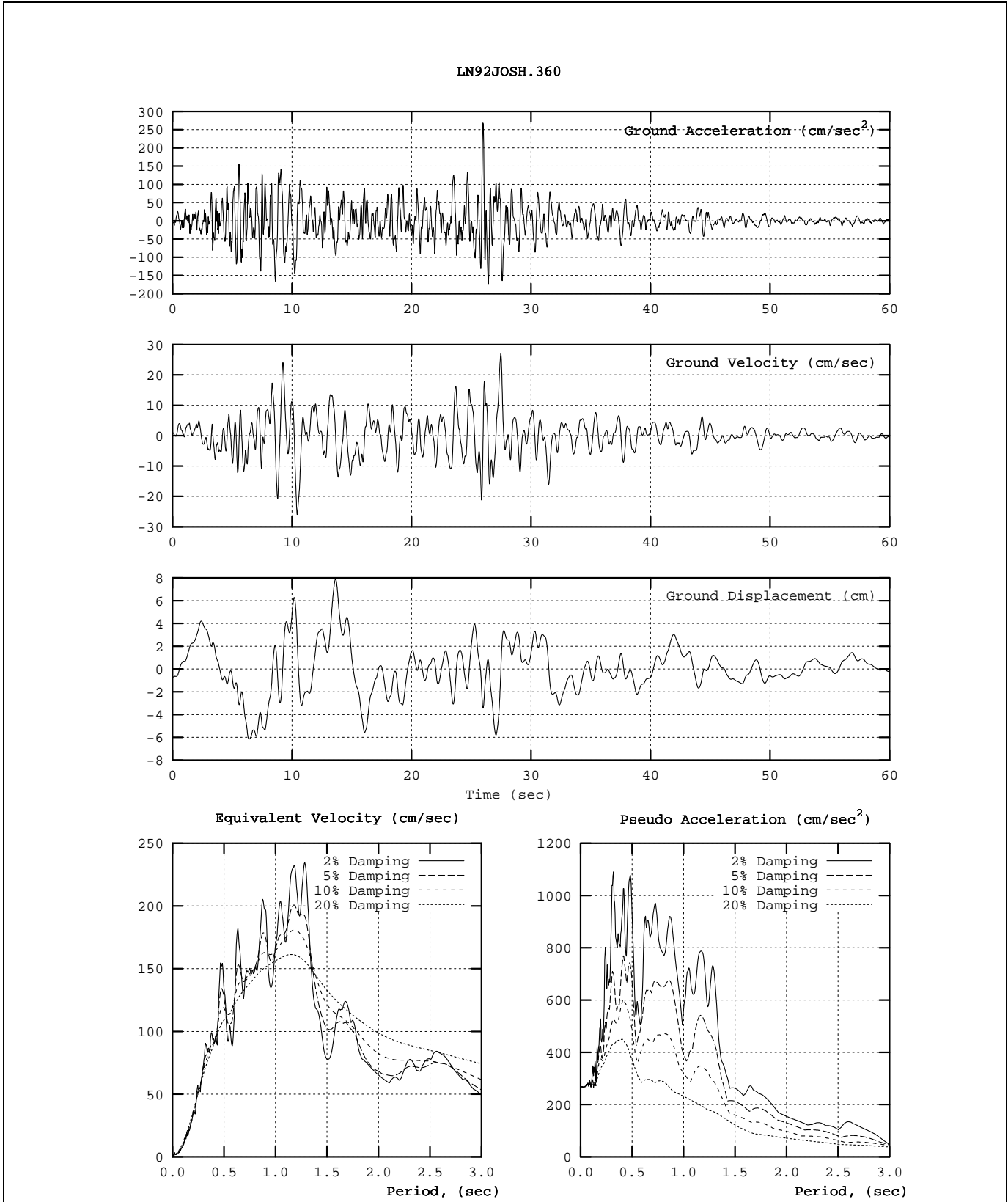


Figure 6-12 Characteristics of the LN92JOSH.360 (Joshua Tree) Ground Motion

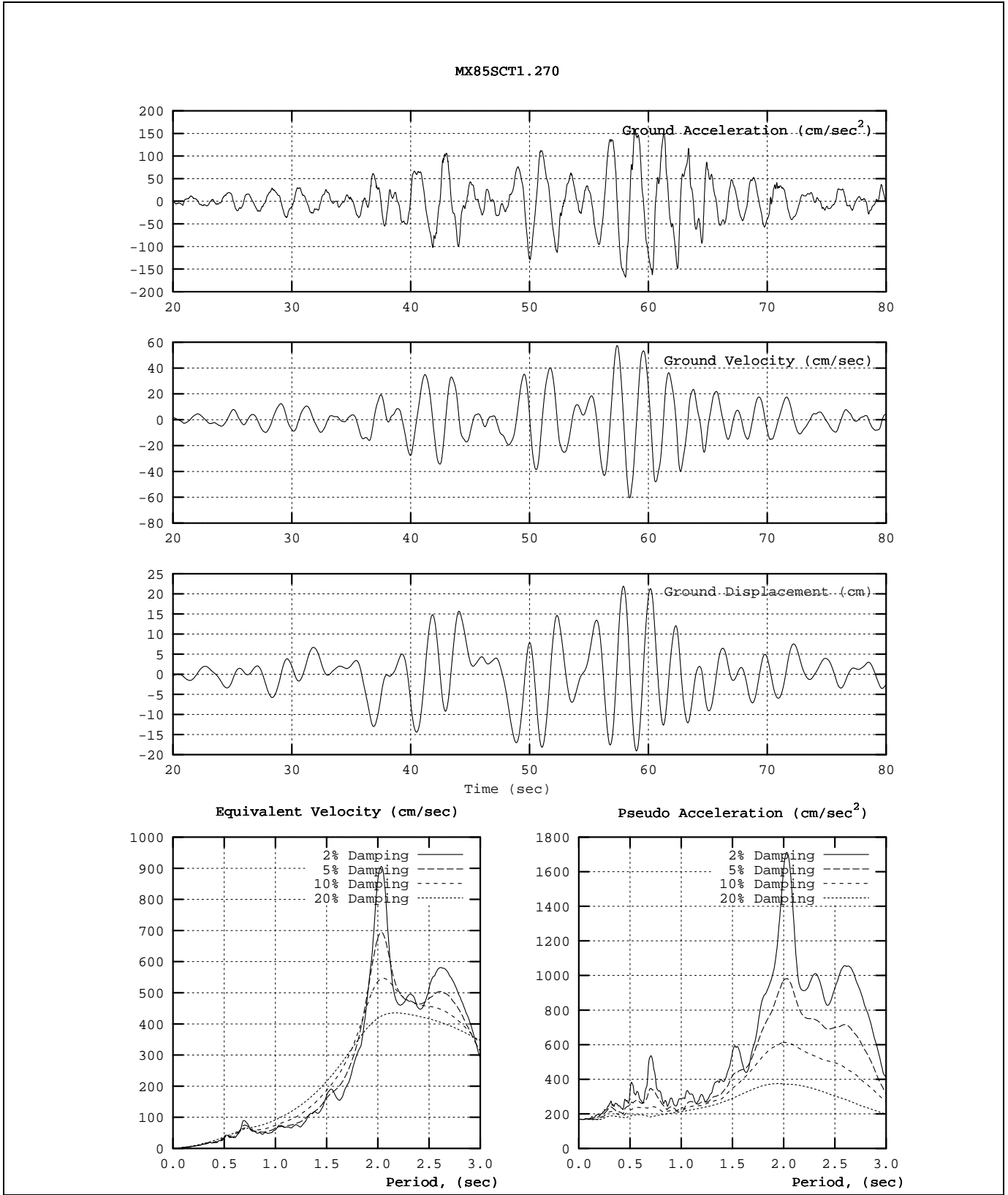


Figure 6-13 Characteristics of the MX85SCT1.270 (Mexico City) Ground Motion

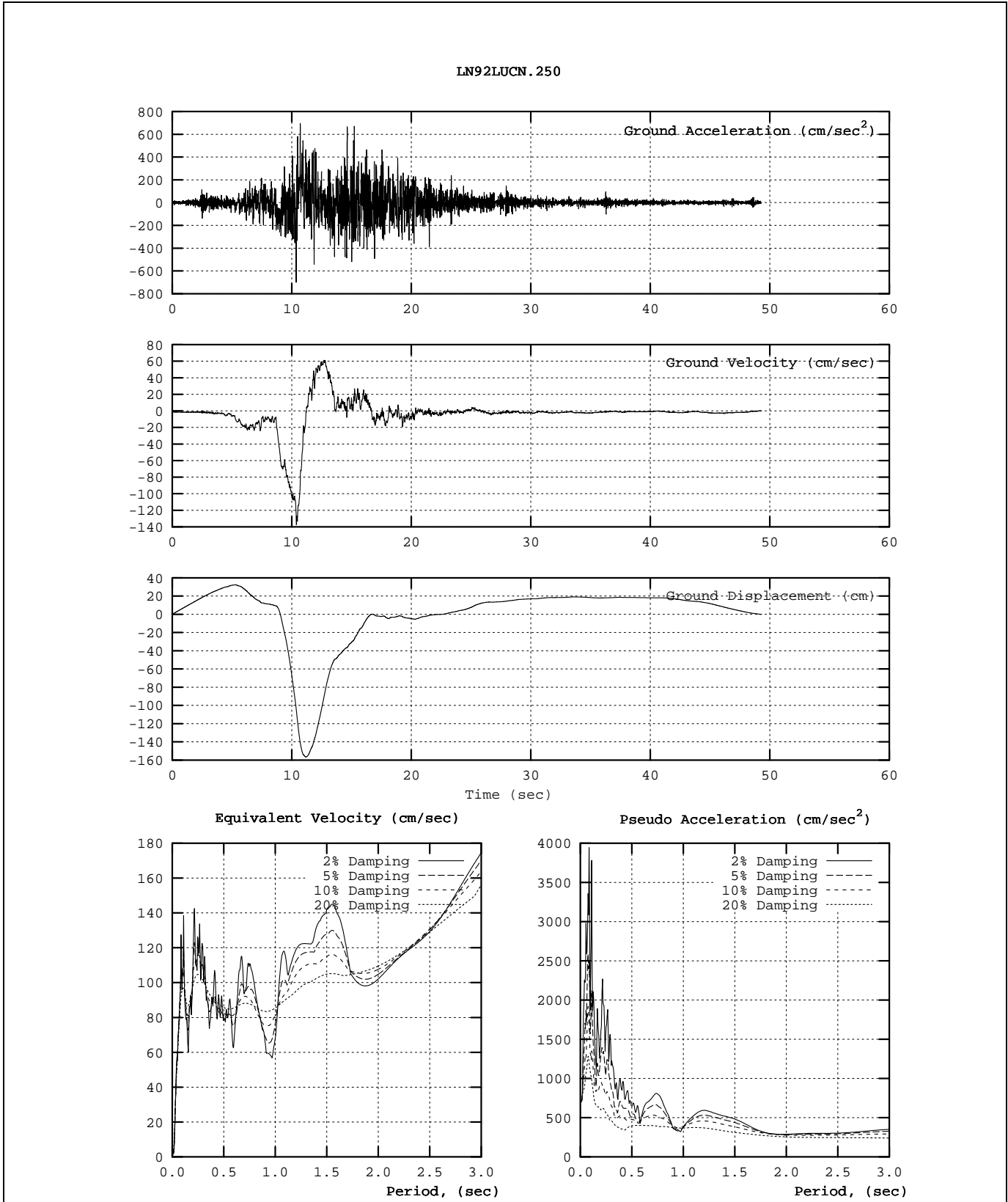


Figure 6-14 Characteristics of the LN92LUCN.250 (Lucerne) Ground Motion

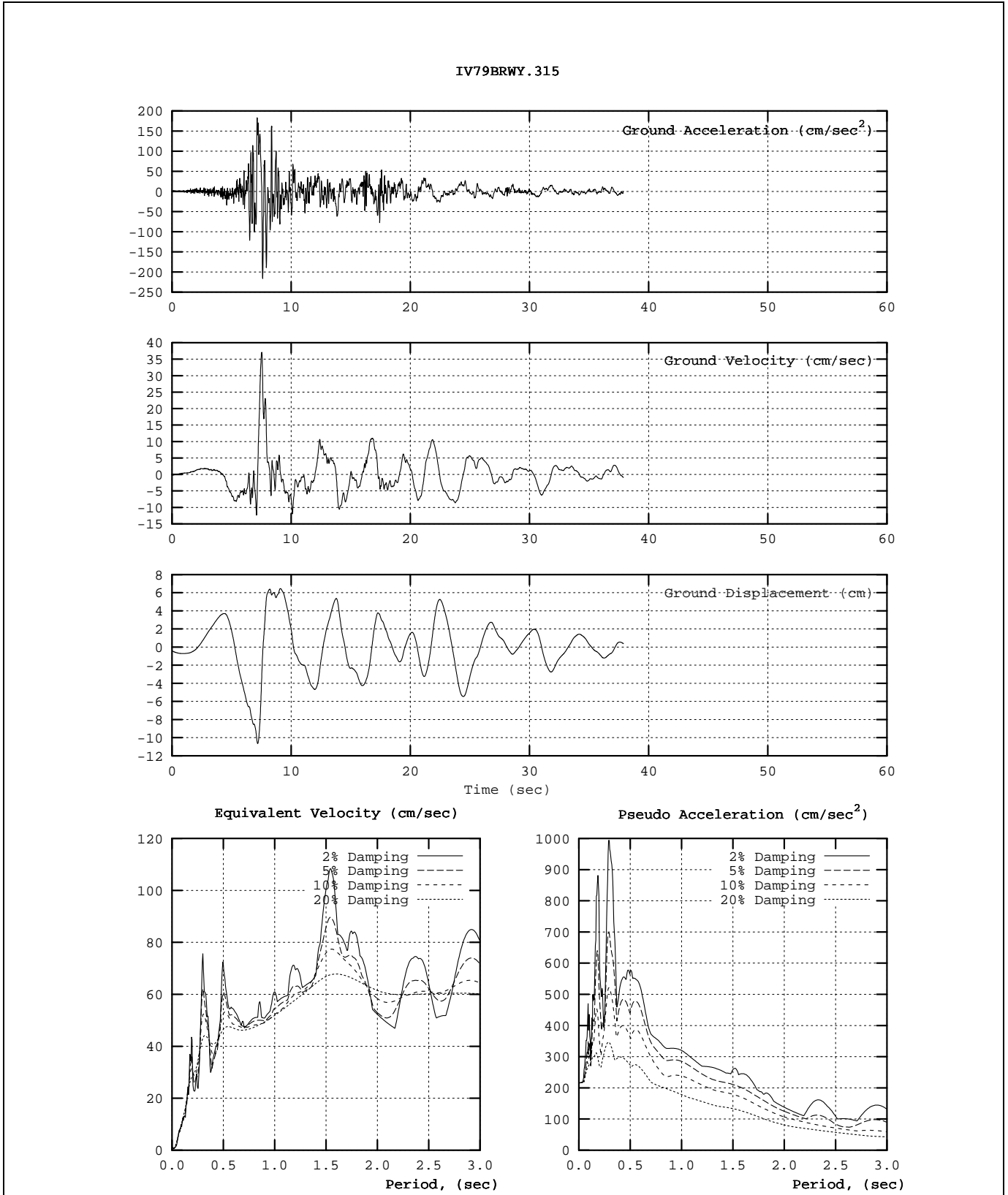


Figure 6-15 Characteristics of the IV79BRWY.315 (Brawley Airport) Ground Motion

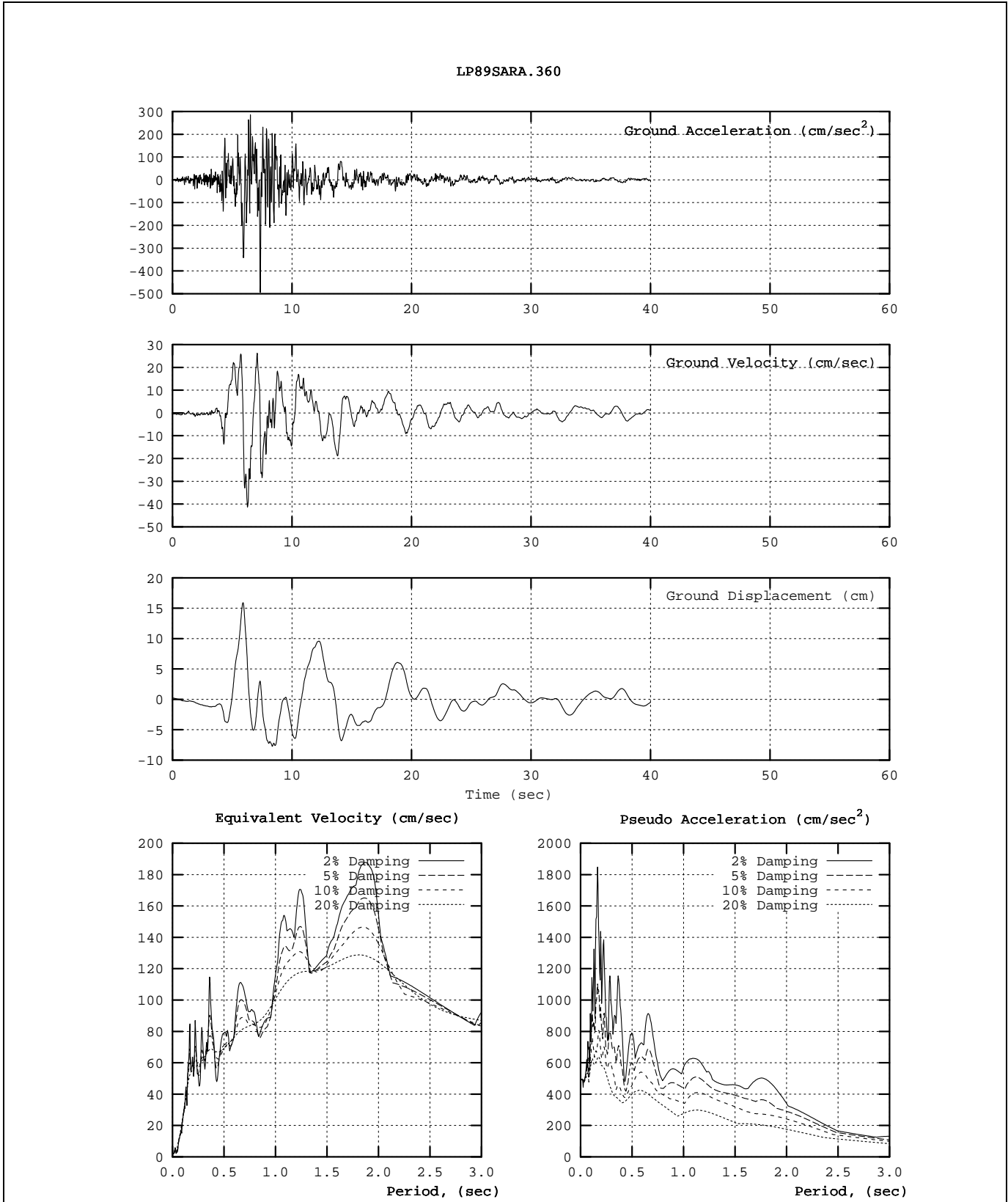


Figure 6-16 Characteristics of the LP89SARA.360 (Saratoga) Ground Motion

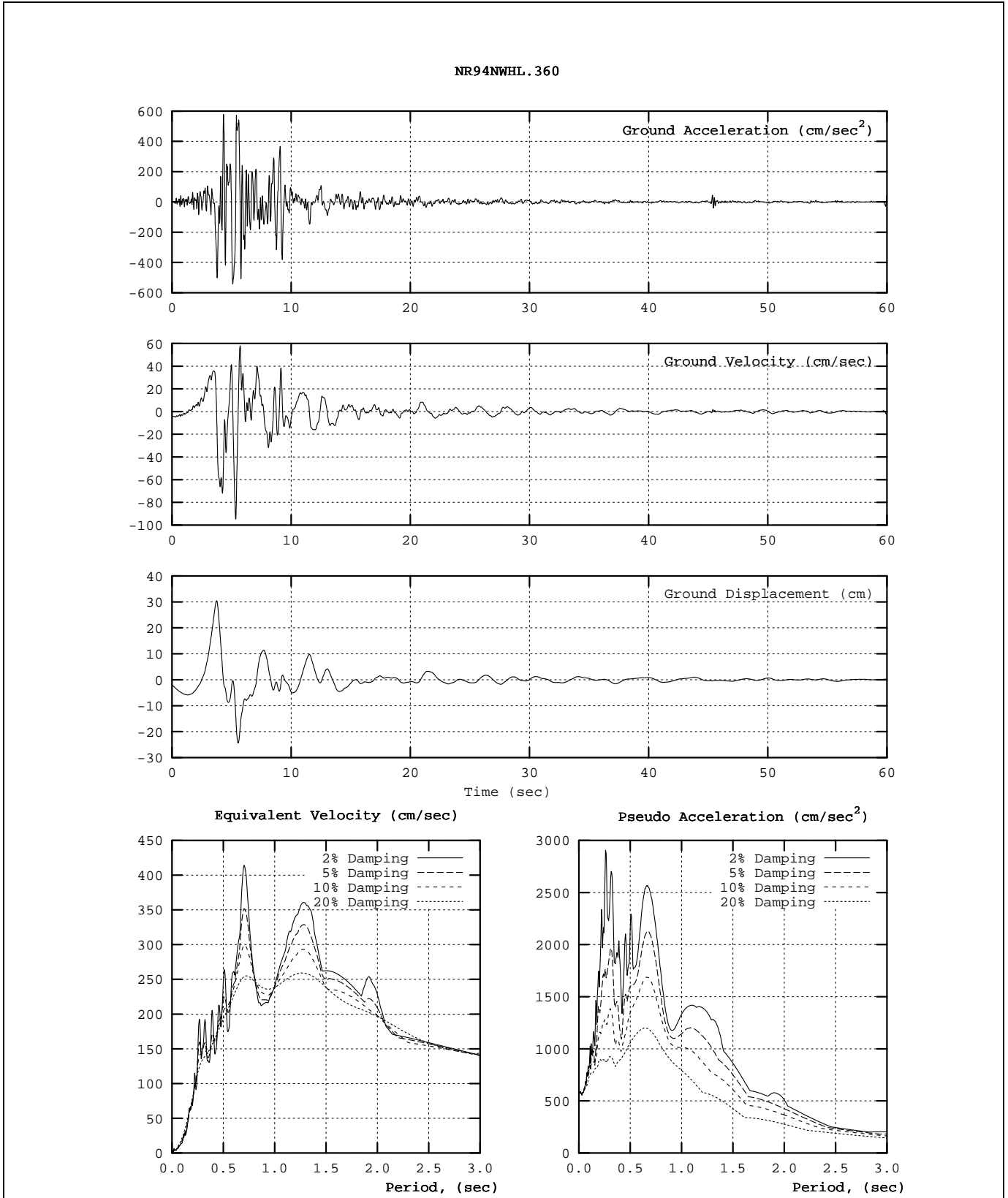


Figure 6-17 Characteristics of the NR94NWHL.360 (Newhall) Ground Motion

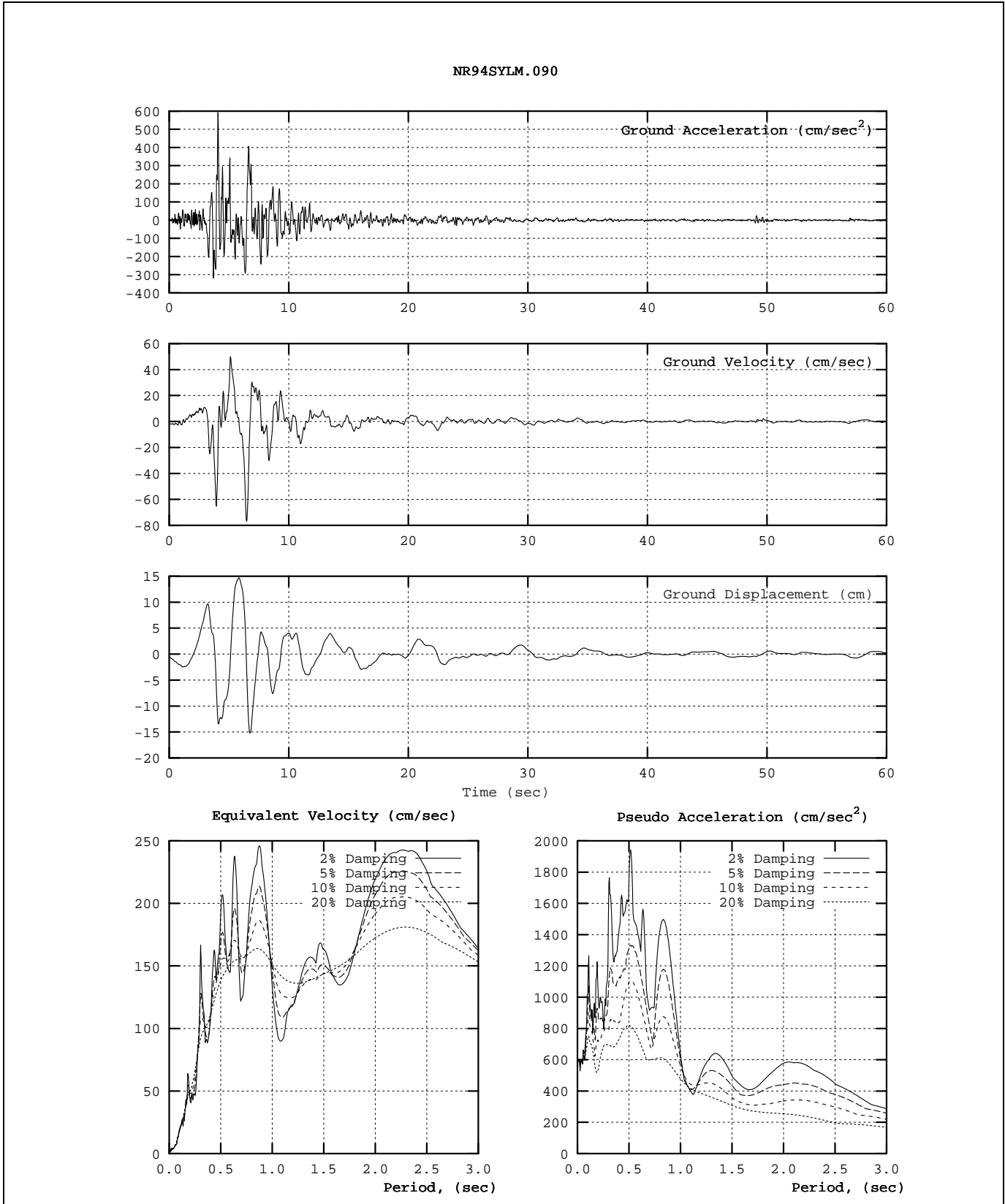


Figure 6-18 Characteristics of the NR94SYLM.090 (Sylmar Hospital) Ground Motion

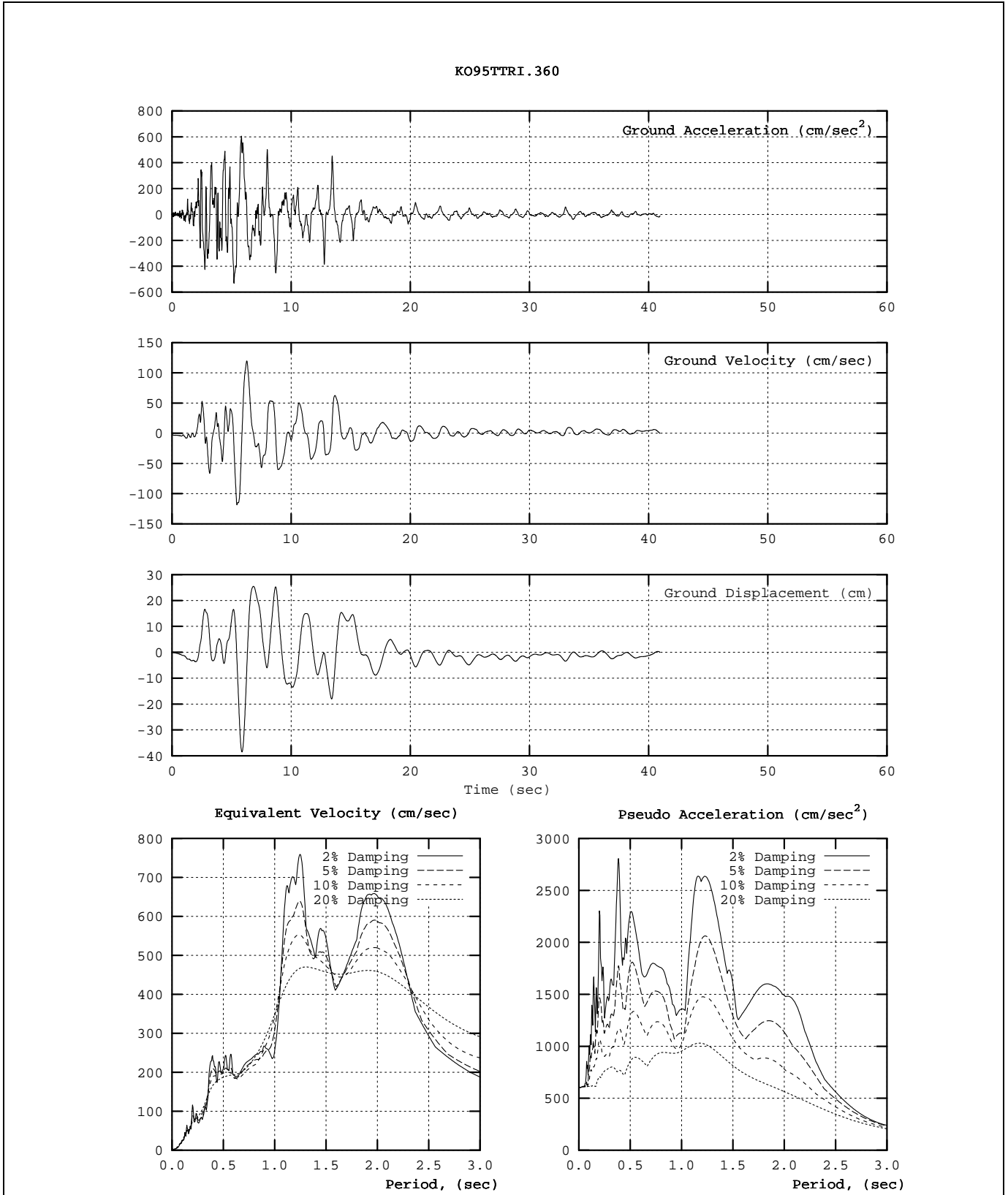


Figure 6-19 Characteristics of the KO95TTRI.360 (Takatori) Ground Motion

The characteristic period, T_g , of each ground motion was established assuming equivalent-velocity spectra and pseudo-acceleration spectra for linear elastic oscillators having 5% damping. The equivalent velocity, V_m , is related to input energy, E_m , and ground acceleration and response parameters by the following expression:

$$\frac{1}{2} m V_m^2 = E_m = m \int \ddot{x}_g \dot{x} dt \quad (6-1)$$

where m = mass of the single-degree-of-freedom oscillator, \ddot{x}_g = the ground acceleration, and \dot{x} = the relative velocity of the oscillator mass (Shimazaki and Sozen, 1984). The spectra present peak values calculated over the duration of the record.

The characteristic periods were determined according to engineering judgment to correspond approximately to the first (lowest-period) peak of the equivalent-velocity spectrum, and, at the same time, the period at which the transition occurs between the constant-acceleration and constant-velocity portions of a smooth design spectrum fitted to the 5% damped spectrum (Shimazaki and Sozen, 1984; Qi and Moehle, 1991; and Lepage, 1997). Characteristic periods were established prior to the dynamic analyses.

Other criteria are available to establish characteristic periods. For example, properties of the site, characterized by variation of shear-wave velocity with depth, may be used to establish T_g . Alternatively, the characteristic period may be defined as the lowest period for which the equal-displacement rule applies,

and thus becomes a convenient reference point to differentiate between short- and long-period systems.

6.3.4 Force/Displacement Models

The choice of force/displacement model influences the response time-history and associated peak response quantities. Ideally, the force/displacement model should represent behavior typical of wall buildings, including strength degradation and stiffness degradation.

Actual response depends on the details of structural configuration and component response, which in turn, depend on the material properties, dimensions, and strength of the components, as well as the load environment and the evolving dynamic load history (which can influence the type and onset of failure). The objective of the dynamic analyses is to identify basic trends in how prior damage affects system response in future earthquakes. Fulfilling this objective does not require the level of modeling precision that would be needed to understand the detailed response of a particular structure or component. For this reason, we selected relatively simple models that represent a range of behaviors that might be expected in wall buildings. Three broad types of system response can be distinguished:

- Type A: Stiffness-degrading systems with positive post-yield stiffness (Figure 6-20a).
- Type B: Stiffness-degrading systems with negative post-yield stiffness (Figure 6-20b).
- Type C: Pinched systems exhibiting strength and stiffness degradation (Figure 6-20c).

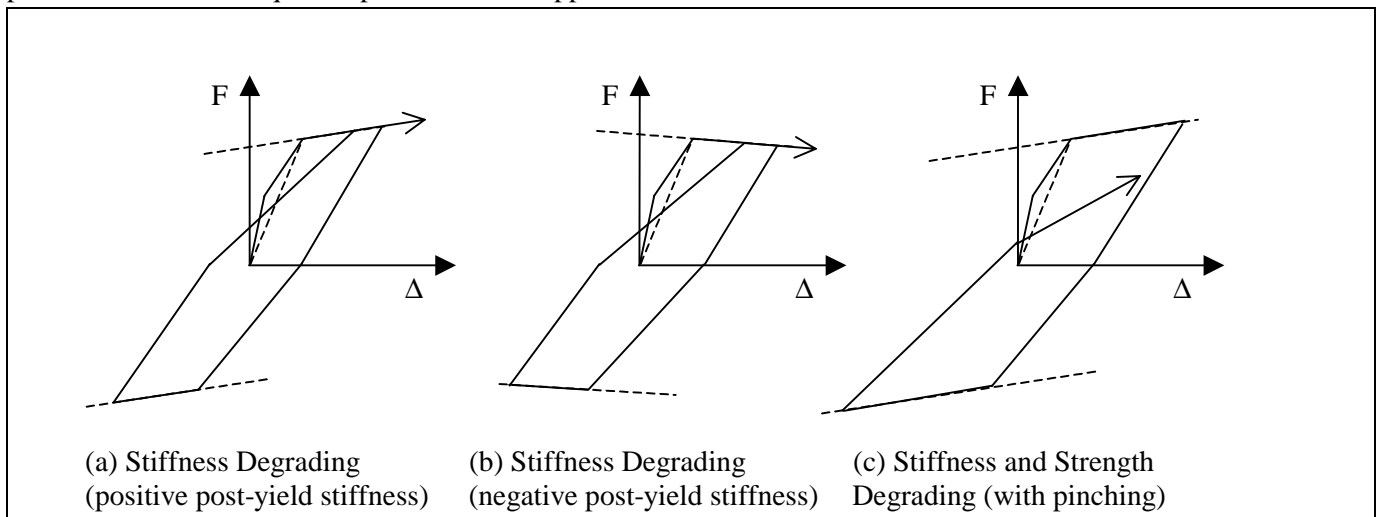


Figure 6-20 Force-Displacement Hysteretic Models

Type A behavior typically represents wall systems dominated by flexural response. Type B behavior is more typical of wall systems that exhibit some degradation in response with increasing displacement; degradation may be due to relatively brittle response modes. Type C behavior is more typical of wall systems that suffer degradation of strength and stiffness, including those walls in which brittle modes of response may predominate.

Type A behavior was represented in the analyses using the Takeda model (Takeda et al., 1970) with post-yield stiffness selected to be 5% of the secant stiffness at the yield point (Figure 6-21a). Previous experience (Section 6.2.1) indicates that this model represents stiffness degradation in reinforced concrete members exceptionally well. In addition, it is widely known by researchers, and it uses displacement ductility to parameterize stiffness degradation. The Takeda model features a trilinear primary curve that is composed of uncracked, cracked, and yielding portions. After yielding, the unloading stiffness is reduced in proportion to the square root of the peak displacement ductility. Additional rules are used to control other aspects of this hysteretic model. This model is subsequently referred to as “Takeda5”.

Type B behavior was represented in the analyses using the Takeda model with post-yield stiffness selected to be -10% of the yield-point secant stiffness (Figure 6-21b). This model is subsequently referred to as “Takeda10”.

Type C behavior was represented in the analyses by a modified version of the Takeda model (Figure 6-21c). The behavior is the same as for Type A, except for modifications to account for pinching and cyclic strength degradation. The pinching point is defined independently in the first and third quadrants (Figure 6-22). The pinching-point displacement is set equal to 30% of the current maximum displacement in the quadrant. The pinching-point force level is set equal to 10% of the current maximum force level in the quadrant. Cyclic strength degradation incorporated in this model is described in Section 6.3.6. This model is subsequently referred to as “TakPinch”.

Collectively, the Takeda5, Takeda10, and TakPinch models are referred to as degrading models in the body of this section. For these models, dynamic analyses were used to identify the effects of prior damage on response to future earthquakes. The analyses covered a number of relative strength values, initial periods of vibration, damage intensities, and performance-level earthquakes. For all dynamic analyses, damping was set equal to 5% of critical damping, based on the period of vibration that corresponds to the yield-point secant stiffness.

In addition, a bilinear model (Figure 6-23) was selected to establish the strength of the degrading oscillators, which were set equal to the strength required to achieve bilinear displacement ductility demands of 1 (elastic), 2, 4, and 8 for each reference period and for each of the 18 ground motions. The bilinear model does not exhibit stiffness or strength degradation. Besides establishing

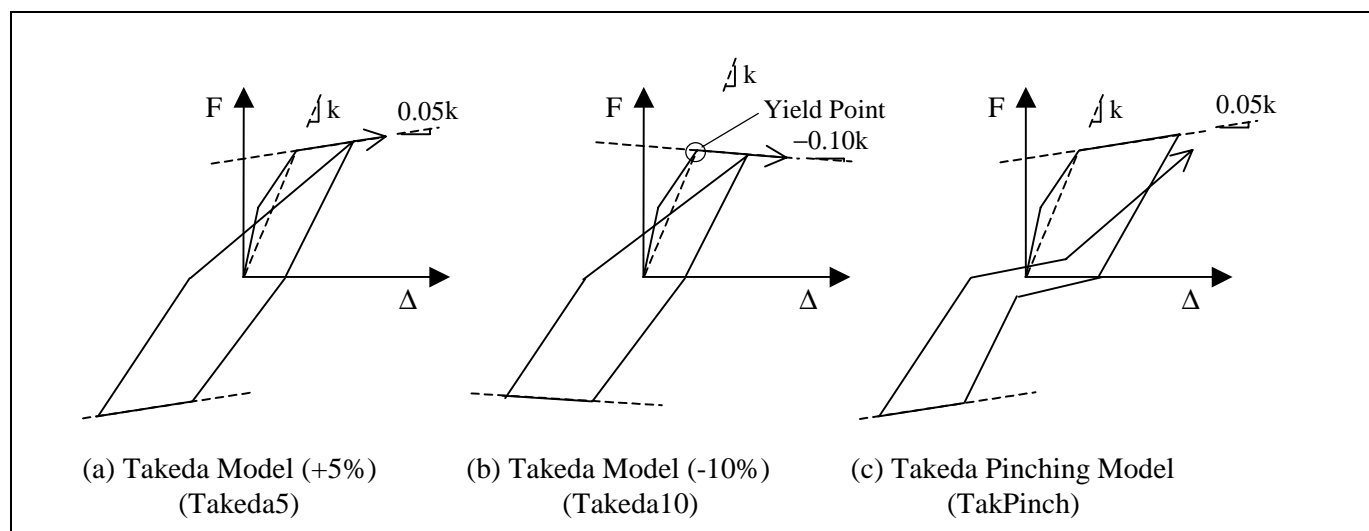


Figure 6-21 Degrading Models Used in the Analyses

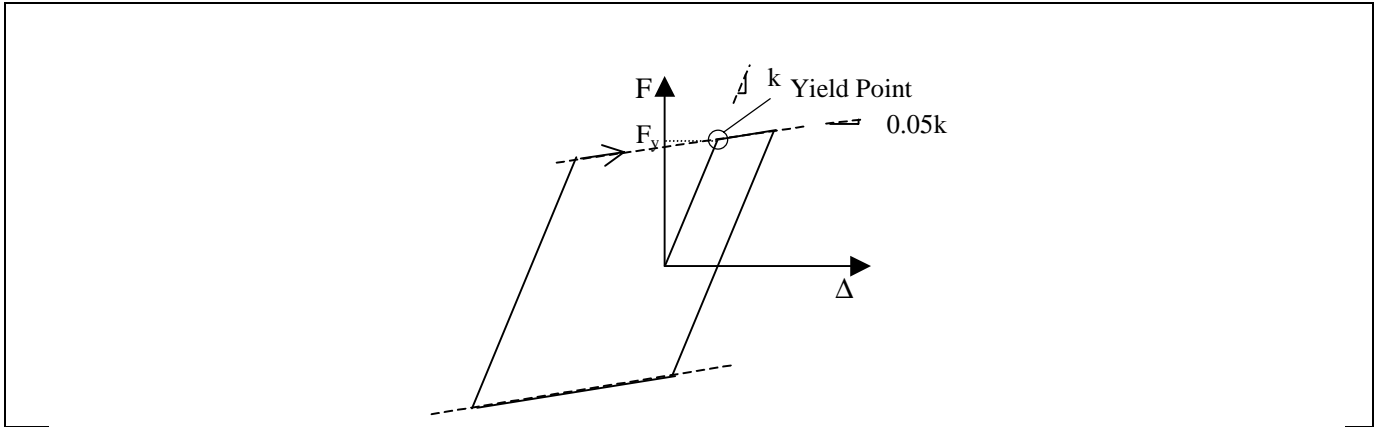


Figure 6-22 Bilinear Model Used to Determine Strengths of Degrading Models

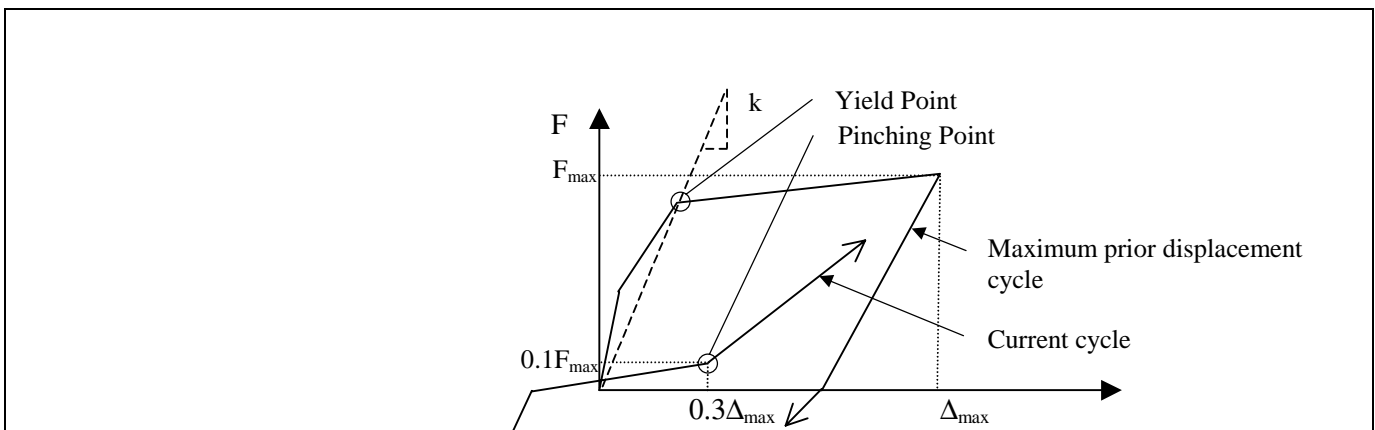


Figure 6-23 Specification of the Pinching Point for the Takeda Pinching Model

the strength of the oscillators, this model serves two additional purposes. First, results obtained in this study with the bilinear model can be compared with those obtained by other researchers to affirm previous findings and, at the same time, to develop confidence in the methods and techniques used in this study. Second, the bilinear model provides a convenient point of departure from which the effects of stiffness and strength degradation can be compared.

6.3.5 Undamaged Oscillator Parameters

To identify effects of damage on response, it is first necessary to establish the response of initially-undamaged oscillators to the same ground motions. The response of the undamaged oscillators is determined using the degrading models of Figure 6-21 for the performance-level ground motions.

The yield strength of all degrading models is set equal to the strength required to achieve displacement

ductility demands (DDD) of 1 (elastic), 2, 4, and 8 using the bilinear model. This is done at each period and for each ground motion. For any period and ground motion considered, the yield strength of the initially-undamaged models is the same, but only the bilinear model achieves the target displacement ductility demand. Where the same target displacement ductility demand can be achieved for various strength values, the largest strength value is used, as implemented in the computer program PCNSPEC (Boroschek, 1991).

The initial stiffness of the models is established to achieve initial (reference) vibration periods of 0.1, 0.2, 0.3, 0.4, 0.5, 0.6, 0.8, 1.0, 1.2, 1.5, and 2.0 seconds. These periods are determined using the yield-point secant stiffness for all the models considered.

For the undamaged Takeda models, the cracking strength is set equal to 50% of the yield strength, and the uncracked stiffness is set equal to twice the yield-point secant stiffness (Figure 6-24).

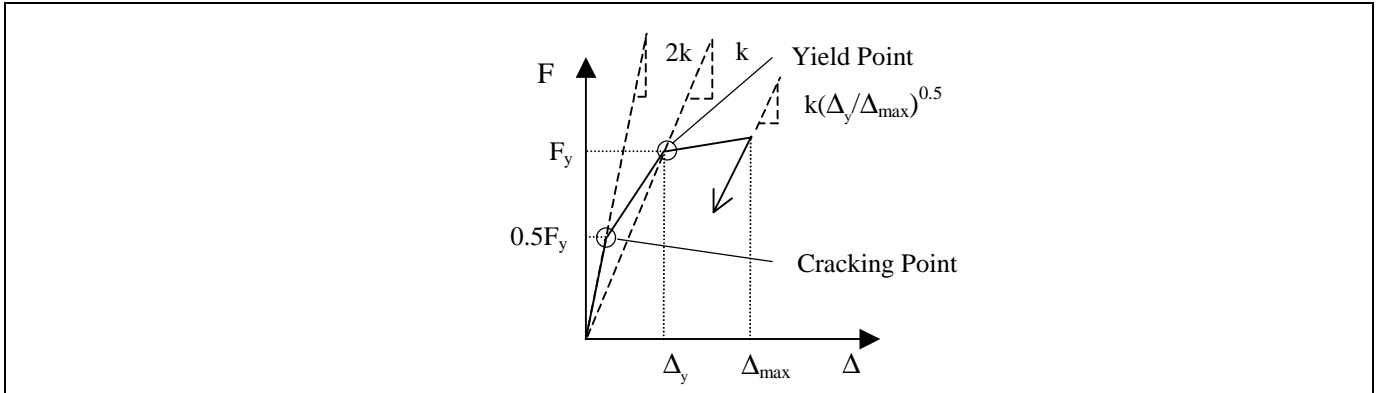


Figure 6-24 Specification of the Uncracked Stiffness, Cracking Strength, and Unloading Stiffness for the Takeda Models

6.3.6 Damaged Oscillator Parameters

Damage is considered by assuming that the force-displacement curves of the oscillators are altered as a result of previous inelastic response. Reduction in stiffness caused by the damaging earthquake is parameterized by prior ductility demand. Strength degradation is parameterized by the reduced strength ratio.

Each of the initially-undamaged degrading oscillators is considered to have experienced prior ductility demand (PDD) equal to 1, 2, 4, or 8 as a result of the damaging earthquake. The construction of an initially-damaged oscillator force/displacement curve is illustrated for a value of PDD greater than zero in Figure 6-25. The prior ductility demand also regulates the unloading stiffness of the Takeda model until larger displacement ductility demands develop.

The analytical study considered damaging earthquakes of smaller intensity than the performance-level earthquake. Consequently, the PDD values considered must be less than or equal to the design displacement ductility (DDD). Thus, an oscillator with strength established to achieve a displacement ductility of 4 is analyzed only for prior displacement ductility demands of 1, 2, and 4. The undamaged Takeda oscillators sometimes had ductility demands for the performance-level earthquake that were lower than their design values (DDD). Again, because the damaging earthquake is considered to be less intense than the performance-level event, oscillators having PDD in excess of the undamaged oscillator response were not considered further.

The Takeda models of the undamaged oscillators represent cracking behavior by considering the uncracked stiffness and the cracking strength. The effects of cracking in a previous earthquake were assessed by comparing the peak displacement response

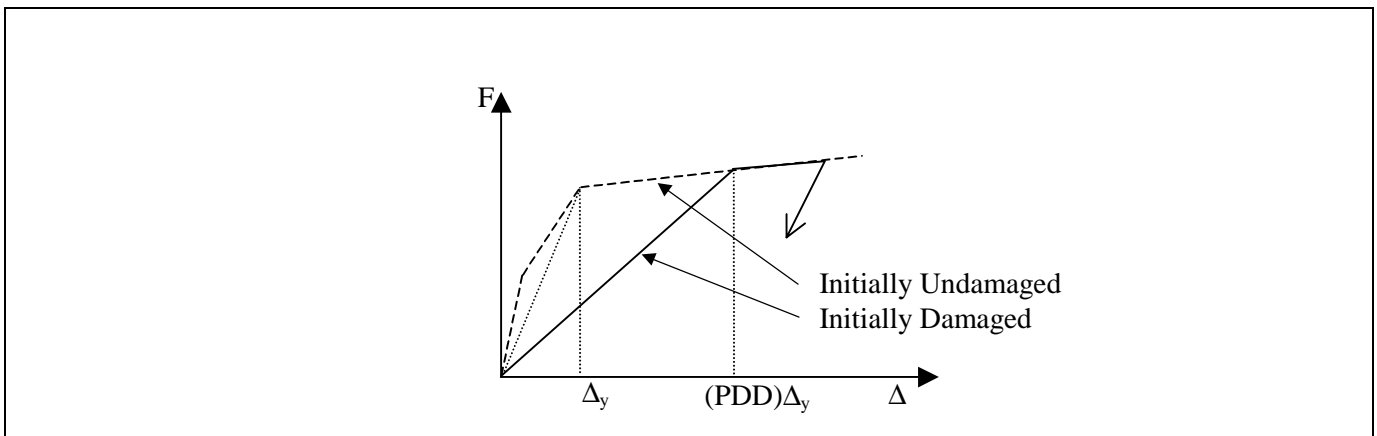


Figure 6-25 Construction of Initial Force-Displacement Response for Prior Ductility Demand > 0 and Reduced Strength Ratio = 1

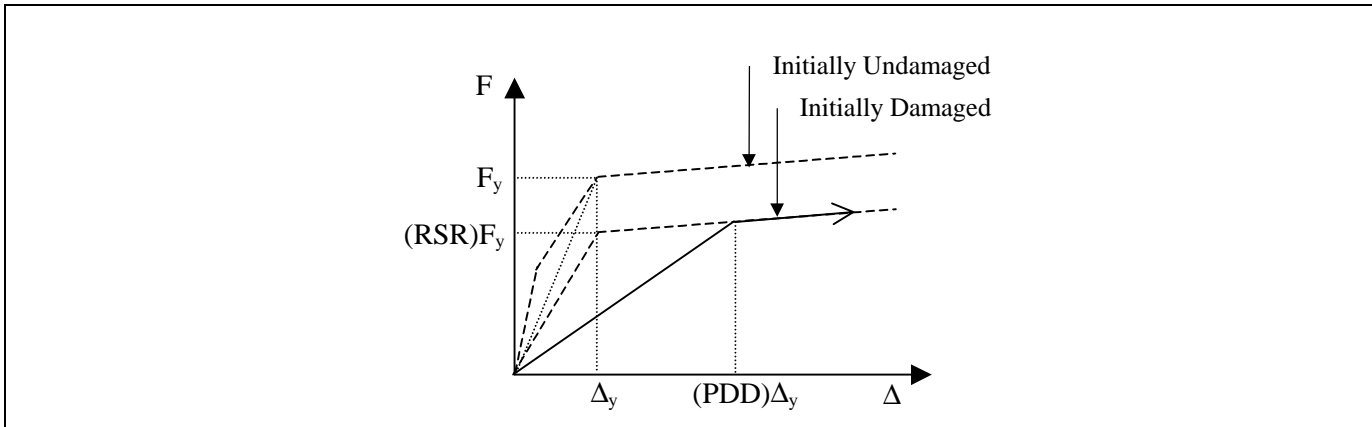


Figure 6-26 Construction of Initial Force-Displacement Response for $PDD > 0$ and $RSR < 1$ for Takeda5 and Takeda10 Models

of initially-uncracked oscillators to the response of oscillators that are initially cracked; that is, Takeda oscillators having a PDD of one. When larger PDD values are considered, the reductions in initial loading and unloading stiffness are determined in accordance with the Takeda model.

It is not obvious what degree of strength degradation is consistent with the PDDs, nor just how the degradation of strength should be modeled to represent real structures. We used two approaches to gauge the extent to which strength degradation might affect the response:

1. **Takeda5 and Takeda10 Oscillators:** The initial strength of the damaged models was reduced to try to capture the gross effects of strength degradation on response. The initial response of the damaged oscillator was determined using the construction of Figure 6-26. The resulting curve may represent a backbone curve that is constructed to approximate the response of a strength-degrading oscillator. For example, a structure for which repeated cycling causes a 20% degradation in strength relative to the primary curve may be modeled as having an initial strength equal to 80% of the undegraded strength.

If the backbone curve is established using the expected degraded-strength asymptotes, then the modeled structure tends to have smaller initial stiffness and larger displacement response relative to the ideal degrading structure. Consequently, the modeled response is expected to give an upper bound to the displacement response expected from the ideal model. If, instead, the backbone curve is selected to represent an average degraded response, using typical degraded-strength values rather than the lower asymptotic values, the computed response

should more closely approximate the response of the ideal model.

2. **TakPinch Oscillators:** Rather than begin with a reduced strength, a form of cyclic strength degradation was explicitly modeled for the Takeda Pinching oscillators. A trilinear primary curve was established (Figure 6-27), identical to the envelope curve used in the Takeda5 model. The curve exhibits cracking, a yield strength determined from the response of the bilinear models, and a post-yield stiffness equal to 5% of the yield-point secant stiffness. A secondary curve is established, having the same yield displacement and post-yield stiffness as the primary curve, but having yield strength equal to the reduced strength ratio (RSR) times the primary yield strength. For displacements less than the current maximum displacement in the quadrant, a reduced-strength point is defined at the maximum displacement at $0.5^n(1-RSR)F_y$, above the secondary curve strength, where n is the number of cycles approaching the current maximum displacement. The oscillator may continue beyond this displacement, and once it loads along the primary curve, n is reset to one, to cause the next cycle to exhibit strength degradation. The term $(1-RSR)F_y$ is simply the strength difference between the primary and secondary curves, and the function 0.5^n represents an asymptotic approach toward the secondary curve with each cycle. In each cycle, the strength is reduced by half the distance remaining between the current curve and the secondary curve. Pinching and strength degradation are modeled independently in the first and third quadrants.

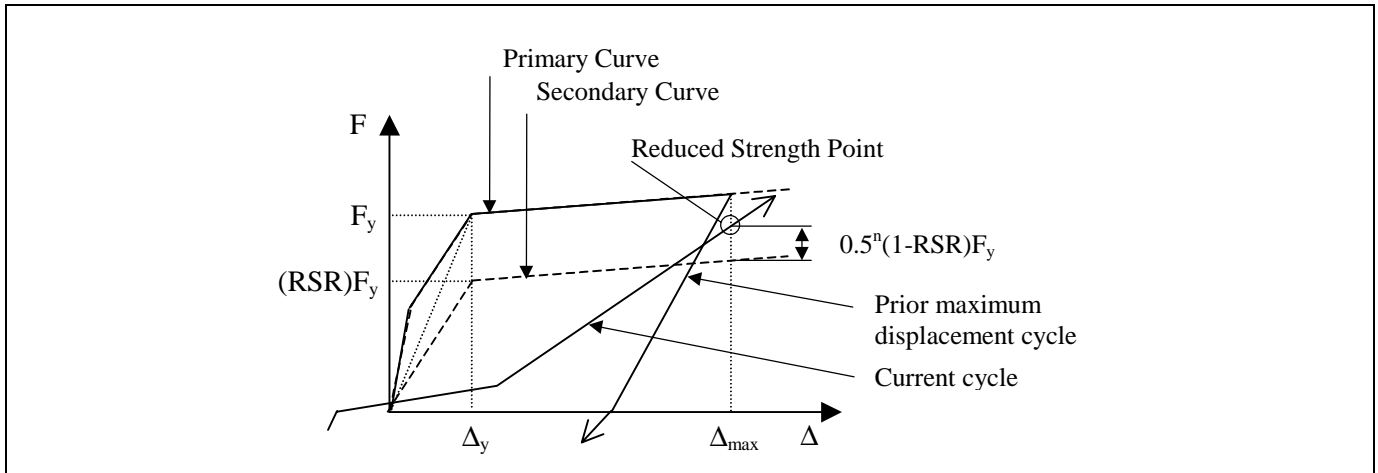


Figure 6-27 Strength Degradation for Takeda Pinching Model

For the TakPinch models, strength degradation is modeled with and without PDD. When PDD is present, the oscillator begins with n equal to one. This represents a single previous cycle to the PDD displacement, and corresponds to initial loading towards a reduced-strength point halfway between the primary and secondary curves at the PDD displacement (Figure 6-28).

For the other degrading models, strength reduction is considered possible only for PDDs greater than zero.

The parameter RSR is used to describe strength degradation in the context of the Takeda Pinching models and strength reduction in the context of the other degrading models. For this study, values of RSR were arbitrarily set at 100%, 80%, and 60%.

Oscillators were referenced by their initial, undamaged vibration periods, determined using the yield-point secant stiffness, regardless of strength loss and PDDs. Note that changes in strength further affect the initial stiffness of the damaged oscillators.

While the values of the parameters used to model Type A, B, and C behaviors, as well as the hysteresis rules themselves, were chosen somewhat arbitrarily, they were believed to be sufficiently representative to allow meaningful conclusions to be made regarding the effects of prior damage on response characteristics of various wall structures. Values of RSR and PDD were selected to identify trends in response characteristics, not to represent specific structures.

6.3.7 Summary of Dynamic Analysis Parameters

Nonlinear dynamic analyses were conducted for SDOF systems using various force/displacement models, various initial strength values, and for various degrees of damage. The analyses were repeated for the 18 selected ground-motion records. The analysis procedures are summarized below.

1. Initially-undamaged oscillators were established at eleven initial periods of vibration, equal to 0.1, 0.2, 0.3, 0.4, 0.5, 0.6, 0.8, 1.0, 1.2, 1.5, and 2.0 seconds. At these periods, the strength necessary to obtain design displacement ductilities (DDD) of 1 (elastic), 2, 4, and 8 were obtained using the bilinear model for each earthquake. This procedure establishes 44 oscillators for each of 18 ground motions.
2. The responses of the oscillators designed in step 1 were computed using the three degrading models (Takeda5, Takeda10, and TakPinch). The yield strength of the degrading oscillators in this step is identical to that determined in the previous step for the bilinear model. The period of vibration of the degrading oscillators, when based on the yield-point secant stiffness, matches that determined in the previous step for the bilinear model.
3. Damage is accounted for by assuming that the force/displacement curves of the oscillators are altered as a result of previous inelastic response. The extent of prior damage is parameterized by PDD. For some cases, the strength of the oscillators is reduced as well. Each of the initially-undamaged, degrading oscillators was considered to have experienced a PDD equal to 1, 2, 4, or 8, but not in excess of the ductility demand for which the oscilla-

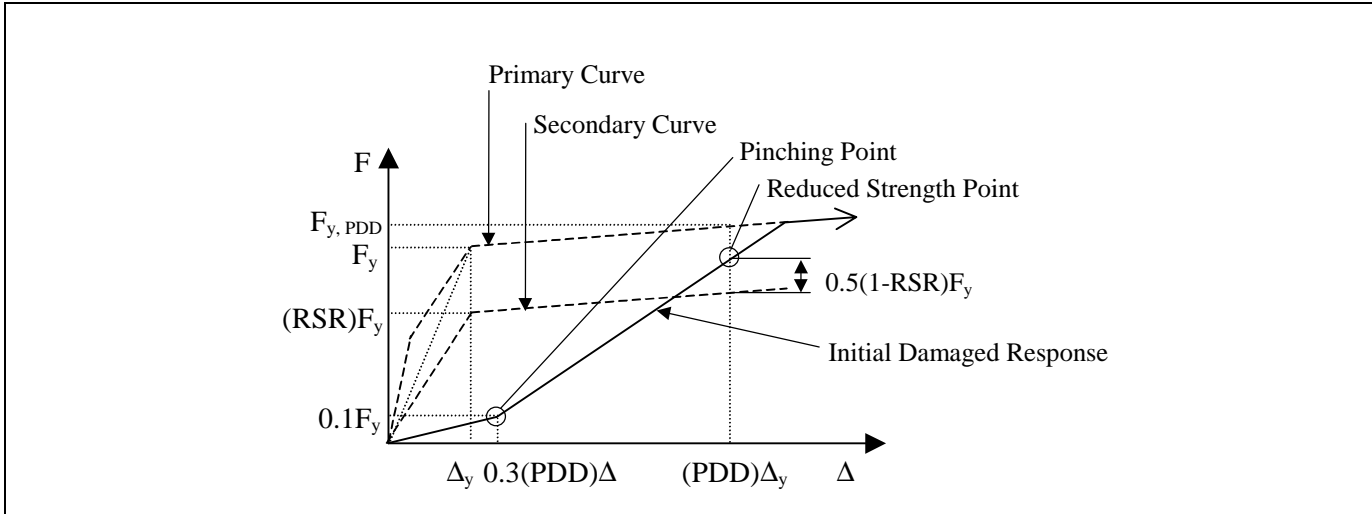


Figure 6-28 Construction of Initial Force-Displacement Response for $PDD > 0$ and $RSR < 1$ for Takeda Pinching Model

tor was designed. The effects of cracking on response were determined by considering a PDD of one. Where larger PDDs are considered, reductions in the initial loading and unloading stiffness were determined in accordance with the Takeda model.

4. Strength degradation was modeled explicitly in the TakPinch model. In the Takeda5 and Takeda10 models, strength degradation was approximated by reducing the initial strength of the damaged Takeda5 and Takeda10 models. RSRs equal to 100%, 80%, and 60% were considered. Although the strength reduction considered in the Takeda 5 and Takeda10 models does not model the evolution of strength loss, it suggests an upper bound for the effect of strength degradation on response characteristics.

6.3.8 Implementation of Analyses

Over 22,000 inelastic SDOF analyses were conducted using a variety of software programs. The strength of the oscillators was determined using constant-ductility iterations for the bilinear oscillators using the program PCNSPEC (Boroschek, 1991), a modified version of NONSPEC (Mahin and Lin, 1983). Response of the Takeda models was computed using a program developed by Otani (1981). This program was modified at the University of Illinois to include the effects of PDD, pinching, and strength degradation and to identify collapse states for models with negative post-yield stiffness.

6.4 Results Of Dynamic Analyses

6.4.1 Overview and Nomenclature

This section describes results obtained from the dynamic analyses. Section 6.4.2 characterizes the ground motions in terms of strength and displacement demand characteristics for bilinear oscillators, in order to establish that the ground motions and procedures used give results consistent with previous studies. Section 6.4.3 discusses the response of the Takeda models in some detail, for selected values of parameters. Section 6.4.4 presents summary response statistics for the Takeda models for a broader range of parameter values.

Several identifiers are used in the plots, as follows:

Records:

- SD= Short-duration ground motions.
- LD= Long-duration ground motions.
- FD= Forward-directivity ground motions.

DDD: Design Displacement Ductility. Strength was determined to achieve the specified DDD response for bilinear oscillators having post-yield stiffness equal to 5% of the initial stiffness. Values range from 1 to 8.

PDD: Prior Ductility Demand. This represents a modification of loading and unloading stiffness, to simulate damage caused by

previous earthquakes. Values range from 1 to 8, but not in excess of DDD.

RSR: Reduced Strength Ratio. This represents a reduction or degradation of strength and associated changes in stiffness. Values range from 100% to 60%, as detailed in Figures 6-26, 6-27, and 6-28.

Displacements:

d_d = Peak displacement response of undamaged oscillator

d'_d = Peak displacement response of damaged oscillator

d_e = Peak displacement response of elastic oscillator having stiffness equal to the yield-point secant stiffness of the corresponding Takeda oscillator

Space constraints limit the number of included figures. Selected results for oscillators designed for a displacement ductility of 8 are presented below. Elastic response characteristics are presented as part of the ground motion plots in Figures 6-2 to 6-19.

6.4.2 Response of Bilinear Models

Figures 6-29 to 6-31 present the response of bilinear models to the SD, LD, and FD ground motions, respectively. The ratio of peak displacement of the inelastic model to the peak displacement response of an elastic oscillator having the same initial period, d_d/d_e , is presented in the upper plot of each figure. The lower plot presents the ratio of elastic strength demand to the yield strength provided in order to attain the specified DDD, which in this case equals 8.

When the strength reduction factor, R , has a value of 8, the inelastic design strength is 1/8 of the elastic strength. For DDD = 8, an $R = 8$ means that the reduced inelastic design strength and the resulting oscillator ductility are equal. If R is greater than 8, say 12, for DDD = 8, then the reduced inelastic design strength of the structure can be 1/12 of the expected elastic strength to achieve an oscillator ductility of 8. That is, for any R , the structure can be designed for 1/ R times the elastic needed strength to achieve a ductility of DDD.

Response to each ground motion is indicated by the plotted symbols, which are ordered by increasing characteristic period, T_g . It was found that the displacement and strength data are better organized when plotted against the ratio T/T_g instead of the reference period, T . The plots present data only for

$T/T_g < 4$ in order to reveal sufficient detail in the range $T/T_g < 1$.

The trends shown in Figures 6-29 through 6-31 resemble those reported by other researchers, for example, Shimazaki and Sozen (1984), Miranda (1991), and Nassar and Krawinkler (1991). However, it can be observed that the longer-period structures subjected to ground motions with forward-directivity effects show a peak displacement response in the range of approximately 0.5 to 2 times the elastic structure response, somewhat in excess of values typical of the other classes of ground motion. Additionally, strength-reduction factors, R , tend to be somewhat lower for the FD motions, representing the need to supply a greater proportion of the elastic strength demand in order to maintain prespecified DDDs.

6.4.3 Response of Takeda Models

The Takeda models were provided with lateral strength equal to that determined to achieve specified DDDs of 1, 2, 4, and 8 for the corresponding bilinear models, based on the yield-point secant stiffness.

Prior damage was parameterized by prior ductility demand (PDD), possibly in conjunction with strength reduction or strength degradation, which is parameterized by RSR. PDD greater than zero (damage present) and RSR less than one (strength reduced or degrading) both cause the initial period of the oscillator to increase. When previous damage has caused displacements in excess of the yield displacement (PDD > 1), even small displacements cause energy dissipation through hysteretic response. No further attention is given to those oscillators for which the imposed PDD exceeds the response of the undamaged oscillator, and these data points are not represented on subsequent plots.

6.4.3.1 Response of the Takeda5 Model

It is of interest to observe how structures proportioned based on the bilinear model respond if their force/displacement response is represented more accurately by a Takeda model. This interest is based in part on the widespread use of the bilinear model in developing current displacement-based design approaches.

Figures 6-32 through 6-34 present the response of Takeda5 models in which the oscillator strength was set to achieve a bilinear displacement ductility demand of 8. The upper plot of each figure shows the ratio of peak displacement response to the peak response of an elastic

(Text continued on page 134)

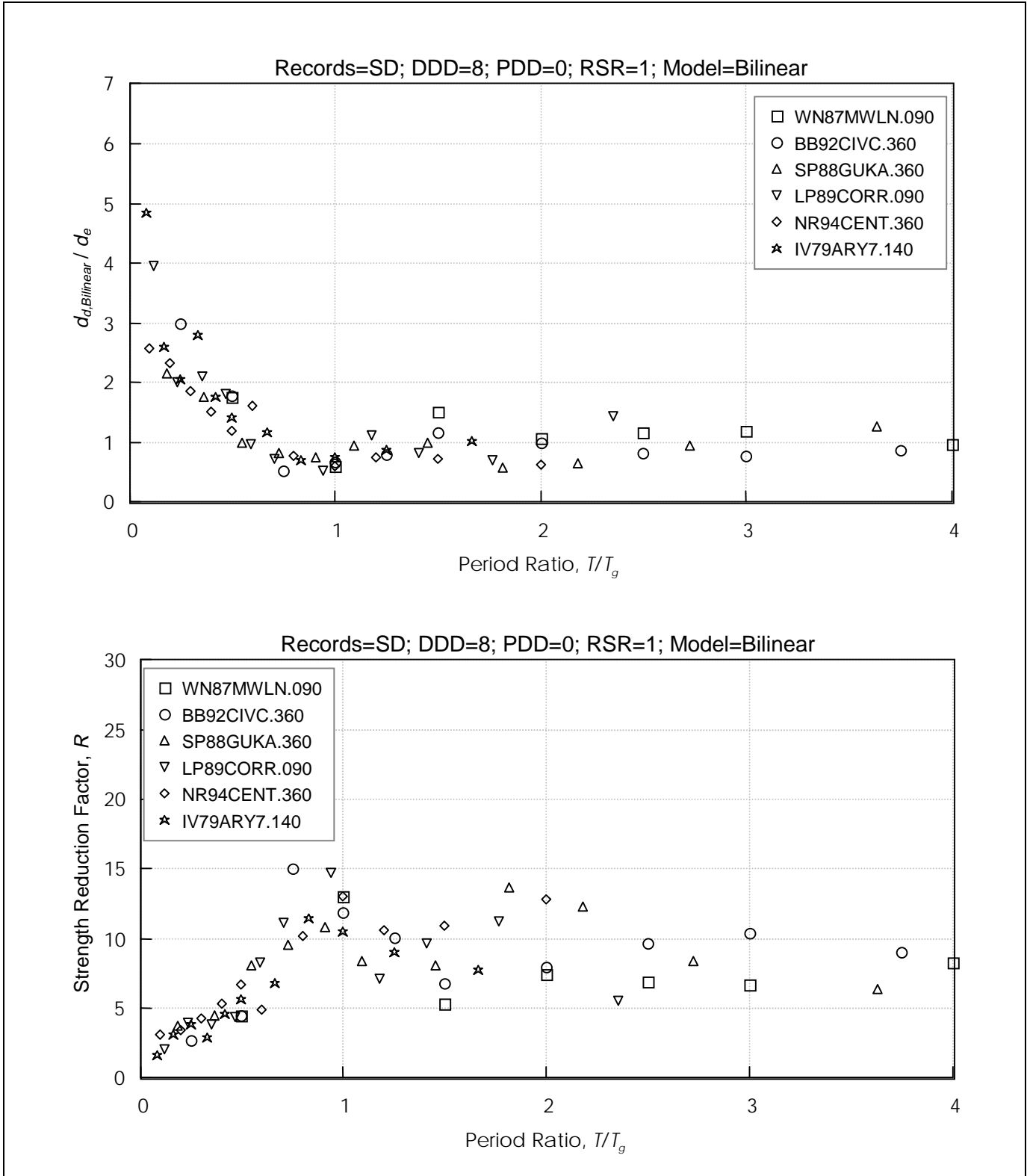


Figure 6-29 Response of Bilinear Oscillators to Short Duration Records (DDD= 8)
 DDD = Design Displacement Ductility; PDD = Prior Ductility Demand; RSR = Reduced Strength Ratio

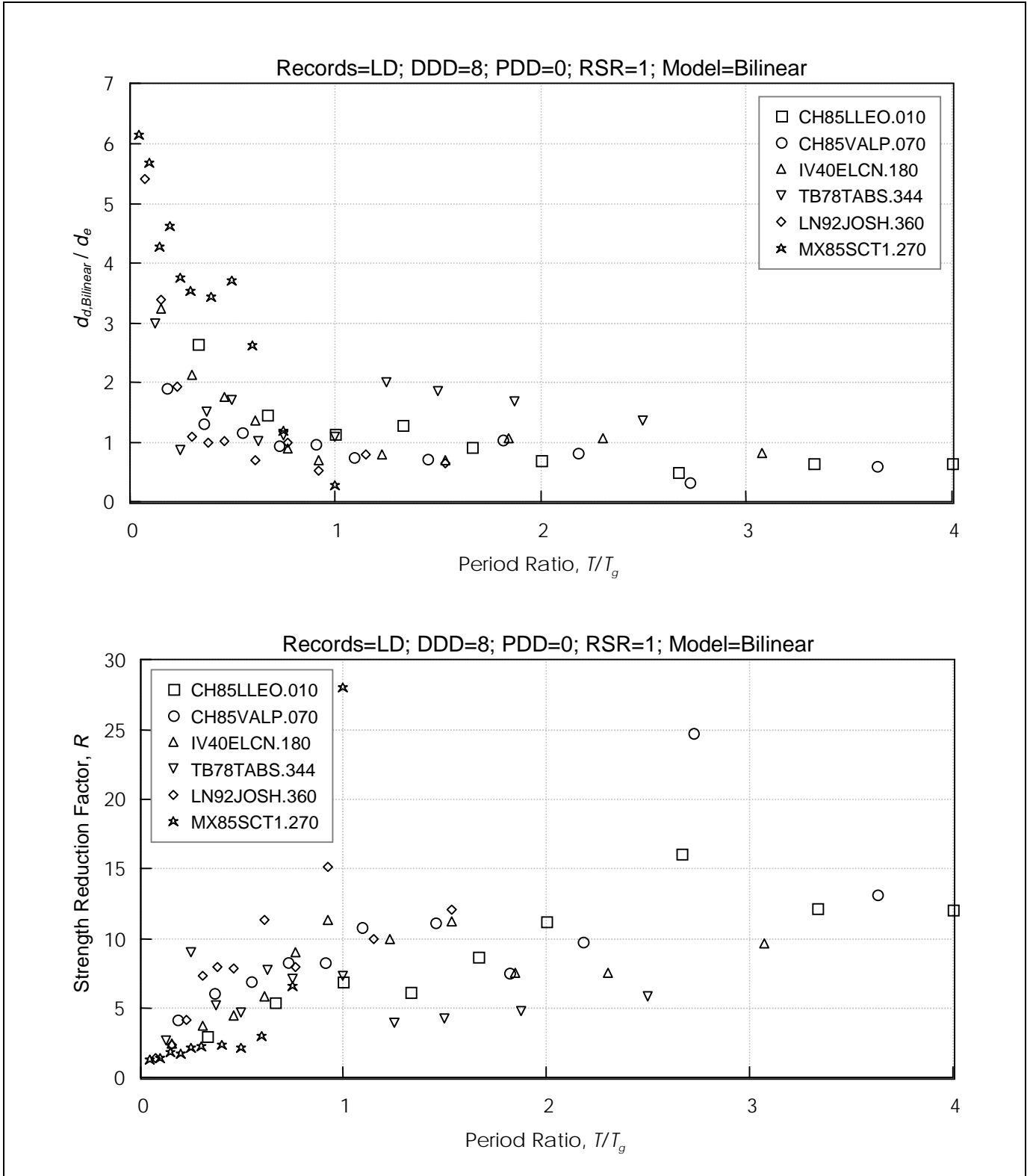


Figure 6-30 Response of Bilinear Oscillators to Long Duration Records (DDD= 8)
 DDD = Design Displacement Ductility; PDD = Prior Ductility Demand; RSR = Reduced Strength Ratio

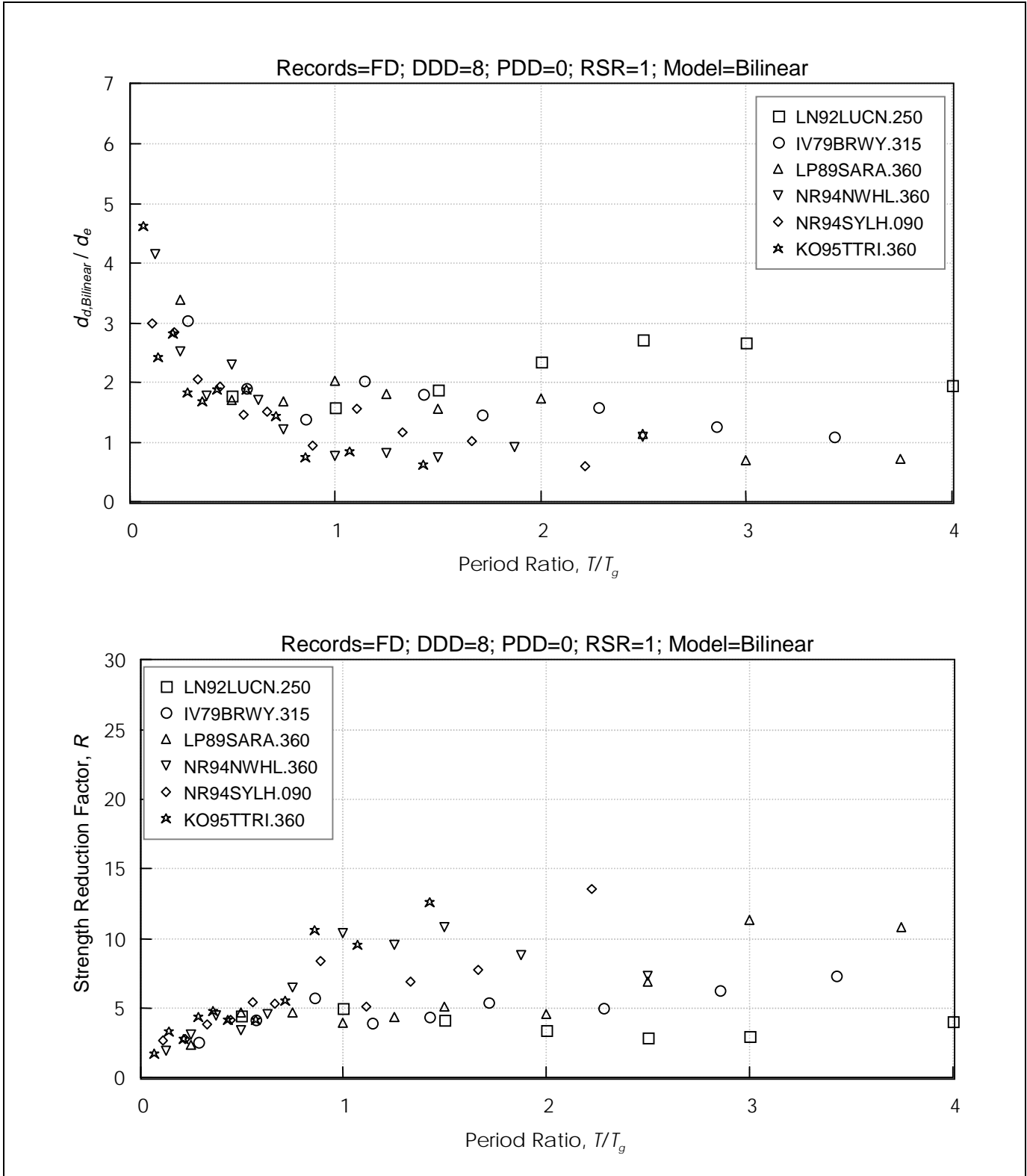


Figure 6-31 Response of Bilinear Oscillators to Forward Directive Records (DDD= 8)
 DDD = Design Displacement Ductility; PDD = Prior Ductility Demand; RSR = Reduced Strength Ratio

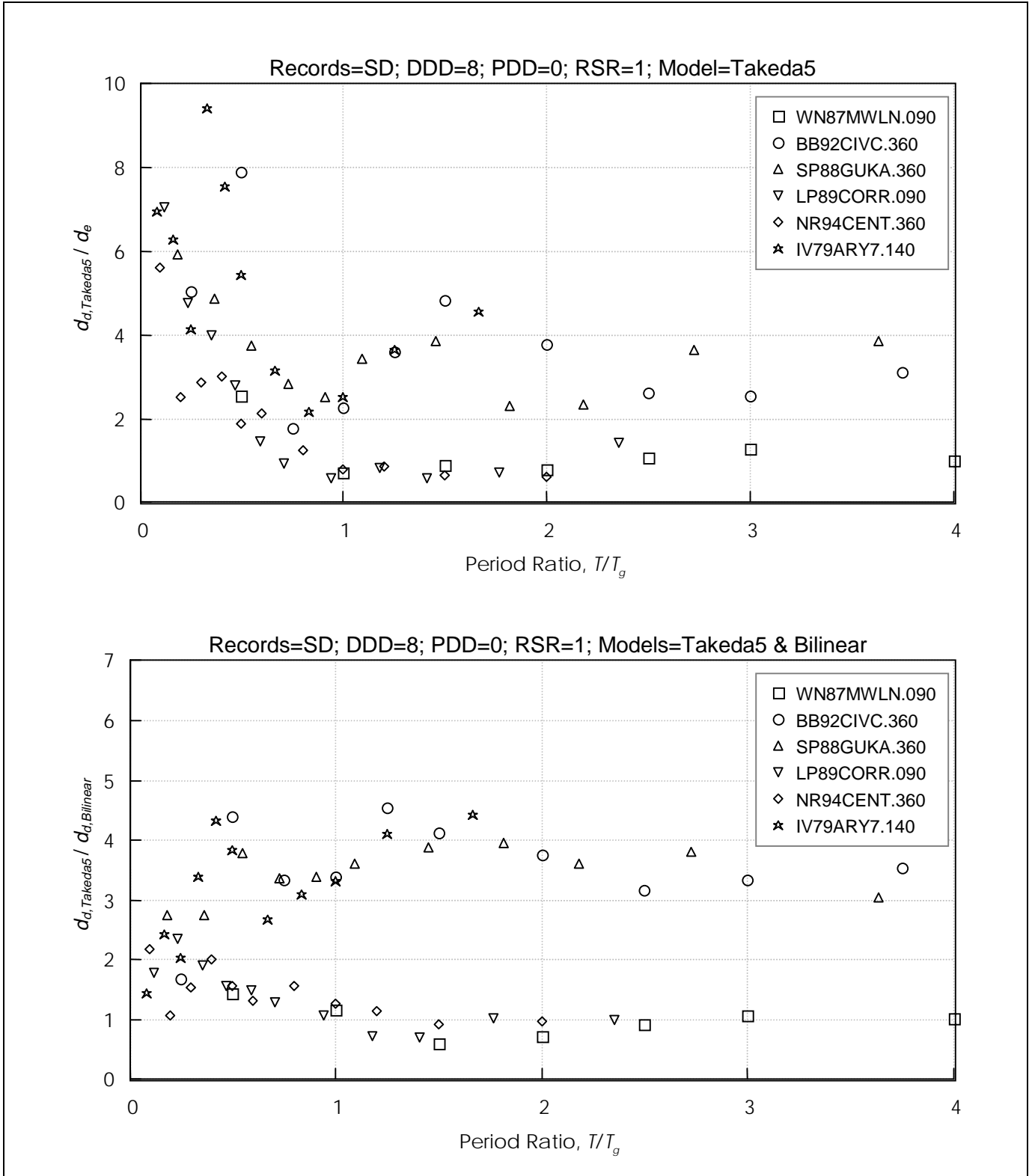


Figure 6-32 Displacement Response of Takeda Models Compared with Elastic Response and Bilinear Response, for Short-Duration Records (DDD= 8 and RSR= 1)
 DDD = Design Displacement Ductility; PDD = Prior Ductility Demand; RSR = Reduced Strength Ratio

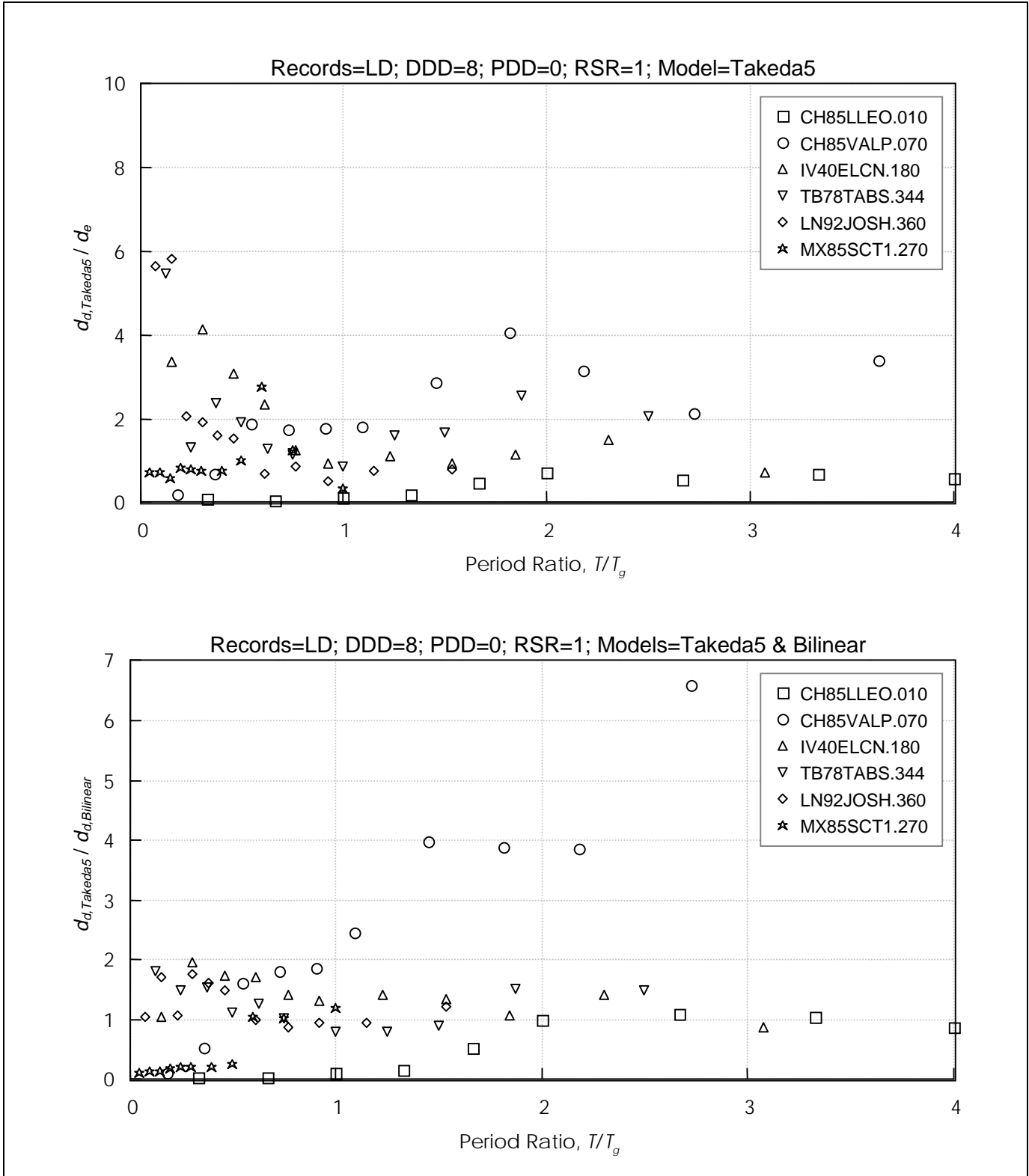


Figure 6-33 Displacement Response of Takeda Models Compared with Elastic Response and Bilinear Response for Long-Duration Records (DDD= 8 and RSR= 1)
 DDD = Design Displacement Ductility; PDD = Prior Ductility Demand; RSR = Reduced Strength Ratio

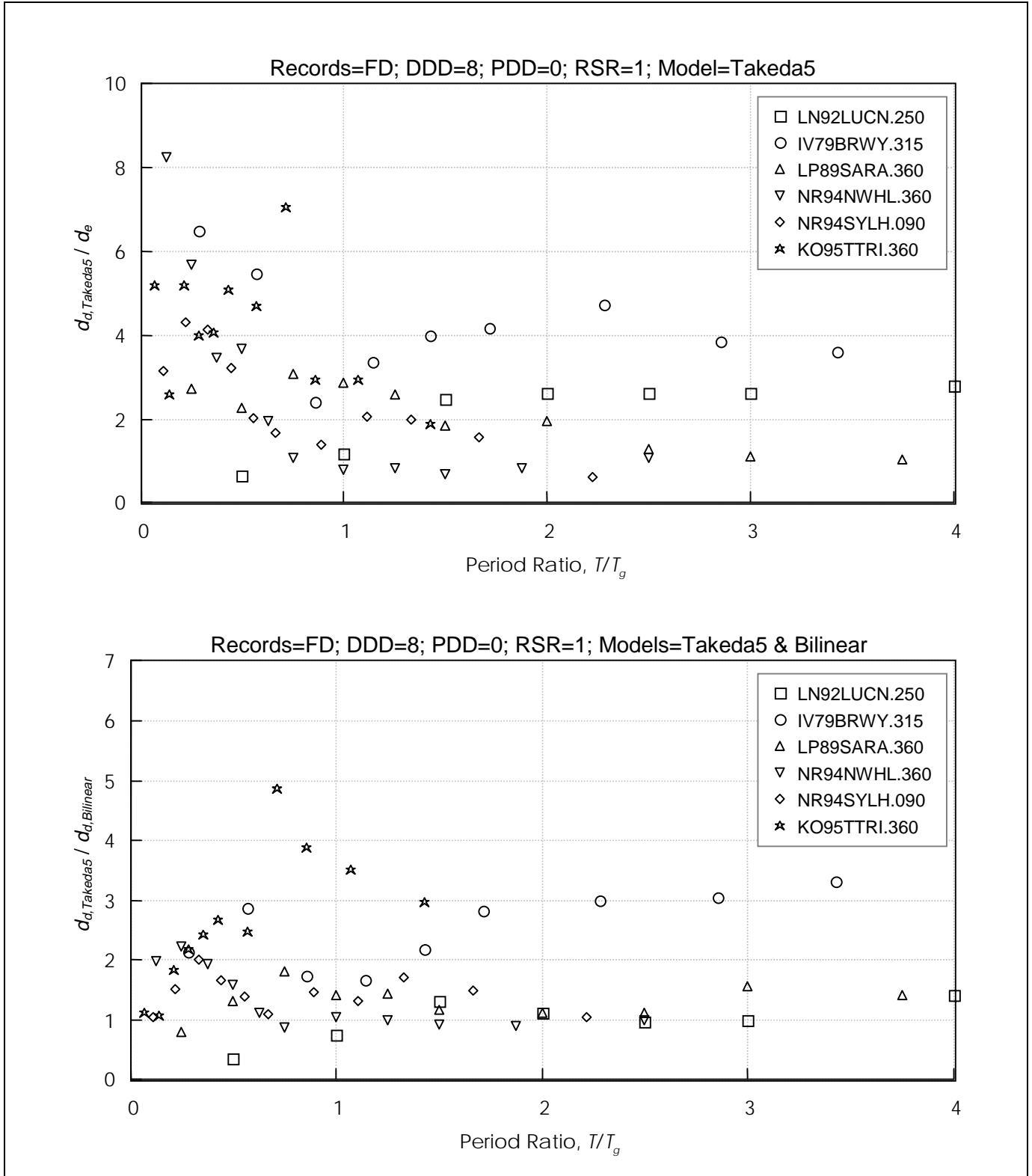


Figure 6-34 Displacement Response of Takeda Models Compared with Elastic Response and Bilinear Response for Forward Directive Records (DDD= 8 and RSR= 1)
 DDD = Design Displacement Ductility; PDD = Prior Ductility Demand; RSR = Reduced Strength Ratio

analog, d_d/d_e . The upper plots of Figures 6-32 through 6-34 are analogous to those presented in Figures 6-29 through 6-31.

The lower plots of Figures 6-32 through 6-34 show the ratio of the Takeda5 and bilinear ultimate displacements, $d_{d,Takeda5}/d_{d,Bilinear}$. It is clear that peak displacements of the Takeda model may be several times larger or smaller than those obtained with the corresponding bilinear model.

The effect of damage on the Takeda5 model is shown in Figures 6-35 through 6-40, for Takeda5 oscillators that were initially designed for a bilinear DDD of 8. The upper plot of each figure shows the response without strength reduction (RSR = 1); the lower plot shows response for RSR = 0.6.

Figures 6-35 through 6-37 show the effect of cracking on response. The displacement response, d'_d , of Takeda5 oscillators subjected to a PDD of one is compared with the response of the corresponding undamaged Takeda5 oscillators, d_d . Where no strength degradation occurs (RSR = 1), cracking rarely causes an increase in displacement demand; for the vast majority of oscillators, cracking is observed to cause a slight decrease in the peak displacement response. Reductions in strength typically cause a noticeable increase in displacement response, particularly for low T/T_g .

Figures 6-38 through 6-40 show the effect of a PDD of 8 on peak displacement, d'_d , relative to the response of the corresponding undamaged oscillators. Prior damage is observed to cause modest changes in displacement response where the strength is maintained (RSR = 1); displacements may increase or decrease. Where displacements increase, they rarely increase more than about 10% above the displacement of the undamaged oscillator for the short-duration and long-duration motions. For the forward directivity motions, they rarely increase more than about 30% above the displacement of the undamaged oscillator. The largest displacements tend to occur more frequently for $T < T_g$.

The above discussion concerned oscillators for which the strength is maintained. When strength is reduced (RSR = 0.6), prior ductility demand may cause displacements to increase or decrease, but the tendency for displacements to increase is more prominent than for RSR = 1. Furthermore, the increase in displacement tends to be larger than for RSR = 1. Reduction in strength, as represented in Figure 6-26, also causes

reduction in stiffness, and both effects contribute to the tendency for displacements to increase.

To understand the effects of prior damage on the response of the Takeda5 models, it is helpful to consider several oscillators exposed to the IV40ELCN.180 (El Centro) record. Figures 6-41 to 6-45 plot the response of oscillators having initial (reference) periods of 0.2, 0.5, 1.0, 1.5, and 2.0 sec, respectively, to this ground motion. The oscillators have yield strength equal to that required to obtain displacement ductility demands of 8 for the bilinear model. Oscillators having PDD of 0 (undamaged), 1, 4, and 8 are considered. Displacement time-histories (40 sec) of the oscillators are plotted at the top of each figure. Details of the first 10 seconds of response are shown below these. The solid lines represent the response of the initially-undamaged oscillators, and the dashed and dotted lines represent oscillators with PDD > 0. Force/displacement plots for the first 10 sec of response of each oscillator are provided in the lower part of the figure, using the same PDD legend. It can be observed that even though the undamaged oscillators initially have greater stiffness, their displacement response tends to converge upon the response of the initially-damaged oscillators within a few seconds. The displacement response of the damaged oscillators tends to be in phase with that of the initially-undamaged oscillators, and maximum values tend to be similar to and to occur at approximately the same time as the undamaged oscillator peaks. Thus, it appears that prior ductility demands have only a small effect on oscillator response characteristics and do not cause a fundamentally different response to develop.

6.4.3.2 Response of the TakPinch Model

Figures 6-46 to 6-48 plot the ratio, d'_d/d_d , of damaged and undamaged displacement response for the TakPinch models having DDD = 8 and PDD = 8, for RSR = 1 and 0.6. Figure 6-49 plots the displacement time-history of TakPinch oscillators subjected to the NS component of the 1940 El Centro record, and Figure 6-50 plots results for oscillators having cyclic strength degradation given by RSR = 0.6. These oscillators have a reference period of one second, DDD = 8, and various PDDs.

By comparison with the analogous figures for the Takeda5 model (Figures 6-38 to 6-40 and 6-43), it can be observed that: (1) for RSR = 1 (no strength degradation), the effect of PDD on displacement response is typically small for the Takeda5 and TakPinch oscillators, and (2) the effect of cyclic strength degradation, as implemented here, is also relatively small. Thus, the observation that prior

(Text continued on page 151)

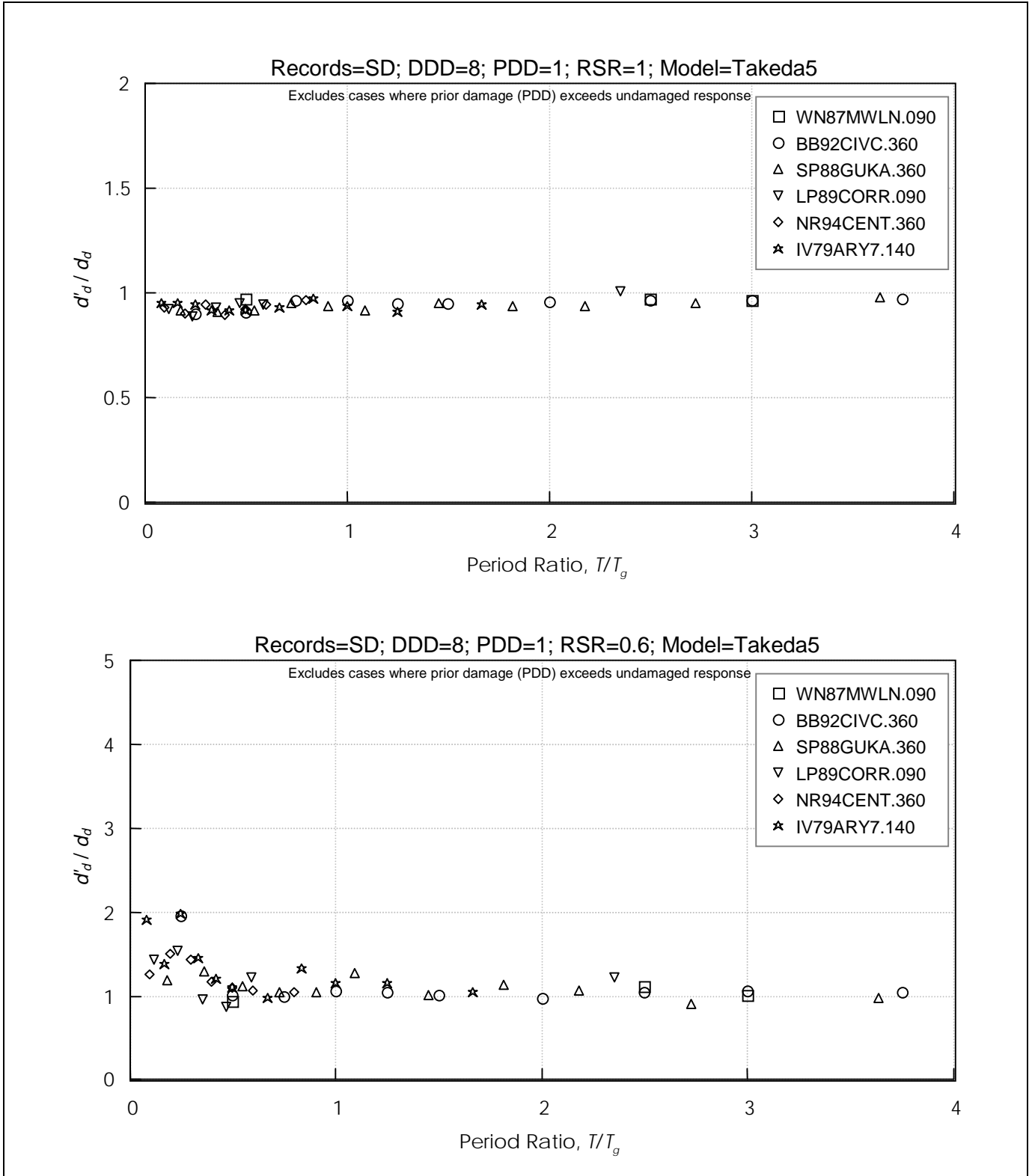


Figure 6-35 Effect of Cracking Without and With Strength Reduction on Displacement Response of Takeda5 Models, for Short-Duration Records (DDD= 8 and PDD= 1)
 DDD = Design Displacement Ductility; PDD = Prior Ductility Demand; RSR = Reduced Strength Ratio

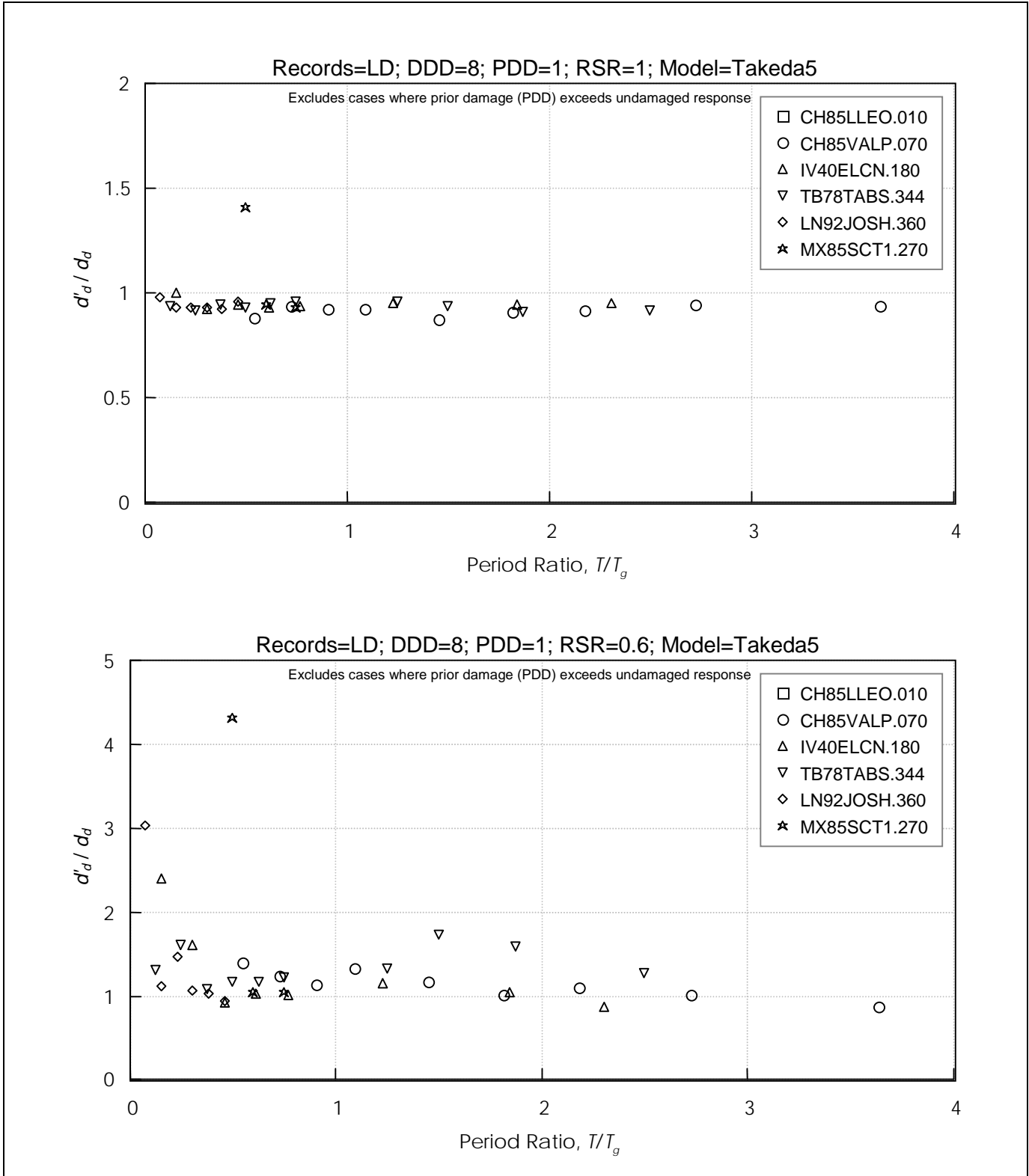


Figure 6-36 Effect of Cracking Without and With Strength Reduction on Displacement Response of Takeda5 Models, for Long-Duration Records (DDD= 8 and PDD= 1)
 DDD = Design Displacement Ductility; PDD = Prior Ductility Demand; RSR = Reduced Strength Ratio

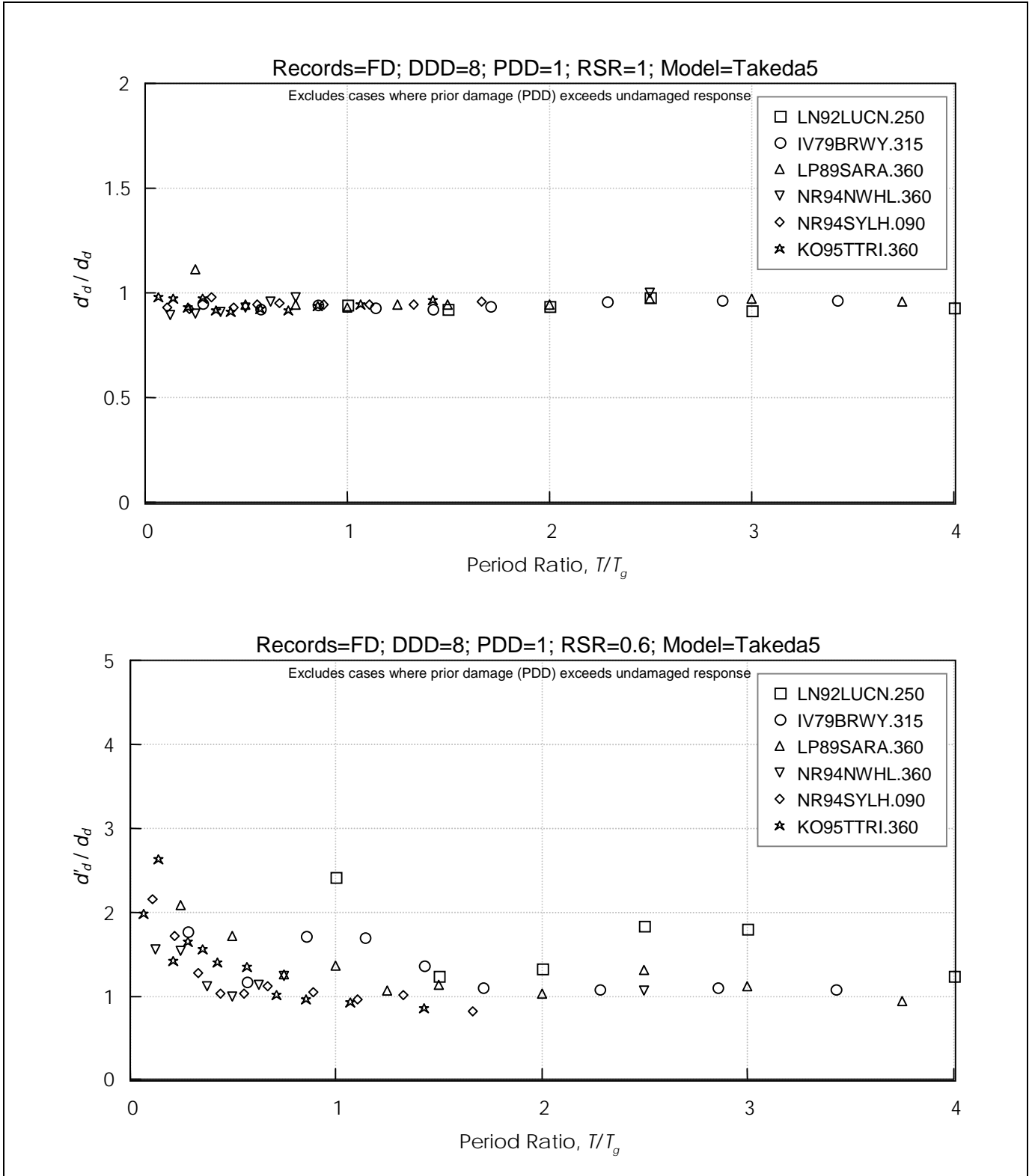


Figure 6-37 Effect of Cracking Without and With Strength Reduction on Displacement Response of Takeda5 Models, for Forward Directive Records (DDD= 8 and PDD= 1)
 DDD = Design Displacement Ductility; PDD = Prior Ductility Demand; RSR = Reduced Strength Ratio

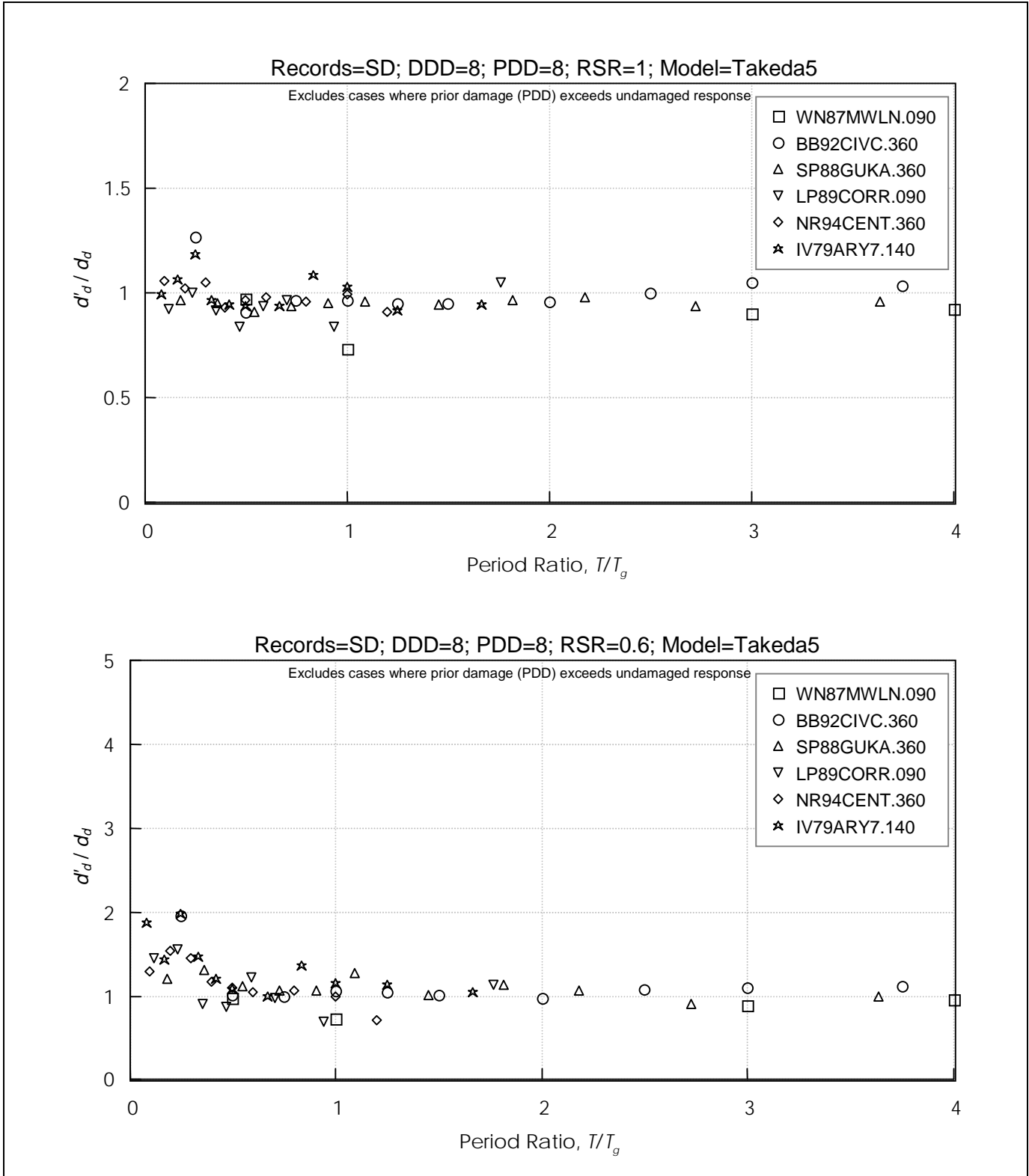


Figure 6-38 Effect of Large Prior Ductility Demand Without and With Strength Reduction on Displacement Response of Takeda5 Models, for Short Duration Records (DDD= 8 and PDD= 8)
 DDD = Design Displacement Ductility; PDD = Prior Ductility Demand; RSR = Reduced Strength Ratio

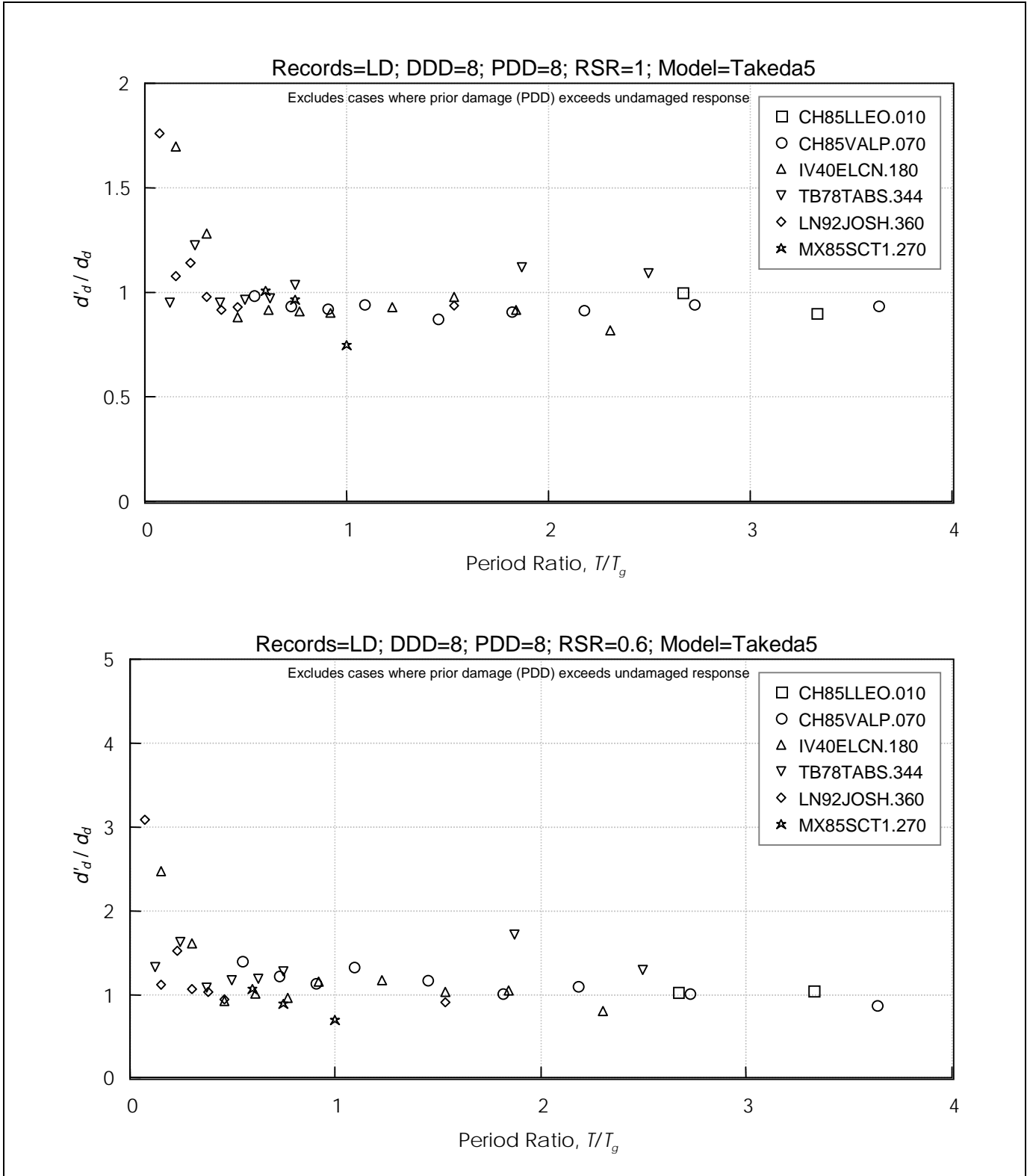


Figure 6-39 Effect of Large Prior Ductility Demand Without and With Strength Reduction on Displacement Response of Takeda5 Models, for Long Duration Records (DDD = 8 and PDD = 8)
 DDD = Design Displacement Ductility; PDD = Prior Ductility Demand; RSR = Reduced Strength Ratio

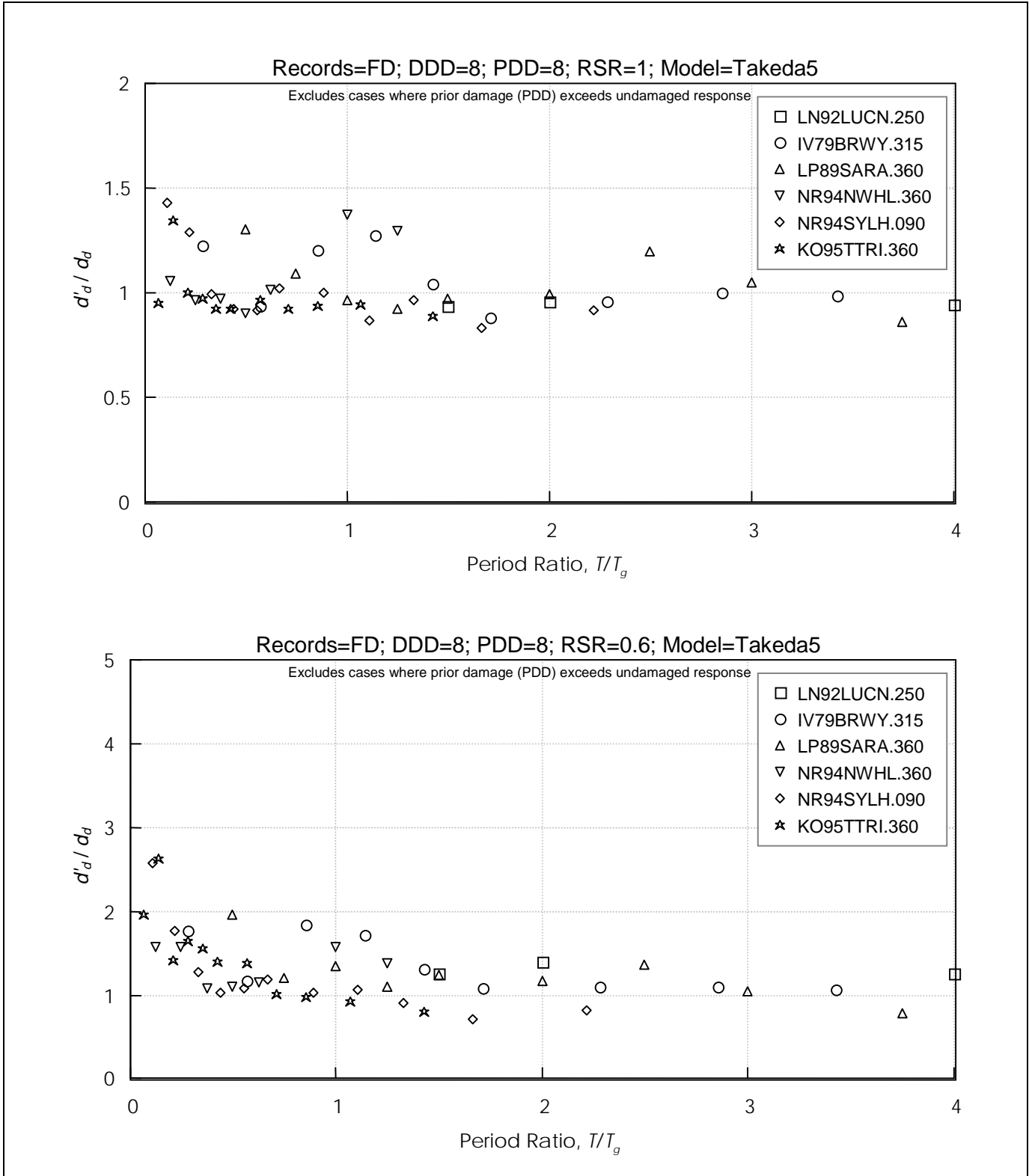


Figure 6-40 Effect of Large Prior Ductility Demand Without and With Strength Reduction on Displacement Response of Takeda5 Models, for Forward Directive Records (DDD= 8 and PDD= 8)
 DDD = Design Displacement Ductility; PDD = Prior Ductility Demand; RSR = Reduced Strength Ratio

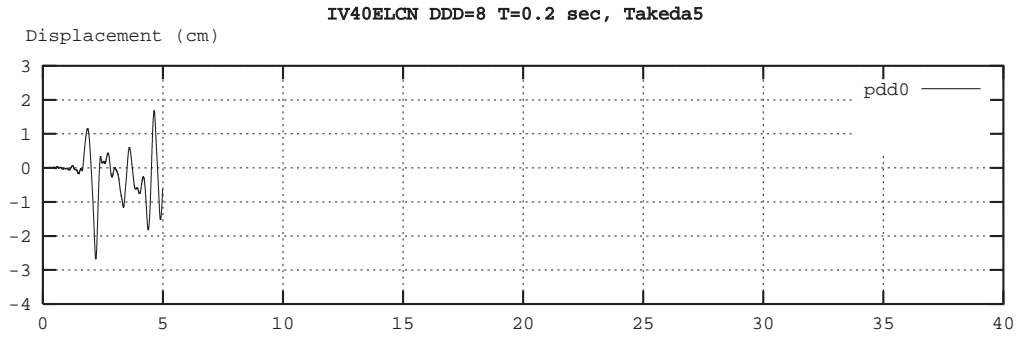


Figure 6-41 Effect of Damage on Response to El Centro (IV40ELCN.180) for Takeda5, T=0.2 sec (DDD= 8)
DDD = Design Displacement Ductility

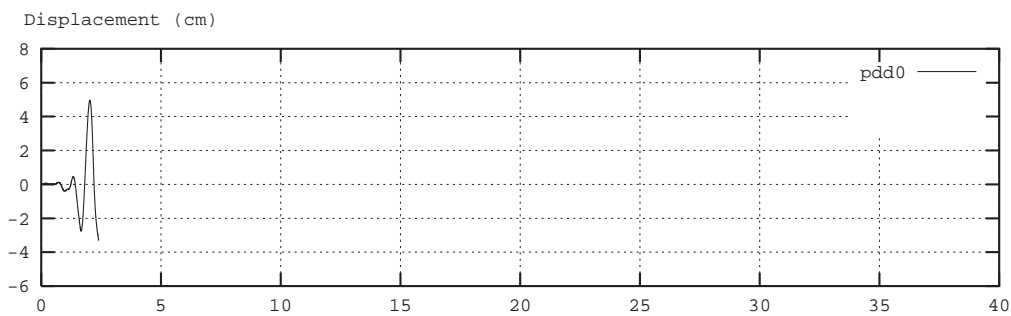


Figure 6-42 Effect of Damage on Response to El Centro (IV40ELCN.180) for Takeda5, $T=0.5$ sec (DDD= 8)
DDD = Design Displacement Ductility

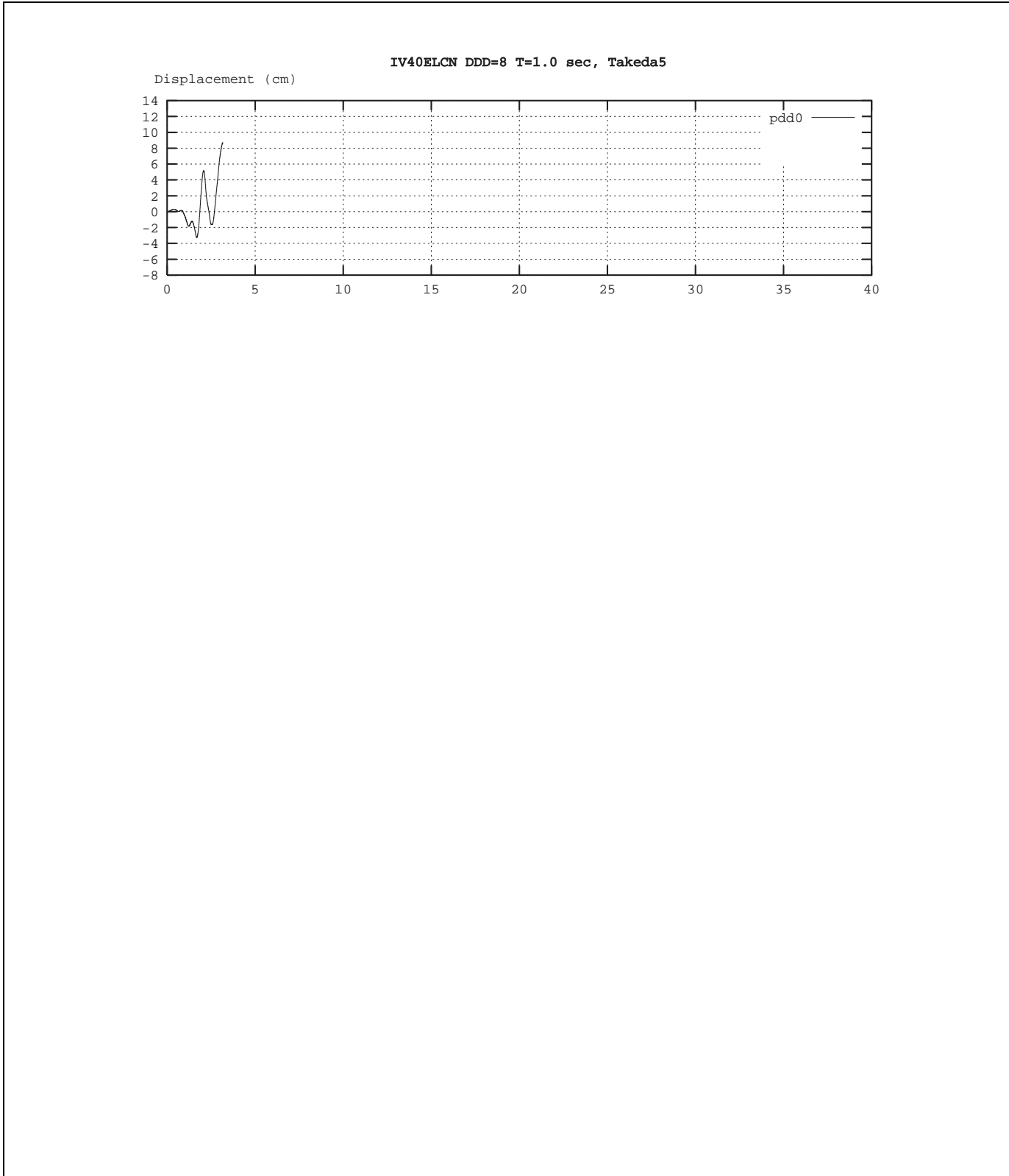


Figure 6-43 Effect of Damage on Response to El Centro (IV40ELCN.180) for Takeda5, T=1.0 sec (DDD= 8)
DDD = Design Displacement Ductility

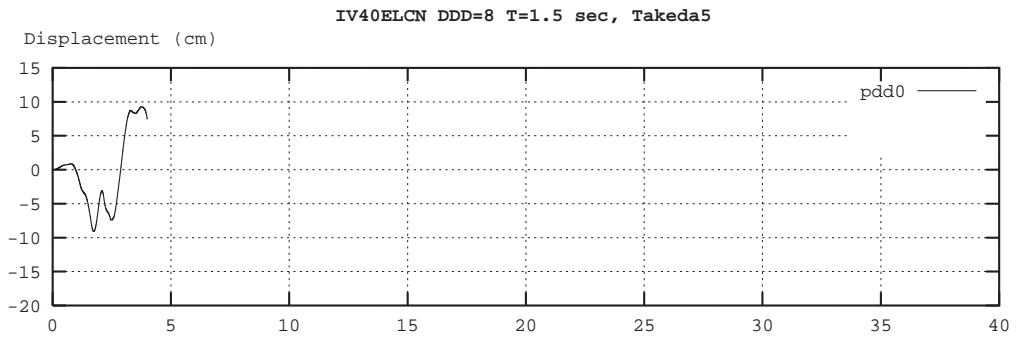


Figure 6-44 Effect of Damage on Response to El Centro (IV40ELCN.180) for Takeda5, T=1.5 sec (DDD= 8)
DDD = Design Displacement Ductility

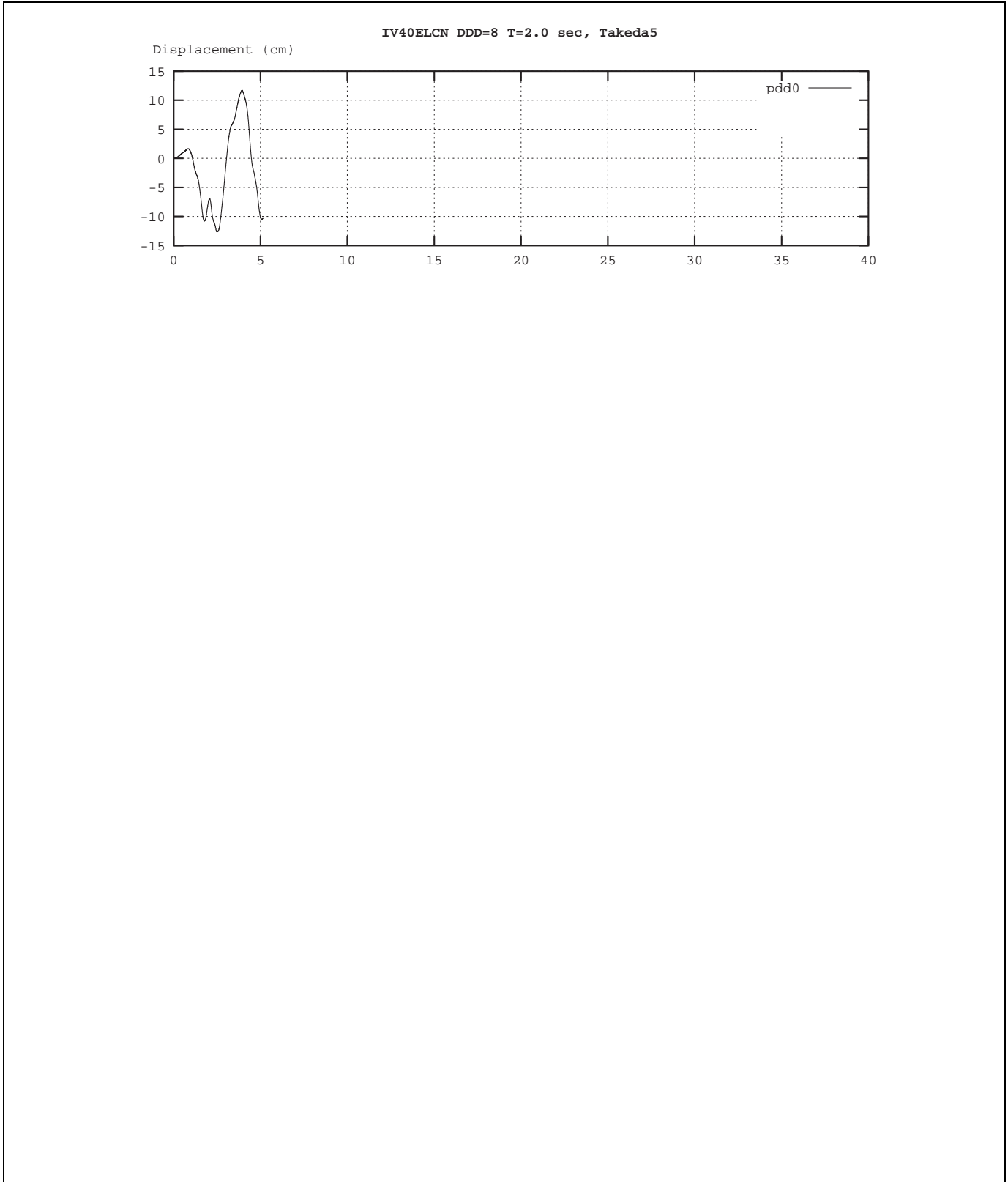


Figure 6-45 Effect of Damage on Response to El Centro (IV40ELCN.180) for Takeda5, T=2.0 sec (DDD= 8)
DDD = Design Displacement Ductility

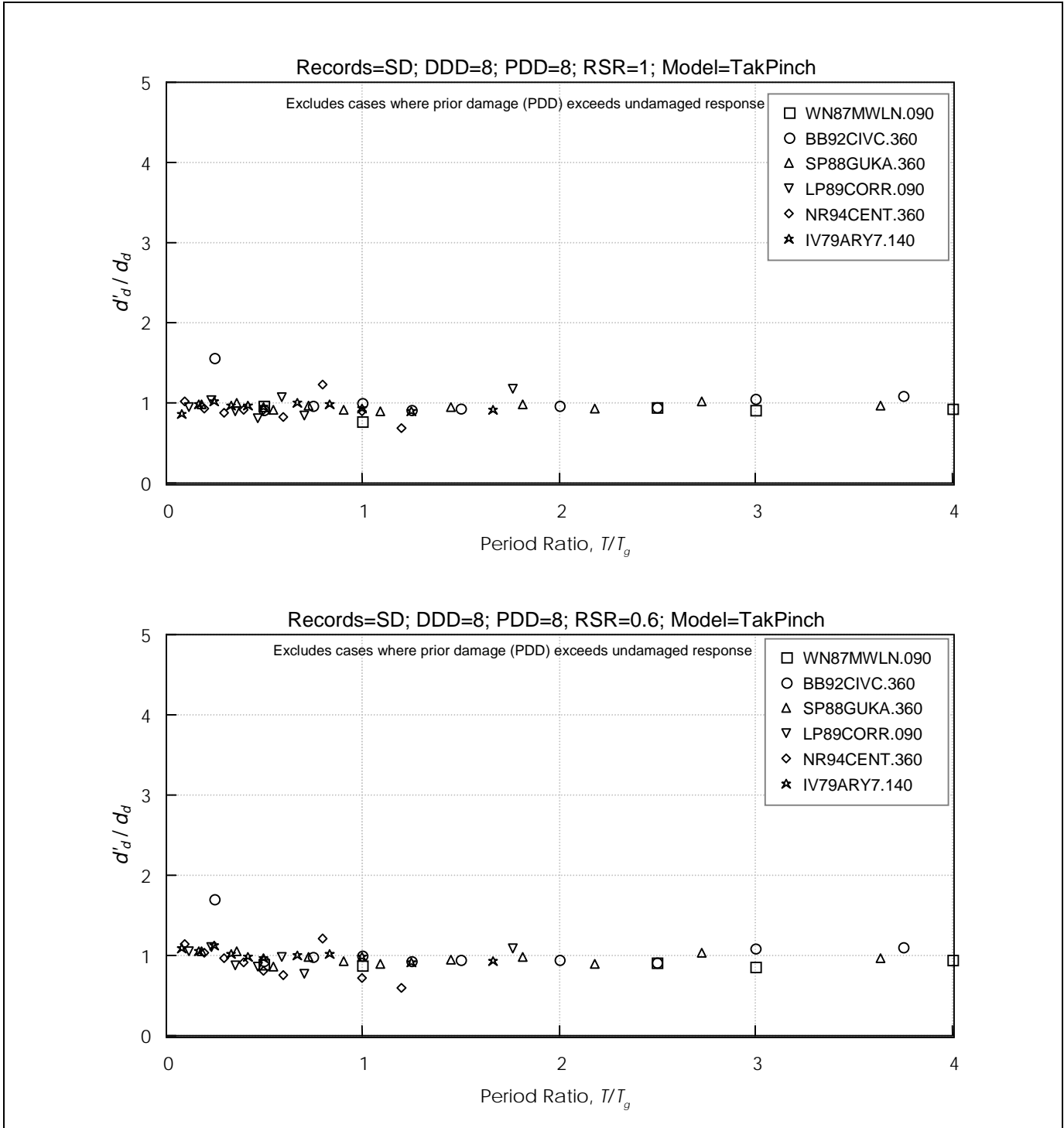


Figure 6-46 Effect of Large Prior Ductility Demand Without and With Strength Reduction on Displacement Response of TakPinch Models, for Short Duration Records (DDD= 8 and PDD= 8)
 DDD = Design Displacement Ductility; PDD = Prior Ductility Demand; RSR = Reduced Strength Ratio

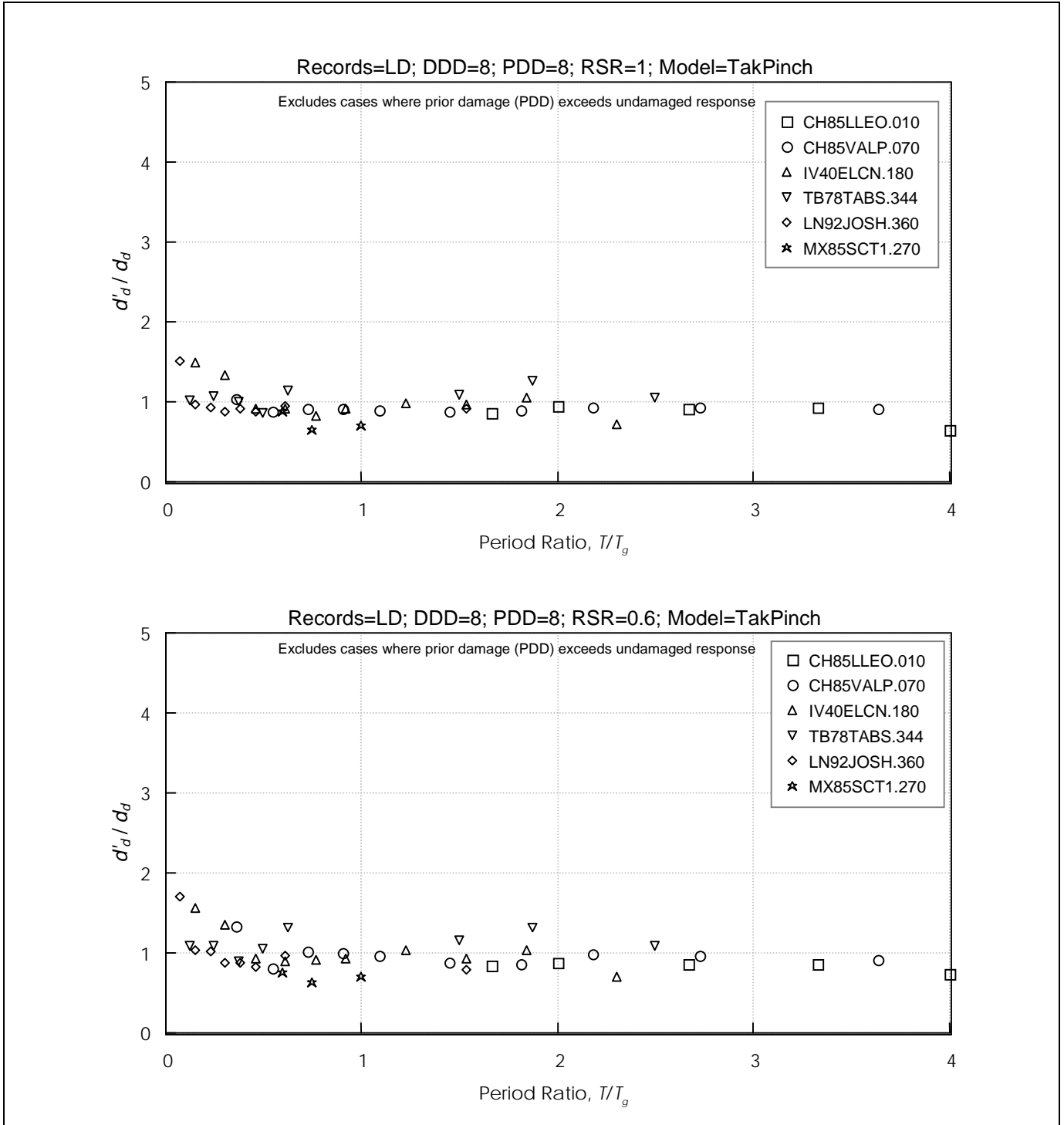


Figure 6-47 *Effect of Large Prior Ductility Demand Without and With Strength Reduction on Displacement Response of TakPinch Models, for Long Duration Records (DDD= 8 and PDD= 8)*
DDD = Design Displacement Ductility; PDD = Prior Ductility Demand; RSR = Reduced Strength Ratio

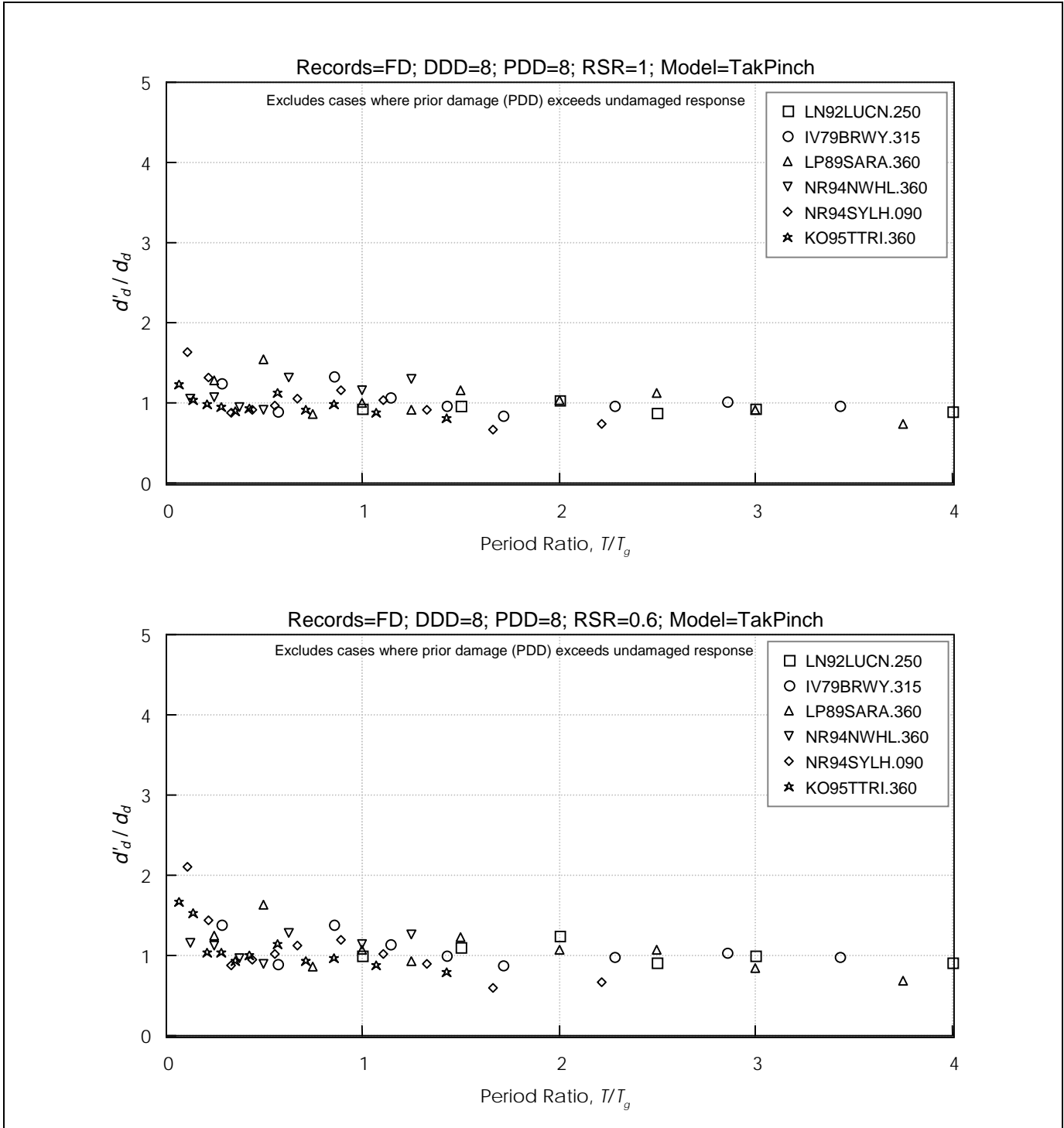


Figure 6-48 Effect of Large Prior Ductility Demand Without and With Strength Reduction on Displacement Response of TakPinch, for Forward Directive Records (DDD = 8 and PDD = 8)
 DDD = Design Displacement Ductility; PDD = Prior Ductility Demand; RSR = Reduced Strength Ratio

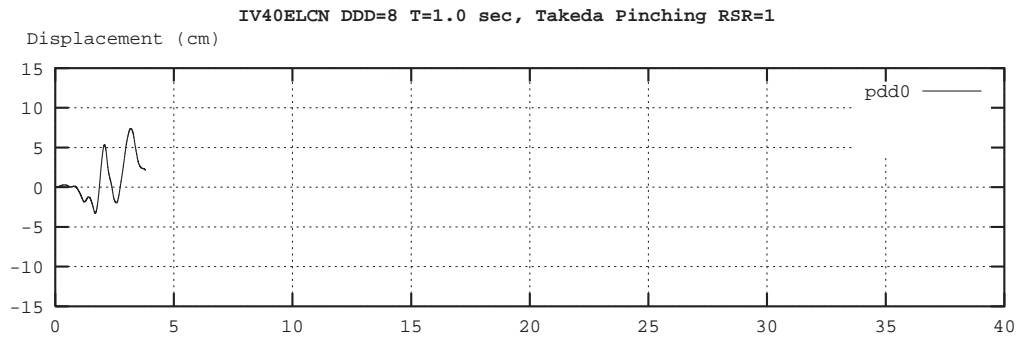


Figure 6-49 Effect of Damage on Response of TakPinch Model to El Centro (IV40ELCN.180) for T=1.0 sec and RSR= 1 (DDD= 8)
DDD = Design Displacement Ductility

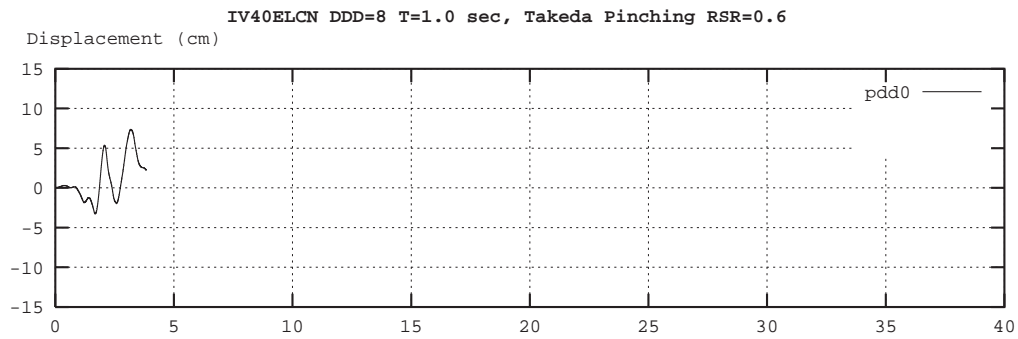


Figure 6-50 Effect of Damage on Response of TakPinch Model to El Centro (IV40ELCN.180) for T=1.0 sec and RSR = 0.6 (DDD= 8)
DDD = Design Displacement Ductility

ductility demand has, in general, only a small effect on displacement demand applies equally to the standard Takeda oscillator and to Takeda oscillators that exhibit pinching. The Takeda5 oscillators with initially reduced strength, given by $RSR = 0.6$, tended to have a response amplified to a much greater extent than is observed for the TakPinch model, reflecting the more dramatic form of strength degradation that was implemented in the Takeda5 model.

6.4.3.3 Response of Takeda10 Model

The Takeda10 model is a Takeda model having post-yield stiffness equal to -10% of the yield-point secant stiffness. As has been found previously by others, models with negative post-yield stiffness are prone to collapse, where collapse is defined as the point at which the displacement is large enough that the force resisted by the oscillator decreases to zero. Comparisons of peak displacement response are of limited value when collapse occurs. Instead, the likelihood of collapse is used to assess the impact of prior damage on response for the Takeda10 models.

Figures 6-51 to 6-53 plot the ratio, d'_d/d_d , of damaged and undamaged peak displacement response for the

Takeda10 oscillators having $DDD = 2$. Collapse of the damaged oscillators (whether the corresponding undamaged oscillator collapsed or not) is indicated by a ratio equal to six, and collapse of the undamaged oscillators is indicated by a ratio equal to zero. Approximately 10% of the oscillators having $DDD = 2$ collapsed with no prior damage. This indicates that structures characterized by negative post-yield stiffnesses must remain nearly elastic if collapse is to be avoided. Prior ductility demand may cause displacement response to either increase or decrease for those oscillators that do not collapse.

Figure 6-54 plots the displacement time-history of a one-second oscillator having $DDD = 8$ and PDD ranging from 0 (undamaged) to 8, subjected to the NS component of the 1940 El Centro record. It can be observed that prior ductility demand helps to avoid collapse in some cases, and may cause collapse in others.

6.4.4 Response Statistics

Summary response statistics were prepared to identify general trends in the data.

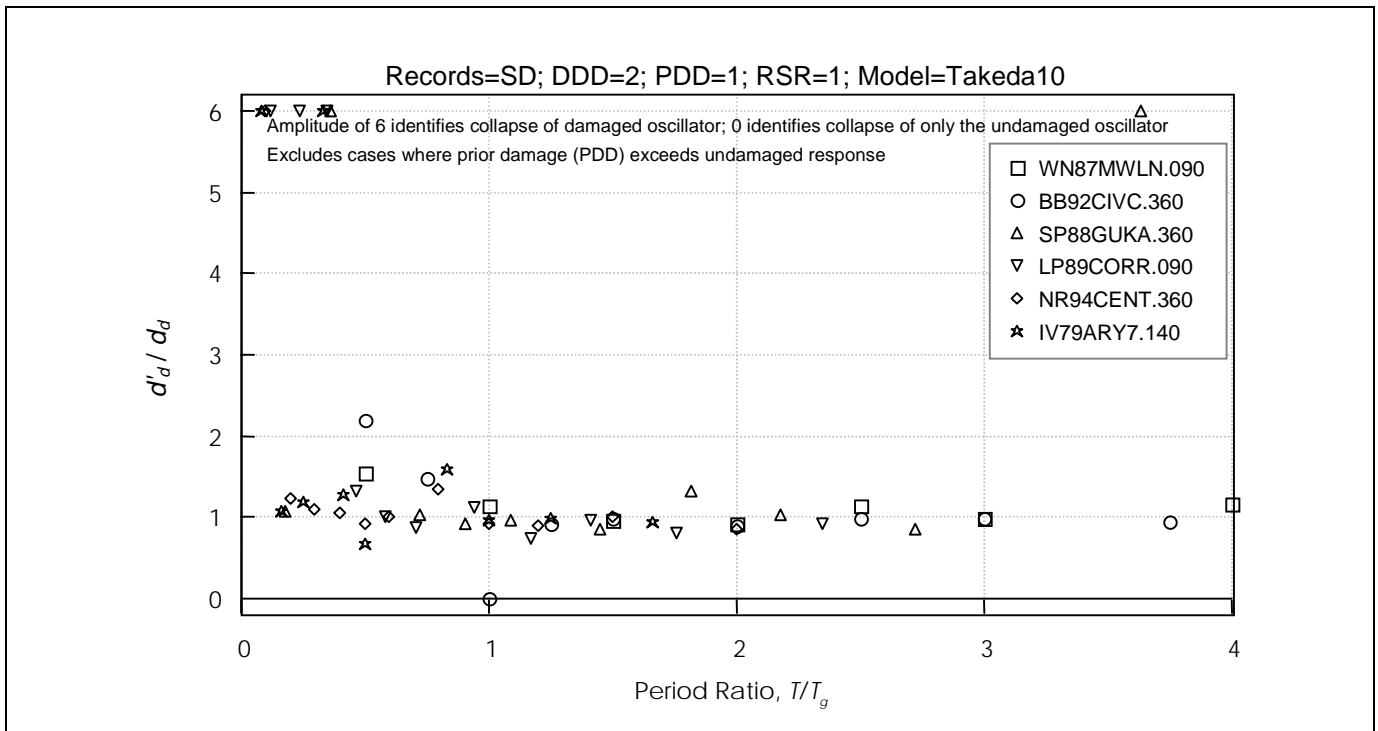


Figure 6-51 Effect of Cracking on Displacement Response of Takeda10 Model for Short Duration Records ($DDD = 8$ and $PDD = 1$)
 $DDD =$ Design Displacement Ductility; $PDD =$ Prior Ductility Demand; $RSR =$ Reduced Strength Ratio

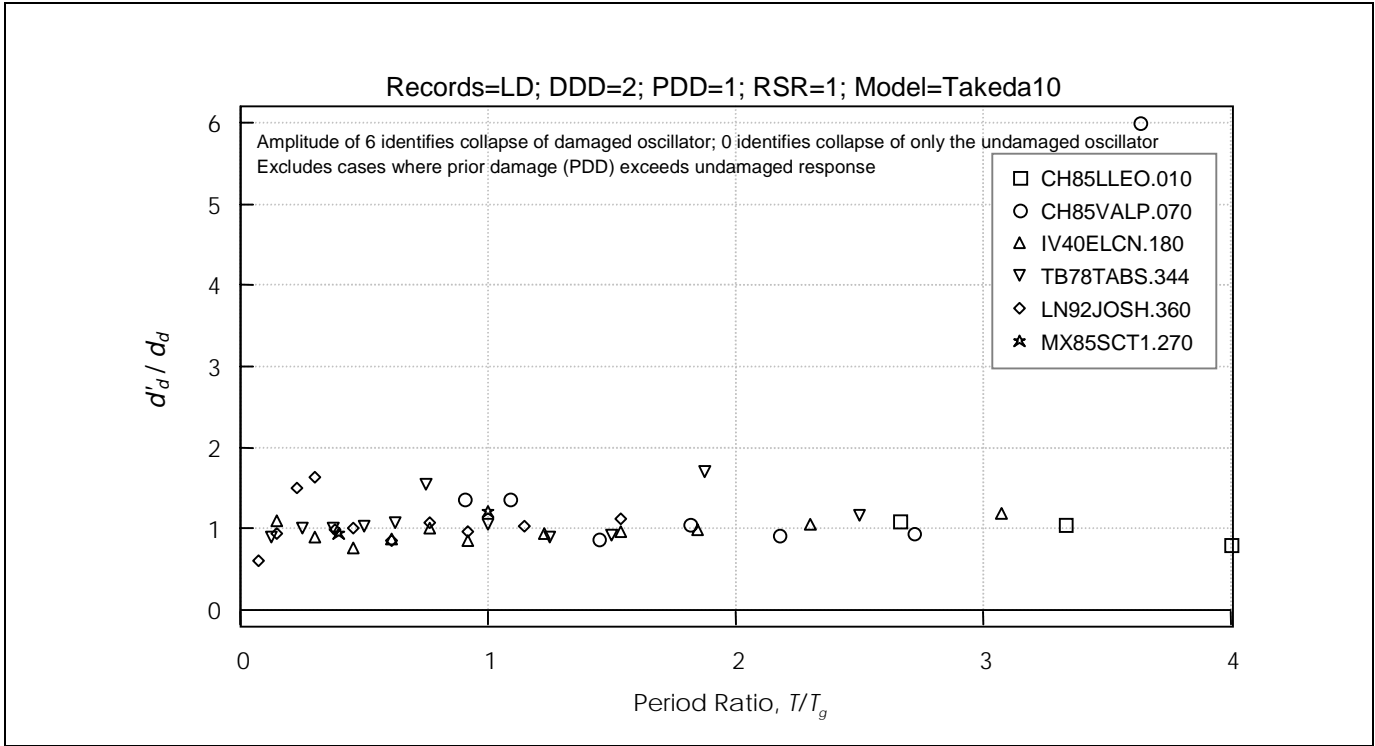


Figure 6-52 Effect of Cracking on Displacement Response of Takeda10 Model for Long-Duration Records (DDD= 8 and PDD=1)
 DDD = Design Displacement Ductility; PDD = Prior Ductility Demand; RSR = Reduced Strength Ratio

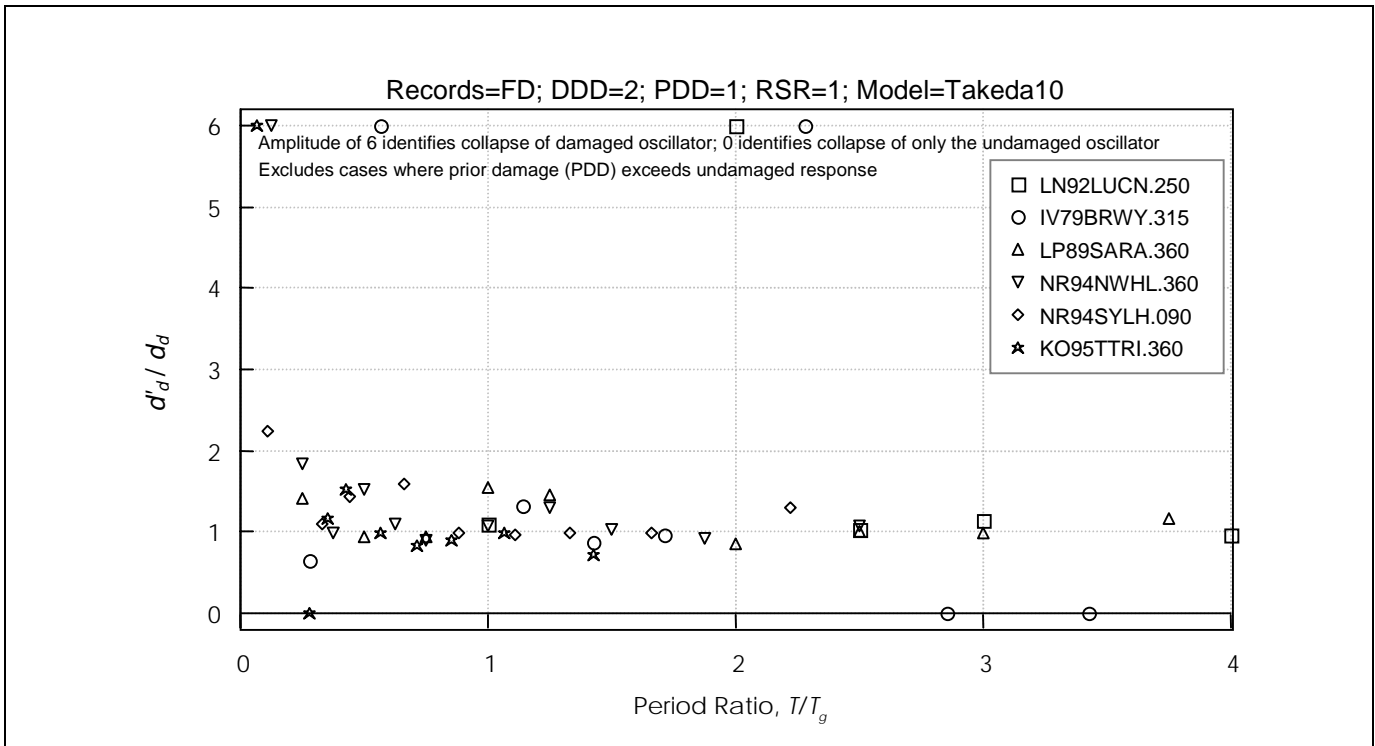


Figure 6-53 Effect of Cracking on Displacement Response of Takeda10 Model for Forward Directive Records (DDD= 8 and PDD=1)
 DDD = Design Displacement Ductility; PDD = Prior Ductility Demand; RSR = Reduced Strength Ratio

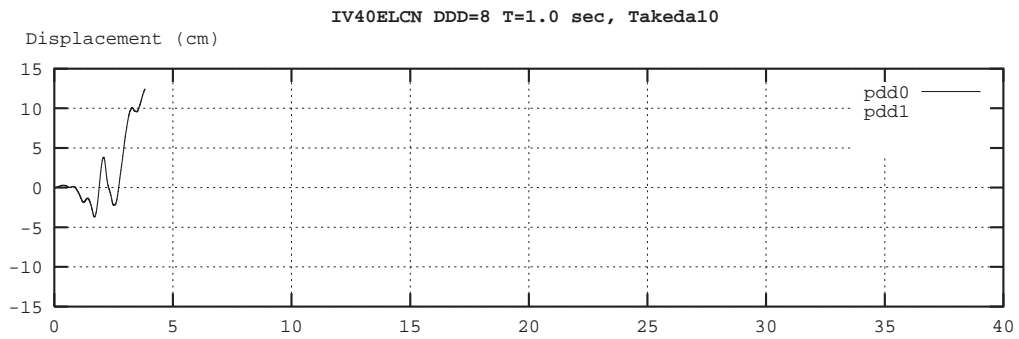


Figure 6-54 Effect of Damage on Response of Takeda10 Model to El Centro (IV40ELCN.180) for T=1.0 sec and RSR= 1 (DDD= 8)
DDD = Design Displacement Ductility

The left side of Figure 6-55 plots mean values of the ratio of damaged and undamaged oscillator peak displacement response, d'_d/d_d , as a function of DDD and PDD, for RSR = 1, 0.8, and 0.6, for the Takeda5 model. The right side of this figure plots mean-plus-one standard deviation values of d'_d/d_d . Figure 6-56 plots similar data, but for the TakPinch model. Mean displacement ratios d'_d/d_d for the Takeda5 and TakPinch models are only slightly affected by PDD and DDD, for RSR = 1. Mean displacement ratios of the TakPinch oscillators increase slightly as RSR decreases.

In Figure 6-55 it can be seen that strength reduction can have a significant effect on the mean displacement ratio d'_d/d_d for the Takeda5 oscillators. However, if the damaging earthquake reduces oscillator strength, then surely the undamaged structure would experience

strength degradation during the performance-level event. Thus, the comparison of d'_d with d_d does not provide a sufficient basis to determine the effect of strength degradation on response. Comparing response of structures having reduced strength, both with and without prior ductility demands would provide more meaningful information. Comparing data for RSR = 0.6 or 0.8, one can see in Figure 6-55 that the effect of PDD is to reduce the mean displacement ratio for Takeda5 oscillators. The capacity curve developed for a structure should incorporate strength degradation when it is anticipated.

The above discussion has focused on mean ratios of d'_d/d_d . Variability of this ratio, plotted as mean plus one standard deviation values on the right sides of Figures 6-55 and 6-56, indicates that response of a

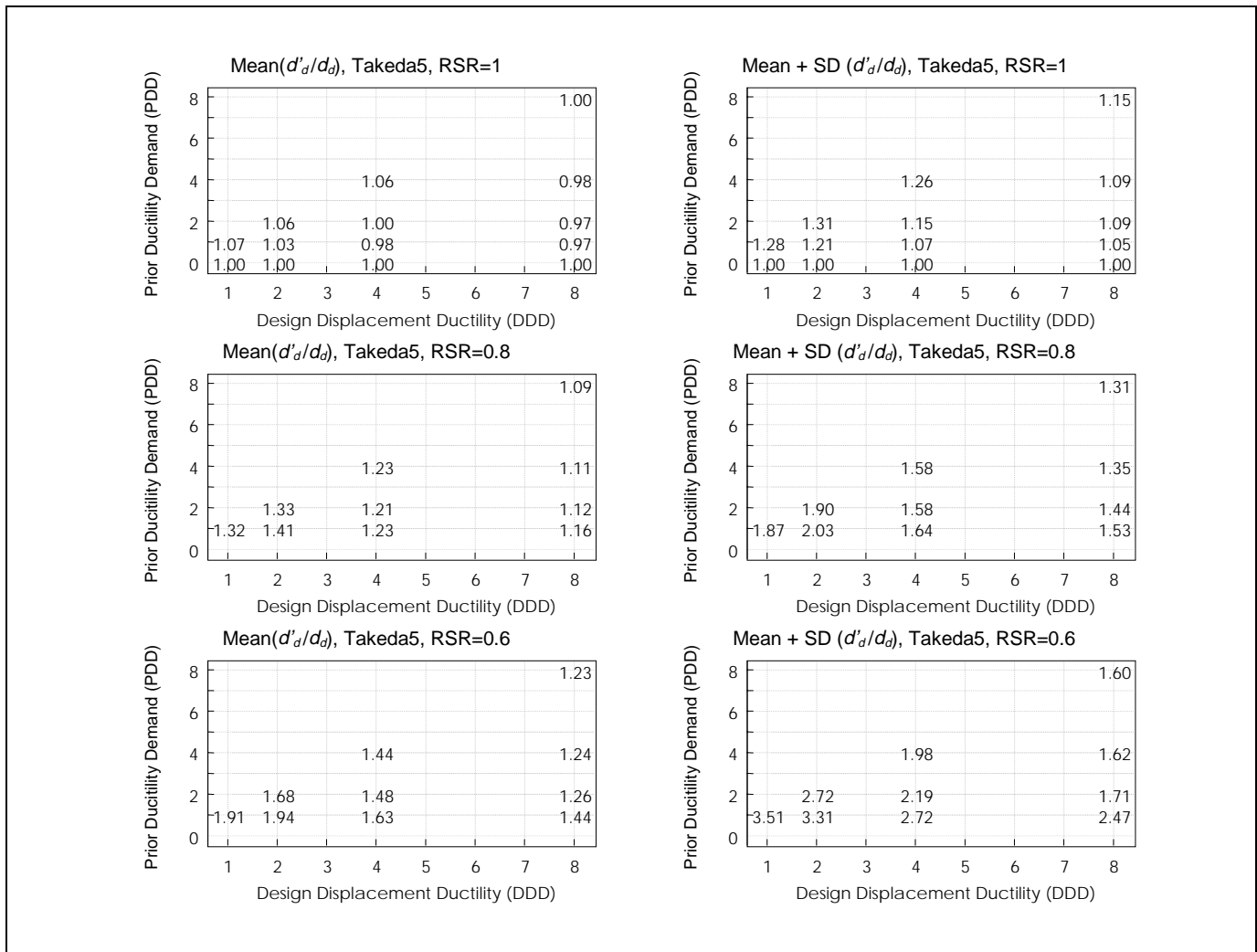


Figure 6-55 Mean and Standard Deviation Values of d'_d/d_d for Takeda5 Model.

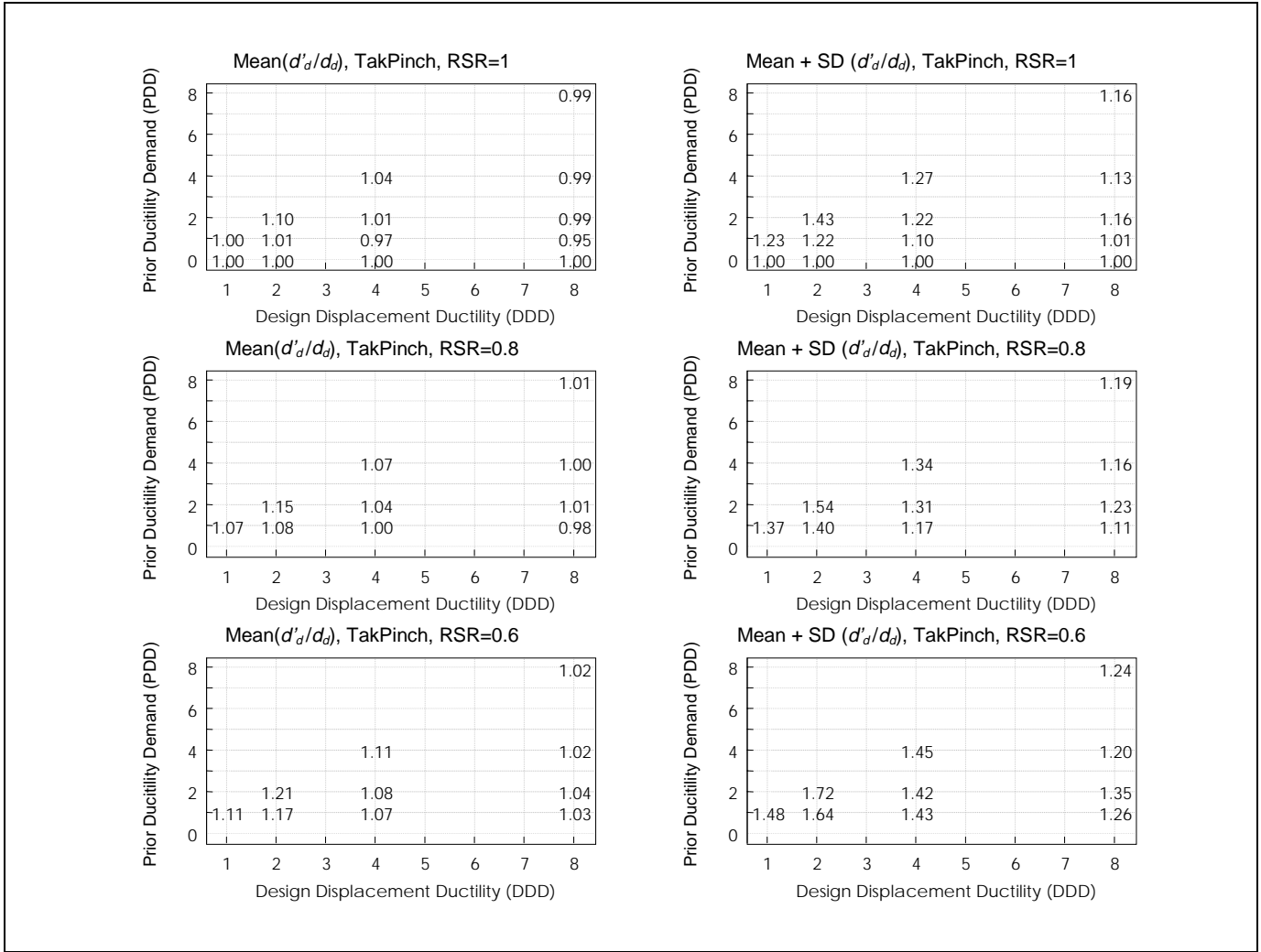


Figure 6-56 Mean and Standard Deviation Values of d'_d/d_d for TakPinch Model.

damaged structure to a given earthquake varies relative to the response in the initially-undamaged state. However, this variability is insignificant in the context of variability arising from other sources. For example, the hysteresis model and earthquake ground motion have a greater effect on response displacements than the variability arising due to prior damage. Figures 6-32 to 6-34 indicate how different the peak displacement response of undamaged Takeda and bilinear models can be to a given earthquake.

Figure 6-57 shows the percentage of Takeda10 oscillators that reached their collapse displacement. It can be observed that 10% or more of those structures designed to achieve a displacement ductility of two collapsed. This indicates the need to ensure that structures having negative post-yield stiffnesses remain nearly elastic if collapse is to be avoided. Strength

reduction tends to increase the tendency of the oscillators to collapse. No clear trend emerges as to the effect of PDD on the tendency of these oscillators to collapse.

6.5 Nonlinear Static Procedures

6.5.1 Introduction

Nonlinear static analysis is used to estimate inelastic response quantities without undertaking the effort required for inelastic dynamic analyses. Several methods are presently in use. No consensus has emerged as to the applicability and relative accuracy of the methods, which are collectively known as nonlinear static procedures (NSP). These procedures each focus

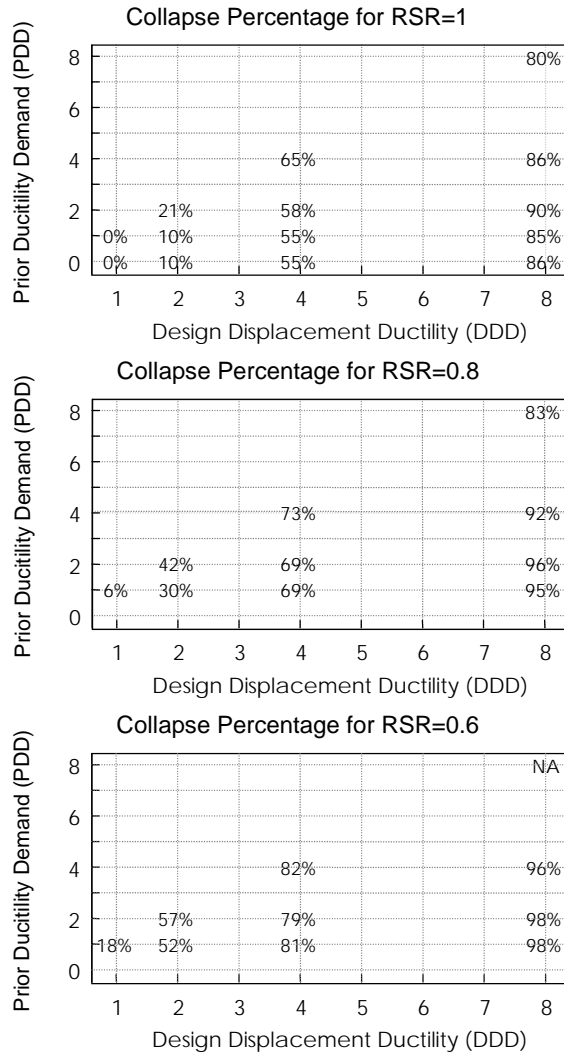


Figure 6-57 Percent of Takeda10 Oscillators that Collapsed

on different parameters for determining estimates of peak displacement response. Consequently, NSP displacement estimates may be affected to different degrees by differences in hysteretic model, initial stiffness, lateral strength, and post-yield stiffness.

Section 6.5.2 describes three nonlinear static methods; displacement coefficient, secant, and capacity spectrum methods. Differences among the methods and the implications for estimating displacements are discussed in Section 6.5.3. Assumptions made to extend the methods to cases with prior damage are discussed in Section 6.5.4. Displacement estimates obtained using

NSP are compared with values computed from dynamic analyses in Section 6.6.

6.5.2 Description of Nonlinear Static Procedures

The methods are briefly described in this section for cases assumed to correspond most closely to the dynamic analysis framework of Section 6.3.3, representing wall buildings at the collapse prevention performance level. The reader is referred to FEMA 273 for greater detail on the displacement coefficient method, and to ATC-40 for greater detail on the secant and capacity spectrum methods. The displacement

coefficient method described here is the same as in FEMA 273.

6.5.2.1 Displacement Coefficient Method

The displacement coefficient method estimates peak inelastic displacement response as the product of a series of coefficients and the elastic spectral displacement. The peak displacement estimate, d_d , is given by

$$d_d = C_0 C_1 C_2 C_3 S_a \left(\frac{T_e}{2\pi} \right)^2 \tag{6-2}$$

where coefficients C_0 through C_3 modify the spectral displacement, given by the product of the elastic spectral acceleration, S_a , and $(T_e/2\pi)^2$, where T_e is an effective period based on the effective stiffness determined using the construction of Figure 6-58. In the above, C_0 relates the spectral displacement and the expected roof displacement, and is set at 1 for SDOF systems. The coefficient C_1 accounts for the amplification of peak displacement for short-period systems, is set at 1 for $T_e > T_g$, and is computed as follows for $T_e < T_g$:

$$C_1 = \frac{1}{R} + \left(1 - \frac{1}{R} \right) \frac{T_g}{T_e} \tag{6-3}$$

where R = the strength-reduction factor, given by the ratio of the elastic base shear force and the effective

yield strength, F_{ye} , illustrated in Figure 6-58. An optional limit of 2 on C_1 was not applied in the analyses described here.

The coefficient C_2 accounts for the type of hysteretic response. At the collapse prevention performance level, C_2 varies linearly between 1.5 at 0.1 sec and 1.2 at T_g , and remains at 1.2 for T_e greater than T_g .

The coefficient C_3 accounts for increases in displacements that arise when $P-\Delta$ effects are significant. Because the dynamic analyses did not include second-order effects, C_3 was assigned a value of 1. However, the Takeda 10 models had a negative post-yield stiffness of 10 percent, which approximates $P-\Delta$ effects

6.5.2.2 Secant Method

The secant method assumes that the peak displacement response of a nonlinear system can be estimated as the peak response of an elastic system having increased period. An idealized lateral-force/displacement curve for the structure is developed using a static “pushover” analysis. The elastic response of the structure is computed using a response-spectrum analysis, using initial component stiffness values. The resulting elastic displacements are used to obtain revised stiffness values for the components, set equal to the secant stiffness defined at the intersections of the component force/displacement curves and the elastic displacements obtained from the response-spectrum analysis. Using these revised stiffness values, another response-spectrum analysis is performed, and iterations continue

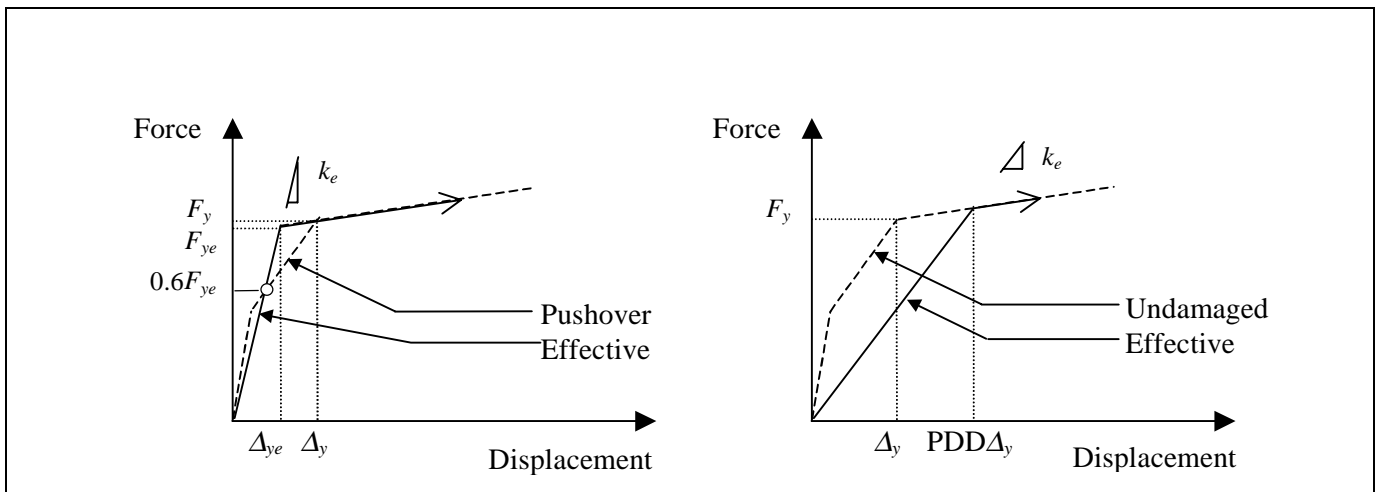


Figure 6-58 Construction of Effective Stiffness for use with the Displacement Coefficient Method

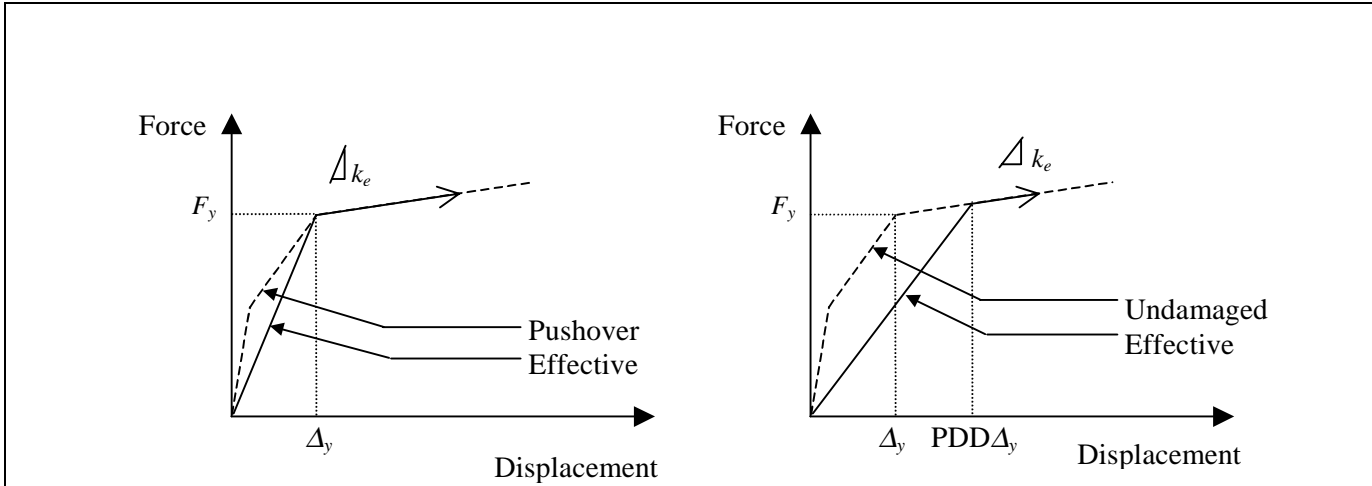


Figure 6-59 Initial Effective Stiffness and Capacity Curves Used in the Secant and Capacity Spectrum Methods

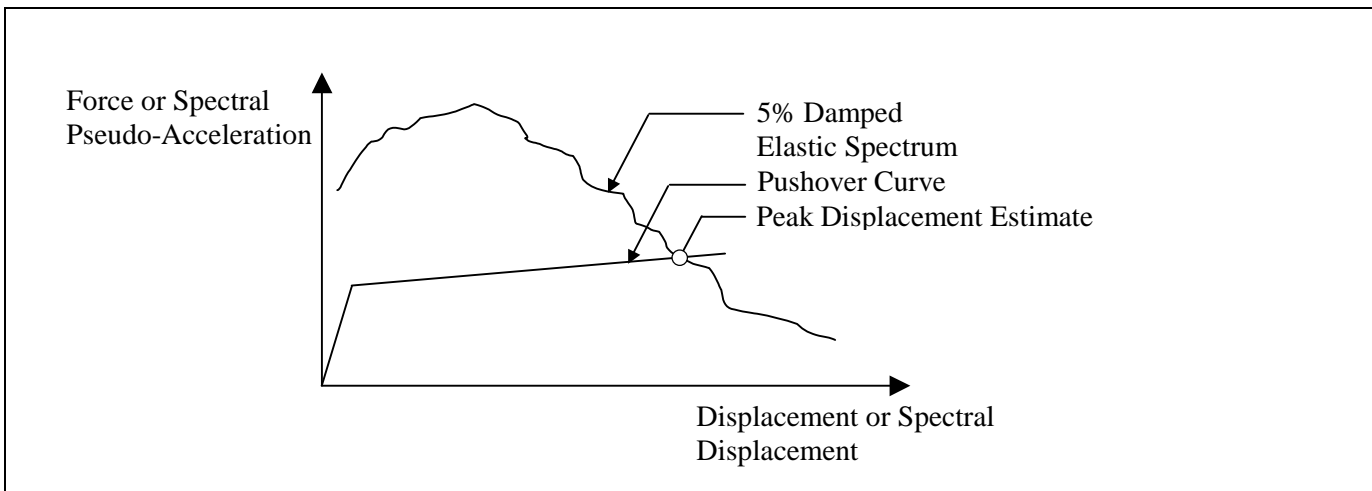


Figure 6-60 Schematic Depiction of Secant Method Displacement Estimation

until the displacements converge. All response-spectrum analyses are made for 5% damping in the secant method, as described in ATC-40. For SDOF structures, the secant method can be implemented in spectral pseudo-acceleration–spectral displacement space, much like the capacity spectrum method. The force/displacement curve may be determined using the constructions of Figure 6-59 for both the undamaged and damaged oscillators. This curve is plotted together with the elastic response spectrum for 5% damping in Figure 6-60. An estimate of peak displacement is indicated in the figure. For the undamaged oscillators, an initial estimate of peak displacement response is the peak response of an elastic oscillator having stiffness equal to the initial stiffness of the oscillator. The intersection of the previous displacement estimate with the idealized force/displacement curve of the structure defines a new secant

stiffness. This stiffness may be used to obtain a revised estimate of peak displacement response. These iterations continue until satisfactory convergence occurs. This is shown schematically in Figure 6-61.

6.5.2.3 Capacity Spectrum Method

Like the secant method, the capacity spectrum method assumes that the peak displacement response of a nonlinear system can be estimated by an elastic system having reduced stiffness. The difference is that the elastic spectral-response values are modified to reflect increases in damping associated with inelastic response. A lateral force “pushover” curve is developed for the structure and plotted on spectral pseudo-acceleration–spectral displacement coordinates. The structure is assumed to displace until it reaches an elastic demand curve that has damping that corresponds to a value based on the current displacement estimate.

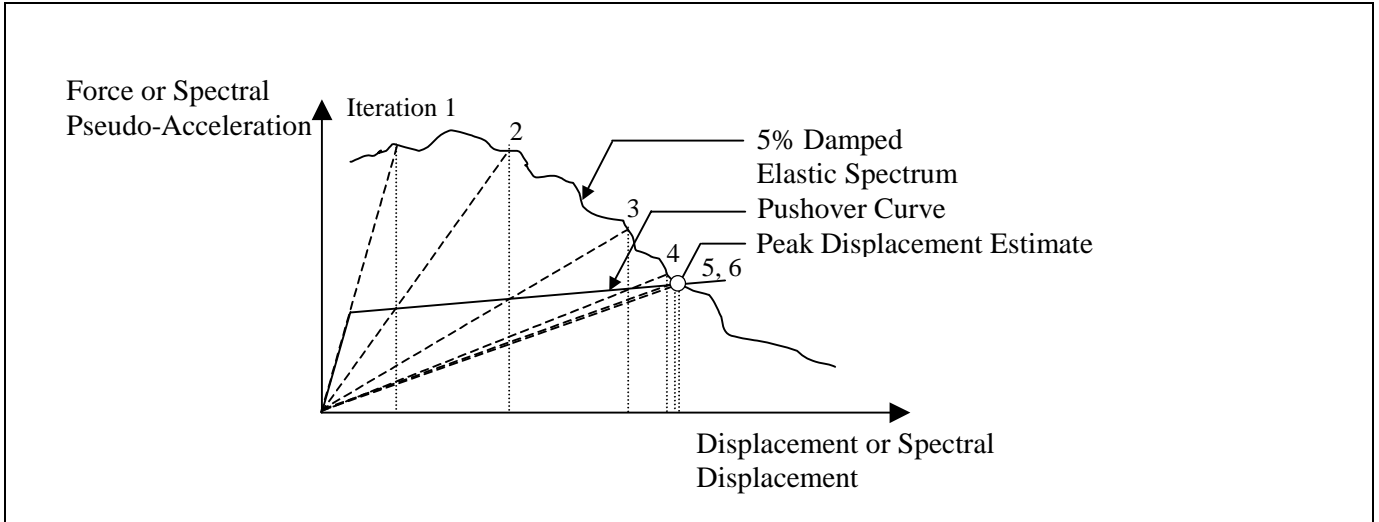


Figure 6-61 Schematic Depiction of Successive Iterations to Estimate Displacement Response Using the Secant Method for Single-Degree-of-Freedom Oscillators

The method may be implemented by successively iterating displacement response. The initial displacement is estimated using the initial stiffness of the structure and assuming elastic response for damping equal to 5% of critical damping. The intersection of the displacement estimate and the idealized force/displacement curve determines a revised estimate of the secant stiffness. Effective viscous damping is revised prescriptively, based on the displacement estimate. This calculation represents the increase in effective damping with increased hysteretic losses. The iterations continue until satisfactory convergence is obtained. Figure 6-62 illustrates the application of the method.

6.5.3 Comments on Procedures

From the above descriptions, it is clear that there are fundamental differences among the various NSPs. The displacement coefficient method primarily relies on the initial effective stiffness to determine a baseline spectral displacement, and it considers strength to a lesser extent for short-period structures.

The secant and capacity spectrum methods are insensitive to initial stiffness (for structures that yield), and displacement estimates depend primarily on yield strength and post-yield stiffness. Effective damping varies with displacement amplitude in the capacity

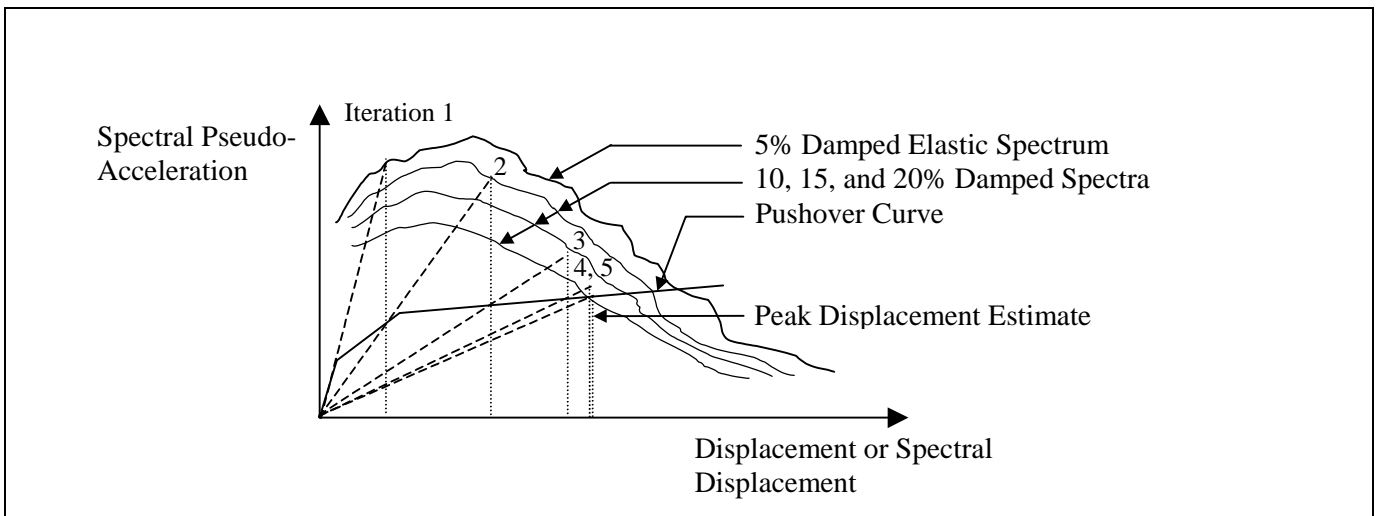


Figure 6-62 Schematic Depiction of Successive Iterations to Estimate Displacement Response Using the Capacity Spectrum Method

spectrum method, while it is invariant in the secant method. In the form presented in ATC-40, secant method displacement estimates are independent of hysteretic model. Through changes in coefficient C_2 , changes in the force/displacement model may be incorporated in the displacement coefficient method. Differences in hysteresis model are accounted for in the capacity spectrum method adjusting effective damping for three “structural behavior types.”

6.5.4 Application of Procedures to Undamaged and Damaged Oscillators

Each procedure presumes that a smoothed, elastic design response spectrum is to be used in practice. To avoid uncertainties in interpretation of results, the actual pseudo-acceleration spectra were used in place of a smoothed approximation in this study. For the capacity spectrum method, the actual pseudo-acceleration spectra were computed for a range of damping levels, and the spectral reduction factors that are prescribed for use with smoothed design spectra were not employed. These modifications introduce some scatter in the resulting displacement estimates that would not occur if smoothed spectra had been used. Thus, some “smoothing” of the data may be appropriate when interpreting the results.

The NSPs were developed for use with undamaged structures. In this study, the NSPs were applied to the initially-damaged structures using the assumptions described below, representing one of many approaches that can be taken. Recommended procedures for estimating displacements are described in Section 4.4 of FEMA 306.

For the displacement coefficient method, the capacity curve was obtained by the procedure described in FEMA 273. For the uncracked oscillators, a bilinear curve was fit, crossing at 60% of the bilinear curve yield strength. For the damaged oscillators, the effective period of vibration was set at the initial period of the damaged oscillators. Displacements were amplified by the factor C_1 without imposing the optional limit of 2 specified in the provisions.

The secant method was applied iteratively. For undamaged oscillators, the initial stiffness was the yield-point secant stiffness. For damaged oscillators, it was set at the secant stiffness obtained at the displacement imposed by prior ductility demands. The

initial stiffness of the damaged oscillators therefore reflected the previous damage.

The capacity spectrum method was also applied iteratively, beginning with the same initial oscillator stiffness used in the secant method. Effective damping was determined by using the yield point of the undamaged oscillators. The capacity spectrum method was implemented for an intermediate “building characteristic,” identified as Type B. This type is considered to represent average existing buildings subjected to short-duration motions and new buildings subjected to long-duration motions. For this type, effective damping is limited to 29% of critical damping.

For both the capacity spectrum and the secant stiffness methods, 10 iterations were performed for each structure. These iterations generally converged on a single result, and differences in successive approximations were typically less than 1%. On occasion, differences in successive approximations were large, suggesting a lack of convergence due to the jagged nature of the actual (not smoothed) spectra. Where these differences occurred, the displacement estimate at the tenth iteration was retained.

6.6 Comparison of NSP and Dynamic Analysis Results

6.6.1 Introduction

In evaluating the utility of the NSPs, attention may be directed at two estimates. The first is peak displacement response; it could be expected that an acceptable procedure would estimate the peak displacement response, d_d , of a nonlinear system within acceptable limits of accuracy. Second, it is possible that a procedure may be systematically biased, and hence may estimate displacement response poorly while providing reasonable estimates of displacement ratio; that is, the ratio of damaged structure displacement to undamaged structure displacement, d'_d/d_d . These response indices, d_d and d'_d/d_d , are examined in detail in the following sections for Takeda oscillators designed for bilinear DDDs of 8.

6.6.2 Displacement Estimation

Peak displacement response of the undamaged Takeda oscillators was estimated for each earthquake record. The ratio of the peak displacement estimate from NSP

and the value computed for each Takeda5 oscillator, at each period and for each ground motion record, is plotted in Figure 6-63 for $DDD = 8$ and $RSR = 1$. The log scale plots the ratio of estimated and computed displacement, $d_{d,NSP}/d_d$. Plots are presented for each ground motion category and for each NSP.

In Figure 6-63, it can be observed that the ratio of the estimated and computed displacements, $d_{d,NSP}/d_d$, can vary significantly, ranging from less than 0.3 to more than 100. At any period ratio, the ratio $d_{d,NSP}/d_d$ may approach or exceed an order of magnitude. Because the trends tend to be consistent for each ground motion record, the jaggedness of the actual spectra does not appear to be the source of most of the variability.

Figure 6-64 plots mean values of ratios $d_{d,NSP}/d_d$ determined for each NSP, for all ground motions and all DDD values. Results for short- and long-period Takeda5 oscillators are plotted separately. In Figure 6-64, it can be observed that the NSP procedures tend to overestimate, in a mean sense, the displacements computed for the short-period Takeda5 oscillators for all DDD . Takeda oscillators having $DDD = 1$ often displaced less than their bilinear counterparts because the Takeda oscillators had initial stiffness equal to twice that of their bilinear counterparts. The difference in initial stiffness explains the tendency of the NSP methods to overestimate displacements for low DDD . This is particularly true for the secant method estimates of short-period oscillators, for which mean ratios exceeded six for DDD greater than 1. The period ratio, T_e/T_g , marking the boundary of the elevated estimates tends to be less than one, possibly reflecting the effective increase in period of Takeda5 oscillators as their stiffness reduces (Figure 6-63).

Figure 6-64 indicates that each NSP tends to overestimate the displacement response of short-period oscillators and that the capacity spectrum method is most accurate for long-period Takeda5 oscillators, in a mean sense. Nevertheless, Figure 6-63 indicates the substantial variability in displacement estimates and the potential to overestimate or underestimate displacements with all methods. A single estimate cannot capture the breadth of response variability that may occur at a given site.

Based on Figures 6-63 and 6-64, the coefficient and capacity spectrum methods appear to be reasonably accurate and to have the least scatter. The secant method

tended to overestimate displacement and exhibited more scatter in values of $d_{d,NSP}/d_d$.

6.6.3 Displacement Ratio Estimation

The ratio of damaged oscillator displacement, d'_d , and the displacement of the corresponding Takeda oscillator having no initial damage, d_d , was estimated using the NSP methods for each Takeda oscillator/earthquake pair, as described in Section 6.5.4. This estimated displacement ratio is compared with the ratio computed from the dynamic analyses in Figures 6-65 through 6-73.

It can be observed that simple application of the displacement coefficient method using the initial stiffness of the undamaged oscillator to calculate d_d and using the reduced stiffness of the damaged oscillator to calculate d'_d almost always overestimates the effects of damage for the cases considered.

Application of the secant and capacity spectrum methods, using the initial and reduced stiffness values, typically led to nearly identical displacement estimates: estimates of d'_d/d_d were often approximately equal to one. Figures 6-68 through 6-73, which might appear to testify to the success of the methods, instead tend more to represent the inverse of the d'_d/d_d as computed for the Takeda models. Figures 6-38 through 6-40 indicate that computed values of d_d/d'_d should tend to be around one, decreasing slightly for small periods.

The preceding plots examine the effectiveness of the methods, as implemented here, for estimating the consequences of prior ductility demand. It is also of interest to examine the effectiveness of the methods in accounting for strength loss. To do this, the ratio of the displacement obtained with $RSR = 0.6$ to that with $RSR = 1.0$ was evaluated for the nonlinear Takeda5 oscillators having $DDD = 8$ and $PDD = 1$, in order to compare the NSP estimates of the displacement ratio with the displacement ratio computed for the nonlinear Takeda5 oscillators. The upper plots in Figures 6-74 through 6-82 show the estimated displacement ratio for one of the three NSPs, and the lower plots of these figures normalize this displacement ratio by the displacement ratio computed for the Takeda5 oscillators. It can be observed that the NSP methods tend to account correctly for the effect of strength reduction on displacement response, in a mean sense.

(Text continued on page 177)

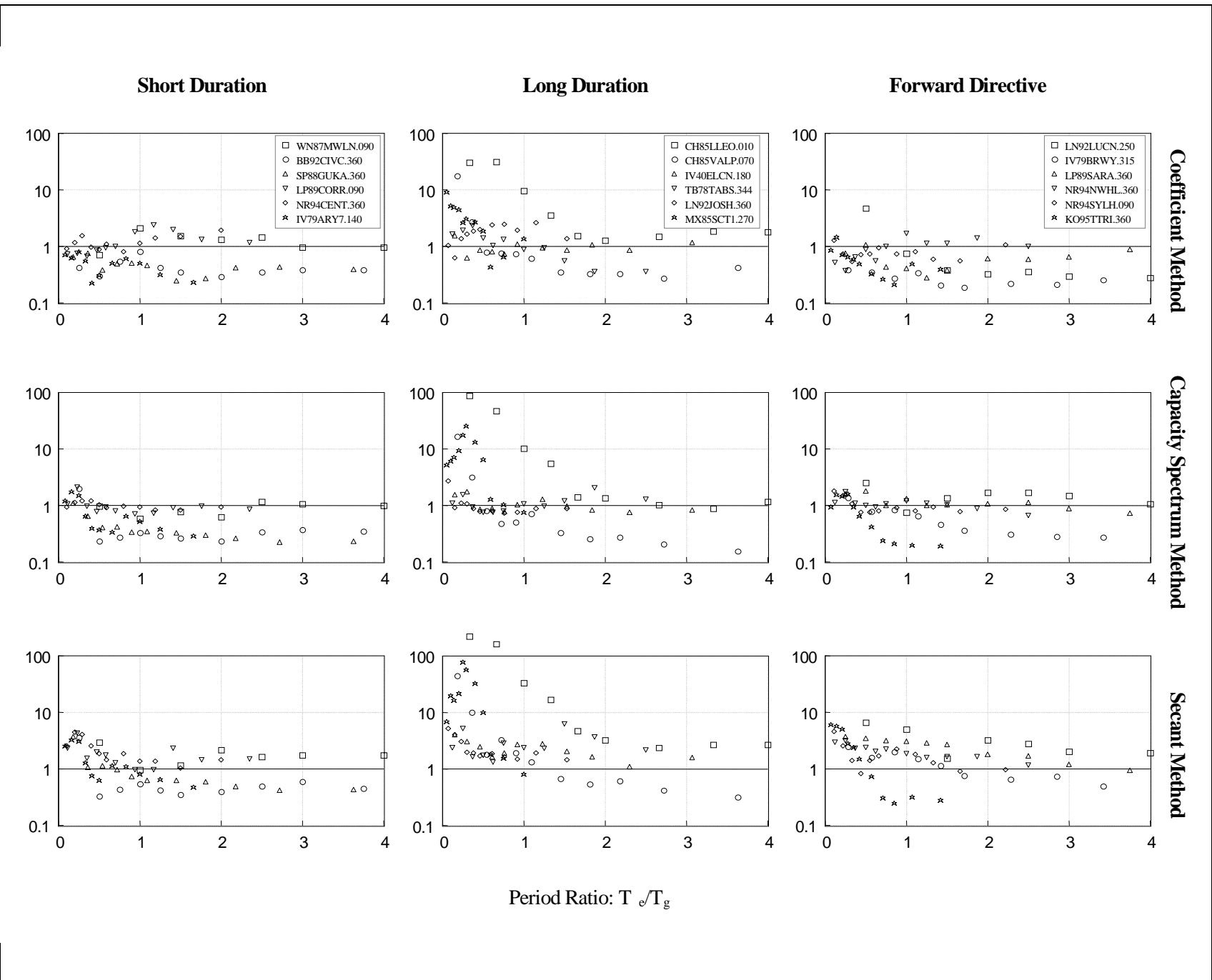


Figure 6-63 Values of d_{nsp}/d_d for the Takeda5 Model

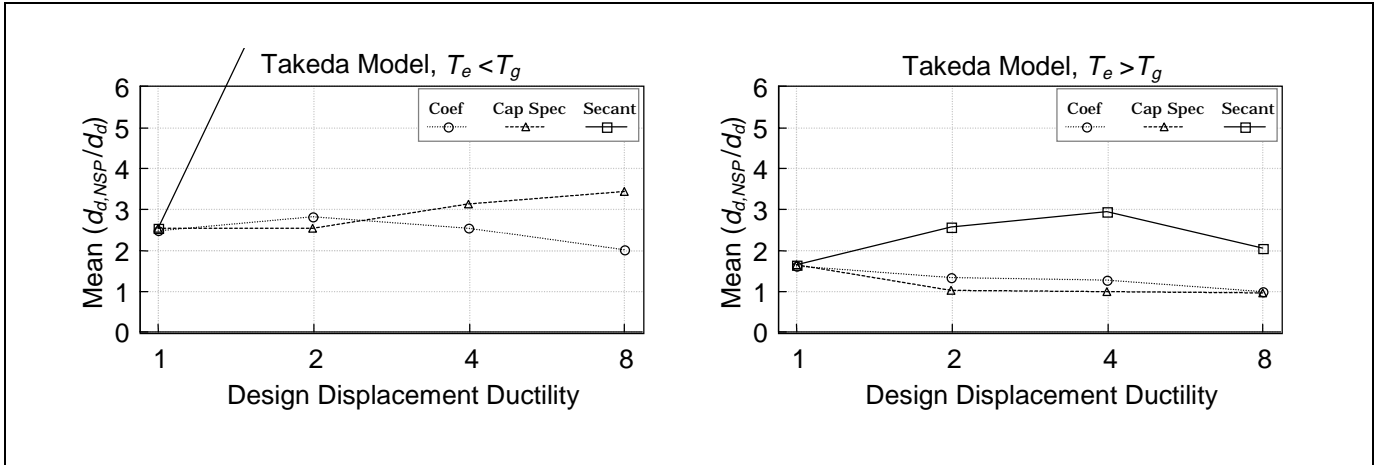


Figure 6-64 Mean values of $d_{d,NSP}/d_d$ for all ground motions for each NSP method, for short and long-period Takeda5 Models. See text in Section 6.6.2.

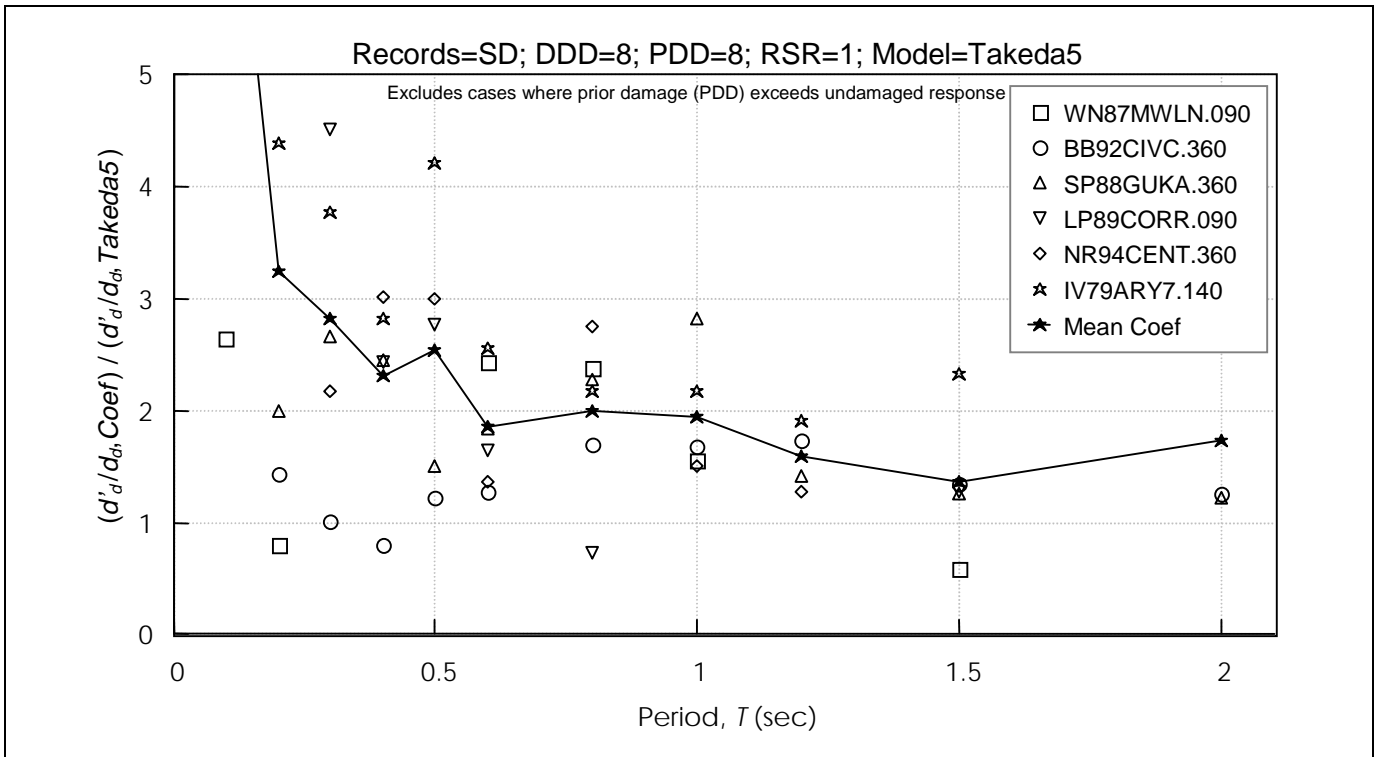


Figure 6-65 Coefficient Method Estimates of Ratio of Damaged and Undamaged Oscillator Displacement Normalized by Computed Ratio, for Short-Duration Records
DDD = Design Displacement Ductility; PDD = Prior Ductility Demand; RSR = Reduced Strength Ratio

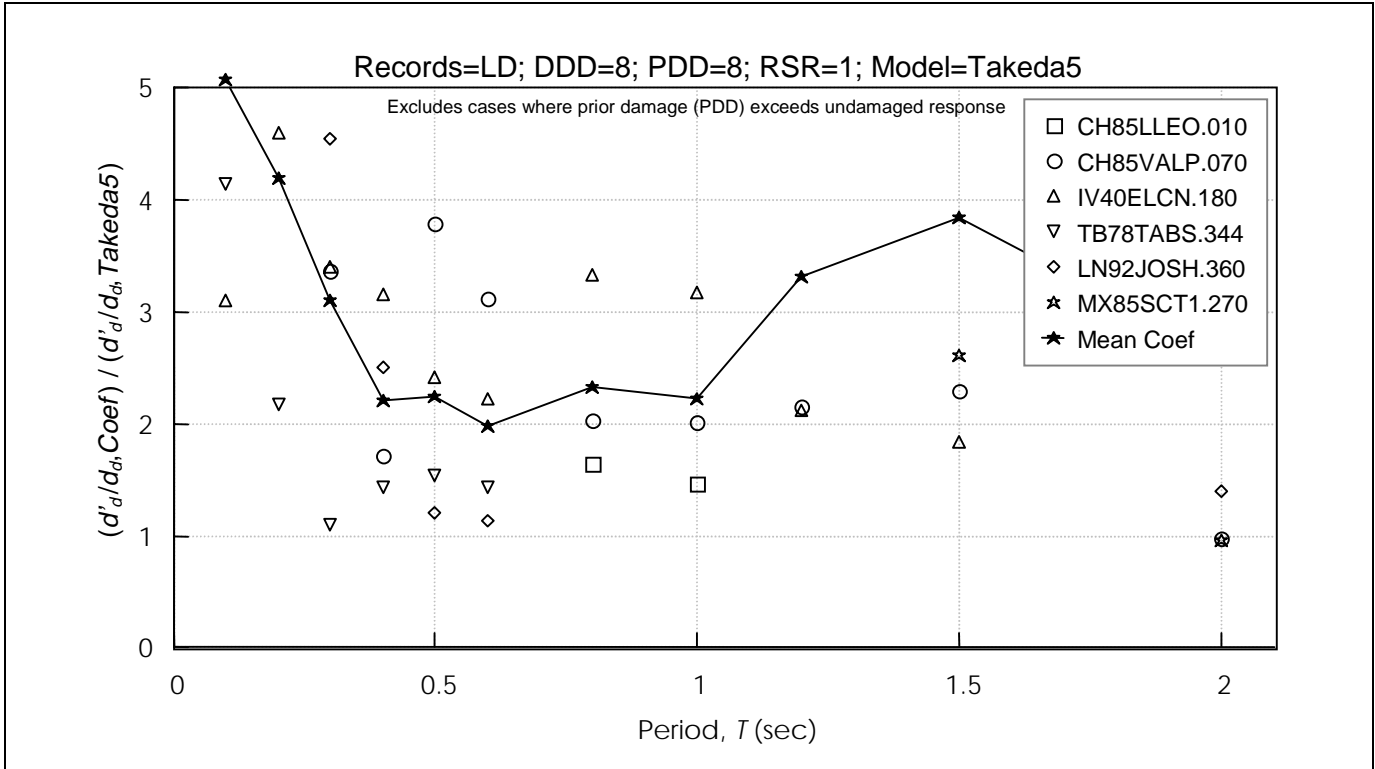


Figure 6-66 Coefficient Method Estimates of Ratio of Damaged and Undamaged Oscillator Displacement Normalized by Computed Ratio, for Long-Duration Records
 DDD = Design Displacement Ductility; PDD = Prior Ductility Demand; RSR = Reduced Strength Ratio

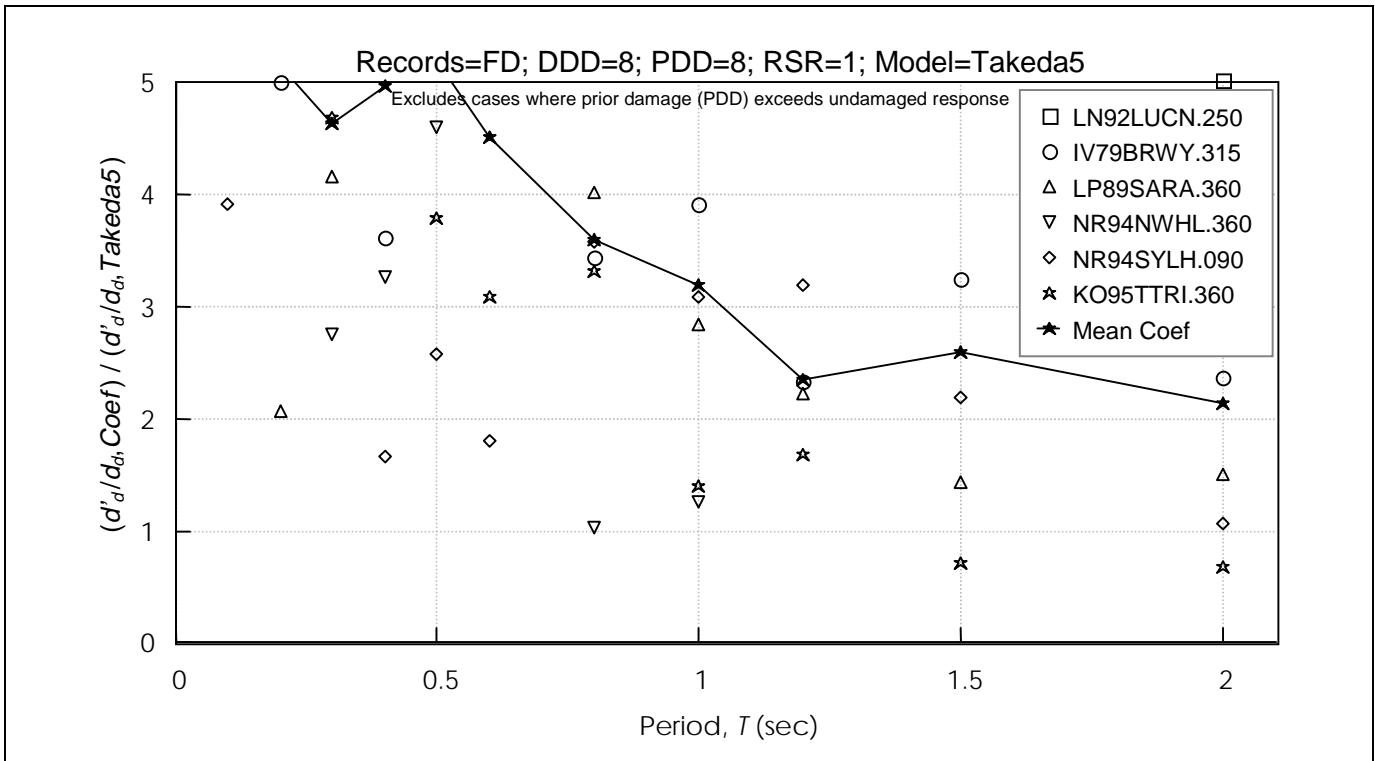


Figure 6-67 Coefficient Method Estimates of Ratio of Damaged and Undamaged Oscillator Displacement Normalized by Computed Ratio, for Forward Directive Records
 DDD = Design Displacement Ductility; PDD = Prior Ductility Demand; RSR = Reduced Strength Ratio

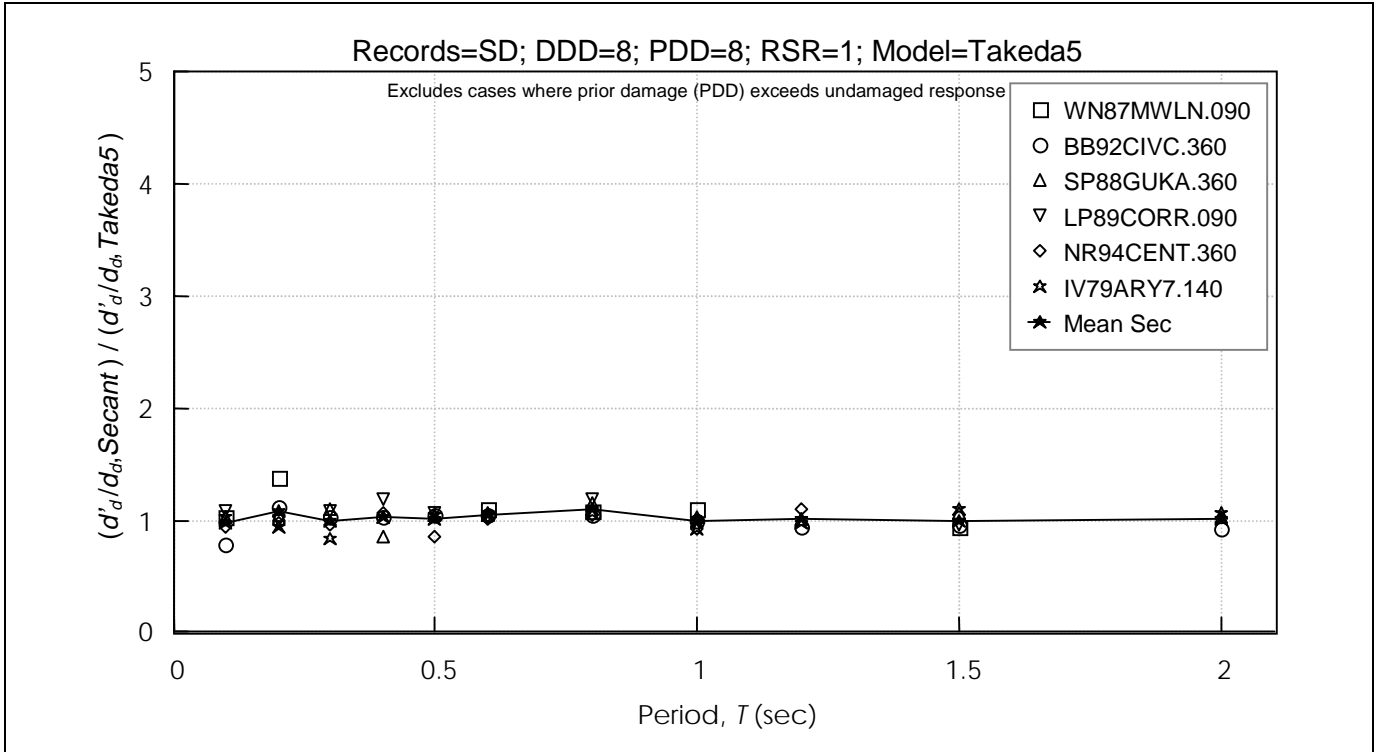


Figure 6-68 Secant Method Estimates of Ratio of Damaged and Undamaged Oscillator Displacement Normalized by Computed Ratio, for Short-Duration Records
DDD = Design Displacement Ductility; PDD = Prior Ductility Demand; RSR = Reduced Strength Ratio

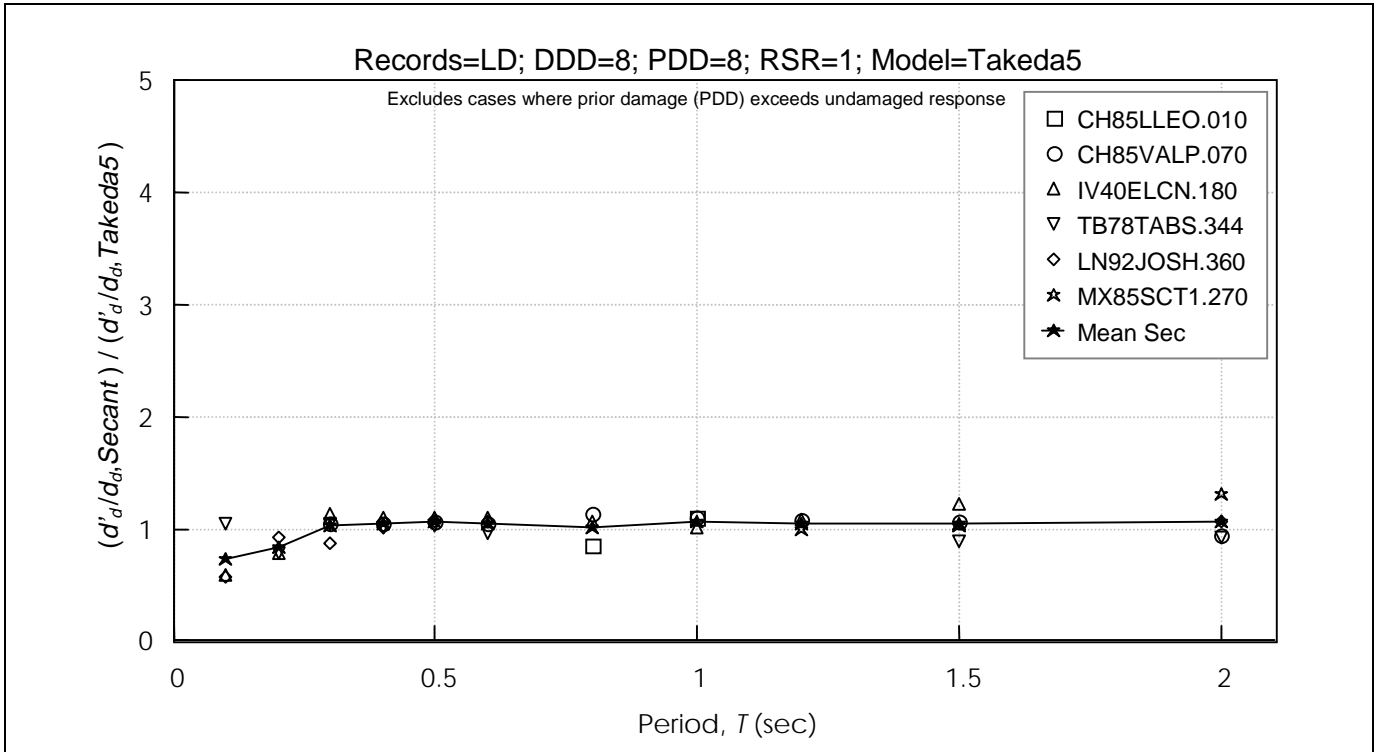


Figure 6-69 Secant Method Estimates of Ratio of Damaged and Undamaged Oscillator Displacement Normalized by Computed Ratio, for Long-Duration Records
DDD = Design Displacement Ductility; PDD = Prior Ductility Demand; RSR = Reduced Strength Ratio

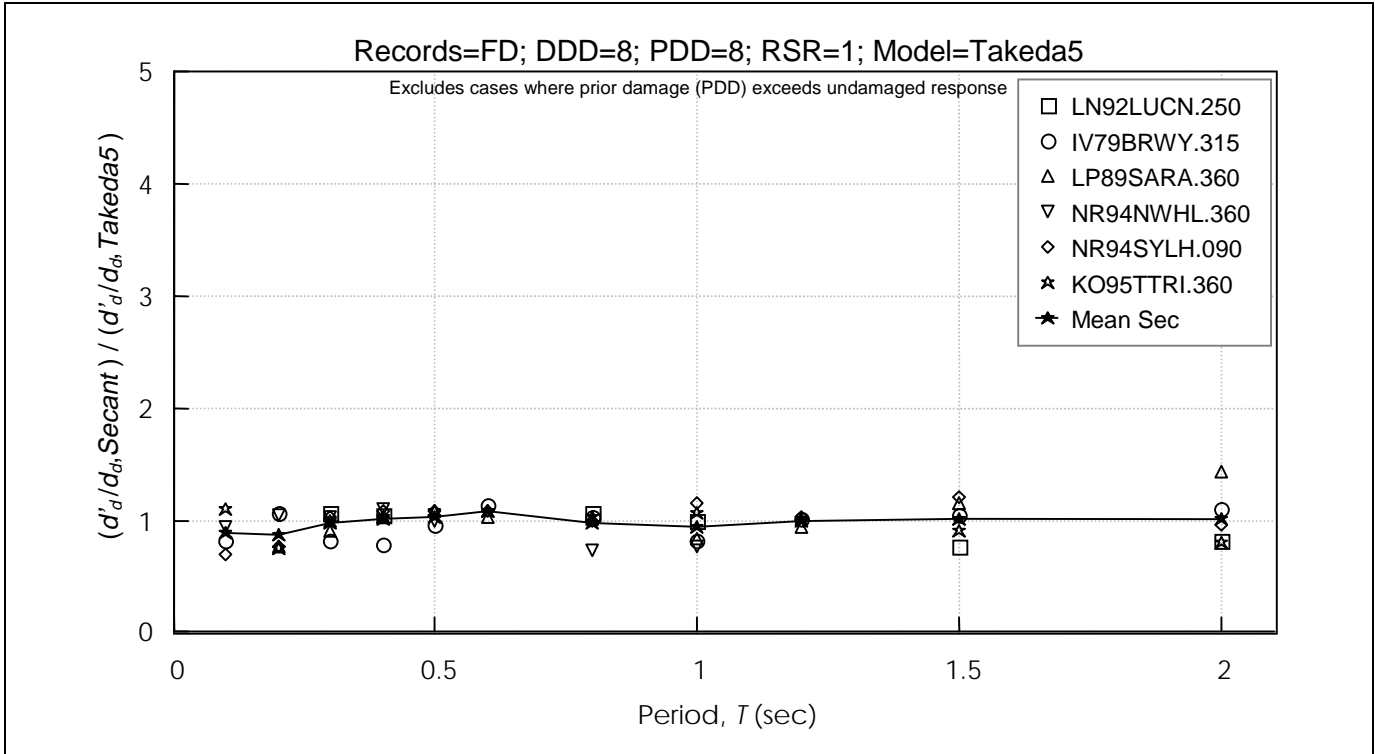


Figure 6-70 Secant Method Estimates of Ratio of Damaged and Undamaged Oscillator Displacement Normalized by Computed Ratio, for Forward Directive Records
 DDD = Design Displacement Ductility; PDD = Prior Ductility Demand; RSR = Reduced Strength Ratio

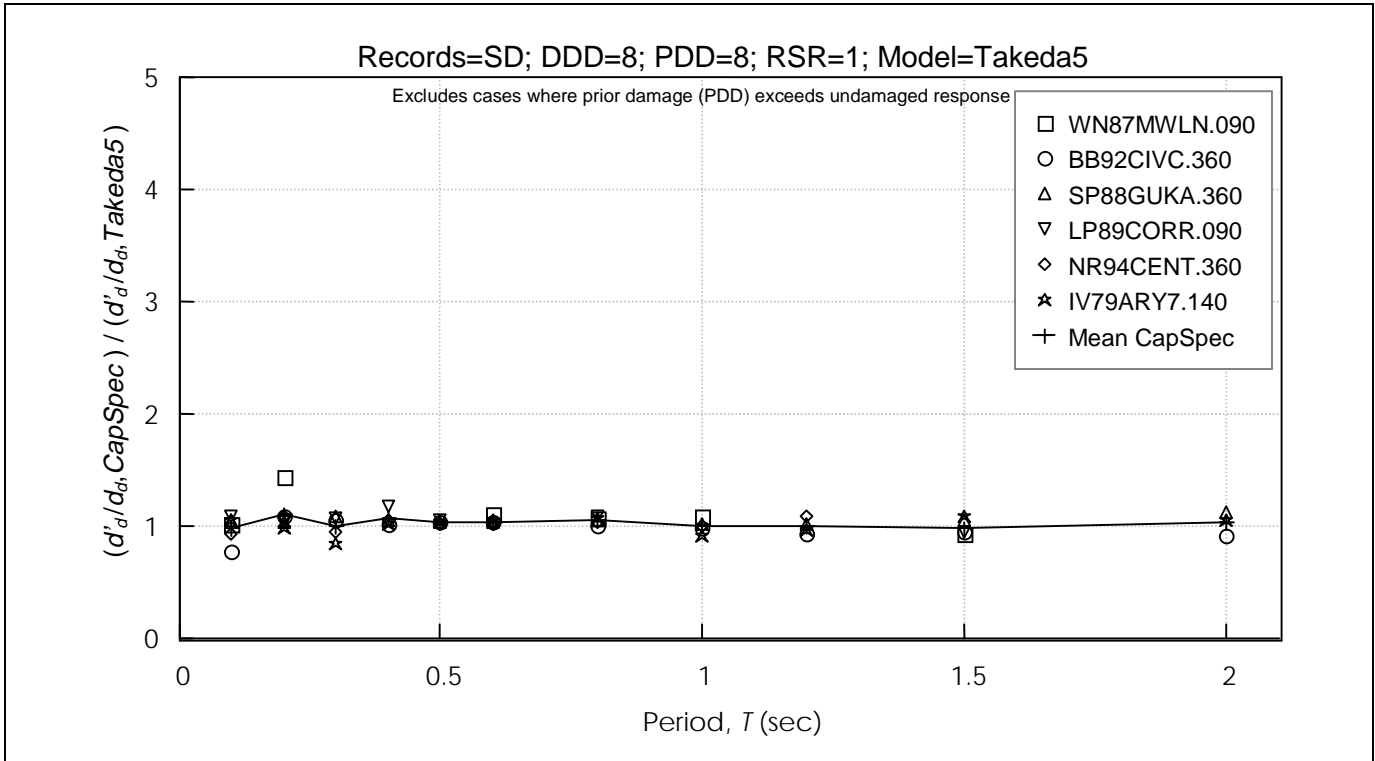


Figure 6-71 Capacity Spectrum Method Estimates of Ratio of Damaged and Undamaged Oscillator Displacement Normalized by Computed Ratio, for Short-Duration Records
 DDD = Design Displacement Ductility; PDD = Prior Ductility Demand; RSR = Reduced Strength Ratio

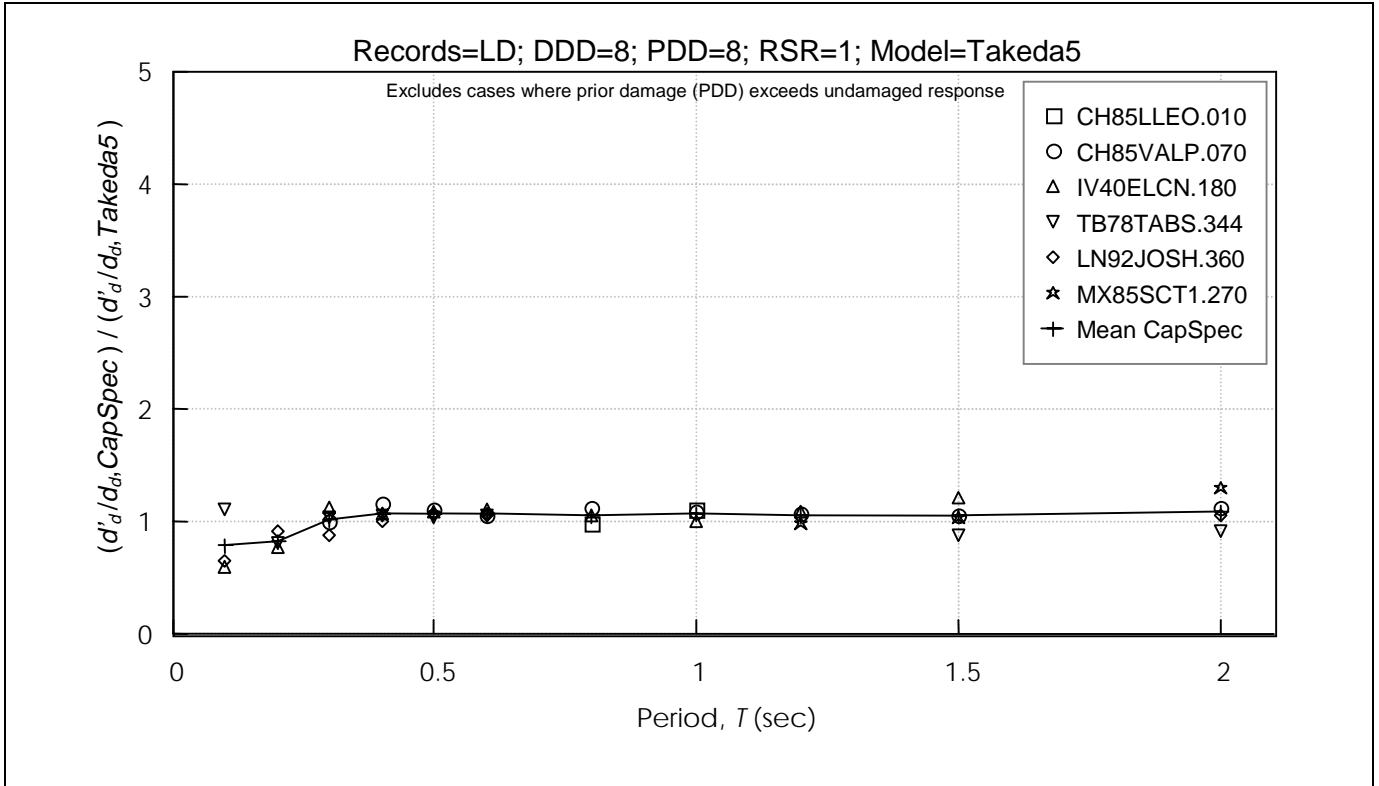


Figure 6-72 Capacity Spectrum Method Estimates of Ratio of Damaged and Undamaged Oscillator Displacement Normalized by Computed Ratio, for Long-Duration Records
 DDD = Design Displacement Ductility; PDD = Prior Ductility Demand; RSR = Reduced Strength Ratio

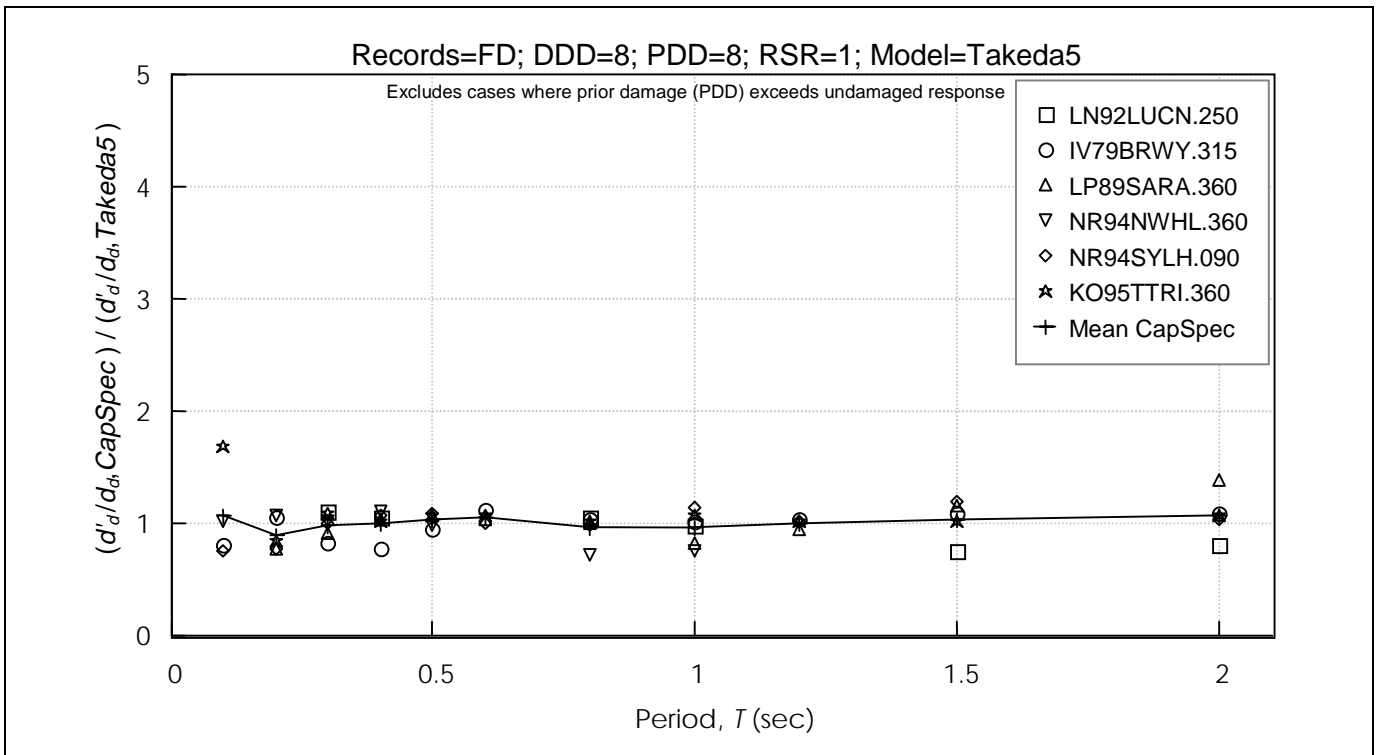


Figure 6-73 Capacity Spectrum Method Estimates of Ratio of Damaged and Undamaged Oscillator Displacement Normalized by Computed Ratio, for Forward Directive Records
 DDD = Design Displacement Ductility; PDD = Prior Ductility Demand; RSR = Reduced Strength Ratio

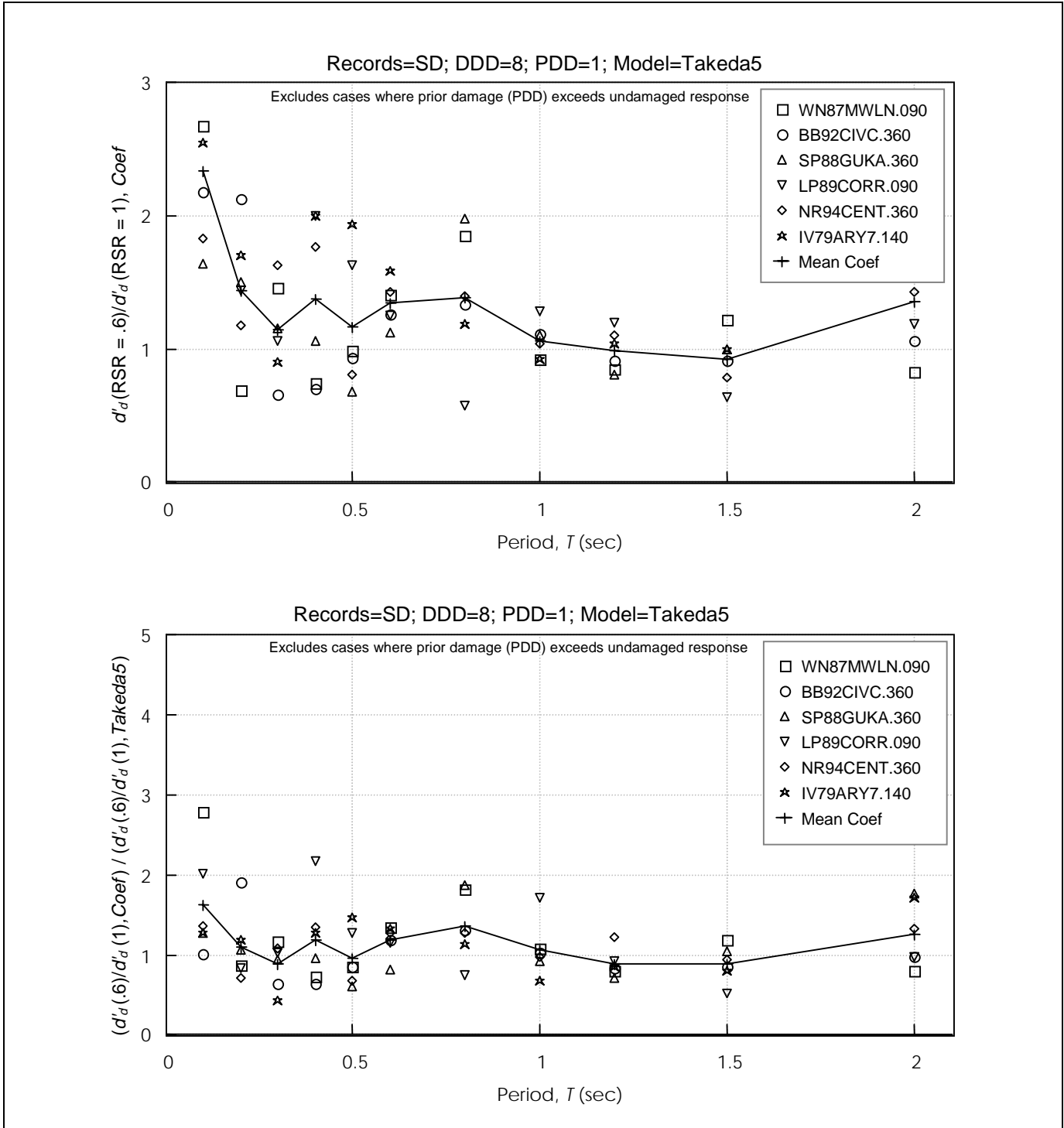


Figure 6-74 Coefficient Method Estimates of Displacement Ratio of RSR=0.6 and RSR=1.0 Takeda5 Oscillators having DDD= 8 and PDD= 1
 DDD = Design Displacement Ductility; PDD = Prior Ductility Demand; RSR = Reduced Strength Ratio

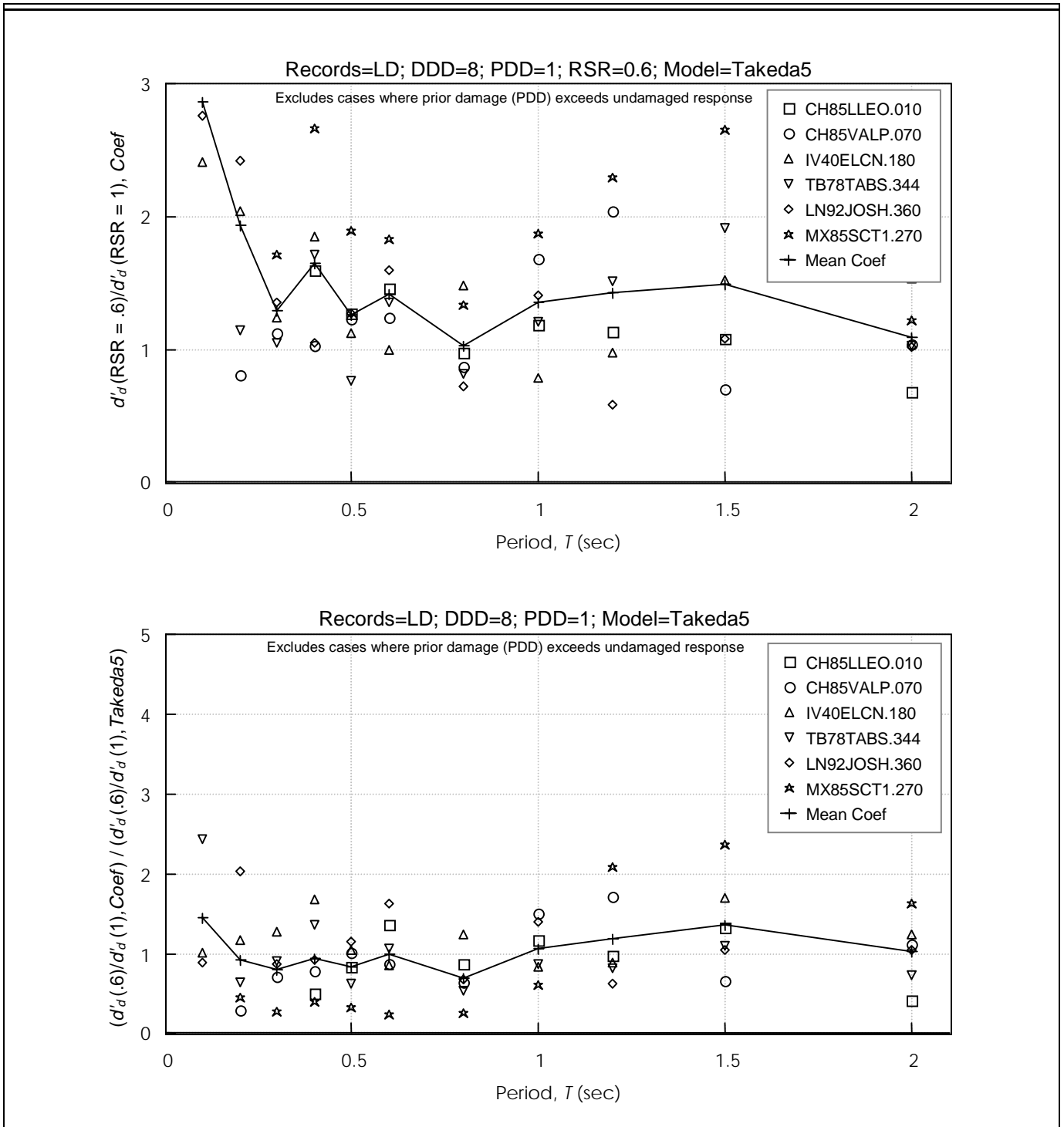


Figure 6-75 Coefficient Method Estimates of Displacement Ratio of RSR=0.6 and RSR=1.0 Takeda5 Oscillators having DDD= 8 and PDD= 1
 DDD = Design Displacement Ductility; PDD = Prior Ductility Demand; RSR = Reduced Strength Ratio

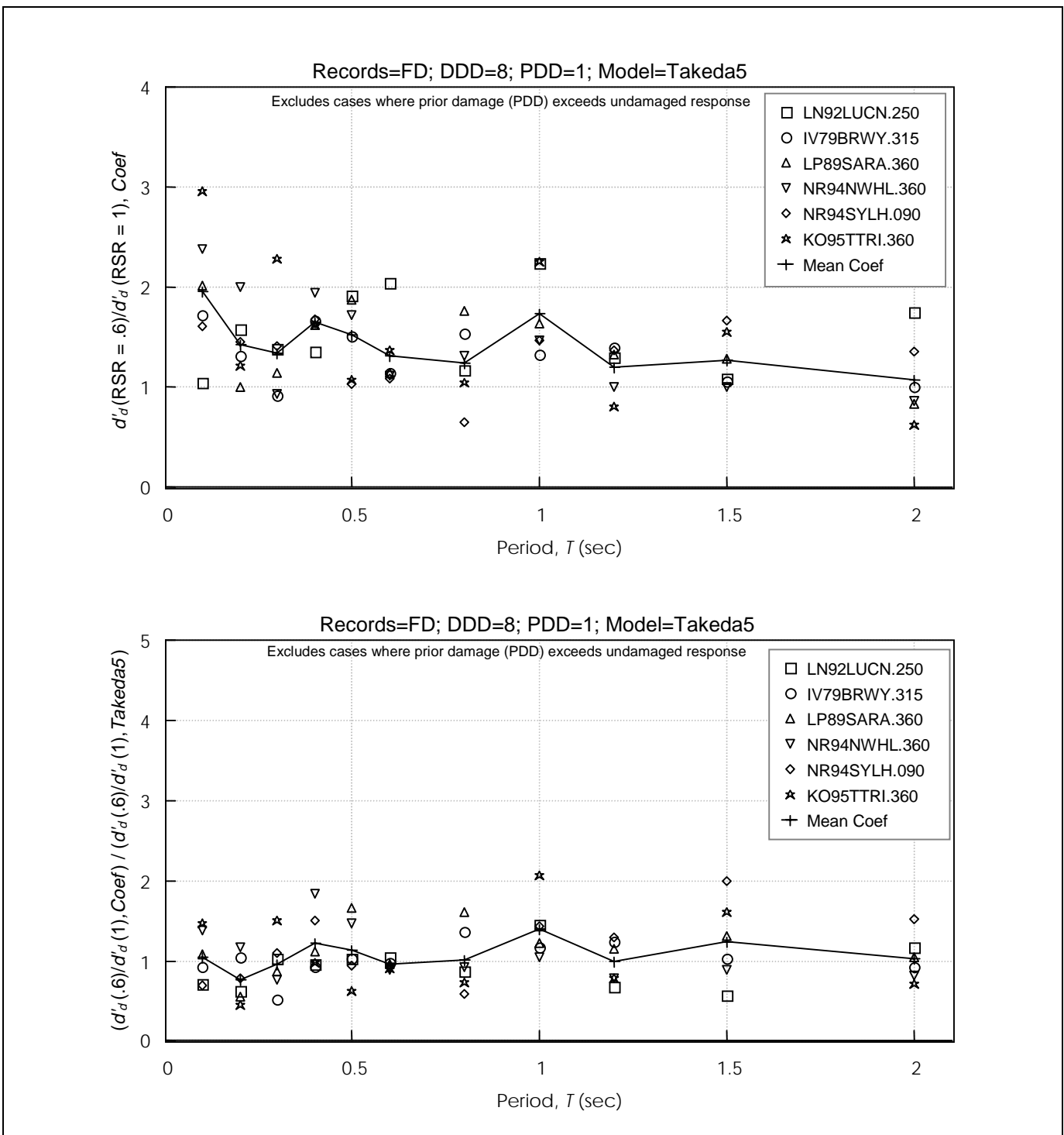


Figure 6-76 Coefficient Method Estimates of Displacement Ratio of RSR=0.6 and RSR=1.0 Takeda5 Oscillators having DDD= 8 and PDD= 1
 DDD = Design Displacement Ductility; PDD = Prior Ductility Demand; RSR = Reduced Strength Ratio

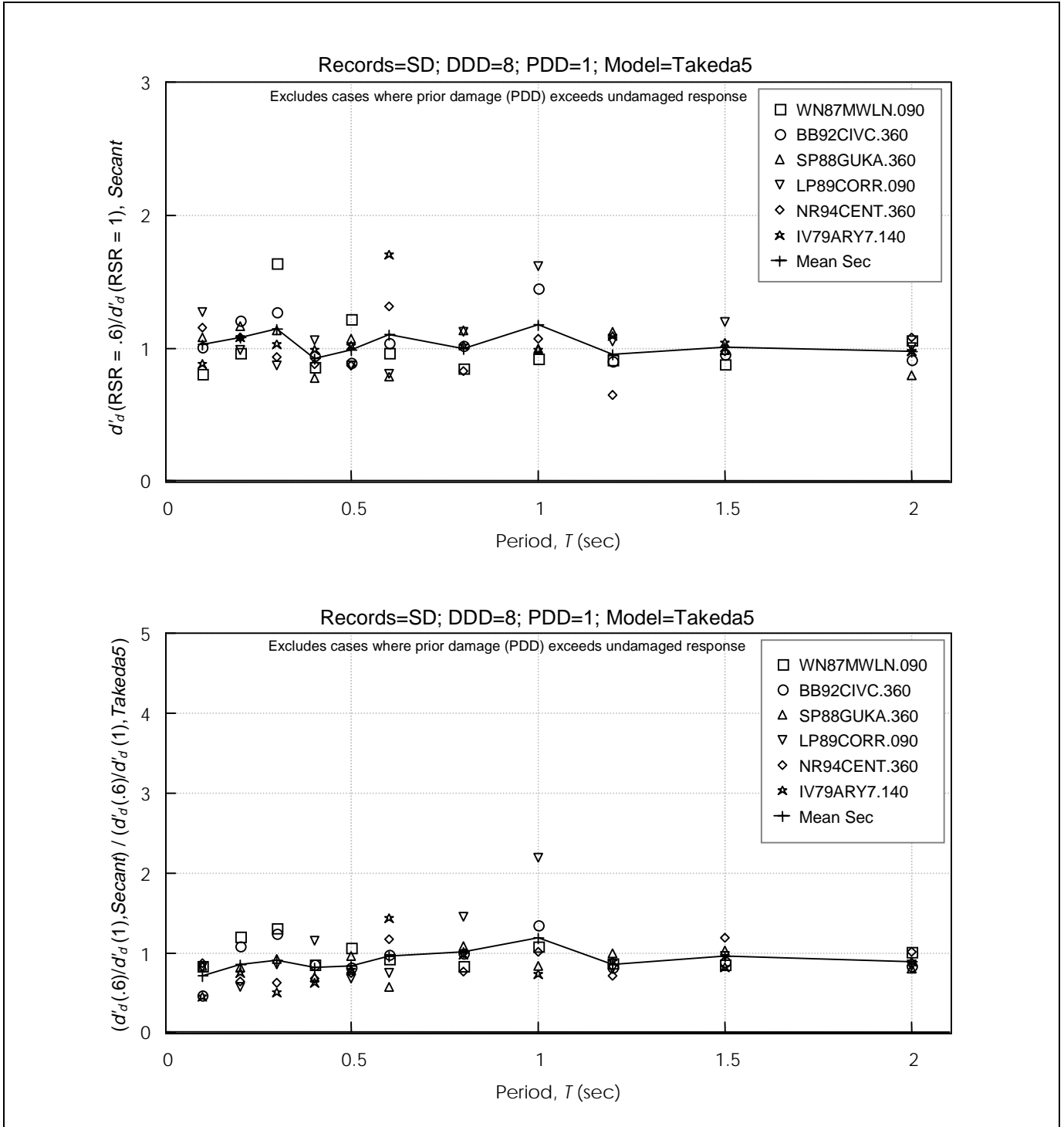


Figure 6-77 Secant Method Estimates of Displacement Ratio of RSR=0.6 and RSR=1.0 Takeda5 Oscillators having DDD= 8 and PDD= 1
 DDD = Design Displacement Ductility; PDD = Prior Ductility Demand; RSR = Reduced Strength Ratio

Chapter 6: Analytical Studies

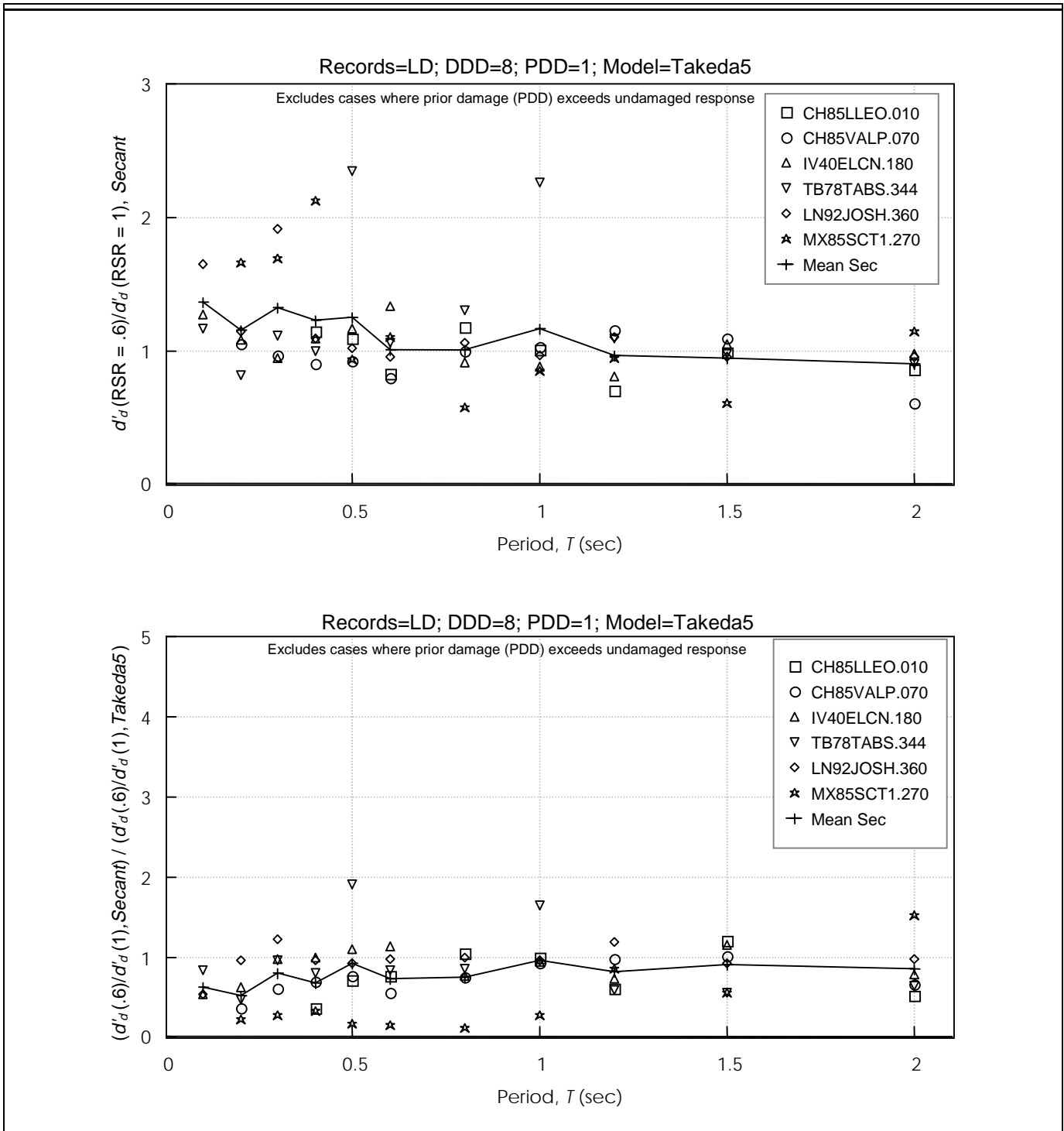


Figure 6-78 Secant Method Estimates of Displacement Ratio of RSR=0.6 and RSR=1.0 Takeda5 Oscillators having DDD= 8 and PDD= 1
 DDD = Design Displacement Ductility; PDD = Prior Ductility Demand; RSR = Reduced Strength Ratio

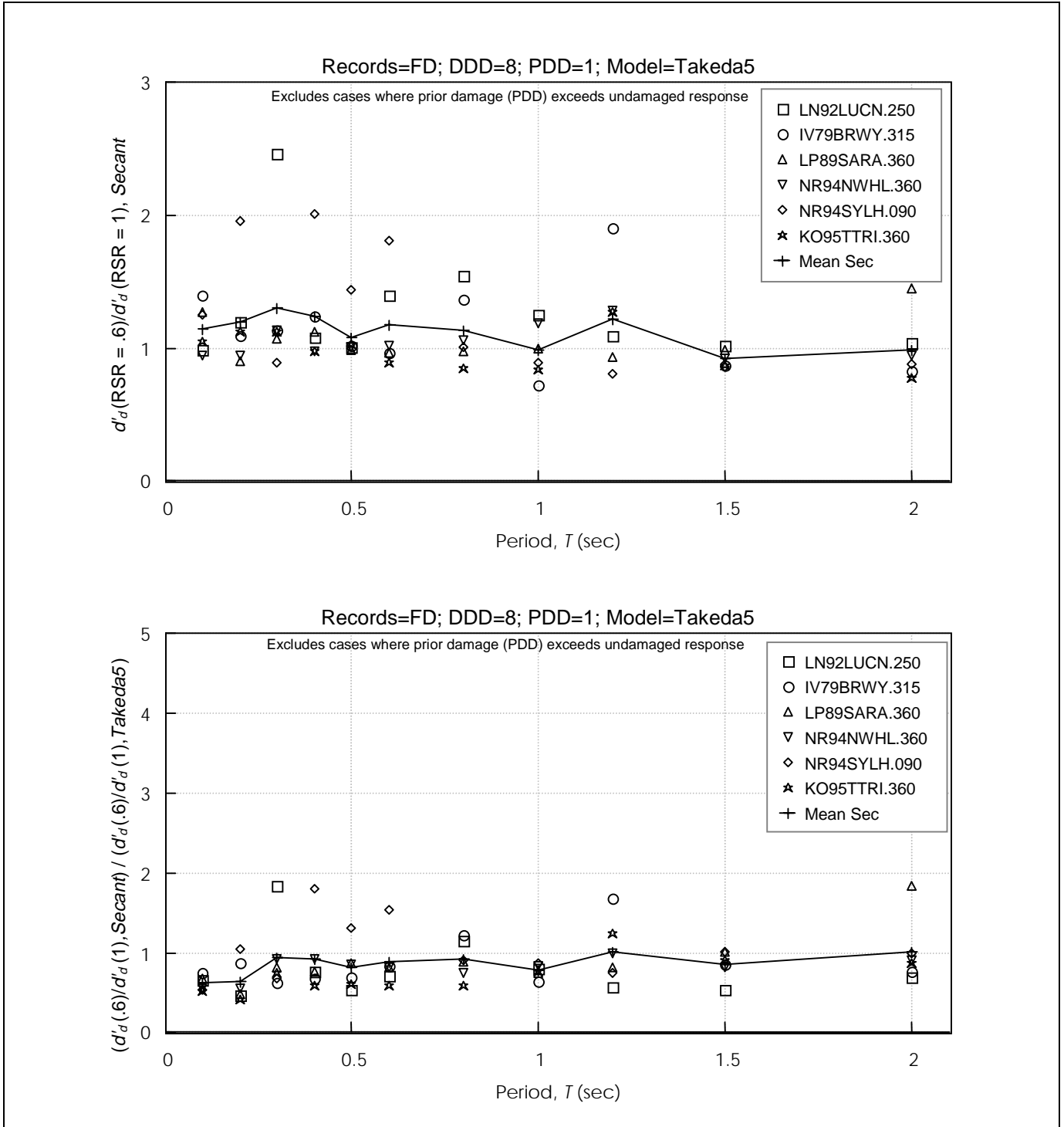


Figure 6-79 **Secant Method Estimates of Displacement Ratio of RSR=0.6 and RSR=1.0 Takeda5 Oscillators having DDD= 8 and PDD= 1**
DDD = Design Displacement Ductility; PDD = Prior Ductility Demand; RSR = Reduced Strength Ratio

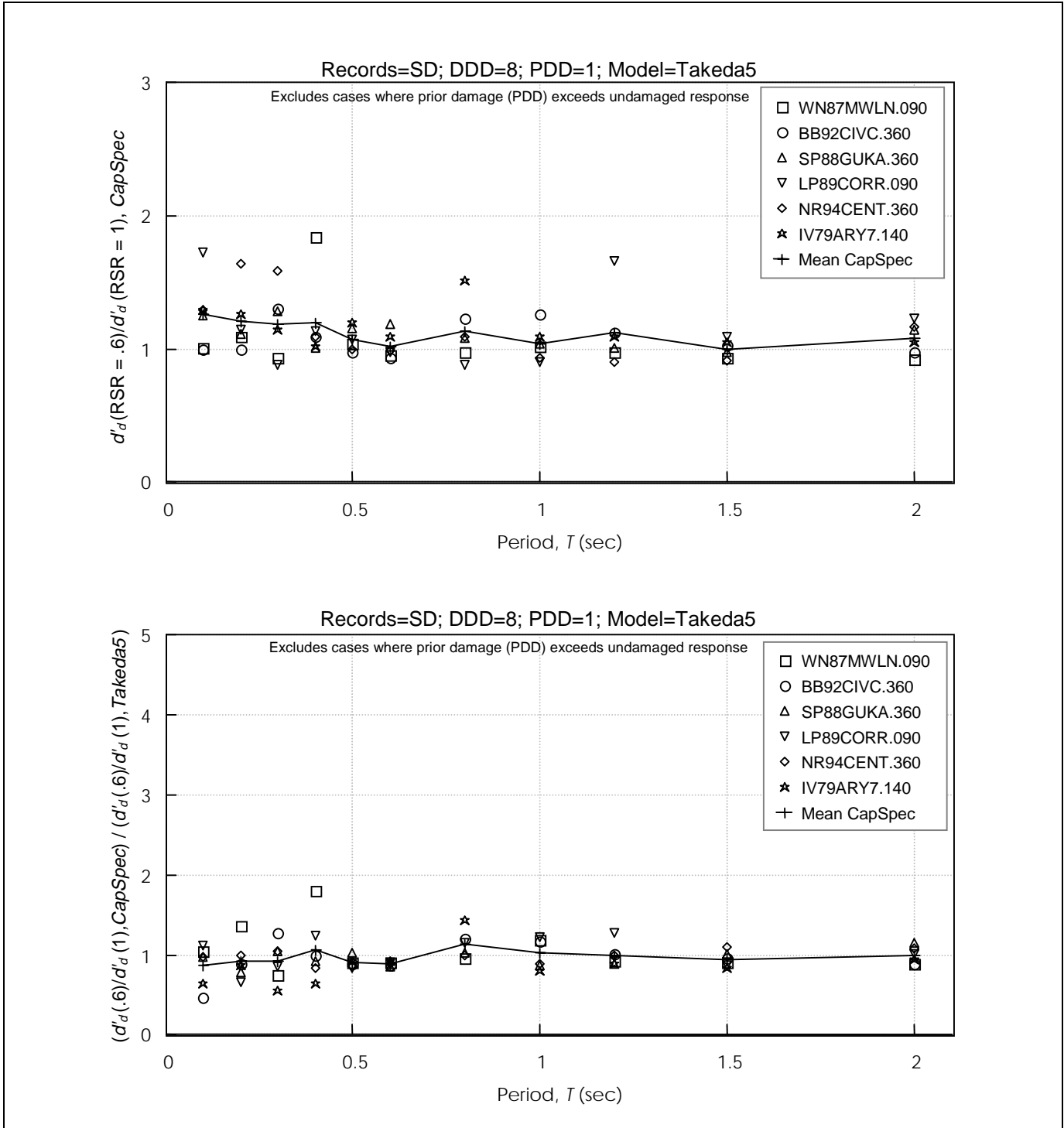


Figure 6-80 Capacity Spectrum Method Estimates of Displacement Ratio of RSR=0.6 and RSR=1.0 Takeda5 Oscillators having DDD= 8 and PDD= 1
 DDD = Design Displacement Ductility; PDD = Prior Ductility Demand; RSR = Reduced Strength Ratio

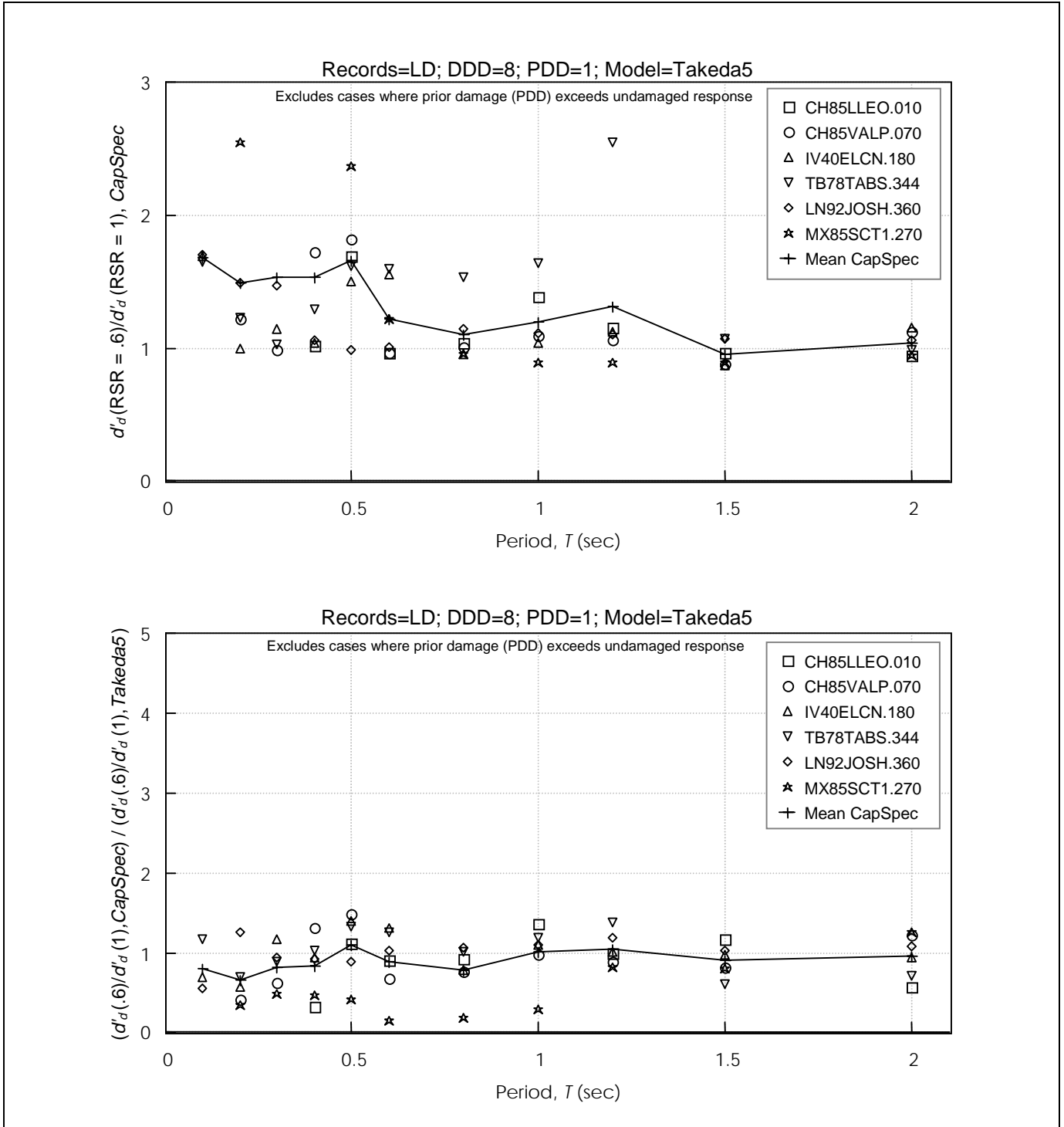


Figure 6-81 Capacity Spectrum Method Estimates of Displacement Ratio of RSR=0.6 and RSR=1.0 Takeda5 Oscillators having DDD= 8 and PDD= 1
 DDD = Design Displacement Ductility; PDD = Prior Ductility Demand; RSR = Reduced Strength Ratio

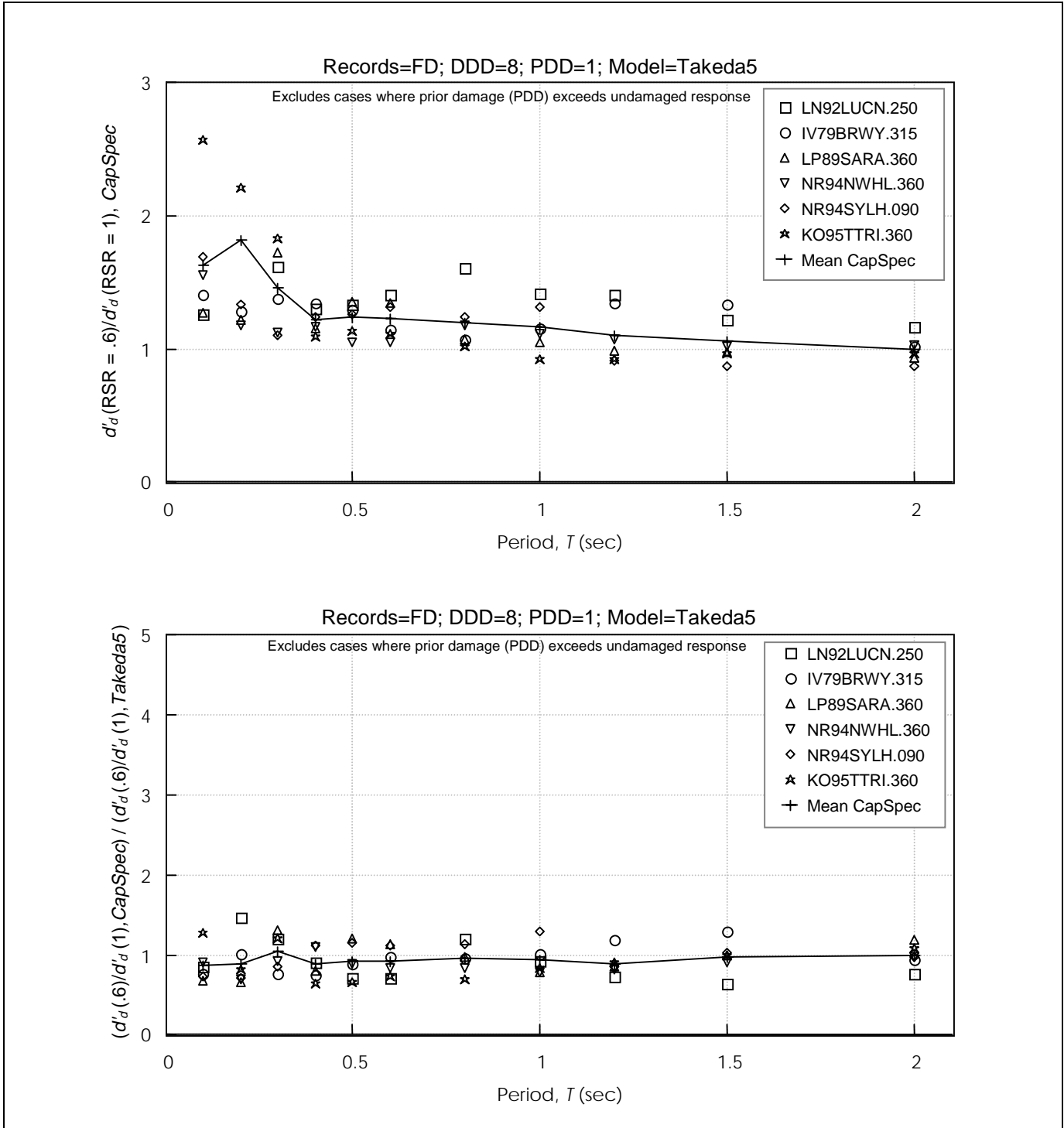


Figure 6-82 Capacity Spectrum Method Estimates of Displacement Ratio of RSR=0.6 and RSR=1.0 Takeda5 Oscillators having DDD= 8 and PDD= 1
 DDD = Design Displacement Ductility; PDD = Prior Ductility Demand; RSR = Reduced Strength Ratio

6.7 Conclusions and Implications

The analyses presented indicate that the displacement response characteristics of the ground motions generally conform to expectations based on previous studies. Forward-directivity motions may have larger displacement response in the long-period range than would be predicted by the equal-displacement rule. The strength-reduction factor, R , appropriate for forward-directivity motions may need to be reduced somewhat relative to other classes of motion if ductility demands are to be held constant.

The displacements of the Takeda oscillators were sometimes several-fold greater or less than those of the bilinear oscillators. Although it is fundamentally important to consider displacements in seismic response, variability of the response estimates as affected by ground motions and hysteresis model must also be considered.

Previous damage, modeled as prior ductility demand, did not generally cause large increases in displacement response when the Takeda models with positive post-yield stiffness were exposed to performance-level earthquakes associated with life safety or collapse prevention. Prior ductility demands were found to cause mean changes in displacement response ranging from -3% to $+10\%$ for the Takeda5 and TakPinch oscillators having no strength degradation (Figures 6-55 and 6-56). PDDs of 8 often caused a slight decrease in the displacement response computed using the Takeda5 and TakPinch models; response infrequently was 20% to 30% or more higher than that for the undamaged oscillator.

For oscillators having cyclic strength degradation, represented by the TakPinch oscillators, the effect of strength degradation was generally to increase the mean displacement response, but only by a few percent. The mean increase was larger for the structures having lower DDD, reaching as much as 21% for oscillators having $RSR = 0.6$. This result merely indicates that strength degradation tends to cause displacement response to increase relative to undamaged or nondegrading systems. Further examination revealed that increasing PDD increases or decreases the mean response of TakPinch systems with strength degradation by only a few percent (Figure 6-56). The weaker oscillators, represented by larger DDD, are more likely to exhibit damage in a real earthquake, and to have smaller increases in displacement due to prior ductility demands.

While prior damage causes relatively small changes in mean displacement response relative to undamaged structures, it also introduces some variability in displacement response. Variability in response is inherent in earthquake-resistant design, and the variability introduced by prior damage should be considered in the context of variability arising from different ground motions, choice of hysteretic models, modeling assumptions, and other sources. For example, Figures 6-32 to 6-34 illustrate the degree to which different earthquakes can cause bilinear and Takeda oscillators of equal strength to have substantially different peak displacement response. Thus, the variability in response introduced by prior damage is not considered significant.

Three NSPs for estimating peak displacement response were applied to the Takeda oscillators. Significant variability in the estimated displacements, when compared with the values calculated from nonlinear dynamic analysis, underscores the difficulty in accurately estimating response of a SDOF system to a known ground motion. The accuracy of the NSP estimates is compared in Figure 6-63. In Figure 6-64 it can be observed that the capacity spectrum and coefficient methods are more accurate, in a mean sense, than the secant method, and that all methods tend to overestimate the displacement response of short-period Takeda5 oscillators.

The NSPs were also used to estimate the change in displacement caused by a prior earthquake. Given the relatively small effect of damage on peak displacement response, it appears that damaged structures should be modeled similar to their undamaged counterparts, in order to obtain identical displacement estimates for performance events that are stronger than the damaging event. This results in damage having no effect on the displacement response, which closely approximates the analytical results.

The accuracy with which an NSP accounts for strength reduction was explored. It was found that each NSP was reasonably able to capture the effect of strength reduction.

The above findings pertain to systems characterized by ductile flexural response having degrading stiffness, with and without pinching. Systems with negative post-yield stiffness were prone to collapse, even with DDD of 2. Such systems should remain nearly elastic if their collapse is to be avoided.

6.8 References

- Araki, H., Shimazu, T., and Ohta, Kazuhiko, 1990, "On Residual Deformation of Structures after Earthquakes," *Proceedings of the Eighth Japan Earthquake Engineering Symposium—1990*, Tokyo, Vol. 2, pp. 1581-1586. (In Japanese with English abstract.)
- ATC, 1996, *Seismic Evaluation and Retrofit of Concrete Buildings*, Applied Technology Council, ATC-40 Report, Redwood City, California.
- ATC, 1997a, *NEHRP Guidelines for the Seismic Rehabilitation of Buildings*, prepared by the Applied Technology Council (ATC-33 project) for the Building Seismic Safety Council, published by the Federal Emergency Management Agency, Report No. FEMA 273, Washington, D.C.
- ATC, 1997b, *NEHRP Commentary on the Guidelines for the Seismic Rehabilitation of Buildings*, prepared by the Applied Technology Council (ATC-33 project) for the Building Seismic Safety Council, published by the Federal Emergency Management Agency, Report No. FEMA 274, Washington, D.C.
- Boroschek, R.L., 1991, *PCNSPEC Manual, (Draft)*, Earthquake Engineering Research Center, University of California at Berkeley.
- Cecen, H., 1979, *Response of Ten-Story Reinforced Concrete Model Frames to Simulated Earthquakes*, Doctoral Thesis, Department of Civil Engineering, University of Illinois at Urbana.
- Fajfar, P. and Fischinger, M., 1984, "Parametric Study of Inelastic Response to Some Earthquakes Recorded in Southern Europe," *Proceedings of the Eighth World Conference on Earthquake Engineering*, Vol. 4, pp. 75-82.
- Humar, J., 1980, "Effect of Stiffness Degradation on Seismic Response of Concrete Frames," *Proceedings of the Seventh World Conference on Earthquake Engineering*, Vol. 5, pp. 505-512.
- Iwan, W.D., 1973, "A Model for the Dynamic Analysis of Deteriorating Structures," *Proceedings of the Fifth World Conference on Earthquake Engineering*, Vol. 2., pp. 1782-1791.
- Iwan, W.D., 1977, "The Response of Simple Stiffness Degrading Systems," *Proceedings of the Sixth World Conference on Earthquake Engineering*, Vol. 2, pp. 1094-1099.
- Kawashima, K., Macrae, G., Hoshikuma, J., and Nagaya, K., 1994, "Residual Displacement Response Spectrum and its Application," *Journal of Structural Mechanics and Earthquake Engineering*, Japan Society of Civil Engineers, No. 501, pp. 183-192. (In Japanese with English abstract.)
- Lepage, A., 1997, *A Method for Drift Control in Earthquake-Resistant Design of RC Building Structures*, Doctoral Thesis, Department of Civil Engineering, University of Illinois at Urbana.
- Mahin, S.A., 1980, "Effects of Duration and After-shocks on Inelastic Design Earthquakes," *Proceedings of the Seventh World Conference on Earthquake Engineering*, Vol. 5, pp. 677-679.
- Mahin, S.A., and Lin, J., 1983, *Construction of Inelastic Response Spectra for Single-Degree-of-Freedom Systems—Computer Program and Applications*, Earthquake Engineering Research Center, University of California at Berkeley, Report No. UCB/EERC-83/17, Berkeley, California.
- Mahin, S.A., and Boroschek, R., 1991, *Influence of Geometric Nonlinearities on the Seismic Response and Design of Bridge Structures*, Background Report to California Department of Transportation, Sacramento, California.
- Minami, T., and Osawa, Y., 1988, "Elastic-Plastic Response Spectra for Different Hysteretic Rules," *Earthquake Engineering and Structural Dynamics*, Vol. 16, pp. 555-568.
- Miranda, E., 1991, *Seismic Evaluation and Upgrading of Existing Buildings*, Doctoral Thesis, Department of Civil Engineering, University of California, Berkeley.
- Moehle, J.P., Browning, J., Li, Y.R., and Lynn, A., 1997, "Performance Assessment for a Reinforced Concrete Frame Building," (abstract) *The Northridge Earthquake Research Conference*, California Universities for Research in Earthquake Engineering, Richmond, California.
- Nakamura, T., and Tanida, K., 1988, "Hysteresis Model of Restoring Force Characteristics of Reinforced Concrete Members," *Proceedings of the Ninth World Conference on Earthquake Engineering*, Paper 6-4-7, Vol. VI.
- Nasser, A.A., and H. Krawinkler, H., 1991, *Seismic Demands for SDOF and MDOF Systems*, John A. Blume Earthquake Engineering Center, Stanford University, Report No. 95, Stanford, California.

- Newmark, N.M., and Riddell, R., 1979, "A Statistical Study of Inelastic Response Spectra," *Proceedings of the Second U.S. National Conference on Earthquake Engineering*, pp. 495-504.
- Otani, S., 1981, "Hysteresis Models of Reinforced Concrete for Earthquake Response Analysis," *Journal (B)*, Faculty of Engineering, University of Tokyo, Vol. XXXVI, No. 2, pp. 125 - 159.
- Palazzo, B., and DeLuca, A., 1984, "Inelastic Spectra for Geometrical and Mechanical Deteriorating Oscillator," *Proceedings of the Eighth World Conference on Earthquake Engineering*, Volume IV, pp. 91-98.
- Parducci, A., and Mezzi, M., 1984, "Elasto-Plastic Response Spectra of Italian Earthquakes Taking into Account the Structural Decay," *Proceedings of the Eighth World Conference on Earthquake Engineering*, Volume IV, pp. 115-122.
- Paulay, T. and Priestley, M.J.N., 1992, *Reinforced Concrete and Masonry Buildings: Design for Seismic Resistance*, Wiley & Sons, New York.
- Qi, X., and Moehle, J.P., 1991, *Displacement Design Approach for Reinforced Concrete Structures Subjected to Earthquakes*, Earthquake Engineering Research Center, Report No. UCB/EERC 91/02, University of California at Berkeley, Berkeley, California.
- Rahnama, M., and Krawinkler, H., 1995, "Effects of P-Delta and Strength Deterioration on SDOF Strength Demands", *Proceedings of the 10th European Conference on Earthquake Engineering*, Vol. 2, pp. 1265-1270.
- Riddell, R., 1980, "Effect of Damping and Type of Material Nonlinearity on Earthquake Response," *Proceedings of the Seventh World Conference on Earthquake Engineering*, Vol. 4, pp. 427-433.
- Saiidi, M., 1980, "Influence of Hysteresis Models on Calculated Seismic Response of R/C Frames," *Proceedings of the Seventh World Conference on Earthquake Engineering*, Vol. 5, pp. 423-430.
- Sewell, R.T., 1992, "Effects of Duration on Structural Response Factors and on Ground Motion Damageability," *Proceedings of the SMIP92 Seminar on Seismological and Engineering Implications of Recent Strong Motion Data*, pp. 7-1 to 7-15.
- Shimazaki, K., and M.A. Sozen, M.A., 1984, *Seismic Drift of Reinforced Concrete Structures*, Research Reports, Hasama-Gumi Ltd., Tokyo (in Japanese), and draft research report (in English).
- Somerville, P.G., Smith, N.F., Graves, R.W. and Abrahamson, N.A., 1997, "Modification of Empirical Strong Ground Motion Attenuation Relations to Include the Amplitude and Duration Effects of Rupture Directivity," *Seismological Research Letters*, Vol. 68, No. 1.
- Takeda, T., Sozen, M.A., and Nielsen, N.N., 1970, "Reinforced Concrete Response to Simulated Earthquakes," *Journal of the Structural Division*, American Society of Civil Engineers, Vol. 96, No. ST12, pp. 2557-2573.
- Wolschlag, C., 1993, *Experimental Investigation of the Response of R/C Structural Walls Subjected to Static and Dynamic Loading*, Doctoral Thesis, Department of Civil Engineering, University of Illinois at Urbana.
- Xie, L.-L., and Zhang, X., 1988, "Engineering Duration of Strong Motion and its Effects on Seismic Damage," *Proceedings of the Ninth World Conference on Earthquake Engineering*, Vol. 2, Paper 3-2-7.

7. Example Application

7.1 Introduction

This section gives an example of the use of FEMA 306 recommendations to evaluate earthquake damage in a two-story reinforced-concrete building. The example is meant to be as realistic as possible and is based on an actual structure.

7.1.1 Objectives

The example is intended to help evaluating engineers understand such issues as:

- the overall process of a FEMA 306 evaluation.
- accounting for pre-existing damage.
- how both observation and analysis are used in the evaluation procedures.
- determining and using the applicable FEMA 306 Component Damage Classification Guides, including cases where an exactly applicable damage guide is not provided.
- foundation rocking of walls, which may be a prevalent behavior mode in many structures.
- some of the ways engineering judgment may need to be applied.
- how restoration measures can be determined based on either the *direct method* or the *performance analysis method*.
- aspects of using a nonlinear static procedure of analysis (pushover analysis).
- establishing displacement capacities and demands.

Reading through the example could be the best introduction to an understanding of the FEMA 306 evaluation process. References to the applicable sections of FEMA 306 or 307 (or to other sources) are given in “bookmark” boxes adjacent to the text. Because the example is meant to be illustrative, it contains more description and explanation than would normally be contained in an engineer’s evaluation report for an earthquake-damaged building.

It should be clear from this example that the FEMA 306 recommendations for evaluating earthquake damage

must be implemented under the direction of a knowledgeable structural engineer, particularly when a performance analysis is carried out. The responsible engineer should have a thorough understanding of the principles behind the FEMA 306 recommendations and should be familiar with the applicable earthquake research and post-earthquake field observations. FEMA 307 provides tabular bibliographies and additional information on applicable research.

A fundamental tenet of the component evaluation methods presented in FEMA 306 is that the severity of damage in a structural component may not be determined without understanding the governing behavior mode of the component, and that the governing behavior mode is a function not only of the component’s properties, but of its relationship and interaction with surrounding components in a structural element. In the following sections, the evaluation of the example building emphasizes the importance of this principle. There may be a temptation among users of FEMA 306 to use the damage classification guides as simple graphical keys to damage, and to complete the analysis by simply matching the pictures in the guides to the observed damage. The example is intended to show that this is not the appropriate use of the guides. It is organized to emphasize the importance of the analytical and observation verification process that is an essential element of the evaluation procedure.

7.1.2 Organization

The example is organized as shown in the flow chart of Figure 7-1. This organization follows the overall evaluation procedure outlined in FEMA 306, beginning with a building description and observations of earthquake damage.

The building has been subjected to a previous earthquake. The damage investigation establishes the pre-existing conditions so that the loss from the recent earthquake can be evaluated. The preliminary classification of component types, behavior modes, and damage severity are made by observing the structure. It is shown, however, that classification of behavior modes, and hence damage severity, may be unclear when based on observation alone. Simple analytical tools provided in the material chapters of FEMA 306 are used to verify the expected component types and behavior modes, and damage severity is assigned accordingly. The steps required to estimate the loss by the direct method are

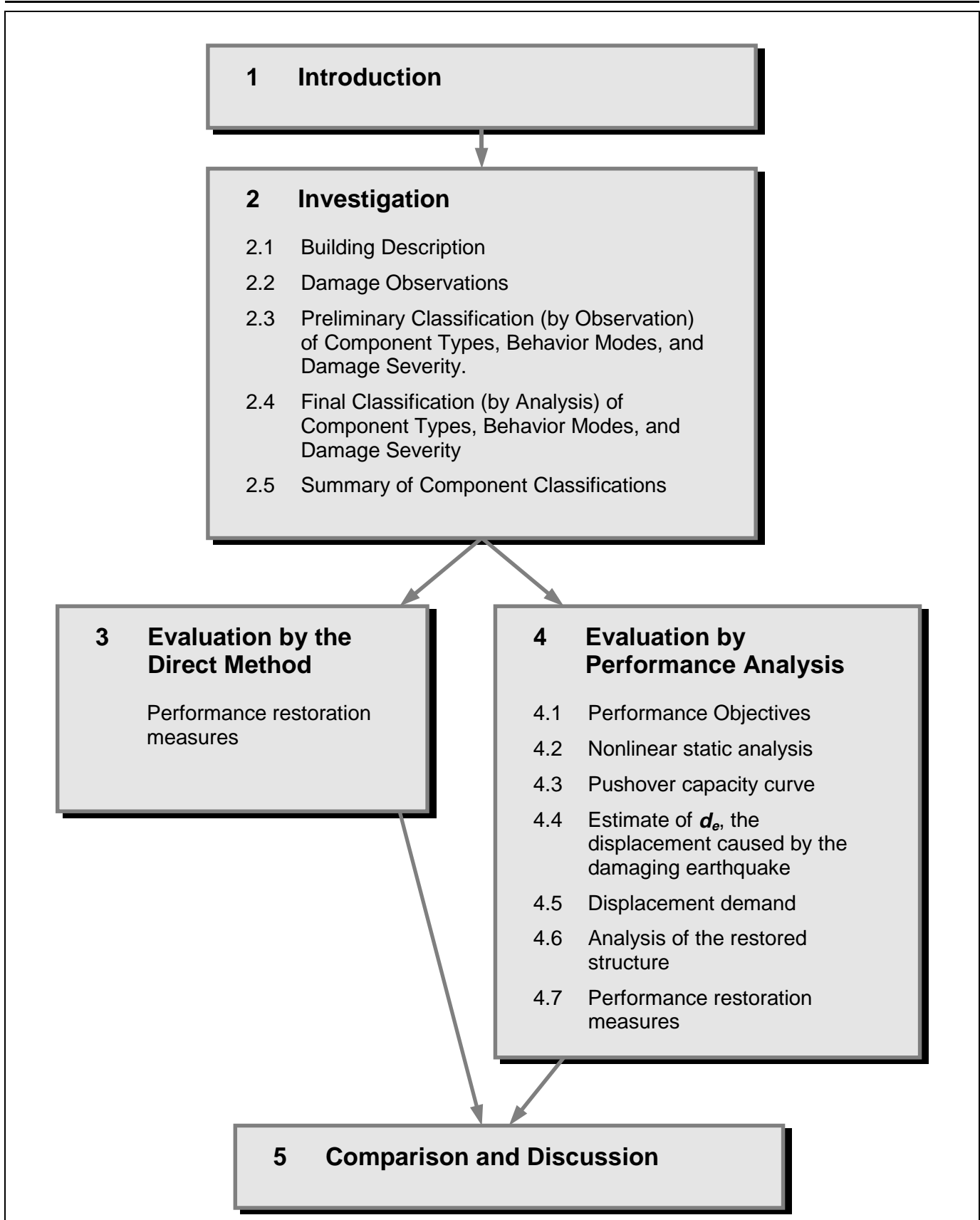


Figure 7-1 Flowchart for example

illustrated, and a relative performance analysis is carried out. It is emphasized that the direct method provides only loss estimation information, and that a relative performance analysis is required in order to make performance-based design decisions.

Damage records for all of the structural walls of the building are included. The damage records for two of the walls are discussed in detail. Damage records for the remaining walls are given at the end of the example.

7.2 Investigation

7.2.1 Building Description

The example building is a two-story concrete building located on a sloping site. The building is a “T” shape in plan with the stem of the T on the downhill side, containing a partial lower story below the other two stories. The building was designed and constructed in the late 1950s. The building is located about 3.6 miles from the epicenter of the damaging earthquake.

The overall plan dimensions of the building are 362 feet in the North-South direction by 299 feet in the East-West direction. The floor slabs cantilever about 6 feet from the perimeter columns forming exterior sun-screens/balconies. The building facade along the perimeter is set back 8 feet from the edge of the slab. For the typical floor, the interior floor area is about 62,600 square feet, and the total slab area is about 70,400 square feet. The lower level encompasses about 20,200 square feet. Floor plans are shown in Figure 7-2 and an elevation is shown in Figure 7-3. The roof of the building supports mechanical equipment.

The floors and roof are constructed with waffle slabs comprised of a 4-½ inch thick slab and 14 inch deep pans (18-½ inches total depth). Columns supporting the slabs are typically spaced at 26 feet in each direction. The interior columns are 18-inch square and the perimeter columns are 18-inch diameter. The columns are supported on spread footings.

Reinforced concrete walls in both directions of the building resist lateral forces. The walls are 12 inches thick and are cast monolithically at each end with the gravity-load-carrying columns. The walls are typically located along corridors, and the corridor side of the wall has a 1-inch thick plaster coat. The typical solid wall configuration and reinforcement are shown in Figure 7-4.

In the lower level there are several reinforced concrete masonry (CMU) walls that are framed between the ground and the first floor slab (basement level) in the three-story section of the building. The CMU walls are attached to the first floor slab. However, these walls were not designed as shear-resisting elements. Because the first floor slab is anchored to the foundation in the two-story portion of the building, the contribution of the CMU walls to the lateral force resistance, particularly in the east-west direction, is minimal.

Several of the reinforced concrete walls have door openings, 7 feet 3 inches tall by 6 feet 6 inches wide, in the middle of the wall, creating a coupled wall. The typical coupled wall configuration and reinforcement are shown in Figure 7-5. In the three-story section of the building (the stem of the T), the walls are discontinued at the lower level. This lower level contains a single reinforced concrete wall in the north-south direction centered between the two walls above.

7.2.2 Post-earthquake Damage Observations

Following the damaging earthquake, the engineers performed a post-earthquake evaluation of the building. The initial survey was conducted one month after the damaging earthquake. The structural drawings for the building were reviewed. The follow-up investigations were conducted about three months following the earthquake.

Visual observation, Guide NDE1, Section 3.8 of FEMA 306

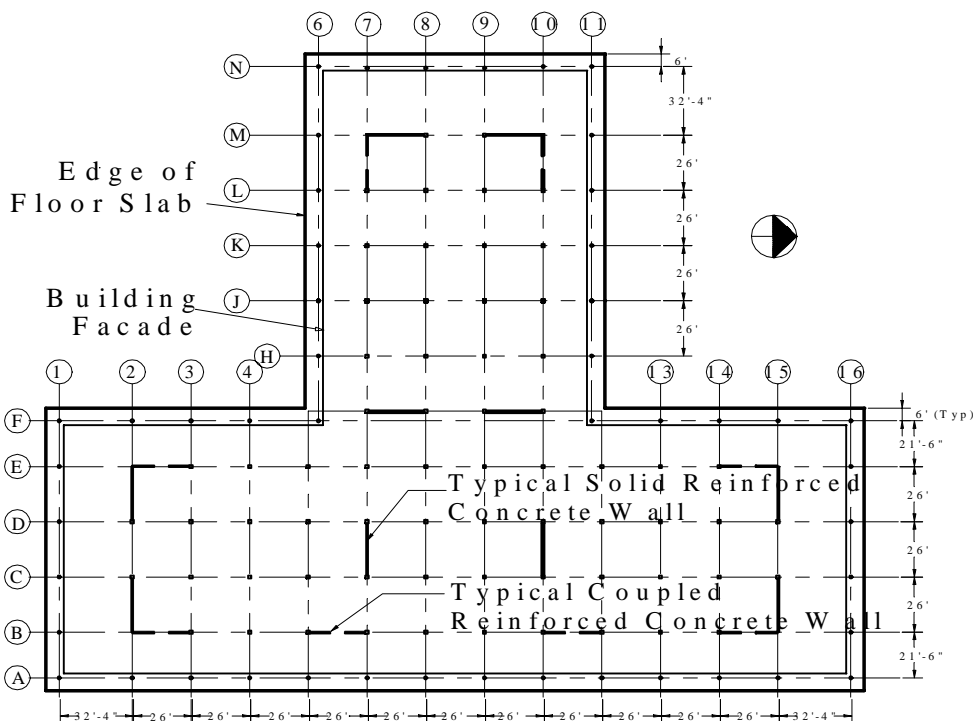
The post-earthquake evaluations were conducted using visual observation techniques on exposed surfaces of the structural elements. The sections of wall above the ceiling were typically observed only where the suspended ceiling tiles had fallen during the earthquake. Crack widths were measured at selected locations using magnifying crack comparators for most of the significant cracks in each wall.

7.2.2.1 Pre-Earthquake Conditions

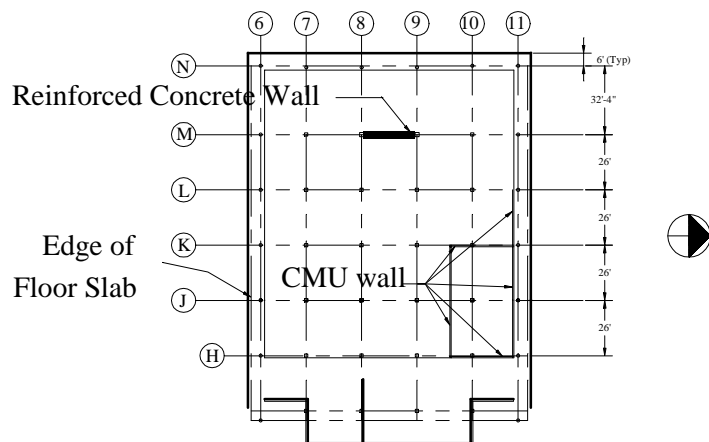
The building had experienced some cracking prior to the damaging earthquake. The pre-existing damage is judged to have been caused by a previous earthquake. The heaviest damage appeared to have been in the coupling beams. The wall cracks above the ceiling line were observed to have been repaired by epoxy injection.

Old cracks vs. new cracks, Section 3.4 of FEMA 306

Chapter 7: Example Application



a) First and Second Floor Plan



b) Basement Floor Plan

Figure 7-2 **Floor Plans**

Chapter 7: Example Application

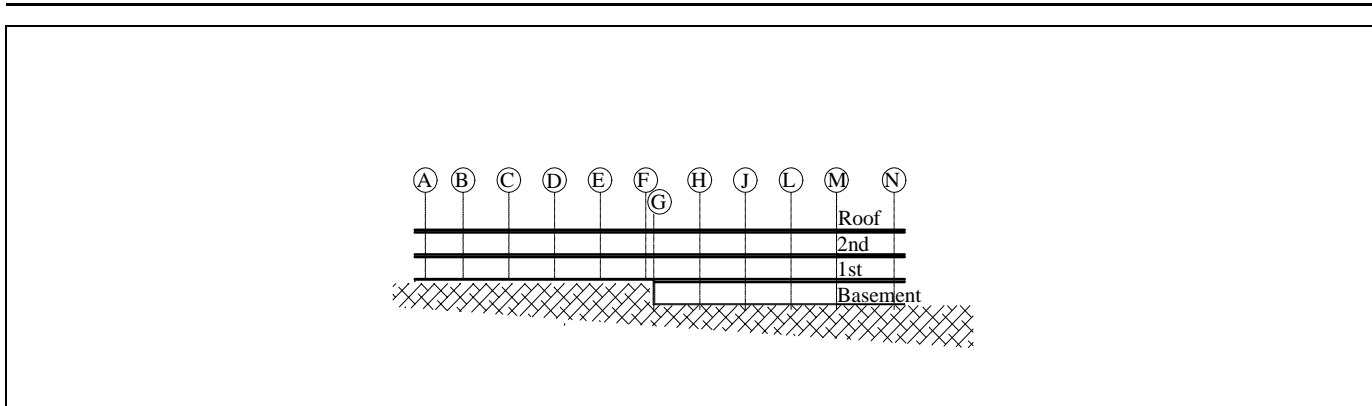


Figure 7-3 Building Cross-section

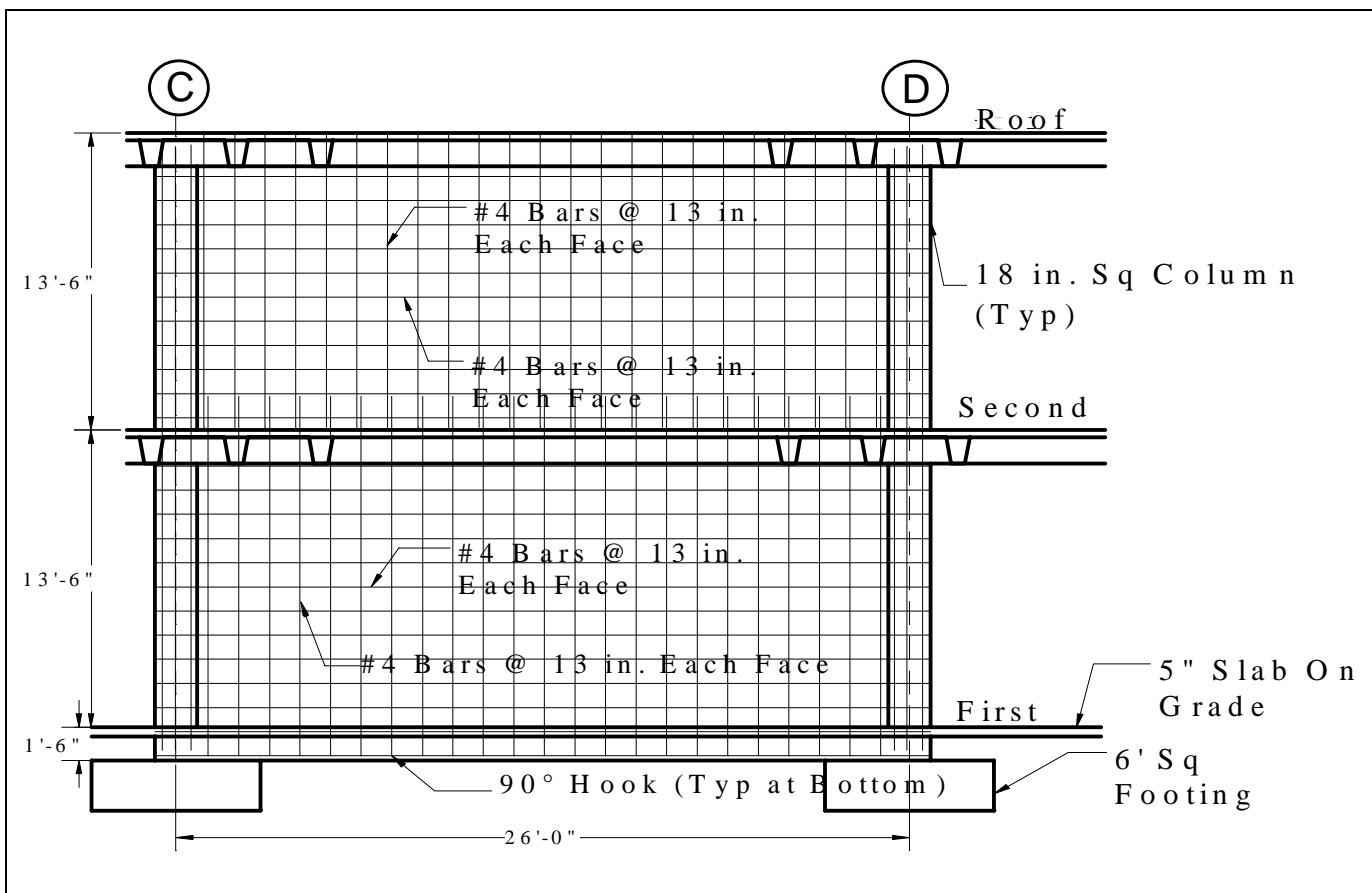


Figure 7-4 Example Solid Wall Detail (Condition at Line 7)

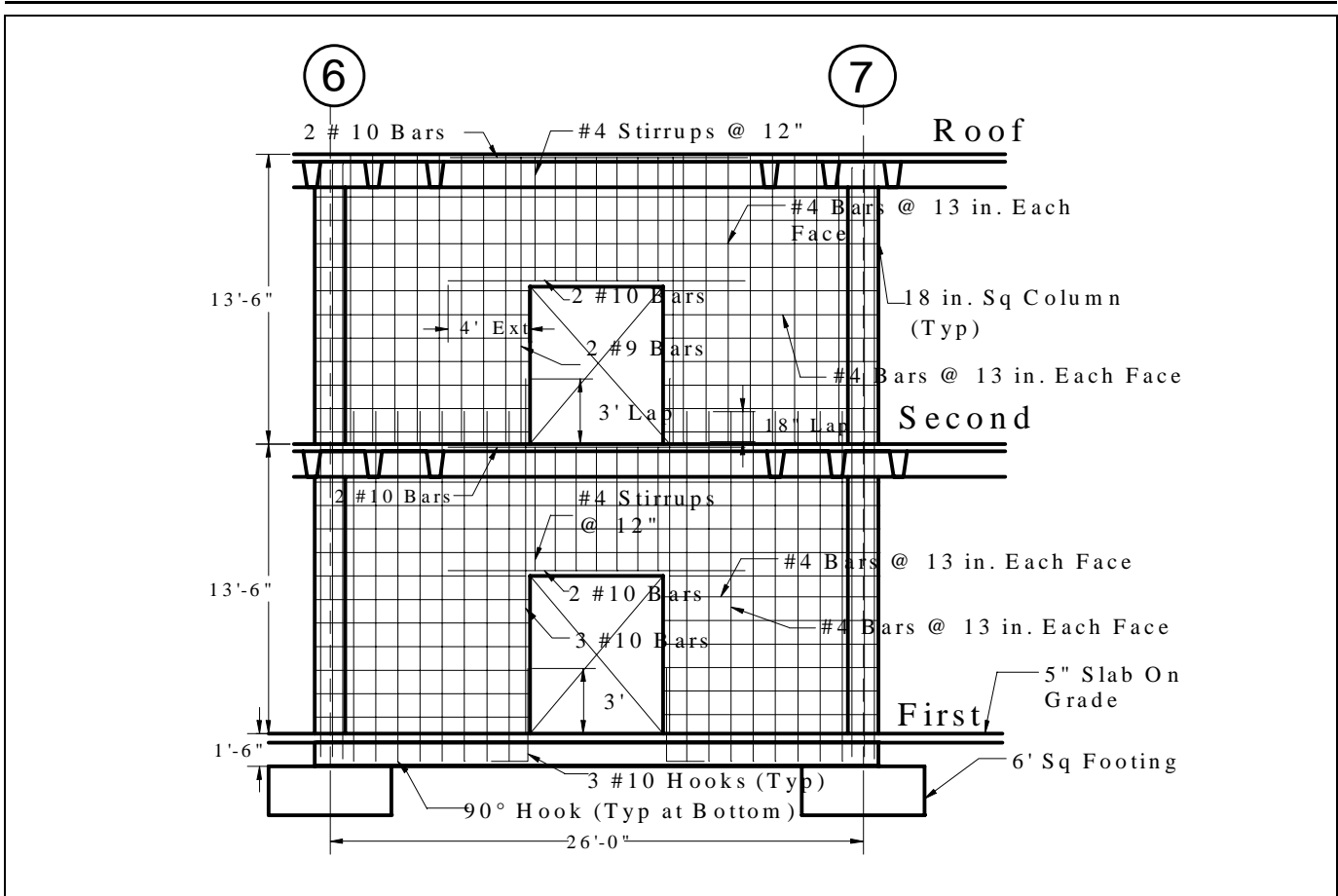


Figure 7-5 Example Coupled Wall Detail (Condition at line B)

Below the ceiling the cracks may also have been injected with epoxy. However, the architectural finishes on those surfaces obscured the evidence of the previous repairs. Many of the cracks in the plaster coat on the walls appeared to have been cosmetically repaired using a strip of fabric and plaster placed over the crack. It was not clear whether the underlying cracks in the concrete had been repaired. Therefore, the building is assumed to have some cracking prior to the damaging earthquake and the pre-existing cracking is taken into account by reducing the pre-event stiffness of the concrete walls.

7.2.2.2 Postearthquake Condition and Damage Documentation

The concrete walls experienced minor to moderate amounts of cracking. Based on the visual observations, component damage records were prepared for each of the walls in the building. These forms are included as Figures 7-6, 7-7, and in Appendix A, Component Damage Records D1 through

Documentation of damage, Section 3.7 of FEMA 306

D19. Each of the component damage records depicts the observations for both stories of a two-story wall, except for the single-story wall on the lower level shown on Record D19. All observable cracks are shown, but only those cracks found to be wider than 30 mils (1/32 inch) have the crack width, in mils, written on the component damage record at the approximate location of the measurement. Cracks found to be previously repaired with epoxy and those with pre-existing surface patches are indicated. Spalls are also noted.

The two first-story coupled walls in the stem of the T section of the building experienced heavy cracking in the coupling beams (Column lines 7 and 10, L to M, Component Damage Records D4 and D6). One of the other coupling beams (Column Line B, 14 to 15, Record D12) also experienced heavy cracking. The damage to the coupling beams included some spalling of the concrete, buckling of reinforcing bars, and cracking of the floor slab adjacent to the wall. Several walls were

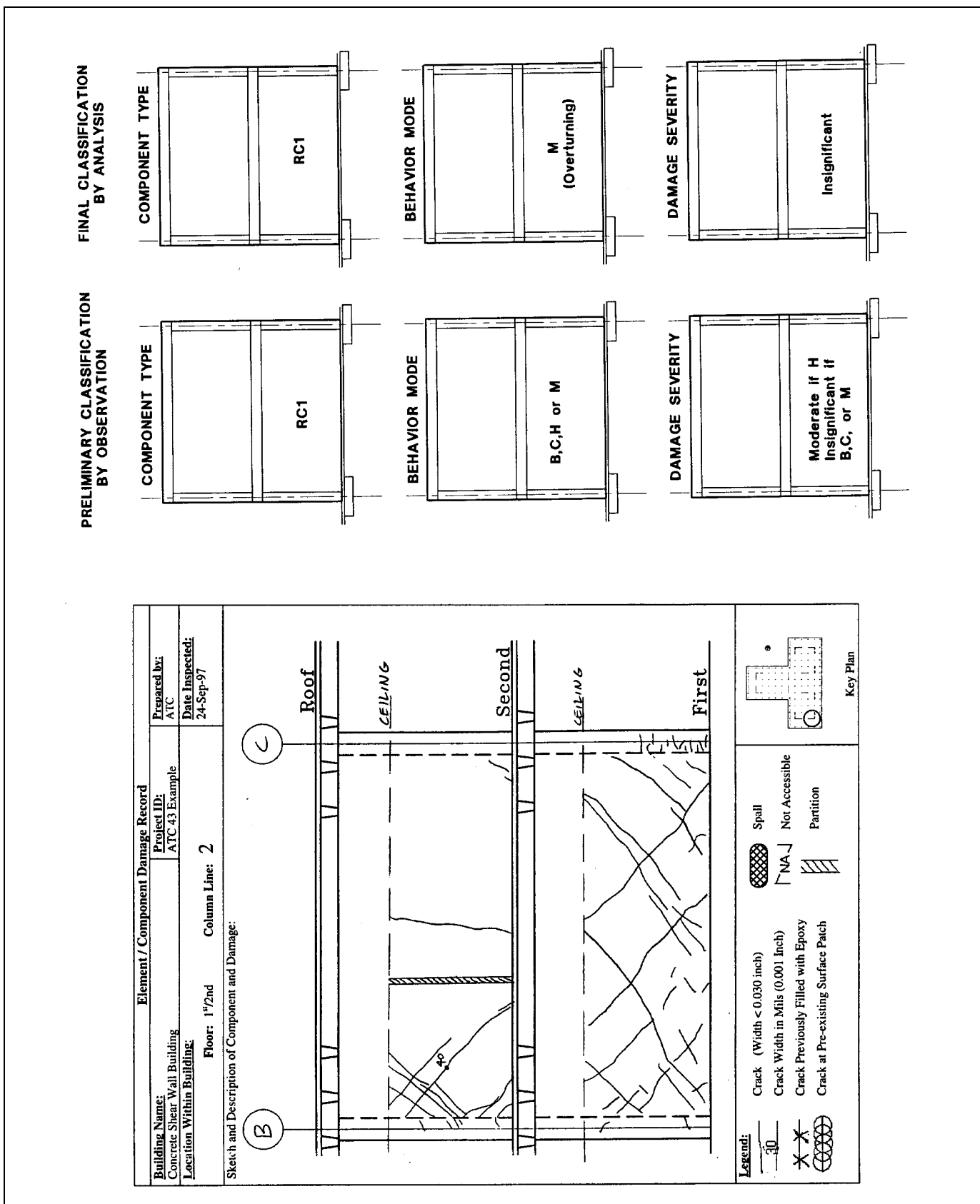


Figure 7-6 Solid Wall Example

FINAL CLASSIFICATION BY ANALYSIS

RC3		RC1	
RC3		RC3	RC1

H		N	
H		H	N

Insignificant		Insignificant	
Moderate		Heavy	

PRELIMINARY CLASSIFICATION BY OBSERVATION

RC3		RC1	
RC3		RC3	RC1

B or H		B, C, H, or N	
B or H		B or H	N

Insignificant or Moderate		Insignificant or Moderate	
Insign. or Moderate		Heavy	

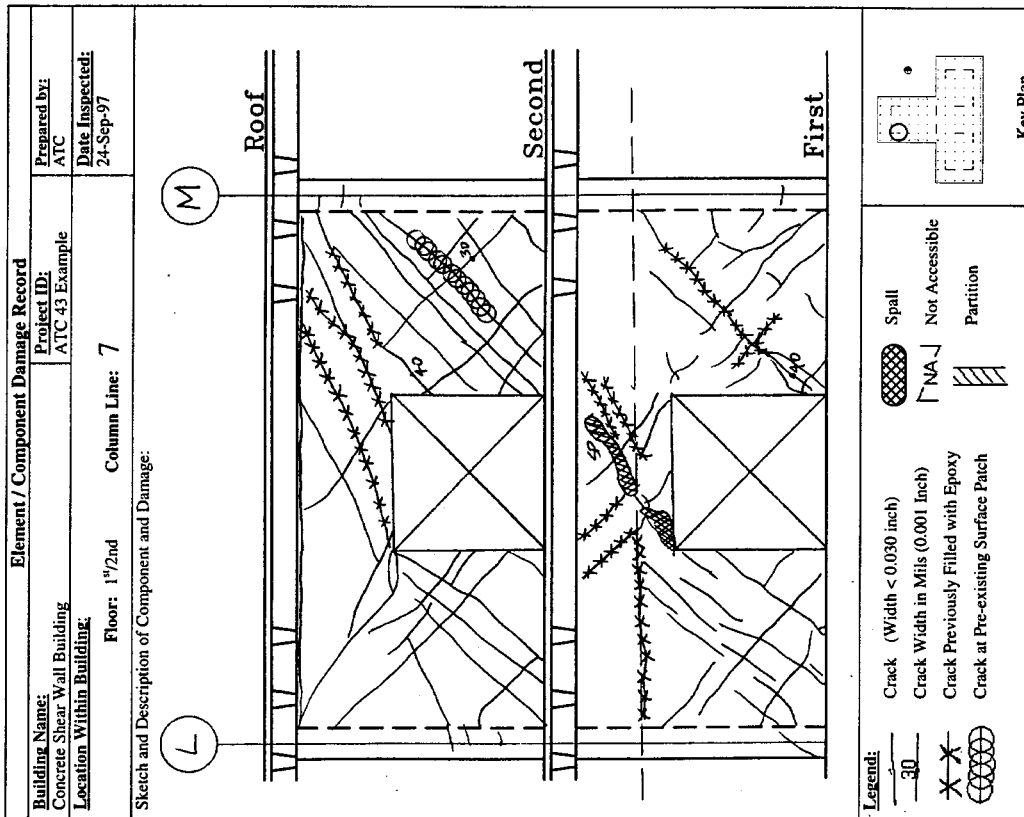


Figure 7-7 Coupled Wall Example

observed to have horizontal cracks along the interface between the top of the wall and the floor slab above.

7.2.3 Preliminary Classification (by Observation) of Component Types, Behavior Modes, and Damage Severity

The first critical step in interpreting component damage records is to identify the components within the structural element under investigation. In this case, the example building is reinforced concrete, so the summary of relevant component types is found in Sections 2.4 and 5.2.1 of FEMA 306.

Component types, Table 5-1 of FEMA 306

7.2.3.1 Component Types

The first pass in the identification process is conducted by observation, keeping in mind that the definition of a component type is not a function of the geometry alone, but of the governing mechanism of lateral deformation for the entire element or structure. Thus the identification of structural components requires consideration of the wall element over multiple floor levels. Complete diagrams showing the crack pattern over multiple floor levels such as the ones shown in the attached damage records shown in Figures 7-6, 7-7 and Damage Records D1 through D19 (Appendix A) are essential.

For the typical coupled wall elements of the example building, shown in Figure 7-7, a survey of the element geometry and the general pattern of damage suggests that the beams over the openings may be classified as weaker coupling beams (RC3), and that the wall piers flanking the openings will behave as two-story cantilever components (RC1). The thought process that leads to this conclusion includes the recognition that the beam elements are likely to be weaker than the walls on either side of the coupling beams, as well as a mental visualization of the lateral deformation of the walls and the attendant large deformation demands on the beams. As shown in Figure 7-6, the solid reinforced concrete wall component is type RC1.

Component identification, Section 2.4 of FEMA 306

7.2.3.2 Behavior Modes and Damage Severity

Once the component types have been identified, an initial classification of the behavior modes and damage severity may be made by inspecting the visible damage with reference to the component damage classification guides. Tables 5-1, 5-2, and

Behavior modes, Table 5-2 of FEMA 306

5-3 of FEMA 306 are also helpful in identifying behavior modes appropriate to the identified components.

For the typical coupled wall shown in Figure 7-7, the coupling beam component (RC3) on the second floor is observed to have light diagonal (shear) cracking, with little or no evidence of flexural cracking. As is typical of a building designed in the late 1950s, the coupling beam does not contain diagonal reinforcement, or even sufficient stirrup reinforcement, so mode A (ductile flexure) may be safely eliminated. The diagonal cracks then suggest that the behavior mode may be either mode B (flexure/diagonal tension) or mode H (preemptive diagonal tension). At the first floor coupling beams, the damage is more severe, but the behavior mode still appears to be either B or H.

In the first floor coupling beam, identification of the damage severity is relatively straightforward: the observed damage would be classified as Heavy regardless of the behavior mode. In many cases, however, the damage severity level may depend on the behavior mode. In the second floor coupling beam, for example, the damage would be classified as Insignificant if the behavior mode is identified as B (flexure followed by diagonal tension), but as Moderate if the behavior mode is identified as H (preemptive diagonal tension).

Component Guides, Section 5.5 of FEMA 306

Similarly, the wall piers of the coupled walls (RC1) have light diagonal cracking, which may be indicative of early stages of mode B (flexure/diagonal tension), early stages of mode C (flexure/diagonal compression) or more advanced stages of mode H (preemptive diagonal tension). In the first two cases, damage would be classified as Insignificant, while in the last case, damage would be classified as Moderate.

It is often not possible to distinguish between the different behavior modes, and hence the damage severity, without some analysis. This is particularly important for lower levels of damage where different modes may look very much alike, but which have different response at higher levels of damage. Consider, for example, modes B and H. The flexural cracks that initiate mode B response may have closed and become nearly invisible. The light diagonal cracking that occurs at the outset of both modes B and H will then be indistinguishable from one another, and only analysis of the section will differentiate the two modes, and hence the severity of damage. In other cases, the differences between modes are of less impor-

Verification loop, Figure 1-3 of FEMA 306

tance. Modes B and C are physically different, but have a similar effect on the stiffness, strength, and deformation capacity of the component at all levels of damage severity.

7.2.4 Final Classification (by Analysis) of Component Type, Behavior Mode and Damage Severity

In the previous section, component type, behavior mode, and damage severity were preliminarily defined based only on observation. In this section, those definitions are verified by calculation. In practice, iterations between observation and analysis may be needed to interpret correctly the seismic response and damage.

7.2.4.1 Expected Strength

The expected pre-earthquake strengths for each of the components were calculated using the FEMA 306 Section 3.6 procedures. The design concrete strength was shown on the drawings to be 3000 psi. According to the discussion in FEMA 306, Section 5.3.2, expected concrete strengths ranging from 1.0 to 2.3 times the specified strength are not unrealistic. In the example building, concrete strength was suspect, so tests were conducted which revealed that expected strength was, in fact, near the specified strength. For the purposes of the following analysis an expected strength of 3000 psi was assumed. Based on the drawing notes, reinforcing bars had a specified yield strength of 40 ksi. The expected strength of the reinforcing bars was assumed to be greater than the nominal yield strength by a factor of 1.25, so a value of 50 ksi was used for the yield strength in all calculations. If, during the course of the analysis, it becomes difficult to reconcile analytically determined behavior modes with observed damage, assumed values for material strength may need to be re-evaluated or verified through tests.

Expected strength, Section 3.6 of FEMA 306

There are two typical element types in the lateral-force-resisting system, solid walls and coupled walls. The following sections describe the details of the calculations and methodology used to classify the components of these elements.

7.2.4.2 Example 1 – Solid Wall (2B-2C)

Once a preliminary damage classification has been made by visual observation, it will generally be neces-

sary to perform some analysis to distinguish between behavior modes that are different but visually similar. As a first example, consider the damage record for the wall shown in Figure 7-6. The wall is 12 inches thick with 18-inch square boundary elements at each end. The wall length from center to center of the boundary elements is 26 feet, and the story height is 13 feet-6 inches. Note that the wall is L-shaped in plan and has a 26-foot return along line B.

Component Type. The definition of this wall as a single RC1 component (isolated wall or stronger wall pier) is easily and intuitively verified by sketching the inelastic deformation mechanism for the wall and its surrounding structure. The slabs framing into the wall clearly do not have the stiffness or strength to force a “weaker wall” type of behavior. The wall is therefore a single component with a height of 27 feet.

Behavior Mode. The preliminary classification identified four possible behavior modes for this component that were consistent with the component type and the observed damage: mode B (flexure/diagonal tension), mode C (flexure/diagonal compression), mode H (preemptive diagonal tension), and mode M (foundation rocking). For each of these behavior modes, Component Guides provide, in addition to the visual description of the different behavior modes, guidance in the analytical steps required to verify a particular behavior mode. See for example the Component Damage Classification Guide RC1B under “How to distinguish behavior mode by analysis”. Based on the recommendations of the guide, the shear associated with the development of the maximum strength in flexure, diagonal tension, web crushing, and foundation rocking were calculated. Calculation results are summarized in Table 7-1. Selected details of the calculations are provided in the box on 192.

Component guides, RC1B, RC1C, and RC2H, Section 5.5 of FEMA 306

The relationship between capacities of the different potential behavior modes defines the governing component behavior mode. Initially, consider the first five modes listed in Table 7-1, temporarily neglecting the overturning (foundation rocking) response. Because the wall is flanged, its response depends on the direction of seismic force, and the flexural capacity must be calculated for each direction. It is possible that a different behavior mode will govern in each of the two different loading directions. In this example, the diagonal tension strength at low ductility is less than the flexural strength

Table 7-1 Capacity of Potential Behavior Modes for Typical Solid Wall (2B-2C)

Behavior Mode	Shear Capacity (kips)	FEMA 306 Reference	Comments
Flexure (modes A & B) – flange in compression $M_e = 31,300$ k-ft	1570*	Sect. 5.3.5	All distributed reinforcement is included in the calculation of flexural strength, as is the contribution of the flange reinforcement.
Flexure (A & B) – flange in tension $M_e = 44,600$ k-ft	2230*	Sect. 5.3.5	
Diagonal Tension (B & H) – at low flexural ductility	1350	Sect. 5.3.6b	Low ductility implies $\mu \leq 2$ and high ductility implies $\mu \geq 5$, but for this example the exact displacement ductility is not important. Capacity at high ductility does not govern, since flexural yielding does not occur.
Diagonal Tension (B) – at high flexural ductility	851	Sect. 5.3.6b	
Web crushing (C)	2560	Sect. 5.3.6c	
Overturning (M) – flange in compression $M_e = 6,860$ k-ft	343	Sect. 5.2.6	When the flange is in tension, the vertical load includes dead load contribution of flange.
Overturning (M) – flange in tension $M_e = 18,000$ k-ft	923	Sect. 5.2.6	

* Shear associated with development of the moment strength

in either loading direction, so mode H (preemptive diagonal tension) appears to be the governing the behavior mode. In either direction, web crushing can be eliminated as a potential behavior mode since its capacity is greater than that of all of the other modes. In the absence of overturning, mode H would therefore be selected as the behavior mode for this component.

Additional calculations indicate, however, that foundation rocking (overturning of the wall and its foundation) will occur before the other failure modes can develop. This is indicated in the last two rows of Table 7-1, where overturning capacity with the flange in compression is shown to be less than other behavior modes. As shown in the example calculations (see sidebar), the foundation rocking capacity is based on the static overturning force associated with all tributary gravity loads. In reality, there are a number of factors that would increase the force required to overturn the wall, so the calculated value may be a lower bound. For example, as the foundation lifts, it will pick up an increasing tributary area of the surrounding slabs, thus increasing the

restoring force. However, the overturning value calculated is sufficiently less than the other behavior modes to suggest that damage will be limited by rocking on the foundation. Mode M is therefore the behavior mode for the wall.

Damage Severity. The identification of the rocking behavior mode is important, because the damage severity is different for mode M than for mode H. While there is no explicit Component Damage Classification Guide provided for the rocking mode—the component may be considered as roughly analogous to the portion of a flexural wall (mode A) above the plastic hinge region—there is a ductile fuse in the structure below the component in question that will prevent the development of the brittle, force-controlled behavior mode H by limiting the development of additional seismic force. Using this analogy, and Component Guide RC1A, the damage severity is classified as Insignificant. Without the rocking mechanism, the behavior mode would be classified as H, and the damage severity would be Moderate rather than Insignificant. It is important to note

Chapter 7: Example Application

EXAMPLE CALCULATIONS FOR DIFFERENT BEHAVIOR MODES EXAMPLE 1 – SOLID WALL

Flexure:

The boundary elements at each end of the wall have 4-#10 and 7-#11 bars. The vertical wall reinforcement is #4 bars at 13" on center in each face. An approximation of the flexural capacity with the flange in compression may be made, assuming that all the steel in the tension boundary and all the wall vertical steel is yielding, as follows:

$$M_{e(comp.)} = \underbrace{A_s f_{ye} l_{wall}}_{\text{Boundary}} + \underbrace{A_{sv} f_{ye} l_{wall} / 2}_{\text{Wall Verts.}} + \underbrace{P_{DL(wall)} l_{wall} / 2}_{\text{Dead Load}}$$

$$= (15.3) 50 (26) + (9.2) 50 (13) + (419) 13$$

$$= 31,300 \text{ k-ft}$$

With the flange in tension the capacity increases because of the yielding of the wall vertical reinforcing in the effective flange width assumed to be one half the effective wall height (M/V) plus the wall thickness, or about ten feet. The capacity also increases because of the additional dead load resistance of the flange. An approximation of the flexural capacity with the flange in tension is then:

$$M_{e(ten.)} = M_{e(comp.)} + \underbrace{A_{sv} f_{ye} l_{wall}}_{\text{Flange Verts.}} + \underbrace{P_{DL(flange)} l_{wall}}_{\text{Flange Dead Load}}$$

$$= 31,317 + (3.8) 50 (26) + (320) 26$$

$$= 44,600 \text{ k-ft}$$

These approximations for moment capacities were checked using strain compatibility calculations and found to be acceptable. Using an M/V ratio of 20 ft the shear forces associated with the moment capacities are 1570 k (flange in compression) and 2230 k (flange in tension).

Diagonal Tension (Shear Strength):

In order to include the effect of axial load on shear strength, and the potential degradation of the shear in plastic hinge zones, the equations recommended in Section 5.3.6b of FEMA 306 were used to calculate the diagonal tension strength.

$$V_n = V_c + V_s + V_p$$

An M/V ratio of 20 feet was used (approximately 0.75 times the component height) based on the analysis results for shear and moment.

$$A_s = 41.2 \text{ in}^2$$

$$A_g = 4176 \text{ in}^2$$

$$\rho_s = 0.0098$$

Thus Equations 5-3 and 5-4 of FEMA 306 yield

$$\alpha = 1.5 \quad k_{rc} = 3.5 \text{ (low ductility)}$$

$$\beta = 0.7 \quad k_{rc} = 0.6 \text{ (high ductility)}$$

and the concrete contribution (Equation 5-2) becomes

$$V_c = \alpha \beta k_{rc} \sqrt{f'_{ce}} b_w (0.8l_w)$$

$$V_c = 605 \text{ kips at low ductility demand}$$

$$V_c = 104 \text{ kips at high ductility demand}$$

The steel contribution is given by Equation 5-5:

$$V_s = \rho_n f_{ye} b_w h_d$$

where $\rho_n = .00256$, $f_{ye} = 50 \text{ ksi}$, $b_w = 12"$, and h_d is limited by the component height of 27'-0". Thus

$$V_s = 498 \text{ kips}$$

The axial load contribution is given by Equation 5-6. Considering only the structure dead load tributary to the wall (419 kips) V_p becomes

$$V_p = \frac{(l_w - c) N_u}{(2M / V)} = 264 \text{ kips (flange in compression)}$$

$$= 249 \text{ kips (flange in tension)}$$

NOTE: $c = 16.8 \text{ in.}$ (flange in compression), $c = 33 \text{ in.}$ (flange in tension)

Therefore, Equation 5-1 for the diagonal tension strength gives a value of 1352 kips at low ductility demand, and 851 kips at high ductility demand, both with the flange in tension.

Diagonal Compression (Web Crushing):

The web crushing strength is given by Equation 5-7. This equation requires an estimate of the drift ratio to which the component is subjected, with increasing drift corresponding to a decrease in capacity. An upper bound estimate of 1 percent drift is assumed, to get a lower bound on the web crushing strength:

$$V_{wc} = \frac{1.8 f'_{ce} b_w (0.8l_w)}{1 + \left(600 - 2000 \frac{N_u}{A_g f'_{ce}} \right) \delta} = 2560 \text{ kips}$$

Foundation Rocking (Overturning):

The static overturning calculation includes not only the dead weight of the wall and tributary slabs at the 2nd floor and roof, but also a tributary area of the slab on grade (496 kips total) and the foundation weight (16 kips per footing). When the wall flange is in tension, the weight of the flange and additional DL are included.

$$V_{or} = \frac{1}{(M / V)} M_{or} = \frac{1}{20} (496k(26' / 2) + 16k(26'))$$

$$= 343 \text{ kips (flange in compression)}$$

$$V_{or} = \frac{1}{(M / V)} M_{or}$$

$$= \frac{1}{20} (496k(26' / 2) + 446k(26') + 16k(26'))$$

$$= 923 \text{ kips (flange in tension)}$$

that the damage severity is not a function of the observed crack pattern alone – the governing behavior mode must be known before a judgement of the damage severity can be made.

7.2.4.3 Example 2 – Coupled Wall (7L-7M)

As an example of the second typical wall element type, consider the damage record for the coupled wall shown in Figure 7-7. Like the solid wall example, the wall is 12 inches wide with 18-inch-square boundary elements at each end. However, there is a 6'-6" wide by 7'-3" tall opening in the center of the wall at each floor. The wall length from center to center of the boundary elements is 26 feet, and the story height is 13'-6". The coupled wall has an L-shaped plan with a 26-foot flange along line M. The coupling beam and wall are similar to the example shown in Figure 7-5, except that this particular coupled wall is discontinuous below the first floor and is supported on 24-inch-square reinforced-concrete columns at the basement.

Component Type. Visual observation leads to the division of this structural element into two RC1 wall piers and two RC3 coupling beams. Analysis will verify that the beams are weaker than the walls, and thus that the initial classification is valid.

Behavior Mode. In the preliminary classification, the coupling beams were designated by observation as

mode B (flexure / diagonal tension) or mode H (preemptive diagonal tension), and the wall piers were designated as mode B (flexure / diagonal tension), mode C (flexure / diagonal compression), mode H (preemptive diagonal tension), or mode N (individual pier rocking). As in the first example, the shears associated with the development of the maximum strength in flexure, diagonal tension, and web crushing were calculated, with results summarized in Tables 7-2 and 7-3. Selected details of the calculations are provided for reference on pages 196 through 198.

Looking first at the RC3 coupling beam component, the calculation results shown in Table 7-2 indicate that the shear strength will be reached before the development of the moment strength, even at low ductility levels, so the behavior mode H (preemptive diagonal tension) governs.

For the RC1 wall pier components, the calculations and discussions that follow show that behavior mode N, individual pier rocking, governs the seismic response. For the piers of the coupled wall, which discontinue below the first floor and are supported on basement columns, this behavior mode involves the yielding in flexure of the basement columns and the coupling beams reaching their capacity in shear. The wall pier rotates about the supporting column in a manner similar to

Table 7-2 Capacity of Potential Behavior Modes for Typical Coupling Beam

Coupling Beams RC3 Behavior Mode	Limiting Component Shear (kips)	FEMA 306 Reference	Comments
Flexure (mode A) $M_e = 1210$ k-ft	373*	Sect. 5.3.5	Note that slab reinforcement was ignored in the calculation of the beam flexure capacity. Since preemptive shear governs ($242 < 373$), this is irrelevant. A more accurate calculation would be warranted if the capacities in the different modes were similar.
Diagonal Tension (B and H) – at low flexural ductility	242	Sect. 5.3.6b	Governing capacity
Diagonal Tension (B) – at high flexural ductility	137	Sect. 5.3.6b	This capacity does not govern since flexural yielding does not occur.
Sliding Shear (D)	150	Sect. 5.3.6c	This mode is unlikely since it typically occurs after flexural yielding. Such yielding is not expected since preemptive diagonal tension governs over flexural response.

* Component shear in beam associated with development of the component moment strength

Chapter 7: Example Application

Table 7-3 Shear Capacities for Potential Behavior Modes of Wall Pier (RC1) Components in Coupled Wall

Potential Behavior Mode	Limiting Component Shear (kips)	FEMA 306 Reference	Notes
<u>Flexure(mode A)</u>	See notes*	Sect. 5.3.5	*In example calculations, moment capacities are compared to moment demands corresponding to mode N. Flexure is shown not to govern.
<u>Diagonal Tension (mode B and H) at Low Flexural Ductility</u> RC1@7L-load to east RC1@7L-load to west RC1@7M-load to east RC1@7M-load to west	690 311 328 692	Sect. 5.3.6b	Limiting shears are compared to those for behavior mode N. To consider redistribution of lateral forces, the sum of shears for the two wall piers is considered.
<u>Diagonal Tension (mode B) at High Flexural Ductility</u> RC1@7L-load to east RC1@7L-load to west RC1@7M-load to east RC1@7M-load to west	470 163 166 472	Sect. 5.3.6b	These capacities do not govern, since flexural yielding does not occur.
<u>Web Crushing (mode C)</u> RC1@7L-load to east RC1@7M-load to west	1710 1810	Sect. 5.3.6c	Web crushing not applicable for low axial load or tension.
<u>Rotation about Column (mode N)</u> RC1@7L-load to east RC1@7L-load to west RC1@7M-load to east RC1@7M-load to west	330 300 300 330		Shear in piers is limited by capacity of coupling beam (RC3) components.

foundation rocking. Free body diagrams corresponding to this mechanism and behavior mode are shown in the example calculations that follow.

Comparison of the moment demands corresponding to the behavior mode N to moment capacities of the wall pier sections is shown in the example calculations. The moment demands are well below the moment capacities, indicating that flexural yielding will not occur. This eliminates modes B (flexure/diagonal tension) and C (flexure/diagonal compression) as possible behavior modes.

The limiting component shears associated with possible behavior modes for the wall piers are summarized in Table 7-3. The table verifies that the web crushing (diagonal compression) can be eliminated as a possible behavior mode because the capacity is much higher than that corresponding to other behavior modes. Behavior mode H, preemptive diagonal tension, is investigated by comparing the limiting shears to those of mode N.

Diagonal tension capacities at high ductility are only relevant for the combined flexure/diagonal tension behavior mode, which will not occur since flexural

yielding and the consequent degradation of the V_c component of shear strength does not occur. The relevant diagonal tension capacities are those at low ductility.

The diagonal tension capacities of 311k (RC1@7L-load to west) to 328k (RC1@7M-load to east) for the wall piers subject to axial tension are similar to the shear demands in the pier rotation mode after failure of the coupling beams; however, there is significant capacity of 690k (RC1@7L-load to east) to 692k (RC1@7M-load to west) in diagonal tension on the corresponding compression sides of the wall. A diagonal tension failure cannot fully develop on one side of the coupled wall without transferring lateral forces to the other side of the wall. Considering that shear can be transferred as axial forces in the coupling beam and slab according to the stiffness and strength of each wall pier, the sum of wall pier component strengths on each side of the coupled wall can be used to determine the governing behavior mode. For the individual pier rotation behavior, the associated total shear demand is 630k on the coupled wall element. For a diagonal tension behavior mode occurring in both wall piers, the associated shear capacity is 1003k to 1018k. Diagonal tension failure will not govern, since the pier rotation behavior mode occurs at a lower total lateral load. Thus, the results of the analytical calculations indicate the pier rotation (N) is the governing behavior mode for the RC1 components. This analytical conclusion agrees with field observation. The degree of diagonal cracking observed in the wall pier RC1 components is consistent with substantial shear stress, but less than that which might be expected for diagonal tension failure.

Damage Severity. For the RC3 components behaving in mode H, the damage classification guides indicate that the observed damage is Moderate in the second story and Heavy in the first story coupling beam. In the wall piers, the protection of the element by a ductile mode (similar to mode N, Foundation Rocking) in surrounding components places them in an Insignificant damage category.

7.2.5 Other Damage Observations

Several of the walls were observed to have horizontal cracks just below the roof slab and/or the second-floor slab. In addition to new cracks of this type, a few walls had pre-existing horizontal cracks below the slabs, which had been repaired by epoxy injection. The widest of these horizontal cracks occurred under the roof slab of the wall on column lines 7C-7D, as shown in the Component Damage Record D3. The engineer in the field indicated that joint movement occurred at this

crack and suspected that sliding shear behavior may have occurred.

Subsequent thinking by the evaluating engineers about this observation, however, weighed against the conclusion of sliding shear behavior. The crack was not observed to extend into the boundary columns of the wall, and there was no evidence of lateral offset at the boundary columns. While the crack is located near a likely construction joint where poor construction practice can exacerbate sliding shear behavior, the crack is not located in the maximum moment region of the wall. As is indicated in FEMA 306, sliding shear behavior is most likely to occur after flexural yielding has occurred. For this wall, flexural yielding would initiate at the base of the wall where moments are at a maximum, not at the top. In any case, foundation rocking preempts flexural yielding for the typical solid wall, as indicated previously in this example. A quick calculation of sliding shear strength shows that the behavior mode is not expected to govern the wall's response.

Given this information, the damage observations are reconsidered, and it is judged that sliding movements did not occur at the horizontal crack. Therefore, the most likely explanation is that these horizontal cracks are caused by earthquake displacements in the *out-of-plane* direction of the wall. It is judged that the horizontal cracks, whose widths are less than 0.03 inches, do not significantly affect seismic response.

7.2.6 Summary of Component Classifications

7.2.6.1 Solid Walls

All wall components of the building are evaluated in a similar manner, as described in the preceding sections. In total, the building has six coupled walls plus five solid walls acting in the North-South direction, and two coupled walls plus six solid walls acting in the East-West direction. The damage records for these walls can be found in Component Damage Records D1–D19 (Appendix A).

Each solid wall is a single structural component (RC1), while each coupled wall has four components: two coupling beams (RC3) and two wall piers (RC1). Thus there are a total of 43 structural wall components in the building, as indicated in Tables 7-4 and 7-5. For each of these, the component type, behavior mode and damage severity is established as described below and shown in the tables.

**EXAMPLE CALCULATIONS FOR DIFFERENT BEHAVIOR MODES
EXAMPLE 2 – COUPLED WALL (7L-7M)**

COUPLING BEAMS

RC3 Flexure:

The moment strength of the coupling beams is calculated as discussed in FEMA 306, Section 5.3.5 using expected values for material properties ($f'_{ce} = 3000$ psi, $f_{ye} = 50$ ksi). The beams are 6'-3" deep, with 3 - #9 bars at top and bottom and #4 bars @ 13" on center at each face. The calculated moment capacity is 1210 k-ft. This capacity is determined using strain compatibility calculations that demonstrate that all longitudinal bars yield. The M/V ratio for the coupling beam is 3'-3", so the shear associated with development of the moment capacity at each end of the beam is 373 kips. Note that slab reinforcement is ignored in the calculation of the beam flexure capacity. It will be shown below that preemptive shear clearly governs, so this is irrelevant. However, a more accurate calculation would be warranted if the capacities in the different modes were similar.

RC3 Diagonal Tension (Shear Strength):

The equations for diagonal tension strength in Section 5.3.6b of FEMA 306 may be used for coupling beams. For beams, the axial load is not significant, thus $V_p = 0$ and Equation 5-1 becomes:

$$V_n = V_c + V_s$$

Using an M/V ratio of 3'-3" (half the clear span of the coupling beams) Equations 5-3 and 5-4 of FEMA 306 yield

$$\alpha = 1.5 \quad \rho_g = 0.0059 \quad \kappa_{rc} = 3.5, 0.6$$

$$\beta = 0.61 \quad \sqrt{f'_{ce}} = 55 \text{ psi}$$

and the concrete contribution Equation 5-2 becomes

$$V_c = \alpha \beta k_{rc} \sqrt{f'_{ce}} b_w (0.8l_w)$$

$$V_c = 127 \text{ kips at low ductility}$$

$$V_c = 22 \text{ kips at high ductility}$$

The steel contribution is given by Equation 5-5

$$V_s = \rho_n f_{ye} b_w h_d$$

where $\rho_n = .00256$ is based on the vertical (stirrup) reinforcement, $f_{ye} = 50$ ksi is the expected steel yield strength, $b_w = 12"$, and $h_d = 75"$ is the horizontal length over which vertical stirrup reinforcement contributes to shear strength, in this case the length of the coupling beam. Thus

$$V_s = 115 \text{ kips}$$

The total diagonal tension strength is then 242 kips at low ductility, and 137 kips at high ductility.

RC3 Sliding (Sliding Shear):

FEMA 306 Section 5.3.6d gives the sliding shear strength for coupling beams at moderate ductility levels as

$$V_{sliding} = 3 \left(\frac{l_n}{h} \right) \sqrt{f'_{ce}} b_w d = 150 \text{ kips}$$

This failure mode is generally associated with beams that are well reinforced for diagonal tension, and that undergo multiple cycles at a moderate ductility level. Since the preemptive shear failure mode governs, the sliding shear mode is not a potential failure mode.

WALL PIERS

RC1 Flexure:

The figures below show the free body diagrams of the wall for lateral forces toward the east and toward the west. In both cases it is assumed that the coupling beams and first floor slab have reached their capacities. It is also assumed that the columns beneath the first floor are yielding in flexure. These assumptions define a potential inelastic lateral mechanism for the coupled wall. If the assumed lateral mechanism for the coupled wall is correct, the flexural capacity of the RC1 components must be sufficient to generate the diagonal tension failure in the RC3 coupling beams. The moment demand diagrams for the RC1 pier components are also shown below.

The boundary elements in the wall piers at lines L and M each contain 8-#11 vertical bars. The vertical wall reinforcing comprises #4 bars at 13" on center in each face. Using strain compatibility calculations, the moment capacities at the top and bottom of the piers (between the first floor and the top of the door opening) corresponding to the appropriate axial loads are calculated.

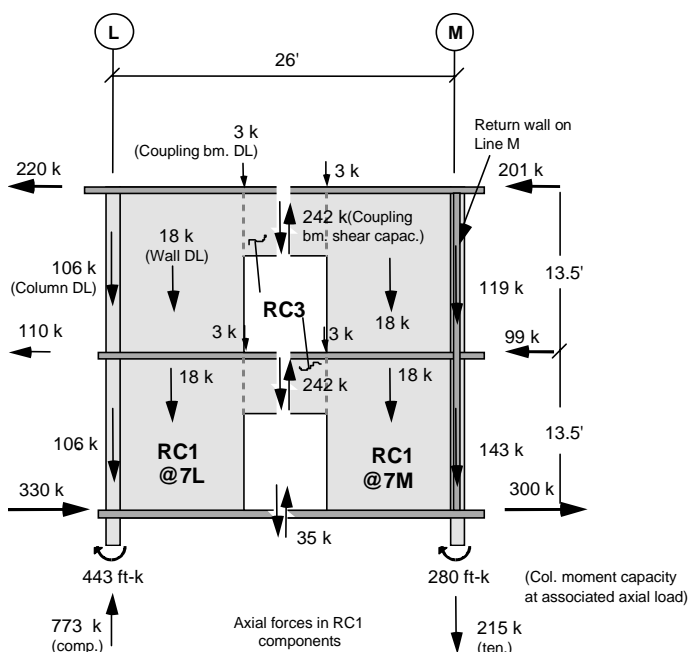
The moment capacity and demand for the RC1 components must be determined with respect to the same axis. For RC1@L the elastic centroid is selected. For RC1@M the elastic centroid of the component neglecting the return wall is used as the axis. When the return wall is in compression it contributes little to the flexural strength of the wall pier. However, when in tension, the reinforcement in the return increases moment strength. Therefore, in the capacity calculations, the vertical reinforcement in approximately 10 ft. of return is included. This distance is estimated in accordance with FEMA 306 Section 5.3.5b as 50% to 100% of the M/V for the entire wall.

The flexural demand and capacity of the RC1 components are summarized in the following table:

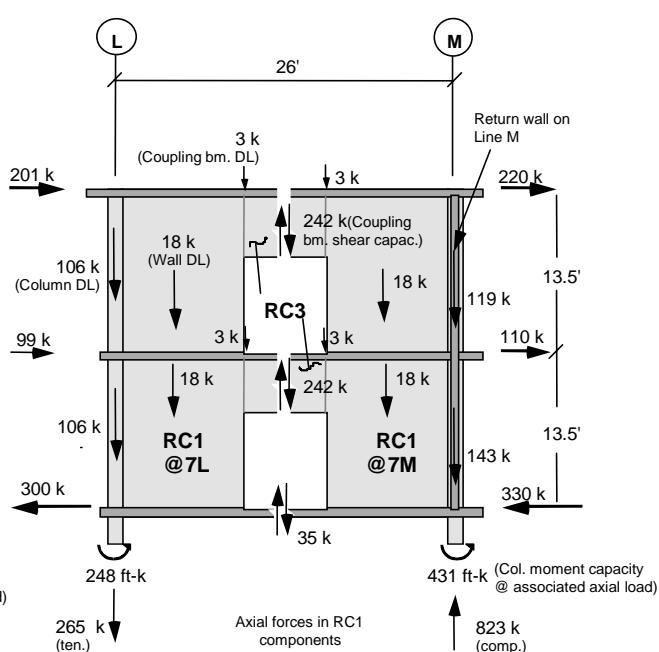
Chapter 7: Example Application

CALCULATIONS FOR EXAMPLE 2 – COUPLED WALL (continued)

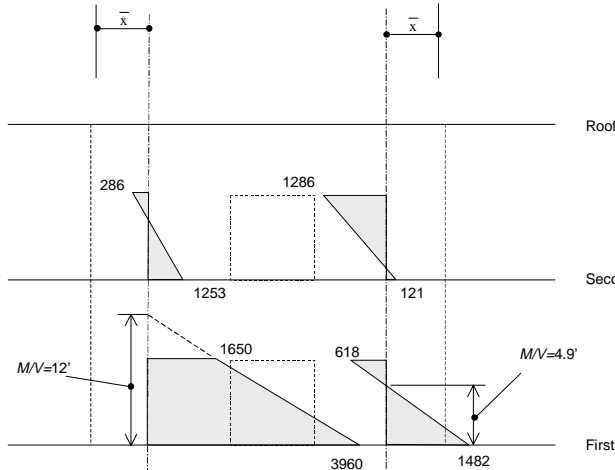
Component	Load Direction	Location on Pier	Axial Load (k, comp.+)	Moment Capacity (k-ft)	Moment Demand (k-ft)
RC1@L	East	Top	773	6470	1650
		Bottom	773	6470	3960
	West	Top	-265	2190	428
		Bottom	-265	2190	1660
RC1@M	East	Top	-215	2400	618
		Bottom	-215	7120	1480
	West	Top	823	6660	1850
		Bottom	823	6660	4160



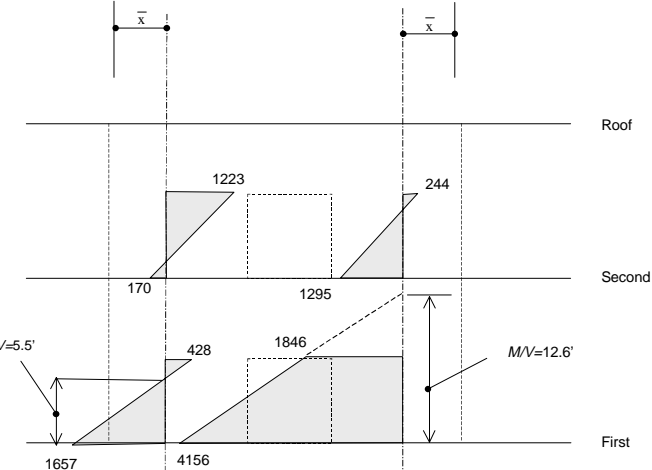
Free Body Diagram for Seismic Forces to East



Free Body Diagram for Seismic Forces to West



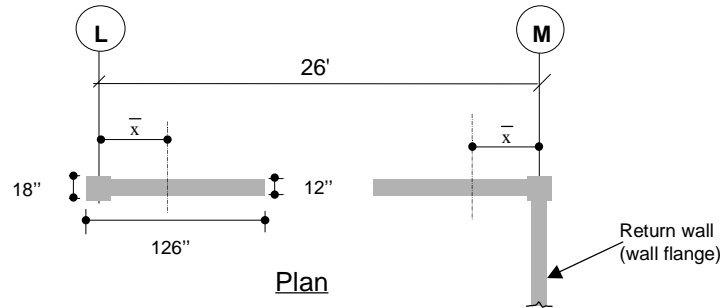
Moment Diagram (@ centroid of piers) for Load to East
(plotted on tension side in k-ft)



Moment Diagram (@ centroid of piers) for Load to West
(plotted on tension side in k-ft)

Chapter 7: Example Application

CALCULATIONS FOR EXAMPLE 2 – COUPLED WALL (continued)



Distance to the elastic centroid from gridline:

$$X = \left\{ \frac{[126(12)126/2 + 2(18)3(9)]}{[126(12) + 2(18)3]} \right\} - 9$$

$$= 50.2" \text{ or } 4.2'$$

Comp.	Load Direct.	Axial Load (k)	V_c	Reduce for Ten.	Net V_c (k)	V_s (k)	V_p (k)	Tot. V (k)	Duct.
RC1@L	East	773 (comp.)	265 45	1.0	265 45	133	292	690 470	low high
	West	-265 (ten.)	265 45	0.67	178 30	133	0	311 163	low high
RC1@M	East	-215 (ten.)	265 45	0.74	195 33	133	0	328 166	low high
	West	823 (comp.)	265 45	1.0	265 45	133	294	692 472	low high

RC1 Diagonal Tension (Shear Strength):

The equations in Section 5.3.6 of FEMA 306 were again used to calculate the diagonal tension strength.

$$V_n = V_c + V_s + V_p$$

Using the component M/V values from the moment diagrams, Equations 5-3 and 5-4 yield

$$\alpha = 1.5 \quad \beta = 0.76 \quad \rho_g = 0.0013$$

and the concrete contribution from Equation 5-2 becomes

$$V_c = \alpha \beta k_{rc} \sqrt{f'_{ce}} b_w (0.8l_w)$$

$$V_c = 265 \text{ kips at low ductility}$$

$$V_c = 45 \text{ kips at high ductility}$$

When the component experiences net axial tension ACI 318-95, eqn. 11-8 specifies the the concrete contribution to shear strength, V_c , be reduced by the factor $1 - [N_u / (500 A_g)]$.

The steel contribution is given by Equation 5-5

$$V_s = \rho_n f_{ye} b_w h_d$$

where $\rho_n = .00256$, $f_{ye} = 50 \text{ ksi}$, $b_w = 12"$, and h_d is limited by the height of the door 7'-3". Thus

$$V_s = 133 \text{ kips}$$

The compressive axial load contribution is given by Equation 5-6.

$$V_p = \frac{(l_w - c)N_u}{\left(2 \frac{M}{V}\right)}$$

Considering all of the above contributions the diagonal tension strengths of the RC1 components are summarized in the table above:

RC1 Diagonal Compression (Web Crushing):

The web crushing strength is given by Equation 5-7. This equation requires an estimate of the drift ratio to which the component is subjected, with increasing drift decreasing the capacity. An upper bound estimate of 1% is assumed to get a lower bound on the web crushing strength:

$$V_{wc} = \frac{1.8 f'_{ce} b_w (0.8l_w)}{1 + \left(600 - 2000 \frac{N_u}{A_g f'_{ce}}\right) \delta}$$

$$= 1710 \text{ kips for RC1@7L load to East}$$

$$= 1807 \text{ kips for RC1@7M load to West}$$

Web crushing is not typically an issue for low axial loads or net tension.

The typical solid walls were calculated to behave in a foundation rocking (or overturning) mode (type M). There are no damage guides for this behavior mode. However, component behavior description in FEMA 306 considers this mode to have moderate to high ductility. The damage associated with this behavior mode may not be apparent based on the observations of the walls. Damage to other structural and nonstructural elements, such as damage to the floor slab at the base or to the beams framing into the ends of the walls, should be used to assess the severity of the mode. Since there was no significant damage to the adjacent structural and nonstructural elements, the damage severity is judged to be Insignificant.

7.2.6.2 Coupling Beams

Based on calculations, the behavior mode of the coupling beams is Preemptive Diagonal Tension (Type H). Based on the damage observations and the component guides, the damage for the coupling beams with spalling, bar-buckling, and/or significant cracking was classified as Heavy. For the coupling beams with shear cracking, but no bar-buckling or significant spalling, the damage is Moderate.

7.2.6.3 Wall Piers

The walls adjacent to the coupling beams are expected to behave in a mode of individual pier rocking (type N). There are no Component Guides for this behavior mode. However, the component behavior description for this mode of behavior considers this mode to have moderate to high ductility. Similar to the solid shear walls, the lack of damage to the adjacent structural and nonstructural elements was used to classify the damage as Insignificant.

7.3 Evaluation by the Direct Method

The effects of damage are quantified by the costs associated with potential repairs (component restoration measures), which if implemented, would restore the components to their pre-event condition. In the direct method, restoration measures are considered on a component-by-component basis without an analysis of global performance. It is intended to be a simple and approximate approach. The Component Damage Classification Guides in FEMA 306 are used to determine

Hypothetical repairs for direct method, Section 4.6 of FEMA 306

the appropriate potential repairs to restore each component.

The potential repairs required to restore the structural performance and nonstructural functionality of the building include both structural and nonstructural (e.g., cosmetic) measures for each damaged component.

7.3.1 Structural Restoration Measures

7.3.1.1 Coupling Beams

As shown in Tables 7-4 and 7-5, three of the coupling beams were classified as component type RC3, behavior mode H, having Heavy damage. As recommended for this component type, behavior mode, and damage severity, the component restoration measure chosen is to replace these components. The proposed repair would be to remove the concrete at the coupling beam and a portion of the floor slab, install new reinforcing bars, and cast new concrete for the wall. The new reinforcing steel in the coupling beams would be detailed in accordance with the current provisions of the governing building code for coupled shear walls, as shown in Figure 7-8.

Damage guide for RC3H, Table 5-2 of FEMA 306

The coupling beams with Moderate damage could be repaired by epoxy injection of all diagonal shear cracks greater than 10 mils wide, since epoxy injection is recommended for structural restoration using the damage guide for RC3H. Although it is possible to inject smaller cracks, the additional cost does not justify the marginal benefit. Since cracks as large as 12 mils can be tolerated in normal concrete structures (ACI, 1994), the unrepaired cracks should not be detrimental. The length of the cracks to be injected is estimated as 100 feet.

7.3.1.2 Solid Walls

The remaining wall components are type N or M. There are no Component Guides for these modes to indicate the appropriate repairs directly. As discussed earlier, these modes have moderate to high ductility capacity. Conservatively, the damage guide for Type B, flexure / diagonal tension, is used since this is a moderate ductility mode, analogous to the actual behavior mode. The Component Guides for the type RC1B components indicate that if cracks are less than 1/16 inch, the damage can be classified as Insignificant, and therefore structural repairs are not necessary. Two of the shear wall components had cracks that exceeded 1/16 inch. This amount of cracking would be classified as Moder-

Chapter 7: Example Application

Table 7-4 Summary of Component Type, Behavior Mode, and Damage Severity for Wall Components (North-South Direction)

Column Line	Floor	Wall Type	Component Type and Behavior Mode	Damage Severity
B / 2-3	First-Second	Coupled	RC1N	Insignificant
	First	Coupled	RC3H	Moderate
	First-Second	Coupled	RC1N	Insignificant
	Second	Coupled	RC3H	Moderate
B / 5-7	First-Second	Coupled	RC1N	Insignificant
	First	Coupled	RC3H	Moderate
	First-Second	Coupled	RC1N	Insignificant
	Second	Coupled	RC3H	Moderate
B / 10-12	First-Second	Coupled	RC1N	Insignificant
	First	Coupled	RC3H	Moderate
	First-Second	Coupled	RC1N	Insignificant
	Second	Coupled	RC3H	Moderate
B / 14-15	First-Second	Coupled	RC1N	Insignificant
	First	Coupled	RC3H	Heavy
	First-Second	Coupled	RC1N	Insignificant
	Second	Coupled	RC3H	Moderate
E / 2-3	First-Second	Coupled	RC1N	Insignificant
	First	Coupled	RC3H	Moderate
	First-Second	Coupled	RC1N	Insignificant
	Second	Coupled	RC3H	Insignificant
E / 14-15	First-Second	Coupled	RC1N	Insignificant
	First	Coupled	RC3H	Moderate
	First-Second	Coupled	RC1N	Insignificant
	Second	Coupled	RC3H	Moderate
G / 7-8	First-Second	Solid	RC1M	Insignificant
G / 9-10	First-Second	Solid	RC1M	Insignificant
M / 7-8	First-Second	Solid	RC1M	Insignificant
M / 9-10	First-Second	Solid	RC1M	Insignificant
M / 8-9	Ground	Solid	RC1B	Insignificant

Table 7-5 Summary of Component Type, Behavior Mode, and Damage Severity for Wall Components (East-West Direction)

Column Line	Floor	Wall Type	Component Type and Behavior Mode	Damage Severity
7 / L-M	First-Second	Coupled	RC1N	Insignificant
	First	Coupled	RC3H	Heavy
	First-Second	Coupled	RC1N	Insignificant
	Second	Coupled	RC3N	Moderate
10 / L-M	First-Second	Coupled	RC1N	Insignificant
	First	Coupled	RC3H	Heavy
	First-Second	Coupled	RC1N	Insignificant
	Second	Coupled	RC3N	Moderate
2 / B-C	First-Second	Solid	RC1M	Insignificant
2 / D-E	First-Second	Solid	RC1M	Insignificant
7 / C-D	First-Second	Solid	RC1M	Insignificant
10 / C-D	First-Second	Solid	RC1M	Insignificant
15 / B-C	First-Second	Solid	RC1M	Insignificant
15 / D-E	First-Second	Solid	RC1M	Insignificant

ate for type B behavior. Epoxy injection is recommended in the Component Damage Classification Guides for these cracks. Thus, for performance restoration by the direct method, these walls would have all of the cracks exceeding 1/16 inch repaired by injection with epoxy. The total length of crack to be injected is estimated at 22 feet.

Spalls (other than at the coupling beams that are being replaced) could be repaired by application of a concrete repair mortar to restore the visual appearance. The total volume of concrete spalls is estimated to be 3 cubic feet.

7.3.2 Nonstructural Restoration Measures

The wall components with visible cracks could be repaired by patching the cracks with plaster, and then painting the entire wall. This repair is only intended to restore the visual appearance of the wall. Restoration of other nonstructural characteristics, such as water tightness and fire protection, are not necessary in this instance.

In addition, many of the suspended ceiling tiles became dislodged and fell during the earthquake. The nonstructural repairs would include replacing the ceiling tiles.

7.3.3 Restoration Summary and Cost

Table 7-6 summarizes the performance restoration measures and estimated costs. Additional costs related to inspection, evaluation, design, management and indirect costs may also be involved.

7.4 Evaluation by Performance Analysis

The use of the direct method is limited to an estimate of the loss associated with the damaging earthquake. It cannot be used to evaluate actual performance. For these purposes, relative performance analysis as described in FEMA 306 is used. The basic procedure comprises a comparison of the anticipated performance of the building in future earthquakes in its pre-event, damaged, and repaired conditions. This comparison may be made for one or more performance objectives.

Chapter 7: Example Application

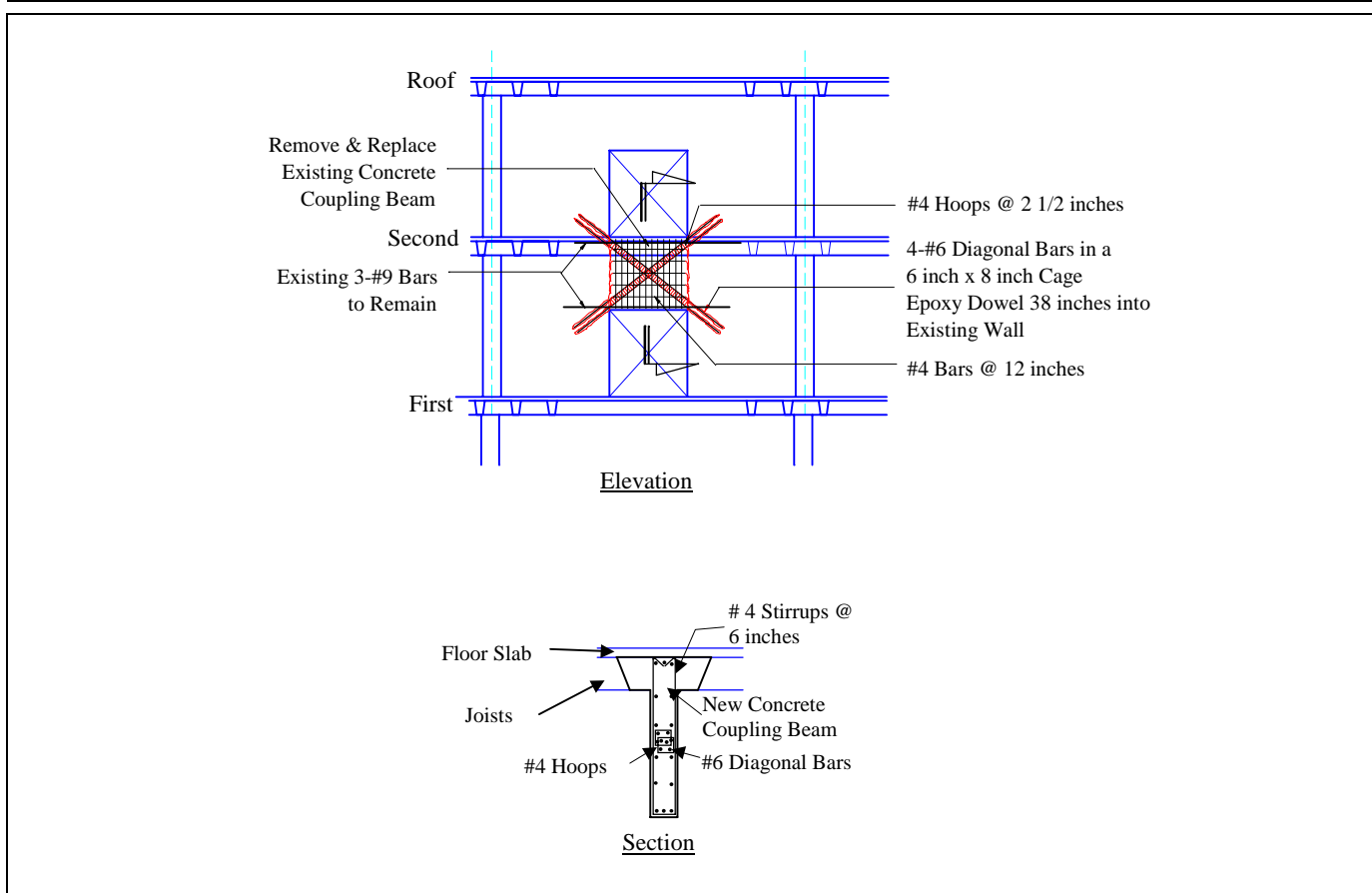


Figure 7-8 Detail of Coupling Beam Replacement

Table 7-6 Restoration Cost Estimate by the Direct Method

Item	Unit Cost (1997 dollars)	Quantity	Cost (1997 dollars)
Epoxy Injection	\$25.00 /lin ft	122 ft	\$ 3,050.
Coupling Beam Removal and Replacement	\$74.00 /cu ft	122 cu ft	\$ 9,028.
Patch and paint walls	\$0.60 /sq ft	10,175 sq ft	\$ 6,105.
Replace ceiling tiles	\$2.00 /sq ft	15,000 sq ft	\$30,000.
General Conditions, Fees, Overhead & Profit (@ 30%)			\$14,455.
Total			\$62,638.

7.4.1 Performance Objectives

Two performance objectives are considered in this example. The first is the *life safety* performance level, as defined in FEMA 273, for an earthquake associated with a 475-year

Performance objectives, Section 4.2 of FEMA 306

return period (10 percent probability of exceedance in 50 years) for this site. The response spectrum for this earthquake is shown in Figure 7-9. The soil at the site was determined to be type S_C . Using the available seismic data, the spectral response at short periods ($T = 0.2$ sec) for this site is 1.0 g and the spectral response at 1 second is 0.56 g.

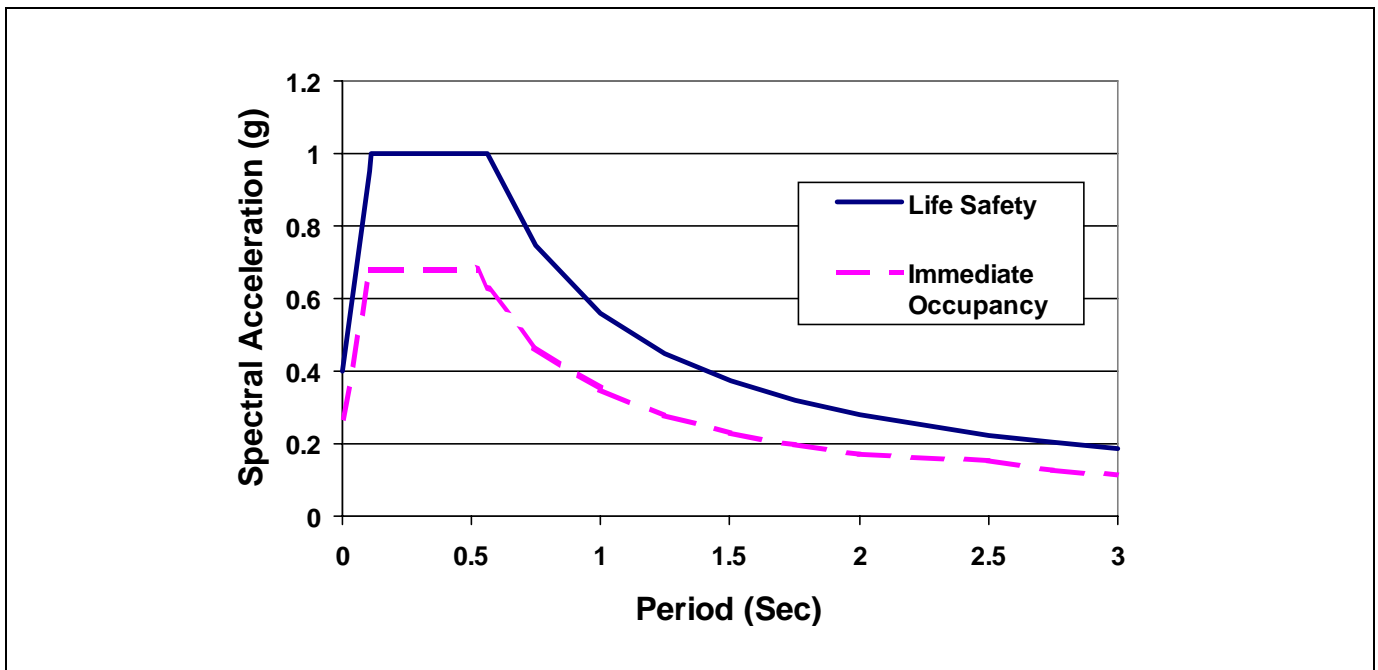


Figure 7-9 Response Spectra for Selected Performance Levels

The building was also checked for *immediate occupancy* performance level using an earthquake with a 50 percent probability of exceedance in 50 years. For this earthquake, the spectral response at short periods at this site is 0.68 g and the spectral response at 1 second is 0.35 g. The response spectra for the immediate occupancy performance level is also shown in Figure 7-9.

It should be noted that these performance objectives do not necessarily correspond to the original criteria used for design of the building.

7.4.2 Nonlinear Static Analysis

7.4.2.1 Computer Model

The building is analyzed in its pre-event, post-event and repaired conditions using a three-dimensional computer model. Modeling of the building is done using the recommendations of FEMA 273 and FEMA 306. The model is subjected to a nonlinear static (pushover) analysis to assess its force/displacement response. For this example, the analysis is run only in the East-West direction, which is the direction that experienced the most significant damage.

The computer analysis program SAP2000 (CSI, 1997) is used to model the structure. The reinforced concrete walls and coupling beams are modeled using beam elements. The beam elements are located at the center of gravity of each wall section, and are given properties

that represent the wall section stiffness. Rigid end offsets are used to model the joint regions in the coupled walls as shown in Figure 7-10. Small models of individual walls are used to verify that the beam elements used to model the walls have approximately the same stiffness and shear distribution as a model using shell elements for the walls. A three dimensional view of the global model is shown in Figure 7-11. The horizontal floor and roof diaphragms are modeled using beam elements, as shown in Figure 7-11, with lumped masses at the nodes.

The pushover analysis is conducted by applying static loads at the locations of the lumped masses in a vertical distribution pattern as described in the second option of Section 3.3.3.2 C, of FEMA 273. Sixty percent of the total lateral force is applied to the roof, thirty percent is applied at the second floor, and ten percent is applied at the first floor. The nodal loads are increased proportionally in progressive iterations. When elements reach their strength limit, their stiffness is iteratively reduced to an appropriate secant stiffness and the model is rerun at the same load level until no elements resist loads in excess of their calculated capacities. (Secant stiffness method, see side bar.)

The pushover analysis is continued to cover the displacement range of interest, which is based on a preliminary estimate of the maximum displacement demand. A global pushover curve is then produced.

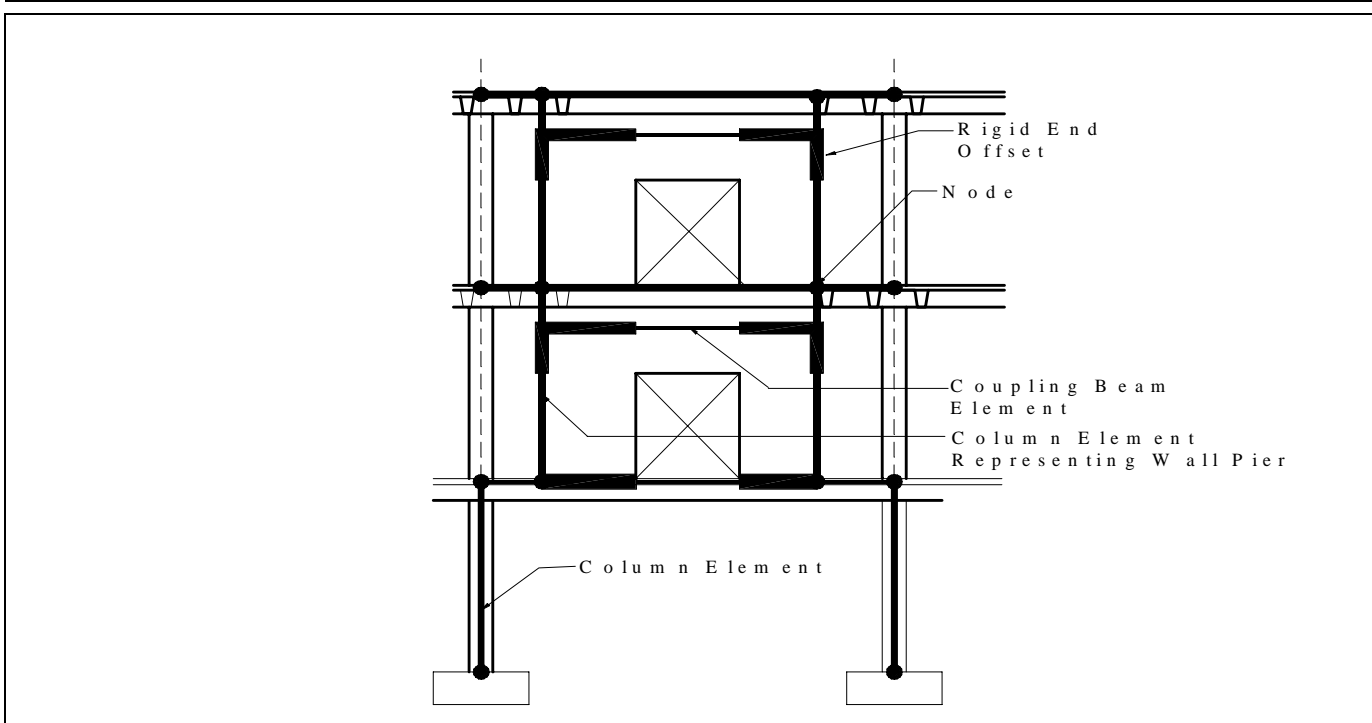


Figure 7-10 Mathematical Model of Coupled Shear Wall

7.4.2.2 Component Force-Displacement Behavior

Component force-displacement curves are developed for each of the typical wall components using the generalized force-displacement curves from Figure 6-1 of FEMA 273. The acceptance limits for the coupling beam components are based on Table 6-17 of FEMA 273 for the case of “nonconforming”, transverse reinforcement, and shear exceeding $6t_w l_w \sqrt{f'_c}$. The pre-event shear-strength-to-

Component force-displacement relations, FEMA 273 and Sections 4.3 and 4.4 of FEMA 306

chord-rotation relationship is shown in Figure 7-12(a). Also shown in this figure are the points representing the displacement limits for immediate occupancy and life safety performance.

The initial slope of the component force/deformation curves is based on the initial elastic stiffness of the component. The pre-event structure is modeled using the effective initial stiffness values recommended in Table 6-4 of FEMA 273. Walls and coupling

Component modeling for pre-event condition, Section 4.4.3.1 of FEMA 306

COEFFICIENT AND CAPACITY SPECTRUM METHODS

Either of two methods are recommended for establishing displacement demands for a nonlinear static analysis: the coefficient method and the capacity spectrum method. A description of these methods is included in ATC 40. The coefficient method is also described in FEMA 273, and the coefficient and capacity spectrum methods are described in FEMA 274. Although either method may be used, it is essential for a valid comparison that the same method be used to assess the performance of the pre-earthquake, post-earthquake, and repaired structure, as outlined in FEMA 306.

In this example, the coefficient method is used. In this method, a target displacement, d_t is calculated and compared to the displacement of a control node, generally located at the roof. The target displacement is determined by multiply-

ing a set of coefficients times a function of the effective building period and the spectral acceleration.

$$\delta_t = C_0 C_1 C_2 C_3 S_a \frac{T_e^2}{4\pi^2} g$$

To use the coefficient method, the nonlinear static analysis must be conducted in order to construct the pushover curve. The pushover curve can be presented as spectral acceleration versus spectral displacement or as base shear versus roof displacement. Once the pushover curve is constructed, an equivalent bilinear curve is fitted to approximate the actual curve. The equivalent bilinear curve is then used to obtain the effective stiffness of the building and the yield base shear needed for calculating the target displacement.

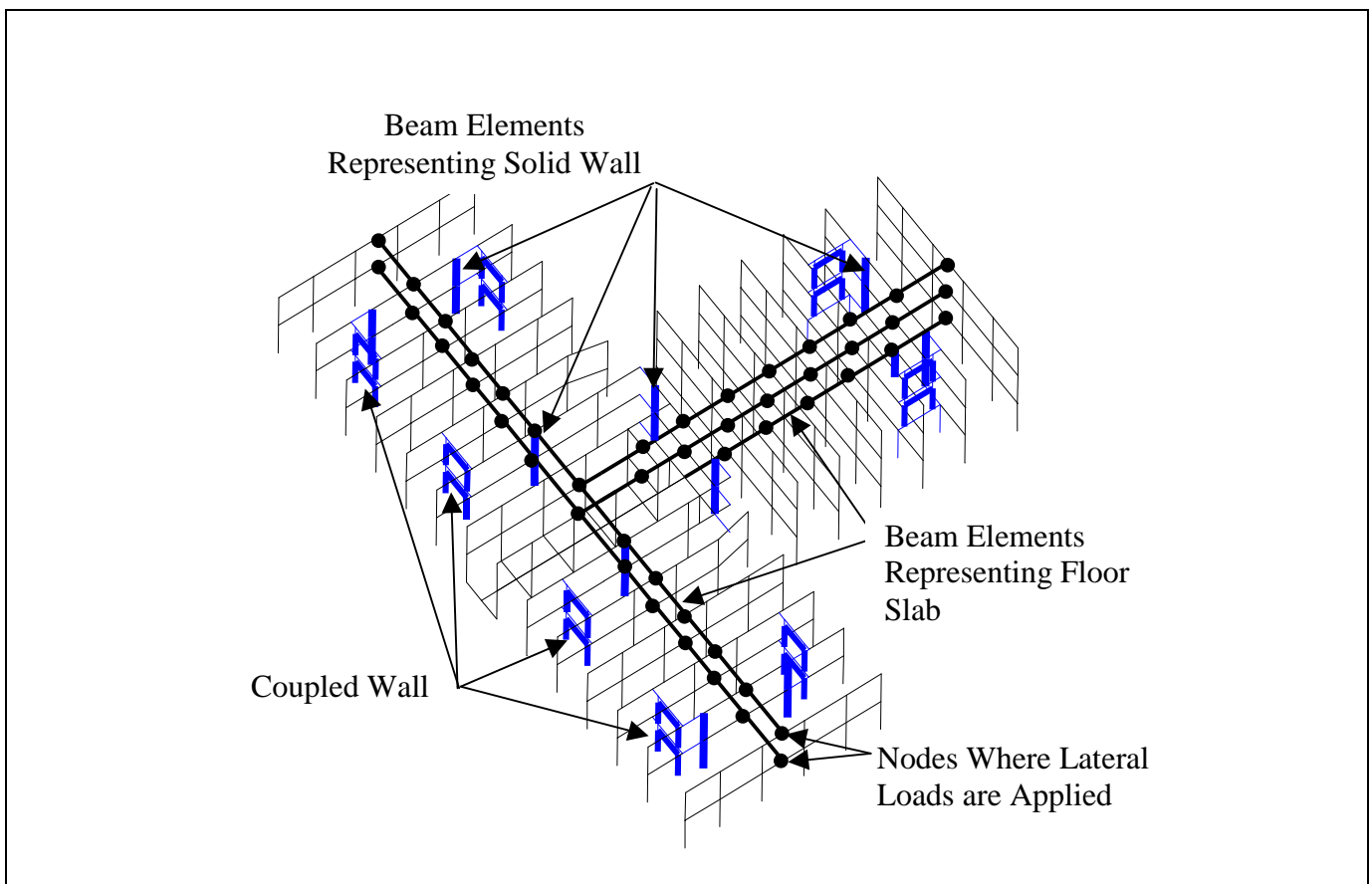


Figure 7-11 Mathematical Model of Full Building

beams are given a flexural rigidity of $0.5E_cI_g$. The base-moment columns of the structure, which support the discontinuous walls, are given a flexural rigidity of $0.7E_cI_g$. As recommended in FEMA 273, the shear rigidities of all components are set equal to gross section values.

The post-event structure is modeled with stiffness values multiplied by the λ_k factors recommended in FEMA 306. Heavily damaged coupling beams have their stiffness reduced to 20 percent ($\lambda_k = 0.2$) of the pre-event value. Moderately damaged coupling beams have their stiffness reduced to 50 percent ($\lambda_k = 0.5$) of the pre-event value. For the solid shear walls, where damage is classified between Insignificant and None, stiffness is reduced to between 80 percent to 100 percent of the pre-event stiffness depending on the amount of cracking.

The horizontal plateau of the component force/deformation curves is based on the strength of the governing behavior mode. For the pre-event structure, the strength

is based on calculations as illustrated in Section 7.2.4 of this example. For the post-event structure, the pre-event strength is multiplied by the λ_Q factors recommended in FEMA 306. Heavily damaged coupling beams have their strength reduced to 30 percent of the pre-event value. Moderately damaged coupling beams have their strength reduced to 80 percent of the pre-event value. For components where damage is classified either Insignificant or None, the strength is not reduced. Figure 7-12(b) shows the force-deformation curves for the moderately and heavily damaged coupling beams.

7.4.2.3 Foundation Rocking

Since the governing behavior mode of the solid concrete walls is identified to be foundation rocking, this behavior is incorporated into the pushover analysis. To model the rocking, the stiffness of the lower story wall elements is reduced when the shear force in those elements reaches the shear force that causes rocking. Once the wall element in the model had started to overturn in the analysis, the stiffness is adjusted so that the wall

NONLINEAR ANALYSIS USING LINEAR ANALYSIS COMPUTER PROGRAMS

Currently, there are few commercially available computer programs for direct implementation of the nonlinear analysis required for a pushover analysis. Many of the nonlinear programs available are sophisticated but can be expensive and difficult to use. For many buildings, a linear elastic analysis program can be used to assess iteratively the nonlinear behavior of the building.

There are two ways to implement a nonlinear static analysis using a linear computer program. Both methods are based on adjusting the stiffness of an element once the analysis indicates that the element has reached its yield level. One method uses the tangential stiffness of the element at the displacement level above yield; the other uses a secant stiffness. The figures below depict the difference between the two methods.

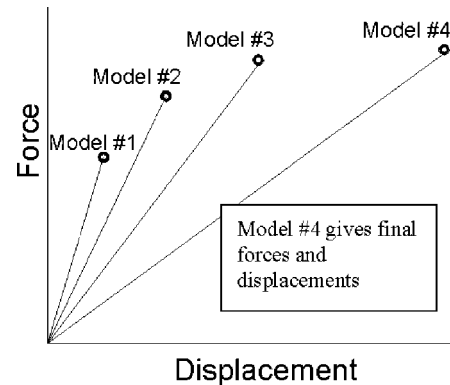


Figure ii – Secant Stiffness Method

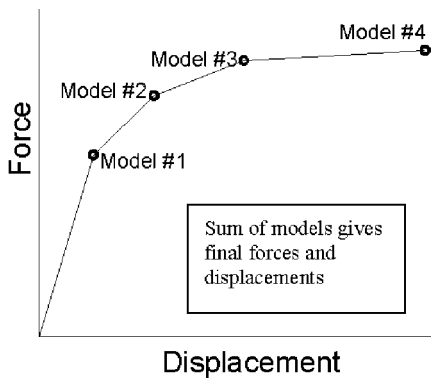


Figure i – Tangential Stiffness Method

The tangential stiffness method is described in detail in ATC 40 (ATC, 1996). Lateral forces are applied to the building and proportionally increased until an element reaches its yield level. A new model is then created in which the yielding component has its stiffness reduced to zero or a small post-yield value. An incremental load is applied to the new

model until another component reaches its yield level. The process continues until a complete mechanism has formed or until the maximum displacement level of interest has been reached. The sum of forces and deformations of each of the incremental models then represent the global behavior of the structure.

In the secant stiffness method, lateral forces are applied to the building and proportionally increased until a component reaches its yield level. A new model is then created in which the yielding element has its stiffness reduced by a value chosen to produce the correct post-yield force in the component. The new model is then rerun at the same force level, and components are checked to verify that the force in the component has not exceeded, or reduced significantly below, its yield level. If necessary, the stiffness of the yielding element may need to be adjusted so that the force in that element is approximately equal to the post-yield force level. Other elements need also be checked since they may be resisting additional load no longer resisted by the yielding element. After iterating until all elements are at approximately the correct force level, a new model is created at a larger lateral force level. The process is repeated at each force level. The behavior of the structure and each element at a given force level is represented directly by the behavior of the appropriate model, rather than combining the results of several models.

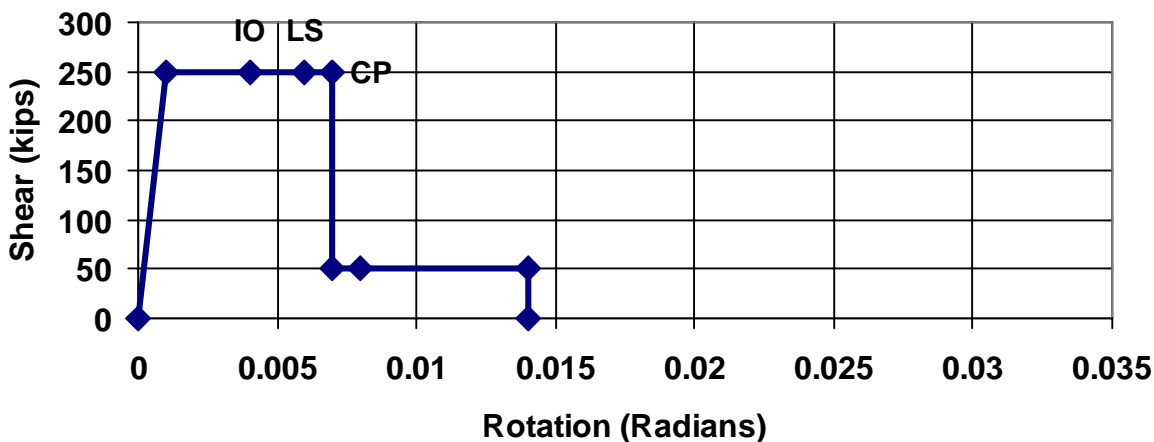
would resist about 10 to 20 percent more shear force than that calculated to cause overturning. This adjustment is made to account for the additional dead weight of the structure that the wall would pick up once it started to uplift. The amount of additional overturning resistance in the wall is based on the shear and moment capacity of the beams framing into the wall.

7.4.3 Force-Displacement Capacity (Pushover Analysis) Results

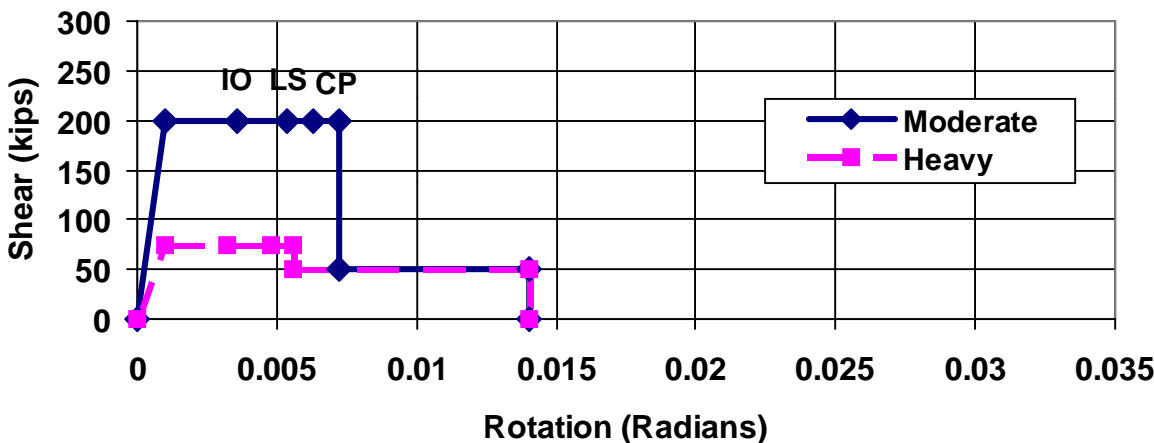
7.4.3.1 Pre-Event Structure

The results of the pushover analysis indicate the progression of displacement events to be as follows for East-West loading (See Figure 7-2 for wall locations):

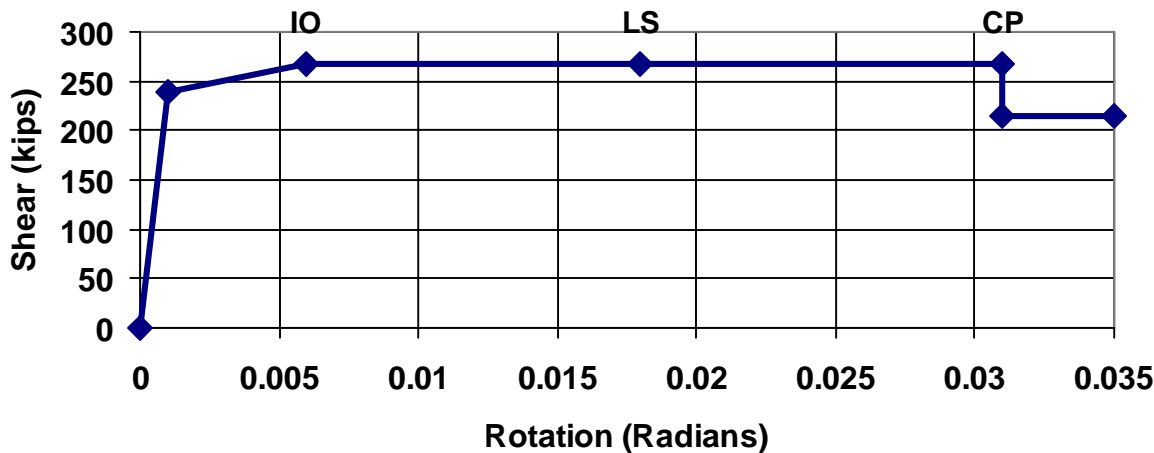
- Initially the two solid walls on lines 7 and 10 between lines C and D reach their rocking capacity.



a) Pre-event



b) Post-event



c) Replacement Coupling Beam with Diagonal Reinforcement

Figure 7-12 Component Force-Displacement Curves for Coupling Beams

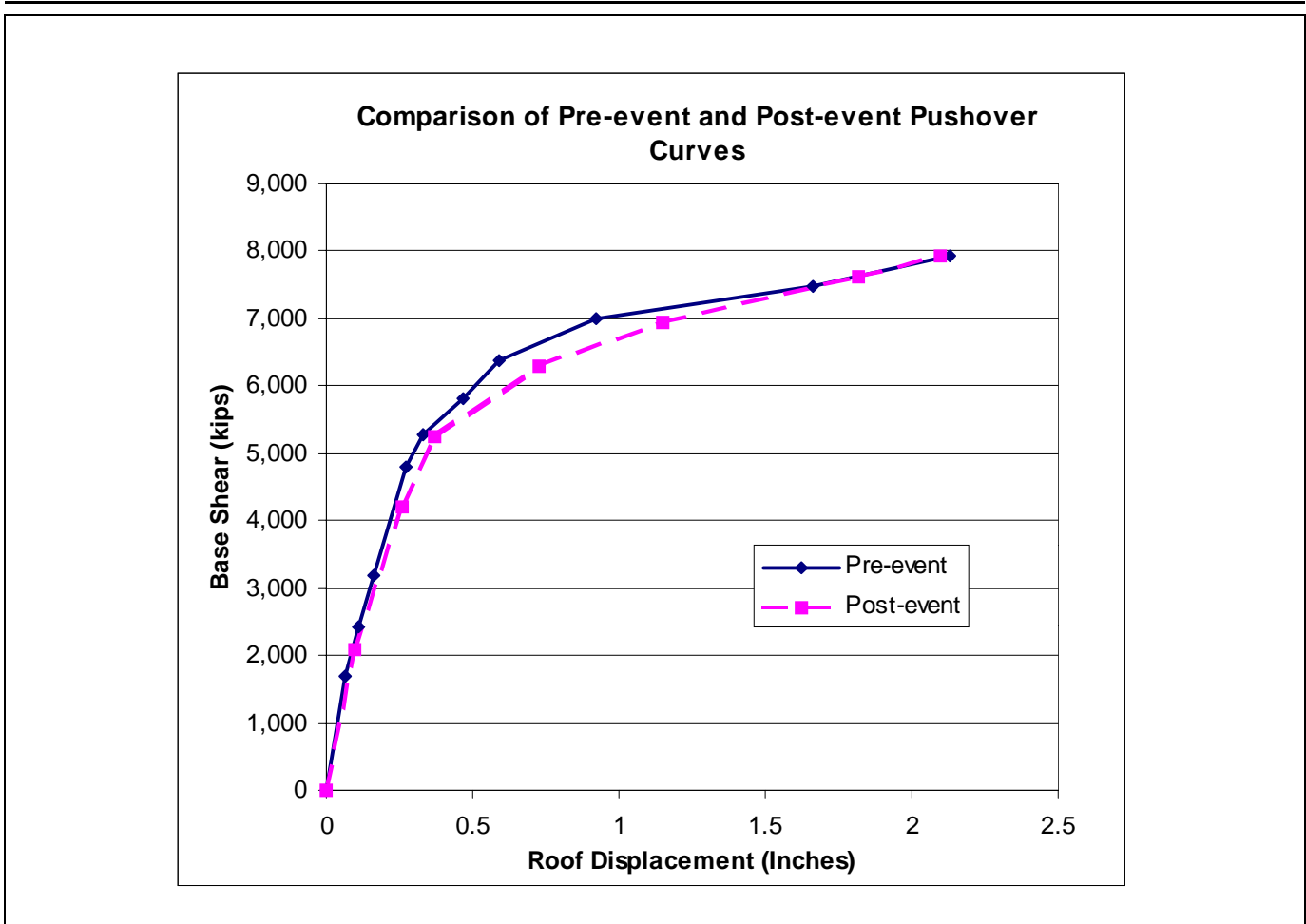


Figure 7-13 Comparison of Pre-event and Post-event Pushover Curves

- When the solid walls between lines C and D are softened, the solid walls on lines 2 and 15 between lines B and C, and between D and E at the first floor pick up additional force and reach their rocking capacity.
- As the solid walls are softened, the coupled walls on lines 7 and 10 between lines L and M resist more force. The first floor coupling beam picks up more force than the second floor coupling beam and reaches its shear capacity first.
- Additional coupling beams reach their capacity and the solid walls continue to rock as the displacement of the structure is increased.
- The approximate target roof displacement is reached after the coupling beams have exceeded their *collapse prevention* acceptability limit, requiring a reduction in their capacity.

As shown in Figure 7-13, the pushover analysis indicates that global nonlinearity begins at a base shear of approximately 5000 k. As lateral displacements increase, the base shear climbs to about 8000 k. Since 10% of the total is applied at the first floor and is transmitted directly into the foundation, the force resisted by the structure above the first floor prior to global nonlinearity is about 4500 k. Allowing for some increase in capacity to reflect rocking behavior more accurately (see Section 7.4.2.3), this agrees well with the hand-calculated capacities of the walls summarized in Tables 7-1 and 7-3. The applied load in excess of the capacity of the walls is resisted by the columns. The magnitude of the increased load is compatible with the capacity of the columns. In the analysis, the first story coupling beams are the first element to reach the immediate occupancy and life safety acceptability limits. The component deformation limit for immediate occupancy occurs when the roof displacement reaches about 0.65 inches and that for life safety is reached at

about 0.88 inch. These displacements are taken as the displacement capacity d_c , as defined in FEMA 306.

The progression of damage shown in the analysis is consistent with the observed damage.

7.4.3.2 Post-Event Condition

For the post-event structure, the progression of displacement events is essentially the same as that outlined for the pre-event structure. The results of the post-event pushover analysis are shown in Figure 7-13. In this analysis, the first story coupling beams reach the immediate occupancy acceptability limit at a roof displacement of 0.47 inches; the beams reach the life safety limit at a roof displacement of 0.66 inches. These values are used for d'_c .

Modeling of the post-event condition, Section 4.4.3.2 of FEMA 306

7.4.3.3 Comparison of Force-Displacement Capacity Curves (Pushover Curves)

The performance of the post-event building was slightly different than the pre-event performance; the overall building is softer since more deflection is obtained for the same magnitude of applied load. The reduced stiffness of the damaged components causes the global reduction of stiffness of the post-event structure. The Moderate and Heavy damage to some of the components corresponds to a reduction in their strength. At

larger displacements (greater than about 1.5 inches) the response of the pre-event and post-event structures are essentially the same.

7.4.4 Estimation of Displacement, d_e , Caused by Damaging Earthquake

The accuracy of the structural model of the building can be verified by estimating the maximum displacement, d_e , that was caused by the damaging event. This is done in two ways. If the data were available, actual ground motion records could be used to predict displacement analytically. Secondly, the pushover curve in conjunction with component capacity data could be used to estimate displacements from the observed damage.

In this case, a spectrum from recorded ground motion at a site approximately 1.5 mi. from the building was available (see Figure 7-14). *FEMA 273* (equation 3-11) uses the displacement coefficient method to estimate maximum displacement from spectral acceleration as follows:

$$d_e = C_0 C_1 C_2 C_3 S_a \frac{T_e^2}{4\pi^2} g \tag{7-1}$$

In this expression the coefficients C_0 to C_3 modify the basic relationship between spectral acceleration and dis-

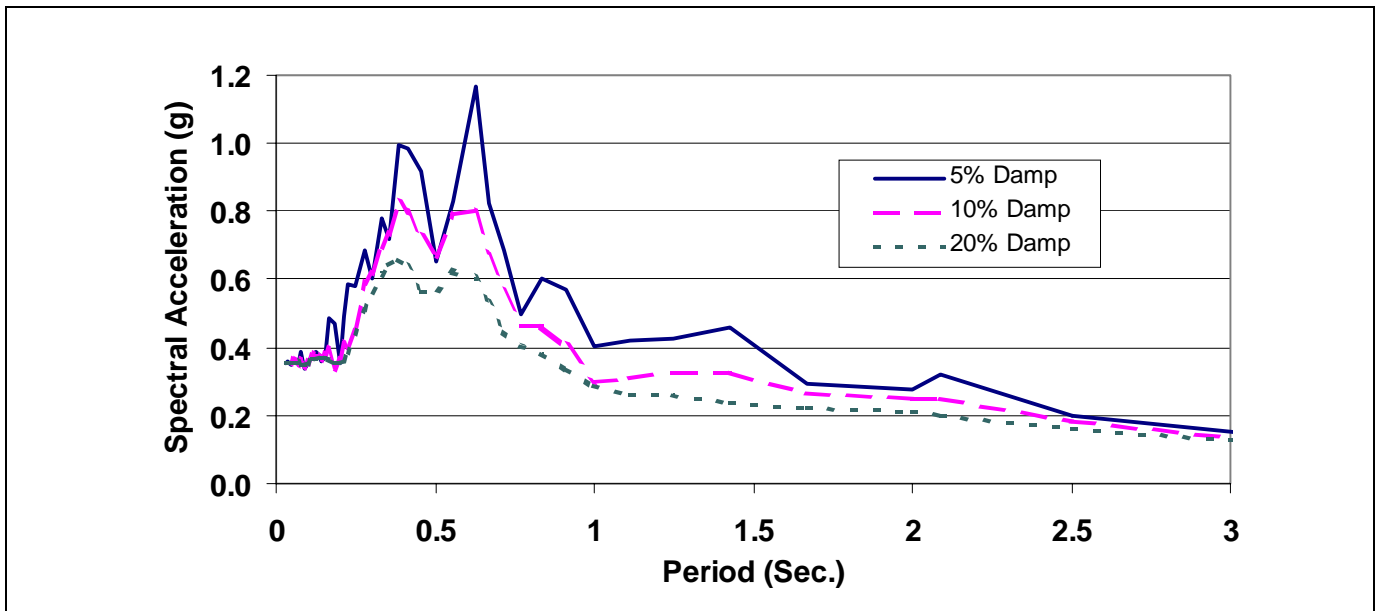


Figure 7-14 Response Spectra from Damaging Earthquake

placement for an elastic system as a function of the effective period of the structure, T_e . The effective period for the pre-event structure is approximately 0.3 sec. The spectral acceleration for this period from Figure 7-14 would be approximately 0.5 to 0.6 g producing an elastic spectral displacement between 0.4 and 0.5 in.

The coefficient C_0 converts spectral displacement to roof displacement and has an approximate value of 1.25 for two- and three-story buildings.

For short-period buildings, the maximum inelastic displacement often is greater than the elastic. *FEMA 273* provides the following expression C_1 to adjust conservatively from elastic to inelastic:

$$C_1 = \frac{\left(1.0 + (R - 1.0) \frac{T_0}{T_e}\right)}{R} \text{ where } R = \frac{S_a}{\left(\frac{V_y}{W}\right) C_0} \quad (7-2)$$

In these expressions, V_y/W is the effective base shear at yield as a portion of the building weight, or about 0.28 in this case. This would result in an R -factor of approximately 1.4 to 1.7. The point where the spectral acceleration transitions from the acceleration to velocity controlled zone occurs at a period of around 0.5 to 0.6 sec. These values would combine to result in a coefficient C_1 of around 1.2 to 1.4.

The coefficient C_2 accounts for the shape of the hysteresis curve and is equal to 1.0 in this case. The coefficient C_3 accounts for dynamic P - Δ effects and is also equal to 1.0 for this case.

Combining all of the coefficients and the elastic spectral displacement results in an estimate for the maximum displacement at the roof, d_e , of between 0.6 to 0.9 in.

From the damage observations, one of the first-floor coupling beams in the east-west direction appeared to reach its capacity, since a severe crack had developed and a transverse bar had buckled. Shear cracking had also developed in the wall piers adjacent to the coupling beams.

From the pushover analysis, at displacement demands between 0.3 inches and 0.5 inches, the coupling beams reach their capacity. The pushover analysis also indicates that the first floor coupling beam would be the first to reach its capacity, which is verified by the observations. Since only the first floor beams were heavily damaged, the displacement demand of the damaging event should not have been much greater than 0.5 in.

The difference between the analytical estimate of d_e and the estimate from the model and observed damage is not large. The difference is acceptable because the building is farther away from the epicenter than the site where the motion was recorded, and actual recorded building response is usually less than that which is predicted analytically. Based on the comparison there is no need to adjust the structural model.

7.4.5 Displacement Demand

7.4.5.1 Estimate of Target Displacement

Estimating the target displacement can be an interactive process. The nonlinear static analysis produces a force-displacement pushover curve covering the displacement range of interest. Based on the procedures of *FEMA 273*, an equivalent bilinear curve is fitted to the pushover curve and a yield point is estimated.

Using this yield point and the associated effective period, the target displacement is calculated using the coefficient method. Given the calculated target displacement, the equivalent bilinear curve can be refitted, adjusting the yield point, and giving a new target displacement. The revised target displacement is close to the original estimate so further iteration is not needed.

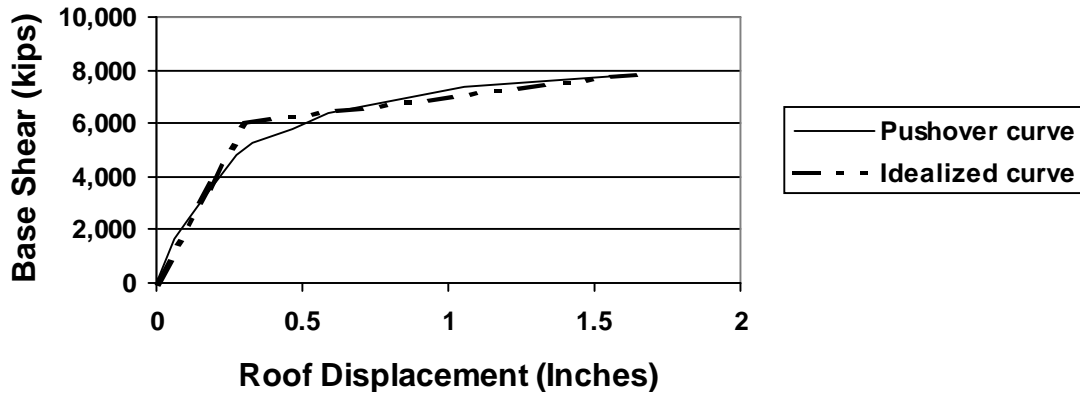
EXAMPLE CALCULATIONS FOR PRE-EVENT AND POST-EVENT DISPLACEMENT DEMANDS

Section 5.4 of *FEMA 306* describes the procedures for calculating the displacement demand for both the pre-event and the post-event structures. The pre-event and post-event pushover curves for this example are shown in Figure 7-13. For this example, the coefficient method is used to calculate the target displacements and *FEMA 306* procedures are used to determine the corresponding displacement demands.

Pre-Event Target Displacement, d_d

An idealized bi-linear capacity curve for the pre-event structure is developed to approximate the actual pushover curve. Based on this idealized curve, the yield level base shear V_y is 6000 kips and the yield level displacement D_y is 0.31 inches. The effective stiffness K_e then becomes 19,400 kips/inch.

EXAMPLE CALCULATIONS FOR PRE-EVENT AND POST-EVENT DISPLACEMENT DEMANDS (continued)



Comparison of idealized bilinear curve to pushover curve

The initial period T_i is 0.25 seconds taken from the initial structural model. The effective period is calculated to be 0.30 seconds using the ratio of the initial to the effective stiffness.

$$T_e = T_i \sqrt{\frac{K_i}{K_e}} = 0.25 \sqrt{\frac{27900}{19400}} = 0.30$$

The spectral acceleration S_a , based on the life safety earthquake response spectra at the effective period is 1.0 g.

The coefficients are:

- $C_0 = 1.25$ for a 2-to-3-story building
- $C_1 = 1.58$ using the equation for T_e in the constant acceleration region of the spectrum
- $C_2 = 1.0$
- $C_3 = 1.0$

Thus the target displacement from Equation 3-11 of FEMA 273 is:

$$d_t = 1.25 (1.58) (1.0g) (386 \text{ in/sec}^2g) (0.30)^2/4\pi^2 = 1.68 \text{ inches}$$

This value is assigned as d_d , the maximum displacement in its pre-event condition.

Post-Event Target Displacement, d'_{d1}

There are two values for the post-event displacement demand that need to be calculated. The first value, d'_{d1} uses

the pre-event effective stiffness and the post-yield stiffness for the post-event curve to calculate a target displacement. In this example, the slopes of the post-yield curves for the pre-event and post-event conditions are similar. Therefore, the target displacements will be essentially the same. The value for d'_{d1} will be taken as the pre-event demand displacement, which is 1.68 inches.

Post-Event Target Displacement, d'_{d2}

Considering the post-event pushover curve, the effective stiffness K_e , with $V_y = 5600$ and $D_y = 0.32$ is 17,500. The initial and effective periods are 0.25 seconds and 0.31 seconds.

The damping coefficient β for the post-event structure is calculated to be 0.06 based on Equation 5-3 of FEMA 306, due to the change in the post-event effective stiffness. The damping adjustments for the response spectrum (B_y and B_1), interpolating from Table 2-15 in FEMA 273, are 1.06 and 1.04 respectively. This changes the spectral acceleration for the post-event structure to 0.97.

The value for C_1 becomes 1.55, and the other coefficients are the same as for the pre-event condition. Using these values, the new target displacement is calculated as:

$$d_t = 1.71 \text{ inches}$$

This value is assigned as d'_{d2} .

The displacement demand from the damaging earthquake d_e was estimated to be 0.6 inches. Since d'_{d1} is greater than d_e , the displacement demand for the post-event structure d'_d is equal to d'_{d1} , which is 1.68 inches.

The target displacement d_d for the pre-event structure for life safety performance against the 475-year-return-period earthquake, based on the coefficient method calculations, is 1.68 inches. The displacement demand for immediate occupancy after the 100-year earthquake is 0.97 inches.

Displacement demand, Section 4.4.4 of FEMA 306

Calculations (see sidebar on previous page) indicate that displacement demand for the post-event structure is essentially the same as for the pre-event structure.

7.4.5.2 Effects of Damage on Performance

The changes in displacement capacity and displacement demand caused by the effects of damage are summarized in Table 7-7. The Performance Indices, P and P' , in Table 7-7 are the ratios of the displacement capacity, d_c or d_c' , to displacement demand, d_d or d_d' , as defined in FEMA 308. The displacement capacities calculated in Section 7.4.3 are based on the assumption that the coupling beams are primary components. FEMA 273 allows coupling beams to be treated as secondary members. Since the global capacity is controlled by the acceptability of the coupling beams, the displacement capacities are determined again assuming that the coupling beams are secondary components and the results are included in Table 7-7. The global displacement capacity, although higher for Life Safety, is still controlled by the coupling beams. The relative change in Performance Index is similar in both cases, indicating that the effects of damage are the same.

The Performance Indices for both the pre-event and post-event structures are less than one for both performance objectives, indicating that the objectives are not met. The effects of damage can be quantified by identifying restoration measures to return the Performance Index to its pre-event value, as outlined in the following sections. The actual course of action to accept, restore, or upgrade the damaged building is a separate consideration for the owner and the local building authority.

7.4.6 Analysis of Restored Structure

7.4.6.1 Proposed Performance Restoration Measures

The primary difference between the pushover models of the pre-event building and the post-event building is the performance of the coupling beams. In their post-earthquake condition, the coupling beams were considered to have less stiffness and strength than in their pre-event condition. The displacement limits were also reduced by the λ_D factor of 0.7. This resulted in the overall reduced stiffness, strength, and displacement capacity of the structure.

To restore the overall performance of the building, various schemes could be investigated, for example, the addition of new concrete walls without repairing damaged components. In this case however, the most straightforward repair appears to be the same component-by-component restoration considered in the direct method. This principally involves the repair of the damaged coupling beams. The coupling beams would be repaired as suggested by the Component Guides in FEMA 306 for the RC3H components. The moderately

Table 7-7 Performance Indices for Pre-event and Post-event Structures

	Displacement Capacity (inches)		Displacement Demand (Inches)		Performance Index (Capacity/Demand)	
	Life Safety	Immediate Occupancy	Life Safety	Immediate Occupancy	Life Safety	Immediate Occupancy
Coupling beams treated as primary components						
Pre-event	$d_c = 0.88$	$d_c = 0.65$	$d_d = 1.68$	$d_d = 0.97$	$P = 0.52$	$P = 0.67$
Post-event	$d_c' = 0.66$	$d_c' = 0.47$	$d_d' = 1.68$	$d_d' = 0.97$	$P' = 0.39$	$P' = 0.48$
Coupling beams treated as secondary components						
Pre-event	$d_c = 1.00$	$d_c = 0.65$	$d_d = 1.68$	$d_d = 0.97$	$P = 0.60$	$P = 0.67$
Post-event	$d_c' = 0.76$	$d_c' = 0.47$	$d_d' = 1.68$	$d_d' = 0.97$	$P' = 0.45$	$P' = 0.48$

damaged coupling beams are repaired by injecting the cracks with epoxy. The heavily damaged coupling beams are repaired by removing the damaged coupling beams and replacing them with new coupling beams. Each new coupling beam will be designed using the provisions of the current building code, which requires diagonal reinforcing bars be installed as the primary shear resistance. A detail of the potential repair is shown in Figure 7-8.

7.4.6.2 Analysis Results

The moderately damaged coupling beams are “repaired” in the model by revising their stiffness and strength based on the Component Damage Classification Guides. The heavily damaged coupling beams that were replaced are given stiffness values for initial, undamaged elements and displacement capacities as in FEMA 273 for flexure-governed beams with diagonal reinforcement, as shown in Figure 7-12(c). The stiffness of the moderately damaged coupling beams is restored to 80 percent of the pre-event stiffness. The strength and displacement limits are restored to the pre-event values. The strength and stiffness of the other components in

the model are unchanged from their post-event condition. The pushover analysis is then conducted using the same procedures and load patterns.

The progression of displacement events for the repaired structure is similar to that for the pre-event structure except that the replaced coupling beam does not reach its collapse prevention displacement limit. Figure 7-15 shows the pushover curve for the repaired structure. Also shown on this curve is the pre-event pushover curve. The overall behavior of the repaired structure closely matches that of the pre-earthquake structure, as it was designed to do. The ratio of displacement capacity to demand, d_c^* / d_d^* , is 0.53 for the life safety performance level and 0.66 for immediate occupancy, which are the same as those for the pre-event performance.

The displacement capacity for the repaired structure is governed by the component deformation limits of the coupling beams that were not replaced. Note that an effective upgrade measure might be to replace all coupling beams, as this would greatly increase global displacement capacity.

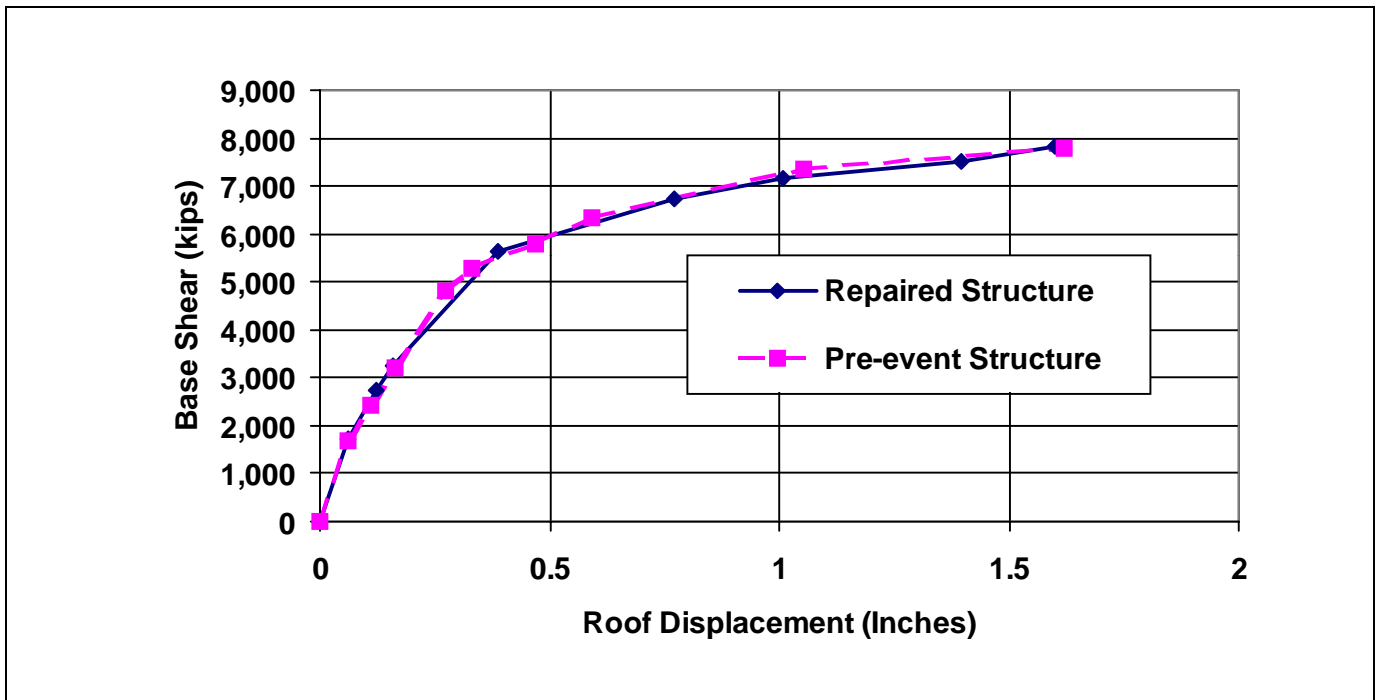


Figure 7-15 Comparison of Pre-event and Repaired Pushover Curves

7.4.7 Performance Restoration Measures

7.4.7.1 Structural Restoration Measures

Based on the relative performance analysis, replacing the three heavily damaged coupling beams and injecting the cracks in the moderately damaged coupling beams restores the performance of the structure. The volume of reinforced concrete coupling beams to be removed is estimated to be about 41 cubic feet per coupling beam. The length of shear cracks to be injected in the moderately damaged coupling beams is estimated to be 100 feet.

Hypothetical repairs for relative performance method, Section 4.5 of FEMA 306

7.4.7.2 Nonstructural Restoration Measures

The Component Guides for the type RC1B components indicate that if cracks are less than 1/8 inch, the damage can be classified as Insignificant, and therefore structural repairs are not necessary. Two of the wall components had cracks that exceeded 1/16 inch. These wall components will have all of the cracks exceeding 1/16 inch repaired by injection with epoxy. The total length of these cracks is estimated to be about 22 feet.

The wall components with visible cracks will be repaired by patching the cracks with plaster and painting the entire wall. This repair is only intended to restore the visual appearance of the wall. Restoration of other nonstructural characteristics, such as water tightness and fire protection, is not necessary.

7.4.7.3 Summary of Restoration Measures and Costs

Table 7-8 summarizes the repairs and estimated costs. Additional costs related to inspection, evaluation, management, and indirect costs may also be involved.

7.5 Discussion of Results

7.5.1 Discussion of Building Performance

The example building contains some typical features found in older concrete wall buildings, such as lightly reinforced concrete elements and discontinuous wall elements. Although the building was designed adequately according to the building code at the time, the design would not be appropriate by current building codes. Because of the improvement in seismic design provisions over the years, it is expected that the building, in its pre-event condition, would not meet the life safety performance level of FEMA 273.

The weak link in the building, as determined by analysis and confirmed with the field observations, is the shear capacity of the coupling beams. Although the analysis indicates that foundation rocking of the solid walls is probably the initial nonlinearity in the building, the rocking of the walls is not detrimental to the global behavior under the anticipated seismic demands.

In the section of the building in which the coupling beams were damaged, the coupled shear walls are discontinuous and are supported by columns at the ends of the walls. Normally, columns supporting discontinuous walls are susceptible to high compressive stresses, and consequently reduced ductility capacity, as the wall overturns. During the pushover analysis, the forces in the columns supporting the coupled walls remained within their capacity. The reason the columns were not overstressed is that the coupling beams acted as fuses for the coupled wall element. The overturning force in the columns could not be greater than the shear capacity of the coupling beams. If the strength of the replaced coupling beams is too large, the overturning force generated could cause failure of the columns below the

Table 7-8 Restoration Cost Estimate by the Relative Performance Method

Item	Unit Cost (1997 Dollars)	Quantity	Cost (1997 Dollars)
Epoxy Injection	\$25.00 /lin ft	122 ft	\$3,050.
Coupling Beam Removal and Replacement	\$74.00 / cu ft	122 ft ³	\$9,028.
Patch and paint walls	\$0.60 /sq ft	10,175 ft ²	\$6,105.
Replace ceiling tiles	\$2.00 /sq ft	15,000 ft ²	\$ 30,000.
General Conditions, Fees, Overhead & Profit (@ 30%)			\$ 14,455.
Total			\$ 62,638.

wall, resulting in a partial collapse of the building. For this reason, the capacity of the repaired coupling beam was designed to be similar to that of the previous coupling beam.

One of the advantages of the relative performance analysis is the ability to assess the behavior of structure and the influence of the behavior of the individual components on the overall behavior. Strengthening a single component may not produce a significant improvement in the overall performance if the progression of failure shifts to a less desirable mode. The pushover analysis of the repaired structure needs to consider the change in overall behavior caused by the repairs.

Because of the improved performance of the first story coupling beams that were replaced, these beams no longer control the global displacement limit of the structure. The force/displacement capacity of the second story coupling beams in their repaired condition is the same as in the pre-event condition. The displacement demand at which the second story coupling beams reach their acceptability limit is very close to the limit at which the first story coupling beams in the pre-event condition reached their limit. Therefore, the overall performance of the building is not improved substantially. The information gained from these analyses can be used to assess whether an upgrade of the building to improve its performance may be cost effective.

7.5.2 Discussion of Methodology and Repair Costs

This example has illustrated some of the important aspects in the FEMA 306 approach to assessing the earthquake damage to concrete and masonry wall buildings. The example building represents an actual building that experienced a damaging earthquake.

FEMA 306 presents two methods for calculating the loss associated with earthquake damage, the direct method and the relative performance method. These methods are used to determine the loss, which is measured as the cost associated with returning the building to its pre-event performance. In this example, the cost of restoring the performance using the two methods produce the same result, principally because the repairs chosen in the relative performance method match those suggested by the direct method. In other buildings, there can be differences between the results obtained by the two methods.

The Nonlinear Static Procedure described in FEMA 273 is used in the relative performance method to assess the performance of the building in the pre-event, post-event and repaired conditions. This analysis method is relatively new and is still subject to further refinements. This procedure can be time-consuming to implement properly. As the method and the analytical tools become further developed, this method should be easier to implement.

7.6 References

- ACI Committee 201, 1994, "Guide for Making a Condition Survey of Concrete in Service," *Manual of Concrete Practice*, American Concrete Institute, Detroit, Michigan.
- CSI, 1997, *SAP2000: Integrated Structural Design & Analysis Software*, Computers and Structures Inc, Berkeley, California
- ATC, 1996, *The Seismic Evaluation and Retrofit of Concrete Buildings*, Applied Technology Council, ATC-40 Report, Redwood City, California.

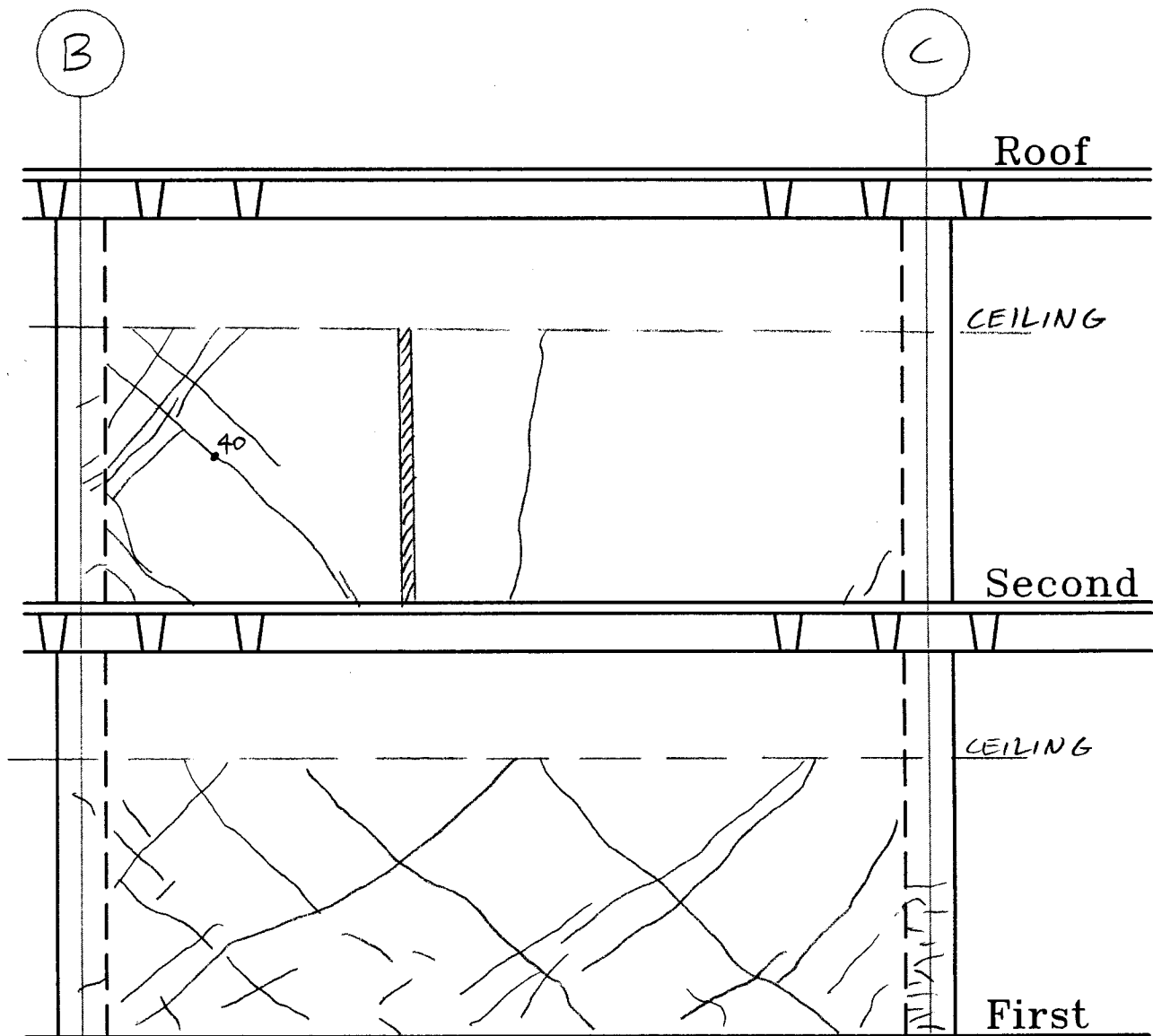
Appendix A. Component Damage Records for Building Evaluated in Example Application

Component Damage Records for Building Evaluated in Example Application

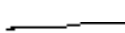


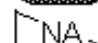
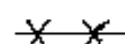
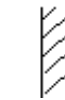
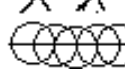
Component Damage Record D1

Building Name: Concrete Shear Wall Building	Project ID: ATC 43 Example	Prepared by: ATC
Location Within Building: Floor: 1 st /2 nd Column Line: 2 Component Type:		Date: 24-Sep-97

Sketch and Description of Damage:



Legend:

- | | | | |
|---|-------------------------------------|---|----------------|
|  | Crack |  | Spall |
|  | Crack Width in Mils (0.001 Inch) |  | Not Accessible |
|  | Crack Previously Filled with Epoxy |  | Partition |
|  | Crack at Pre-existing Surface Patch | | |

Component Damage Records for Building Evaluated in Example Application

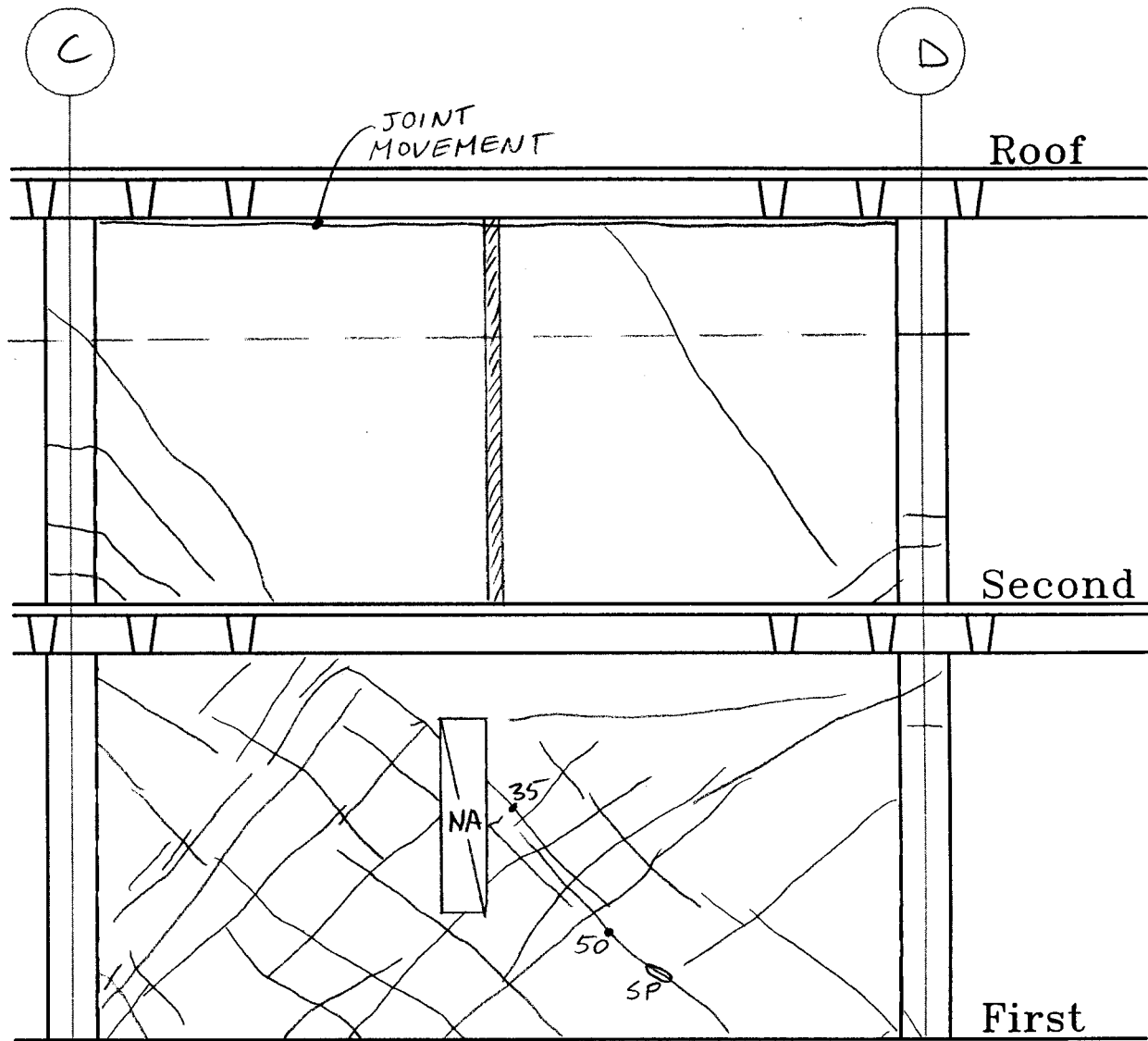
Component Damage Record D2			
Building Name: Concrete Shear Wall Building	Project ID: ATC 43 Example	Prepared by: ATC	
Location Within Building: Floor: 1 st /2 nd Column Line: 2 Component Type:		Date: 24-Sep-97	
Sketch and Description of Damage:			
Legend:			
	Crack		Spall
	Crack Width in Mils (0.001 Inch)		Not Accessible
	Crack Previously Filled with Epoxy		Partition
	Crack at Pre-existing Surface Patch		

Component Damage Records for Building Evaluated in Example Application

Component Damage Record D3

Building Name: Concrete Shear Wall Building		Project ID: ATC 43 Example	Prepared by: ATC
Location Within Building: Floor: 1 st /2 nd Column Line: 7 Component Type:			Date: 24-Sep-97

Sketch and Description of Damage:



Legend:

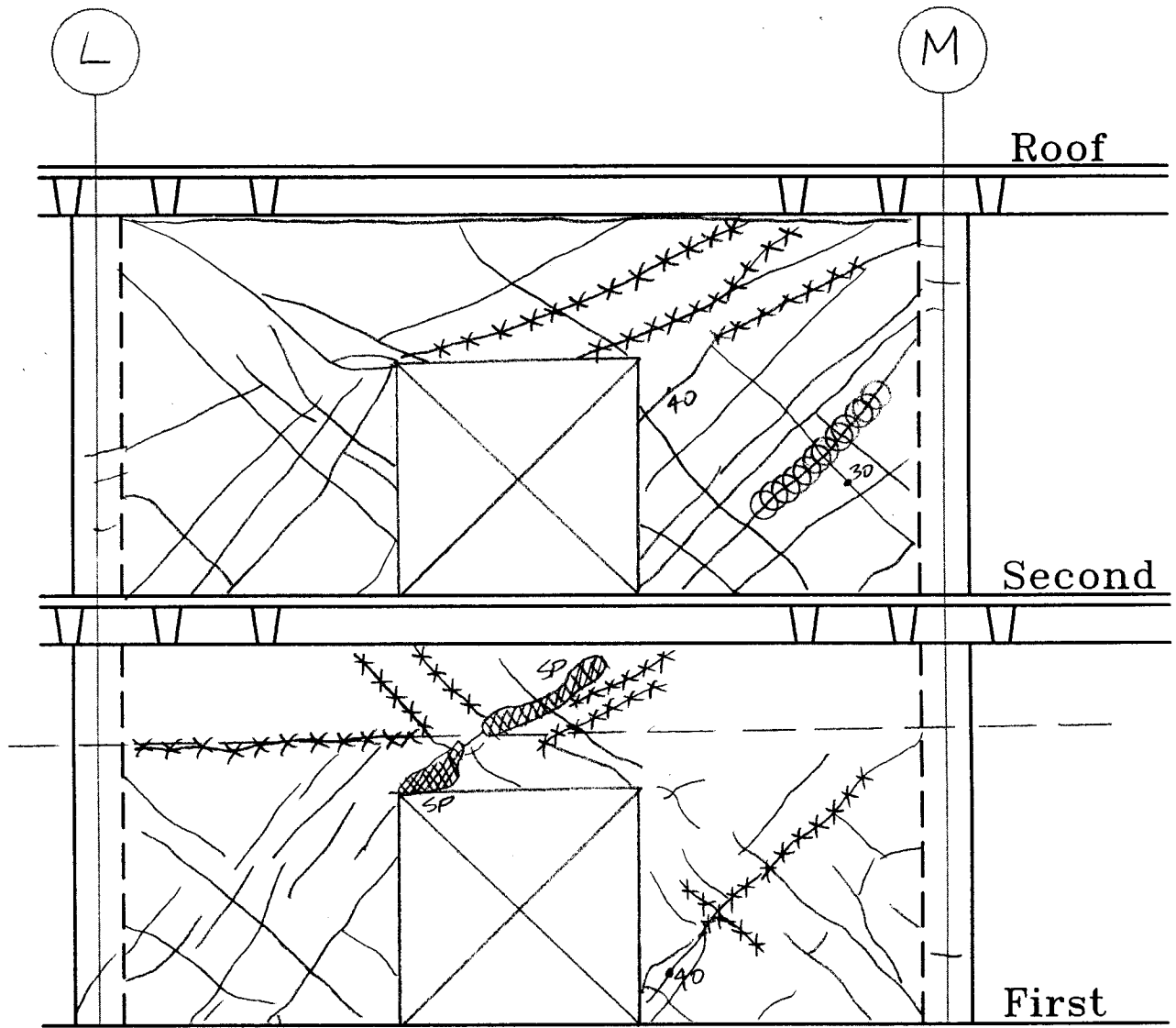
	Crack		Spall
	Crack Width in Mils (0.001 Inch)		Not Accessible
	Crack Previously Filled with Epoxy		Partition
	Crack at Pre-existing Surface Patch		

Component Damage Records for Building Evaluated in Example Application

Component Damage Record D4

Building Name: Concrete Shear Wall Building	Project ID: ATC 43 Example	Prepared by: ATC
Location Within Building: Floor: 1 st /2 nd Column Line: 7 Component Type:		Date: 24-Sep-97

Sketch and Description of Damage:



Legend:

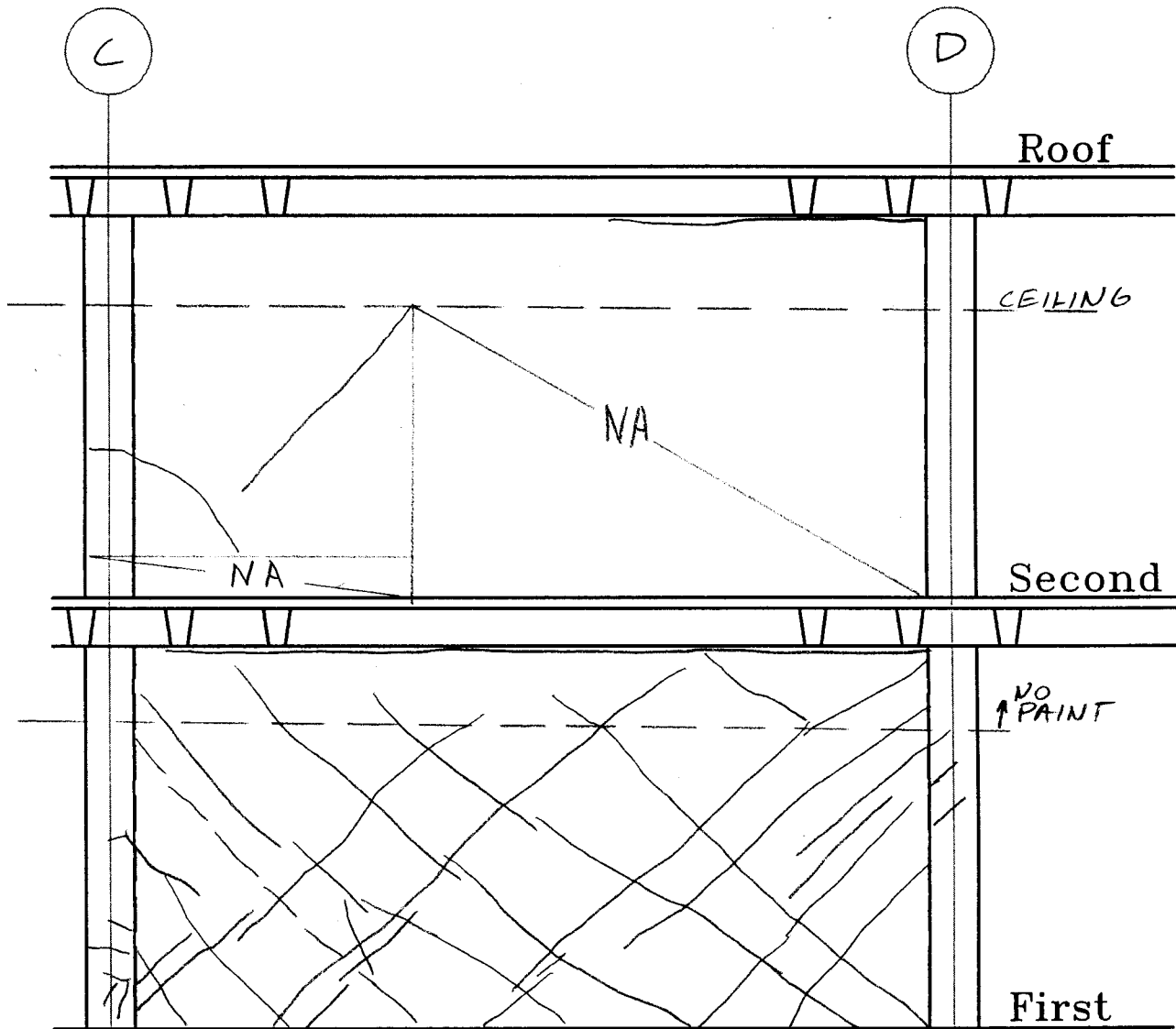
	Crack		Spall
	Crack Width in Mils (0.001 Inch)		Not Accessible
	Crack Previously Filled with Epoxy		Partition
	Crack at Pre-existing Surface Patch		

Component Damage Records for Building Evaluated in Example Application

Component Damage Record D5

Building Name: Concrete Shear Wall Building		Project ID: ATC 43 Example	Prepared by: ATC
Location Within Building: Floor: 1 st /2 nd Column Line: 10 Component Type:		Date: 24-Sep-97	

Sketch and Description of Damage:



Legend:

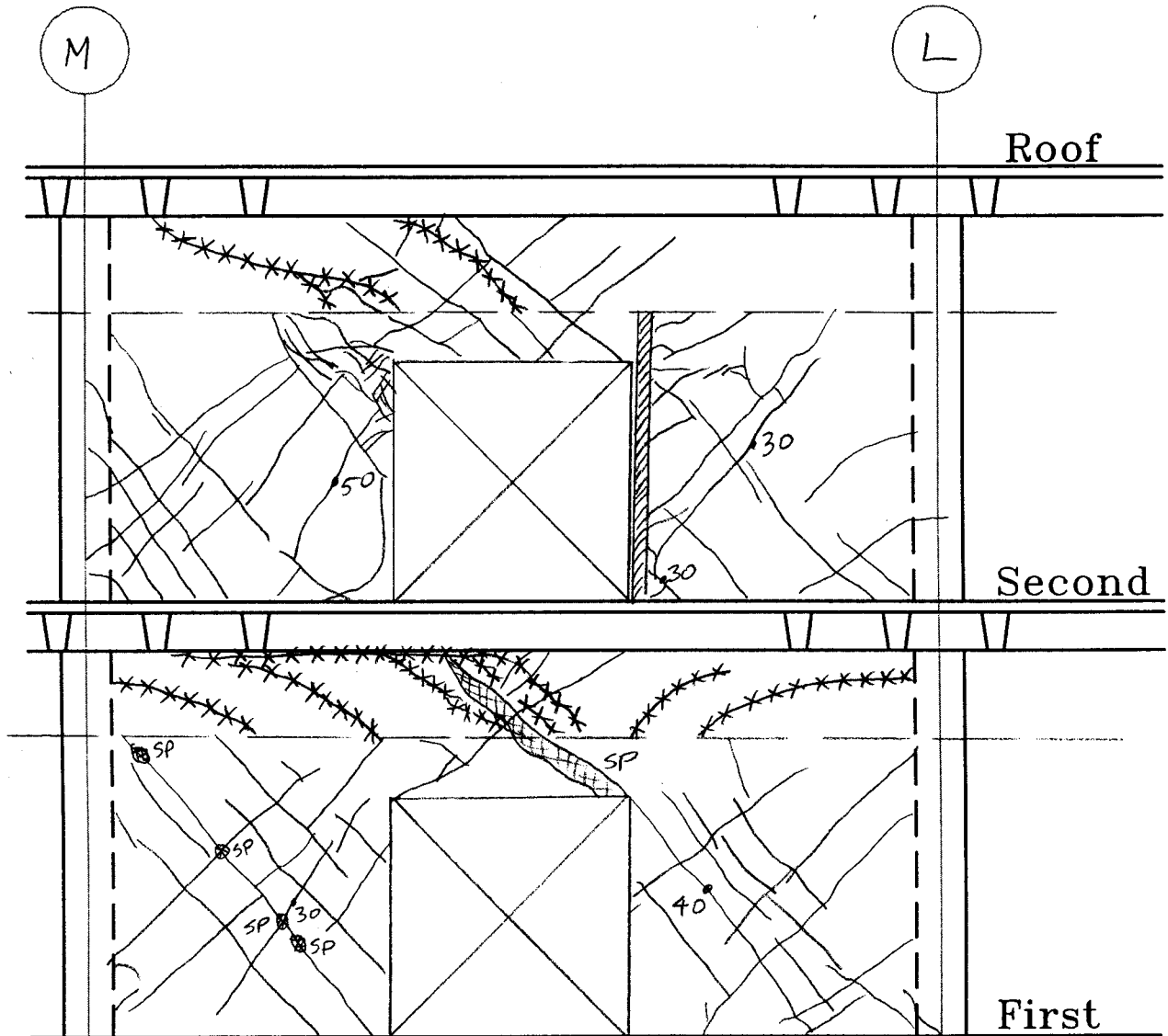
- | | | | |
|--|-------------------------------------|--|----------------|
| | Crack | | Spall |
| | Crack Width in Mills (0.001 Inch) | | Not Accessible |
| | Crack Previously Filled with Epoxy | | Partition |
| | Crack at Pre-existing Surface Patch | | |

Component Damage Records for Building Evaluated in Example Application

Component Damage Record D6

Building Name: Concrete Shear Wall Building	Project ID: ATC 43 Example	Prepared by: ATC
Location Within Building: Floor: 1 st /2 nd Column Line: 10 Component Type:		Date: 24-Sep-97

Sketch and Description of Damage:



Legend:

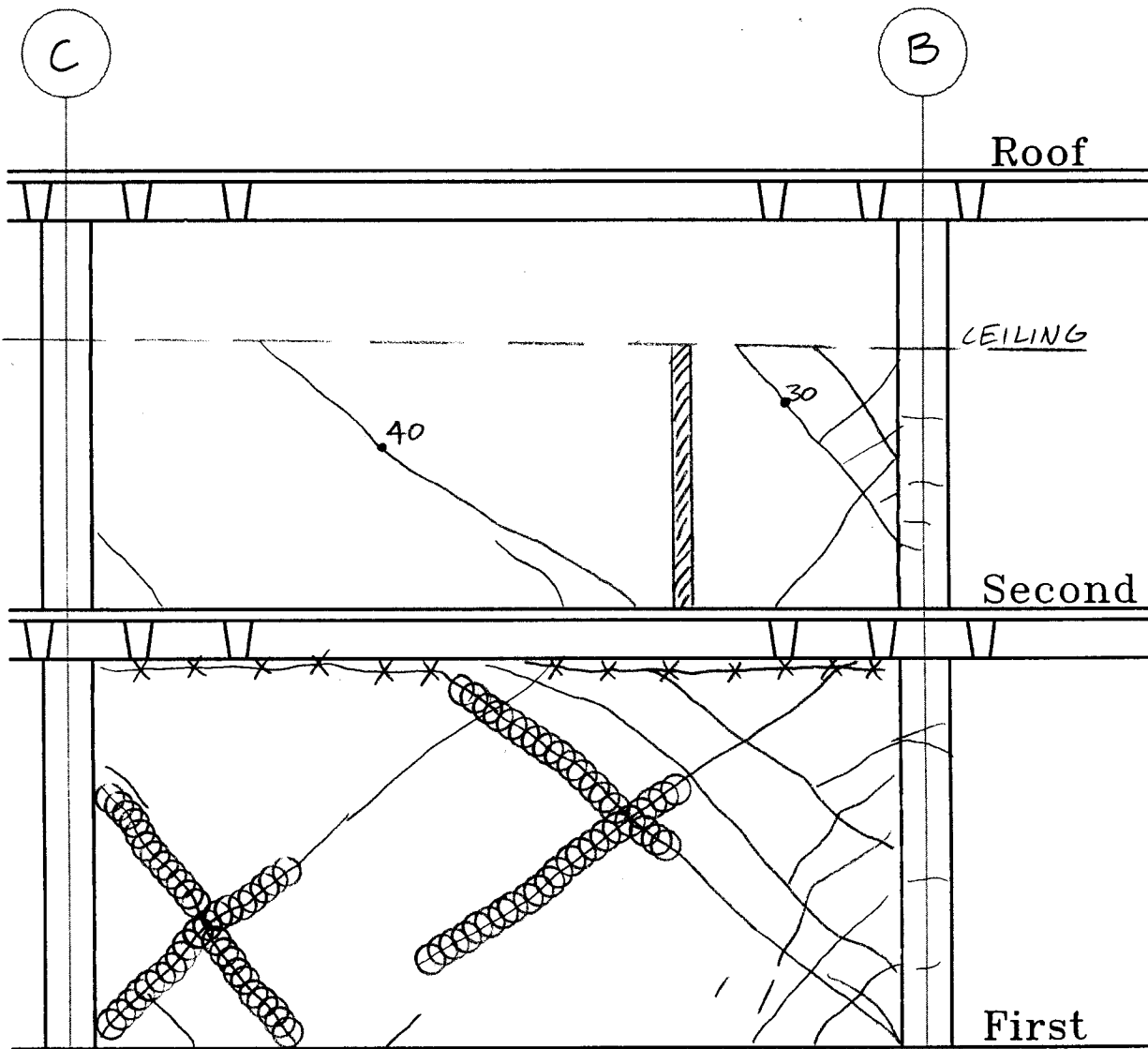
	Crack		Spall
	Crack Width in Mils (0.001 Inch)		Not Accessible
	Crack Previously Filled with Epoxy		Partition
	Crack at Pre-existing Surface Patch		

Component Damage Records for Building Evaluated in Example Application

Component Damage Record D7

Building Name: Concrete Shear Wall Building	Project ID: ATC 43 Example	Prepared by: ATC
Location Within Building: Floor: 1 st /2 nd Column Line: 15 Component Type:		Date: 24-Sep-97

Sketch and Description of Damage:



Legend:

	Crack		Spall
	Crack Width in Mils (0.001 Inch)		Not Accessible
	Crack Previously Filled with Epoxy		Partition
	Crack at Pre-existing Surface Patch		

Component Damage Records for Building Evaluated in Example Application

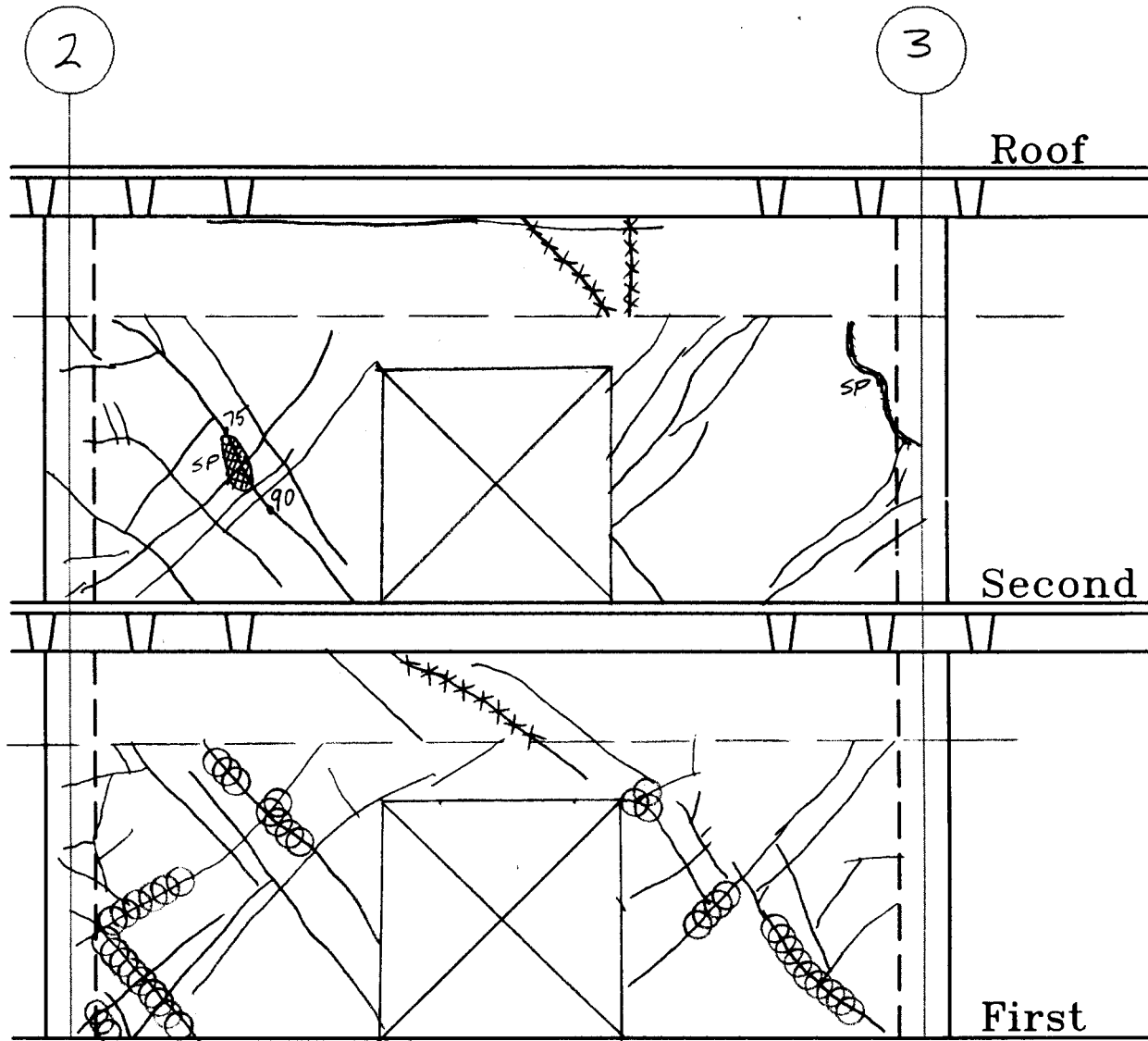
Component Damage Record D8			
Building Name: Concrete Shear Wall Building	Project ID: ATC 43 Example	Prepared by: ATC	
Location Within Building: Floor: 1 st /2 nd Column Line: 15 Component Type:		Date: 24-Sep-97	
Sketch and Description of Damage:			
Legend:			
	Crack		Spall
	Crack Width in Mils (0.001 Inch)		Not Accessible
	Crack Previously Filled with Epoxy		Partition
	Crack at Pre-existing Surface Patch		

Component Damage Records for Building Evaluated in Example Application

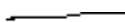


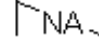



Component Damage Record D9

Building Name: Concrete Shear Wall Building		Project ID: ATC 43 Example	Prepared by: ATC
Location Within Building: Floor: 1 st /2 nd Column Line: B Component Type:		Date: 24-Sep-97	

Sketch and Description of Damage:



Legend:

	Crack		Spall
	Crack Width in Mills (0.001 Inch)		Not Accessible
	Crack Previously Filled with Epoxy		Partition
	Crack at Pre-existing Surface Patch		

Component Damage Records for Building Evaluated in Example Application

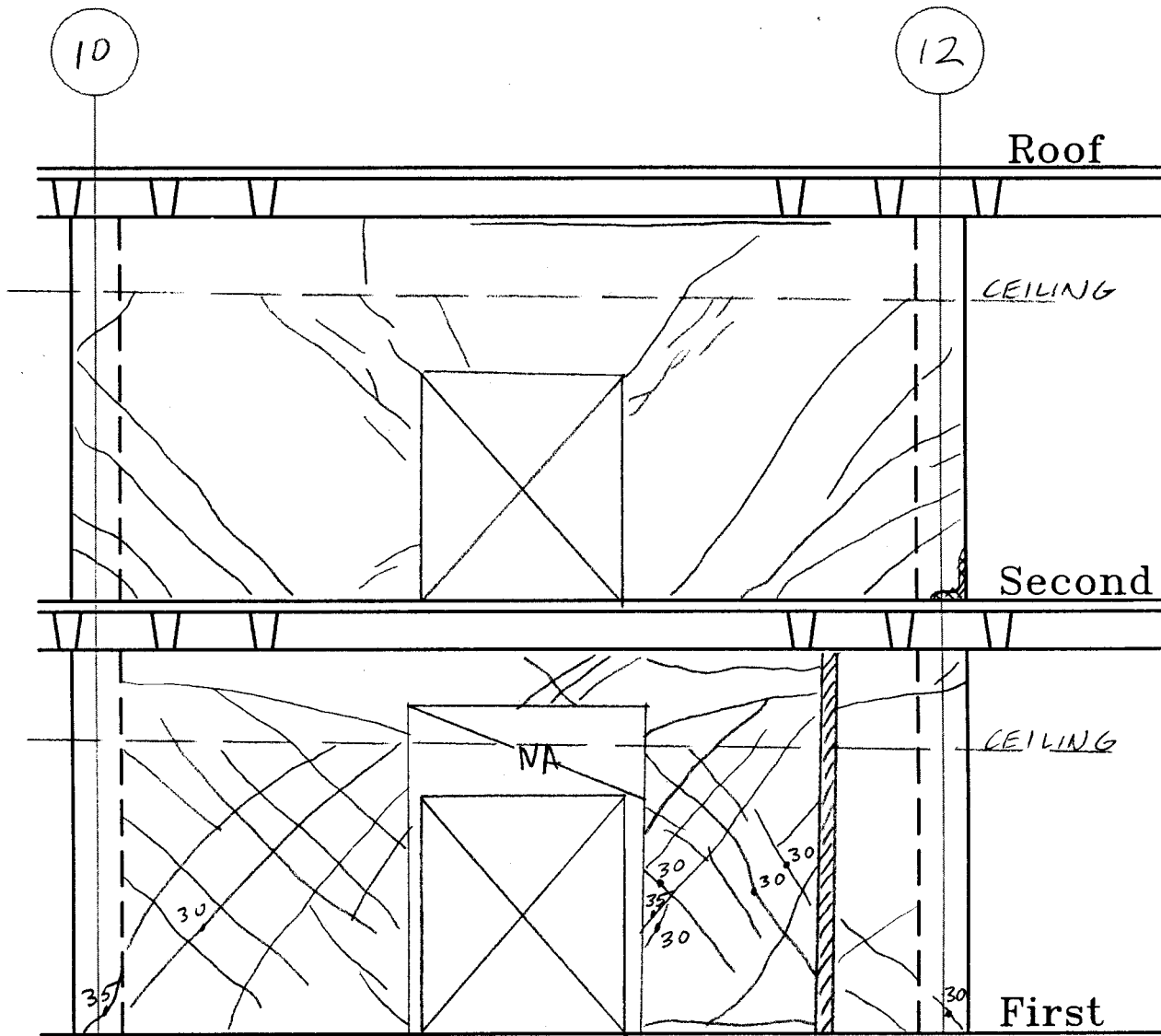
Component Damage Record D10		
Building Name: Concrete Shear Wall Building	Project ID: ATC 43 Example	Prepared by: ATC
Location Within Building: Floor: 1 st /2 nd Column Line: B Component Type:		Date: 24-Sep-97
Sketch and Description of Damage:		
Legend:		
	Crack Crack Width in Mils (0.001 Inch)	
	Crack Previously Filled with Epoxy	
	Crack at Pre-existing Surface Patch	
		Not Accessible
		Partition

Component Damage Records for Building Evaluated in Example Application

Component Damage Record D11

Building Name: Concrete Shear Wall Building	Project ID: ATC 43 Example	Prepared by: ATC
Location Within Building:		Date: 24-Sep-97
Floor: 1 st /2 nd	Column Line: B	Component Type:

Sketch and Description of Damage:



Legend:

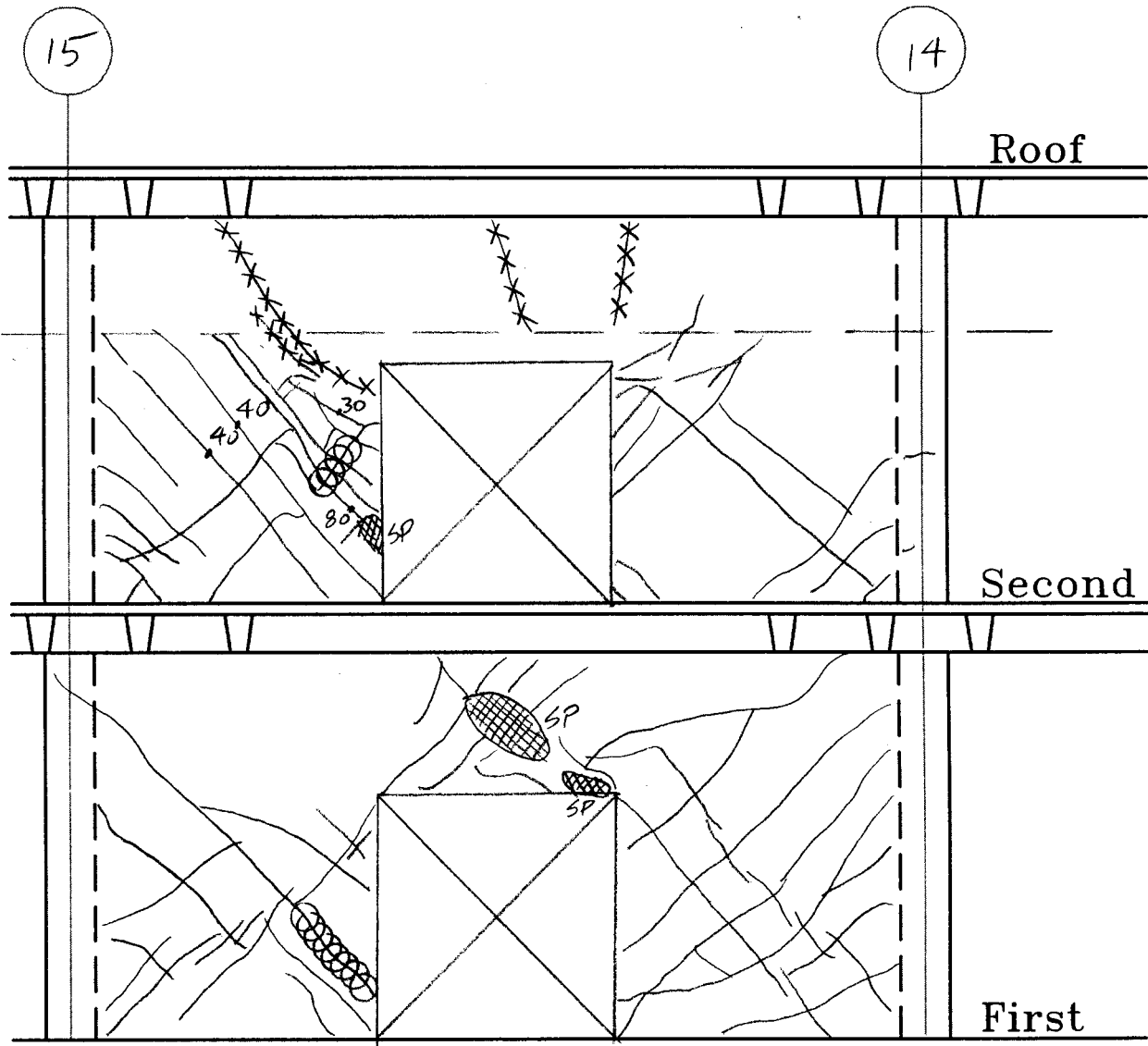
- | | | | |
|--|-------------------------------------|--|----------------|
| | Crack | | Spall |
| | Crack Width in Mils (0.001 Inch) | | Not Accessible |
| | Crack Previously Filled with Epoxy | | Partition |
| | Crack at Pre-existing Surface Patch | | |

Component Damage Records for Building Evaluated in Example Application

Component Damage Record D12

Building Name: Concrete Shear Wall Building	Project ID: ATC 43 Example	Prepared by: ATC
Location Within Building: Floor: 1 st /2 nd Column Line: B Component Type:		Date: 24-Sep-97

Sketch and Description of Damage:



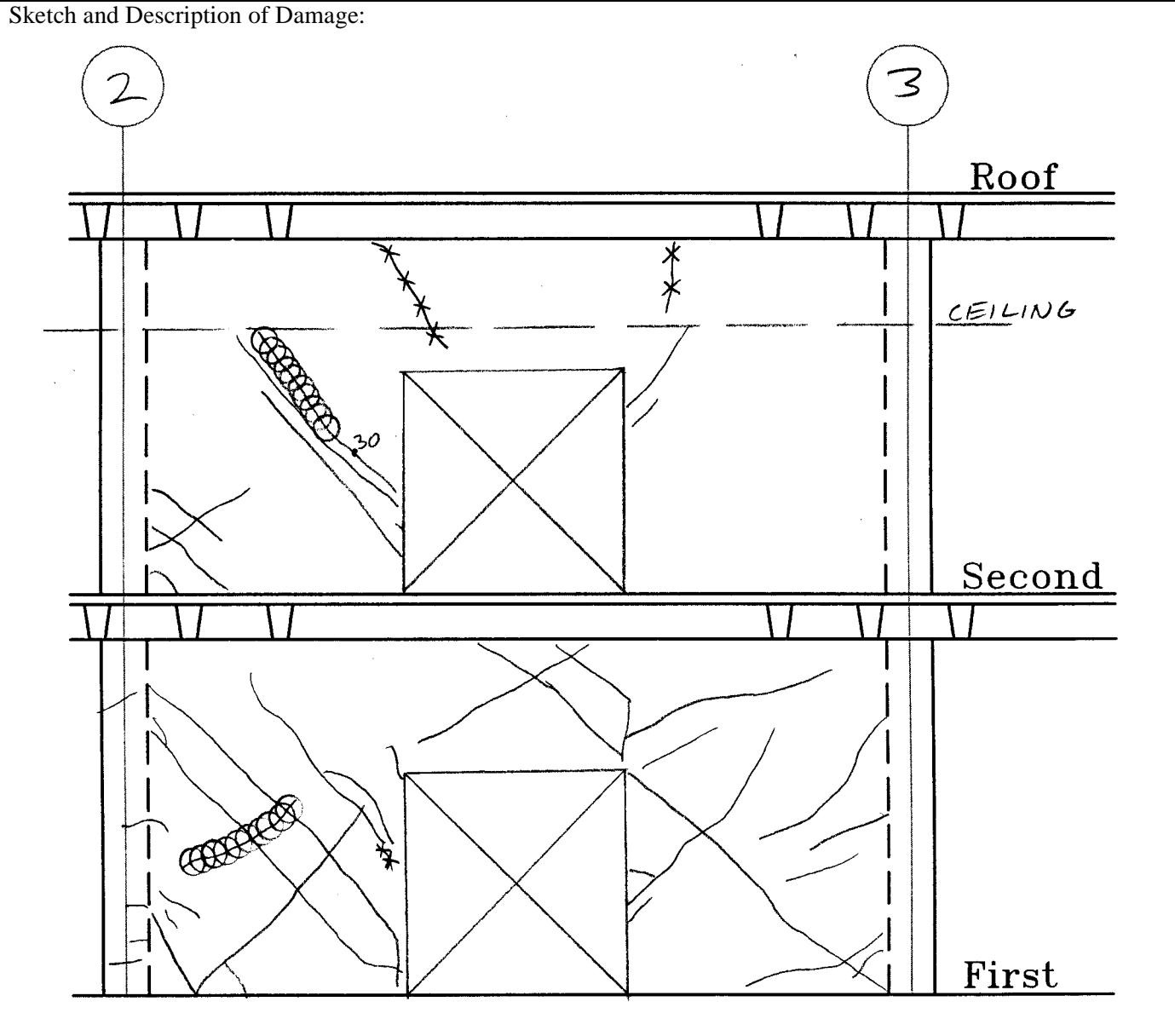
Legend:

	Crack		Spall
	Crack Width in Mils (0.001 Inch)		Not Accessible
	Crack Previously Filled with Epoxy		Partition
	Crack at Pre-existing Surface Patch		

Component Damage Records for Building Evaluated in Example Application

Component Damage Record D13

Building Name: Concrete Shear Wall Building	Project ID: ATC 43 Example	Prepared by: ATC
Location Within Building: Floor: 1 st /2 nd Column Line: E Component Type:		Date: 24-Sep-97



Legend:

	Crack		Spall
	Crack Width in Mils (0.001 Inch)		Not Accessible
	Crack Previously Filled with Epoxy		Partition
	Crack at Pre-existing Surface Patch		

Component Damage Records for Building Evaluated in Example Application

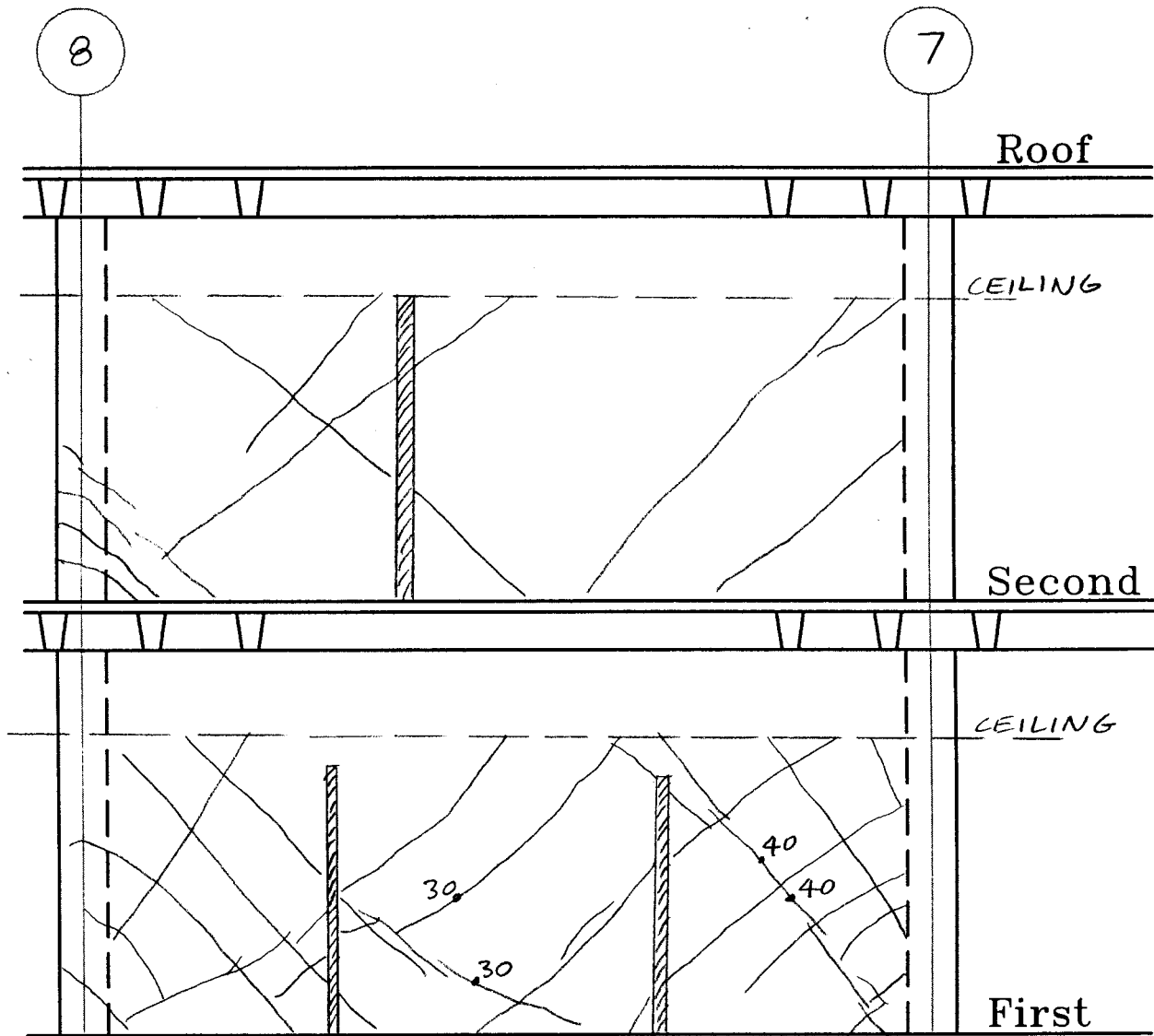
Component Damage Record D14		
Building Name: Concrete Shear Wall Building	Project ID: ATC 43 Example	Prepared by: ATC
Location Within Building: Floor: 1 st /2 nd Column Line: E Component Type:		Date: 24-Sep-97
Sketch and Description of Damage:		
Legend:		
Crack Crack Width in Mils (0.001 Inch) Crack Previously Filled with Epoxy Crack at Pre-existing Surface Patch	Spall Not Accessible Partition	

Component Damage Records for Building Evaluated in Example Application

Component Damage Record D15

Building Name: Concrete Shear Wall Building	Project ID: ATC 43 Example	Prepared by: ATC
Location Within Building: Floor: 1 st /2 nd Column Line: G Component Type:		Date: 24-Sep-97

Sketch and Description of Damage:



Legend:

- | | | | |
|--|-------------------------------------|--|----------------|
| | Crack | | Spall |
| | Crack Width in Mils (0.001 Inch) | | Not Accessible |
| | Crack Previously Filled with Epoxy | | Partition |
| | Crack at Pre-existing Surface Patch | | |

Component Damage Records for Building Evaluated in Example Application

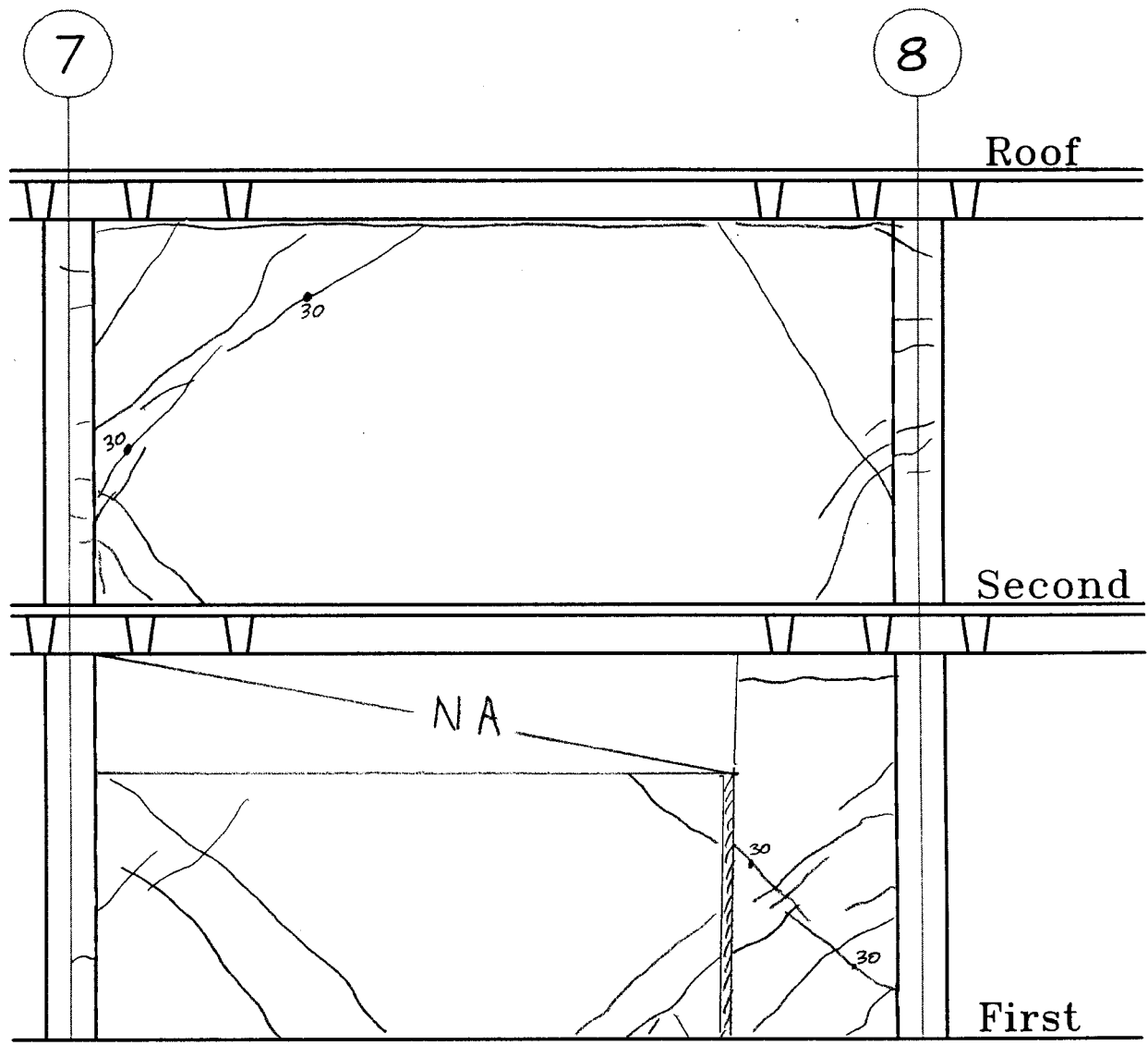
Component Damage Record D16			
Building Name: Concrete Shear Wall Building	Project ID: ATC 43 Example	Prepared by: ATC	
Location Within Building: Floor: 1 st /2 nd Column Line: G Component Type:		Date: 24-Sep-97	
Sketch and Description of Damage:			
Legend:			
	Crack		Spall
	Crack Width in Mils (0.001 Inch)		Not Accessible
	Crack Previously Filled with Epoxy		Partition
	Crack at Pre-existing Surface Patch		

Component Damage Records for Building Evaluated in Example Application

Component Damage Record D17

Building Name: Concrete Shear Wall Building	Project ID: ATC 43 Example	Prepared by: ATC
Location Within Building: Floor: 1 st /2 nd Column Line: M Component Type:		Date: 24-Sep-97

Sketch and Description of Damage:



Legend:

	Crack		Spall
	Crack Width in Mils (0.001 Inch)		Not Accessible
	Crack Previously Filled with Epoxy		Partition
	Crack at Pre-existing Surface Patch		

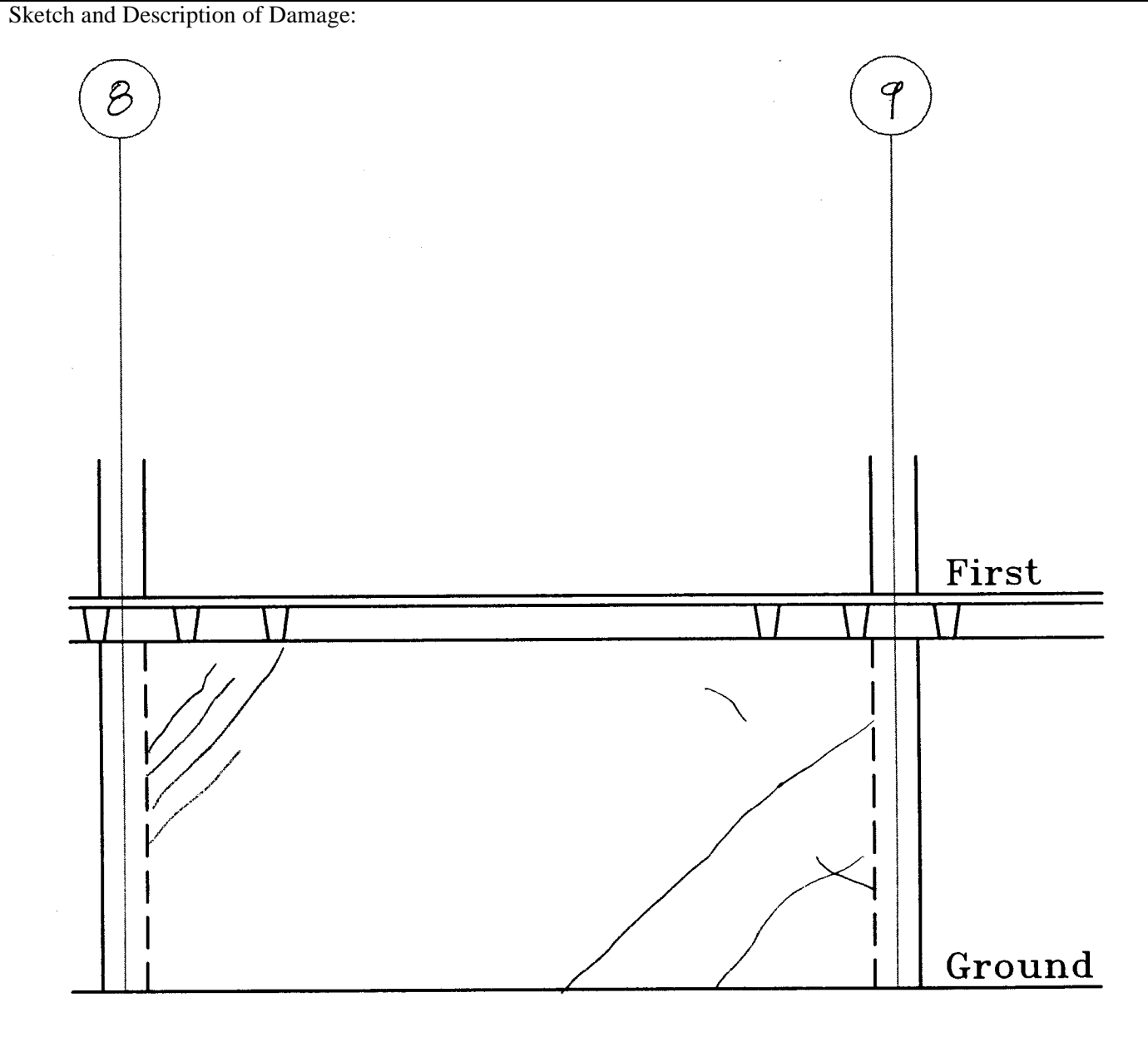
Component Damage Records for Building Evaluated in Example Application

Component Damage Record D18			
Building Name: Concrete Shear Wall Building	Project ID: ATC 43 Example	Prepared by: ATC	
Location Within Building: Floor: 1 st /2 nd Column Line: M Component Type:		Date: 24-Sep-97	
Sketch and Description of Damage:			
Legend:			
	Crack		Spall
	Crack Width in Mills (0.001 Inch)		Not Accessible
	Crack Previously Filled with Epoxy		Partition
	Crack at Pre-existing Surface Patch		

Component Damage Records for Building Evaluated in Example Application

Component Damage Record D19

Building Name: Concrete Shear Wall Building	Project ID: ATC 43 Example	Prepared by: ATC
Location Within Building: Floor: 1 st /2 nd Column Line: M Component Type:		Date: 24-Sep-97



Legend:

	Crack		Spall
	Crack Width in Mils (0.001 Inch)		Not Accessible
	Crack Previously Filled with Epoxy		Partition
	Crack at Pre-existing Surface Patch		

ATC-43 Project Participants

ATC MANAGEMENT

Mr. Christopher Rojahn,
Principal Investigator
Applied Technology Council
555 Twin Dolphin Drive, Suite 550
Redwood City, CA 94065

Mr. Craig Comartin,
Co-PI and Project Director
7683 Andrea Avenue
Stockton, CA 95207

Technical Management Committee

Prof. Dan Abrams
University of Illinois
1245 Newmark Civil Eng'g. Lab., MC 250
205 North Mathews Avenue
Urbana, IL 61801-2397

Mr. Andrew T. Merovich
A.T. Merovich & Associates, Inc.
1163 Francisco Blvd., Second Floor
San Rafael, CA 94901

Mr. James Hill
James A. Hill & Associates, Inc.
1349 East 28th Street
Signal Hill, CA 90806

Prof. Jack Moehle
Earthquake Engineering Research Center
University of California at Berkeley
1301 South 46th Street
Richmond, CA 94804

FEMA/PARR Representatives

Mr. Timothy McCormick
PaRR Task Manager
Dewberry & Davis
8401 Arlington Boulevard
Fairfax, VA 22031-4666

Prof. Robert Hanson
FEMA Technical Monitor
74 North Pasadena Avenue, CA-1009-DR
Parsons Bldg., West Annex, Room 308
Pasadena, CA 91103

Mr. Mark Doroudian
PaRR Representative
42 Silkwood
Aliso Viejo, CA 92656

Materials Working Group

Dr. Joe Maffei, Group Leader
Consulting Structural Engineer
148 Hermosa Avenue
Oakland California

Mr. Brian Kehoe, Lead Consultant
Wiss, Janney, Elstner Associates, Inc.
2200 Powell Street, Suite 925
Emeryville, CA 94608

Dr. Greg Kingsley
KL&A of Colorado
805 14th Street
Golden, CO 80401

Mr. Bret Lizundia
Rutherford & Chekene
303 Second Street, Suite 800 North
San Francisco, CA 94107

Prof. John Mander
SUNY at Buffalo
Department of Civil Engineering
212 Ketter Hall
Buffalo, NY 14260

Analysis Working Group

Prof. Mark Aschheim, Group Leader
University of Illinois at Urbana
2118 Newmark CE Lab
205 North Mathews, MC 250
Urbana, IL 61801

Prof. Mete Sozen, Senior Consultant
Purdue University, School of Engineering
1284 Civil Engineering Building
West Lafayette, IN 47907-1284

Project Review Panel

Mr. Gregg J. Borchelt
Brick Institute of America
11490 Commerce Park Drive, #300
Reston, VA 20191

Dr. Gene Corley
Construction Technology Labs
5420 Old Orchard Road
Skokie, IL 60077-1030

Mr. Edwin Huston
Smith & Huston
Plaza 600 Building, 6th & Stewart, #620
Seattle, WA 98101

Prof. Richard E. Klingner
University of Texas
Civil Engineering Department
Cockbell Building, Room 4-2
Austin, TX 78705

Mr. Vilas Mujumdar
Office of Regulation Services
Division of State Architect
General Services
1300 I Street, Suite 800
Sacramento, CA 95814

Dr. Hassan A. Sassi
Governors Office of Emergency Services
74 North Pasadena Avenue
Pasadena, CA 91103

Mr. Carl Schulze
Libby Engineers
4452 Glacier Avenue
San Diego, CA 92120

Mr. Daniel Shapiro
SOH & Associates
550 Kearny Street, Suite 200
San Francisco, CA 94108

ATC-43 Project Participants

Prof. James K. Wight
University of Michigan
Department of Civil Engineering
2368 G G Brown
Ann Arbor, MI 48109-2125

Mr. Eugene Zeller
Long Beach Department of Building & Safety
333 W. Ocean Boulevard, Fourth Floor
Long Beach, CA 90802

Applied Technology Council Projects And Report Information

One of the primary purposes of Applied Technology Council is to develop resource documents that translate and summarize useful information to practicing engineers. This includes the development of guidelines and manuals, as well as the development of research recommendations for specific areas determined by the profession. ATC is not a code development organization, although several of the ATC project reports serve as resource documents for the development of codes, standards and specifications.

Applied Technology Council conducts projects that meet the following criteria:

1. The primary audience or benefactor is the design practitioner in structural engineering.
2. A cross section or consensus of engineering opinion is required to be obtained and presented by a neutral source.
3. The project fosters the advancement of structural engineering practice.

A brief description of several major completed projects and reports is given in the following section. Funding for projects is obtained from government agencies and tax-deductible contributions from the private sector.

ATC-1: This project resulted in five papers that were published as part of *Building Practices for Disaster Mitigation, Building Science Series 46*, proceedings of a workshop sponsored by the National Science Foundation (NSF) and the National Bureau of Standards (NBS). Available through the National Technical Information Service (NTIS), 5285 Port Royal Road, Springfield, VA 22151, as NTIS report No. COM-73-50188.

ATC-2: The report, *An Evaluation of a Response Spectrum Approach to Seismic Design of Buildings*, was funded by NSF and NBS and was conducted as part of the Cooperative Federal Program in Building Practices for Disaster Mitigation. Available through the ATC office. (Published 1974, 270 Pages)

ABSTRACT: This study evaluated the applicability and cost of the response spectrum approach to seis-

mic analysis and design that was proposed by various segments of the engineering profession. Specific building designs, design procedures and parameter values were evaluated for future application. Eleven existing buildings of varying dimensions were redesigned according to the procedures.

ATC-3: The report, *Tentative Provisions for the Development of Seismic Regulations for Buildings (ATC-3-06)*, was funded by NSF and NBS. The second printing of this report, which includes proposed amendments, is available through the ATC office. (Published 1978, amended 1982, 505 pages plus proposed amendments)

ABSTRACT: The tentative provisions in this document represent the results of a concerted effort by a multi-disciplinary team of 85 nationally recognized experts in earthquake engineering. The provisions serve as the basis for the seismic provisions of the 1988 *Uniform Building Code* and the 1988 and subsequent issues of the *NEHRP Recommended Provisions for the Development of Seismic Regulation for New Buildings*. The second printing of this document contains proposed amendments prepared by a joint committee of the Building Seismic Safety Council (BSSC) and the NBS.

ATC-3-2: The project, *Comparative Test Designs of Buildings Using ATC-3-06 Tentative Provisions*, was funded by NSF. The project consisted of a study to develop and plan a program for making comparative test designs of the ATC-3-06 Tentative Provisions. The project report was written to be used by the Building Seismic Safety Council in its refinement of the ATC-3-06 Tentative Provisions.

ATC-3-4: The report, *Redesign of Three Multistory Buildings: A Comparison Using ATC-3-06 and 1982 Uniform Building Code Design Provisions*, was published under a grant from NSF. Available through the ATC office. (Published 1984, 112 pages)

ABSTRACT: This report evaluates the cost and technical impact of using the 1978 ATC-3-06 report, *Tentative Provisions for the Development of Seismic Regulations for Buildings*, as amended by a joint

committee of the Building Seismic Safety Council and the National Bureau of Standards in 1982. The evaluations are based on studies of three existing California buildings redesigned in accordance with the ATC-3-06 Tentative Provisions and the 1982 *Uniform Building Code*. Included in the report are recommendations to code implementing bodies.

ATC-3-5: This project, Assistance for First Phase of ATC-3-06 Trial Design Program Being Conducted by the Building Seismic Safety Council, was funded by the Building Seismic Safety Council to provide the services of the ATC Senior Consultant and other ATC personnel to assist the BSSC in the conduct of the first phase of its Trial Design Program. The first phase provided for trial designs conducted for buildings in Los Angeles, Seattle, Phoenix, and Memphis.

ATC-3-6: This project, Assistance for Second Phase of ATC-3-06 Trial Design Program Being Conducted by the Building Seismic Safety Council, was funded by the Building Seismic Safety Council to provide the services of the ATC Senior Consultant and other ATC personnel to assist the BSSC in the conduct of the second phase of its Trial Design Program. The second phase provided for trial designs conducted for buildings in New York, Chicago, St. Louis, Charleston, and Fort Worth.

ATC-4: The report, *A Methodology for Seismic Design and Construction of Single-Family Dwellings*, was published under a contract with the Department of Housing and Urban Development (HUD). Available through the ATC office. (Published 1976, 576 pages)

ABSTRACT: This report presents the results of an in-depth effort to develop design and construction details for single-family residences that minimize the potential economic loss and life-loss risk associated with earthquakes. The report: (1) discusses the ways structures behave when subjected to seismic forces, (2) sets forth suggested design criteria for conventional layouts of dwellings constructed with conventional materials, (3) presents construction details that do not require the designer to perform analytical calculations, (4) suggests procedures for efficient plan-checking, and (5) presents recommendations including details and schedules for use in the field by construction personnel and building inspectors.

ATC-4-1: The report, *The Home Builders Guide for Earthquake Design*, was published under a contract with HUD. Available through the ATC office. (Published 1980, 57 pages)

ABSTRACT: This report is an abridged version of the ATC-4 report. The concise, easily understood text of the Guide is supplemented with illustrations and 46 construction details. The details are provided to ensure that houses contain structural features that are properly positioned, dimensioned and constructed to resist earthquake forces. A brief description is included on how earthquake forces impact on houses and some precautionary constraints are given with respect to site selection and architectural designs.

ATC-5: The report, *Guidelines for Seismic Design and Construction of Single-Story Masonry Dwellings in Seismic Zone 2*, was developed under a contract with HUD. Available through the ATC office. (Published 1986, 38 pages)

ABSTRACT: The report offers a concise methodology for the earthquake design and construction of single-story masonry dwellings in Seismic Zone 2 of the United States, as defined by the 1973 *Uniform Building Code*. The Guidelines are based in part on shaking table tests of masonry construction conducted at the University of California at Berkeley Earthquake Engineering Research Center. The report is written in simple language and includes basic house plans, wall evaluations, detail drawings, and material specifications.

ATC-6: The report, *Seismic Design Guidelines for Highway Bridges*, was published under a contract with the Federal Highway Administration (FHWA). Available through the ATC office. (Published 1981, 210 pages)

ABSTRACT: The Guidelines are the recommendations of a team of sixteen nationally recognized experts that included consulting engineers, academics, state and federal agency representatives from throughout the United States. The Guidelines embody several new concepts that were significant departures from then existing design provisions. Included in the Guidelines are an extensive commentary, an example demonstrating the use of the

Guidelines, and summary reports on 21 bridges redesigned in accordance with the Guidelines.

The guidelines have been adopted by the American Association of Highway and Transportation Officials as a guide specification.

ATC-6-1: The report, *Proceedings of a Workshop on Earthquake Resistance of Highway Bridges*, was published under a grant from NSF. Available through the ATC office. (Published 1979, 625 pages)

ABSTRACT: The report includes 23 state-of-the-art and state-of-practice papers on earthquake resistance of highway bridges. Seven of the twenty-three papers were authored by participants from Japan, New Zealand and Portugal. The Proceedings also contain recommendations for future research that were developed by the 45 workshop participants.

ATC-6-2: The report, *Seismic Retrofitting Guidelines for Highway Bridges*, was published under a contract with FHWA. Available through the ATC office. (Published 1983, 220 pages)

ABSTRACT: The Guidelines are the recommendations of a team of thirteen nationally recognized experts that included consulting engineers, academics, state highway engineers, and federal agency representatives. The Guidelines, applicable for use in all parts of the United States, include a preliminary screening procedure, methods for evaluating an existing bridge in detail, and potential retrofitting measures for the most common seismic deficiencies. Also included are special design requirements for various retrofitting measures.

ATC-7: The report, *Guidelines for the Design of Horizontal Wood Diaphragms*, was published under a grant from NSF. Available through the ATC office. (Published 1981, 190 pages)

ABSTRACT: Guidelines are presented for designing roof and floor systems so these can function as horizontal diaphragms in a lateral force resisting system. Analytical procedures, connection details and design examples are included in the Guidelines.

ATC-7-1: The report, *Proceedings of a Workshop of Design of Horizontal Wood Diaphragms*, was

published under a grant from NSF. Available through the ATC office. (Published 1980, 302 pages)

ABSTRACT: The report includes seven papers on state-of-the-practice and two papers on recent research. Also included are recommendations for future research that were developed by the 35 workshop participants.

ATC-8: This report, *Proceedings of a Workshop on the Design of Prefabricated Concrete Buildings for Earthquake Loads*, was funded by NSF. Available through the ATC office. (Published 1981, 400 pages)

ABSTRACT: The report includes eighteen state-of-the-art papers and six summary papers. Also included are recommendations for future research that were developed by the 43 workshop participants.

ATC-9: The report, *An Evaluation of the Imperial County Services Building Earthquake Response and Associated Damage*, was published under a grant from NSF. Available through the ATC office. (Published 1984, 231 pages)

ABSTRACT: The report presents the results of an in-depth evaluation of the Imperial County Services Building, a 6-story reinforced concrete frame and shear wall building severely damaged by the October 15, 1979 Imperial Valley, California, earthquake. The report contains a review and evaluation of earthquake damage to the building; a review and evaluation of the seismic design; a comparison of the requirements of various building codes as they relate to the building; and conclusions and recommendations pertaining to future building code provisions and future research needs.

ATC-10: This report, *An Investigation of the Correlation Between Earthquake Ground Motion and Building Performance*, was funded by the U.S. Geological Survey (USGS). Available through the ATC office. (Published 1982, 114 pages)

ABSTRACT: The report contains an in-depth analytical evaluation of the ultimate or limit capacity of selected representative building framing types, a discussion of the factors affecting the seismic performance of buildings, and a sum-

mary and comparison of seismic design and seismic risk parameters currently in widespread use.

ATC-10-1: This report, *Critical Aspects of Earthquake Ground Motion and Building Damage Potential*, was co-funded by the USGS and the NSF. Available through the ATC office. (Published 1984, 259 pages)

ABSTRACT: This document contains 19 state-of-the-art papers on ground motion, structural response, and structural design issues presented by prominent engineers and earth scientists in an ATC seminar. The main theme of the papers is to identify the critical aspects of ground motion and building performance that currently are not being considered in building design. The report also contains conclusions and recommendations of working groups convened after the Seminar.

ATC-11: The report, *Seismic Resistance of Reinforced Concrete Shear Walls and Frame Joints: Implications of Recent Research for Design Engineers*, was published under a grant from NSF. Available through the ATC office. (Published 1983, 184 pages)

ABSTRACT: This document presents the results of an in-depth review and synthesis of research reports pertaining to cyclic loading of reinforced concrete shear walls and cyclic loading of joint reinforced concrete frames. More than 125 research reports published since 1971 are reviewed and evaluated in this report. The preparation of the report included a consensus process involving numerous experienced design professionals from throughout the United States. The report contains reviews of current and past design practices, summaries of research developments, and in-depth discussions of design implications of recent research results.

ATC-12: This report, *Comparison of United States and New Zealand Seismic Design Practices for Highway Bridges*, was published under a grant from NSF. Available through the ATC office. (Published 1982, 270 pages)

ABSTRACT: The report contains summaries of all aspects and innovative design procedures used in New Zealand as well as comparison of United States and New Zealand design practice. Also included are research recommendations developed

at a 3-day workshop in New Zealand attended by 16 U.S. and 35 New Zealand bridge design engineers and researchers.

ATC-12-1: This report, *Proceedings of Second Joint U.S.-New Zealand Workshop on Seismic Resistance of Highway Bridges*, was published under a grant from NSF. Available through the ATC office. (Published 1986, 272 pages)

ABSTRACT: This report contains written versions of the papers presented at this 1985 Workshop as well as a list and prioritization of workshop recommendations. Included are summaries of research projects being conducted in both countries as well as state-of-the-practice papers on various aspects of design practice. Topics discussed include bridge design philosophy and loadings; design of columns, footings, piles, abutments and retaining structures; geotechnical aspects of foundation design; seismic analysis techniques; seismic retrofitting; case studies using base isolation; strong-motion data acquisition and interpretation; and testing of bridge components and bridge systems.

ATC-13: The report, *Earthquake Damage Evaluation Data for California*, was developed under a contract with the Federal Emergency Management Agency (FEMA). Available through the ATC office. (Published 1985, 492 pages)

ABSTRACT: This report presents expert-opinion earthquake damage and loss estimates for industrial, commercial, residential, utility and transportation facilities in California. Included are damage probability matrices for 78 classes of structures and estimates of time required to restore damaged facilities to pre-earthquake usability. The report also describes the inventory information essential for estimating economic losses and the methodology used to develop loss estimates on a regional basis.

ATC-14: The report, *Evaluating the Seismic Resistance of Existing Buildings*, was developed under a grant from the NSF. Available through the ATC office. (Published 1987, 370 pages)

ABSTRACT: This report, written for practicing structural engineers, describes a methodology for performing preliminary and detailed building seis-

mic evaluations. The report contains a state-of-practice review; seismic loading criteria; data collection procedures; a detailed description of the building classification system; preliminary and detailed analysis procedures; and example case studies, including nonstructural considerations.

ATC-15: The report, *Comparison of Seismic Design Practices in the United States and Japan*, was published under a grant from NSF. Available through the ATC office. (Published 1984, 317 pages)

ABSTRACT: The report contains detailed technical papers describing design practices in the United States and Japan as well as recommendations emanating from a joint U.S.-Japan workshop held in Hawaii in March, 1984. Included are detailed descriptions of new seismic design methods for buildings in Japan and case studies of the design of specific buildings (in both countries). The report also contains an overview of the history and objectives of the Japan Structural Consultants Association.

ATC-15-1: The report, *Proceedings of Second U.S.-Japan Workshop on Improvement of Building Seismic Design and Construction Practices*, was published under a grant from NSF. Available through the ATC office. (Published 1987, 412 pages)

ABSTRACT: This report contains 23 technical papers presented at this San Francisco workshop in August, 1986, by practitioners and researchers from the U.S. and Japan. Included are state-of-the-practice papers and case studies of actual building designs and information on regulatory, contractual, and licensing issues.

ATC-15-2: The report, *Proceedings of Third U.S.-Japan Workshop on Improvement of Building Structural Design and Construction Practices*, was published jointly by ATC and the Japan Structural Consultants Association. Available through the ATC office. (Published 1989, 358 pages)

ABSTRACT: This report contains 21 technical papers presented at this Tokyo, Japan, workshop in July, 1988, by practitioners and researchers from the U.S., Japan, China, and New Zealand. Included are state-of-the-practice papers on various topics,

including braced steel frame buildings, beam-column joints in reinforced concrete buildings, summaries of comparative U. S. and Japanese design, and base isolation and passive energy dissipation devices.

ATC-15-3: The report, *Proceedings of Fourth U.S.-Japan Workshop on Improvement of Building Structural Design and Construction Practices*, was published jointly by ATC and the Japan Structural Consultants Association. Available through the ATC office. (Published 1992, 484 pages)

ABSTRACT: This report contains 22 technical papers presented at this Kailua-Kona, Hawaii, workshop in August, 1990, by practitioners and researchers from the United States, Japan, and Peru. Included are papers on postearthquake building damage assessment; acceptable earth-quake damage; repair and retrofit of earthquake damaged buildings; base-isolated buildings, including Architectural Institute of Japan recommendations for design; active damping systems; wind-resistant design; and summaries of working group conclusions and recommendations.

ATC-15-4: The report, *Proceedings of Fifth U.S.-Japan Workshop on Improvement of Building Structural Design and Construction Practices*, was published jointly by ATC and the Japan Structural Consultants Association. Available through the ATC office. (Published 1994, 360 pages)

ABSTRACT: This report contains 20 technical papers presented at this San Diego, California workshop in September, 1992. Included are papers on performance goals/acceptable damage in seismic design; seismic design procedures and case studies; construction influences on design; seismic isolation and passive energy dissipation; design of irregular structures; seismic evaluation, repair and upgrading; quality control for design and construction; and summaries of working group discussions and recommendations.

ATC-16: This project, Development of a 5-Year Plan for Reducing the Earthquake Hazards Posed by Existing Nonfederal Buildings, was funded by FEMA and was conducted by a joint venture of ATC, the Building Seismic Safety Council and the Earthquake Engineering

Research Institute. The project involved a workshop in Phoenix, Arizona, where approximately 50 earthquake specialists met to identify the major tasks and goals for reducing the earthquake hazards posed by existing non-federal buildings nationwide. The plan was developed on the basis of nine issue papers presented at the workshop and workshop working group discussions. The Workshop Proceedings and Five-Year Plan are available through the Federal Emergency Management Agency, 500 "C" Street, S.W., Washington, DC 20472.

ATC-17: This report, *Proceedings of a Seminar and Workshop on Base Isolation and Passive Energy Dissipation*, was published under a grant from NSF. Available through the ATC office. (Published 1986, 478 pages)

ABSTRACT: The report contains 42 papers describing the state-of-the-art and state-of-the-practice in base-isolation and passive energy-dissipation technology. Included are papers describing case studies in the United States, applications and developments worldwide, recent innovations in technology development, and structural and ground motion issues. Also included is a proposed 5-year research agenda that addresses the following specific issues: (1) strong ground motion; (2) design criteria; (3) materials, quality control, and long-term reliability; (4) life cycle cost methodology; and (5) system response.

ATC-17-1: This report, *Proceedings of a Seminar on Seismic Isolation, Passive Energy Dissipation and Active Control*, was published under a grant from NSF. Available through the ATC office. (Published 1993, 841 pages)

ABSTRACT: The 2-volume report documents 70 technical papers presented during a two-day seminar in San Francisco in early 1993. Included are invited theme papers and competitively selected papers on issues related to seismic isolation systems, passive energy dissipation systems, active control systems and hybrid systems.

ATC-18: The report, *Seismic Design Criteria for Bridges and Other Highway Structures: Current and Future*, was published under a contract from the Multi-disciplinary Center for Earthquake Engineering Research (formerly NCEER), with funding from the

Federal Highway Administration. Available through the ATC office. (Published 1997, 152 pages)

ABSTRACT: This report documents the findings of a 4-year project to review and assess current seismic design criteria for new highway construction. The report addresses performance criteria, importance classification, definitions of seismic hazard for areas where damaging earthquakes have longer return periods, design ground motion, duration effects, site effects, structural response modification factors, ductility demand, design procedures, foundation and abutment modeling, soil-structure interaction, seat widths, joint details and detailing reinforced concrete for limited ductility in areas with low-to-moderate seismic activity. The report also provides lengthy discussion on future directions for code development and recommended research and development topics.

ATC-19: The report, *Structural Response Modification Factors* was funded by NSF and NCEER. Available through the ATC office. (Published 1995, 70 pages)

ABSTRACT: This report addresses structural response modification factors (R factors), which are used to reduce the seismic forces associated with elastic response to obtain design forces. The report documents the basis for current R values, how R factors are used for seismic design in other countries, a rational means for decomposing R into key components, a framework (and methods) for evaluating the key components of R, and the research necessary to improve the reliability of engineered construction designed using R factors.

ATC-20: The report, *Procedures for Postearthquake Safety Evaluation of Buildings*, was developed under a contract from the California Office of Emergency Services (OES), California Office of Statewide Health Planning and Development (OSHPD) and FEMA. Available through the ATC office (Published 1989, 152 pages)

ABSTRACT: This report provides procedures and guidelines for making on-the-spot evaluations and decisions regarding continued use and occupancy of earthquake damaged buildings. Written specifically for volunteer structural engineers and building inspectors, the report includes rapid and detailed

evaluation procedures for inspecting buildings and posting them as “inspected” (apparently safe), “limited entry” or “unsafe”. Also included are special procedures for evaluation of essential buildings (e.g., hospitals), and evaluation procedures for non-structural elements, and geotechnical hazards.

ATC-20-1: The report, *Field Manual: Postearthquake Safety Evaluation of Buildings*, was developed under a contract from OES and OSHPD. Available through the ATC office (Published 1989, 114 pages)

ABSTRACT: This report, a companion Field Manual for the ATC-20 report, summarizes the postearthquake safety evaluation procedures in brief concise format designed for ease of use in the field.

ATC-20-2: The report, *Addendum to the ATC-20 Postearthquake Building Safety Procedures* was published under a grant from the NSF and funded by the USGS. Available through the ATC office. (Published 1995, 94 pages)

ABSTRACT: This report provides updated assessment forms, placards, and procedures that are based on an in-depth review and evaluation of the widespread application of the ATC-20 procedures following five earthquakes occurring since the initial release of the ATC-20 report in 1989.

ATC-20-3: The report, *Case Studies in Rapid Postearthquake Safety Evaluation of Buildings*, was funded by ATC and R. P. Gallagher Associates. Available through the ATC office. (Published 1996, 295 pages)

ABSTRACT: This report contains 53 case studies using the ATC-20 Rapid Evaluation procedure. Each case study is illustrated with photos and describes how a building was inspected and evaluated for life safety, and includes a completed safety assessment form and placard. The report is intended to be used as a training and reference manual for building officials, building inspectors, civil and structural engineers, architects, disaster workers, and others who may be asked to perform safety evaluations after an earthquake.

ATC-20-T: The report, *Postearthquake Safety Evaluation of Buildings Training Manual* was developed under

a contract with FEMA. Available through the ATC office. (Published 1993, 177 pages; 160 slides)

ABSTRACT: This training manual is intended to facilitate the presentation of the contents of the ATC-20 and ATC-20-1. The training materials consist of 160 slides of photographs, schematic drawings and textual information and a companion training presentation narrative coordinated with the slides. Topics covered include: posting system; evaluation procedures; structural basics; wood frame, masonry, concrete, and steel frame structures; nonstructural elements; geotechnical hazards; hazardous materials; and field safety.

ATC-21: The report, *Rapid Visual Screening of Buildings for Potential Seismic Hazards: A Handbook*, was developed under a contract from FEMA. Available through the ATC office. (Published 1988, 185 pages)

ABSTRACT: This report describes a rapid visual screening procedure for identifying those buildings that might pose serious risk of loss of life and injury, or of severe curtailment of community services, in case of a damaging earthquake. The screening procedure utilizes a methodology based on a "sidewalk survey" approach that involves identification of the primary structural load resisting system and building materials, and assignment of a basic structural hazards score and performance modification factors based on observed building characteristics. Application of the methodology identifies those buildings that are potentially hazardous and should be analyzed in more detail by a professional engineer experienced in seismic design.

ATC-21-1: The report, *Rapid Visual Screening of Buildings for Potential Seismic Hazards: Supporting Documentation*, was developed under a contract from FEMA. Available through the ATC office. (Published 1988, 137 pages)

ABSTRACT: Included in this report are (1) a review and evaluation of existing procedures; (2) a listing of attributes considered ideal for a rapid visual screening procedure; and (3) a technical discussion of the recommended rapid visual screening procedure that is documented in the ATC-21 report.

ATC-21-2: The report, *Earthquake Damaged Buildings: An Overview of Heavy Debris and Victim Extrication*, was developed under a contract from FEMA. (Published 1988, 95 pages)

ABSTRACT: Included in this report, a companion volume to the ATC-21 and ATC-21-1 reports, is state-of-the-art information on (1) the identification of those buildings that might collapse and trap victims in debris or generate debris of such a size that its handling would require special or heavy lifting equipment; (2) guidance in identifying these types of buildings, on the basis of their major exterior features, and (3) the types and life capacities of equipment required to remove the heavy portion of the debris that might result from the collapse of such buildings.

ATC-21-T: The report, *Rapid Visual Screening of Buildings for Potential Seismic Hazards Training Manual* was developed under a contract with FEMA. Available through the ATC office. (Published 1996, 135 pages; 120 slides)

ABSTRACT: This training manual is intended to facilitate the presentation of the contents of the ATC-21 report. The training materials consist of 120 slides and a companion training presentation narrative coordinated with the slides. Topics covered include: description of procedure, building behavior, building types, building scores, occupancy and falling hazards, and implementation.

ATC-22: The report, *A Handbook for Seismic Evaluation of Existing Buildings (Preliminary)*, was developed under a contract from FEMA. Available through the ATC office. (Originally published in 1989; revised by BSSC and published as the *NEHRP Handbook for Seismic Evaluation of Existing Buildings* in 1992, 211 pages)

ABSTRACT: This handbook provides a methodology for seismic evaluation of existing buildings of different types and occupancies in areas of different seismicity throughout the United States. The methodology, which has been field tested in several programs nationwide, utilizes the information and procedures developed for and documented in the ATC-14 report. The handbook includes checklists, diagrams, and sketches designed to assist the user.

ATC-22-1: The report, *Seismic Evaluation of Existing Buildings: Supporting Documentation*, was developed under a contract from FEMA. (Published 1989, 160 pages)

ABSTRACT: Included in this report, a companion volume to the ATC-22 report, are (1) a review and evaluation of existing buildings seismic evaluation methodologies; (2) results from field tests of the ATC-14 methodology; and (3) summaries of evaluations of ATC-14 conducted by the National Center for Earthquake Engineering Research (State University of New York at Buffalo) and the City of San Francisco.

ATC-23A: The report, *General Acute Care Hospital Earthquake Survivability Inventory for California, Part A: Survey Description, Summary of Results, Data Analysis and Interpretation*, was developed under a contract from the Office of Statewide Health Planning and Development (OSHPD), State of California. Available through the ATC office. (Published 1991, 58 pages)

ABSTRACT: This report summarizes results from a seismic survey of 490 California acute care hospitals. Included are a description of the survey procedures and data collected, a summary of the data, and an illustrative discussion of data analysis and interpretation that has been provided to demonstrate potential applications of the ATC-23 database.

ATC-23B: The report, *General Acute Care Hospital Earthquake Survivability Inventory for California, Part B: Raw Data*, is a companion document to the ATC-23A Report and was developed under the above-mentioned contract from OSHPD. Available through the ATC office. (Published 1991, 377 pages)

ABSTRACT: Included in this report are tabulations of raw general site and building data for 490 acute care hospitals in California.

ATC-24: The report, *Guidelines for Seismic Testing of Components of Steel Structures*, was jointly funded by the American Iron and Steel Institute (AISI), American Institute of Steel Construction (AISC), National Center for Earthquake Engineering Research (NCEER), and NSF. Available through the ATC office. (Published 1992, 57 pages)

ABSTRACT: This report provides guidance for most cyclic experiments on components of steel structures for the purpose of consistency in experimental procedures. The report contains recommendations and companion commentary pertaining to loading histories, presentation of test results, and other aspects of experimentation. The recommendations are written specifically for experiments with slow cyclic load application.

ATC-25: The report, *Seismic Vulnerability and Impact of Disruption of Lifelines in the Conterminous United States*, was developed under a contract from FEMA. Available through the ATC office. (Published 1991, 440 pages)

ABSTRACT: Documented in this report is a national overview of lifeline seismic vulnerability and impact of disruption. Lifelines considered include electric systems, water systems, transportation systems, gas and liquid fuel supply systems, and emergency service facilities (hospitals, fire and police stations). Vulnerability estimates and impacts developed are presented in terms of estimated first approximation direct damage losses and indirect economic losses.

ATC-25-1: The report, *A Model Methodology for Assessment of Seismic Vulnerability and Impact of Disruption of Water Supply Systems*, was developed under a contract from FEMA. Available through the ATC office. (Published 1992, 147 pages)

ABSTRACT: This report contains a practical methodology for the detailed assessment of seismic vulnerability and impact of disruption of water supply systems. The methodology has been designed for use by water system operators. Application of the methodology enables the user to develop estimates of direct damage to system components and the time required to restore damaged facilities to pre-earthquake usability. Suggested measures for mitigation of seismic hazards are also provided.

ATC-28: The report, *Development of Recommended Guidelines for Seismic Strengthening of Existing Buildings, Phase I: Issues Identification and Resolution*, was developed under a contract with FEMA. Available through the ATC office. (Published 1992, 150 pages)

ABSTRACT: This report identifies and provides resolutions for issues that will affect the development of guidelines for the seismic strengthening of existing buildings. Issues addressed include: implementation and format, coordination with other efforts, legal and political, social, economic, historic buildings, research and technology, seismicity and mapping, engineering philosophy and goals, issues related to the development of specific provisions, and nonstructural element issues.

ATC-29: The report, *Proceedings of a Seminar and Workshop on Seismic Design and Performance of Equipment and Nonstructural Elements in Buildings and Industrial Structures*, was developed under a grant from NCEER and NSF. Available through the ATC office. (Published 1992, 470 pages)

ABSTRACT: These Proceedings contain 35 papers describing state-of-the-art technical information pertaining to the seismic design and performance of equipment and nonstructural elements in buildings and industrial structures. The papers were presented at a seminar in Irvine, California in 1990. Included are papers describing current practice, codes and regulations; earthquake performance; analytical and experimental investigations; development of new seismic qualification methods; and research, practice, and code development needs for specific elements and systems. The report also includes a summary of a proposed 5-year research agenda for NCEER.

ATC-29-1: The report, *Proceedings Of Seminar On Seismic Design, Retrofit, And Performance Of Nonstructural Components*, was developed under a grant from NCEER and NSF. Available through the ATC office. (Published 1998, 518 pages)

ABSTRACT: These Proceedings contain 38 papers presenting current research, practice, and informed thinking pertinent to seismic design, retrofit, and performance of nonstructural components. The papers were presented at a seminar in San Francisco, California, in 1998. Included are papers describing observed performance in recent earthquakes; seismic design codes, standards, and procedures for commercial and institutional buildings; seismic design issues relating to industrial and hazardous material facilities; design, analysis, and test-

ing; and seismic evaluation and rehabilitation of conventional and essential facilities, including hospitals.

ATC-30: The report, *Proceedings of Workshop for Utilization of Research on Engineering and Socioeconomic Aspects of 1985 Chile and Mexico Earthquakes*, was developed under a grant from the NSF. Available through the ATC office. (Published 1991, 113 pages)

ABSTRACT: This report documents the findings of a 1990 technology transfer workshop in San Diego, California, co-sponsored by ATC and the Earthquake Engineering Research Institute. Included in the report are invited papers and working group recommendations on geotechnical issues, structural response issues, architectural and urban design considerations, emergency response planning, search and rescue, and reconstruction policy issues.

ATC-31: The report, *Evaluation of the Performance of Seismically Retrofitted Buildings*, was developed under a contract from the National Institute of Standards and Technology (NIST, formerly NBS) and funded by the USGS. Available through the ATC office. (Published 1992, 75 pages)

ABSTRACT: This report summarizes the results from an investigation of the effectiveness of 229 seismically retrofitted buildings, primarily unreinforced masonry and concrete tilt-up buildings. All buildings were located in the areas affected by the 1987 Whittier Narrows, California, and 1989 Loma Prieta, California, earthquakes.

ATC-32: The report, *Improved Seismic Design Criteria for California Bridges: Provisional Recommendations*, was funded by the California Department of Transportation (Caltrans). Available through the ATC office. (Published 1996, 215 Pages)

ABSTRACT: This report provides recommended revisions to the current *Caltrans Bridge Design Specifications* (BDS) pertaining to seismic loading, structural response analysis, and component design. Special attention is given to design issues related to reinforced concrete components, steel components, foundations, and conventional bearings. The recommendations are based on recent research in the field of bridge seismic design and the performance

of Caltrans-designed bridges in the 1989 Loma Prieta and other recent California earthquakes.

ATC-34: The report, *A Critical Review of Current Approaches to Earthquake Resistant Design*, was developed under a grant from NCEER and NSF. Available through the ATC office. (Published, 1995, 94 pages)

ABSTRACT. This report documents the history of U. S. codes and standards of practice, focusing primarily on the strengths and deficiencies of current code approaches. Issues addressed include: seismic hazard analysis, earthquake collateral hazards, performance objectives, redundancy and configuration, response modification factors (*R* factors), simplified analysis procedures, modeling of structural components, foundation design, nonstructural component design, and risk and reliability. The report also identifies goals that a new seismic code should achieve.

ATC-35: This report, *Enhancing the Transfer of U.S. Geological Survey Research Results into Engineering Practice* was developed under a contract with the USGS. Available through the ATC office. (Published 1996, 120 pages)

ABSTRACT: The report provides a program of recommended "technology transfer" activities for the USGS; included are recommendations pertaining to management actions, communications with practicing engineers, and research activities to enhance development and transfer of information that is vital to engineering practice.

ATC-35-1: The report, *Proceedings of Seminar on New Developments in Earthquake Ground Motion Estimation and Implications for Engineering Design Practice*, was developed under a cooperative agreement with USGS. Available through the ATC office. (Published 1994, 478 pages)

ABSTRACT: These Proceedings contain 22 technical papers describing state-of-the-art information on regional earthquake risk (focused on five specific regions--California, Pacific Northwest, Central United States, and northeastern North America); new techniques for estimating strong ground motions as a function of earthquake source, travel path, and site parameters; and new developments

Applied Technology Council Projects And Report Information

specifically applicable to geotechnical engineering and the seismic design of buildings and bridges.

ATC-37: The report, *Review of Seismic Research Results on Existing Buildings*, was developed in conjunction with the Structural Engineers Association of California and California Universities for Research in Earthquake Engineering under a contract from the California Seismic Safety Commission (SSC). Available through the Seismic Safety Commission as Report SSC 94-03. (Published, 1994, 492 pages)

ABSTRACT. This report describes the state of knowledge of the earthquake performance of nonductile concrete frame, shear wall, and infilled buildings. Included are summaries of 90 recent research efforts with key results and conclusions in a simple, easy-to-access format written for practicing design professionals.

ATC-40: The report, *Seismic Evaluation and Retrofit of Concrete Buildings*, was developed under a contract from the California Seismic Safety Commission. Available through the ATC office. (Published, 1996, 612 pages)

ABSTRACT. This 2-volume report provides a state-of-the-art methodology for the seismic evaluation and retrofit of concrete buildings. Specific guidance is provided on the following topics: performance objectives; seismic hazard; determination of deficiencies; retrofit strategies; quality assurance procedures; nonlinear static analysis procedures; modeling rules; foundation effects; response limits; and nonstructural components. In 1997 this report received the West-

ern States Seismic Policy Council "Overall Excellence and New Technology Award."

ATC-44: The report, *Hurricane Fran, South Carolina, September 5, 1996: Reconnaissance Report*, is available through the ATC office. (Published 1997, 36 pages.)

ABSTRACT: This report represents ATC's expanded mandate into structural engineering problems arising from wind storms and coastal flooding. It contains information on the causative hurricane; coastal impacts, including storm surge, waves, structural forces and erosion; building codes; observations and interpretations of damage; and lifeline performance. Conclusions address man-made beach nourishment, the effects of missile-like debris, breaches in the sandy barrier islands, and the timing and duration of such investigations.

ATC-R-1: The report, *Cyclic Testing of Narrow Plywood Shear Walls*, was developed with funding from the Henry J. Degenkolb Memorial Endowment Fund of the Applied Technology Council. Available through the ATC office (Published 1995, 64 pages)

ABSTRACT: This report documents ATC's first self-directed research program: a series of static and dynamic tests of narrow plywood wall panels having the standard 3.5-to-1 height-to-width ratio and anchored to the sill plate using typical bolted, 9-inch, 5000-lb. capacity hold-down devices. The report provides a description of the testing program and a summary of results, including comparisons of drift ratios found during testing with those specified in the seismic provisions of the 1991 *Uniform Building Code*.

ATC BOARD OF DIRECTORS (1973-Present)

Milton A. Abel	(1979-85)	John F. Meehan*	(1973-78)
James C. Anderson	(1978-81)	Andrew T. Merovich	(1996-99)
Thomas G. Atkinson*	(1988-94)	David L. Messinger	(1980-83)
Albert J. Blaylock	(1976-77)	Stephen McReavy	(1973)
Robert K. Burkett	(1984-88)	Bijan Mohraz	(1991-97)
James R. Cagley	(1998-2001)	William W. Moore*	(1973-76)
H. Patrick Campbell	(1989-90)	Gary Morrison	(1973)
Arthur N. L. Chiu	(1996-99)	Robert Morrison	(1981-84)
Anil Chopra	(1973-74)	Ronald F. Nelson	(1994-95)
Richard Christopherson*	(1976-80)	Joseph P. Nicoletti*	(1975-79)
Lee H. Cliff	(1973)	Bruce C. Olsen*	(1978-82)
John M. Coil*	(1986-87, 1991-97)	Gerard Pardoen	(1987-91)
Eugene E. Cole	(1985-86)	Stephen H. Pelham	(1998-2001)
Edwin T. Dean	(1996-99)	Norman D. Perkins	(1973-76)
Robert G. Dean	(1996-2001)	Richard J. Phillips	(1997-2000)
Edward F. Diekmann	(1978-81)	Maryann T. Phipps	(1995-96)
Burke A. Draheim	(1973-74)	Sherrill Pitkin	(1984-87)
John E. Droeger	(1973)	Edward V. Podlack	(1973)
Nicholas F. Forell*	(1989-96)	Chris D. Poland	(1984-87)
Douglas A. Foutch	(1993-97)	Egor P. Popov	(1976-79)
Paul Fratessa	(1991-92)	Robert F. Preece*	(1987-93)
Sigmund A. Freeman	(1986-89)	Lawrence D. Reaveley*	(1985-91)
Barry J. Goodno	(1986-89)	Philip J. Richter*	(1986-89)
Mark R. Gorman	(1984-87)	John M. Roberts	(1973)
Gerald H. Haines	(1981-82, 1984-85)	Charles W. Roeder	(1997-2000)
William J. Hall	(1985-86)	Arthur E. Ross*	(1985-91, 1993-94)
Gary C. Hart	(1975-78)	C. Mark Saunders*	(1993-2000)
Lyman Henry	(1973)	Walter D. Saunders*	(1975-79)
James A. Hill	(1992-95)	Lawrence G. Selna	(1981-84)
Ernest C. Hillman, Jr.	(1973-74)	Wilbur C. Schoeller	(1990-91)
Ephraim G. Hirsch	(1983-84)	Samuel Schultz*	(1980-84)
William T. Holmes*	(1983-87)	Daniel Shapiro*	(1977-81)
Warner Howe	(1977-80)	Jonathan G. Shipp	(1996-99)
Edwin T. Huston*	(1990-97)	Howard Simpson*	(1980-84)
Paul C. Jennings	(1973-75)	Mete Sozen	(1990-93)
Carl B. Johnson	(1974-76)	Donald R. Strand	(1982-83)
Edwin H. Johnson	(1988-89, 1998-2001)	James L. Stratta	(1975-79)
Stephen E. Johnston*	(1973-75, 1979-80)	Scott Stedman	(1996-97)
Joseph Kallaby*	(1973-75)	Edward J. Teal	(1976-79)
Donald R. Kay	(1989-92)	W. Martin Tellegen	(1973)
T. Robert Kealey*	(1984-88)	John C. Theiss*	(1991-98)
H. S. (Pete) Kellam	(1975-76)	Charles H. Thornton*	(1992-99)
Helmut Krawinkler	(1979-82)	James L. Tipton	(1973)
James S. Lai	(1982-85)	Ivan Viest	(1975-77)
Gerald D. Lehmer	(1973-74)	Ajit S. Virdee*	(1977-80, 1981-85)
James R. Libby	(1992-98)	J. John Walsh	(1987-90)
Charles Lindbergh	(1989-92)	Robert S. White	(1990-91)
R. Bruce Lindermann	(1983-86)	James A. Willis*	(1980-81, 1982-86)
L. W. Lu	(1987-90)	Thomas D. Wosser	(1974-77)
Walter B. Lum	(1975-78)	Loring A. Wyllie	(1987-88)
Kenneth A. Luttrell	(1991-98)	Edwin G. Zacher	(1981-84)
Newland J. Malmquist	(1997-2000)	Theodore C. Zsutty	(1982-85)
Melvyn H. Mark	(1979-82)		
John A. Martin	(1978-82)	* President	

ATC EXECUTIVE DIRECTORS (1973-Present)

Ronald Mayes	(1979-81)	Roland L. Sharpe	(1973-79)
Christopher Rojahn	(1981-present)		

Applied Technology Council

Sponsors, Supporters, and Contributors

Sponsors

Structural Engineers Association of California
James R. & Sharon K. Cagley
John M. Coil
Burkett & Wong

Supporters

Charles H. Thornton
Degenkolb Engineers
Japan Structural Consultants Association

Contributors

Lawrence D. Reaveley
Omar Dario Cardona Arboleda
Edwin T. Huston
John C. Theiss
Reaveley Engineers
Rutherford & Chekene
E. W. Blanch Co.

